Durham University

Durham E-Theses

An assessment of fluid flow and overpressure modelling m selected North Sea and Laramide basins

Stephen Cross Edwards

How to cite:

Edwards, Stephen Cross (1994) An assessment of fluid flow and overpressure modelling m selected North Sea and Laramide basins. Doctoral thesis, Durham University.

Use policy

The full-text may be used and/or reproduced, and given to third parties in any format or medium, without prior permission or charge, for personal research or study, educational, or not-for-profit purposes provided that:

- a full bibliographic reference is made to the original source
- a https://etheses.durham.ac.uk/id/eprint/5881/ is made to the metadata record in Durham E-Theses
- the full-text is not changed in any way

The full-text must not be sold in any format or medium without the formal permission of the copyright holders.

Please consult the full Durham E-Theses policy for further details.

Academic Support Office, The Palatine Centre, Durham University, Stockton Road, Durham, DH1 3LE
e-mail: e-theses.admin@durham.ac.uk Tel: +44 0191 334 6107
https://etheses.durham.ac.uk

An Assessment of Fluid Flow and Overpressure Modelling in Selected North Sea and Laramide Basins

Stephen Cross Edwards (University College)

A thesis submitted to the University of Durham
for the degree of Doctor of Philosophy

The copyright of this thesis rests with the author.
No quotation from it should be published without
his prior written consent and information derived
from it should be acknowledged.

February 1994

27 JUN 1994

To Mum, Dad and Zac

The greater the prize
the greater the effort
the greater the pain
the greater the pleasure

Paul von Hindenberg

Declaration

The contents of this thesis is the original work of the author and has not been previously published for a degree at this university or any other institution. The work of others is acknowledged throughout this thesis by reference.

Stephen .C. Edwards BSc. (Hons) St.A.
Department of Geological Sciences
University of Durham
England

Copyright

The copyright of this thesis rests with the author. Any information taken from it should be acknowledged. Otherwise, no quotation should be published without prior written permission from the author.

An Assessment of Fluid Flow and Overpressure modelling in selected North Sea and Laramide Basins

Abstract

The occurrence of overpressure observed in petroleum bearing basins must be understood in terms of generation and distribution in order to build up a fluid flow history. Overpressure influences expulsion and migration of hydrocarbons from source rocks. This thesis details and interprets observations and results of a case study into aspects of overpressure distribution, fluid flow patterns, causative mechanisms, palaeo-pressure and subsequent pressure history, the surface expression of overpressure and the mechanical strength relationships of sealing rocks.

One of the principle study areas was the Alwyn field in the Northern North Sea. The overpressure distribution over the field area was seen not to be uniform. Organic geochemical data indicated that the source of reservoired hydrocarbons and associated fluids was the Viking Graben depocentre. Fluid inclusion data recorded in specific diagenetic mineral phases interpreted fluid flow conditions of hydrocarbons into the reservoir under normal pressures but elevated temperatures. When combined with computer generated pressure models, these diagenetic events were exclusive of modelled overpressure periods. The greatest contribution of overpressure was modelled as being a result of compaction disequilibrium but with a likely contribution from the thermal cracking of oil to gas which would also account for the present day distribution of overpressure across the Alwyn field area.

The Uinta Basin with its relatively simple burial and thermal history allowed the production of a model involving a temporal history of overpressure generation, fracture development, regional tectonism, hydrocarbon maturation and expulsion and the process of Gilsonite emplacement. It is inferred that initial hydraulically induced fracturing of the Green River and overlying formations was a result of combined overpressure due to disequilibrium and regional extension with a possible contribution from the maturation of the source rock. This study recognised that the hydrocarbon was emplaced under a high pressure regime with evidence provided by the existence of forcibly injected hydrocarbon sills. Hydrocarbons fractionated in the pre-existing vertical fractures to leave residual highly viscous and immobile hydrocarbons in veins seen at the present day.

The third major component of this study detailed results from an assessment of the mechanical capacity of sealing rocks with respect to specific composition and mineralogy. It was found that increasing organic carbon decreased the compressive strength of the tested shale specimens. This relationship was interpreted as a possible result of the interaction of alkaline fluids to produce a dispersant which acts to reduce the cohesion of the organic rich shale.

Acknowledgements

This Ph.D. would not have been initiated without the financial and logistical support of Shell International and the Petroleum Science and Technology Institute (PSTI). Linda Armstrong and Howard Johnson for selecting my Ph.D. proposal. Michelle Martin, Sharon Munro, Jim Docherty, Martin Eves, Rick Preston and Peter Ashford of Shell are all thanked (especially for the Audi Quattro!!). Stewart Brown and Pauline Torley of PSTI are gratefully thanked for their swift response to 'yet another expenses claim'. James Iliffe of PSTI for the loan of his snake boots.

Dick Swarbrick, my supervisor, is gratefully thanked for his initial acceptance of supervising the project and continued advice and support throughout my three and a half year sentence.

Ian Inglis, of Total Oil Marine, for consistently supplying all requested data for the Alwyn field study is thanked for his patience and goodwill. Half of this thesis would not exist without his help.

Gordon McLeod, Stewart Pech and Steve Larter of NRG for providing the geochemical analyses of the petroleum fluid inclusions and for general good advice. Linda Stalker for providing the 'Ladybird Guide to Biomarkers'.

Rob Marsden and John Dennis of the Department of Mineral Resources Engineering at Imperial College deserve medals for triaxially testing the Uinta Basin core samples. I wouldn't have known which was the 'on button' - a big cheers to them.

The Utah Saints - B.J. McPherson, Phil and Tish Armstrong, Jackie Bott and David Chapman of the University of Utah are thanked for help, accommodation, office space and beer in Salt Lake City. Also for the trip to Capitol Reef National Park is remembered for turning me into a rock lobster in 24 hours.

Roy Fitzsimmons and Steve Johnson for the crash course in high resolution sequence stratigraphy in Wyoming - It was 'famous potatoes' in Powder River with 'McPike The Vietnam Vet'.

Carolyn Olsen of the Utah Geological Survey for unlimited access to core and well records. Tom Chidsey of the UGS for base grids. Virginia Peterson of the Econolodge, Vernal for very reasonable rates in such harsh accommodation (air con,

cable T.V., swimming pool and free pizza). Alamo car hire at Denver Airport for upgrading my field vehicle to a Pontiac Firebird convertible. The Royal Mail are gratefully thanked for losing my field shots - a return trip to Utah would not have been possible without their uselessness and incompetence.

Dave Asbery for exposing a few of us to the exotic dancers of Gilesgate Moor. Alan Carr and Jon Booler for their behaviour on the above mentioned night in Gilesgate. Gerry Dresser for photographic work. Carol and Lynne for unlimited stationary and general banter.

Gary Lancaster, of Anadrill and the most outstanding statistic of the St. Andrews University beer festival, is thanked for remaining in Alaska throughout the duration of this Ph.D. Ian 'the village idiot' Cloak for putting his Access Card behind the bar in the Lamb and Flag in London. St. Chads RFC are thanked for socially enlightening rugby club dinners. Eric Halliday for coaching myself and the other members of the St. Chads Boat Club 1st IV SII crew.

All the Durham lads who were 'Damed - Gary, Andy, Mikey, Mark, Nilpf, Spod and Booler.

My office mates throughout my time in Durham - Microscope Billing, Chimera, Marsh and grateful thanks to Billy Butler and Timmy A. (The Word Wizard) for not complaining about my monopoly on the computer whilst writing up. Also, ex-St. Andrews old boys John Bole and Jon Freeman. Thanks must also go to Zoë for unfailing support and help in finishing this thing. Also, I gratefully acknowledge my brother's chequebook.

To British Rail for providing a one-way ticket out of Durham.

Finally to my Mum and Dad. I am endebted to you both on an unrealistic scale.

Contents

Chapter 1
Introduction and thesis outline

1.1 Introduction

Ever since the early days of oil well drilling and the bringing in of the 'gusher' to the present day multi-million dollar oil field and satellite developments, the existence of overpressure down hole has been treated with great importance. Successful well planning, efficient recovery programmes and reservoir integrity must include an understanding of sub surface pressure if the drilling process is to go ahead with the minimum of risk and hazard. Overpressure, although the understanding of the generation processes, distribution and detection is better understood with increasing technology and application, is still a largely unknown phenomenon. The mechanisms of overpressure generation and the maintenance of overpressure is largely individual and unique to the particular geological scenario.

This thesis details the existence of overpressure in two differing geological settings. Overlapping techniques have been used in the two case studies to constrain the pressure history and any associated processes of the two areas. Also, this thesis details the results of a mechanical test programme to observe any correlation of a sealing formation, which serves to contain overpressured reservoirs, with respect to its mineralogical and compositional characteristics.

The main aspects to this thesis are principally the assessment of likely generative overpressure mechanisms, the mechanics and effects of fluid flow, the estimation of palaeopressure and temperature using fluid inclusions, the development of a model which links diagenetic processes to reservoir pressure conditions, the value of computer based basin modelling and the correlation of mechanical and compositional data of seal formations.

Methodology and techniques employed in this thesis include organic geochemical maturity information, seismic modelling, basin modelling incorporating burial history analysis, pressure, maturity and kinetic modelling. Also fluid inclusion microthermometry, direct field observations, triaxial compressive testing, X-Ray diffraction and Total Organic Carbon analyses constitute the original data created in this study..

The thesis is (basically) divided into 3 principal chapters on which the pressure and fluid flow study is based: (Chapter 3) The fluid flow and overpressure modelling of

the Alwyn Field, North Sea; (Chapter 4) The evaluation of overpressure induced Gilsonite veins in the Uinta Basin, Utah; (Chapter 5) The multiple failure compression tests on the Green River Formation, Uinta Basin, Utah. Chapter 2 provides and overview of overpressure and Chapter 6 documents the main conclusions to this thesis.

1.2 Thesis outline

1.2.1 Chapter 2

This chapter introduces the principles and mechanisms of overpressure generation, maintenance and evaluation. Since basin modelling is used as the main tool of interpretation throughout this thesis, the variables and assumptions used in compaction, fluid flow, thermal and hydrocarbon generating processes have been defined and described.

1.2.2 Chapter 3

The Alwyn Field, an intermediate sized oil field, in the Northern North Sea provided one of the principal areas on which this thesis is based. The field is introduced in terms of overpressure distribution at the present day as well as the field structure and stratigraphy. The fluid flow pattern is then assessed using organic geochemical information to model maturity patterns. A generalised paragenetic sequence for the field is presented and within this framework, (2 phase) fluid inclusions containing both brine and petroleum were identified for microthermometry analyses. These analyses were then used to assess the pressure and temperature representative of reservoir conditions at the time of entrapment. This information is combined with published K-Ar dates to constrain these conditions in time. A model is presented to combine the rock data with the computer based simulations of pressure through time, which leads to a link between the pressure differential operating between pressure source and reservoir and the diagenetic process.

1.2.3 Chapter 4

The Uinta Basin is a petroliferous basin situated in the Rocky Mountain region of the Western Interior of the United States. Its tectonic and thermal evolution differs greatly from the Alwyn Field. Gilsonite (a solid hydrocarbon) filled veins occur in the eastern part of the Uinta Basin provides a unique surface expression, and are attributed to an earlier period, of previous overpressure. The field relations of these veins with respect to structure and wall rock interaction are discussed. Geochemical information, utilising vitrinite reflectance and biomarker trends are discussed with respect to likely petroleum source horizons. The identified source horizon is modelled in terms of pressure evolution and maturation/kinetic development. When combined with field

observations a basin evolution is proposed to account for the initiation and filling of these veins. The effects of time dependant strain associated with differential fractionation is discussed to account for the present day form of the veins and their constituents.

1.2.4 Chapter 5

This chapter investigates the mechanical capacities of selected shale rich samples from the Green River Formation, which acts as a seal for overpressured Tertiary reservoirs in the Uinta Basin. The aim of this study is to infer any possible correlation between peak strength of the samples with respective compositional differences of the bulk mineralogy and clay mineral assemblages. Total Organic Carbon (TOC) analyses were also run to provide a further possible constraint of any trend in the mechanical dataset.

1.2.5 Chapter 6

The principal conclusions to the thesis are presented in this chapter.

Chapter 2
An overview of overpressure mechanics and basin modelling parameters

2.1 Introduction

Anomalous pore fluid pressures frequently occur during the development and evolution of a sedimentary basin. The generation, maintenance and distribution of this abnormal pressure, or overpressure, is of great importance to the drilling process from aspects of safety and well planning and development. Overpressure also has the potential to exist both in porous and permeable rocks as well as in source rocks where it can influence expulsion and migration from source rocks and the respective behaviour of fluids through the carrier system.

This chapter will review previous key studies of petroleum provinces where overpressure has been experienced. Basin modelling techniques and assumptions, which have been used throughout this study, are also documented in this chapter. Several of these previous studies of overpressure offer theories regarding the likely causative mechanisms and distribution of the overpressure. Each major mechanism of overpressure generation is summarised in this chapter. Maintenance and retention of overpressure is also critically assessed.

2.1.1 Terminology and Definitions

Any pressure which exists in a state either negative or positive relative to the ambient pressure conditions describes either a surpressure (below normal ambient pressure) or an overpressure (above normal ambient pressure). As all pressures described and referred to in this study (unless specifically noted otherwise) are subject to the physical forces governing natural systems, any surpressure or overpressure must be inferred to be a physically metastable phenomenon. As the surpressured or overpressured system continually readjusts to equilibrate with the ambient pressure state, these overpressures must also be thought to be transient through time. Some definitions and terminology which are referred to in this study are given below (also Fig.2.1.1):

Hydrostatic pressure:
is the pore pressure that is recorded when the pore fluids only support the weight of the overlying pore fluids and the weight of the pore fluid displaced by the rock matrix (Mann and Mackenzie, 1990). The pore fluids will obviously have specific properties dependant largely on the density of the fluids. Pore fluid salinity will determine the specific hydrostatic pressure gradient.

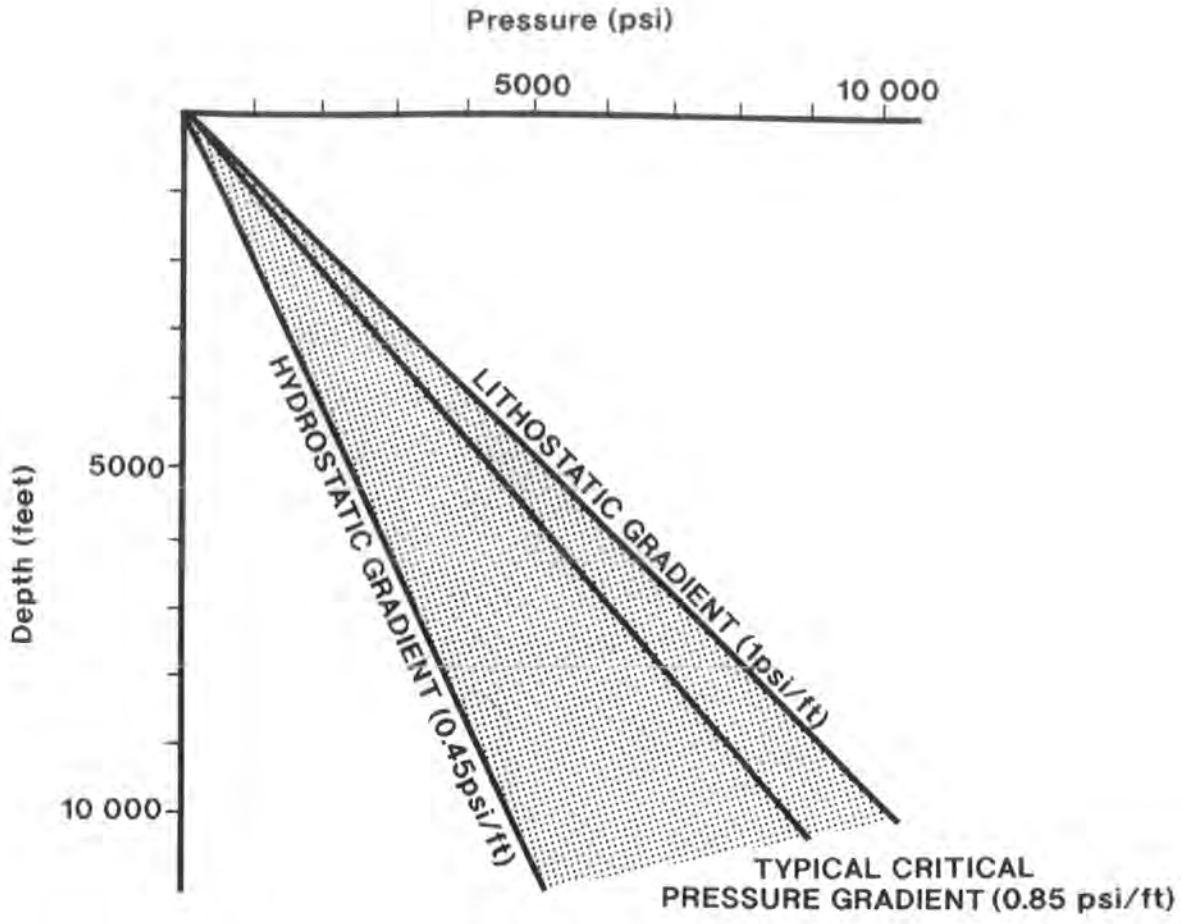

Fig.2.1.1a - Pressure versus depth plot showing the hydrostatic gradient, typical critical pressure gradient and lithostatic gradient. Stipled area depicts overpressure

Overpressure (otherwise referred to as abnormal pressure or geopressure):
is defined as the zone of pressure which lies above the gradient describing the hydrostatic regime but below the lithostatic gradient.

Lithostatic pressure:
is the theoretical maximum that the pore fluids can attain in the absence of any tensile strength in the rock. If this limit is surpassed, the shear strength of the rock is reached and fracturing occurs with the associated loss of fluids. Mud volcanoes, involving flowage, occur when the pore pressure transiently exceeds lithostatic pressure. The commonly quoted lithostatic gradient is 1.0psi/ft (Barker, 1972: Buhrig, 1989).

Critical pressure:
is the fluid pressure at which fractures are induced perpendicular to the direction in which minimum compressive stress acts (Mann and Mackenzie, 1990). Typically, this critical pressure lies in the region of 70-90% of the lithostatic pressure (Du Rochet, 1981) and observed to be approximately 85% or greater for pore fluids in the Gulf of Mexico (Stuart, 1960). Therefore, this critical pressure gradient is in the range of 0.7-0.9 psi/ft. At this pressure transition, cohesion is lost in the material and any pre-existing fractures initiate perpendicular to the minimum compressive stress fields. Fluids and pressure will leak from the system as the pressure equilibrium readjusts.

Effective stress:
can be expressed as the difference between the vertical stress borne by the sediment and the internal fluid pressure. It is described by Terzaghi (1948) in the form:

$$\sigma = S - \rho$$ where σ = effective stress
S = vertical stress/overburden stress
ρ = pore fluid pressure

If the effective stress is less than would be obtained by a hydrostatic system then the pore fluids are described as overpressured.

The hydrostatic gradient describes the fluid pressure at any depth where there is complete vertical fluid communication throughout the pore network to the surface. The hydrostatic gradient varies with salinity and in the North Sea, 0.44-0.45psi/ft is commonly used (Buhrig, 1989: Mann and Mackenzie, 1990) reflecting the pore waters being relatively fresh (fresh water = 0.43psi/ft; saturated brine = 0.53psi/ft, Whittaker, 1980).

To enjoy any anomalous amount of pore pressure, an overpressured regime must be intrinsically discrete or compartmentalised with respect to the hydrostatic regime. Therefore, a critical condition for the development and maintenance of overpressure is the restriction of fluid, vapour and gas flow (Jansa and Noguera, 1990). These

conditions require that the overpressured zone is separate from the adjacent hydrostatic regime and an impermeable barrier, or seal, must exist normally separated by a zone between the overpressured and hydrostatic systems. The following sections will review overpressure mechanisms and maintenance.

2.2 Overpressure Mechanics

This section reviews and discusses theories and postulated ideas on generative overpressure mechanisms and the controls on abnormal pore pressure. Historically, overpressure existence has been cited as a consequence of one of the following mechanisms of generation, which are ranked in terms of primary or secondary importance in the potential contribution to develop overpressure:

1) Compaction disequilibrium (primary)
2) Hydrocarbon thermal maturation (primary)
3) Montmorillonite/Smectite dehydration or The chemical transformation of mixed layered clays to illite (primary) and anhydrite to gypsum.
4) Aquathermal pressuring (secondary)
5) Osmosis (secondary)
6) Tectonism (secondary)

2.2.1 Compaction Disequilibrium (rapid sediment loading)

The recognition and association of abnormally pressured shales with undercompaction or an 'higher than expected' porosity has been intimated by various workers (Ruby and Hubbert, 1959; Hottman and Johnson, 1965 Magara, 1968; Carstens and Dypvik, 1980). This correlation lays the basis of a critical principle for recognising undercompaction in shales and its common, but not exclusive, association with overpressure. Many detection and overpressure evaluation techniques also base the ability of an instrument's capability to respond to an abnormal shale porosity as a parameter and function of the amount of overpressure generated. Although a number of studies observe this correlation, Carstens and Dypvik (1980) describe a shale sequence in which the onset of abnormal formation pressure does not seem to be coincident with any increase in shale porosity. However, the intimate relationship in areas particularly where massive argillaceous sequences are observed and the burial history records a relatively rapid burial rate for these sediments (such as the Gulf of Mexico - Plumley, 1980) suggests that this potential generative mechanism of overpressure should be seriously considered.

The mechanism operates, basically, by the inability of compacting shales to expel interlayer and interpore fluid quickly enough to maintain a normal pressure state. When argillaceous sediments first settle onto a medium such as the sea floor, this sediment undergoes initial compaction as a result of continued deposition and settling of material from the substrate. During initial compaction, the argillaceous components of this sediment adopts a 'house of cards' structure (Fig.2.2.1a) in which only primitive ordering of constituent members exists (mainly ionic ordering at this level). The initial result is the loss of interlayer fluid as the sediment reorganises and this fluid is lost to the surrounding hydraulic system (ie. expelled upward, Bethke, 1985). At this stage, the entire system remains in the hydrostatic regime. Further compaction takes place under continued burial and, depending upon specific sedimentation rate, porosity loss and coherence to loading, the argillaceous layers will adjust to the additional load by expelling interlayer and interpore fluid thus constantly re-equilibrating the pressure system to achieve an hydrostatic condition.

With a high porosity and permeability in its initial state, argillaceous sediments (such as one composed of flocculating clays) will allow the expulsion of ionically bound interlayer (lying between individual clay layers as opposed to internally and chemically bound water within individual clay crystals) fluid in the direction of least resistance. Flow will be directed towards a lower pressure zone. Such a zone may be a porous sand layer or a similar conduit such as a fault or fracture zone. However, such structural heterogenieties are uncommon at initial compaction depths (0-500m). Therefore, hydrostatic conditions will operate in the compacting sediment as long as interlayer and interpore fluid can escape. This state of equilibrium can only be maintained by following and adhering to critical criteria during compaction and if the following conditions are upset then the sediment pile will proceed into a state described as compaction disequilibrium. This condition will display itself as an undercompacted and, very often, overpressured sequence. The conditions of equilibrium are:

1) The sedimentation and compaction rate must remain slow enough to allow free and bound water to escape from the compacting sediment (Fig.2.2.1a). Thus, the permeability afforded by the sediment must be sufficient to allow and transport the interstitial fluid out of the system.

2) The expelling fluids must have access to the greater hydrostatic network. Therefore pressure communication must exist between compacting and dewatering units to the surface or to an interface such as carrier beds or by structural conduits.

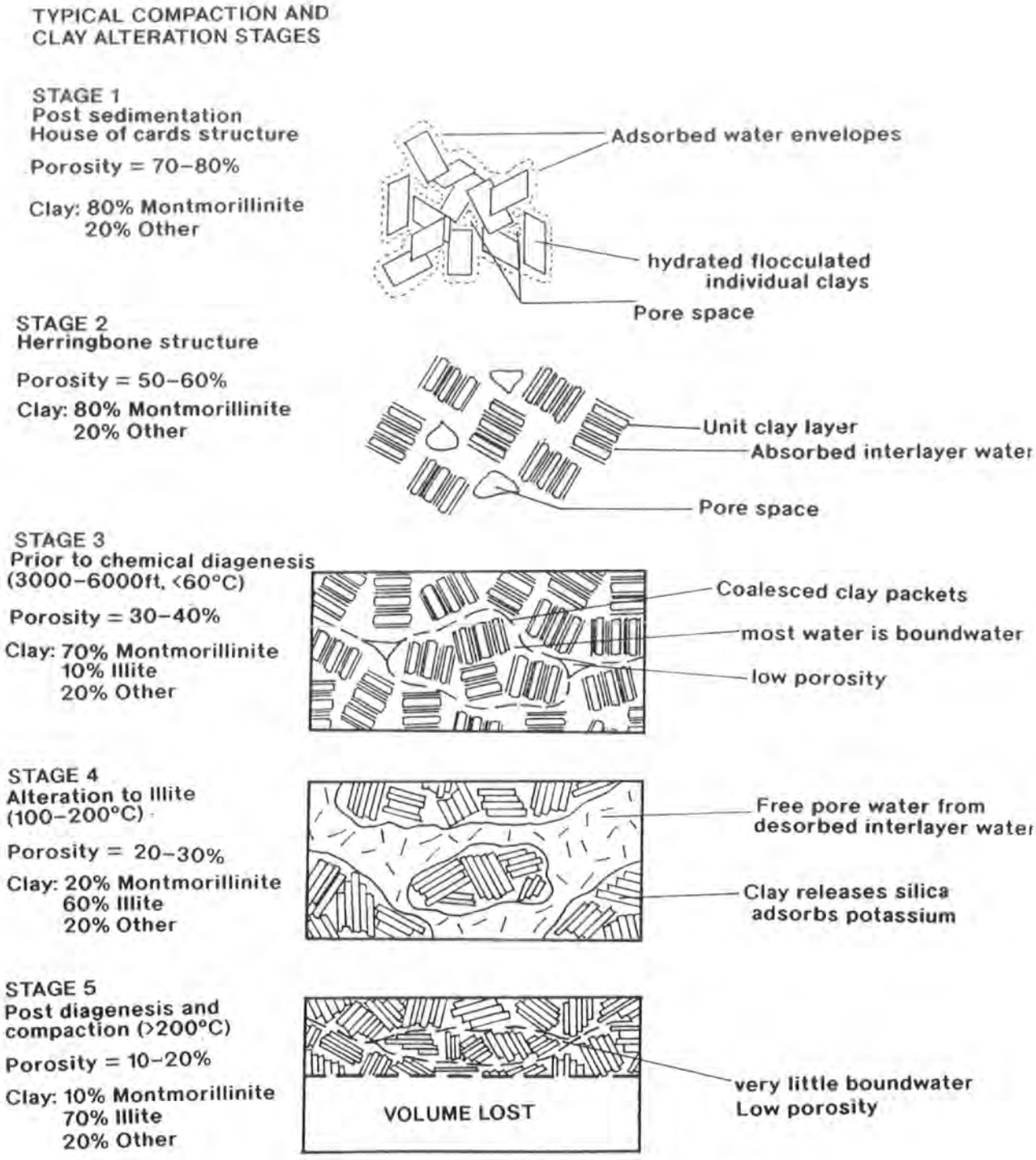

Fig.2.2.1a - Compaction stages of an argillaceous sediment and the clay transformation of smectite to illite with increasing burial, temperature and ion exchange. Modified from Powers (1967)

If any of these variables and their associated parameters are denied dynamic reorganisation due to a change in conditions then the expulsion of excess pore fluid will be impeded with a resultant increase in pore pressure. Another effect of this onset and generation of overpressure is that excess pore fluids contribute to support an increasing overburden load but further compaction of the sediment need not occur as, if the pore fluid is a brine or water, pore fluids are almost incompressible and normal compaction will not resume until hydraulic communication with the hydrostatic regime is re-established or pressure dissipation takes place.

Because of the inherent correlation and occurrence of overpressure with thick shale sequences which have been deposited in a relatively rapid period (eg. Green River Formation, Uinta Basin, Utah - Spencer, 1987), this mechanism would be thought of as being a primary process in low permeability sequences. Although shale sequences are of low permeability and the fact that perfect seals over geological time scales do not exist in the natural system, leakage due to the pressure differential across shale interfaces is to be expected. This is indicative of the dynamic and hydraulic potential of these overpressured zones. Therefore, over a series of shale/sand intervals, the pressure gradient would be expected to deviate in association with the hydraulic potential across the lithological boundary (Fig.2.2.1b). Flow will be transmitted from the shales to the sand horizons if these sands are linked to a hydraulic head and under these conditions the sands will reflect hydrostatic conditions. These dramatic changes in pressure can cause problems in borehole drilling.

2.2.2 Thermal Maturation of Hydrocarbons

Overpressures identified in normally compacted sediments must be explained by mechanisms other than compaction disequilibrium. This particular scenario of overpressured but normally compacted rocks has been identified by Jansa and Noguera (1990) in the Venture Gas field, offshore Canada. Jansa and Noguera (1990) identified the co-occurrence of peak wet gas generation with the top of an overpressured zone and cite this as compelling evidence for the pressure increase to be caused by the thermal alteration of kerogens to wet gas within a sealed reservoir of constant volume. There are principally two stages of the hydrocarbon thermal maturation process have been considered to generate overpressure.

Maturation of kerogen to liquid oil and associated gas has been cited by Meisnner (1987), Hunt (1979) and Spencer (1987) as generating a volume increase during the thermal reaction.

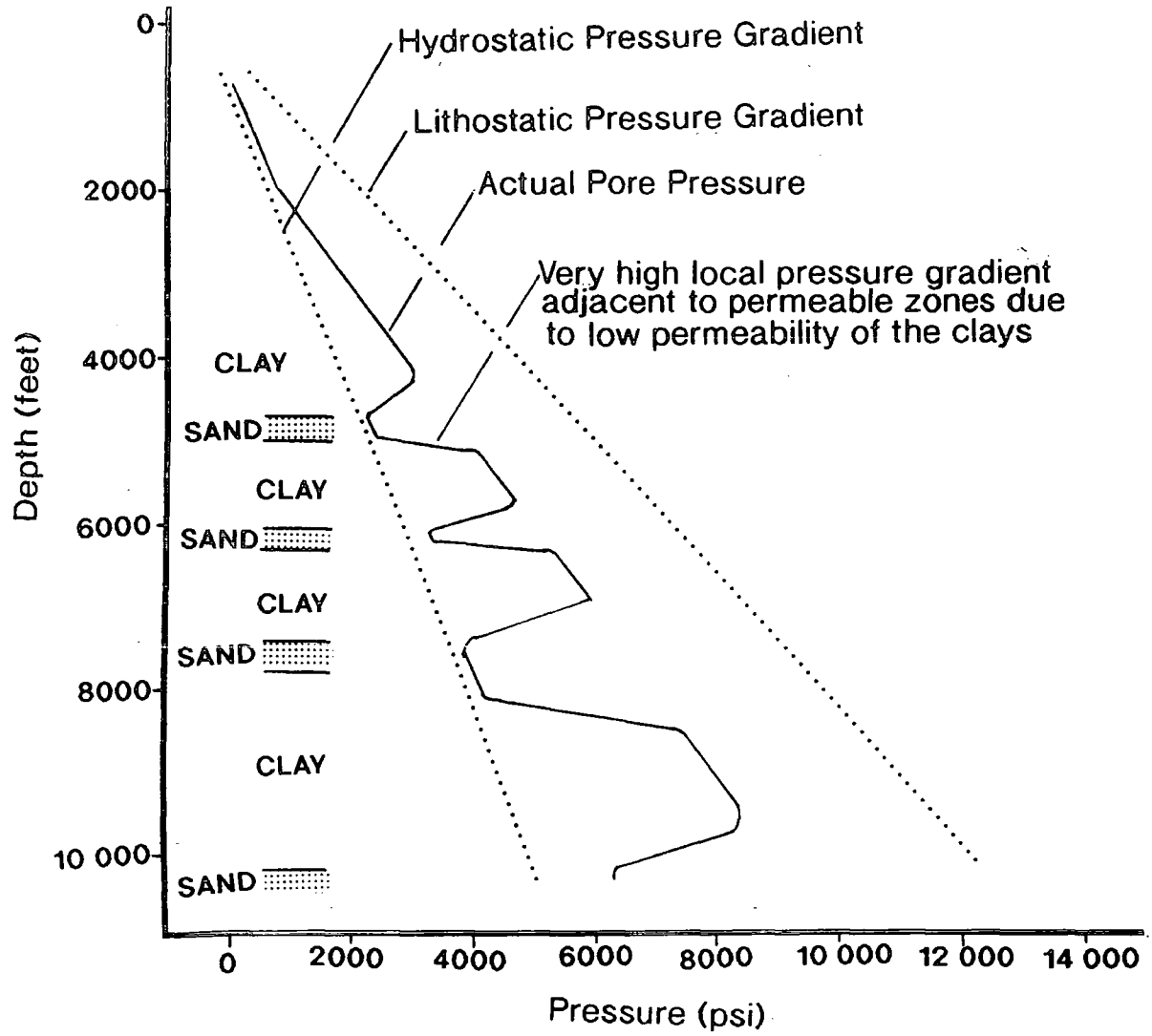

Fig.2.2.1b - Typical pre pressure versus depth plot of compaction disequilibrium derived overpressures also illustrating the drainage of overpressure to hydrostatically pressured sand units. From Whittaker (1980)

Also, the thermal cracking of oil to gas has been calculated by Barker (1990) as producing a vast increase in products compared to reactants.

Spencer (1987) also attributes basin wide, deep overpressure to the active generation of hydrocarbons in the Rocky Mountain region. Spencer (1987) has observed several types of sedimentary successions have significant overpressuring in the Uinta Basin, Utah and in the Williston, Powder River and Wind River Basins, Wyoming. The common observation between these basins is the existence of overpressured Cretaceous reservoirs which have been filled from organic source beds still capable of hydrocarbon generation at the present (Spencer, 1987), indicating that these overpressured reservoirs are experiencing recent to present day overpressure charge.

Barker (1990) calculates that one arbitrary volume of oil thermally cracks to 534.3 volumes of gas (at standard temperature and pressure). Barker (1990) also states that the rising temperature that accompanies increasing burial will convert oil in a reservoir into thermal gas by cracking. Therefore, if liquid hydrocarbons are thermally cracked in a sealed reservoir unit the associated volume expansion will create a greater pressure within the sealed unit. Barker (1990) considers the hydrocarbon balance during this thermal alteration and calculates that approximately $3000ft^3$ ($85m^3$) will be generated from one barrel of oil. In addition to the generated gas, another by by-product of the thermal alteration is a graphitic precipitate which has a lower volume than the parent oil. Barker (1990) combines data for gas solubility in pore water and gas non-ideality so that volumetric, and hence pressure, relationships can be calculated for any degree of thermal cracking.

Although these calculations conducted by Barker (1990) will favour large amounts of generated overpressure during the thermal alteration of oil to gas, other variables at work in the natural system must be considered. Solubility of the gaseous product from the reaction will depend upon composition, salinity of the pore water and the compressibility of the gas. Similarly, other compounds and reactants available to the cracking oil such as sulphur must be considered. Sulphur can strip large quantities of hydrogen from crude oil producing H_2S. This reaction is likely to be particularly important for oils in carbonate reservoirs because they are often associated with evaporites containing abundant sulphur bearing minerals (eg. anhydrite) (Barker, 1990). The calculations conducted by Barker (1990) assume standard temperature and pressure (STP). The effect of overburden pressure will obviously have an effect on the expandability of gas that is being produced. Thus, the arbitrary unit of 534.3 volumes of gas may seriously be reduced upon the introduction of overburden and confining

pressure. Calculations taking this factor into account have been conducted in the Alwyn Field study (section 3.5.5).

Barker (1990) summarises with a theoretical calculation whereupon within a completely oil filled reservoir, only 1% of that oil needs to thermally crack to gas to sufficiently raise the internal pore pressure to surpass the lithostatic gradient. This would suggest very little oil is required to crack to gas to initiate fractures in the seal. However, once the onset of gas generation is reached, in terms of temperature, the likely effect would be to crack a vastly greater amount than 1% of the available liquid hydrocarbon. This would then cause fracturing in the seal and associated dissipation of any overpressure and gas.

Clearly, from studies conducted by Spencer (1987); Mudford (1990) and Jansa and Noguera (1990), other independent variables such as overburden stress must be considered to effectively contain the generated volumes of gas from the thermal reaction of oil to gas.

The thermal alteration of kerogen to oil and associated gas has been recognised as a potential overpressure mechanism. Other dependant variables which may be significant include kerogen type and associated kinetics, hydrocarbon yield of the source rock, rate of maturation and expulsion efficiency of the source rock.

2.2.3 Chemical Transformation of Smectite to Illite

It has originally been suggested that illite is formed as a diagenetic product from smectite (Burst, 1969) and that this clay transformation can occur over a very small depth range. Burst (1969) suggested also that the reaction can occur over lithostratigraphic boundaries indicating that the reaction is not dependant on lithology or stratigraphic interval. The rate of alteration appears to increase and occur at shallower depths in areas of high geothermal gradients (Burst, 1969) suggesting that the reaction is dependant on the depth of burial and therefore is temperature dependant. Magara (1975) also recognised that the reaction occurred with increasing temperature and burial. Boles and Franks (1979) proposed that the reaction is also dependant upon the presence of K^+ ions which, when adsorbed, completes the transformation to illite (Fig.2.2.3a). Also, the presence of K^+ ions at temperatures lower than that necessary for thermal dewatering also causes the collapse of the smectite lattice and thus illite may be formed at lower temperatures (Whittaker, 1980). Freed and Peacor (1989) suggested that in addition to heat and ion exchange, the

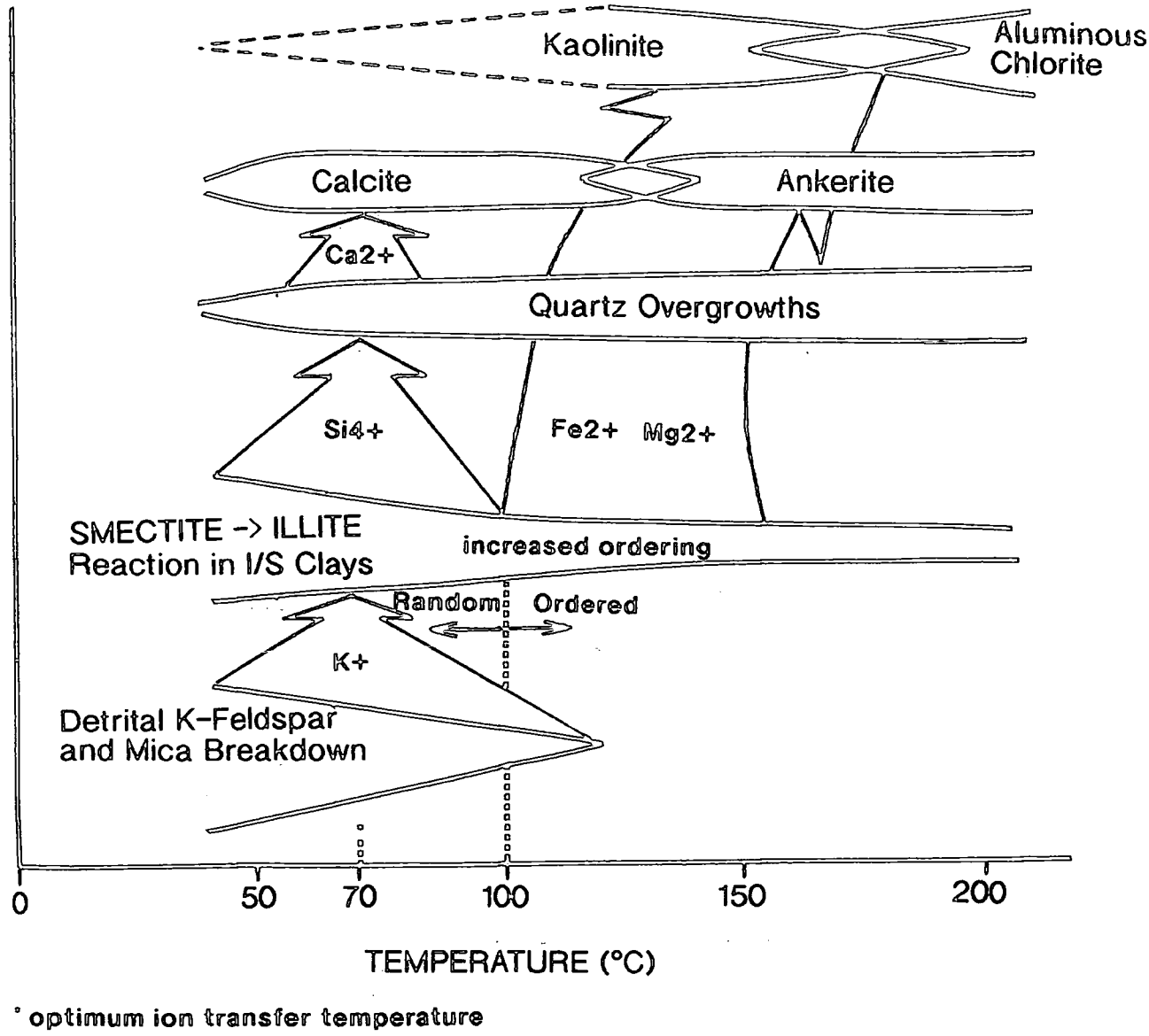

Fig.2.2.3a - Schematic diagram of I/S clay ordering, reactants and products. Vertical arrows depict ion transfer between I/S clay reactions and phases in sandstones. Temperature range of ordering suggest 100°C as the threshold of ordering and the transformation to illite. Modified from Boles and Franks (1979)

dissolution of smectite and the crystallisation of illite at crystal interfaces will only take place in the presence of water.

With reference to Fig.2.2.1a it is observed that after initial deposition, smectite is hydrated during shallow burial and adsorbs interlayer water. The structural lattice of smectite expands to its maximum. Further burial (with an increasing overburden stress) causes compaction and expulsion of free pore water so that the clay structure adopts a 'herringbone' type rather than the initial 'house of cards' structure. With further compaction, the clay is subjected to increasing temperature due to burial whereupon structured interlayer water is expelled to free pore space. At elevated temperatures (100-200°C as pore fluids at depth will require higher temperatures to achieve their boiling point due to increased confining pressure) all structured water becomes liberated. At elevated temperatures, Boles and Franks (1979) proposed the following reactions for the smectite to illite transformation:

1) $4.5\ K^{+} + 8Al^{+3} + \text{smectite} = \text{illite} + Na^{+} + 2Ca^{+2} + 2.5Fe^{+3} + 2Mg^{+2} + 3Si^{+4} + 10H_2O$

2) $3.93K^{+} + 1.57\text{smectite} = \text{illite} + 1.57Na^{+} + 3.14Ca^{+2} + 4.28Mg^{+2} + 4.78Fe^{+3} + 24.66Si^{+4} + 57O^{-2} + 11.4OH^{-} + 15.7H_2O$

The amount of water released in forming 1 mole of illite in reaction 2) is more than 50% greater than the water released during reaction 1). The produced desorbed water expands due to a density reduction when the interlayer water becomes available to the pore network causing the internal pore pressure to increase. The amount of water released to the pores is volumetrically greater than the volume reduction caused by lattice collapse (Whittaker, 1980). These chemical mass balance equations can substantiate the potential of generating excess fluid and, hence by implication, overpressure in clay rich formations. However, in addition, as neoformational illite is the main product of this reaction, the permeability in the clay will be reduced as illite is identified as a major permeability occluding mineral. This will accentuate the effect of the inability of desorbed interlayer water to escape from clay rich sequences by reducing the permeability of these clay units.

Observed relations of smectite diagenesis and abnormal pressure indicate that the smectite-illite transformation is a principal mechanism for the development of abnormal pore pressure in the Tertiary section of the United States Gulf Coast (Bruce, 1984). Freed and Peacor (1989) also relate the importance of the mechanism in generating overpressure in Brazoria and Hildago Counties, Texas and suggest a relationship of the

amount of illite being proportional and corresponding to the fluid pressure gradient determined by the local geological setting. However, Colton-Bradley(1987) documents the changes in clay stability with interlayer water loss and concludes that simple dehydration of smectite probably is not involved in the generation of abnormally high subsurface pressures. Instead, Colton-Bradley (1987) suggests that the by-products (K^+ and Si^{+4}) of the smectite-illite transformation may be important in forming a permeability barrier above overpressured zones.

2.2.4 Aquathermal Pressuring

Aquathermal pressuring has been described as a potentially significant overpressure generating mechanism in shallow basins with high geothermal gradients (Daines, 1982). Barker (1972) describes the theoretical pressure increase associated with a relatively small increase in temperature acting on a sealed body of fluid. Barker (1972) hypothesised that pore water is trapped in a closed system through permeability reduction or some form of sealing. The rock unit is then progressively buried with exposure to increasing temperature. A pressure-temperature-density diagram for water is used (Fig.2.2.4a) to explain the theory but the following restrictions were placed on the system:

1) Any porous volume must be completely isolated.
2) The porous volume that will become overpressured due to a temperature increase must have a constant volume.
3) Isolation and sealing of the rock unit must have occurred at a lower temperature than observed at present.

With reference to Fig.2.2.4a (Barker, 1972) at 2000ft, there is a recorded temperature of 54.4°C (point A on Fig.2.2.4a), experiencing a hydrostatic pore pressure of 893psi, before the unit is isolated. Sealing takes place at this temperature and the rock unit is subjected to elevated temperatures, at constant volume, by burial. Sealing at the original depth and temperature is a pre-requisite of the mechanisms operation. Fluid will respond to increase temperature at constant volume by moving up the appropriate isochore (line of equal density) to the point where a temperature (corresponding to a certain burial depth) records a unique pressure. In this case, at a burial depth of 5000ft, a temperature of 93.3°C (point B on Fig.2.2.4a) is observed with a resultant pore pressure of 8893psi. The rate of pressure increase in this example is 2.67psi/ft. Therefore, the overburden pressure would be balanced by the pore pressure at approximately 2500ft with an associated temperature of 64.1°C. Therefore, by applying Barker's (1972) diagram, it is seen that if a rock unit is completely sealed,

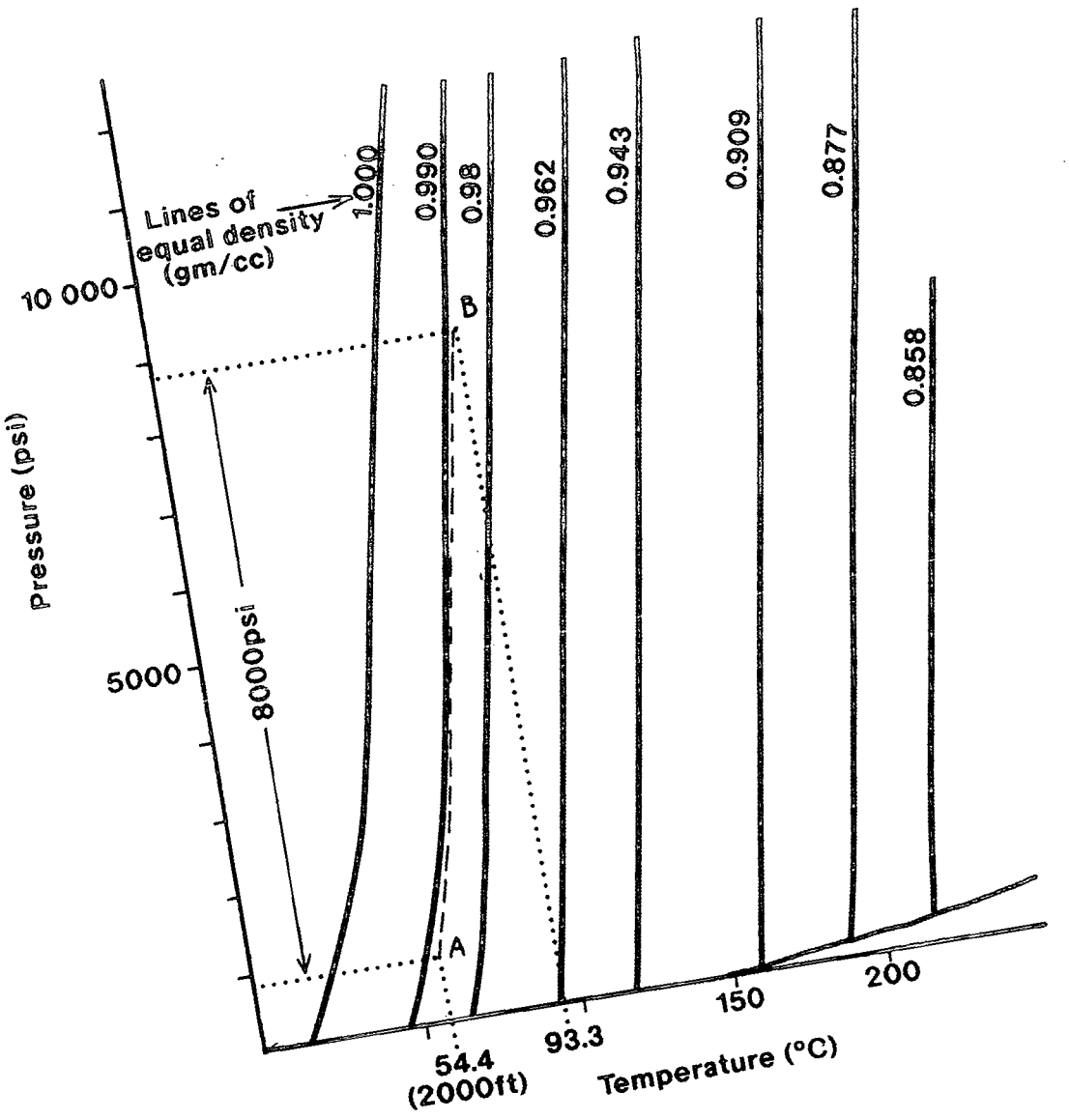

Fig.2.2.4a - Pore pressure increase with aquathermal effect (see text for discussion). From Barker (1972)

only a small incremental increase in temperature is required to raise the internal pore pressure to overcome the overburden stress (effective stress = 0) and initiate fracturing.

Aquathermally generated pressure depends largely on the geothermal gradient, salinity of water and depth of burial after unit isolation. High geothermal gradients, low saline fluids and rapid burial all enhance higher pressures (Whittaker, 1980). The existence of such an isolated unit, however, could only exist for a short period of geological time in a subsiding basin as basin evolution processes such as tectonism would tend to rupture any seal. Evaporites and some limestones could provide the necessary near zero permeability for isolation but the ductility and flow characteristics associated with such sequences would question the practical ability to compartmentalise compacting units.

Lou and Vassuer (1992) have simplified the equations which describe basin compaction and the effect of aquathermal pressuring in generating overpressures. The methodology and calculations utilised by Lou and Vasseur (1992) simplify the equations for the reduction of effective stress of sediment, considering only highly compressible or totally incompressible rocks. Lou and Vassuer (1992) conclude that aquathermal pressuring plays only a small part in the generation of overpressure in sedimentary basins. However, Miller and Luk (1993) used a more general model of sediment compaction and material properties that are more representative of conditions at depth. Miller and Luk (1993) calculate, that using intermediate compressibilities corresponding to measured values for the majority of rocks, that aquathermal affects can be significant. The material properties of pore fluids also play an important role in aquathermal pressuring (Miller and Luk, 1993) and change with temperature, pressure and salinity. In response, Lou and Vassuer (1993), using calculations based on Darcy-flow terms varying the effective stress, permeability, pressure and porosity of compacting sediments, to conclude and reiterate that for the vast majority of cases, aquathermal pressuring has minimal effect in contributing to overpressure in sedimentary basins.

Aquathermal pressure can be conceived as an overpressure mechanism which could be operational and important during the early stages of burial (Daines, 1982) as any subsequent temperature increase, after this initial burial and temperature increase, may cause the release of excess water volume through the formation of fractures. It is unlikely, however, that a coherent seal could develop at shallow depths and remain so to deep reservoir levels where overpressures are experienced at the present day. It is

now generally agreed that aquathermal pressuring plays a subordinate role in overpressure generation (Hermanrud, 1993). Daines (1982) concludes that any overpressure developed by this mechanism would likely be geologically transient.

2.2.5 Osmosis

Osmosis is defined as the spontaneous flow of water into a solution, or from a dilute to a more concentrated solution, when separated from each other by a suitable membrane (Whittaker, 1980). It appears that the osmotic pressure differential at constant temperature is almost directly proportional to the concentration differential and for a given concentration differential, it increases with the absolute temperature (Jones, 1969).

Hanshaw and Zen (1965) proposed that osmosis may be influential in generating abnormal pore pressures. Hanshaw and Zen (1965) suggested that if ions in pore water were filtered out by clays acting as semi-permeable membranes, then when equilibrium had been attained, the pore pressure should be anomalously high on the influx side of the membrane. Upon reaching osmotic balance, the higher salt concentration is balanced by higher pressure, resulting in an equal water chemical potential across the membrane.

A generated osmotic pressure is dependant upon the efficiency of the membrane (Whittaker, 1980). Young and Low (1965) conducted osmotic experiments using shale samples and variable concentration solutions and found that the resulting osmotic pressures were far below those suggested by theory. Young and Low (1965) concluded that the shales used as semi-permeable membranes were highly inefficient due to the possible existence of microcracks, large pore sizes, weakly charged pore throats and a relatively high concentration of fine silica in the clay interstices. In many overpressured units, however, these overpressures are associated with thick, massive shales within which the overpressures occur and the pore water is lower in ionic concentration in the shales than in the adjacent sandstones (Whittaker, 1980).

This mechanism is recognised as generating overpressure theoretically but no major published study on overpressured zones have reported this mechanism as important in the development of overpressure.

2.2.6 Tectonism

The mechanism of generating overpressure due to tectonic compression is similar to the process involved in compaction disequilibrium with the exception that the time factor is a function of strain rate and of rate of deposition.

In neotectonic geosynclinal basins, porosity may be directly related to the effective weight of the overlying sediments if the pore water can escape in response to increasing overburden pressures (Whittaker, 1980). However, in a tectonic environment, additional tectonic stress is applied horizontally. Tectonically produced overpressures will behave and appear much the same as those resulting from vertical compaction (Whittaker, 1980) but tectonic movement such as slip along fault planes will tend to aid dissipation of any developed overpressure. However, there are instances where faults are seen as important features in their ability to act as lateral seals or fluid conduits.

Grauls and Cassignol (1993) have recognised a zone of anomalous minimum effective stress and high permeability. The recorded high permeability is a direct result of open fractures. These fractures are thought to have been induced by high fluid pressure caused by compressive tectonics. Grauls and Cassignol (1993) suggest that competing compressive tectonics, induced at the base of a decollement zone, and high sedimentation rates, since the Miocene, have produced an increase in the fluid pressure to initiate fracturing. These fractures have been seen to have a significant effect on the migration pathway of reservoir fluids.

Tectonism, however, is thought to contribute negligible amounts of overpressure in the majority of documented areas where overpressures have been identified and studied.

2.3 Pore pressure maintenance and seal efficiency

Hunt (1990) noted that a vast number of identified overpressured zones are confined to relatively young rocks - Triassic and younger (but not necessarily at shallow depths). This suggests the possibility that these phenomena are unstable and transitionary in the development and history of a sedimentary basin. An existing overpressure must question at which stage of development the overpressure is at, the causes and controls and the maintenance mechanisms assuming that the seal is not perfect and dissipation is active.

Since an overpressured zone represents a dynamic imbalance in the natural system, the overpressure must be seen to be in a state of development, depletion or recharge. By

identifying the likely causative mechanism of the overpressure, it is possible to draw some assumptions regarding the maintenance of any abnormal pressure which exists.

The mechanism of compaction disequilibrium can theoretically continue to overpressure a sequence if any of the parameters controlling the sedimentation and loading rate, efficiency of pore water expulsion and sealing mechanism remain in or increase the state of non-equilibrium. Like the controls for compaction disequilibrium, aquathermal pressuring can theoretically continue to develop an overpressure at a rate dependant upon the burial rate and geothermal gradient.

Considering overpressure developed by the clay transformation of smectite to illite, it must be considered that there is a finite limit on the amount of smectite available to transform to illite (with the associated loss of interlayer and bound water to consequently increase the pore pressure of a compartmentalised rock unit). Therefore, the ultimate pressure generated by this process has a ceiling and once the transformation has been halted by the availability of smectite, any developed overpressure cannot be 'topped up' unless by transference from another source.

Overpressure developed by the thermal alteration of liquid hydrocarbons to gas is a more likely mechanism to maintain abnormal pressure. Continued burial and development of a basin would increase geothermal temperatures imposed on a subsiding rock unit (or reservoired oil). Liquid hydrocarbons, depending upon their stage of maturity, will respond to time and temperature effects of a subsiding basin to thermally alter to a gas causing an increase in pressure. Therefore, exposure of a suitably mature oil to increased burial will provide the necessary primary conditions for maintaining overpressure in an oil bearing reservoir which is sealed.

Overpressured zones identified in subsiding basins may be considered to be developing, stable or dissipating. Shallow overpressure zones are recognised to be in the early stages of development with compaction disequilibrium and, less likely, aquathermal pressuring the primary mechanisms of overpressure generation. Smectite to illite reactions would not occur at these depths nor would oil thermally crack to gas unless very high geothermal gradients were in operation such as recorded in the Pattani Trough, Gulf of Thailand - 4.8°C/km (Lundegard, et al., 1987).

If dissipation is occurring, zones of sufficient hydraulic conductivity must be present and must have a lower hydraulic potential than the overpressured zone, or the rate of

overpressure increase must be less than the dissipation rate through the sealing membrane.

Abnormal pressures (high and low) generated must be isolated and are not in harmony with the overall pressure regime of the basin. The dynamic nature of the pressure system will try to equalise this imbalance. Therefore, for an overpressured unit to exist an impermeable barrier, or seal, must exist to effectively discommunicate any fluid or pressure connectivity. Several types of seal have been documented (Plumley, 1980; Hunt, 1990). Recognised seals include low permeability lithological seals such as shale and evaporite sequences, structural features such as fault planes and seals initiated by diagenetic processes such as illitisation.

Seals have been reported to exist where there is no obvious structural or lithostratigraphic discontinuities (Hunt, 1990), also occurring over a range of depth intervals. The existence of a seal therefore does not seem to conform to any particular set of regulations or patterns with respect to lithostratigraphy or structure. Hunt (1990), however, noted in the North Sea the existence of a seal with a planar top around a depth of 3000m. This depth interval is also coincidental with an abnormal temperature increase (Paxton et al 1993). This is due to the insulating effect of an overpressured zone and that the seal would act as a transition zone in the temperature profile resulting in the temperature response noted by Paxton et al (1993).

An overpressured reservoir must be sealed in three dimensions and it is unlikely that there would be structural enclosure with faults or fracture networks operating on all sides of an overpressured unit. Therefore, seals are mainly thought to be controlled by lithology with the possible contribution from diagenesis (Hunt, 1990). Diagenesis is largely controlled by burial effects such as compaction and temperature. Hunt (1990) recognises the existence of a laterally extensive planar top seal in the North Sea but fails to address the problem of how this top seal can constantly remain at a depth of 3000m in a subsiding basin. This would involve a mechanism whereby the diagenetic seal would be in a constant state of transition effectively reprecipitating and resealing in response to continued subsidence. Buhrig (1989) suggests, in the North Sea, that lateral sealing efficiency increases with depth. Buhrig (1989) recognises that the Lateral Drainage Efficiency Factor (LDEF) increases away from the Viking Graben axis possibly in response to the overpressure generation potential that is distributed across the graben.

It is more likely on the recognition in this study and in Buhrig's (1989) study that pressure compartments are smaller in size than Hunt (1990) suggests and that these compartments exist with their own hydraulic potential, circulation and sealing capacity.

2.4 Basin Modelling Review and Assumptions

Procedures (Mann and Mackenzie, 1990; Audet and McConnell, 1992) have been devised for forward modelling and predicting fluid pore pressures in sedimentary basins. These procedures may be based around mathematical modelling (Audet and McConnell, 1992) or based on equations to account for fluid flow (Mann and Mackenzie, 1990). However, studies for real case histories use the aspect of dynamic burial histories, thermal models and hydrocarbon generation, migration and accumulation histories (Lerche, 1993). The interactive and fully integrated quantitative geological modelling attempts to quantify the formation and evolution of a basin using all available knowledge and data from plate tectonics, sedimentology, geothermics and organic geochemistry in an integrated manner (Yukler and Dahl, 1993). Once the geological evolution of the basin is optimised by minimising the differences between the computed and measured sedimentary thicknesses, porosity, pressure, temperature and maturity indicator values a quantified generation, migration and accumulation of the hydrocarbons is calculated as a function of time and space (Yukler and Dahl, 1993). Various computer software programmes have been written, based on large databases and incorporating the ability to vary parameters such as functions of compaction, permeability, maturity and kinetics, and have become commercially available.

In this study Platte River's BasinMod™ has been utilised on the Alwyn Field and the Uinta Basin in this thesis to model various processes such as compaction, hydrocarbon maturation and kinetics and pore pressure. Williamson and Smyth (1992) have also used BasinMod™ to evaluate the timing of gas and overpressure generation in the Sable Basin, offshore Nova Scotia. Williamson and Smyth (1992) utilised the software to refine the conclusions made by Jansa and Noguera (1990), Mudford (1990) and Forbes et al (1992) in the assessment of overpressure generation and distribution in the Sable Basin. Forbes et al (1992) and Mudford (1992) undertook a numerical approach to observe the overpressure history and concluded that compaction disequilibrium is likely to be the main mechanism of generating overpressure. Jansa and Noguera (1990) taking more qualitative observations describe how hydrothermal cracking is the most likely overpressure mechanism. Williamson and Smyth (1992) used BasinMod™ to conclude that, among other observations, gas generation is coincidental with overpressure generation at specific periods in the burial history but that compaction

disequilibrium accounts for the majority of abnormal pressuring in the Sable Basin. Williamson and Smyth (1992) describe the possible correlation and implications with the computer derived models which suggest that compaction disequilibrium generates most of the excess pressures with hydrocarbon generation contributing minor amounts.

Many basin modelling programmes, such as BasinMod™, rely on mass and thermal energy balance equations which incorporate fluid flow, apply Darcy's law. Because of the amount of error between processes and quantitative mathematical functions describing these processes in basin modelling, the main variables are described and justified. This has consequences in this study. The main variables in the modelling are:

1) Compaction
2) Thermal Processes
3) Fluid Flow and Overpressuring
4) Hydrocarbon Generation

2.4.1 Compaction Modelling

Since publication of the consolidation theory (Terzaghi, 1923), the consolidation of soils has been described by the effect of increasing frame pressure or effective stress. Later, in Smith (1971), the theory of soil consolidation was extended to the compaction of sedimentary rocks. The relationship of depth/porosity for a compacting lithofacies is given by both empirical and polynomial functions. This approach of evaluating porosity at a certain depth is physically valid under certain hypotheses but may be criticised because of choice of function. This choice is partly constrained by the data available which can be used to calibrate the function (Schneider et al 1993). Effective stress has been computed by Schneider et al (1993) according to the concept put forward by Terzaghi (1923). Schneider et al (1993) observed similar considerations that the effective stress/porosity relation has a physical meaning when mass transfers (diagenesis) are neglected. Therefore, the mechanism of compaction disequilibrium displaying an underconsolidated character in typically low permeability lithofacies will not conform to an effective stress/porosity relationship and porosity/depth functions as proposed by various authors. The documented functions do not recognise undercompaction and the generation of overpressure which would give an abnormal porosity for a given depth. However, the basin modelling package must conform to some mathematical function to simulate the compaction process in sediments.

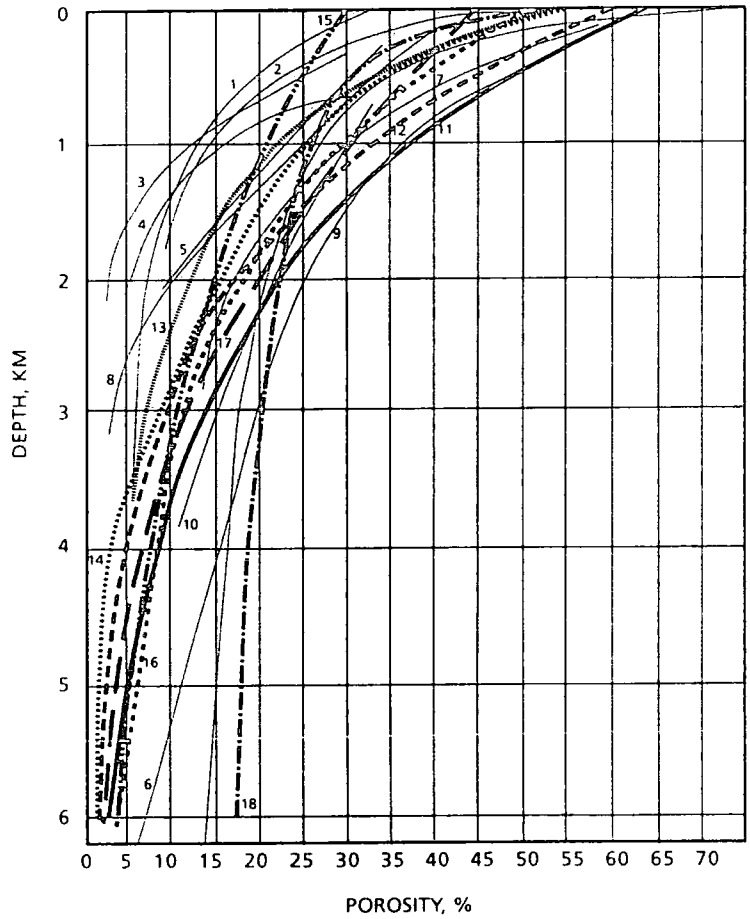

The thin curves (and their labelling) are those presented by Rieke and Chilingarian (1974, their fig. 17). *1* = Proshlyakov (1960); *2* = Meade (1966); *3* = Athy (1930a); *4* = Hosoi (1963); *5* = Hedberg (1936); *6* = Dickinson (1953); *7* = Magara (1968); *8* = Weller (1959); *9* = Ham (1966); *10* = Foster and Whalen (1966); *11* = Sclater and Christie (1980); *12* = Bethke (1985); *13* = Doligez et al. (1986); *14* = England et al. (1987); *15* = Deming and Chapman (1989); *16* = Burnham and Braun (1990); *17* = Hermanrud et al. (1990a); *18* = Lerche (1990a).

Fig.2.4.1a - Suggested porosity versus depth relationships. From Hermanrud (1993)

There is a definite need to constrain porosity decrease with depth relationships as shales dominate most sequences volumetrically (Hermanrud, 1993) and due to the fact that hydrocarbon generation and expulsion takes place in shales. Fig.2.4.1a summarises the quantitative approaches and functions proposed by various workers. The spread and degree of error between these functions is likely an attribute of compositional and textural variations of the sediment being modelled, measurement techniques employed and tectonic stress history. Depending upon which compaction function is chosen, the overall burial history and associated processes will be affected. Therefore, some inherent consistency is needed and the following functions have been utilised throughout this study and justified where appropriate. These functions were available and interactive with other processes in BasinMod™:

1) Sclater and Christie (1980)
2) Falvey and Middleton (1981)
3) Baldwin and Butler (1985)

2.4.1.1 Depth versus Porosity function as proposed by Sclater and Christie(1980)

From an extensive study of 8 wells in the middle and on the flanks of the Central Graben of the North Sea, an empirical function was derived. Sclater and Christie (1980) observed an exponential increase in thickness with shallowing depth upon compaction. Their equation relating porosity to depth in this data is:

$$P = Po \exp^{(-Kz)}$$

where P = porosity
Po= Initial porosity
K = Compaction factor to adjust for varying compressibility of different lithologies
z = depth

Parameters used by Sclater and Christie (1980) for calculations in the exponential relationship were:

Lithology	**Po**	**Exponential Factor (K)**
Shale	0.63	0.51 x 10^{-5}/cm
Sand	0.49	0.27 "
Chalk	0.70	0.71 "
Shaley Sand	0.56	0.39 "

2.4.1.2 Depth versus Porosity function as proposed by Falvey and Middleton (1981)
Based on data from wells drilled in the shallow carbonate Perth Basin, offshore Western Australia. The basin history experienced significantly lower sedimentation rates with lower clay content (Falvey and Middleton, 1981) than for the exponential porosity/depth relationship of Sclater and Christie (1980) which did not fit the shallower depths. Thus, Falvey and Middleton (1981) formulated a reciprocal relationship that assumes porosity changes proportionally to the change of the sediment load:

$1/P = (1/Po) + Kz$ where P = porosity
Po= initial porosity
K = compaction factor
z = depth

Lithology	**Po**	**Compaction Factor (K)**
Sands	40-50%	1.5-2.0 km^{-1}
Shale	50-70%	2.0-2.5 km^{-1}

2.4.1.3 Depth versus Porosity function as proposed by Baldwin and Butler (1985)
The work developed by Baldwin and Butler (1985) is based on a composite of published compaction data for argillaceous sediments. Shale composition data was taken from a range of published curves which all fell within an error range of 5%. Baldwin and Butler (1985) concluded that their calculated relationship was applicable for most normally pressure shales up to 200m in thickness. They noted that thick shales (>200m/700ft) do not lose pore water as readily, so thick shales tend to be overpressured and undercompacted.

For normally pressured shales, Baldwin and Butler (1985) present a power relationship:

$z = 6.02\ S^{6.35}$ where z = depth (km)
S = solidity, the inverse of porosity (1-P)

This relationship assumes sedimentation has 0% solidity (or 100% porosity) at the surface which rapidly increases and reaches 100% solidity at a defined depth. BasinMod™ sets a lower limit of 0.0001%.

In the following basin modelling simulations of the Alwyn Field and the Uinta Basin, the above compaction functions are used depending upon the depth of reservoir and main lithology. Baldwin and Butler (1985) has been used for calculating shale rich sections, Sclater and Christie (1980) for sand dominated sections in the Alwyn Field (Chapter 3) and Falvey and Middleton (1981) for relatively shallow wells in the Uinta Basin (Chapter 4).

2.4.2 Thermal Processes

Thermal modelling may incorporate discrepancies as a result of geological interpretations, heat flow equations, coupling of heat flow to other equations (such as compaction), thermal parameters, boundary conditions and calibrations to well data (Hermanrud, 1993). Geological interpretations include possible discrepancies in the age of a specific horizon and correct timing and amount of any hiatus or erosion in the burial history. This particular variable is demonstrated with a marked effect in both modelled studies of the Alwyn field (section 3.5.5) and Uinta Basin (section 4.6.4).

Heat flow equations in the BasinMod™ programme includes terms for heat conduction, heat storage, convective heat transfer and heat generation within the sediments and throughout this study heat flow is based upon the boundary conditions of surface temperature as a function of time, corrected bottom hole temperatures and regional geothermal gradients. These specific values are documented at appropriate points in the study. Heat flow equations do contribute with unequal amounts to the thermal budget (Hermanrud, 1993). Heat conduction is considered to be the most important heat transporting process (Kappelmyer and Haenel, 1974) with the exception of active hydrothermal areas (Didyk and Simoneit, 1989). Hydrodynamic ground water has been seen as significant in producing thermal effects (Smith and Chapman; Willet and Chapman, 1988) and has been considered in the Uinta Basin study (Chapter 4).

Free convection in sediments in terms of thermal effect is negligible where temperatures are dominated by burial heating (Ludvigson, et al., 1993) as is the influence of radiogenic heat flow from sediments (Rybach, 1986).

The coupling of heat flow equations to other functions, such as compaction, also influences the modelled thermal history. Models that do take any account of compaction will produce markedly different thermal histories from ones that do not (Hermanrud, 1993). Empirical relationships that are calibrated to thermal histories based on non-compacting sediments (such as the TTI calculations of Waples, 1980)

should not be used by models which include compaction (Dykstra, 1987). BasinMod™ allows the capacity for TTI calculations but as this study incorporates compaction factors this empirical function is not used.

Thermal conductivity differs with lithology and BasinMod™ allows the use of defaulted end member standards with predefined thermal matrix conductivities as well as other defaulted parameters such as initial porosities and permeabilities. The defaulted values used in this study are:

Lithology	Relative%	Thermal Conductivity (W/m °C)
Shale	100	1.5
Sandstone	100	4.4
Siltstone	100	2.0
Limestone	100	2.9

BasinMod™ does not incorporate a calculation of transient thermal effects due to rapid deposition and large scale crustal movements (such as stretching and thrusting) simultaneously. However, the programme does allow the input of a heat flow history. Such data was not inputted in this study due to data unavailability.

2.4.3 Fluid Flow and Overpressure Modelling

Hermanrud (1993) describes the role of fluid flow as subordinate in transporting thermal energy but in studies conducted by Jourdan et al (1987), Burley et al (1989) and in this study, hot fluid circulation is deemed an important process. This is apparent when considering diagenetic phases in the reservoir section (sections 3.6 and 3.7). Fluid flow also interacts with other processes such as compaction and therefore must be assessed in basin modelling. The simulation of fluid flow (single phase) modelled by BasinMod™ in this study, is through porous media using Darcy's flow equation which was developed to observe water flow through a sand medium. Experimental work varying fluids and materials showed that viscosity and density of the fluid plus the size of the grains affect the rate of flow. The function permeability with depth (effective stress) used in this study is the modified Kozeny-Carman method (Ungerer et al 1990). This equation has been derived for use when modelling low permeability rocks such as compacted rocks and is described by:

$$k = \frac{20\,\phi^5}{So^2\,(1-\phi)^2}$$

where k = permeability (m^2)
ϕ = porosity (dimensionless)
So=specific surface area of the rock, 1/m

and where ϕ is less than 10%

The basin modelling programme assesses excess pressure build up as a result of compaction disequilibrium only and does not acknowledge any contribution from other mechanisms. This , however, is a restriction and limitation of the programme and is not a reflection on the recognition of other mechanisms. BasinMod™ models compaction using a simultaneous basin modelling engine where porosity is calculated as a function of both depth and pressure. The procedure first calculates a burial history using the Sclater and Christie (1980) exponential equation. The resulting burial history is then modified by the coupled fluid flow compaction equation (incorporating the permeability function) to calculate excess pressure. A second iteration is performed to adjust the porosities and depths in consideration of the excess pressure. Excess pressure is calculated at each time step and coupled into the pressure calculation for the next time step. There is a minimum of two iterations.

2.4.4 Hydrocarbon Generation

Many mathematical approaches for modelling oil and gas generation have been proposed. Lopatin (1971) developed a time-temperature index (TTI) to describe the process of coalification. This was subsequently applied to petroleum source rocks to simulate the maturation of kerogen (Hunt, et al., 1991). The index proposes that the reaction rate doubles for every 10°C rise in temperature. Waples (1980) took this TTI to relate to hydrocarbon generation with correlation to vitrinite reflectance and thermal indicators. Bostick (1973) modified a chemical-kinetic model for coalification established by Karweil (1955) to relate thermal history to vitrinite reflectance (Ro). Ro is the reflectance of vitrinite particles that occur in organic matter deposited in sediments (Hermanrud, 1993). Ro is now used extensively in the assessment of maturity in hydrocarbon formations. However its accuracy is diminished in samples where the organic fraction has been subjected to erosional processes. Indeed, Price (1982, 1983) compiled Ro data for sedimentary basins presently at maximum temperature and could not find any correlation between increasing Ro and increasing burial time for any temperature interval. Thus, Price (1982, 1983) concluded that heating time had no observable effect on hydrocarbon generation and that Ro could only be used as a palaeo-thermometer. However, TTI which is based on the assumed correspondence between Ro and hydrocarbon generation is still widely used in basin modelling. This is mainly due to the wide availability of Ro data and it can be used in combination with other thermal maturation indices such as TAI (Thermal Alteration Index), spore colour and biomarkers.

Tissot (1969) and Tissot and Espitalie (1975) developed a simulation of the degradation process of kerogen to hydrocarbons by parallel, first order, kinetic reactions. This application of kinetic modelling to simulating hydrocarbon generation is now generally accepted for basin modelling purposes and is summarised by Ungerer (1993). The kinetic approach considers the diversity of composition and distribution of the original kerogens. The kinetic reaction calculates multiple parallel reactions that occur as organic matter undergoes degradation. Of these multiple reactions, each reaction has specific parameters including the reaction fraction (percentage of kerogen with a specific activation energy), activation energy (energy required for chemical bond breakage) and Arrhenius constant (frequency with which a certain reaction takes place). BasinMod™ stores a library of defaulted values of kerogen types based on established data from the main oil provinces including the North Sea (Type II kerogen) and the Uinta Basin (Type I kerogen). Reaction scenarios are also simulated in conjunction with the imported thermal and burial histories to assess the kinetics. BasinMod™ holds a library of kinetic parameters based on a large number of studies due to the variation in results from various source rocks using different equipment to calculate the pyrolysis of the source rock and under different heating conditions (Burnham et al 1987; Sweeney et al 1987; Horsfield et al 1989; Burnham and Braun, 1990; Klomp and Wright, 1990; Burnham, 1991; Burnham et al 1991 and Reynolds et al 1991).

The methodology and calculations used in this study to ascertain the hydrocarbon generation and stage of maturity of the source rock utilises BasinMod™ kinetic model - LLNL Easy %Ro. This provides a kinetics model developed at Lawrence Livermore National Laboratory (LLNL) to calculate maturity in the form of %Ro. The model uses a distribution of Arrhenius rate constants to calculate global vitrinite maturation, then correlates maturation with reflectance. This is similar to the VITRIMAT model (Sweeney and Burnham, 1990) which calculates Vitrinite elemental composition, then correlates composition with reflectance. The form in which the kinetic model is calculated and displayed in this study allows instant interpretation in terms of %Ro and stage of maturity with respect to the oil window (immature <0.5 %Ro, early mature 0.5-0.7 %Ro, main mature 0.7-1.2 %Ro, main gas generation phase >1.2 %Ro, based on Tissot et al.,1987).*

2.5 Summary of main modelling data and assumptions

Using a similar approach to Williamson (1992), the basin modelling data and assumptions are listed for the Alwyn Field study as:

Observational Data	Source	Utility
LITHOLOGY	Well Composite Logs Well History Reports	Burial History and Compaction Corrections
AGE/DEPTH CHRONOSTRAT.	Composite Logs Electric Logs Harland et al (1982)	Burial History
BOTTOM HOLE TEMPERATURES	Log Header Information Geochemical Reports	Matching of computed thermal histories
VITRINITE REFLECT.	Geochemical Reports	Matching of computed thermal histories
BOTTOM HOLE PRESSURES	Log Header Information	Present day reference for modelled pressure history
Modelling Assumptions	**Source**	**Utility**
COMP. FUNCTIONS	Sclater and Christie (1980) Baldwin and Butler (1985) Falvey Middleton (1981)	Compaction effects due to loading and porosity reduction with depth
THERMAL CONDUCT,	BasinMod™ defaulted library based on Brigaud and Vassuer (1989)	Computation of thermal histories
HEAT FLOW	Constant isotherms through time	Computation of thermal and maturation histories
SURFACE TEMP. Palaeo " "	Burley et al (1989) Buchardt (1978)	Computation of thermal and maturation histories
PRESSURE HISTORY	Sclater and Christie (1980) Mod. Kozeny-Carman	Computation of pressure history
MATURITY/KINETICS	LLNL Easy %Ro	Maturation/ Kinetics of hydrocarbon generation

Summary data and assumptions of the Uinta Basin:

Observational Data	**Source**	**Utility**
LITHOLOGY	USGS Central Files Anders et al (1992)	Burial History and Compaction Corrections
AGE/DEPTH CHRONOSTRAT.	Pitman et al (1982) Anders et al (1992) Harland, et al. (1982)	Burial History
BOTTOM HOLE TEMPERATURES	Log Header Information UGS Reports	Matching of computed thermal histories

VITRINITE REFLECT.	Anders et al (1992)	Matching of computed thermal histories
BOTTOM HOLE PRESSURES	Lucas and Drexler (1976) Spencer (1987)	Present day reference for modelled pressure history
Modelling Assumptions	**Source**	**Utility**
COMP. FUNCTIONS	Sclater and Christie (1980) Baldwin and Butler (1985) Falvey Middleton (1981)	Compaction effects due to loading and porosity reduction with depth
THERMAL CONDUCT,	BasinMod™ defaulted library based on Brigaud and Vassuer (1989)	Computation of thermal histories
HEAT FLOW	Willet and Chapman (1988) Sweeney et al (1989)	Computation of thermal and maturation histories
SURFACE TEMP.	Willet and Chapman (1988)	Computation of thermal
Palaeo " "	Anders et al (1992)	and maturation histories
PRESSURE HISTORY	Sclater and Christie (1980) Mod. Kozeny-Carman	Computation of pressure history
MATURITY/KINETICS	LLNL Easy %Ro	Maturation/ Kinetics of hydrocarbon generation

2.6 Conclusions to Chapter 2

This chapter served to review and explain the processes involved in the generation, maintenance and depletion of abnormal pressure which is described in the following chapters. Also, as basin modelling is used as a primary tool of interpreting observational data in this study, the major regulations, assumptions and limitations have been documented in this chapter to act as a reference base for the subsequent interpretations made in and utilised in this thesis.

Chapter 3
Overpressure and fluid flow modelling in the Alwyn Field, Northern North Sea

3.1 Introduction

This chapter describes and reviews the interpretation of regional, field scale and microscopic observations to document the distribution of the areal and stratigraphic occurrence of overpressure within an oil field in the Northern North Sea of the U.K. The general and detailed characterisation of overpressure in the Alwyn Field area has been undertaken with geochemical, petrophysical, diagenetic, basin modelling and structural analysis. This study of overpressure distribution, genesis and likely causative mechanisms shows the necessary work to constrain local overpressure occurrence with the regional framework and the basin evolution history.

The regional setting allows the Alwyn Field to be placed in the regional geological framework as is the stratigraphy of the reservoir sections. The present day pressure distribution is documented followed by maturation modelling, diagenesis and pressure modelling which together allow the reconstruction of a fluid flow model. The overpressure evolution through time in the reservoir section has been correlated with likely causative mechanisms utilising a combination of the analysis and observations employed in the aforementioned sections.

3.2 Regional Setting

The Alwyn Field area constitutes, in this context, blocks 3/9, 3/14 and 3/15 referred to as Alwyn North, South and South East respectively. The field lies south east of the Ninian field in the East Shetland Basin in the Northern North Sea with the Shetland Isles being the nearest landfall 140km west. The East Shetland Basin is a sub basin of the North Viking Graben, an intermediate faulted terrace flanking the East Shetland Platform which sits to the west and also strikes sub parallel to the Viking Graben axis which is situated to the east (Fig 3.2a).

Structurally, the field is influenced by two sets of faults developed in response to the initiation of graben systems under a tensional regime in the Permo-Triassic periods (Inglis and Gerard, 1991). The dominant Viking Graben NNW-SSE fault system is complimented by a second E-W set of smaller cross faults which combine to generate the westward dipping rotation of the fault blocks (Inglis and Gerard, 1991). Tectonic activation and reactivation has supplied the necessary component to constitute the main structural trapping style for the Mesozoic reservoirs throughout the Brent

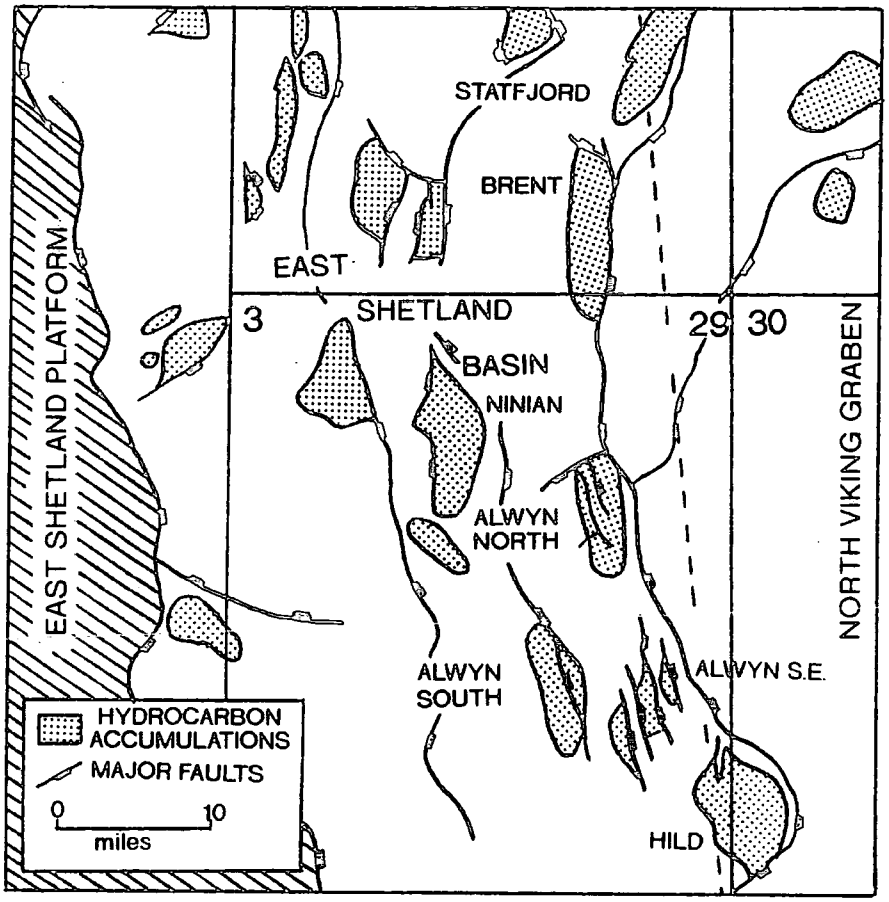

Fig.3.2a - Regional location and structural map of the Alwyn field (modified from Inglis and Gerard, 1991)

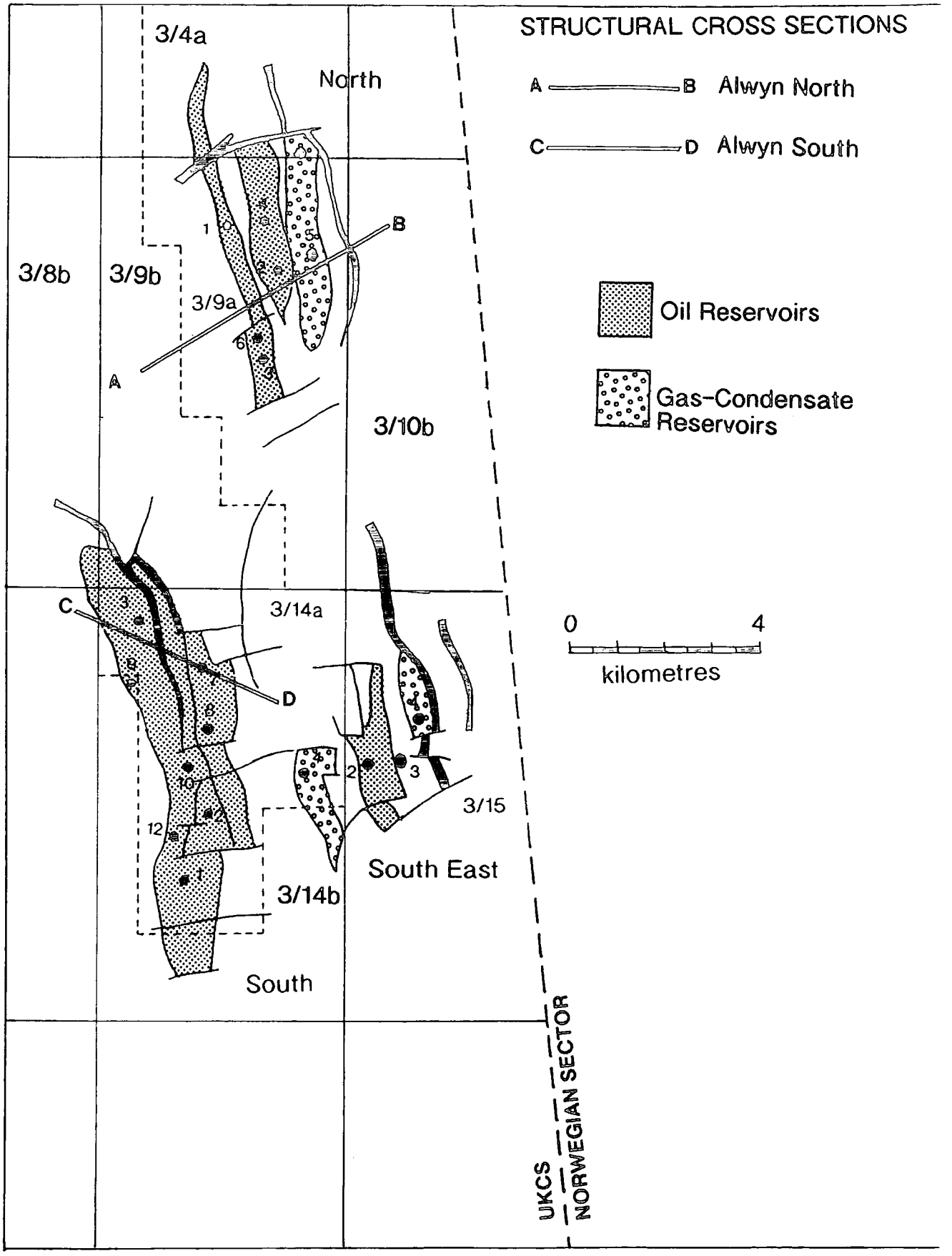

Fig.3.2b - Detailed structural map of the Alwyn field area showing showing hydrocarbon accumulations. Cross sections A-B and C-D represented on Figs.3.2c and 3.2d.

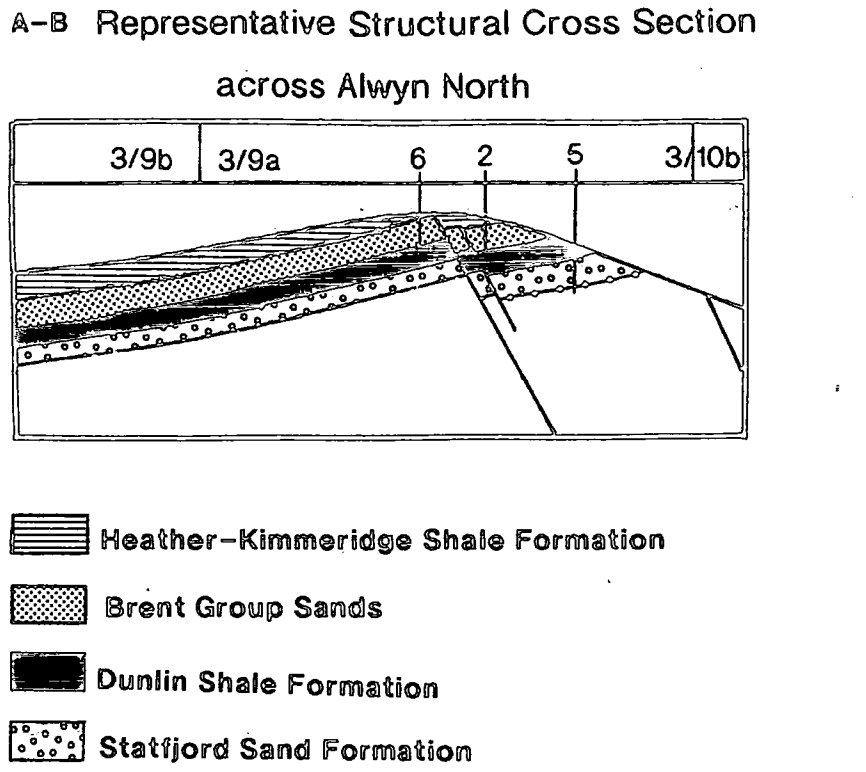

Fig.3.2c - Representative structural cross section A-B (see Fig.3.2b for location of A-B)

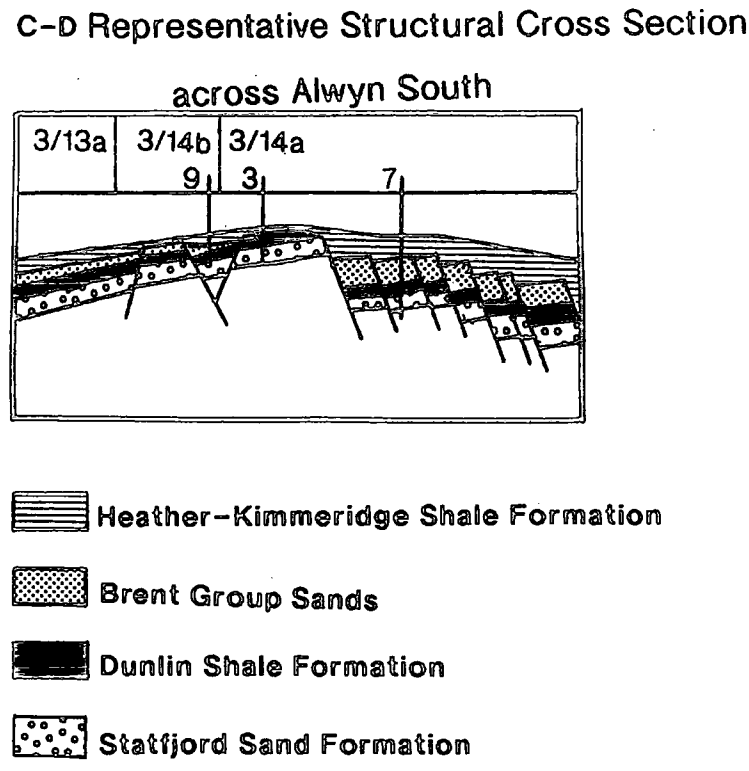

Fig3.2d - Representative structural cross section C-D (see Fig.3.2b for location of C-D)

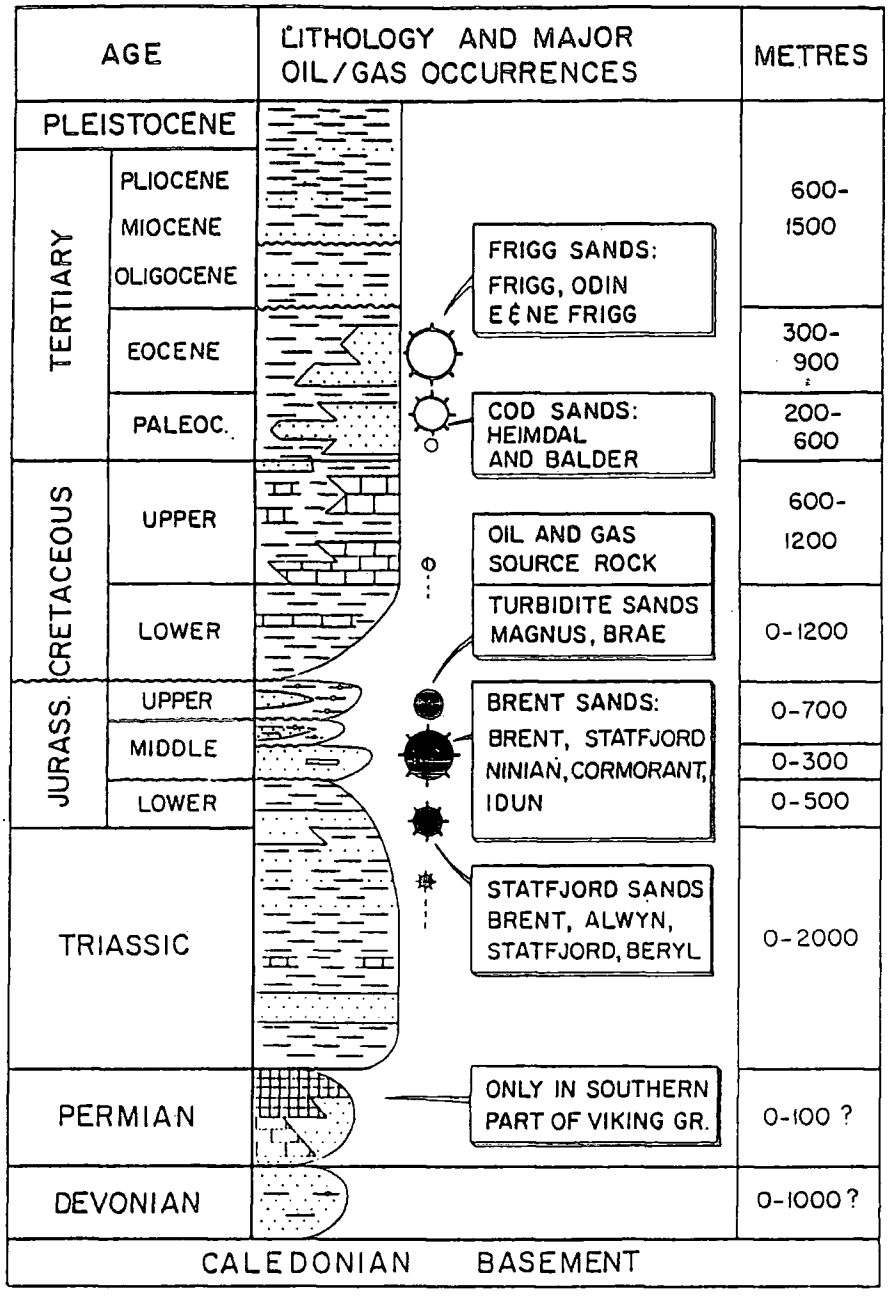

The hydrocarbon bearing Brent and Statfjord Formations in the context of the regional lithostratigraphy of the Northern North Sea.

Province. It is these faults which effectively compartmentalise both the reservoirs and the pressure which is observed in Alwyn (Fig 3.2b, c and d).

Hydrocarbons are produced from the Brent Group and the Statfjord Formation. Production so far is limited to the 3/9 block (Alwyn North) with the Alwyn South and South East fields still in the appraisal and planning stage. Alwyn North has initial recoverable reserves estimated at 176MMBbl oil and condensate and $22x10^9Sm^3$ of gas (Inglis and Gerard, 1991). Closure in the Brent Group affords the trap for the oil whereas the older Statfjord Formation provides the reservoir for the condensate. There is apparently no communication between the two stratigraphic intervals as the Mid Jurassic Dunlin Shale provides an effective bottom seal for the Brent reservoired oils and a top seal for the condensate in the Statfjord Formation. This agrees with the pressure information discussed in section 3.4.

3.3 Stratigraphy

Both the Middle Jurassic Brent Group and the Lower Jurassic Statfjord Formation are the principal reservoirs in the Alwyn area. The stratigraphy of the Brent Group and its interpreted position in a sequence stratigraphic framework has been well documented (Morton et al., 1991). It is necessary in this study to briefly describe the lithostratigraphy to constrain the temporal framework when correlating the fill up history, field diagenesis and fluid flow model.

The Mid Jurassic Brent Group formations extend areally over much of the Northern North Sea East flank fields (the Brent Province). The Brent Group has been subdivided using borehole log character and lithofacies as follows:

Heather
TARBERT
NESS
ETIVE
RANNOCH
BROOM
Dunlin

where **BOLD TYPE** indicates the Brent Group Formations.

The thickness of the group and its member formations vary according to depositional and structural influence. Inglis and Gerard (1991) as well as Jourdan et al. (1987) and Johnson and Eyssautier (1987) have described the formations. Inglis and Gerard

(1991), referring to well 3/9a-4, summarise the formations of the Brent Group as follows:

Broom - combined with the relatively thin Rannoch Formation, which sits comformably above, represents a prograding shoreface sand.
Etive - conformably overlies the Broom and is interpreted as a progradational barrier sand.
Ness - contains the petroliferous rich thick Ness D Member which combines minor and shoreface sands before passing into a back barrier lagoonal depositional sand sequence. The Ness Formation is interpreted as being deposited in the deltaic to alluvial/lower delta plain environment.
Tarbert - the youngest member of the Brent Group shows a retrogressive character in the lower part of the sequence of a prograding shoreface and bar sands being accentuated and amplified in the Upper Tarbert which shows a lower to upper shoreface sand set.

The Statfjord Formation is classified, based on observations made from the 3/9a-5 well (Inglis and Gerard, 1991), into:

Dunlin
NANSEN
EIRIKSSON
RAUDE
Cormorant

where BOLD TYPE indicates the Statfjord Formation Members

The Statfjord Formation can also be summarised based on the observations made by Inglis and Gerard (1991):

Raude - represents a coarsening upward sequence, unconformable on the underlying Cormorant Formation, deposited in floodplain to point bar deposits.
Eiriksson - marks the transition from the underlying Raude Member to an alluvial plain environment with interspersed and fluctuating braided channel sands and floodplain deposits. A progressive flooding event is inferred from the interpretation that the Upper Eiriksson is a fan delta sand.
Nansen - unconformably overlies the Eiriksson and is interpreted as a reworked high energy fluvial deposit.

The Lower Jurassic Statfjord Formation, which acts as a gas condensate reservoir in the Alwyn area, shows an interspersed set of deposits fluctuating from braided channel deposits to alluvial plain and overbank sands. The Brent Group Formations reflect responses to changes in eustacy and tectonism documented in the depositional style. However, the Brent group represents an overall deltaic to lagoonal/marginal marine depositional setting.

Depths to top reservoir range from 3129m (3/9a-3) in Alwyn North to 3687m (3/14a-8) in Alwyn South for the top of the Brent Group (Tarbert Formation) and for the top of the Statfjord reservoirs from 3356m (3/9a-5) in the North field to 4044m in Alwyn South (3/14a-8). All depths quoted are TVD SS.

3.4 Pressure Recognition and Distribution

Pressure data were assimilated from 23 wells in the Alwyn area penetrating the Brent and Statfjord reservoirs. These data were mostly taken from corrected DST, FIT and RFT measurements. All pressure data are documented in Appendix 4.1. Each well was observed in terms of pressure versus depth referenced against hydrostatic (taken at 0.45 psi/ft - see section 2.2). It is also noteworthy that none of the data in any of the measured wells lie on the hydrostatic gradient indicating then that the whole of the Alwyn area is overpressured. This observation is common with the study made by Buhrig (1989). When representative pressure data are plotted and referenced to a common depth on a structure map, the Alwyn area can be shown to contain 3 distinct pressure cells or compartments (Fig. 3.4a). The compartments can be classified into:

Alwyn North: experiencing the lowest overpressures in the order of 1600-2200psi.
Alwyn South: shows an overpressure range of between 2700-3000psi.
Alwyn South East: overpressures in the range of 3300-3600psi.

There appears to be a slight deviation in overpressure from the Brent to the Statfjord reservoirs (Fig. 3.4b). The Statfjord reservoirs observe slightly greater overpressures in the region of approximately 100psi (well 3/14a-8) to 200psi (well 3/9a-3). This difference may be the result of long hydrocarbon columns with the Statfjord reservoirs being condensate prone and the Brent reservoirs oil bearing giving different pressure gradients over a vertical interval. A subsequent result of this would be to observe differing amounts of overpressure.

Buhrig (1989) also recognised the overpressure differential between North and South Alwyn for reservoirs in the same range of depth and with similar burial histories.

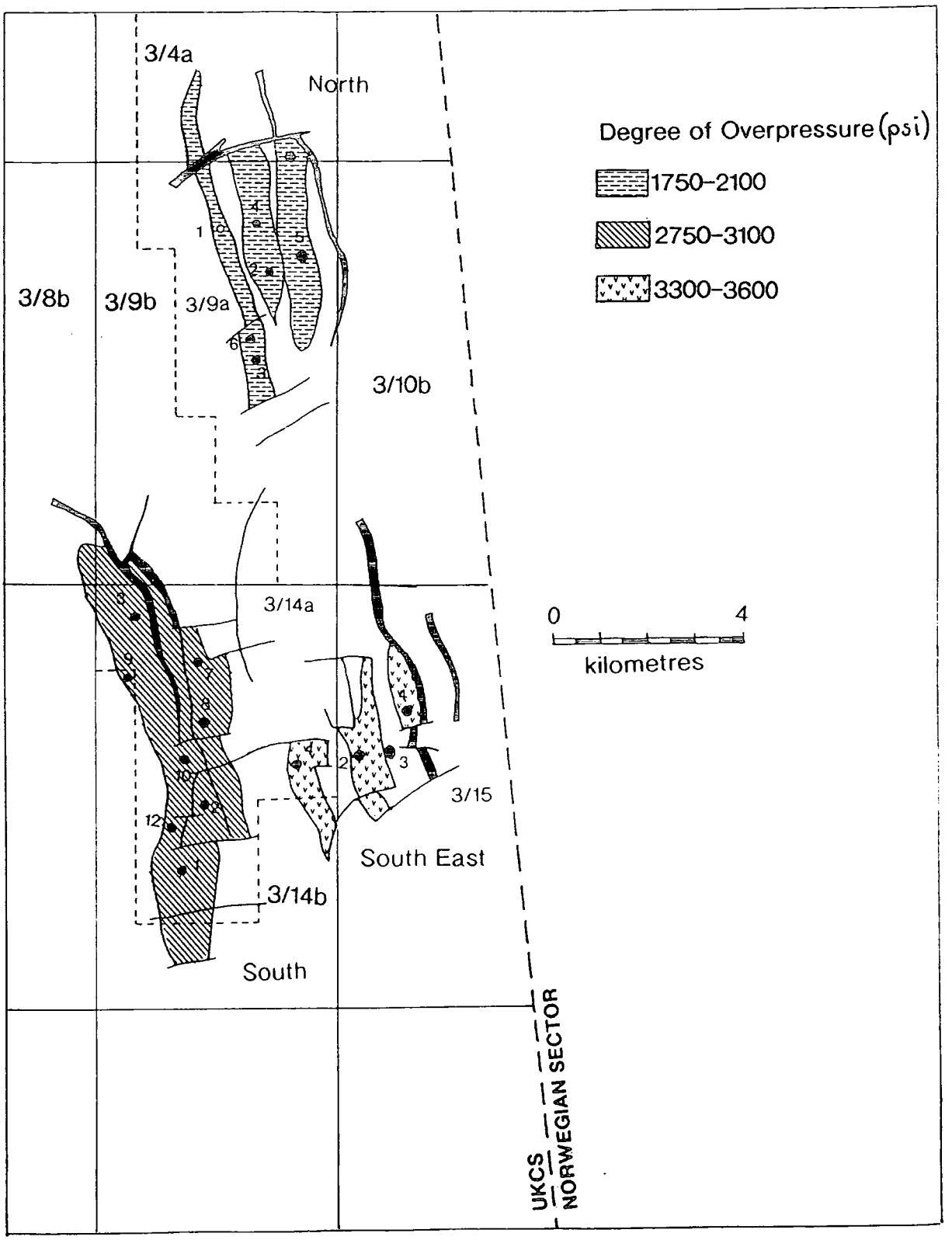

Fig.3.4a - Areal distribution of overpressure in the Alwyn field

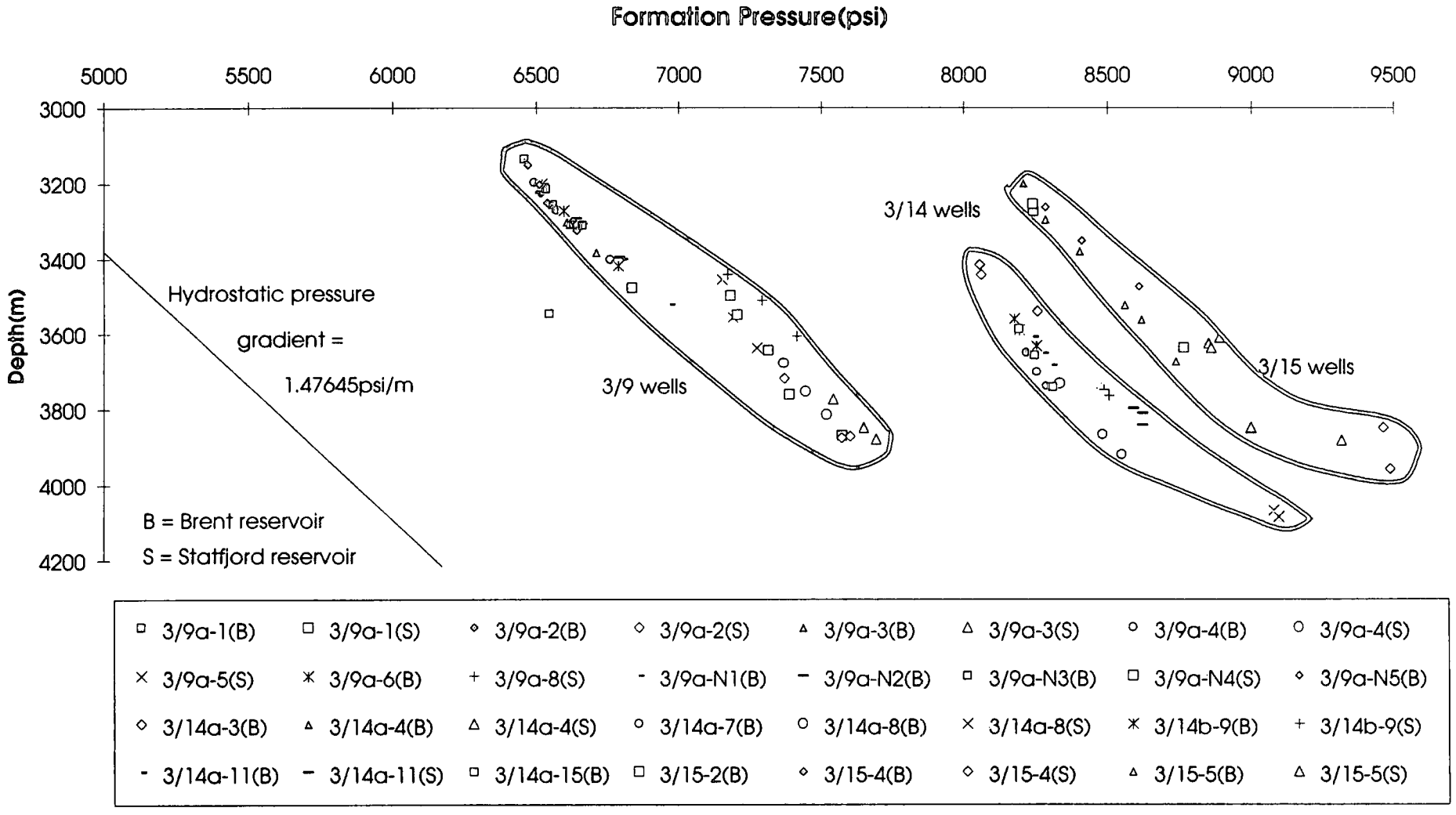

Fig.3.4b - Pressure versus depth plot of representative downhole pressures. Data from DST, FIT and RFT.

Buhrig (1989) classified the pressure compartments of Alwyn, as with many other fields in the Northern North Sea, into a regional framework. A series of pressure cells were defined on the basis of their lateral drainage efficiency and the amount of restriction of fluid flow linked to the structural downthrow of the fault blocks reservoirs.

Pressure leak off or dissipation between these recognised compartments is prevented by either a lithostratigraphic change such as a stratigraphic pinch out or a permeability decline. An obvious lateral sealing mechanism would be the well documented Kimmerian normal faults. It is these faults which seem to control the pressure distribution and define the 3 pressure compartments in the Alwyn area with the more discrete pressure differentials observed between individual wells also linked to incomplete pressure communication across smaller local fault planes. There appears to no obvious correlation between a particular fault set or trend with sealing capacity (Fig.3.4a). Both the larger and regional Graben sub parallel NNW-SSE faults and the smaller E-W cross faults appear to inhibit pressure.

There appears, then, to be a general trend that overpressure increases from Alwyn North to Alwyn South East with the Alwyn South field experiencing intermediate overpressures. Therefore, a pressure differential appears to be in operation heading south and east across the field. When observed in a structural and areal sense, it appears that overpressure increases toward the Viking Graben.

3.5 Fluid Flow and Maturation Modelling

3.5.1 Introduction

In order to understand the migration of oil and gas condensate as well as the present distribution of overpressure, it is necessary to identify any indicators of fluid flow through the reservoir system. From inferencesthat overpressure in the area increases toward the deeper Viking Graben which is situated to the east (section 3.4), observations and correlations of the organic rich rocks in the Alwyn area and the reservoired oils were defined. A similar approach was taken here to the Gullfaks field on petroleum heterogeneity using biochemical and other organic geochemical data (Horstad et al., 1990). The burial history, maturation characteristics and timing of hydrocarbon generation was also modelled.

If hydrocarbons have migrated into the Alwyn area, they may have done so with an associated pressure drive. The identification of any maturity profile or organic geochemical trend across the area may reveal the likely source area for the reservoired

hydrocarbons and suggest a carrier system available for fluid transference from a distal source area to the structural traps of the Alwyn field. Timing of such a fluid flow event is critical in the analyses of reservoir diagenesis and fill-up history of the field and therefore a time constraint is important in the evaluation of any fluid migration and its effects. If this source area can be identified, then burial history and maturation modelling could be used to simulate the hydrocarbon generation potential, any associated developed overpressure (due to the thermal cracking of liquid to gaseous hydrocarbons - section 2.1) of this source area and provide a constraint on the timing of maturation.

Work has been conducted by Pittion (1987) on the geochemical signatures of the reservoired oils, extracts and the organic potential source rocks in the area as part of a geochemical investigation of the Alwyn area. Total Organic Carbon(TOC), Hydrogen Index(HI), Productivity Potential(S2), Vitrinite Reflectance(Ro) and Tmax(Rock-Eval) studies have been conducted and the results are documented for the Kimmeridge Shale, Heather Formation, Dunlin Shale, Brent Coals and Statfjord Coals from the Alwyn North, South and South East fields. Discussion and interpretation of the results run concurrent with the observations to ascertain any correlation and trend which may become apparent.

3.5.2 - Source Rock Potential

The Kimmeridge Clay Formation - the most likely source rock for oil and gas condensate in the immediate vicinity (Jourdan et al., 1987) and also in the region of the Viking Graben, was analysed in terms of TOC, HI and S2 in wells of Alwyn North, South and South East (Pittion, 1987).

Fig.3.5.2a shows that TOC varies from 1-8% with typical values around 3-4%. The Hydrogen Index (HI) values shows a trend (Fig 3.5.2b) where the HI seems to decrease in the deeper wells indicating a decrease in the quality and therefore humic input of the organic component reflecting a possible change in depositional conditions. Below 3900m, the HI drops rapidly indicating a maturity change around this point. 3900m equates to a temperature of 132.6°C (using a geothermal gradient of 34°C/km calculated from bottom hole temperature data). In wells Norwegian 30/4-1 and 30/7-8 (outside the Alwyn area, lying more proximal to the Viking Graben axis) the HI would indicate a maturity higher than those recorded for rocks of the Kimmeridge Formation, with similar TOC, in the Alwyn field.

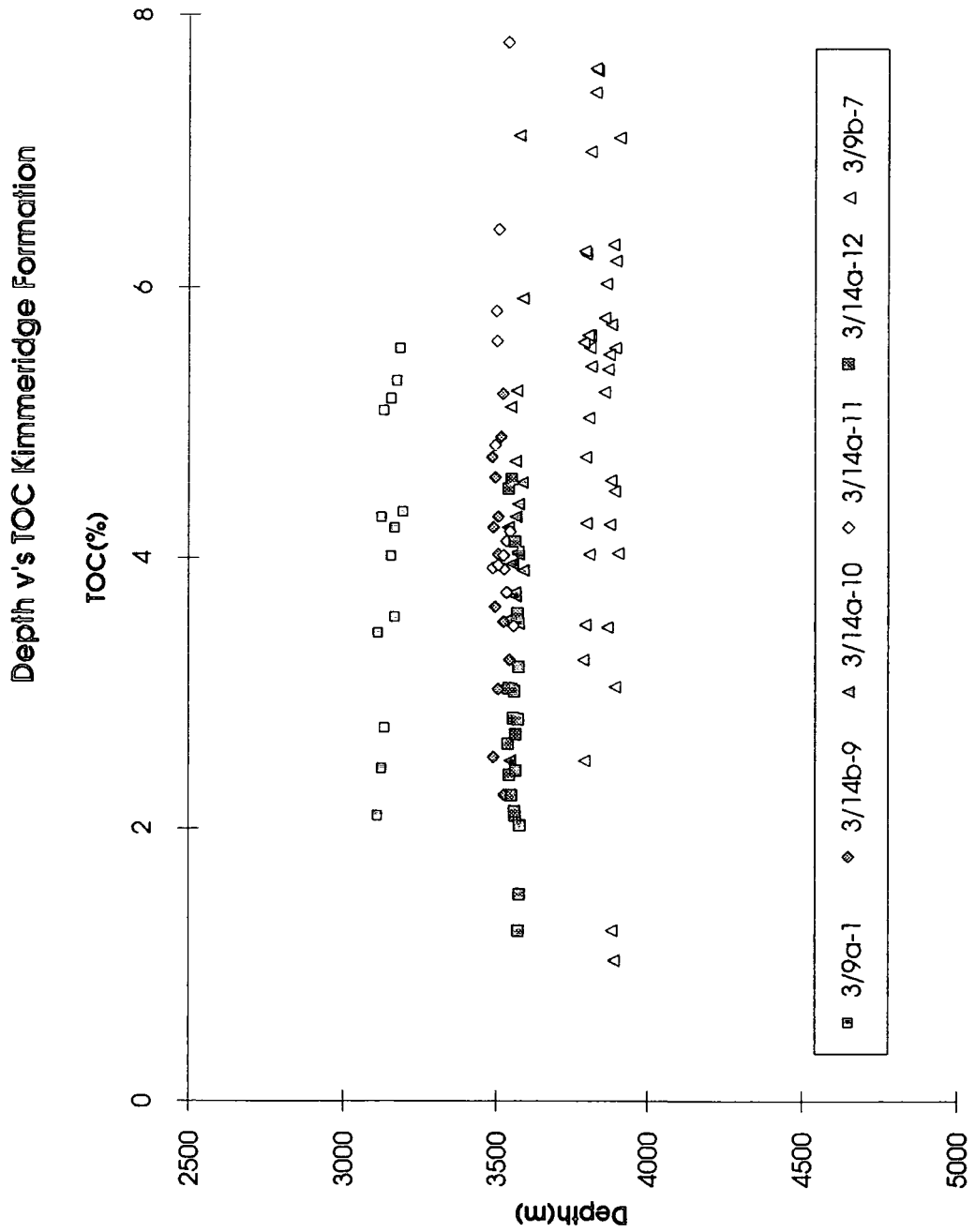

Fig.3.5.2a - Depth versus Total Organic Carbon (TOC) for the Kimmeridge Formation. Data from Pittion (1987).

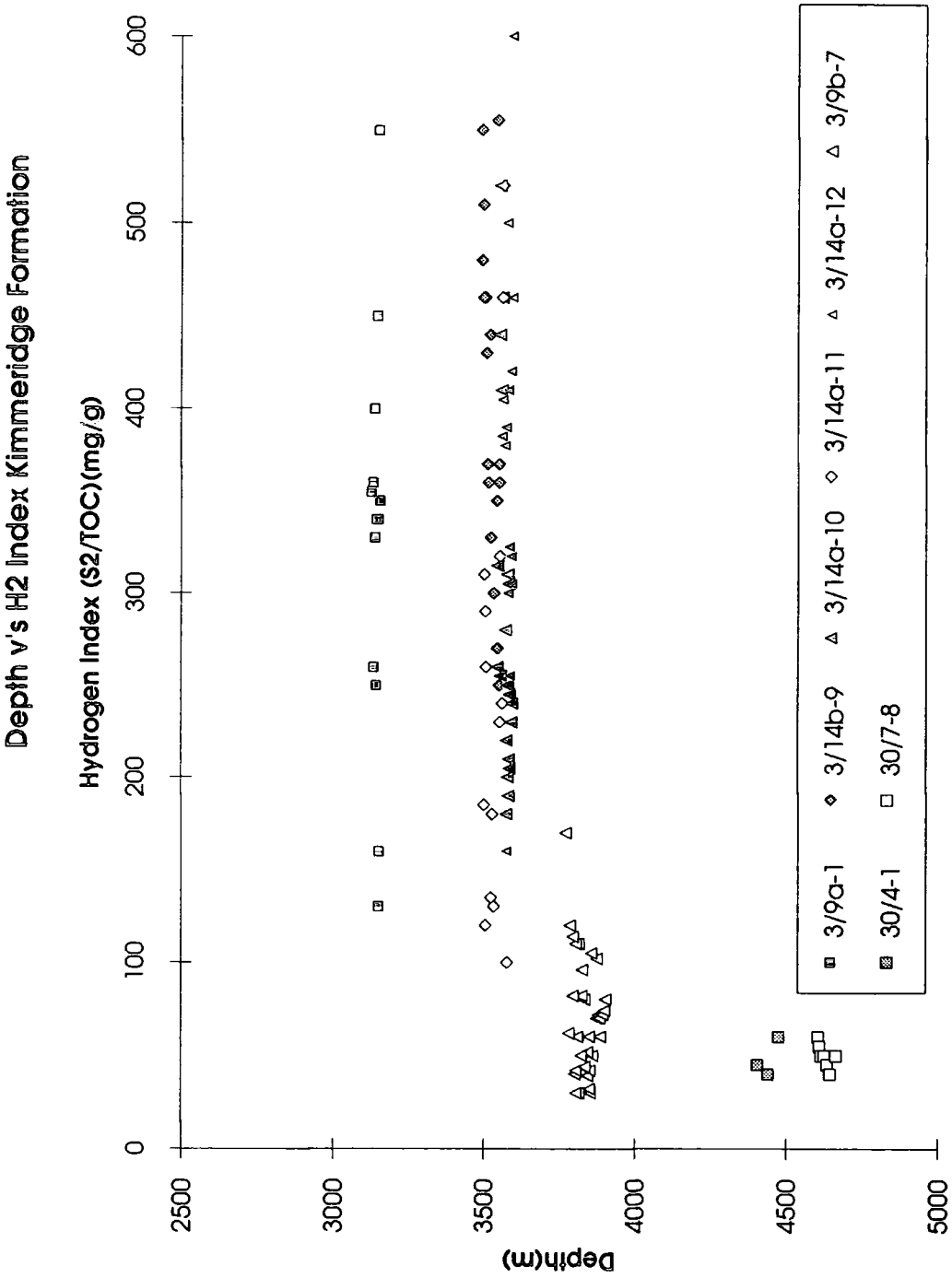

Fig.3.5.2b - Depth versus Hydrogen Index for the Kimmeridge Formation. Data from Pittion (1987).

Since the HI indicates a residual quality (Pittion, 1987), the trend of decreasing HI might indicate the cracking of organic matter to oil was effective below the 3900m transition zone based on observations in Fig 3.5.2b. Pittion (1987) describes this point as being an indicator of the peak of the oil window. The Potential Productivity (S2) (Fig.3.5.2c) also reflects a similar pattern to the previous observation. Fig.3.5.2c shows a marked decrease in S2 below 3900m possibly due to an increase in maturity and cracking of base organic matter and kerogen into liquid hydrocarbons.

Comprehensive analyses of the source rock potential of the Heather, Brent, Dunlin and Statfjord formations were also undertaken (Pittion, 1987).

Heather Formation has a low potential (TOC range of 1-4%, HI of 50-200mg/g, S2<10kg/t) but lower than the overlying Kimmeridge. However, it is generally considered a lean source rock.

Dunlin shows a similar potential as a source rock to the values and trends in Heather for oil.

Brent, the major reservoir formation in the Alwyn area, showed a lower potential but interstitial coal horizons proved high TOC's of up to 50%. However, due to the sporadic and varying occurrence of these relatively very thin coals, an overall low TOC reflects the overall low potential of Brent.

The **Statfjord Formation** is an alternating sequence of shales and sands. The potential of the Statfjord is uncertain. Only cuttings were analysed and hence the true potential of the shales is biased due to unbalanced mixing of the two lithologies (Pittion, 1987). TOC analyses are in the range of 1-2% and unlikely that the Statfjord is a major potential source rock for the area.

In summary, the Kimmeridge Shale Formation is the only significant source rock for oil.

3.5.3 - Maturity

To assess and compare the maturation characteristics of the organic rich rocks in the area and the reservoired oils in the Alwyn fields, an observation was firstly made on the maturity of the likely source rock. Analyses were performed on the entire Jurassic section with two main parameters: Vitrinite Reflectance(Ro) and Tmax(Rock-Eval Pyrolysis). The analytical work was documented by Pittion (1987). From the analyses, the following points have been noted:

3.5.3.1 - Vitrinite Reflectance -

Fig.3.5.3.1a shows the plotted reflectance values for analyses carried out on coals and kerogens in the Jurassic section. Data supplied in Pittion (1987) does not differentiate

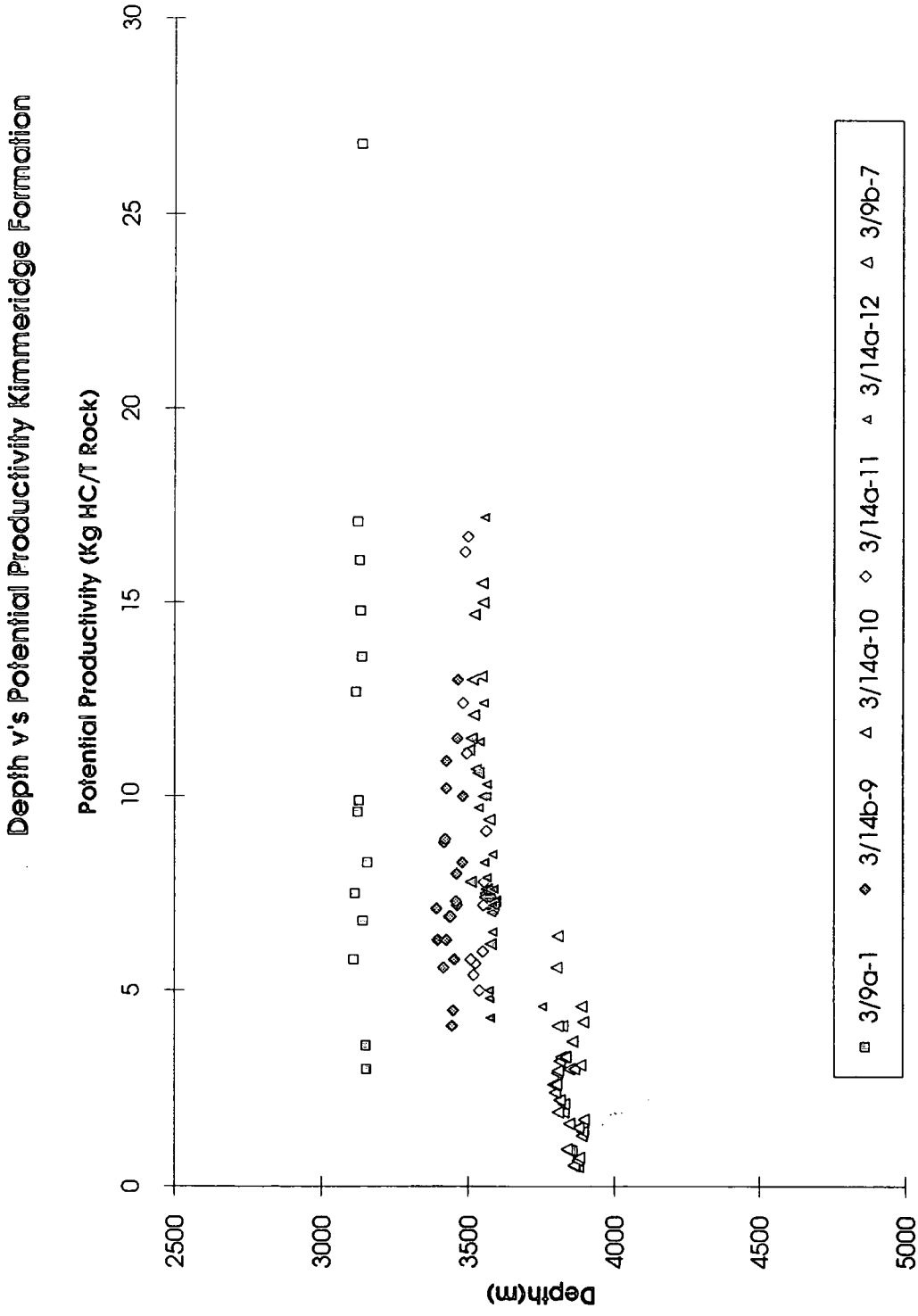

Fig.3.5.2c - Depth versus Potential Productivity for the Kimmeridge Formation. Data from Pittion (1987).

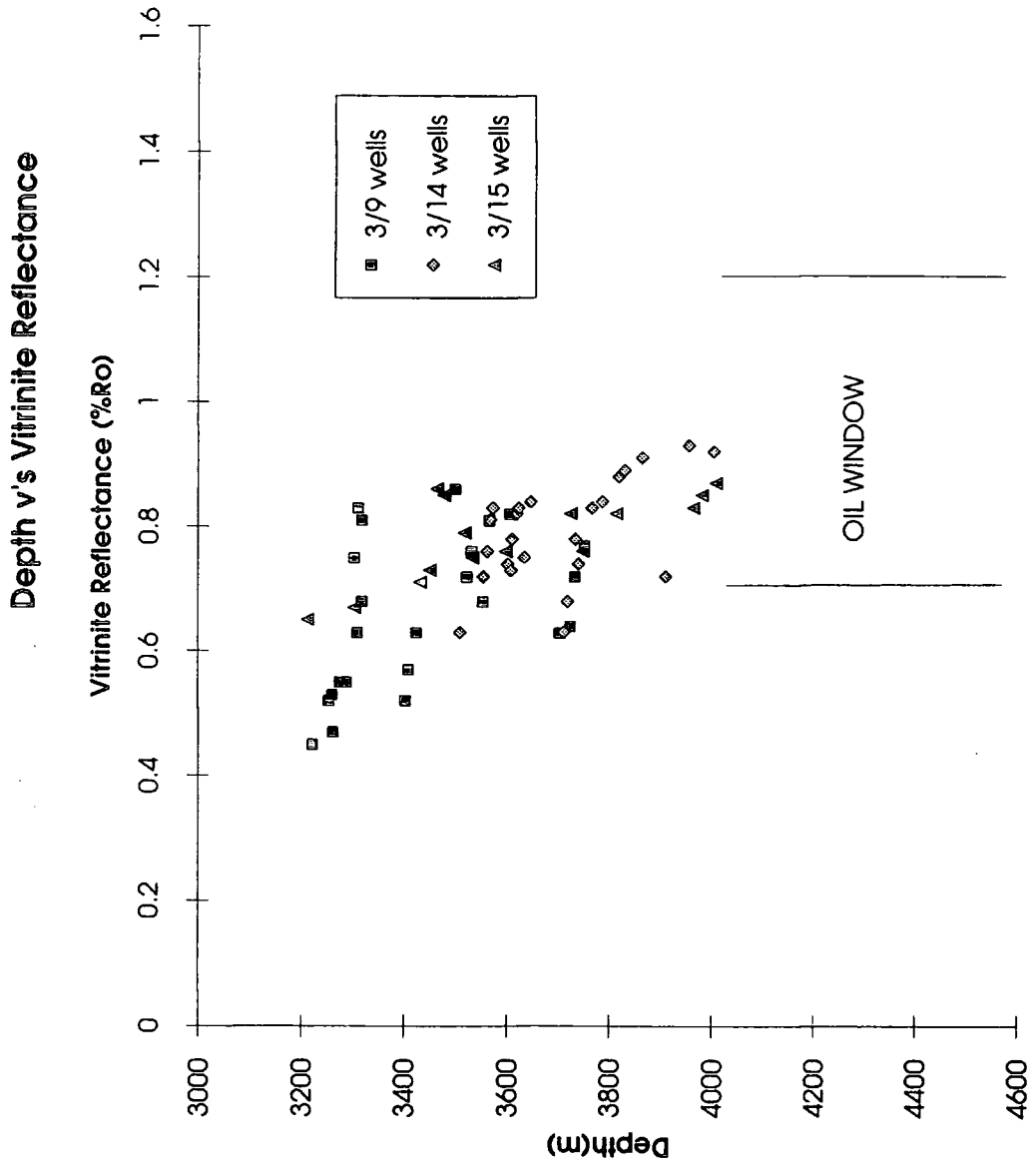

Fig.3.5.3.1a - Depth versus Vitrinite Reflectance (%Ro) for coals and kerogens in the Jurassic section. Data from Pittion (1987). Oil window defined by Tissot et al. (1987).

between formations for Ro versus depth data, except that values for the 3/9b-7 well were from coals in the lower Brent section. However, it is possible to correlate these Ro values with depths for the Kimmeridge Shale Formation using information from well logs. These depth intervals for the Kimmeridge Shale Formation are tabulated in t3.5.3.1a.. Correlating Kimmeridge depth information with Ro in the Alwyn North wells (Fig.3.5.3.1b), it is clear that the Kimmeridge Formation does not record values greater than 0.52%Ro. Fig.3.5.3.1b details the pattern of increasing maturity with depth in the 3/9 structure with values up to 0.9% Ro. However, these higher values reflect coals analysed from the lower Brent section in the 3/9b-7 well rather than from the favoured and more likely source rock (the Kimmeridge Shale Formation). If the oil window is described as being in the mature stage of generation between 0.7-1.2%Ro equivalent (VRE) (Tissot et al 1987; Anders and Gerrild, 1988) then the wells of the Alwyn North Fault block which have been drilled updip on the structure, the Ro values of the likely source rock (the Kimmeridge Formation) are therefore described as immature to early mature(<0.5%Ro - immature, 0.5-0.7%Ro - early mature, Tissot et al., 1987; Anders and Gerrild, 1988).

This pattern of increasing reflectance and maturity with depth is also depicted in Alwyn South (3/14)(Fig.3.5.3.1c) and Alwyn South East (3/15)(Fig.3.5.3.1d).

Alwyn South observes reflectance values which lie in the oil window for all samples in the Jurassic Formations (Fig.3.5.3.1c) being Ro 0.55-1.1% for a depth between 3200-4100m. However, when considering the Kimmeridge Formation, the correlation between depth and Ro shows Ro values from 3354m (3/14a-3) to 3571m (3/14a-8) in the range of 0.65-0.73%Ro.

Alwyn South East (Fig.3.5.3.1d) shows a range of Ro between 0.5-1.1% for a given depth range of 3150-4000m. When correlated to a similar depth range (3300-3400m) with Alwyn North (Fig.3.5.3.1b), the values in the South East structure have slightly higher reflectance values. The Kimmeridge Formation has a depth range in the Alwyn South East field of between 3119m (3/15-2) to 3228m (3/15-3). Corresponding Ro values in the Kimmeridge Formation gives values of 0.57-0.75%Ro (mode 0.67%Ro).

It can be inferred, when considering observations based on Ro, that only the Upper Jurassic formations of the Kimmeridge (the likely source rock in the area) in the 3/14 fault block would provide the necessary maturity to fall in the oil window (Ro of 0.7-1.2%). Based on vitrinite reflectance then, the Kimmeridge in the Alwyn North and South East fields would be immature and unlikely to yield hydrocarbons in sufficient

North Wells	Depth (TVD, m)	South Wells	Depth (TVD, m)	S.E. Wells	Depth (TVD, m)
3/9a-1	3077-3196	3/14a-1	3124-3156	3 15-2	3119-3226
3/9a-2	3124-3176	3/14a-2b	3166-3173	3 15-3	3182-3228
3/9a-3	3099-3129	3/14a-3	3354-3375	3 15-4	3135-3219
3/9a-4	3118-3121	3/14a-4	3369-3433	3 15-5	3109-3166
3/9a-5	3139-3160	3/14a-7	3411-3509		
3/9a-6	3095-3108	3/14a-8	3449-3571		
3/9a-7	3169-3220	3/14b-9	3453-3527		
3/9a-8	3124-3152	3/14a-11	3440-3556		
		3/14a-15	3423-3498		

Table t.3.5.3.1a - Depth range of the Kimmeridge Formation in Alwyn field wells. Data from available well logs.

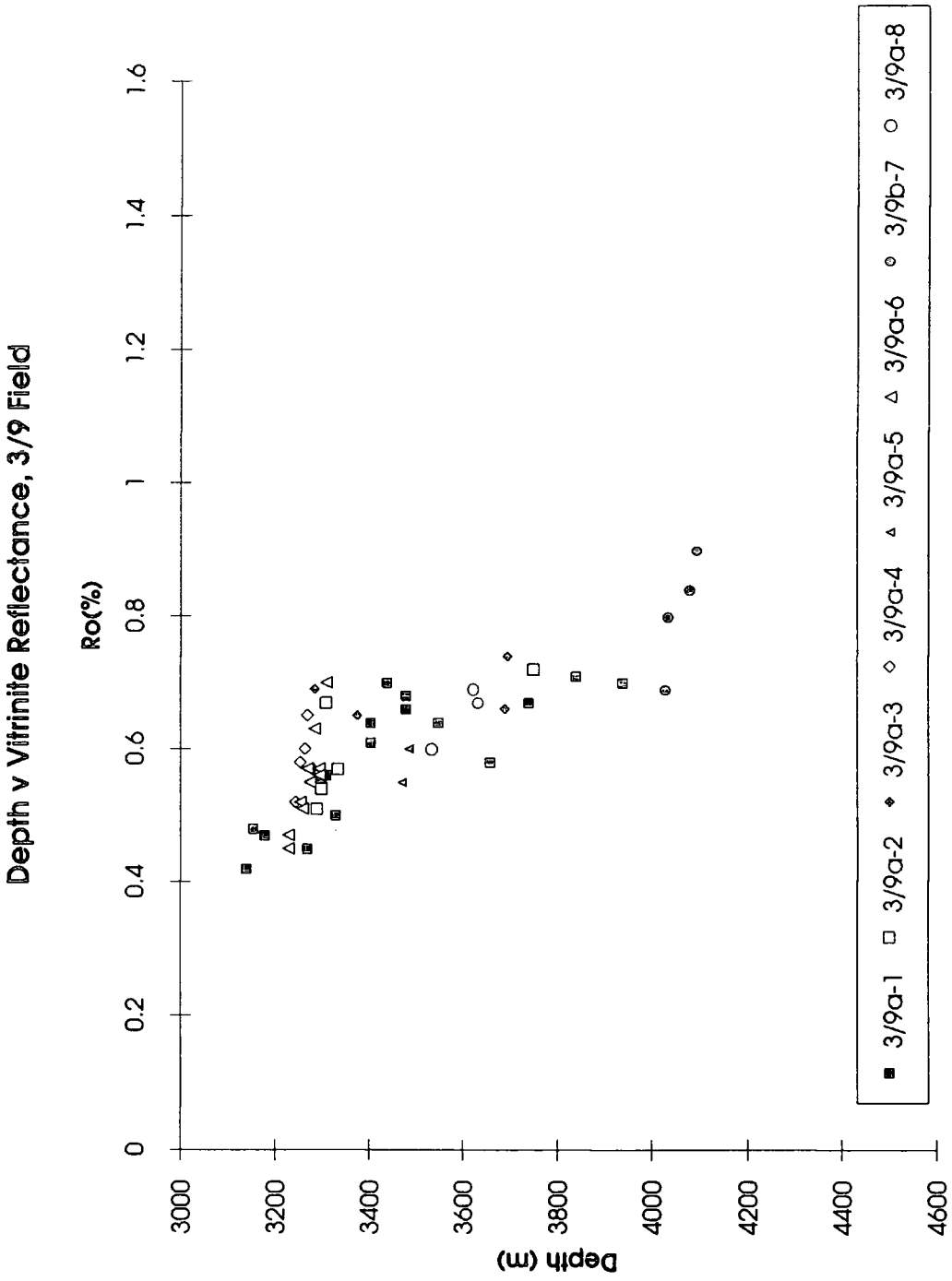

Fig.3.5.3.1b - Depth versus Vitrinite Reflectance (%Ro) for Alwyn North wells. Data from Pittion (1987).

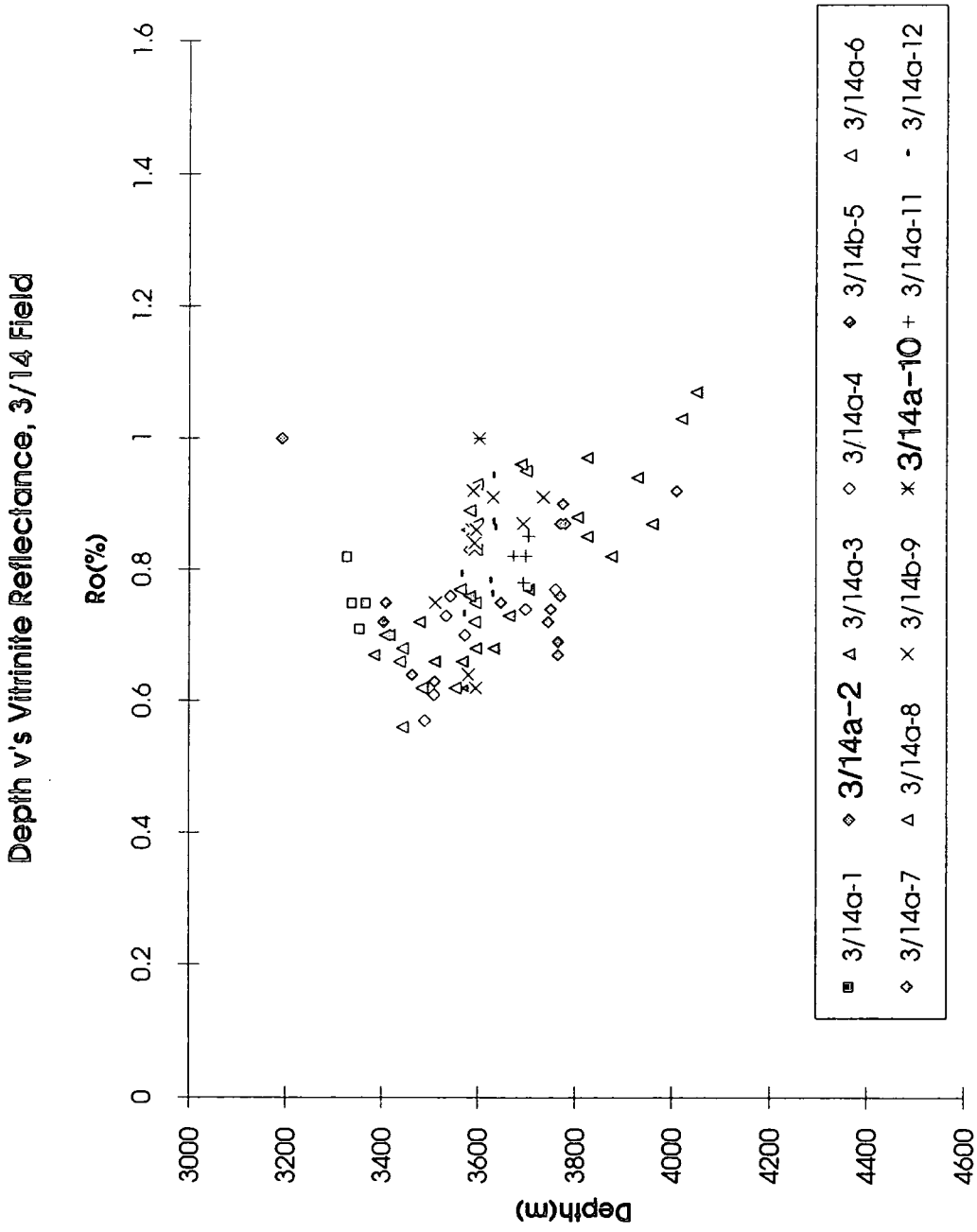

Fig.3.5.3.1c - Depth versus Vitrinite Reflectance (%Ro) for Alwyn South wells. Data from Pittion (1987).

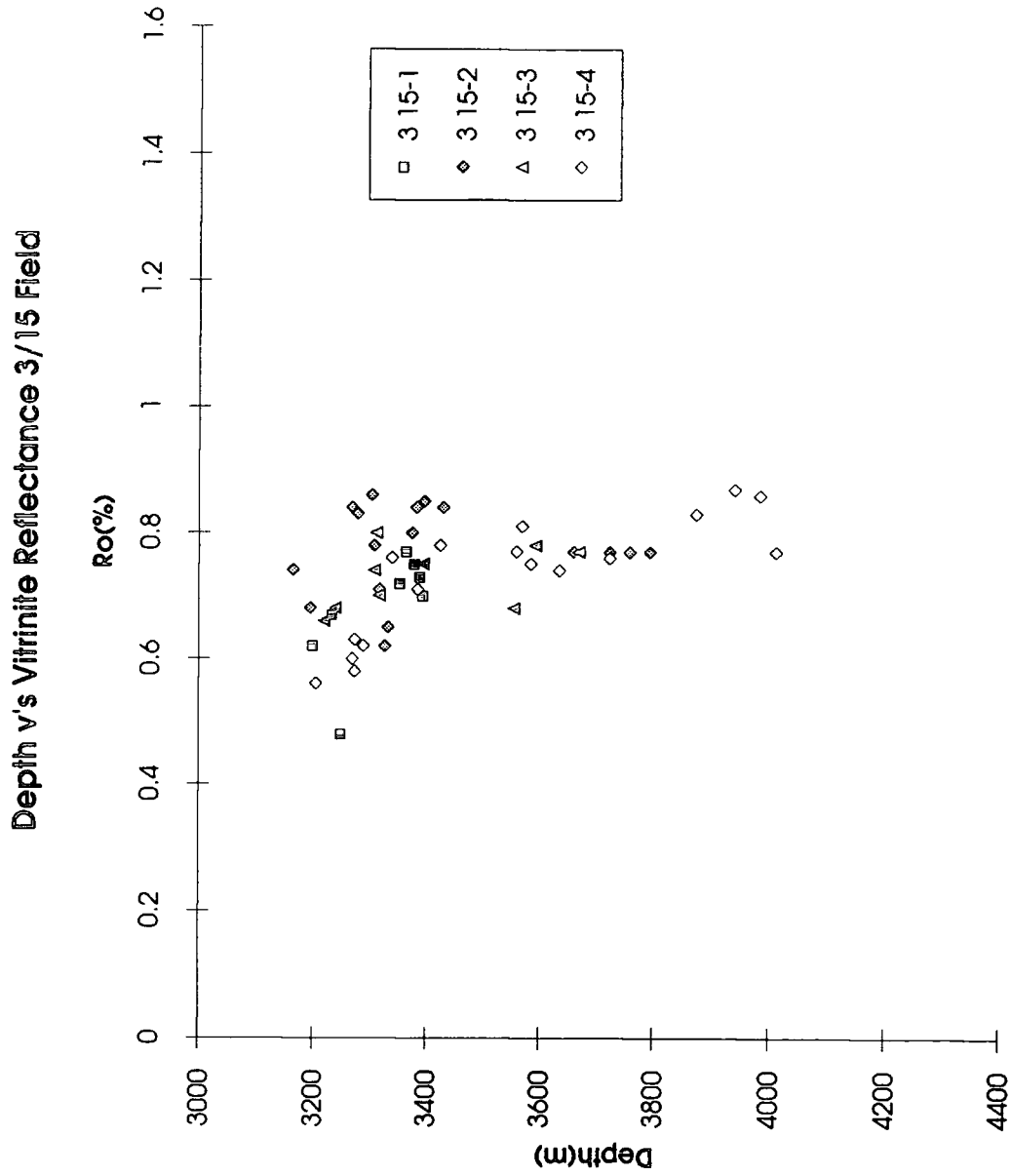

Fig.3.5.3.1d - Depth versus Vitrinite Reflectance (%Ro) for Alwyn South East wells. Data from Pittion (1987)

quantity and only the Alwyn South field can be envisaged as possibly generating oil at the depths which the Kimmeridge Formation is recorded in the field. However, there is a general correlation in all three fields that there is an increase in maturity with depth.

3.5.3.2 - Tmax -

Tmax has been reviewed as a maturity indicator in section 2.2. Tmax pyrolysis temperature reflects the measurement of temperature (°C) of the maximum formation of hydrocarbons by cracking of kerogen. Tmax can be affected by factors such as low critical amount of organic matter, the mineral matrix in which the organics are set, hydrocarbon staining and contamination by cavings (Pittion, 1987).

Analysis for Tmax were also carried out on coals with the recognised limits of the oil window at 435°C and 465°C for the beginning and end respectively (Karlsen, 1990). From Fig.3.5.3.2a, a similar pattern emerges as seen in the vitrinite reflectance observations where Tmax values for updip Alwyn North wells lie in the immature zone as does the Upper Jurassic formations of the Alwyn South East field.

3.5.3.3 - Maturity Conclusions -

The trends offered by both vitrinite reflectance and Tmax studies indicate strongly that the maturity increases and is therefore controlled primarily by increasing temperature (associated with burial). Therefore, this observation would deny any explanation that lithological and stratigraphic parameters would control maturity. However, there are several slight variations - maturity in Alwyn South East (3/15) appears to be slightly higher than in Alwyn North (3/9) for the same depth range (3200-3300m). This may be due to higher heat flow from local circulating fluids being hotter in the Alwyn South East field.

The three fault blocks of Alwyn North, South and South East can be classified in terms of maturity and it is observed that only the South field boasts a structural configuration where the mean Ro values recorded in the Kimmeridge Formation falls within the main oil window VRE 0.7-1.2%Ro. This is obviously important when assessing the likelihood of local maturation and primary migration of hydrocarbons from a source rock. In the North and South East fields, the Kimmeridge Shale Formation does not approximate to a maturity whereupon hydrocarbons would be expelled from the organic rich rocks. In the Lower Jurassic section of these structures which lies within the oil window, the previous interpretation of TOC, HI and S2 would argue against any local maturation of hydrocarbons in quantities observed to be present in the

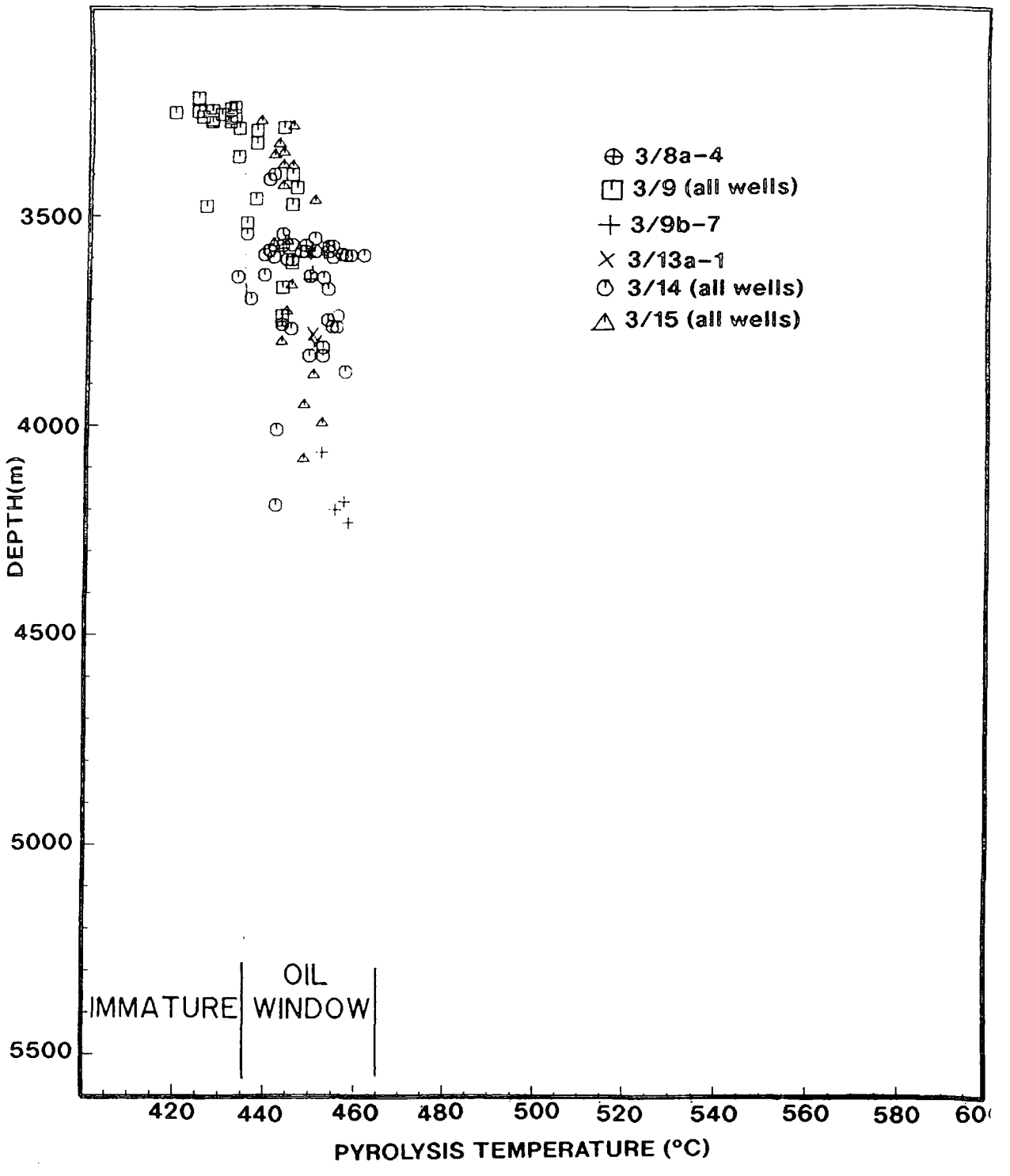

Fig.3.5.3.2a - Tmax (Pyrolysis) temperatures of selected wells in the Alwyn area. Data from Pittion (1987). Oil window defined by Tissot et al (1987).

reservoirs (section 3.2). In clonclusion, local sourcing seems unlikely and a source of hydrocarbons from adjacent depocentres is the most probable alternative.

3.5.4 - Oil Analysis

The reservoired oils in the Alwyn area were analysed geochemically to ascertain their maturation and geochemical signatures relative to the organic rich rocks in the fault blocks.

Whilst drawing information on oil-source rock correlation, it is worthwhile and potentially revealing to look for any oil-oil compositional variations within and between reservoirs. Although many mechanisms serve to homogenise reservoir fluids, petroleum populations of varied composition can be defined and related to reservoir continuity and history of field filling (Karlsen and Larter, 1991). Indeed, if a reservoir is filled from one end in a sequential manner, as proposed by England et al (1987) and a field size similar to Alwyn is considered, the most mature petroleum in the reservoir should be located nearest the source rock basin or probable filling point (England et al., 1987; England and Mackenzie, 1989; Larter et al., 1990). Horstad et al., (1989) have shown that there is a relationship between reservoir scale and filling time since continuos hydrocarbon diffusion through the reservoir over time tends to homogenise the composition of the petroleum and destroy compositional gradients in the field. This homogenisation effect will have a tendency to influence the vertical column rather than causing lateral heterogeneities (Karlsen and Larter, (1991) based on data from England et al., 1987).

3.5.4.1 - C15+ Saturates Analyses -

The heavier components (C15+) were analysed and three main parameters are considered (data documented in Pittion, 1987): Pristane/C17 (Pr/C17), Phytane/C18 (Ph/C18) and Pristane/Phytane (Pr/Ph). The ratios of these 3 parameters are discussed.

Fig.3.5.4.1a shows the relationship of Pr/C17 versus Ph/C18 in the Alwyn oils where these two ratios decrease when maturity increases. Indication from the plotted data suggests that the oils in Alwyn North (3/9) are less mature than the reservoired oils in the South (3/14) field and to a lesser extent the oils in the South East (3/15) field. Two wells - 3/9a-3 and 3/9a-6 - show an anomaly to this trend but Pittion (1987) notes that the analysed fluids in these wells are in a state of equilibrium between gas and liquid (in a critical state).

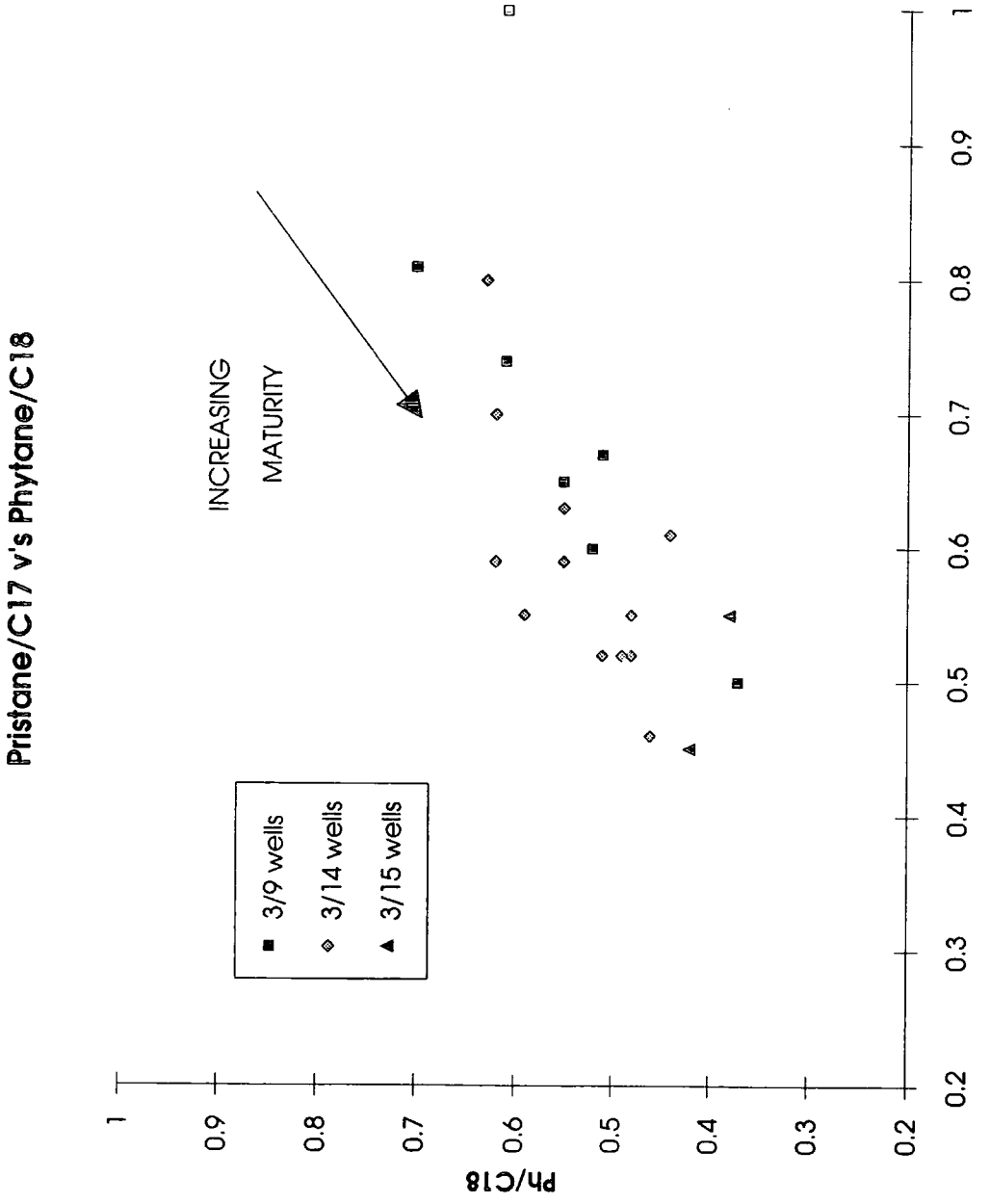

Fig.3.5.4.1a - Pristane versus Phytane ratios of Alwyn field reservoired oils. Data from Pittion (1987)

Thermovaporisation Fraction -

The technique of thermovaporisation allows analysis of the C5 - C15 part of the oils with the two ratios - Ip and Ih - being observed

where

$$Ip = \frac{\text{2Methyl C6 + 3Me C6}}{\text{3isomer of Di Methyl cyclo C5}}$$

$$Ih = \frac{\text{nC7 x 100}}{\text{Cyclo C6 <peaks< Methyl cyclo C6}}$$

These two ratios record the lighter fraction of oils (C5 - C15) and increase systematically as result of increasing maturity (Peters and Moldowan, 1992). It is seen from Fig.3.5.4.1b samples from Alwyn North (3/9) wells have a broad spread in terms of maturity but tend to cluster in the field defining a sapropelic origin for the oils. Statistically, the Alwyn North samples have a mean Ih ratio of 24 and Ip ratio of 1.4. Fig.3.5.4.1b observes the oils reservoired in Brent sands of Alwyn South (3/14) cluster around a mean Ih ratio of 23 and Ip ratio of 1.9. Samples corresponding to the Alwyn South East field only return 2 values and have a mean Ih ratio of 16 and Ip ratio of 1.45. Summarising the data, it can be inferred that oils of the Alwyn South have a more mature signature than oils from reservoired oils from Alwyn North and South East.

The lighter fraction (Ip and Ih ratios) of the oils in the Alwyn area follow a similar pattern, with the more mature oils being reservoired in the Alwyn South field, relative to those seen in the C15+ analyses. Hence the Alwyn South oils are of a higher maturity than oils reservoired in the North and South East fields. The oils, however, in these two latter fields show compositional and maturity differences, albeit slight, to infer a higher maturity in Alwyn South East (3/15) oils which are also of a humic organic source (Fig.3.5.4.1b). This is in contrast to the oils of the 3/9 reservoirs which fall on or above the sapropelic trend line (possibly as a result of migration effect or a specific matter such as source - Pittion, 1987).

3.5.4.2 - Steranes - Triterpanes Biomarkers -

Mass spectrometry of the sterane and triterpane fraction of the oils have been analysed as parameters of maturity and these values are documented and interpreted fully in the discussion with respect to basin fill point and overall fluid flux throughout the field (section 3.5.4.3). All the data follow a similar maturity conclusion as in the C15+ and C5 - C15 analyses: The Alwyn North (3/9) and South East (3/15) reservoired oils are less mature than their counterparts in the Alwyn South (3/14) field.

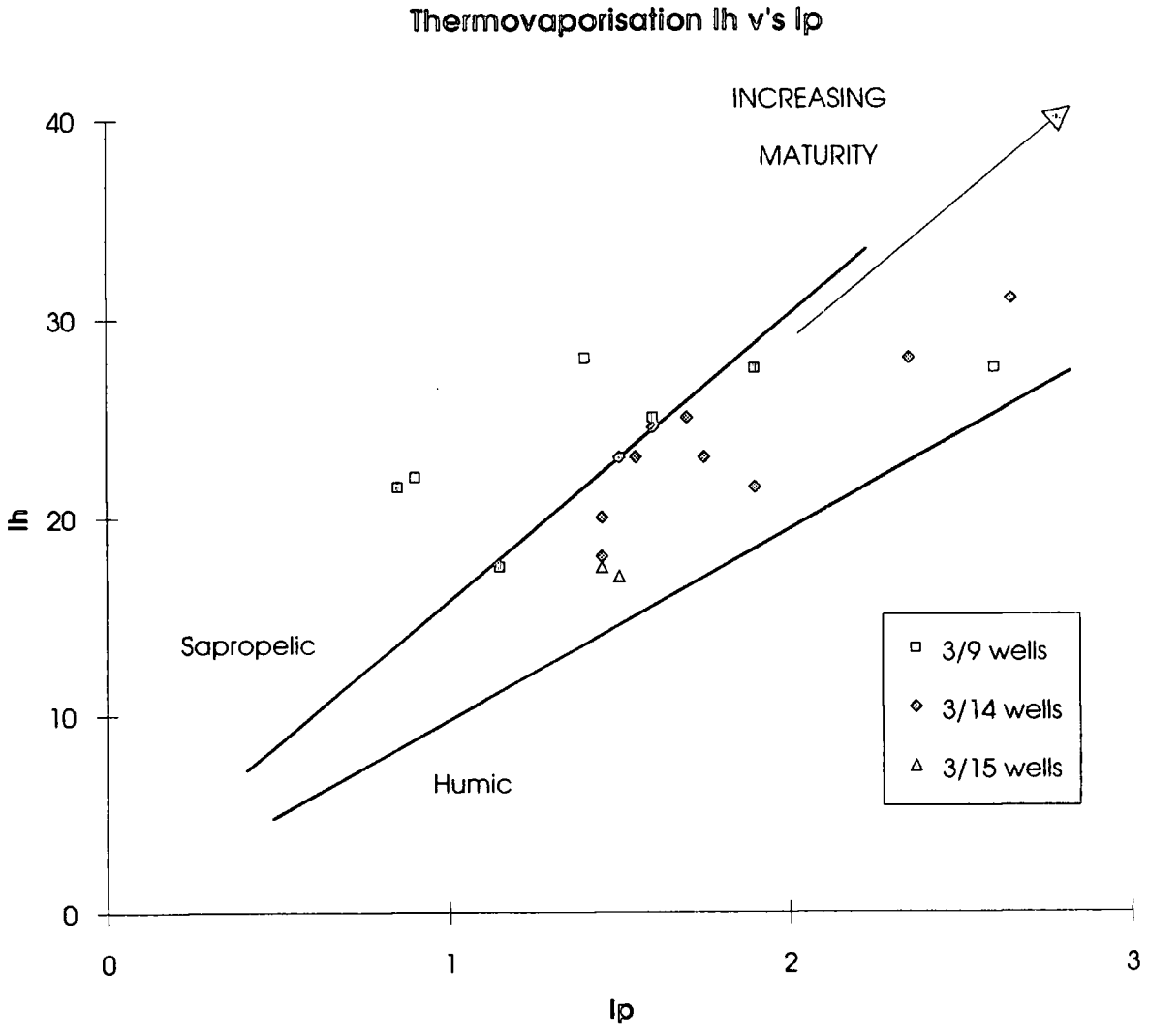

Fig.3.5.4.1b - Thermovaporisation ratios Ih versus Ip (see text for definitions) for reservoired oils. Data from Pittion (1987)

Oil - Extract Correlation -

A similar suite of analyses were carried out on the rock extract components from the 3 Alwyn areas. Extracts are the soluble organic components from the organic rich rocks (Karslen, 1990) in the formation of interest. In order to assess whether the oils have the same chemical signature as the source rocks, Fig.3.5.4.2a and b observes a correlation between the extracts and the oils. It is seen that almost all Kimmeridge extracts lie within the same range as the oils confirming that the oils are sourced only from the Kimmeridge Shale Formation.

Summarising all maturity characteristics and values from the extracts (Figs.3.5.4.2b, c, d and e) against the values for the oils (Figs.3.5.4.1a, 3.5.4.2f, g and h), the conclusion is that the extracts from all the wells of the Alwyn North structure (3/9) show that all the analysed formations are immature and are indeed less mature than the reservoired oils in the same fault block. Although there is a lack of data to positively conclude, with respect to the extracts/oils correlation (that there is such a) for Alwyn South East wells, a similar pattern emerges for the wells that were studied. This would then indicate that the oils were sourced from outside the immediate area in keeping with the observations made from the previous maturity (Ro and Tmax) interpretations.

Alwyn South (3/14) shows a maturity suite of extracts which approximately correlates in terms of chemical signature with that of the oils in the reservoirs. Therefore this implies that the present day oils in the structure were derived from organic rich rocks in the Kimmeridge Shale Formation within its own fault block.

3.5.4.3 Fluid Flow modelling based on Sterane - Triterpane Biomarkers -

The use of biomarkers is widely used to reveal trends with respect to lateral heterogeneities, basin fill points and possible source kitchen (Horstad et al., 1989).

Figs.3.5.4.2f, g and h show the correlation of specific biomarker compounds with respect to maturity of the reservoired oils. However, as documented by Horstad et al (1989) and Karlsen and Larter (1991) it is possible to plot the biomarker values from Figs.3.5.4.2f, g and h on a field map and mark these values areally to assess any trends in maturity. Biomarkers reveal trends in maturity as a consequence of their ability to record the intensity of biodegradation which these compounds have undergone. If a field is filled first with respect to another then the oils will be more severely degraded in the first filled reservoir in relation to the later filled reservoir. Obviously, early mature oils will fill a reservoir first and subsequently be subjected to a higher degree of biodegradation than oils generated at a later time with a correspondingly higher

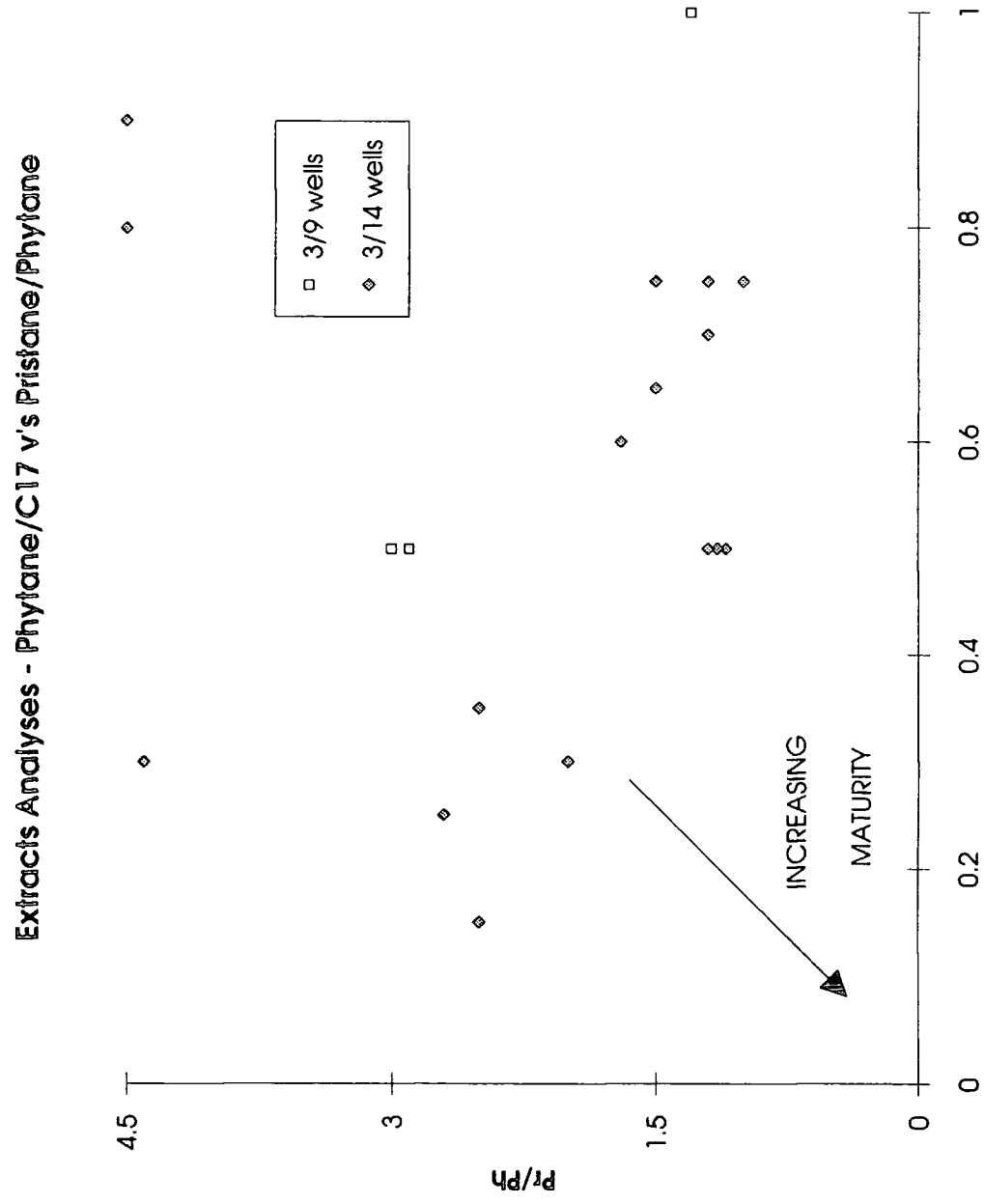

Fig.3.5.4.2a - Phytane/C17 versus Pristane/Phytane ratios of rock extracts. Data from Pittion (1987)

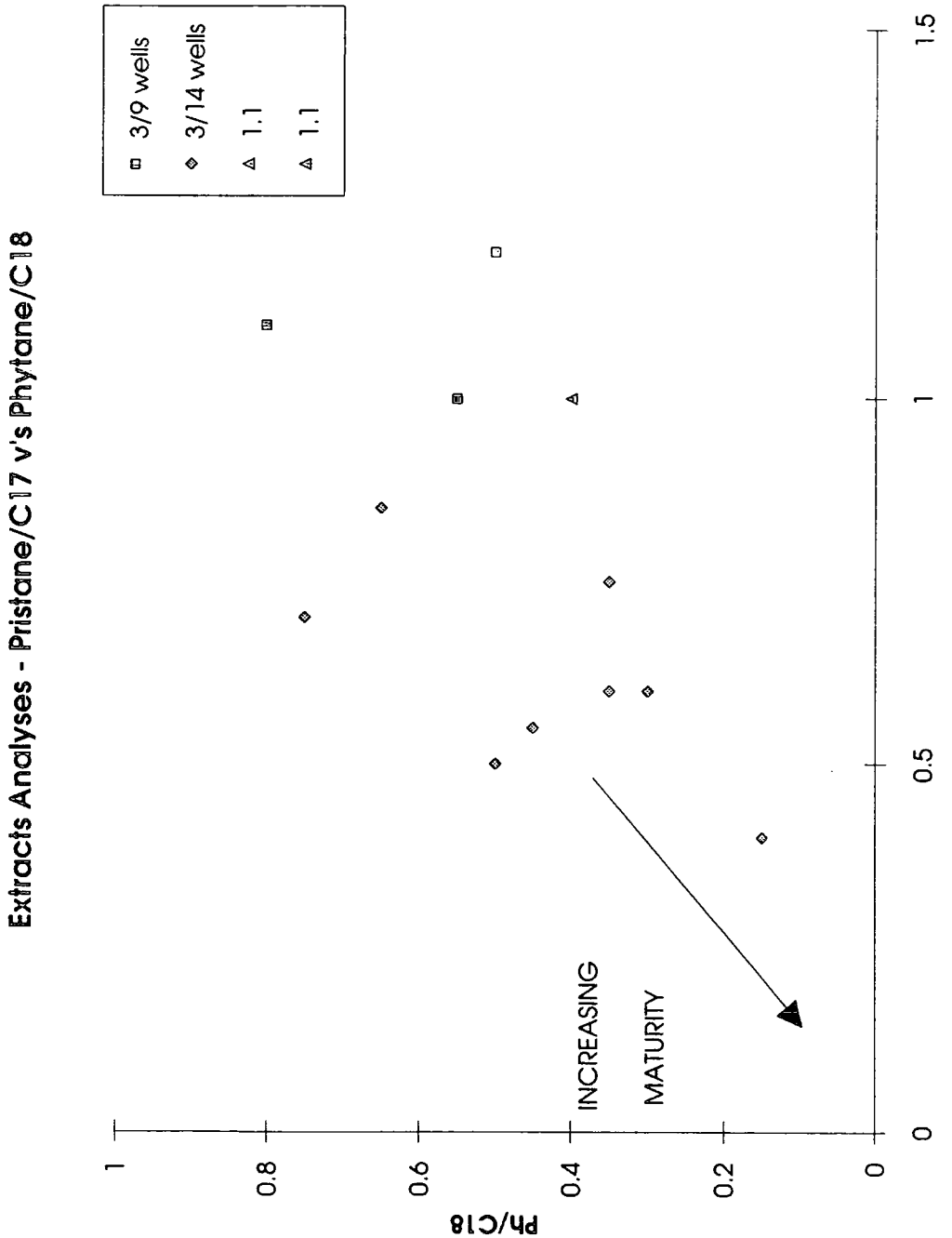

Fig.3.5.4.2b - Pristane/C17 versus Phytane/C18 ratios of rock extracts. Data from Pittion (1987)

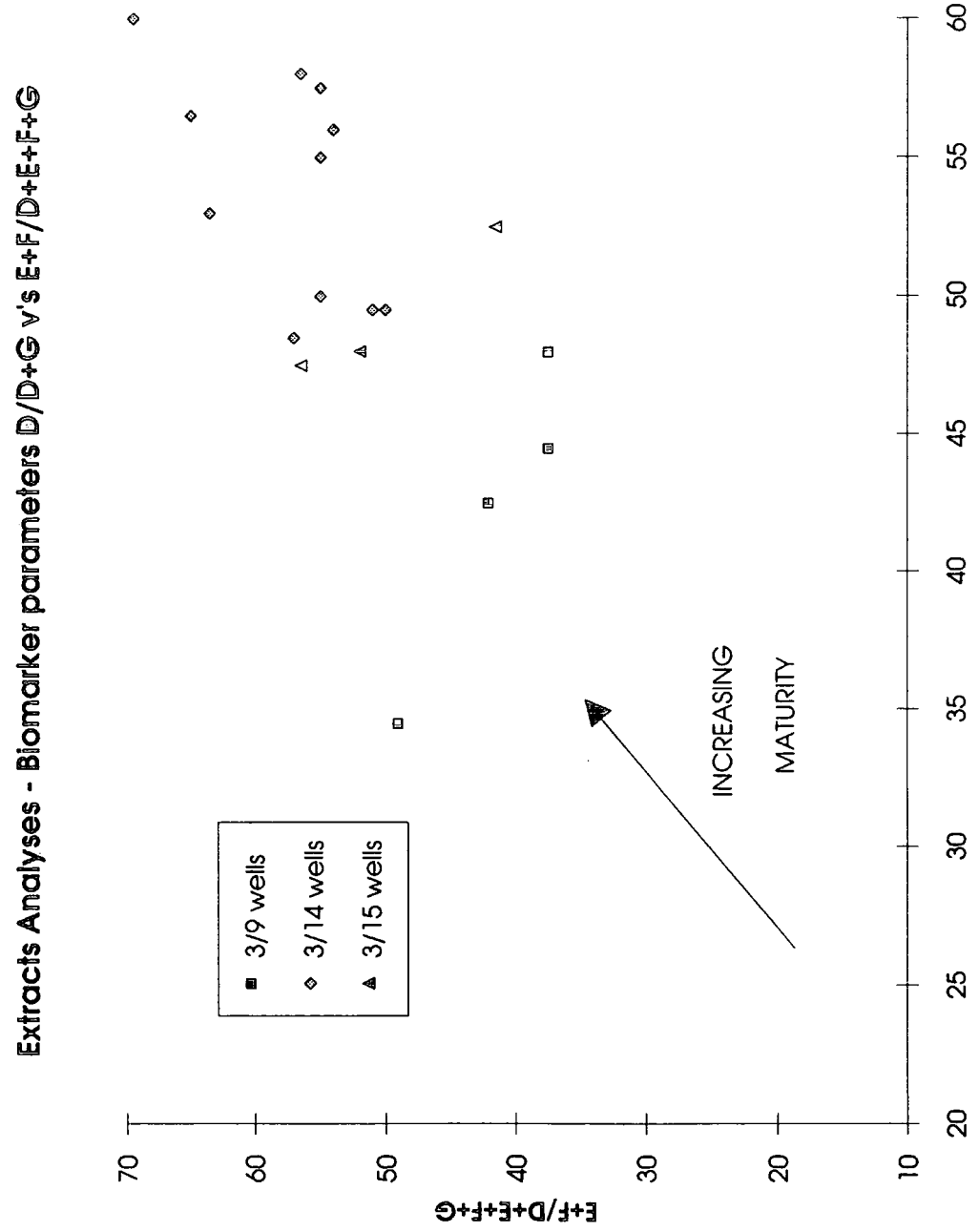

Fig.3.5.4.2c - Biiomarker ratios D/D+G versus E+F/D+E+F+G (see text for definitions) of rock extracts. Data from Pittion (1987)

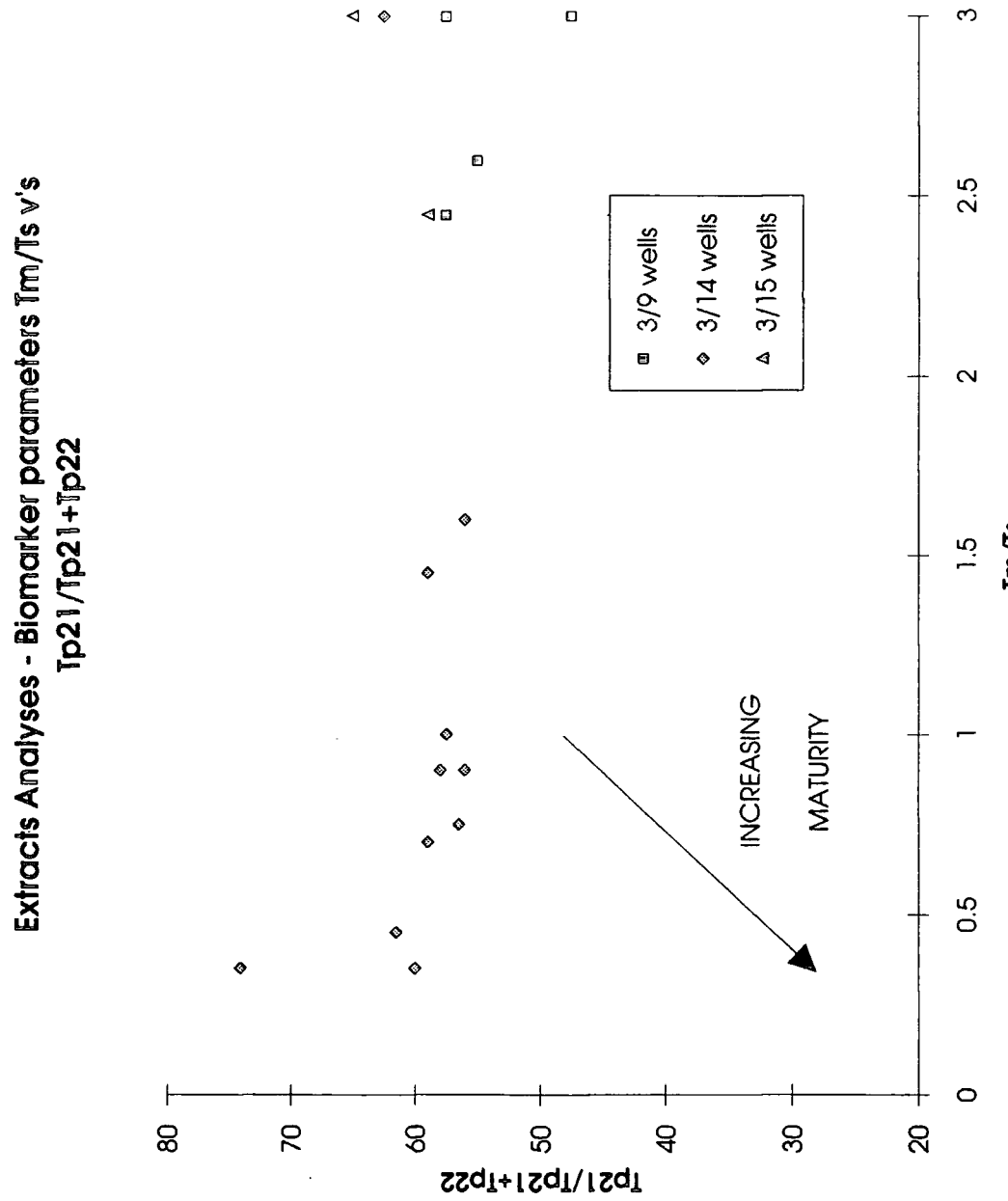

Fig.3.5.4.2d - Biomarker ratios Tm/Ts versus Tp21/Tp21+Tp22 (see text for definitions). Data from Pittion (1987)

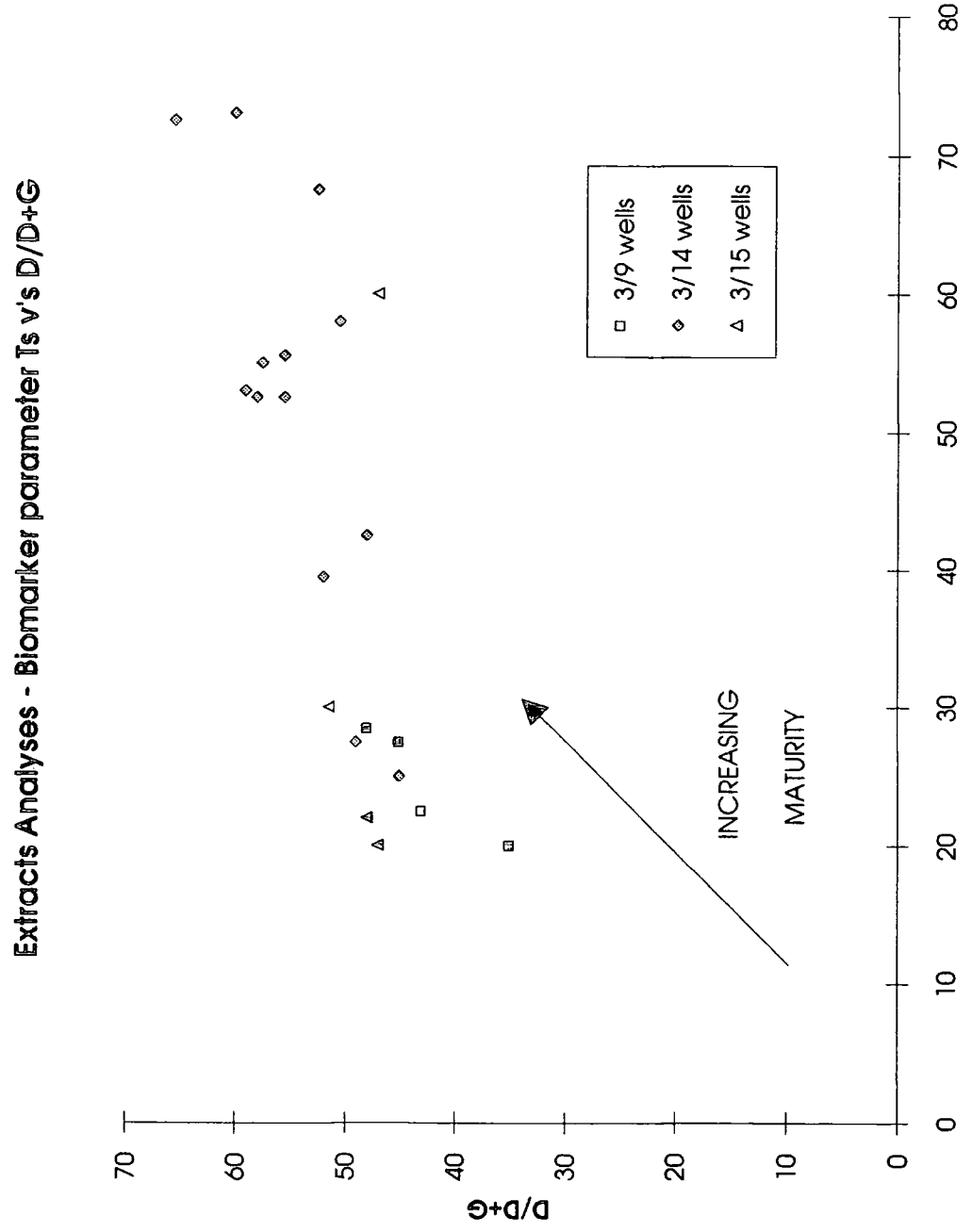

Fig.3.5.4.2e - Biomarker ratios Ts versus D/D+G (see text for definitions). Data from Pittion (1987)

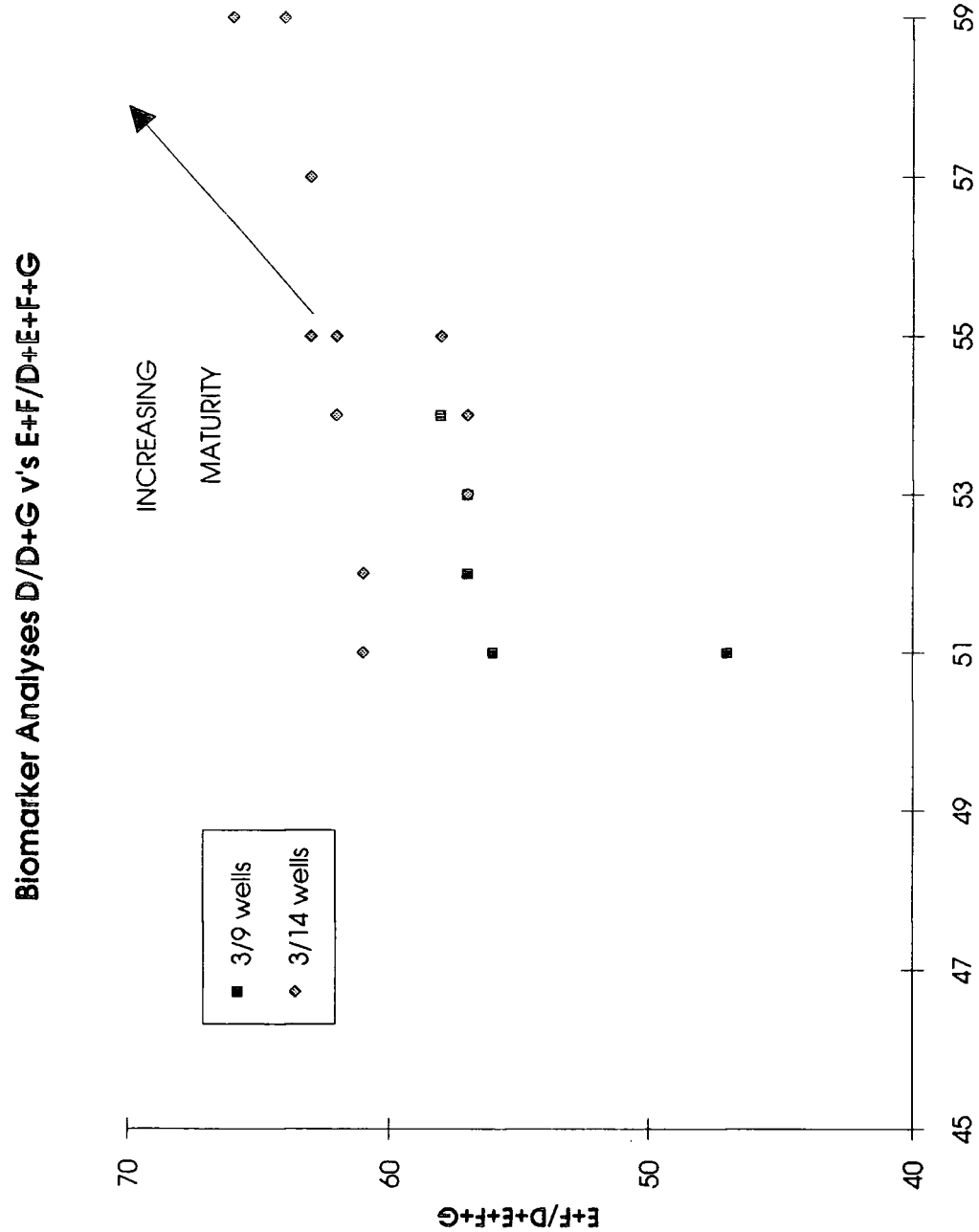

Fig.3.5.4.2f - Biomarker ratios D/D+G versus E+F/D+E+F+G (see text for definitions). Data from Pittion (1987)

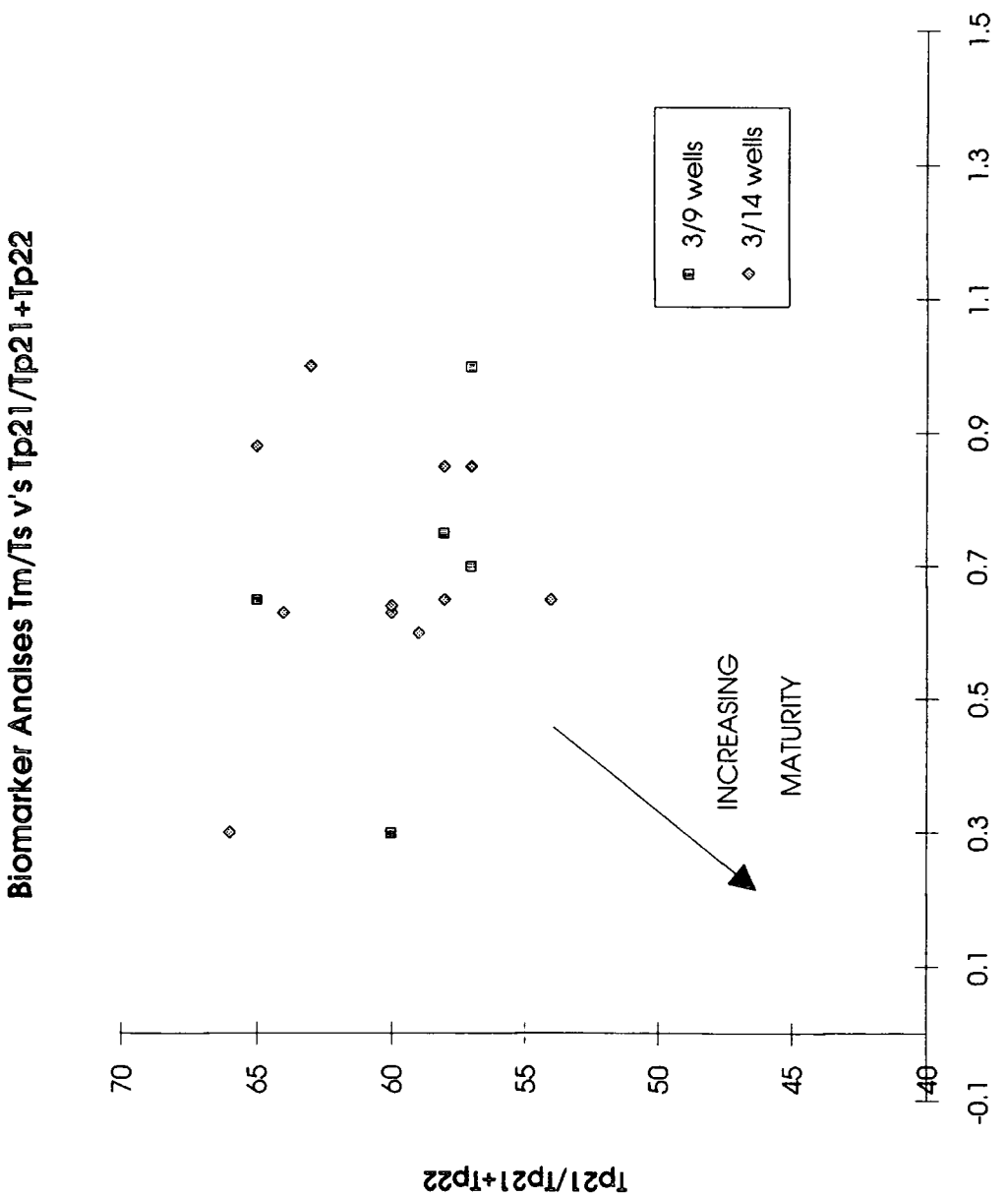

Fig.3.5.4.2g - Biomarker ratios Tm/Ts versus Tp21/Tp21+Tp22 (see text for discussion). Data from Pittion (1987)

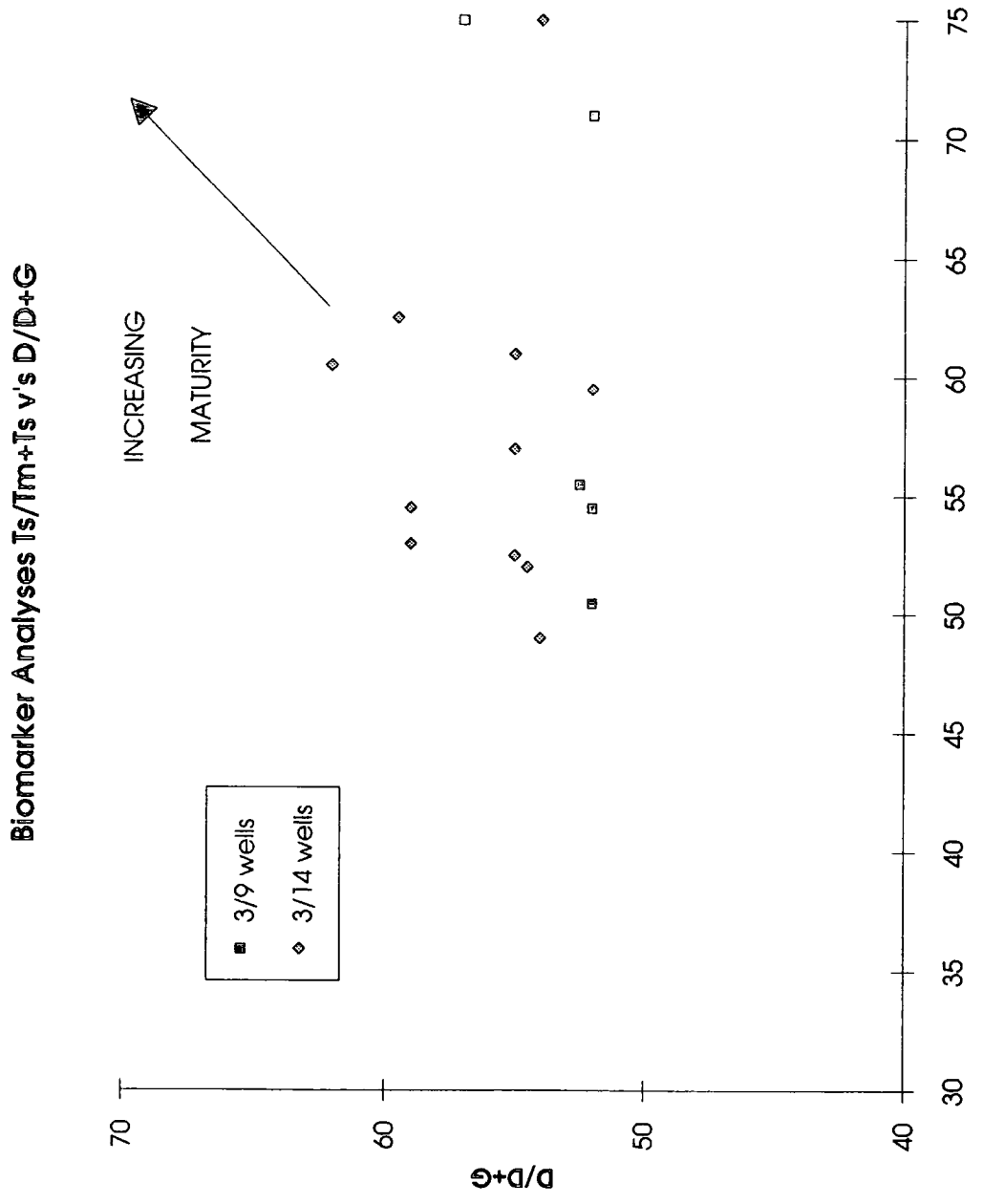

Fig.3.5.4.2h - Biomarker ratios of Ts/Tm+Ts versus D/D+G (see text for definitions). Data from Pittion (1987)

maturity. These degradation trends can then be used as maturity parameters and hence indicate filling direction (in the opposite sense to increasing maturity, Horstad et al 1989). Figs.3.5.4.3a, b, c and d show the areal distribution of these parameters. The parameters used for this interpretation were

Tm (Fig.3.5.4.3a)	D (Fig.3.5.4.3b)	Ts (Fig.3.5.4.3c)
Ts	D+G	Tm+Ts

and also the thermovaporisation parameter Ip ratio (Fig.3.5.4.3d)

where

Sterane series:

D = 24 ethyl-5 α(H), 14 α(H), 17 α(H) Cholestane C29H52 with (20S) config.

G = 24 ethyl-5 α(H), 14 α(H), 17 α(H) Cholestane C29H52 with (20R) config

Hopanes in Triterpane series:

Tm = Trisnorphane C27H46 with R configuration

Ts = Trisnorphane C27H46 with S configuration

The maturity characterisation illustrated on Figs.3.5.4.3a, b and c shows that lateral heterogeneities can be observed from data plotted areally throughout the Alwyn North structure. An increase in maturity is seen progressively toward wells located in the south east of the structure implying a filling direction in the opposite sense, that is, from the south east approximately from the 3/9a-3 well through wells 3/9a-6, 3/9a-2,3/9 a-4 and north west to 3/9a-1. This is possibly due to more severe biodegradation of the oils near the point of entry in a field (Horstad et al 1989). The source area for the 3/9 structure can be inferred as being south east of the immediate area. The Brent and Statfjord reservoirs of the 3/9 structure are faulted but continuous aquifers (although local habit and intra-structure permeability and hydraulic connectivity is largely controlled by faults) and extends from the area down dip of the Alwyn South East (3/15) field (Brooks and Glennie, 1987). From the maturity data and the observed trends, hydrocarbons may have migrated from south east of the Alwyn structures and that, if the sands of the Brent group and Statfjord Formation acted as carrier beds, a hydrocarbon migration pathway could be envisaged to account for the maturity patterns seen in Figs.3.5.4.3a, b, c and d .

Very limited biomarker analyses were carried out on the oils of the Alwyn South East wells but analyses on the extracts of the 3/15 fault block (Fig.3.5.4.2c) show that they are more mature than extract samples from the North field. However, analyses carried out on the Ip ratio of the oils in two wells in the South East field - 3/15-2 and 3/15-4 (Fig.3.5.4.3d) indicate a trend of increasing maturity toward the south and east off-structure. It is observed that oils in these wells follow a maturation increase toward

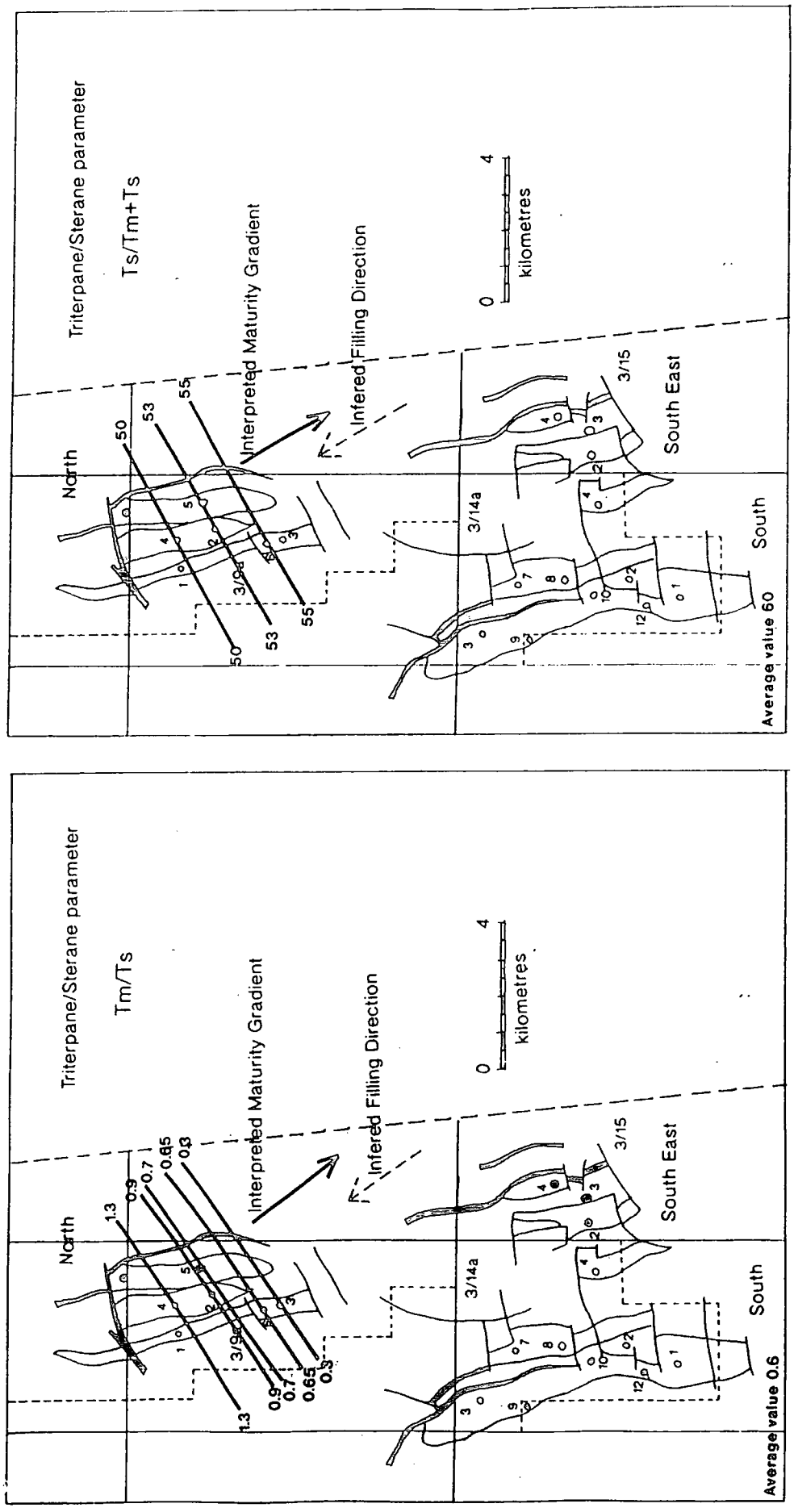

Figs.3.5.4.3a (left) and b (right) - Maturity trends based on selected maturity indicators.

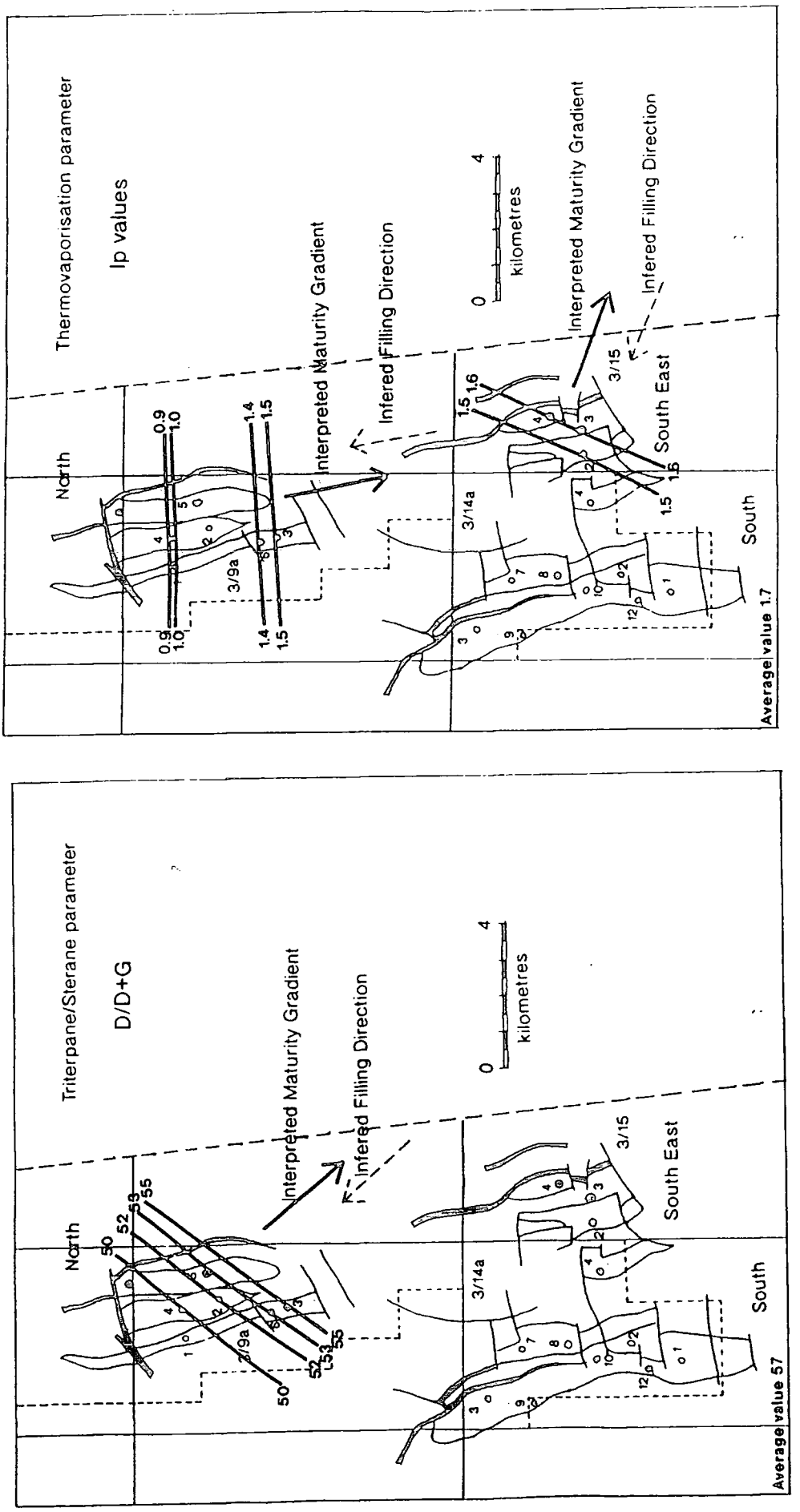

Figs.3.5.4.3c (left) and d (right) - Maturity trends based on selected maturity indicators

the south east with an inferred filling direction toward the south east off-structure (Fig.3.5.4.3). Therefore, the filling point for reservoired oils in the North (3/9) and South East (3/15) fields is most likely to be the most south easterly down dip part of the Alwyn field heading structurally down dip toward the Viking Graben axis (Fig.3.2d).

The source rocks on the vicinity of Alwyn South (3/14) field has already been inferred as locally sourcing the reservoired oils in the Alwyn South accumulation. This biomarker dataset, shows a set of values which average a higher maturity value in all of the observed parameters than either data point averages from the North or South East fields. No emergent pattern or trend of the biomarker values is evident in Alwyn South (Figs.3.5.4.3a, b and c). This may be the result of the local sourcing of hydrocarbons from within the fault block; without the single source point the type of trend seen in Alwyn North and South East would be absent.

3.5.5 Basin Modelling

Recreating and modelling the maturation potential of the three fields in the Alwyn area was made possible by burial history and maturation modelling. This modelling would then allow an independent reconstruction of the potential maturation and the onset and timing of any hydrocarbon generation within the fields to be correlated with the geochemical data and interpretations.

A summary of the basin modelling data sources and assumptions have been documented in section 2.2.

The reconstructed burial histories and predicted maturation modelling for each of the fault blocks of Alwyn North, South and South East are represented by typical example wells from each field (Figs. 3.5.5a, c and e). These reconstructions assume constant temperature through time using the present day geothermal gradient of 34°C/km(from corrected bottom hole temperatures)and a surface temperature of 5°C. The burial rate and history in the three representative wells follow approximately similar pathways but a much more rapid burial rate at the mid Cretaceous (approximately 90-80Ma) is observed in well 3/14a-8 (Fig. 3.5.5c) in comparison to wells 3/9a-2 and 3/15/4. Stratigraphic and lithological information was well constrained using well log information with the exception of the top hole section (Quaternary, Pliocene, Miocene and Oligocene). This section was constrained by utilising electric log characteristics for wells across the Alwyn area (section 3.7.11).

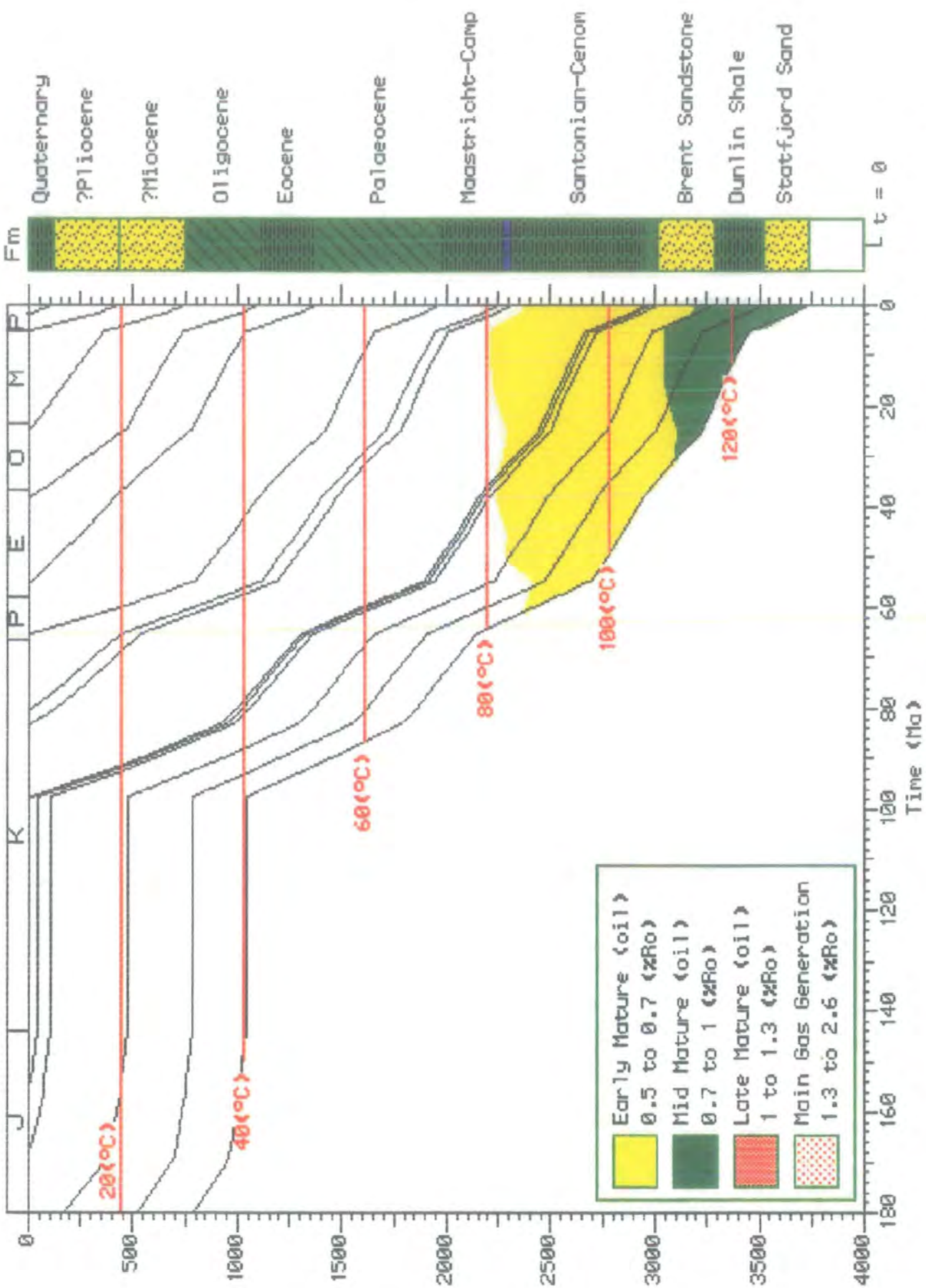

Fig.3.5.5a - Burial history plot, with superimposed maturation windows, for Alwyn North well 3/9a-2, assuming constant temperature through time

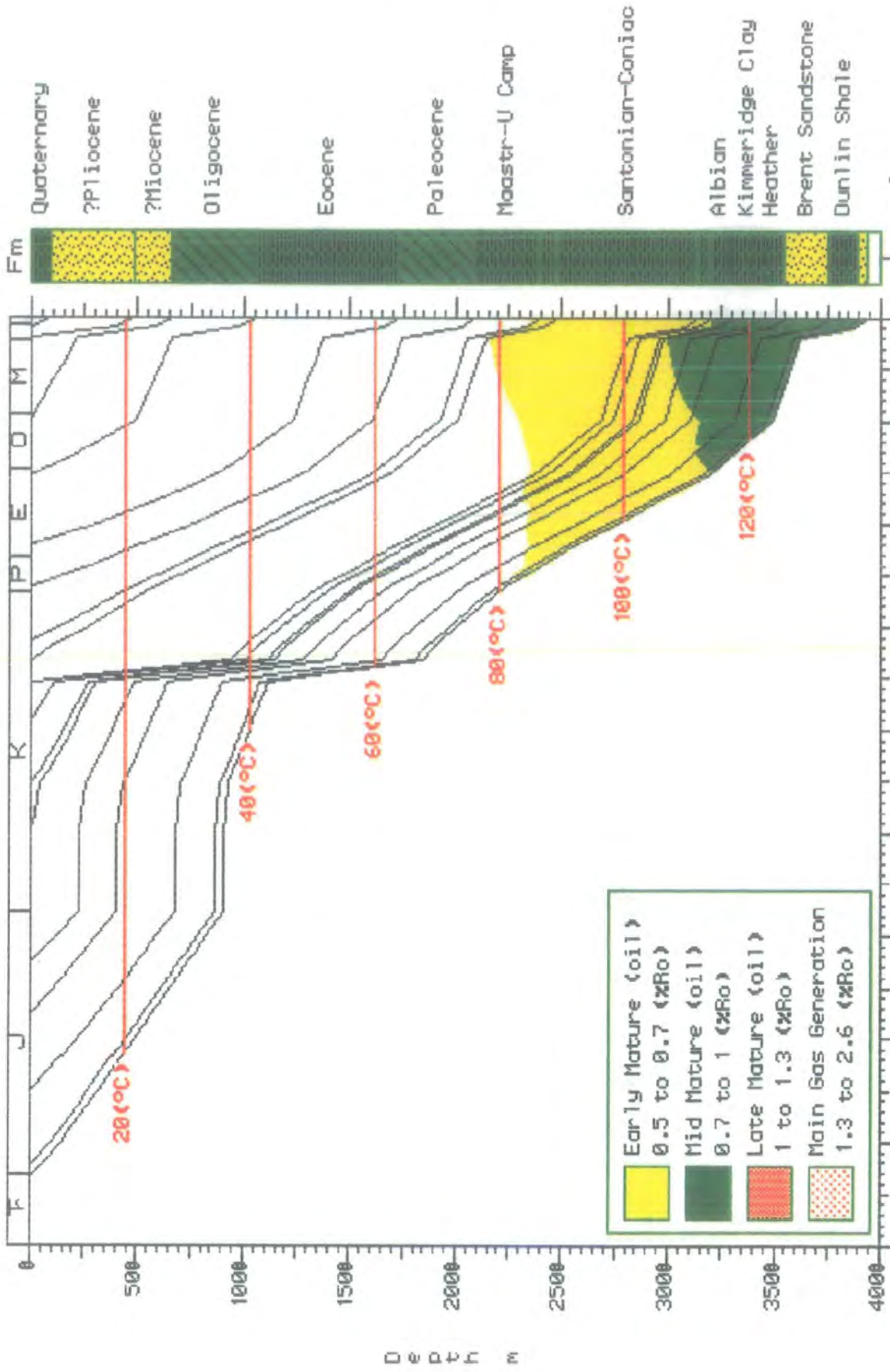

Fig.3.5.5c - Burial history plot, with superimposed maturation windows, for Alwyn South well 3/14a- 8, assuming constant temperature through time

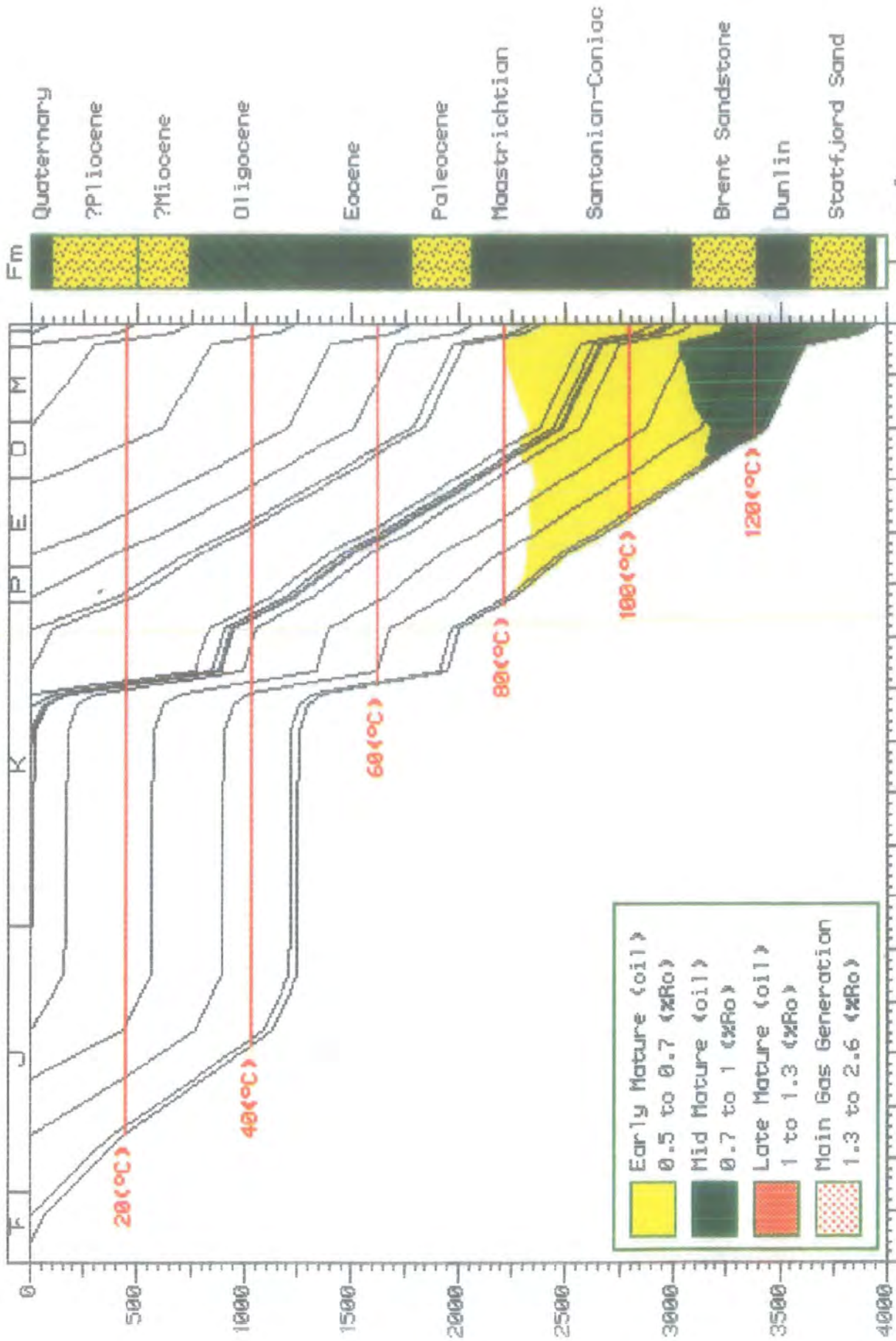

Fig.3.5.5e - Burial history plot, with superimposed maturation windows, for Alwyn South East well 3/15-4, assuming constant temperature through time

*Maturation in the Alwyn Field area was modelled with respect to sensitivity in fluctuating palaeo-surface temperature. Heat flow was assumed to be constant through time. This assumption was based mainly on the lack of data to constrain a heat flow history. Local heat flow effects such as those caused by igneous intrusions can have a considerable effect on the thermal history and therefore timing of maturation of the source rock. Transient heat flow is also recognised as having a potential effect on the maturation history of the source rock. In the study of the Alwyn Field, there was not a sufficient data set available to accurately assess sensitivity of introducing pulsed or transient heat flow through the evolution of the basin.

Maturation modelling is largely dependant upon temperature information (section 2.2). When constant temperature gradient and heat flow is assumed through the burial history, only the 3/14a-8 (Alwyn South, Fig.3.5.5.c) well models the entry of the organic rich Kimmeridge Shale Formation into the early mature field (0.5-0.7%Ro) at approximately 47Ma and then, through progressive heating due to increased burial, into the mid mature oil window at approximately 15Ma assuming a maturity equivalent to 0.7-1.2%Ro (Tissot et al 1982). The wells of the Alwyn North (3/9a-2 - Fig.3.5.5a) and Alwyn South East (3/15-4 - Fig.3.5.5e) show only an early mature character for the Kimmeridge Shale Formation throughout the burial profile. In Alwyn North the Kimmeridge Formation enters the early mature field (0.5-0.7%Ro equivalent) at approximately 43Ma (Fig.3.5.5a) and at approximately 33Ma (Fig3.5.5e) in Alwyn South East. Previous interpretations made on the maturity indicator data and trends using Ro, Tmax and biomarkers (sections 3.5.3.3 and 3.5.4.3) inferred that only the organic source rock (Kimmeridge Shale Formation) in the Alwyn South field is capable of maturing and locally generating hydrocarbons. The models generated by BasinMod ™ (Figs.3.5.5a, c and e) also observe these present day maturation references.*

Although these maturity modelling and observations agree with geochemical rock data in that only the organic rich Kimmeridge Formation in the Alwyn South fault blocks may possess the ability to locally mature and expel oils, any constraint on temperature would likely enhance greater accuracy on the maturation modelling. From work conducted by Buchardt (1978) using the temperature-induced δO^{18} recorded in carbonate shells, surface temperature variations were imported into the basin model at 5My intervals back to 60Ma. Further constraints on the surface temperature were defined using interpretations made by Anderton et al. (1980) based on palaeo flora and fauna information. These data were imported into the model from 60 to 200Ma at 20My intervals. Both sets of approximate palaeo-surface temperature data are summarised as:

Table t3.5.5a, data from Buchardt (1978)

Time	Surface Temperature(°C)
5	8
10	8
15	13
20	10
25	9
30	6
35	8
40	21

Table t3.5.5b, data from Anderton (1980)

Time	Surface Temperature(°C)
80	20
100	20
120	20
140	22
160	22
180	22
200	22

45	25
50	25
55	22
60	14

The resultant maturity windows calculated for the burial history profiles for the same three wells are depicted in Figs.3.5.5b, d and f (3/9a-2, 3/14a-8 and 3/15-4 respectively). The effect of this surface temperature fluctuation through time is, observed in 3/14a-8 (Fig.3.5.5c), to allow the entry of the Kimmeridge Shale Formation into the mid mature window at a much earlier time (approximately 35Ma for the base of the formation compared to approximately 15Ma assuming constant surface temperature through time). The effect on calculating the maturity windows using Buchardt's (1978) and Anderton et al (1980) data is to allow the onset of maturation earlier in the burial history. The Alwyn North well 3/9a-2 models maturation of the Kimmeridge Formation at approximately 54Ma (Fig.3.5.5b) for the early mature oil as opposed to 43Ma when constant temperature is assumed (Fig.3.5.5a). Similarly, the Kimmeridge Formation of the 3/15-4 well is now modelled to commence oil generation in the early mature window at approximately 44Ma as opposed to 33Ma assuming constant temperature. The overall effect of using the fluctuating surface temperature seems to cause an earlier onset of maturation in all wells studied from the three Alwyn fields.

Since rock data, particularly Vitrinite Reflectance (Ro) data, was available and correlatable with depth in these wells (section 3.5.3.1), the Ro data was imported into the basin modelling programme and plotted against the modelled maturity profile. In each case Figs. 3.5.5a', b', 3.5.5c', d' and 3.5.5e' and f', the maturity profile modelled against depth shows that maturation history plotted assuming constant heat flow through time provides a better fit with the rock data (Ro) in the depth profile than the fit using the fluctuating temperature data. This would infer that although the surface temperature fluctuations interpreted by Buchardt (1978) may be correct, the effect on modelled maturity is erroneous. This would suggest that a further constraint or assumption must be detailed in the basin model to allow the predicted maturity and the maturity calculated using Buchardt (1978) and Anderton et al. (1980) to correlate. For this study, however, the modelled maturity gives a very reasonable fit to the geochemical rock data assuming constant temperature through the burial history.

This preference is carried over into the interpretation of palaeo-pressure from fluid inclusion microthermometry when describing the palaeo-conditions of fluid entrapment at reservoir level (section 3.7.8.3)

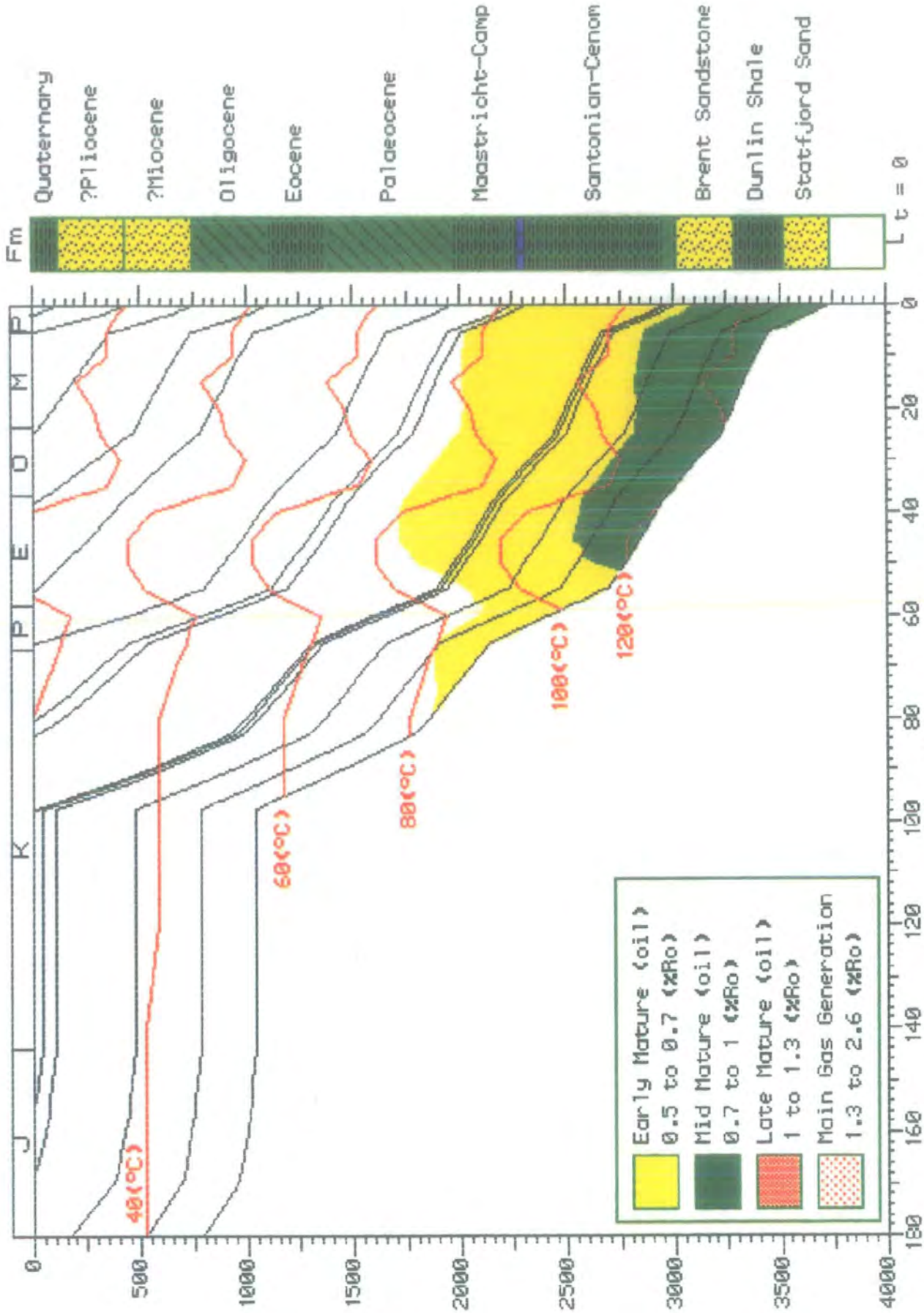

Fig.3.5.5b - Burial history plot of 3/9a-2, assuming palaeo surface temperature fluctuations using data from Buchardt (1978) and Anderton et al. (1980)

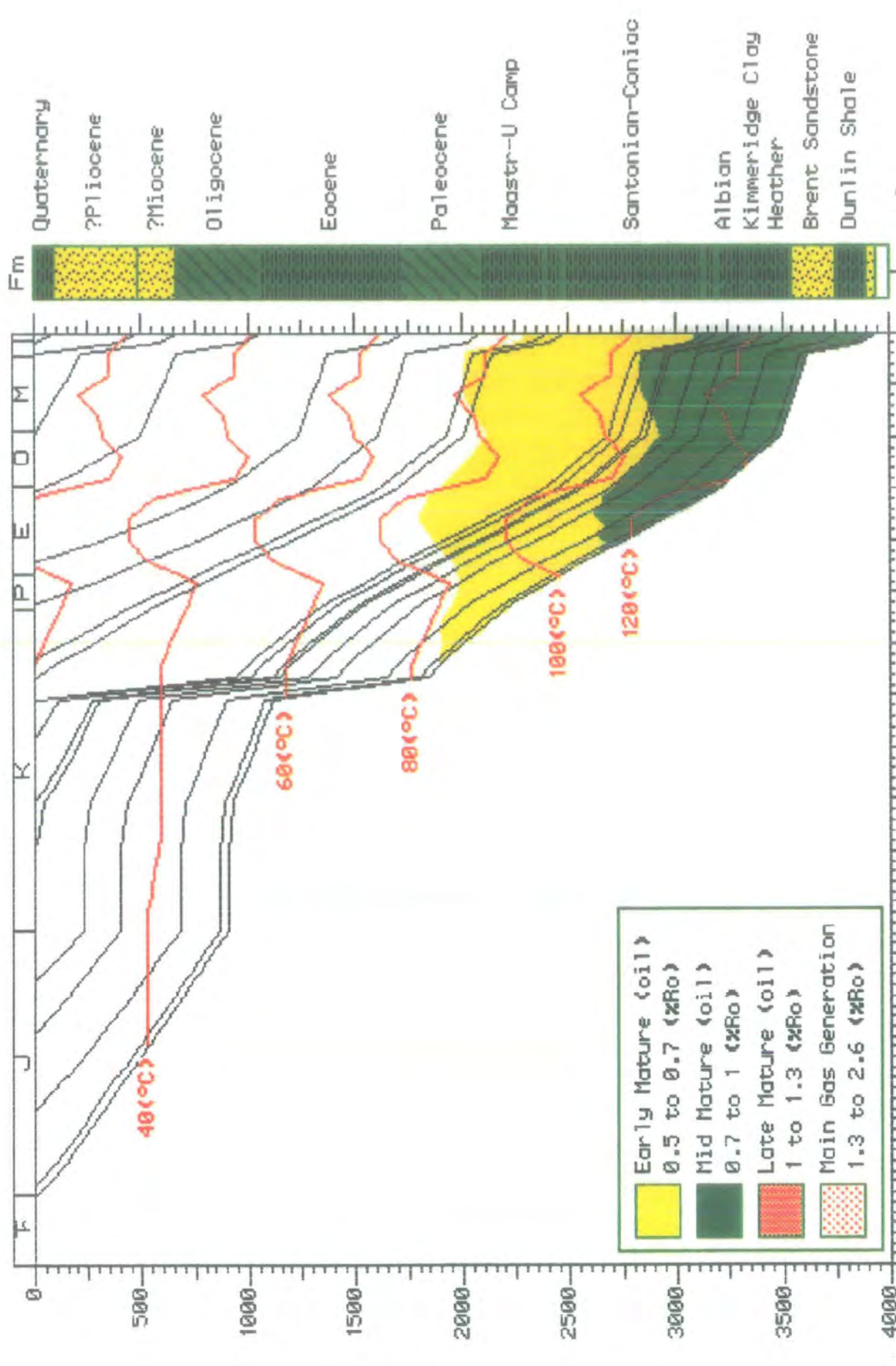

Fig.3.5.5d - Burial history plot of 3/14a-8, assuming palaeo surface temperature fluctuations using data from Buchardt (1978) and Anderton et al. (1980)

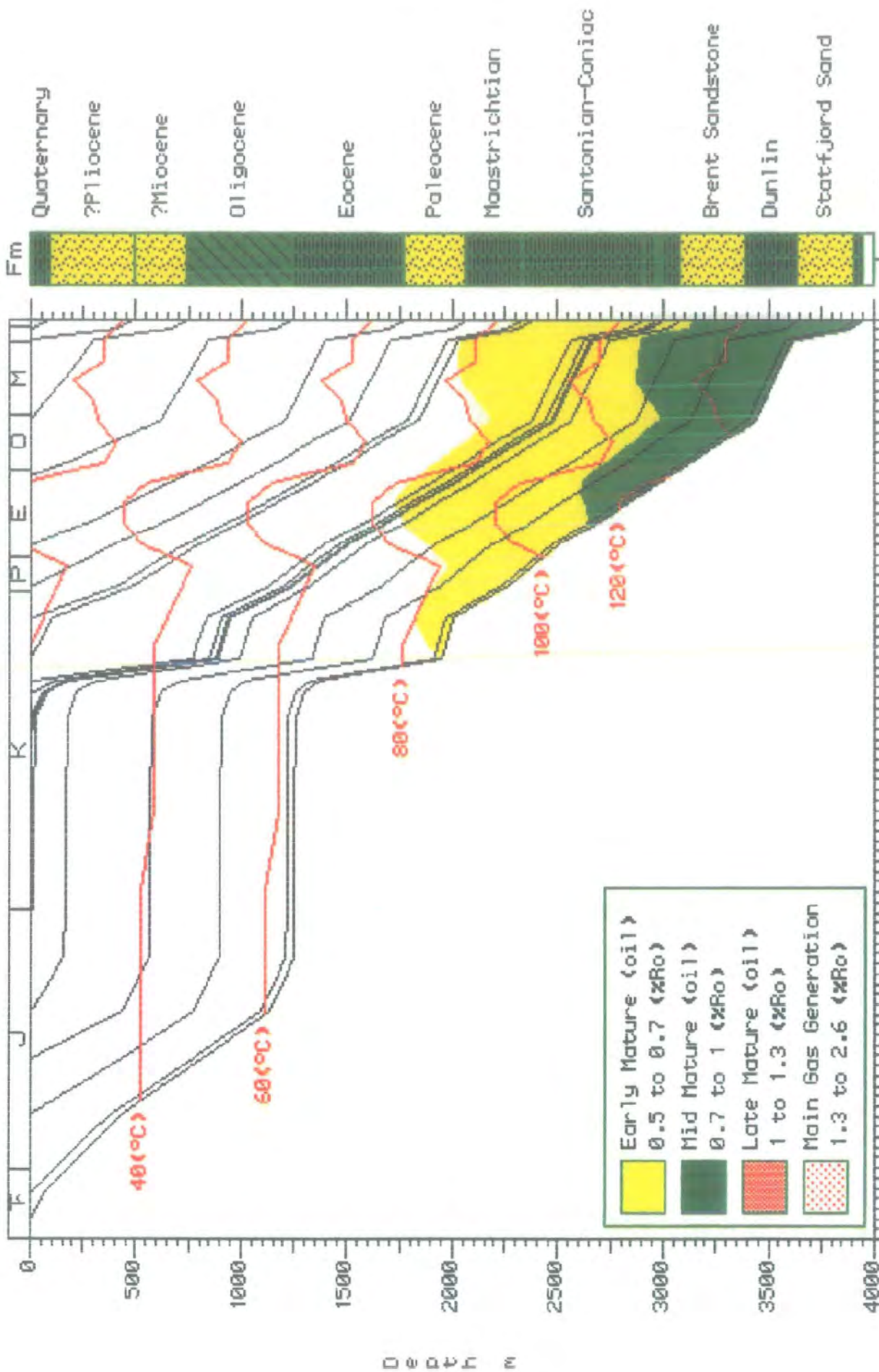

Fig.3.5.5f - Burial history plot of 3/15-4, assuming palaeo surface temperature fluctuations using data from Buchardt (1978) and Anderton et al. (1980)

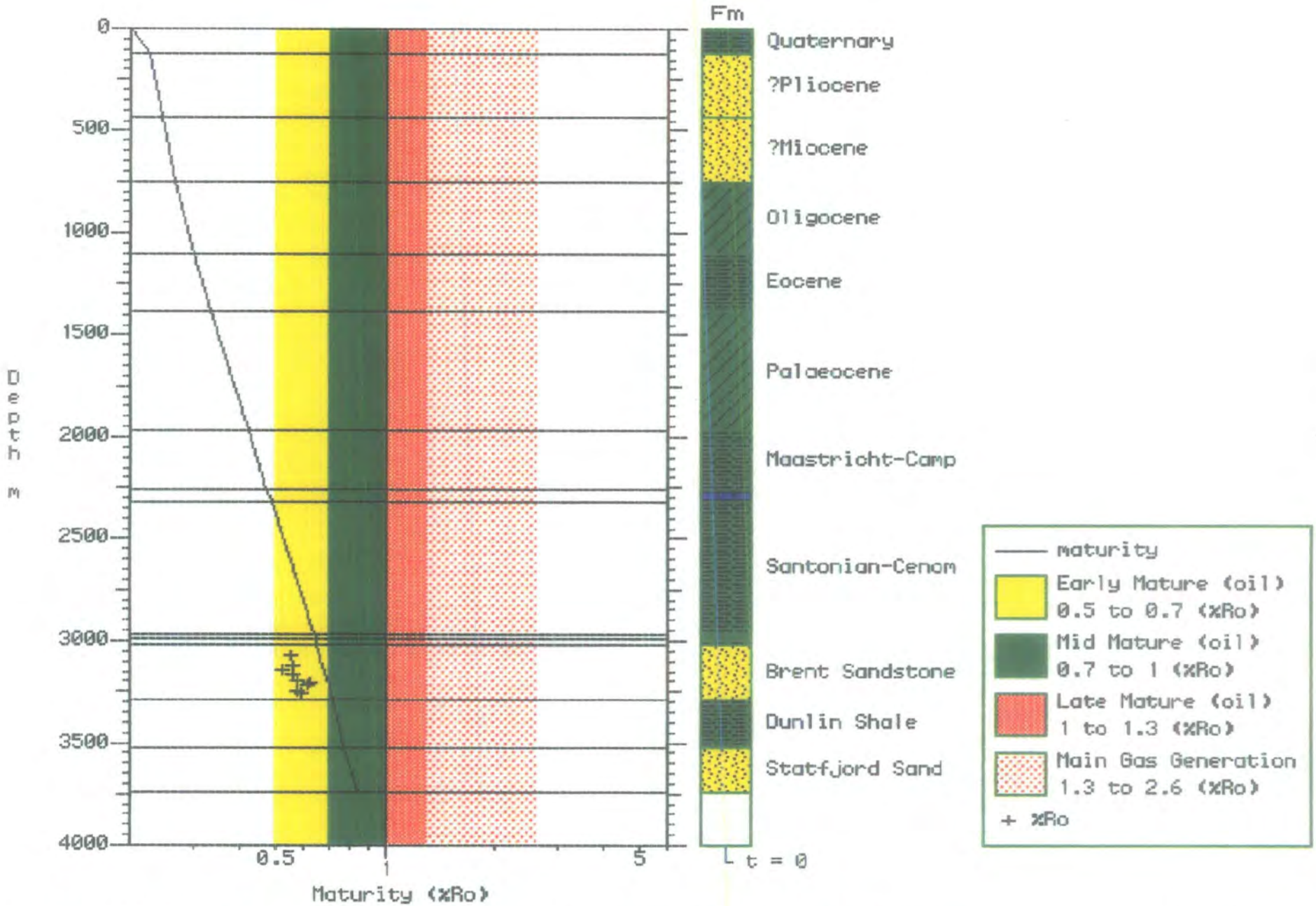

Fig.3.5.5a' - Modelled maturity versus depth with superimposed Vitrinite Reflectance (%Ro) data for 3/9a-2. Constructed from Fig.3.5.5a assuming constant temperature through time

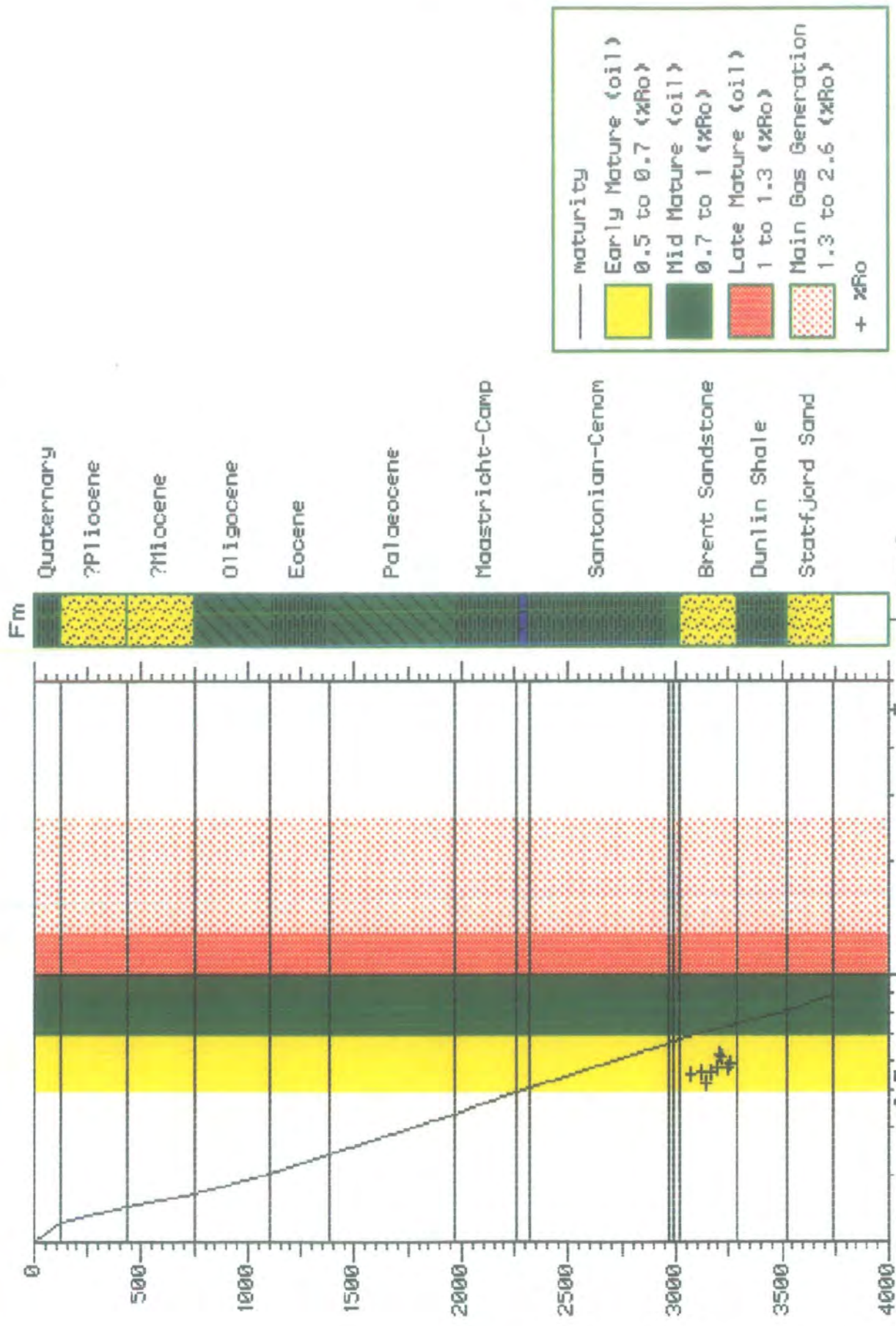

Fig.3.5.5b' - Modelled maturity versus depth with superimposed Vitrinite Reflectance (%Ro) data for 3/9a-2. Constructed from Fig.3.5.5b assuming fluctuating surface temperature through time

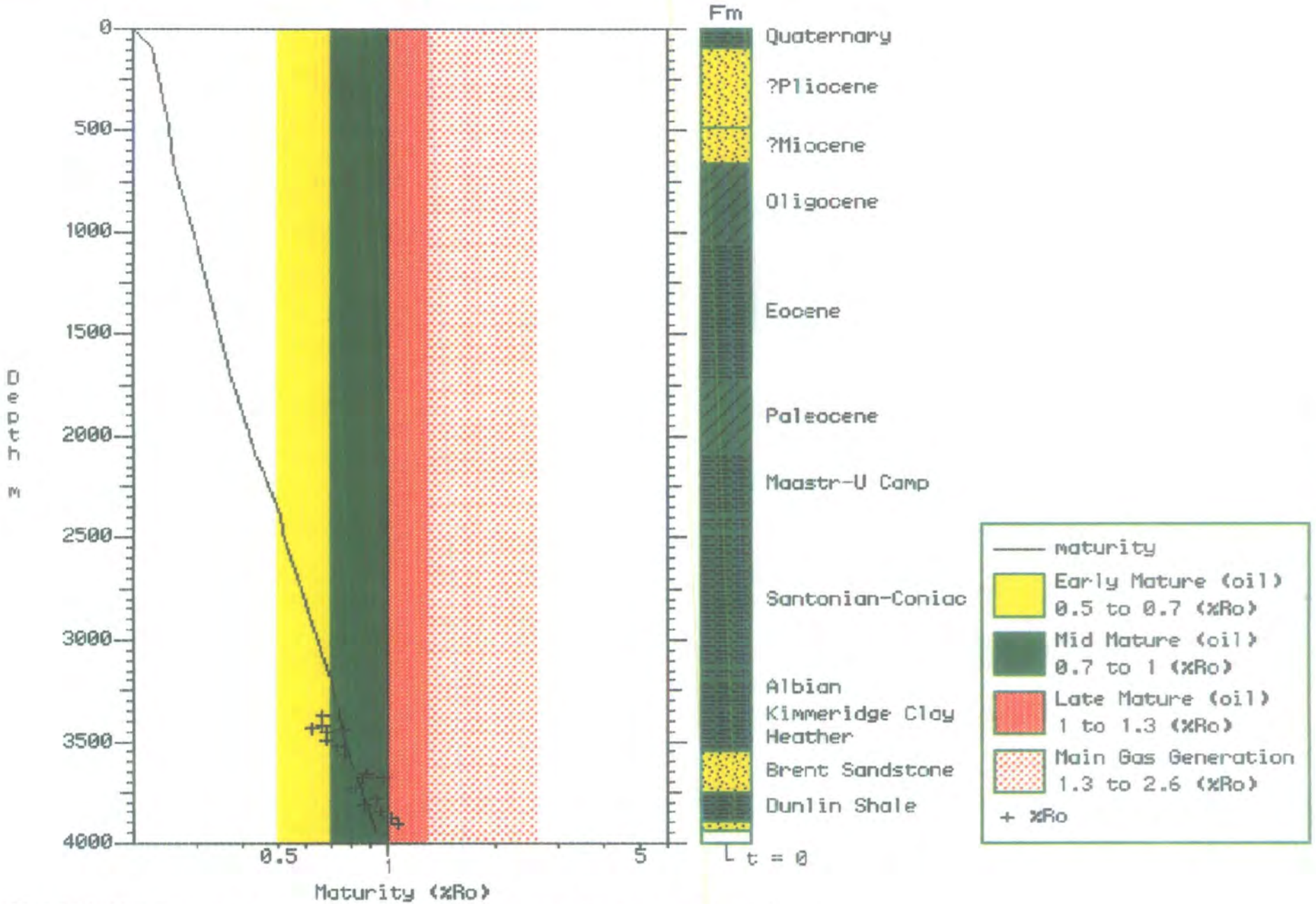

Fig.3.5.5c' - Modelled maturity versus depth with superimposed Vitrinite Reflectance (%Ro) data for 3/14a-8. Constructed from Fig.3.5.5c assuming constant temperature through time

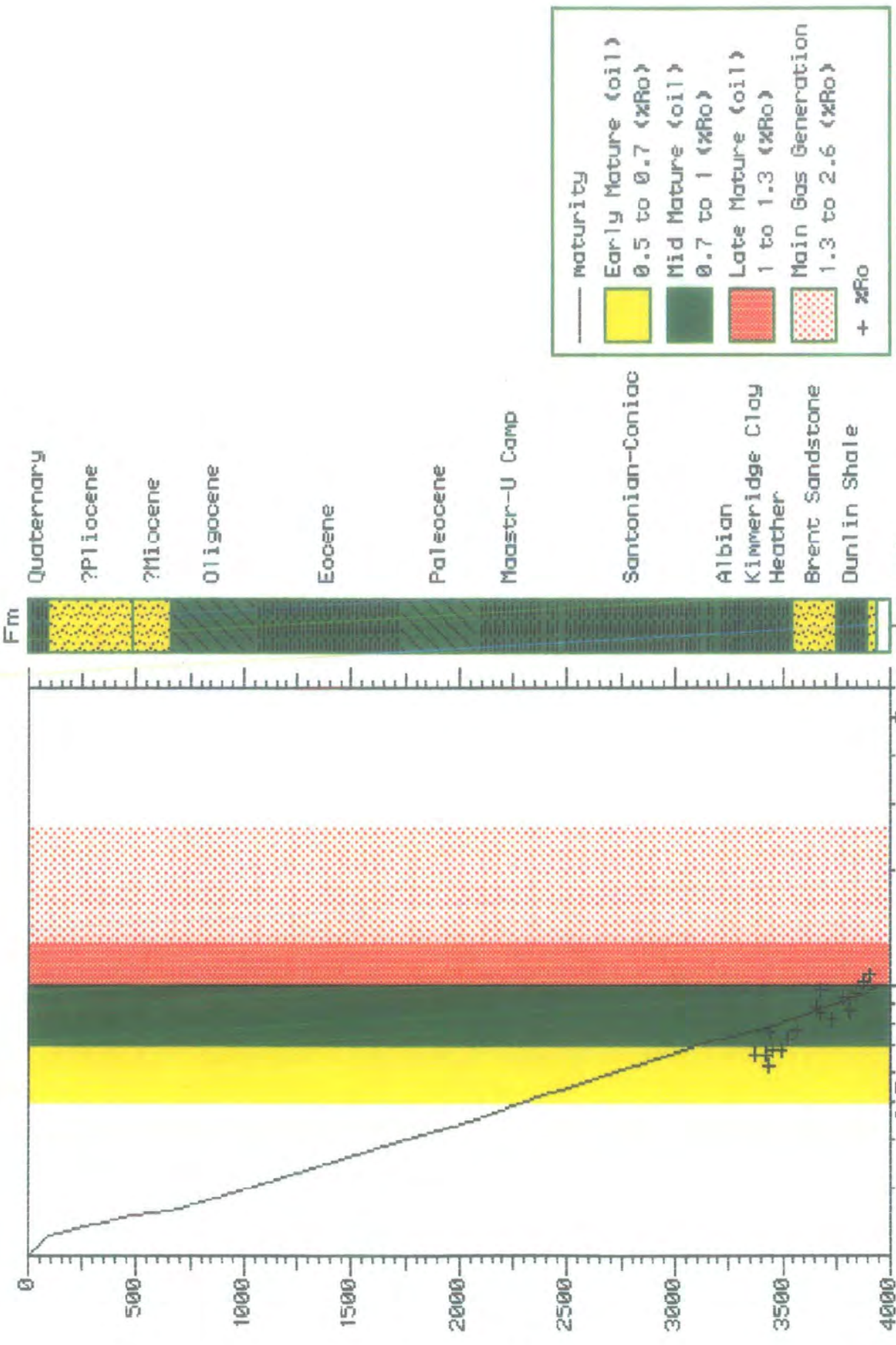

Fig.3.5.5d' - Modelled maturity versus depth with superimposed Vitrinite Reflectance (%Ro) data for 3/14a-8. Constructed from Fig.3.5.5d assuming fluctuating surface temperature through time

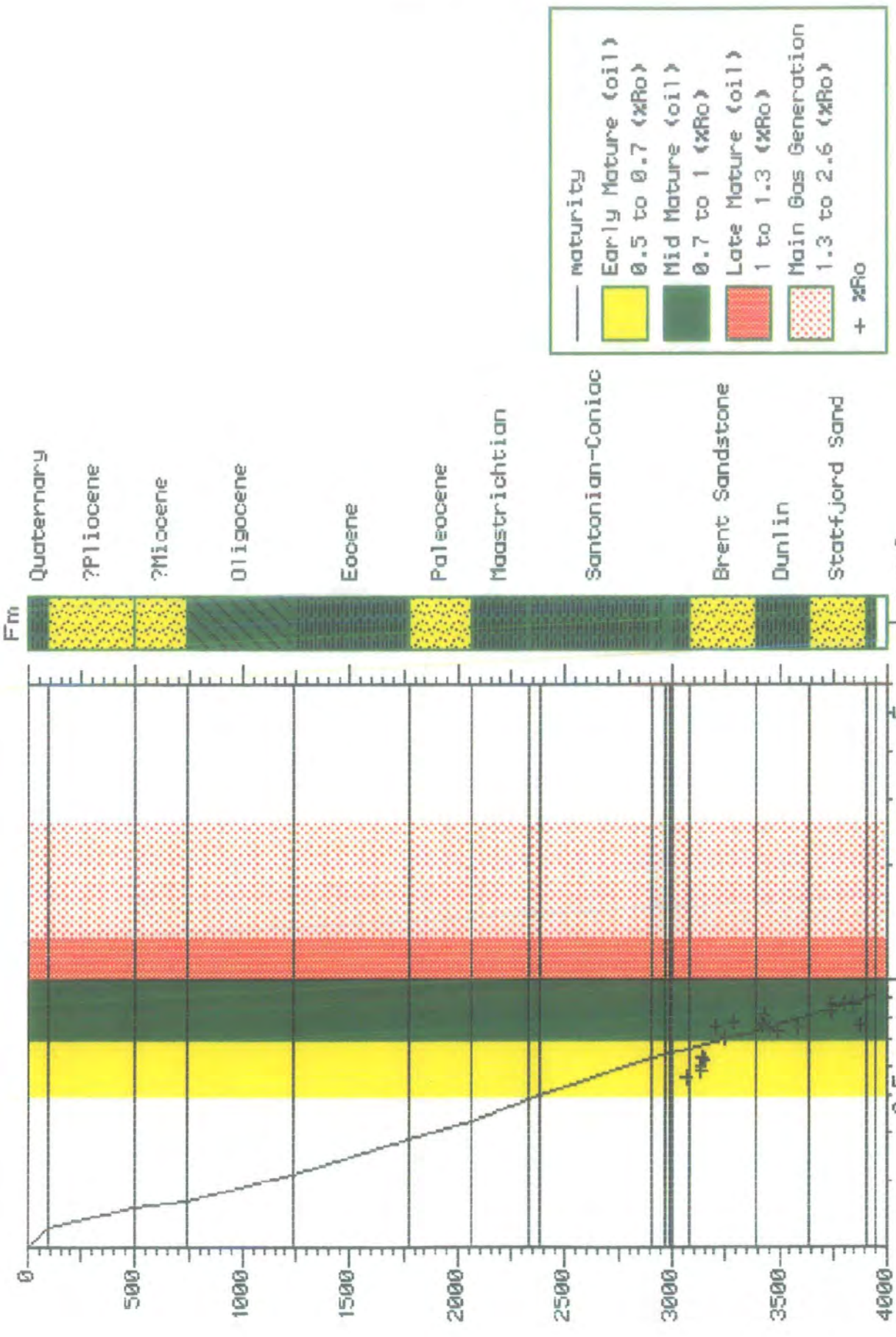

Fig.3.5.5e' - Modelled maturity versus depth with superimposed Vitrinite Reflectance (%Ro) data for 3/15-4. Constructed from Fig.3.5.5e assuming constant temperature through time

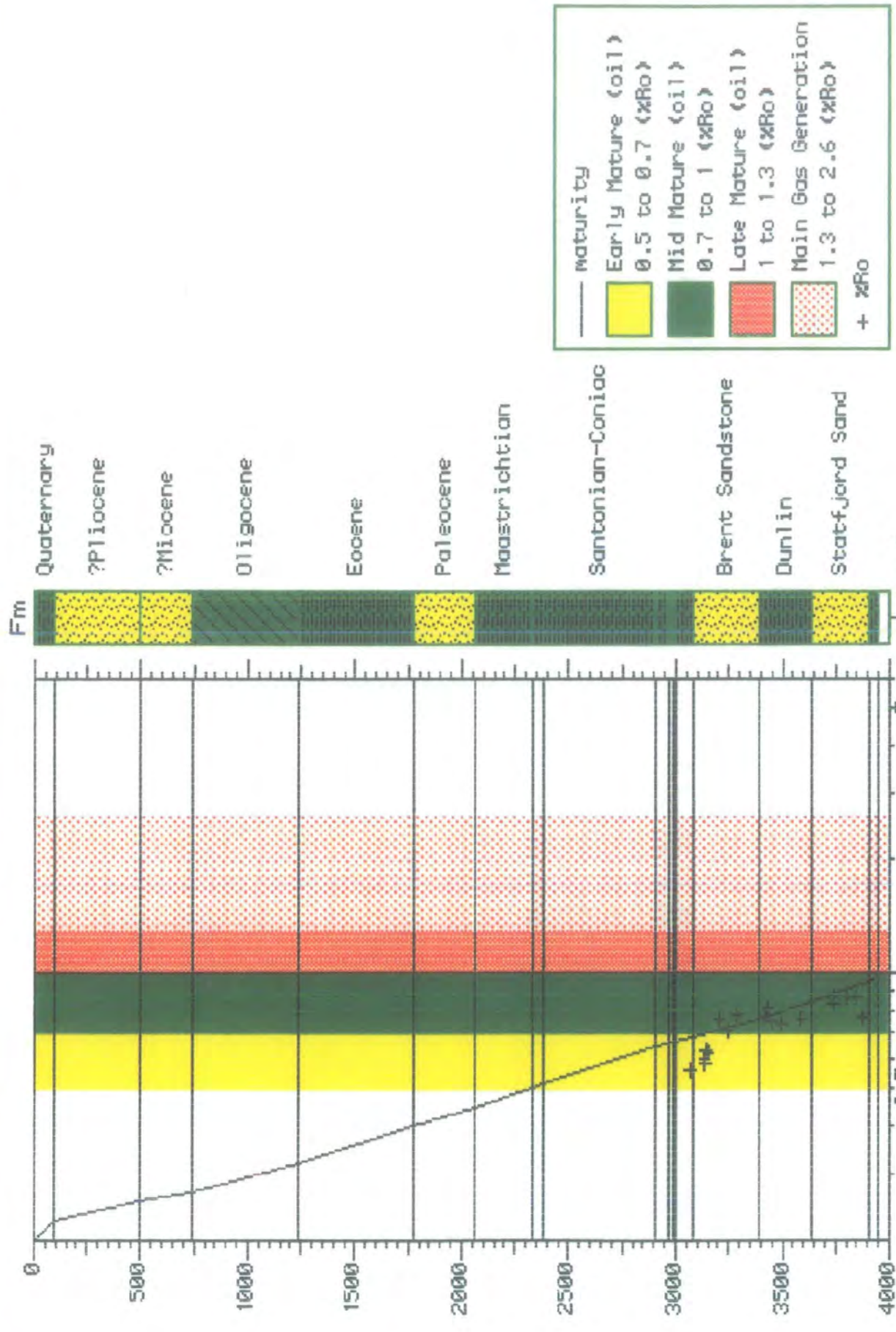

Fig.3.5.5f - Modelled maturity versus depth with superimposed Vitrinite Reflectance (%Ro) data for 3/15-4. Constructed from Fig.3.5.5f assuming fluctuating surface temperature through time

3.5.6 Offstructure Modelling - Seismic Modelling

The geochemical modelling strongly suggests that reservoired oils in the 3/9 and 3/15 structures have been filled from outside the immediate Alwyn area. The fill point is located south and east of the 3/15 structure (section 3.5.4.3) in the hotter and deeper Viking Graben.

To assess the timing of the maturation stages of a Kimmeridge Clay source rock in the Viking Graben to the east, a stratigraphic model was constructed from seismic data and geochemical data imported from the Alwyn area.

3.5.6.1 Seismic Modelling

A comprehensive grid of data is available across blocks 3/9, 3/14 and 3/15 including Survey 774, which was shot SW-NE (lines 01-111) and SE-NW (lines 02-14). The survey was carried out by CCG in August 1977 for the operators - Total Oil Marine. All sections are migrated and filtered. In addition, a non-proprietary survey of regional seismic lines is available in this part of the North Sea including the Nopec 1984 survey line NNST 05 which runs E-W through the Alwyn field across the Viking Graben area into the Norwegian sector. Fig.3.5.6.1a shows a summary map of the specific Alwyn survey (774), orientation of the lines of interest and the location of line NNST84-05. Significant lines which tie wells drilled on the structure are:

Line No.	Well Tie
774 - 19	3/9a-1
774 - 21	3/9a-4
774 - 29	3/9a-2, 3/9a-5
774 - 43	3/9a-3

Stratigraphic and depth correlation is therefore possible over the area by mapping the reflectors across the blocks of interest tied to significant stratigraphic horizons in the wells. Depth conversion was achieved by taking identifying key horizons in wells which were drilled close to available seismic and transferring these horizons onto the seismic sections at the appropriate time horizons thus constraining the individual horizons in time as well as depth. These horizons were then extrapolated from the field area to the Viking Graben depocentre. Since time values for individual horizons were tied to depth values in field area a mathematical polynomial function could be used to depth convert for extrapolated stratigraphy off structure into the depocentre Fig.3.5.6.1b).

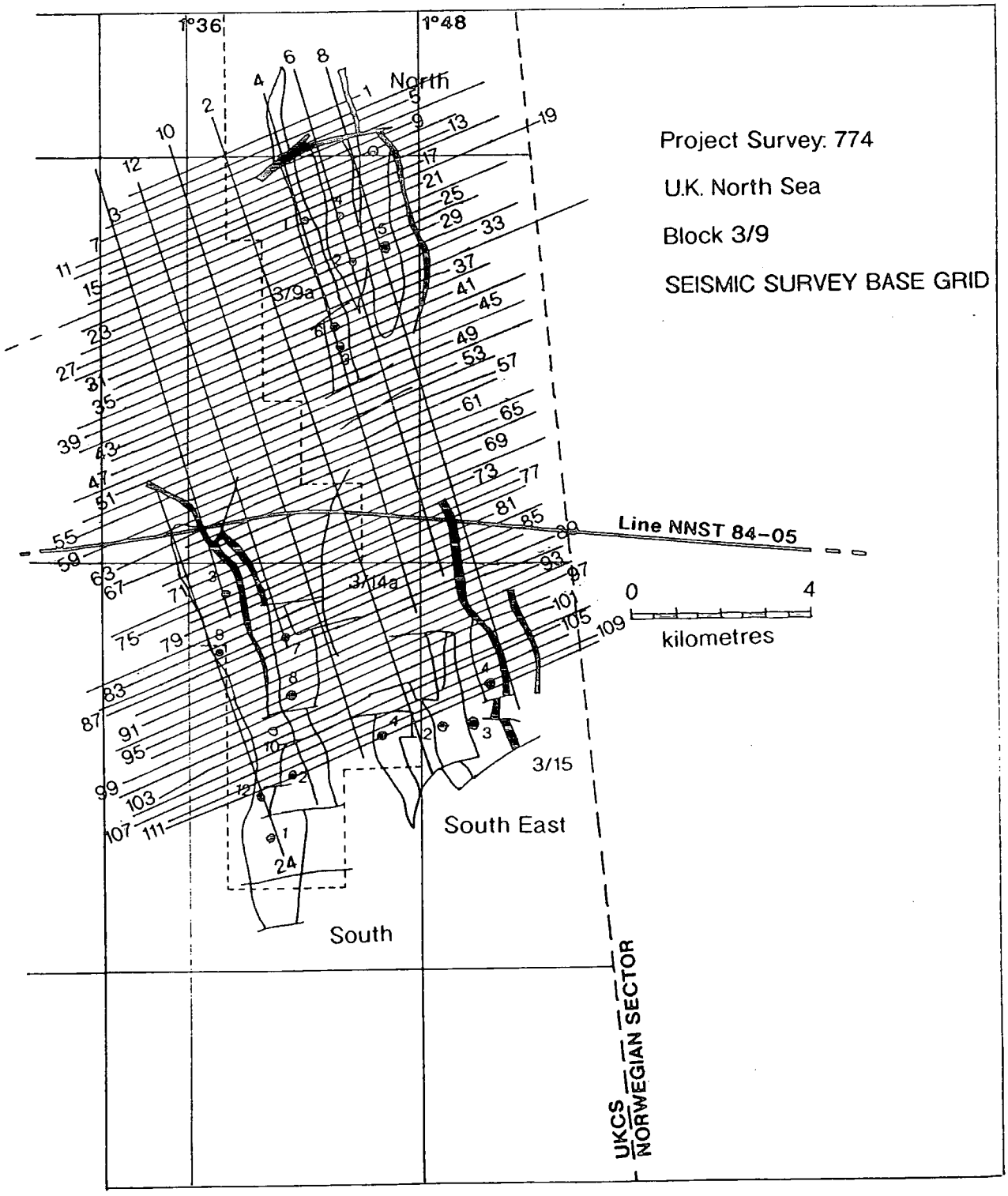

Fig.3.5.6.1a - Summary base grid of seismic line locations

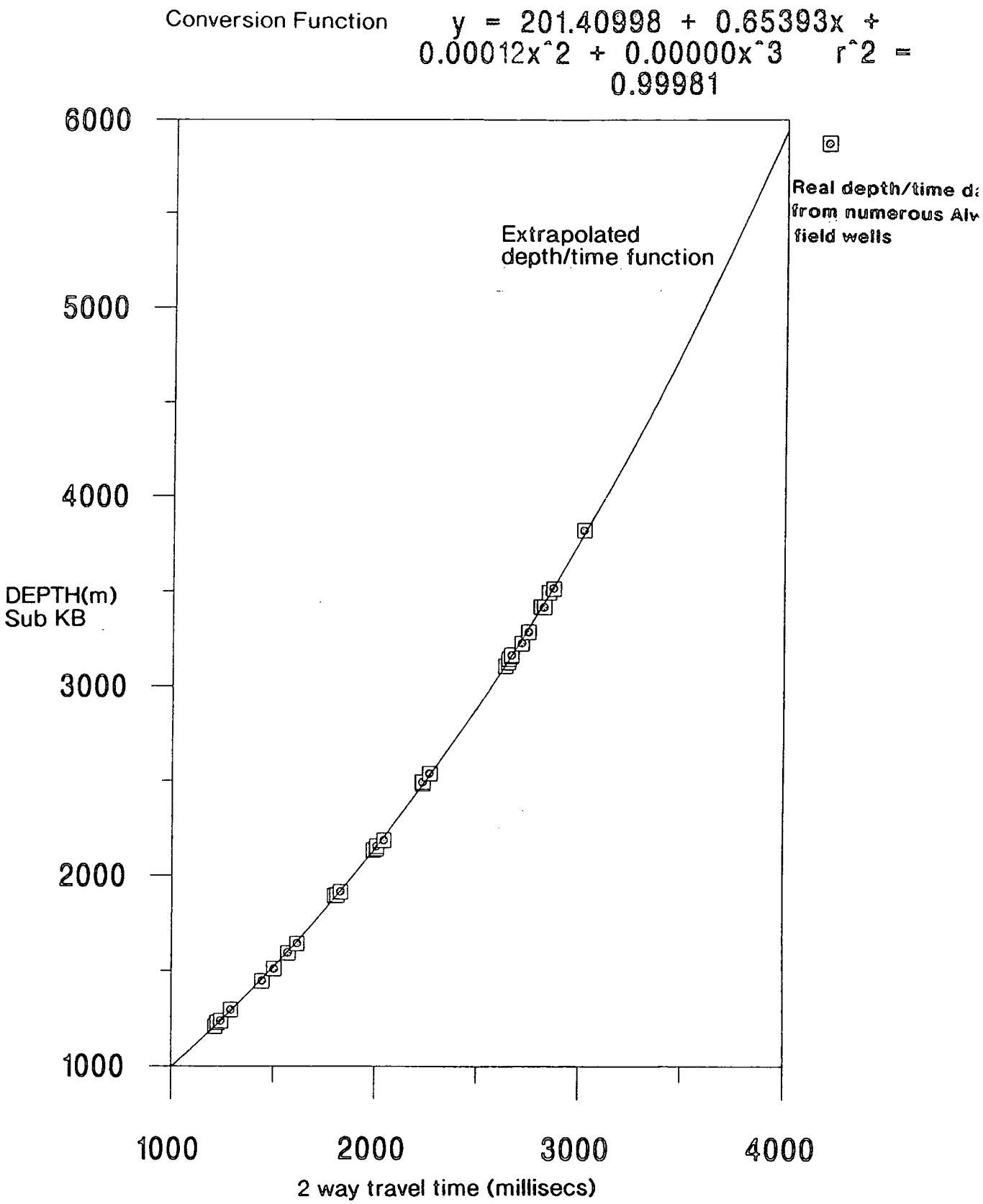

Fig.3.5.6.1b - Depth versus two way travel time. Polynomial function plotted through actual data and extrapolated to provide depth conversion function

The depth conversion function was achieved by importing controlled time/depth data from wells - 3/9a-1, 3/9a-3, 3/9a-4 and 3/9a-5, for the following horizons - Eocene, Palaeocene, Danian, Lower Cretaceous, Santonian, Upper Cretaceous, Kimmeridge, Brent, Heather and Middle Jurassic. These wells were tied on lines 774 - 19, 29, 43, 21 and 29 respectively.

Fig.3.5.6.1b shows the plot for this tied data with the calculated polynomial function for the curve fit which links all the data points. The function was computed using CricketGraph™ software. The function allowed extrapolation past the last data point so that any further time value (interpreted and picked from the regional seismic line) could be assigned a depth value.

Line NNST - 05 (Fig.3.5.6.1a) was used due to its proximity, running E-W, to wells 3/9a-3 and 3/14a-3 and its projection off into basinal areas to the east (Viking Graben) and west (East Shetland Basin). Shot Point (S.P.) 3400 was chosen as representative of the axial part of the basin west of the Alwyn area and S.P. 4650 representative of the deepest part of the Viking Graben (east of the Alwyn area). Two way travel times were measured from the section for these two S.P.'s. The 2 way travel times and calculated depths for these two separate depocentres are given in tables t3.5.6.2a and t3.5.6.2b:

Table t3.5.6.2a. S.P. 3400 (west of Alwyn):

Horizon	2 way t.t.	Depth(m) (calc. from function *)
Oligocene	600	610
Eocene	1200	1210
Palaeocene	1530	1580
Danian	1900	1995
Upp.Cretaceous	2050	2270
Santonian	2240	2490
Lr. Cretaceous	2850	3380
Kimmeridge	3280	4270
Heather	-	-
Middle Jurassic	3620	5010

* Function for depth conversion (Fig...):

$$y = 201.40998 + 0.65393x + 0.00012x^2 + r^2 = 0.99981$$

Table t3.5.6.2b. S.P. 4650 (east of Alwyn, Viking Graben):

Horizon	2 way t.t.	Depth(m) (calc. from function *)
Oligocene	600	610
Eocene	1350	1365
Palaeocene	1945	2055
Danian	2020	2200
Upp. Cretaceous	2190	2405
Santonian	2410	3220
Lr. Cretaceous	3100	3920
Kimmeridge	3770	5310
Heather	4000	5890
Middle Jurassic	4360	6750

The calculated depths provided the necessary information to allow these respective depocentres to be modelled in terms of burial histories and maturation.

3.5.6.2 Burial History and Pressure Potential of Pseudowell Depo B.B.1 (back basin, Fig.3.5.6.2a) - East Shetland Basin / west of Alwyn

3.5.6.2.1 Burial History Modelling

A burial history curve shows that for the formations of interest and hydrocarbon potential - Upper Jurassic Kimmeridge Formation - the calculated oil maturation window is entered at approximately 70Ma with entry into the mid-mature and late mature regions of the oil window at approximately 58Ma and 22 Ma respectively. The rapid burial phases are during the Middle-Upper Cretaceous and Pliocene-Recent. The effects of these sustained periods of rapid burial, with respect to temperature, is to increase the geothermal effect upon the rocks undergoing burial, effectively allowing them to enter the oil window at a faster rate.

3.5.6.2.2 Overpressure potential due to hydrocarbon maturation in the depocentre

Increasing temperature allows the organic rich Kimmeridge Formations to pass through the early to mid to late mature stage with the potential for an associated volume increase in liquid hydrocarbon component (Barker, 1987). The organic rich rocks enter the main gas generation phase at approximately 5Ma (Fig.3.5.6.2a). It has already been documented that the volume increase associated with the thermal cracking of liquid hydrocarbons could create overpressure (section 2.1 - Barker, 1990). Calculations have been made using the same assumptions as documented by Barker (1990) (section 2.1).

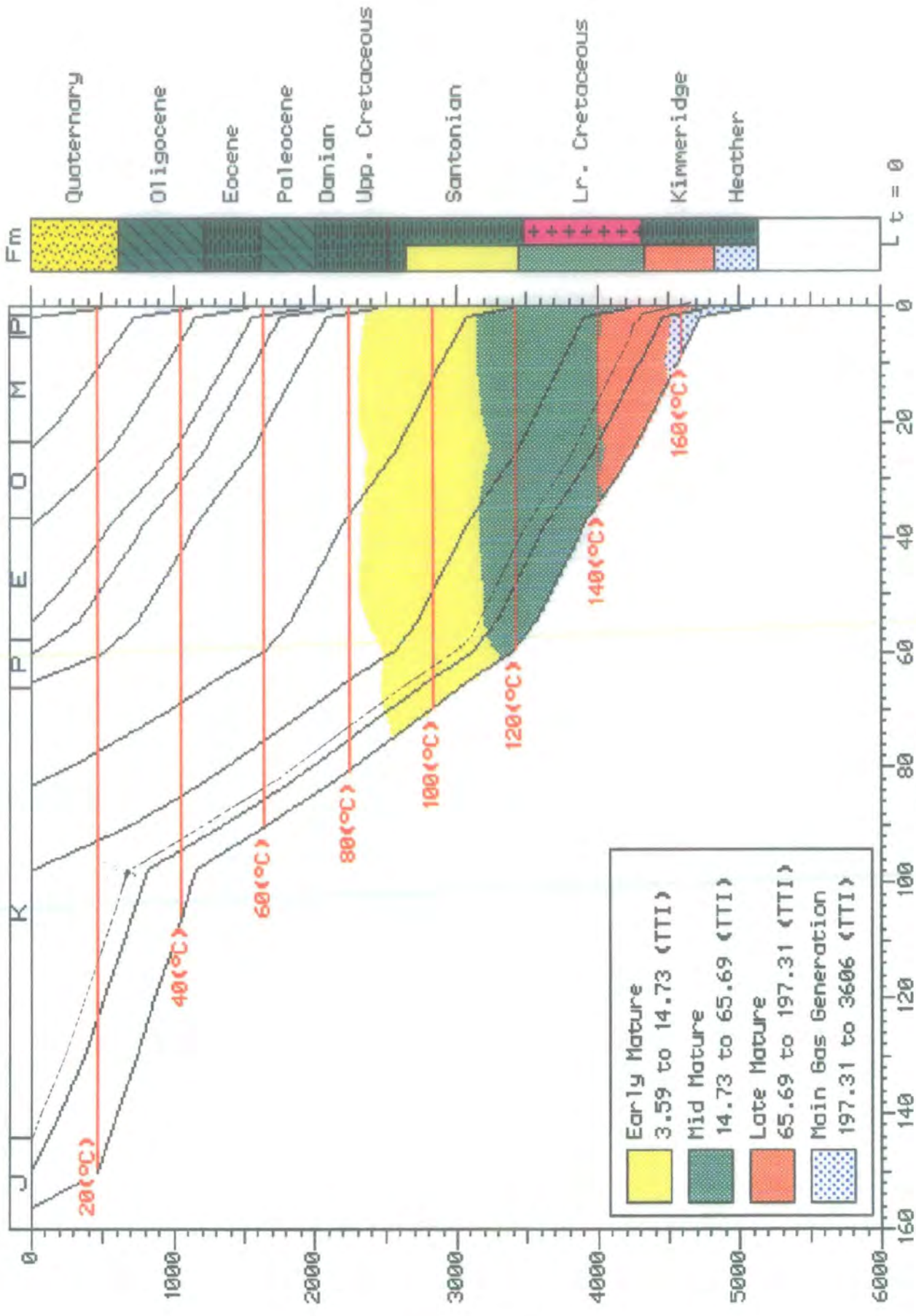

Fig.3.5.6.2a - Burial history plot, with superimposed maturity windows, for a pseudowell located in the depocentre west of the Alwyn field area

The following information has been applied to the function PV = ZnRT (the modified non ideal gas law) for the Kimmeridge Formation (Fig.3.5.6.2a) where:

P = Pressure of system (psi)

V = Volume occupied (constant arbitrary units)

Z = Compressibility of methane(from Barker, 1987, based on data from Brown, et al., 1948)

n = number of moles of methane that occupies one thermally altered volume of oil.

R = constant

T = Temperature of system (°C)

To calculate the volume expansion associated with the depth and temperature when the Kimmeridge Formation enters the gas window (Fig.3.5.6.2a):

P = 6644psi (assumed hydrostatic at a depth of 4500m and a hydrostatic pressure gradient of 1.47645psi/m)

V = Unknown

Z = 1.19 (recalculated from Barker, 1987 based on hydrostatic pressure and geothermal gradient of 34°C/km)

n = 8.43 (number of moles of gas that occupies the volume created by the thermal cracking of one barrel (bbl) of oil at S.T.P.)

R = 8.314

T = 153°C (4500m at 34°C/km)

$$PV = ZnRT, \quad 6644 \times V = 1.19 \times 8.43 \times 8.314 \times 153$$

$$V = 1.92$$

Therefore, one bbl of oil would thermally alter to 1.92x its volume at hydrostatic pressure (pressure is fixed, volume is the variable) at a depth of 4500m and a temperature of 153°C.

If, however, volume remained stable and therefore pressure acted as the variable, the following information can be used to calculate the pressure created by thermally cracking one bbl of oil at the above depths and temperatures:

P = Unknown — Depth = 4500m

V = 1 (fixed) — Hydro = 6644psi

Z = 1.17 (hydrostatic) → 1.76 (lithostatic) (calculated from Barker, 1987) — Litho = 14 776psi

n = 8.43

R = 8.314

*Another important parameter in the transference of overpressured fluid from low permeability rocks such as thick shale sequences is the expulsion efficiency of the rock. The expulsion efficiency is a term primarily dependant upon the pore throat connectivity and the viscosity of the pore fluid. Also, when organic rich rocks are considered, specific kerogen type is also important in terms of kinetics (activation energy and transformation ratio) which has an inherent effect on the expulsion efficiency.

T = 153°C

at hydrostatic pressure conditions:

PV = ZnRT, P x 1 = 1.17 x 8.43 x 8.314 x 153

P = 12 546psi (overpressure of 5902psi)

at lithostatic pressure conditions:

PV = ZnRT, P x 1 = 1.76 x 8.43 x 8.314 x 153

P = 18 873psi (overpressure of 12 229psi)

Therefore, pressure calculations for the thermal cracking of one bbl of oil to gas at 4500m (153°C) lies between 12 546psi (overpressure of 5902psi) assuming Z = 1.17 and 18873psi (which surpasses the lithostatic gradient by 4107psi) assuming Z = 1.76.

It is therefore important to specify the compressibility of methane, which is unknown unless a down-hole pressure is known. Pressure, being the variable and the unknown, cannot be defined and is actually calculated by assuming a value for Z. Therefore, in the case of the onset of gas generation in the depocentre east of Alwyn, gas would have the potential to produce overpressure assuming that a cumulative 100% of oil has thermally altered in a perfectly sealed unit, reacting to produce pure methane, to lie in the range of:

	5902psi overpressure	assuming	Z = 1.17 (hydrostatic)
@4500m/153°C	↓		↓
	4107psi over lithostatic	assuming	Z = 1.76 (lithostatic)

No account has been made to specify kerogen types, reaction kinetics, solubilities of oil/gas and seal retention of the container (porosity and permeability relationships and mechanical properties).*

From the above calculations it is possible that maturing hydrocarbons in this depocentre could develop overpressures of a magnitude needed to expel fluid and pressure out of the maturing Kimmeridge Formation. However, although sufficient hydrocarbon and associated pressure generation in this area has been modelled, by observing the timing of the onset of the gas window it is seen that the Heather Formation enters the main phase of gas maturation at approximately 15Ma (Fig.3.5.6.2a). The Kimmeridge Formation lies outside the main gas generation phase until approximately 5Ma (Fig.3.5.6.2a). Any developed overpressure associated with the thermal cracking of oil, generated from the Kimmeridge Formation, to gas therefore will not commence until 5Ma.

It is known that hydrocarbons reservoired in the Alwyn area, from K-Ar dating methods (Jourdan et al., 1987; section.3.6.8) and diagenetic observations (section.3.6.5, 6 and 7), are dated between 75-35Ma for the initial phase of oil saturation. Oil has been modelled as generating in this area from approximately 70Ma (Fig.3.5.6.2a) and oils expelled from this depocentre could have migrated up flank to proximal structural highs such as the Alwyn field area. However, previously documented geochemical information would tend to eliminate any hydrocarbon input from this westerly source from data interpretation in the Alwyn North and South East fields (Fig.3.5.4.3a, b, c and d). It is feasible, however, that some Alwyn South wells that, from the geochemical data, reservoired oils have been predominantly sourced locally but also with mixing and contamination from other areas (section 3.5.4.3).

3.5.6.3 Burial History and Pressure Potential of Pseudowell Depo V.G.1 (Viking Graben, Fig.3.5.6.3a) - east of Alwyn

3.5.6.3.1 Burial History Modelling

Using the same seismic line (NNST 84-05), formations were modelled offstructure from the Alwyn area to the east into the Viking Graben. Geochemical interpretation has already cited this region as a likely source area for the hydrocarbons reservoired in Alwyn North and South East. Similar applications were used in modelling the Viking Graben area as were used west of Alwyn South.

Shot Point (S.P.) 4650 represented the deepest, most axial part of the rift basin and a pseudowell was constructed and modelled in terms of burial history and maturation potential. It is clear that the burial history from the Jurassic to end Cretaceous approximately follows a similar trend to that of the back basin indicating similar styles of rifting, deposition and burial. Rates of burial are, however, relatively more rapid in the Viking Graben area (Fig.3.5.6.3a). The effect of this faster burial is to accelerate the onset of early maturation, by exposing the formations to higher temperatures more quickly, which is modelled at approximately 90 and 82Ma for the Heather and Kimmeridge Formations respectively. Generation of oil commenced, then, as early as 90Ma. Secondary migration would transport generated fluids up dip out of the depocentre. It is feasible that the first oil saturation in the Alwyn area, dated at 75Ma (Jourdan et al., 1987) in the Alwyn North field, was sourced from the Graben area. This would imply, if the maturation history for the depocentre and that hydrocarbons reservoired in the Alwyn fields were sourced in this depocentre is correct, and the dates proposed by Jourdan et al. (1987) are accurate, that there was a lag time of 15Ma to

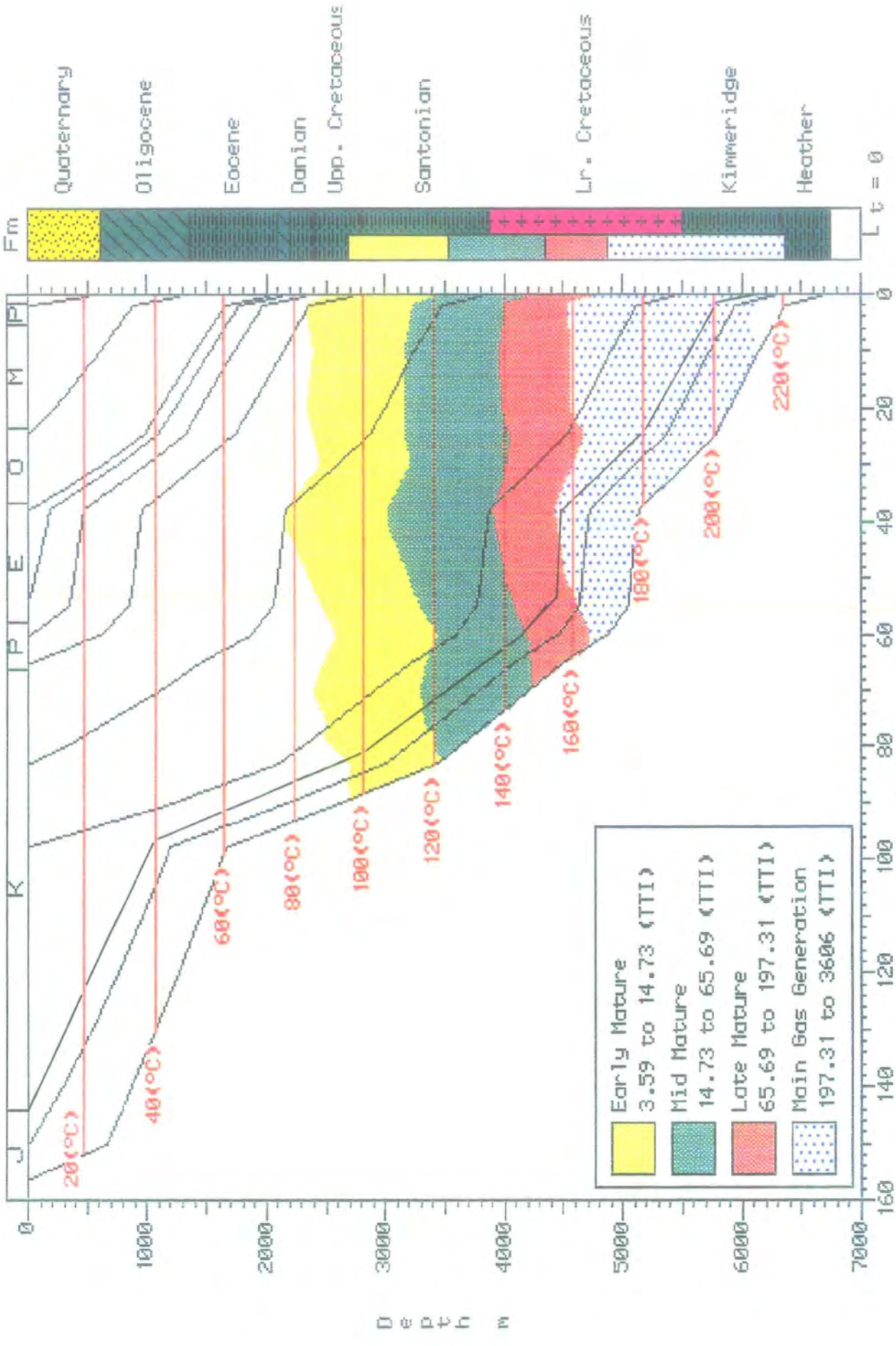

Fig.3.5.6.3a - Burial history plot, with superimposed maturity windows, for a pseudowell located in the Viking Graben depocentre east of the Alwyn field area

allow for migration of hydrocarbons from the modelled depocentre to the Alwyn North field.

The maturation characteristics, timing and expulsion potential (secondary migration) coupled with geochemical observations allow the postulation that there has been sufficient amounts of hydrocarbons generated, expelled and emplaced to fit all of the observed criteria for the reservoired hydrocarbons in the Alwyn North and South East fields and that the oils have been sourced from the Viking Graben area. The main gas generation phase in this depocentre has been timed at 55Ma for the Kimmeridge formation (Fig.3.5.6.3a), with the horizons entering the gas phase at respective depths and temperatures of 4800m/163°C and 4500m/153°C.

3.5.6.3.2 Overpressure potential due to hydrocarbon maturation in the depocentre

Calculating the overpressure potential at the onset of gas generation in the Viking Graben area, the Kimmeridge Formation gave the following information:

P = 7087psi (assumed hydrostatic at a depth of 4800m and a hydrostatic pressure gradient of 1.47645psi/m)

V = Unknown

Z = 1.22 (recalculated from Barker, 1987 based on hydrostatic pressure and a geothermal gradient of 34°C/km)

n = 8.43

R = 8.314

T = 162°C (4800m at 34°C/km)

$PV = ZnRT, \quad 7087 \times V = 1.22 \times 8.43 \times 8.314 \times 162$

$V = 1.95$

Therefore, one bbl of oil would thermally alter to 1.95x its volume at hydrostatic pressure at a depth of 4800m and a temperature of 162°C.

If, however, volume remained stable and therefore pressure acted as the variable, the following information can be used to calculate the pressure created by thermally cracking one bbl of oil at the above depths and temperatures:

P = Unknown	Depth = 4800m
V = 1 (fixed)	Hydro = 7087psi
Z = 1.22 (hydrostatic) → 1.83 (lithostatic)	Litho = 15749psi
n = 8.43	
R = 8.314	
T = 162°C	

at hydrostatic pressure conditons:

$$PV = ZnRT \quad P \times 1 = 1.22 \times 8.43 \times 8.314 \times 162$$
$$P = 13\,852\text{psi (overpressure of 6765psi)}$$

at lithostatic pressure conditions:

$$PV = ZnRT \quad P \times 1 = 1.83 \times 8.43 \times 8.314 \times 162$$
$$P = 20778\text{psi (overpressure of 13 691psi)}$$

Pressure, due to the thermal cracking of oil to gas in this temperature/depth regime, created by the reaction of one bbl of oil to gas would create an overpressure between 6765psi (Z = 1.22) and 20778psi (Z = 1.83). The assumptions made in these calculations are identical to those made in 3.5.6.2.2.

It is has been inferred that the organic rich Kimmeridge Formation has been subjected to a sufficient amount of heating to generate hydrocarbons. The generated oils have been calculated to develop significant amounts of overpressure when thermally altered to gas through continued exposure to increased heating as a consequence of burial. This pressure could affect primary migration by fracturing sealing rocks before transferring this pressure and associated fluids out of the depocentre as the hydrodynamic system in this area tries to reachieve a pressure equilibrium in the rock and fluid framework.

It could be inferred that fluids, and possibly overpressure, are sourced in this depocentre and are transferred by buoyancy, diffusion or some other drive mechanism up to distal areas such as Alwyn. The structural style of the Alwyn field tilted fault blocks provides a trap to contain these migrating fluids and any associated overpressure. It is possible to observe these migrating fluids in relation to the diagenetic sequence in the reservoir. These observations can be applied when interpreting the hydrocarbon fill-up and pressure history of the Alwyn reservoirs.

3.5.7 Conclusions

Previous geochemical modelling have cited likely hydrocarbon generating source areas (section 3.5.4.3). It has been shown that by using local seismic information and stratigraphic and lithological controls provided by well ties, that this information can be utilised off-structure via regional seismic lines into these likely hydrocarbon source areas. By applying a computed depth conversion function to manually extrapolated key stratigraphic horizons, it was possible to assign depths for these horizons. The burial history was modelled for a specific shot point in these source areas. The burial

history was modelled and the stage and timing of maturation of the organic rich Kimmeridge Formation was calculated.

It was evident that both basinal areas lie proximal (in a regional sense) to the Alwyn field; the depocentre to the west and the Viking Graben to the east both have the potential to generate and expel hydrocarbons. The main gas generation phase is entered by the Kimmeridge Formation at approximately 56Ma in the Viking Graben whereas it is not until 5Ma that this phase of gas generation is realised in the maturation history of the depocentre west of Alwyn. It has been calculated from modified equations and work based on Barker (1987, 1990) that, even accounting for the effects of confining pressure by overburden and local geothermal and hydrostatic gradients, the thermal reaction of oil to gas with an associated pressure increase within an enclosed volume, at modelled depths and temperatures, is sufficient to create a significant overpressure in the depocentres. It is however, more likely, that due to the timing of the maturation and the geochemical trends (section 3.5.4.3) that the reservoired hydrocarbons in Alwyn would be expelled from the Viking Graben.

3.6 Diagenesis

3.6.1 Introduction

Since the overpressure can effectively be described and defined into 3 pressure cells - Alwyn North, South and South East - it then follows to observe the diagenetic phases in each of these areas to ascertain any diagenetic relationship to the overpressure distribution. The purpose of describing and interpreting the petrography is to establish a diagenetic framework for the fluid inclusion study and the estimation of palaeopressure. Also, it is fundamental to establish the relative timing of diagenetic events to produce a paragenetic sequence which, in part, relates to the fluid flow history in the reservoirs.

The diagenesis is also considered with respect to the age-dating of illite as illite is part of the suite of the authigenic minerals. This has implications for the timing of hydrocarbon migration into the various reservoirs in the Alwyn field and could provide a valuable temporal constraint on the fluid flow history.

A description is given of the compositional analyses incorporating constitutional grains, porosity and permeability characteristics, texture and fabric. This lays the basis for the interpretation of diagenesis in each of the Alwyn fields.

Information and data used in the interpretation of the diagenesis comes from various sources. The diagenetic sequence in the Alwyn reservoirs has been previously documented by Johnson and Eyssautier (1987), Jourdan et al. (1987) and Hogg et al. (1992). Petrographic and diagenetic observations from these studies are incorporated in this interpretation and illite age-dates interpreted by Jourdan et al. (1987) and Hogg et a. (1992) are also used to provide timing constraints in the diagenetic sequence. In addition, various analytical techniques including thin section petrography and microprobe analyses were conducted on reservoir sandstone samples. These samples were cut from well core (specific well and depth sampling locations are documented in Appendix 4.2). A total of 35 samples were analysed petrographically.

It is the oil-bearing Brent Group reservoir sandstones which this study focuses upon although observations have previously been made by other workers for the Statfjord Formation (Johnson and Eyssautier, 1987; Jourdan et al., 1987; Hogg et al., 1992). The diagenetic observations and interpretations are made exclusively for sands of the Brent Group due to material and data availability. Rock data was not available for the water-bearing section.

Analytical equipment and techniques are documented in Appendix 2.

3.6.2 Previous Diagenetic Studies

Many models have been described for the diagenesis of the Brent Group summarised in the generalised sequence proposed by Haszeldine (1992) (Fig.3.6.2a). However, Johnson and Eyssautier (1987) report that the intensity and nature of diagenesis varies over the Alwyn area. Indeed, such are the local variations between each structure both between the fields and individual fault blocks that Hogg et al. (1992) has investigated the zonation and cementation characteristics of 4 wells in Alwyn South to ascertain information on local fluid flux and the degradational effect on porosity and permeability. Hogg et al. (1992), has identified and classified a paragenetic pathway of diagenetic minerals in the Brent Group sandstones in Alwyn South (Fig.3.6.2b; Hogg et al. 1992). Jourdan et al. (1987), has attempted to document and generalise the chronological evolution of diagenetic sequences in the reservoir sequence for the entire Alwyn area (Fig.3.6.2b) but for the purpose of this study, it is necessary to classify the diagenesis in relation to the overpressure distribution.

Early diagenetic effects are largely linked to mechanical compaction within the first few hundred metres of burial. Porosity loss is greatest during this first phase of burial and the rate of porosity loss in the reservoir sands of the Brent Group in the Alwyn

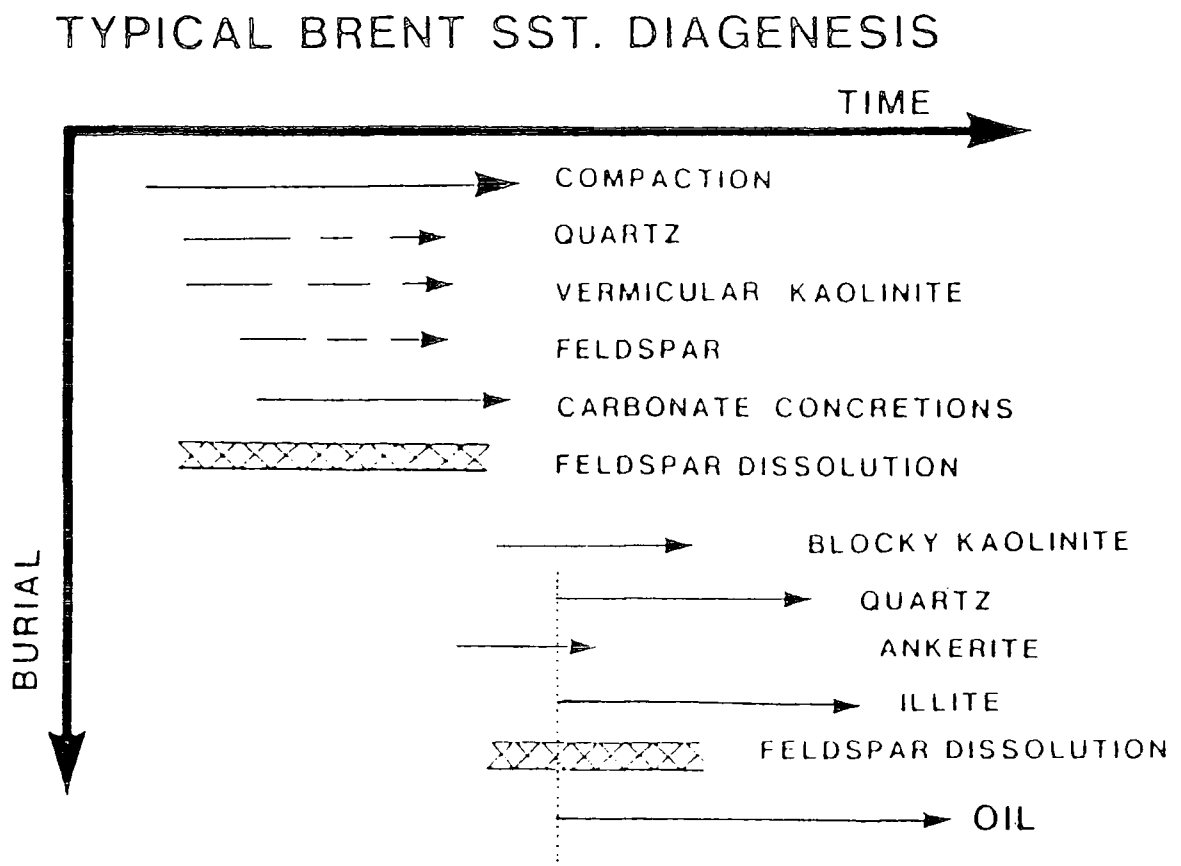

Fig.3.6.2a - Sequence of events representative of Brent sandstone diagenesis. Vertical dotted line highlights the common synchroneity of quartz, illite and oil. Modified after Haszeldine et al. (1992)

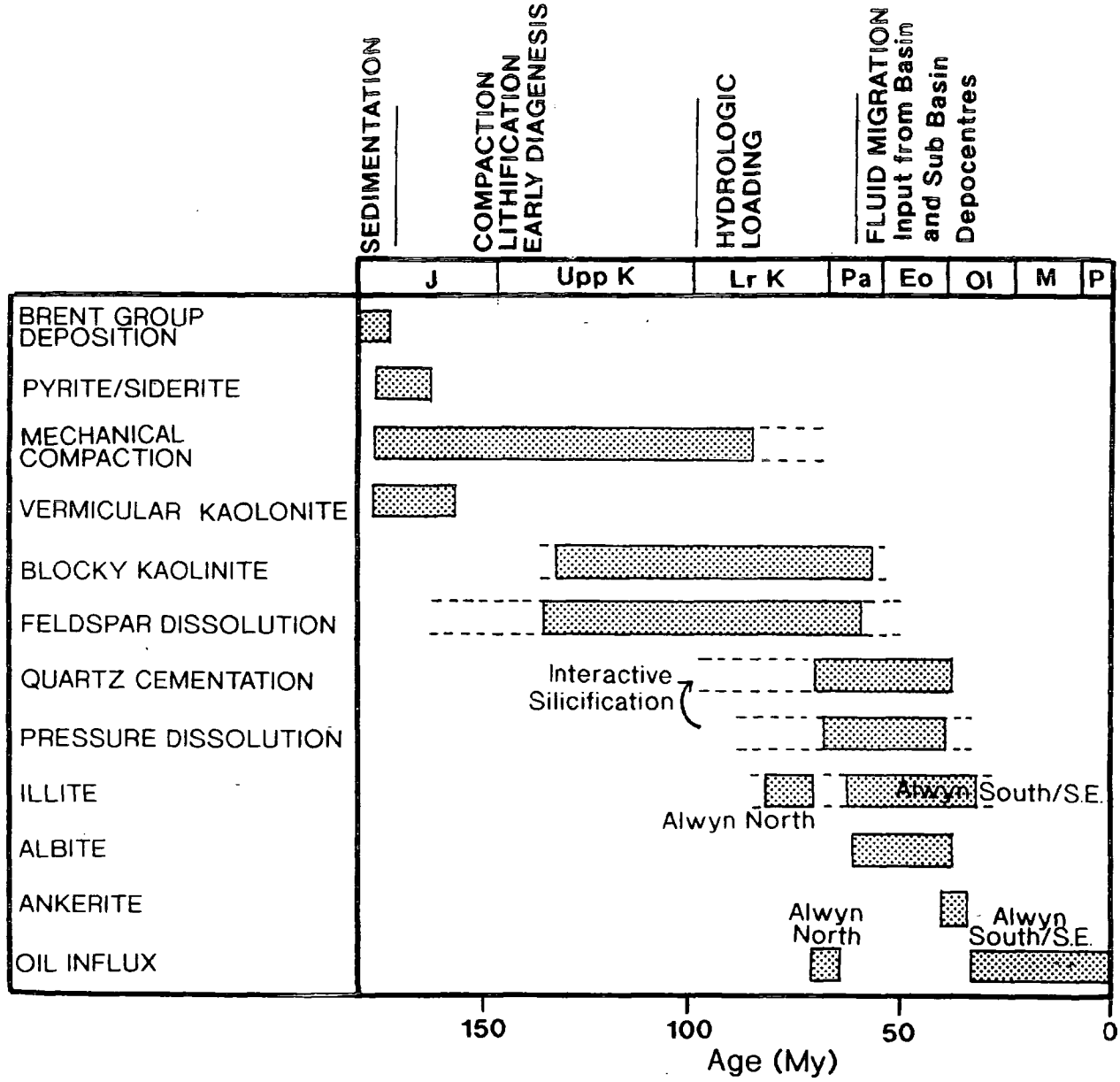

Fig.3.6.3b - Chronological evolution of the diagenetic sequences in the Alwyn reservoirs. Associated processes are documented along along the top of the diagram. Modified from Jourdan et al. (1987) and Hogg et al. (1992)

fields would be best represented by porosity/depth relationships based on formulae such as proposed by Sclater and Christie (1980) and Falvey and Middleton (1981). During this early phase of diagenesis, chemical effects would take place in the medium of water related to the environment of deposition (Tucker, 1981). In the case of the Alwyn area, Sommer (1978) described an early silification phase which effectively protected the sands from severe compactional effects. This primary silicification would most likely be the result of circulating meteoric waters enriched in silica precipitating through the course of the fluid movement. However, there is confusion as to the nature of this early silica being amorphous or crystalline (Johnson and Eyssautier, 1987).

Compactional effects are suppressed in the later stages of diagenesis as primary compaction and porosity loss occurs over the first few hundred metres of burial. Late diagenesis is largely associated with the chemical transfer of solutes and the precipitation of these solutes in the mineral and grain framework. These solutes may become available to the host rock through the effects of pressure solution whereby minerals dissolve or partly dissolve through very high pressure contact with each other. The resultant solutes may remobilise and reprecipitate as part of the authigenic phase. Mass transfer of solutes as part of a static or moving fluid body may also contribute to the solute budget available for diagenetic mineral growth. The flow of fluid rich in mineral solutes through the reservoir sands will also promote diagenetic growth phases if conditions necessary for precipitation are correct. The source of any incoming and recharging fluid is also important with respect to the interpretation of the diagenetic sequence. Hogg et al. (1992) has identified a fault zone as a likely point of entry into the Brent Group reservoir sands of Alwyn South field. Hogg et al. (1992) interprets the relationship of authigenic illite growth to the proximity of a fluid entry point causing late stage and intense illitisation in Alwyn South wells close to a fault zone. Similarly, Jourdan et al. (1987) and Burley et al. (1989) (in the Tartan field) have used evidence from anomalously high fluid inclusion temperatures recorded in the diagenetic sequence in reservoir sands as evidence for hot fluid circulation sourced from a deeper area. The associated authigenic quartz overgrowth phases which contain, and are co-eval, with these fluid inclusions are therefore interpreted by Jourdan et al. (1987) as being attributed to incoming fluid providing the precipitates now recorded as late stage diagenetic overgrowths.

3.6.3 Petrography of Alwyn North (wells 3/9a-5 and 3/9a-6) - Plates p3.6.3a, b and c

In Alwyn North, the reservoir sands are moderate to poorly sorted with a dominance of medium grained sub-angular to sub-rounded grains (Plate p3.6.3a). Texturally, the sands show sub-maturity with occasionally preserved and deformed micas and eroded/dissolved feldspar grains. The fabric of the sands record a semi-homogenous population of mono but dominantly polycrystalline quartz grains with interstitial clays and semi-corroded and etched feldspars. Compositionally, quartz grains amount to up to 80% of the component grains with an average of 72%. Feldspars constitute approximately 6%, micas 6%, interstitial clays 12% and the remainder being lithic fragments. Packing characteristics show that there is grain-grain contact, compactional suturing and grain slip rotation. Later compaction and diagenetic effects show pressure solution arcs and the possible remobilisation of this diagenetic silica into pore filling cement and overgrowths.

Quartz overgrowths are easily identifiable due to the dominantly polycrystalline quartz which shows different extinction angles under cross-polarised light. These overgrowths, however, are difficult to define with respect to one another. A thin peloidal or microstalactitic quartz overgrowth (Plate p3.6.3b) which serves to envelope detrital quartz grains is a recurrent feature on quartz grains which are not largely affected by suturing or other grain contacts. However, it is occasionally seen that this first quartz overgrowth has been affected by mechanical compaction with other grains appearing to 'puncture' the thin envelope of quartz. This, however, may be later effect of pressure solution rather being due to early compaction. This first quartz overgrowth may be described, for purposes of notation and reference here and in the fluid inclusion section (3.7), as QA1. Syntaxial and epitaxial quartz overgrowths are also identified as being a later stage overgrowth than QA1. These syntaxial overgrowths develop, where allowed, into free pore space but appear to be suppressed at grain contacts and compromise boundaries with other overgrowths and also occasionally appear to terminate in pore space (Plate p3.6.3c). These syntaxial overgrowths which use QA1 as a template for growth are termed QA2. Later quartz overgrowths do appear to exist but their relationship to QA2 is uncertain due to the irregularity of occurrence and growth patterns that they possess.

Clay development appears to be a late stage phenomenon. Unidentified fine grained muddy clays are identified as lining pore space and occur occasionally at quartz overgrowth terminations. Eroded feldspars also appear to blend into clay interstices and the definition between these two types of mineral groups is difficult. Overall these unidentified clays constitute approximately 12% of the constituent minerals.

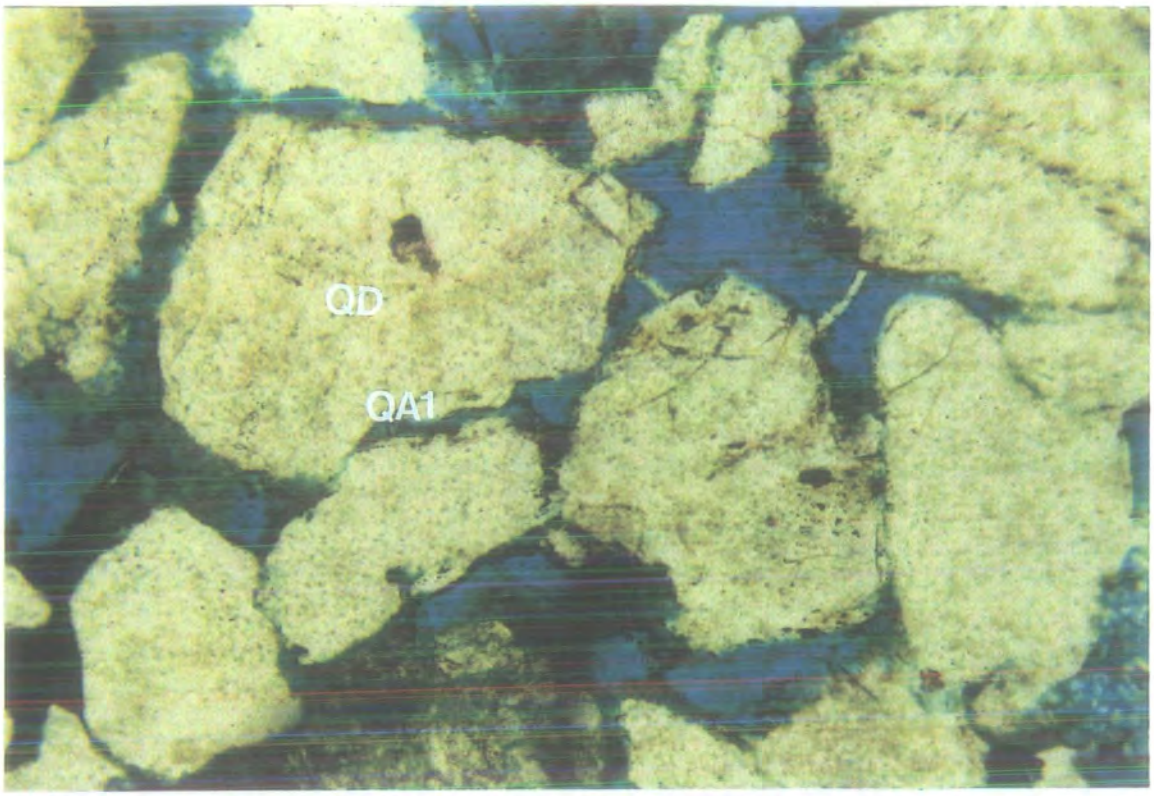

Plate p3.6.3a - 3/9a-6 (3230m). Peloidal cement 'shadowing' and appearing drusey to detrital grains. This peloidal overgrowth is described as QA1 but does not envelope detrital grains in the way that QA2 syntaxial overgrowths do (QA2 overgrowths frequently contain the fluid inclusions - Plate p3.6.3c). Field of view 1.2mm.

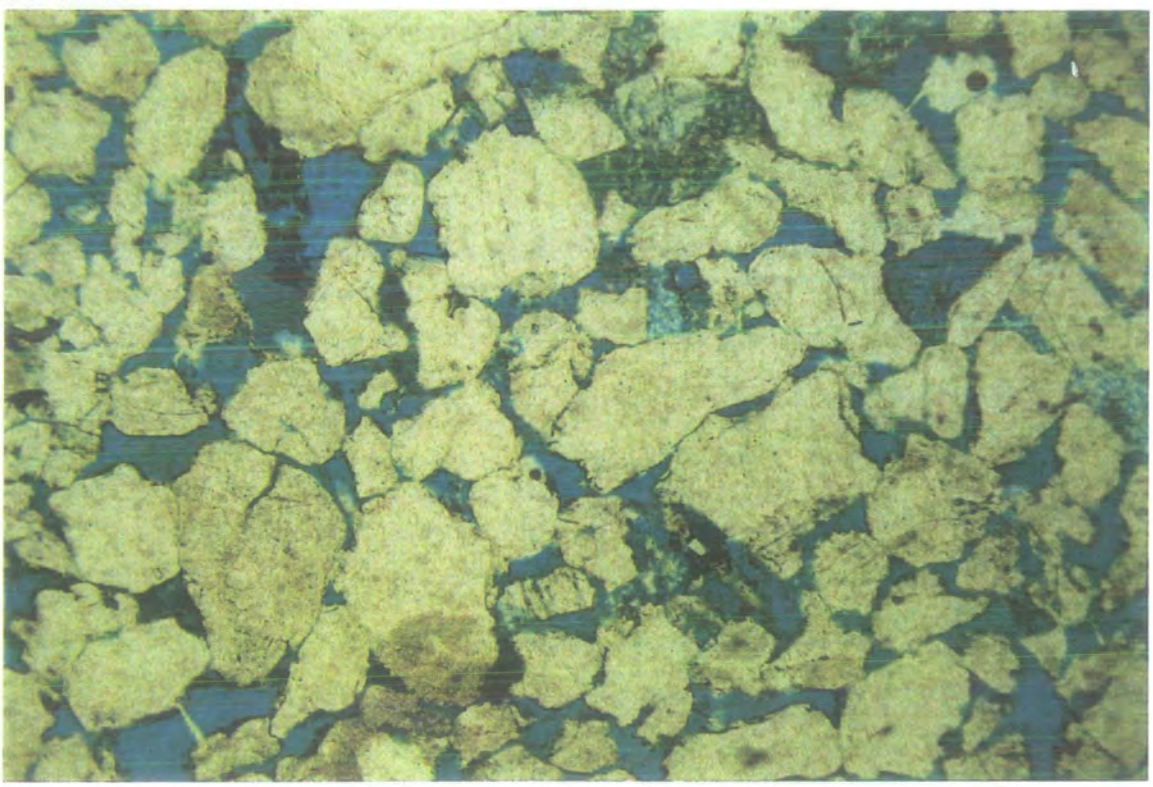

Plate p3.6.3b - 3/9a-6 (3190m). Relatively high porosity and permeability shown by blue stain. Average compaction is 2/3 contacts per quartz grain. Relatively little clay except for contribution from feldspar dissolution. Field of view 3mm.

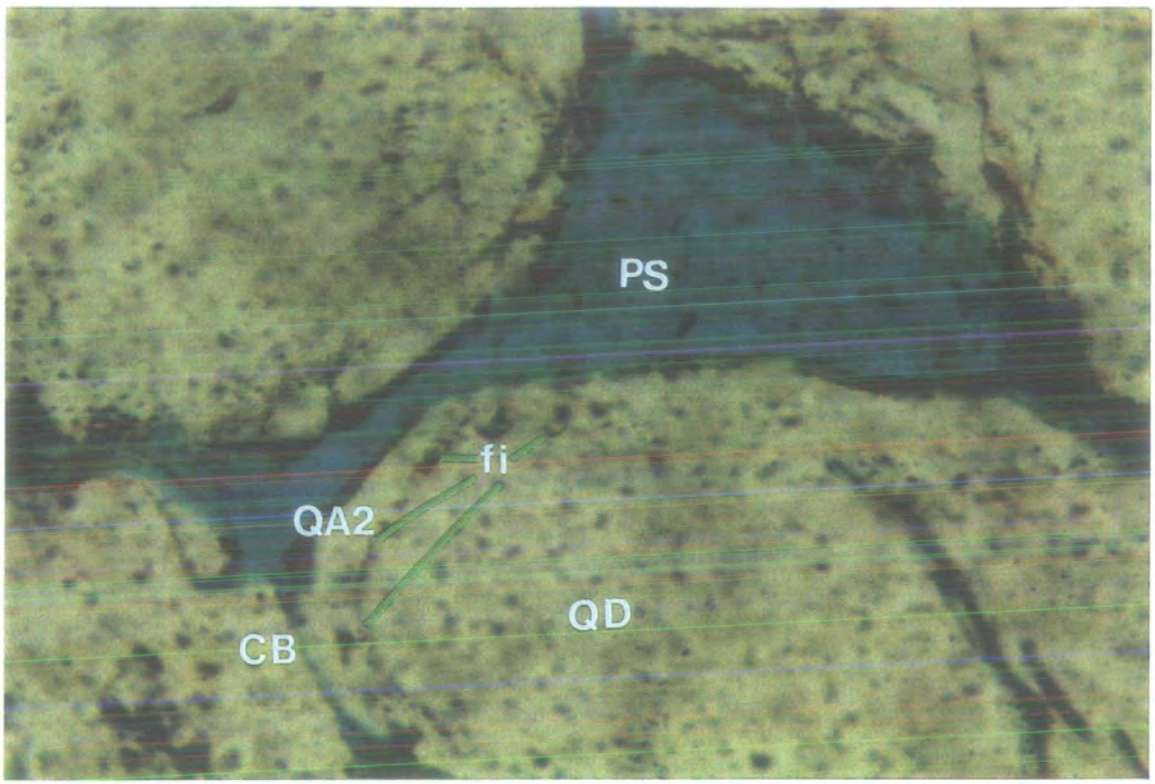

Plate p3.6.3c - 3/9a-6 (3200m). Close up of elongate prominant fluid inclusions with gas bubbles (marked fi). Trail of inclusions show the detrital grain boundary. Syntaxial (marked QA2) overgrowth grows into free pore space except where terminated by compromise boundary (marked CB) with another grain/overgrowth. Field of view 0.48mm

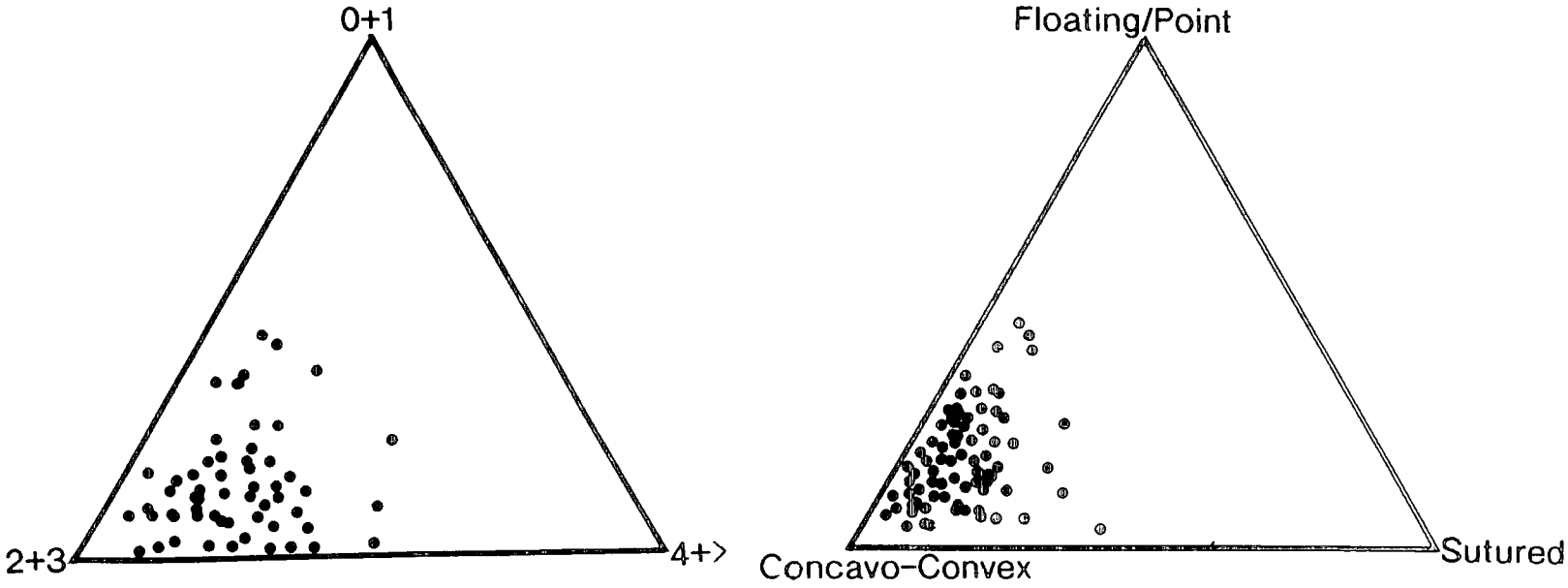

Fig.3.6.3a (left) - Compaction Index of Alwyn North (3/9a-6, 3288m) reservoir sandstone. Compaction Index after Taylor (1950) and **3.6.3b (right)** - Tight Packing Index (3/9a-6, 3288m) reservoir sandstone. Tight Packing Index after Wilson and McBride (1988)

Overall effective porosity averages approximately 16% in the reservoir sands with primary porosity in some cases being severely reduced by mechanical compaction and associated pressure solution effects accentuated by highly deformed allogenic micas and also sutured contacts. However, the Compaction Index (C.I.) (Taylor, 1950) and the Tight Packing Index (T.P.I.) (Wilson and McBride, 1988) suggest, for the moderately to well sorted sands of Alwyn North, moderate to high overall preservation of primary porosity with the C.I. showing a clustering around the 2+3 contacts per quartz grain area Fig.3.6.3a) and a T.P.I. bias toward the concavo convex pressure solution contact field (Fig.3.6.3b). Grain slippage and rearrangement has occurred but with limited interpenetration due, possibly, to an early phase of silicification as recorded by Sommer (1978).

3.6.4 Diagenesis of Alwyn North -

Although pressure solution effects are seen in quartz grains, the relationship of the grain contacts observing a trend toward 2/3 contacts per grain and the lack of sutured contacts suggest that mechanical compaction effects have been suppressed. Micas were relatively undeformed and feldspars (usually one of the first minerals to succumb to primary diagenetic effects) are seen to be etched and corroded but largely physically deformed. This relative preservation of primary porosity allowing the grains to compact at a rate which would give these packing characteristics must be attributed to a mechanism operating to limit the effects of early compaction.

The identification of the thin peloidal quartz overgrowth (QA1) around detrital quartz grains may have acted to limit the early mechanical compaction effects by strengthening the grain framework. Therefore, this silicification phase could be inferred as being early occurring contemporaneous with early compaction (within the first 500 metres of burial).

The etching and corrosion of feldspars appears to approximate to the timing of the syntaxial quartz overgrowths which includes QA2 (describing the overgrowth which uses QA1 as a growth template) as no direct relationship could be ascertained between the two minerals. If the erosion and precipitation of feldspars is contemporaneous with the syntaxial quartz overgrowths, then secondary porosity may be a result of the feldspar dissolution. However, dissolution of the feldspars would provide solutes which could be remobilised and contribute to the authigenic phase and thus counteract any secondary porosity developed. However, observations of these authigenic quartz overgrowths occluding free pore space suggest that a contribution from another source to account for the volume and amount of authigenic quartz recorded. Even accounting

for precipitates available from dissolution of feldspars and micas and from pressure solution effects, another contributory source for diagenetic quartz must be inferred. This chemical transfer of fluids is described, typically, as being a late stage diagenetic phenomenon. It is then that these quartz overgrowths can be described as being relatively late in the paragenetic sequence.

The pore lining occurrence of thin clay envelopes on feldspar and occasionally quartz grains suggest that the development of these clays are contemporaneous with the dissolution of the feldspars. The majority of the clay component is largely interstitial with eroded micas and feldspars and therefore can be inferred to be relatively late stage diagenetic growth phases. Individual clays could not be identified to ascertain a more rigorous relationship with respect to specific diagenetic position.

3.6.5 Petrography of Alwyn South (wells 3/14a-3 and 3/14b-9) Plates p3.6.5a, and b

The sands of Alwyn South are observed to be well to moderately sorted and form fine to coarse grain size sandstones. Compositionally, the sands compare favourably with those of Alwyn North except for the clay content which increases markedly in the sands of the Alwyn South field. This clay content is observed to occlude free pore space and occasionally invade pore throats. The fabric and texture of the sands are akin to those in Alwyn North showing submaturity containing approximately 8-15% interstitial clays. Less stable members of the sediment population, such as feldspars have been etched and corroded (Plate p3.6.5a). Overall porosity varies in the samples analysed for the wells in Alwyn South. Values for the 3/14a-3 well gave porosity values ranging from 9% (3550m sample) to 17% (3520m sample). Values for the 3/14b-9 well observed a wide spread of porosity values from as low as 7% (3731m sample) to 21% (3600m).

Texturally, the sands show a differing packing character to the sands of the Alwyn North field. In the sands of the Alwyn South, there appears to be a higher coincidence of grain-grain contacts and compactional suturing. Also, detrital quartz grains show an increase in pressure solution arcs and concavo-convex boundaries.

Polycrystalline quartz dominates the quartz population as a result mainly of suturing and mechanical compactional effects but also as result of apparently complex generations of overgrowths. There is no recognisable thin peloidal quartz overgrowth around detrital grains in the sands of the Alwyn South as was observed in Alwyn North. The identified authigenic quartz growth phases appears to be a series of individual syntaxial, epitaxial and overgrowths which have an apparent random growth pattern.

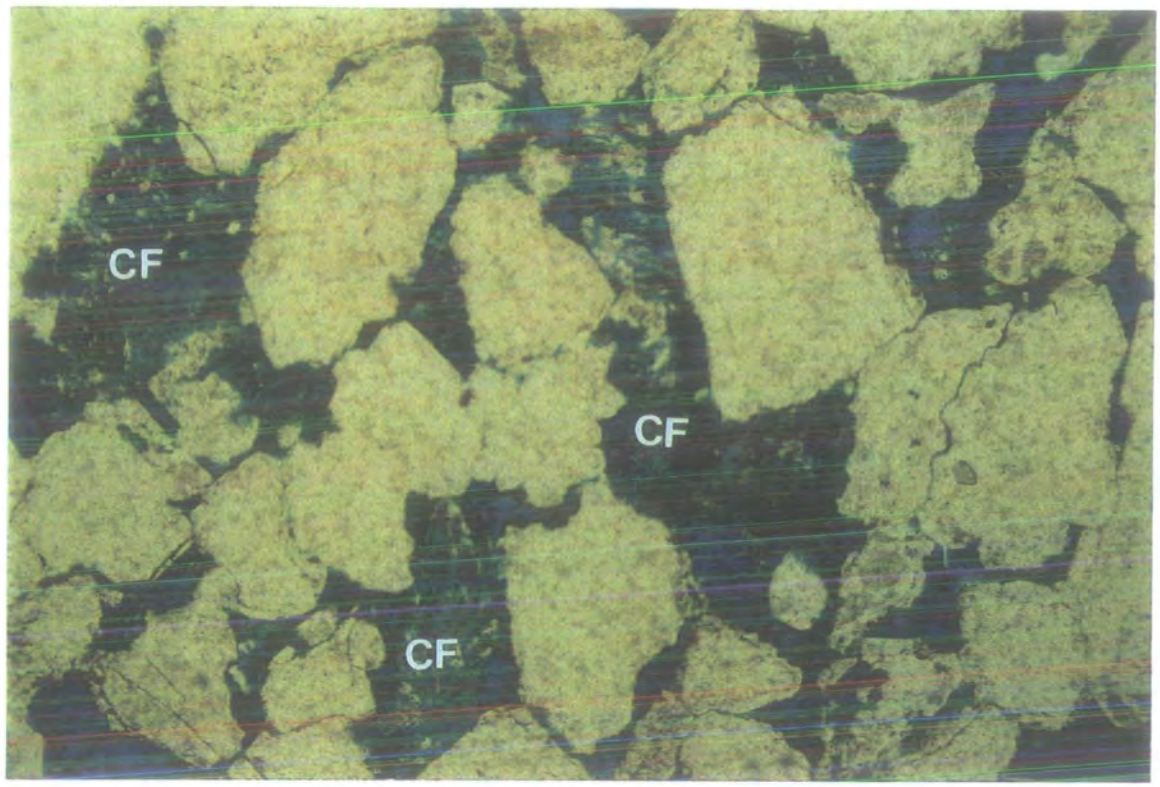

Plate p3.6.5a - 3/14a-3 (3410m). Sutured quartz grains and pressure solution and pressure contacts are seen. Main observation is the highly corroded feldspars (marked CF) giving secondary porosity and contributing to the clay matrix. Field of view 1.2mm

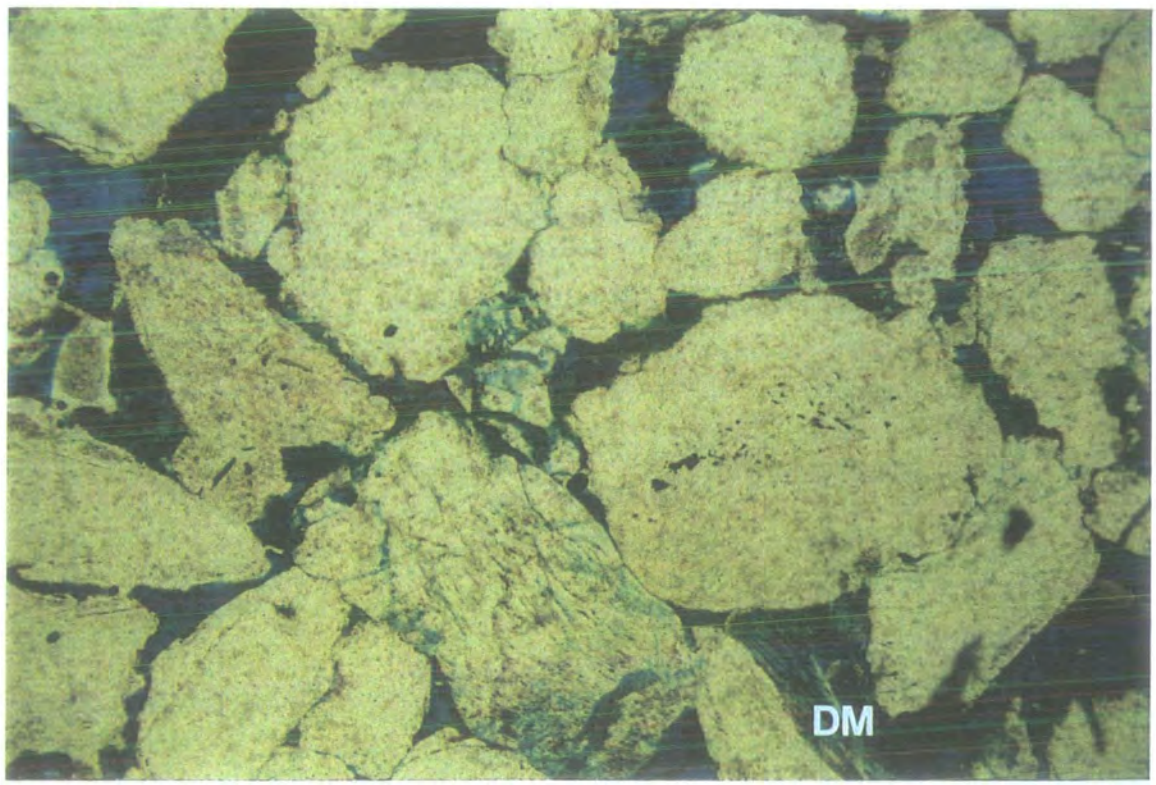

Plate p3.6.5b - 3/14a-3 (3410m). Sub-angular to sub-rounded quartz grains with relatively complex overgrowths. Corroded and deformed mica grains (marked DM) are seen to be interstitial with the clay matrix. Field of view 1.2mm

This random growth involves overgrowths terminating in irregular fashion being curved and occasionally etched at the termination boundaries. The quartz overgrowths, as a whole, vary in thickness and continuity ranging from well developed syntaxial overgrowths projecting into free pore space and identified by well defined euhedral to subhedral faces to poorly developed thin and irregular shaped overgrowths. It was not possible to assign a notation to individual quartz overgrowths due to the uncertainty of repetitive correct identification.

Mica grains were seen to be in a stage of high corrosion and any discrete mica flakes which could be identified were highly deformed typically bent between grain contacts (Plate p3.6.5b). Similarly, feldspars were seen to be in advanced alteration to finer groundmass identified as interstitial clay. Largely, feldspars could not be resolved to being specifically identified. The fine clay fraction was recorded as being interstitial to corroded micas and feldspars and appeared to occlude free pore space and line quartz overgrowth and detrital grain boundaries to reduce porosity.

3.6.6 Diagenesis of Alwyn South

Early diagenetic features observed in the reservoir sands of Alwyn South differ slightly from the succession recorded in Alwyn North. Mechanical compaction effects are more evident in the sands of Alwyn South with a tighter packing character and more sutured grains being observed. Micas which are preserved show a high degree of deformity and feldspars also appear to be etched. No early silification phase was recorded and thus the potential porosity protection from mechanical compaction effects was not afforded in the Alwyn South sands.

Deformation of micas and feldspars coincidental with the suturing and packing of quartz grains would likely be followed in the paragenetic sequence by the dissolution of the micas. As micas tend to be susceptible to alteration upon interaction with hydrous fluids, this dissolution phase would tend to occur on exposure to fluid saturation. This stage of chemical diagenesis would free some pore space through the dissolution of the micas and then by the dissolution of the feldspars to create a degree of secondary porosity. However, any porosity developed by this process is masked by the subsequent and dominant authigenic quartz overgrowths.

These quartz overgrowths are seen to be a complex arrangement of differing growth patterns and intensities. The complexity of these individual quartz growth phases may suggest the periodic precipitation of solutes to develop an overgrowth. Then the source of the precipitates is retarded or that conditions in the reservoir sequence for

the precipitation of these minerals alters to inhibit authigenic growth. The pattern and complexity of the overgrowths suggests such a mechanism whereby the authigenic quartz part of the diagenetic sequence grows in relatively distinct phases. Such a mechanism may invoke a periodic exposure to a migrating fluid rich in solutes or a fluctuation in reservoir conditions and that the diagenesis is sensitive to such fluctuations.

Similar to the quartz overgrowths in Alwyn North, the relative amount of authigenic quartz identified in Alwyn South sands is unlikely to support a local source for the precipitating solutes. A more reasonable inference is that solutes available to precipitate as authigenic quartz in the reservoir section have been migrated into the area of diagenetic occurrence.

3.6.7 Petrography of Alwyn South East (wells 3/15-3 and 3/15-4) Plates p3.6.7a, b and c

The petrography observed in the two observed Alwyn South East wells constitute a mineral framework similar to that of Alwyn South. Texturally, the sands of Alwyn South East observed here shows a sub-maturity composed of a largely polymodal sediment population but the quartz grain population shows an overall unimodal grain size (medium grained). The sands can be described as moderately well sorted. Grain shape is largely based on the dominant population of quartz grains which show a sub-rounded to sub-angular shape. There appears to be no fabric and grains are not oriented in any fashion. The packing characteristics of the sands show the presence of deformed and sutured grains but less so than recorded in Alwyn South (Plate p3.6.7a).

The mineral composition is similar to that of Alwyn South but a notable difference is the lack of complexity of quartz overgrowths. The overgrowth pattern appears relatively consistent for at least the first two overgrowths which grow in a regular fashion outward into free pore space. In similar notation to that used for the quartz overgrowths identified in Alwyn North, a QA1 and QA2 overgrowth can be observed (Plates p3.6.7b and c). QA1 is identified as an enveloping authigenic quartz phase which tends to be a thin but euhedral faced overgrowth dissimilar to the peloidal QA1 overgrowth of Alwyn North. QA2 typically uses QA1 as a template for syntaxial growth into pore space and also is terminated by euhedral to subhedral boundaries except where these boundaries are compromised by another authigenic phase. QA1 and QA2 are used for fluid inclusion location and reference in section 3.7.

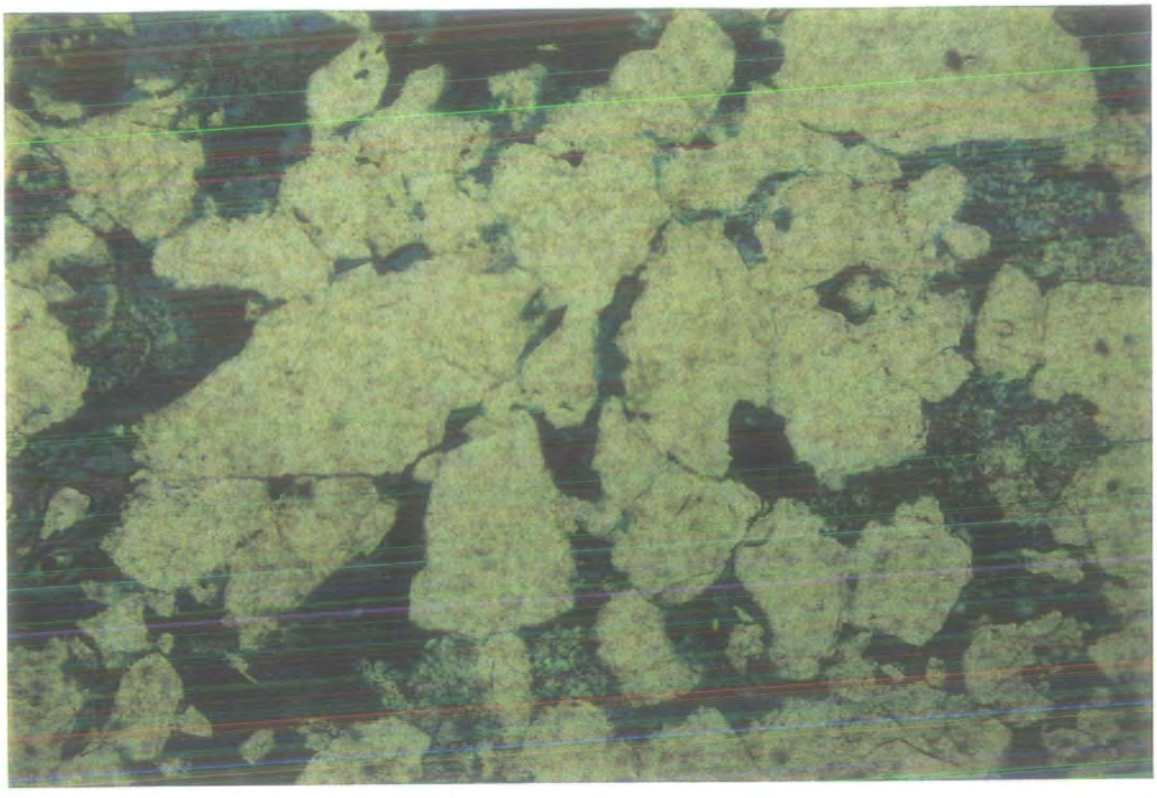

Plate p3.6.7a - 3/15-4 (3266m). Greater compaction effects and contacts per grain compared to 3/9a-6 (3190m). Also higher clay content lines pore throats reducing permeability. Field of view 3mm

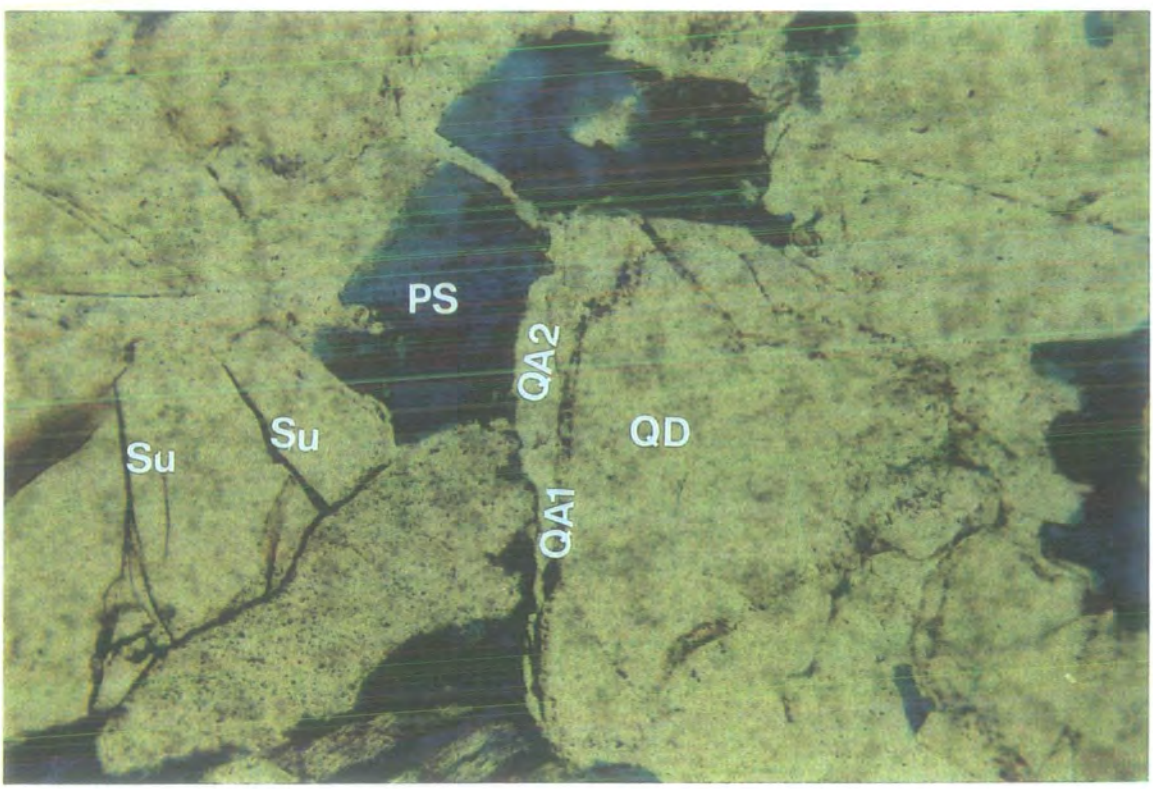

Plate p3.6.7b - 3/15-4 (3250m). Original detrital quartz grain (marked QD) depicted in outline by dust rim of fluid inclusions of QA1. A second more prominent QA2 syntaxial overgrowth grows into free pore spce (marked PS). High amount of suturing and grain fracturing seen by sutures (marked Su). Field of view 1.2mm

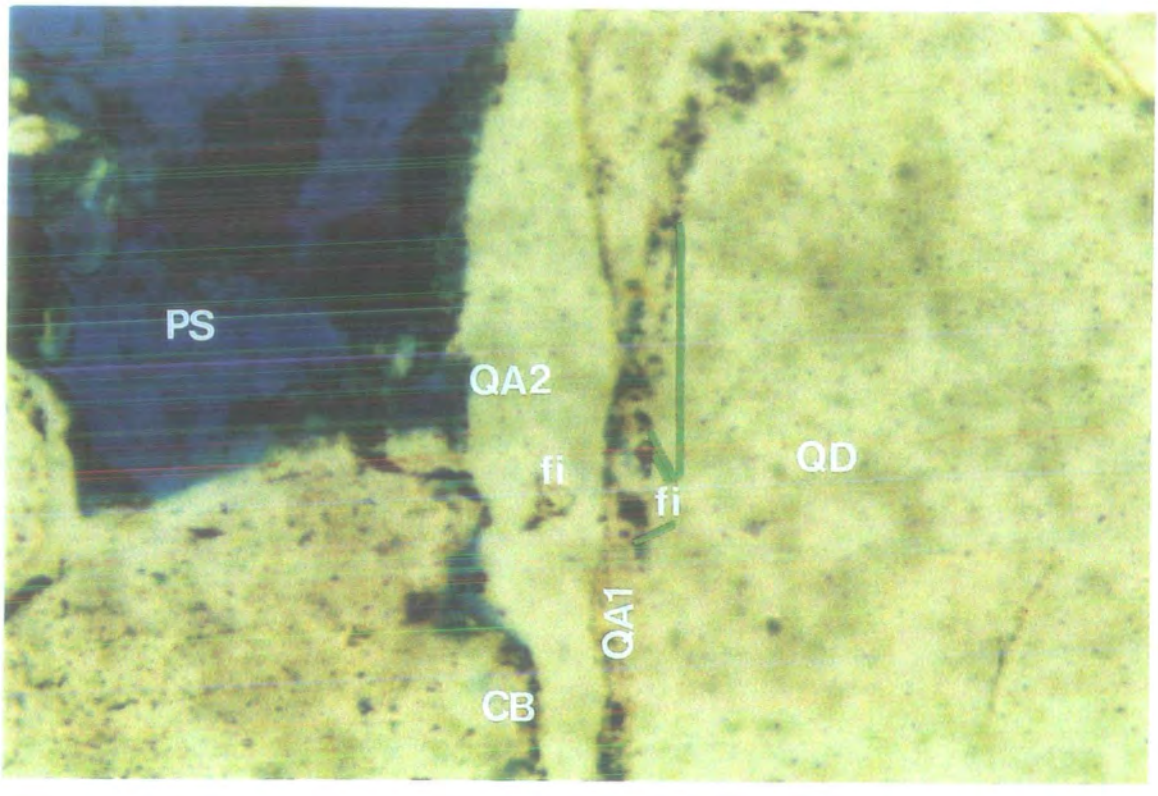

Plate p3.6.7c - 3/15-4 (3250m). Close up of Plate p3.67b showing the QA1 and QA2 fluid inclusion relationship. QA1 inclusions located along and sub-parallel to detrital grain (marked QD). QA2 inclusion is oblate in shape and is located interstitially in the larger QA2 syntaxial overgrowth. Field of view 0.48mm

The clay matrix is recognisable as a fine ground mass but does not constitute as much of the mineral composition as was seen in Alwyn South. The clays appear to have an intimate relationship with corroded and etched feldspars and micas but also appear to occlude and line free pore space without any apparent relationship to a parent grain. This is a similar observation to that seen in the clays of Alwyn South.

Porosity relationships are observed in the range of 11% (3352m sample, well 3/14-3) to 20% (3250m sample, well 3/14-4)

3.6.8 Diagenesis of Alwyn South East

The interpretation for the paragenetic sequence observed in Alwyn South is also interpreted to be similar to that of the Alwyn South East. However, the complexity of the quartz overgrowths noted in Alwyn South is less well developed in the Alwyn South East. The overgrowths are defined as QA1 and QA2 and are relatively consistent in occurrence. The inference is that these overgrowths developed in response to two separate events whereby solutes became available to the mineral framework to precipitate these overgrowths. The growth patterns showing euhedral face terminations also suggest relatively unrestricted growth into free pore space and only apparently limited by the amount of solutes available to precipitate.

The clay matrix was seen to have an even distribution between pore lining localities – being intimate with minerals such as feldspars and micas, suggesting that growth of authigenic clay was distributed between being alteration products of allogenic minerals and separate authigenic growth phases. The clay fraction not associated with a direct parent mineral may also infer growth due to precipitation from solution, perhaps the same fluid as that which is postulated to carry the silica solutes for quartz precipitation.

3.6.9 Summary and Discussion of Diagenesis

Early Diagenesis -

The three fields have each undergone a similar phase of early diagenesis where initial porosity loss was brought about by increasing burial stress and mechanical compaction. Effects of this mechanical compaction is to severely reduce primary porosity. Pressure solution arcs and grain suturing records this process in all fields. Early chemical diagenesis has also recorded a thin peloidal quartz overgrowth which coats detrital quartz grains. This observation is particularly apparent in Alwyn North. The early silicification has also been reported by Sommer (1978). The source of this early silica may be from remobilised quartz undergoing pressure solution. However, as the Brent Group sands are thought to represent facies born in a coastal to transitional marine

setting (Jourdan et al., 1987) circulating silica enriched meteoric waters could provide the silica precipitating at this early stage. However, Jourdan et al. (1987) suggest that the Alwyn reservoir sands were sealed by lower Cretaceous shales and thus were protected from any circulating meteoric waters. The Brent Group sands, being a widely dispersed facies group, could provide access to meteoric waters through sub-crops and subsequent flow through continous sand sequences. Oxygen isotopes may provide information as to the source of this early quartz cement to constrain the likely source of the fluid. Primary corrosion of unstable minerals such as micas may also have been influenced by early fluid movements.

Any secondary porosity created by pressure solution effects would largely be cancelled by mineral precipitation from these solute rich fluids. An effect of this precipitation would be to limit free pore space. However, as this early silicification phase does not follow any recognisable growth patterns and is relatively thin, this suggests a limited supply of precipitating silica.

Late Diagenesis -

Dominated by chemical effects, the late diagenetic phases record mineral precipitation and reprecipitation. Petrographic observations record the dissolution of feldspars and micas. However, the presence of multi-stage overgrowths around detrital quartz grains has been seen. Alwyn North and South East sands were observed to possess relatively well defined syntaxial overgrowths projecting into free pore space. It has been observed that the volume occupied by this authigenic quartz appears to be larger than the volume lost through feldspar dissolution and pressure solution effects. This suggests the import of mineral solutes from another area. Overgrowths define discrete mineral growth phases and therefore may record the availability of silica rich fluid in separate events. Jourdan et al. (1987) suggest an external fluid input from a distal source to account for these authigenic quartz overgrowths. External fluids may periodically invade the reservoir sequence at separate intervals to account for the repeated quartz overgrowths.

The complexity of quartz overgrowth development in Alwyn South sands suggests a similar type of diagenetic mechanism operating for Alwyn North and South East. However, the complexity of the authigenic quartz suggests the reservoir sands were subjected to many silicification events. Hogg et al. (1987) using CL techniques also recognises this overgrowth pattern in Alwyn South. Hogg et al. (1992) detailed complex zonation and although these zones could not be verified in this study, it is likely that they result from separate fluid events to cause complex diagenetic growth.

The relatively high clay content recorded in Alwyn South agrees with observations made by Hogg et al. (1992) who observe increasing authigenic illite in wells in close proximity to a fault zone. Hogg et al. (1992) interpret this intense illite growth as a result of focused fluid flow along the fault plane which acts as a conduit for fluids rich in diagenetic solutes. This type of fluid movement, accessing fault planes, suggest that the imported source of silica and other diagenetic minerals are from distal areas. Jourdan et al. (1987) record the poorest porosity and permeability in well 3/14a-8. This well also lies in close proximity to a fault zone and may account for the intense diagenetic sequence recorded in this field.

3.6.10 Implications from diagenesis for fluid flow

Identification of the source of the solutes and mineral phases in section 3.6.9 is important as the source of diagenetic fluids could identify likely migration pathways and a fluid flow history.

In common with observations made in sections 3.6.3, 3.6.5 and 3.6.7, Bjorlykke and Egeberg (1993) cite evidence for local dissolution of quartz by pressure solution but observe that the volume of silica released is difficult to quantify. Therefore authigenic quartz is difficult to interpret with respect to silica source. However, Bjorlykke and Egeberg (1993) have provided calculations to show if externally sourced quartz is introduced to a reservoir sandstone, the flux required for significant silica precipitation could be obtained on a local scale. Bjorlykke and Egeberg (1993) also calculate that a vast amount of calcite dissolution occurs with the introduction of a distally sourced advective flow of cooling quartz rich pore water. Bjorlykke and Egeberg (1993) conclude that the source of quartz cements in sandstones is predominantly local (<10m), sourced from within the sandstones, mainly by pressure solution. Aplin et al. (1993), using ^{18}O isotopes in Tertiary cements from North Sea reservoir sands show that compositional patterns of mineralising fluids also agree with Bjorlykke and Egeberg (1993) in suggesting silica transport mechanisms are restricted to reservoir-scale convection and diffusion. Bjorlykke and Egeberg (1993) argue that the import of silica by advection transport from sources outside the reservoir would require very large pore water fluxes ($>10^8 cm^3/cm^2$) to supply significant volumes of silica and that diffusion of silica in pore water is insignificant as a mechanism for long distance (>10-100m) transport of silica.

Robinson and Gluyas (1992) interpret fluid inclusion data which indicates that quartz cements in sandstones grow during discrete, geologically rapid events and not

constantly through the burial history of the sandstone. Such geological events may be similar to that described by Burley et al. (1989) whereby intense diagenesis is a result of mass fluid flow entering a reservoir under pressure typically acting through a fault zone. This would suggest a distal source for diagenetic fluids and minerals such as silica, entering the reservoir through repeated injections of silica rich fluids. Hogg et al. (1992) suggest that such a fluid injection mechanism may be represented by the complex and multiple zonation of quartz cements identified in the reservoir sands of Alwyn South.

There appears, then, to be two schools of thought on the source of imported authigenic silica into the reservoir sands. The calculations made by Bjorlykke and Egeberg (1993) and ^{18}O isotope interpretation by Aplin et al. (1993) infer a local source of silica. Burley et al. (1989) and Hogg et al. (1992) explain observations of anomalously high fluid inclusion temperatures and complex authigenic quartz zonation as a result of repetitive fluid pulses..

3.6.11 K-Ar dating of authigenic illite

It is possible to constrain certain diagenetic mineral phases, and therefore constrain the paragenetic sequence, in a temporal sense. Increasing the saturation of hydrocarbons in a reservoir has the effect of retarding quartz diagenesis before eventual termination (Saigal et al., 1992). Bjorlykke and Egeberg (1993) also recognise that quartz cementation will progress at a reduced rate under oil saturation and that increased oil saturation will have the effect of terminating any further quartz cement growth. Oil saturation may, therefore, halt reservoir diagenesis and the effect of early oil influx into a reservoir sand will tend to protect porosity and permeability by restricting/halting mineral phase growth by precipitation from circulating diagenetic fluids.

Authigenic illite, which has grown co evally with quartz (Hogg et al., 1992) can be used for K-Ar dating. This dating of the illite can effectively date the influx and saturation of hydrocarbons into the reservoir. Hamilton et al. (1989) report that authigenic illite is suitable for radiometric age determination by the K-Ar method and ceases to form if ambient aqueous pore water is displaced by hydrocarbons.

Dalrymple and Lanphere (1969) report the theories and assumptions of K-Ar dating which are summarised by Faure (1986) and Montigny (1985).

K-Ar dating of illites have been interpreted for wells in the Alwyn area. Jourdan et al. (1987) have ascribed dates of 65-75Ma in Alwyn North wells 3/9a-1, 3/9a-4, 3/9a-6

and 3/9a-8. Dates for the Alwyn South structure vary between 45-35 and 55-45Ma (Jourdan et al., 1987). Hogg et al. (1992) have investigated the authigenic illite fraction from four Alwyn South wells (3/14a-7, 3/14a-8, 3/14a-11 and 3/14b-9). Hogg et al (1992) interpreted a range of dates for illite formation between 66-38. These dates are summarised in Fig.3.6.12a. Age dates documented by Jourdan et al. (1987) for wells 3/15-2 and 3/15-4 are in the range of 55-45Ma which are similar to illite ages from nearby wells west of the Alwyn South East structure (3/14a-4 and 3/14a-6).

The information that can be interpreted from illite ages in the three Alwyn fields can be used to time the influx of hydrocarbons into the three structures. From the above information, Alwyn North is interpreted as being saturated with oil at 75-65Ma, Alwyn South at 55-45 (wells 3/14a-8, 3/14a-11, 3/14a-7, 3/14a-3) and 45-35 (wells 3/14b-9, 3/14a-10, 3/14a-12); these data are a combination from Jourdan et al. (1987) and Hogg et al. (1992). The Alwyn South East structure is interpreted as being filled with oil at 55-45Ma.

3.6.12 Reconstruction of fluid movements from geochemical, basin modelling, diagenetic and illite age dating interpretations

From the interpretations made on maturity data, burial history and maturation modelling, diagenetic observations and illite age data, it is possible to combine these various parameters to develop a model for the overall fluid flow pattern in the Alwyn area.

Maturity Information -

Sections 3.5.4 and 3.5.5 detailed and interpreted data trends based on Ro, Tmax and biomarker information. Ro and Tmax inferred that only the Kimmeridge Formation in the Alwyn South structure was at an equivalent stage of maturity to generate and expel oils (0.7-1.2%Ro). Ro and Tmax data recorded early mature equivalent maturities for the organic rich Kimmeridge Formation in the Alwyn North and South East wells. This inferred that oils reservoired in the Alwyn North and South East reservoirs were not generated locally and had migrated from another source area. Biomarker information on the reservoired oils showed a pattern of increasing maturity through the Alwyn North and South East fields toward the south and east. The likely source area was inferred to be the Viking Graben from these maturity trends for reservoired oils in the Alwyn North and South East fields. Biomarker analyses of the Alwyn South oils did not define any trend in maturity. This may be a consequence of local oil

generation, as suggested by the Ro and Tmax data, or by contamination and mixing of the reservoired oils through internal fluid circulation.

Basin Modelling -

Modelling of the three Alwyn fields seemed to agree with the maturity data from the geochemical analyses. Only the Alwyn South field was modelled to generate hydrocarbons from the Kimmeridge Formation and that this formation in the Alwyn North and South East fields are modelled as being in the early mature window only.

Using the geochemical interpretations to cite the likely source area for the reservoired oils of the Alwyn North and South East fields, seismic information was used to provide the information to model the Viking Graben depocentre. The burial history and superimposed maturation history was calculated. Calculations show that the Kimmeridge Formation was expelling hydrocarbons in the depocentre from approximately 90Ma. Transference of these hydrocarbons could be envisaged as migrating up dip to structural highs such as the Alwyn North and South East traps.

Diagenetic Interpretations -

The diagenetic sequence recorded, amongst other observations, the consistent and dominant occurrence of authigenic quartz cements. These quartz overgrowths are interpreted to have developed late in the diagenetic sequence. The source of this silica necessary to precipitate the quartz overgrowths is uncertain. It is inferred that pressure solution effects, alone, could not supply the necessary volume and amount of authigenic quartz now observed in the reservoir sands. However, whether the imported silica and associated solutes are from a local source (<10m) or distal (10-100m or greater) source is uncertain.

Using the interpretations of hydrocarbon flow from the geochemical information and the relationship of increasing intensity of diagenesis near fault zones acting as fluid entry points noted by Hogg et al. (1992), it is possible to infer a distal source for the silica rich diagenetic fluids. In the Alwyn field area, the relationship of diagenesis with increasing illitisation and repetitive authigenic quartz zones observed by Hogg et al. (1992) would infer a distal rather than local source for the diagenetic fluids. These fluids may be operating under similar mechanisms and controls of migration as the hydrocarbons.

K-Ar dating

The dating of authigenic illite infers different timing of oil saturation into the reservoirs of the three Alwyn fields. Alwyn North is interpreted to have filled first followed by Alwyn South and South East reservoirs which are approximately contemporaneous with each other. No distinct trends can be observed within individual fields but illite dates recorded by Hogg et al. (1992) suggest that hydrocarbons and associated diagenetic fluids have migrated up the Ninian Fault Zone (Fig.3.6.12a) and then invade the structures in a sequential manner. This would account for the distribution and trend of illite dates becoming progressively older heading north and west away from this entry point.

The geochemical, basin modelling, diagenetic and K-Ar dating observations and interpretations infers that the hydrocarbons have been sourced in the Viking Graben depocentre to the south and east of the Alwyn field area. Migration pathways are identified as heading north and west across the three individual fields to fill the reservoirs in the structural traps at different times. The fluid flow inferred for the Alwyn South, North and South East fields are shown in Figs.3.6.12a, b and c respectively.

3.7 Pressure Modelling

3.7.1 Introduction

Constraints have been put on the origin of the hydrocarbons in the Alwyn reservoirs and fluid movements have been postulated for these hydrocarbons and also associated diagenetic fluids (section 3.6.12). The fluid flux into the three fields has been interpreted and reconstructed using data and information provided by petrophysical observations and associated secondary mineralogical work tied with independent basin modelling. All of these previous observations have tended to support the influx of hydrocarbons into the reservoir, at least for the Alwyn North and South East fields, from a distal off-structure source area to the east. Geochemical, basin modelling and diagenetic observations identified the source of the fluids as being from the Viking Graben which was inferred to be the source area for compactional fluids as well as hydrocarbons. Apart from being the origin of these fluid phases, the area was also identified as being a possible and likely source of overpressure generation due to the thermal alteration of hydrocarbons undergoing progressive heating. The genesis of the overpressure in the reservoirs has been postulated and associated with various mechanisms (section 2.1); Rapid burial of argillaceous sequences can build anomalous amounts of pressure due to compaction disequilibrium (Magara, 1974; Dutta, 1983; Mann and Mackenzie, 1988). The potential of hydrocarbon cracking during the

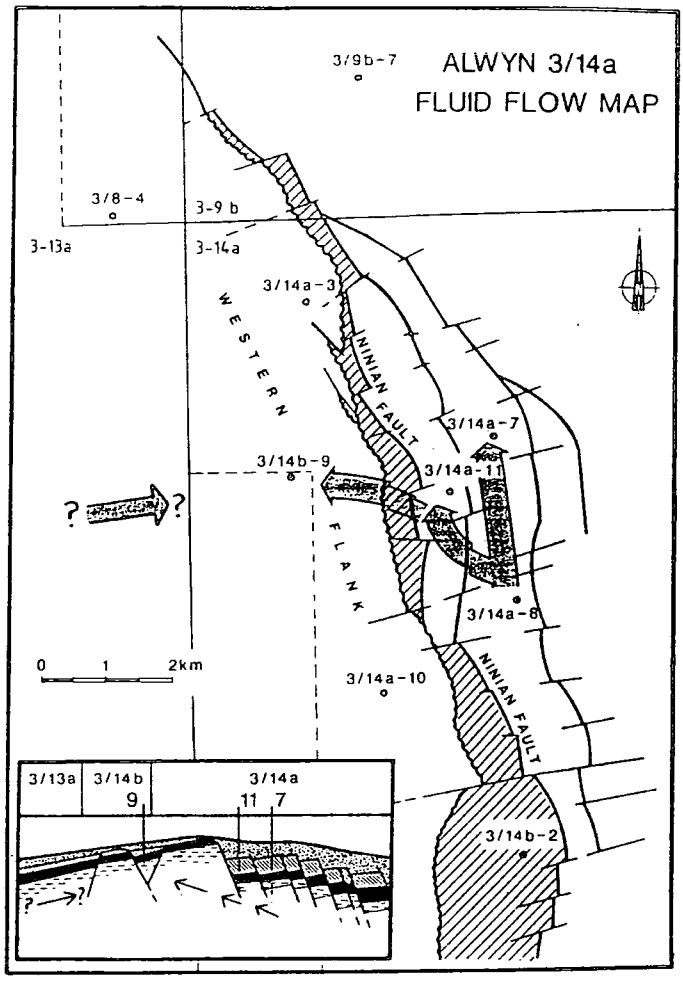

Geochemical Parameter

Well	Illite Ages	Tm/Ts	Ts/Tm+Ts	D/D+G	Ip
3/14a-8	60.3-47.1	0.65	60.5	55	
3/14a-11	59-43	0.85	52.5	55	1.45
3/14a-7	56.2-37.9	0.6	52.5	51	1.5
3/14b-9	47-38.8	0.65	61	53	1.7

Illite data from Hogg, et al. (1992)

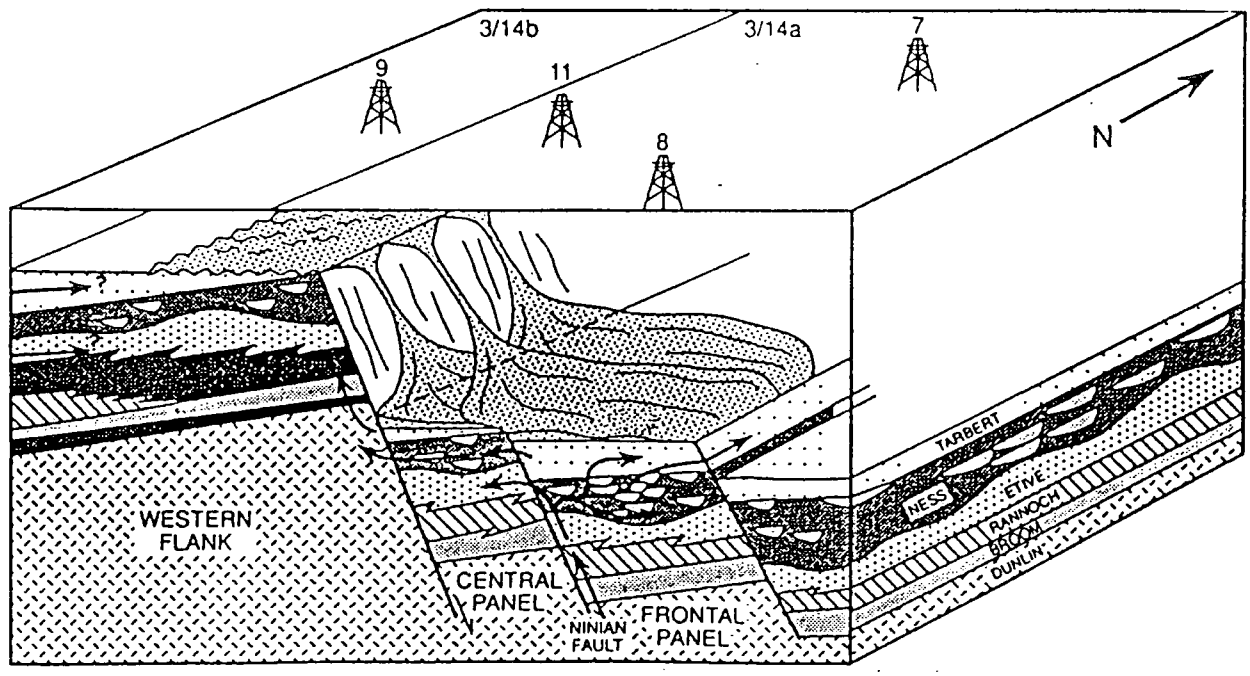

Fig.3.6.12a - Fluid flow map for Alwyn South constructed the combination of illite age dates, geochemical maturity modelling, diagenetic interpretation and basin modelling

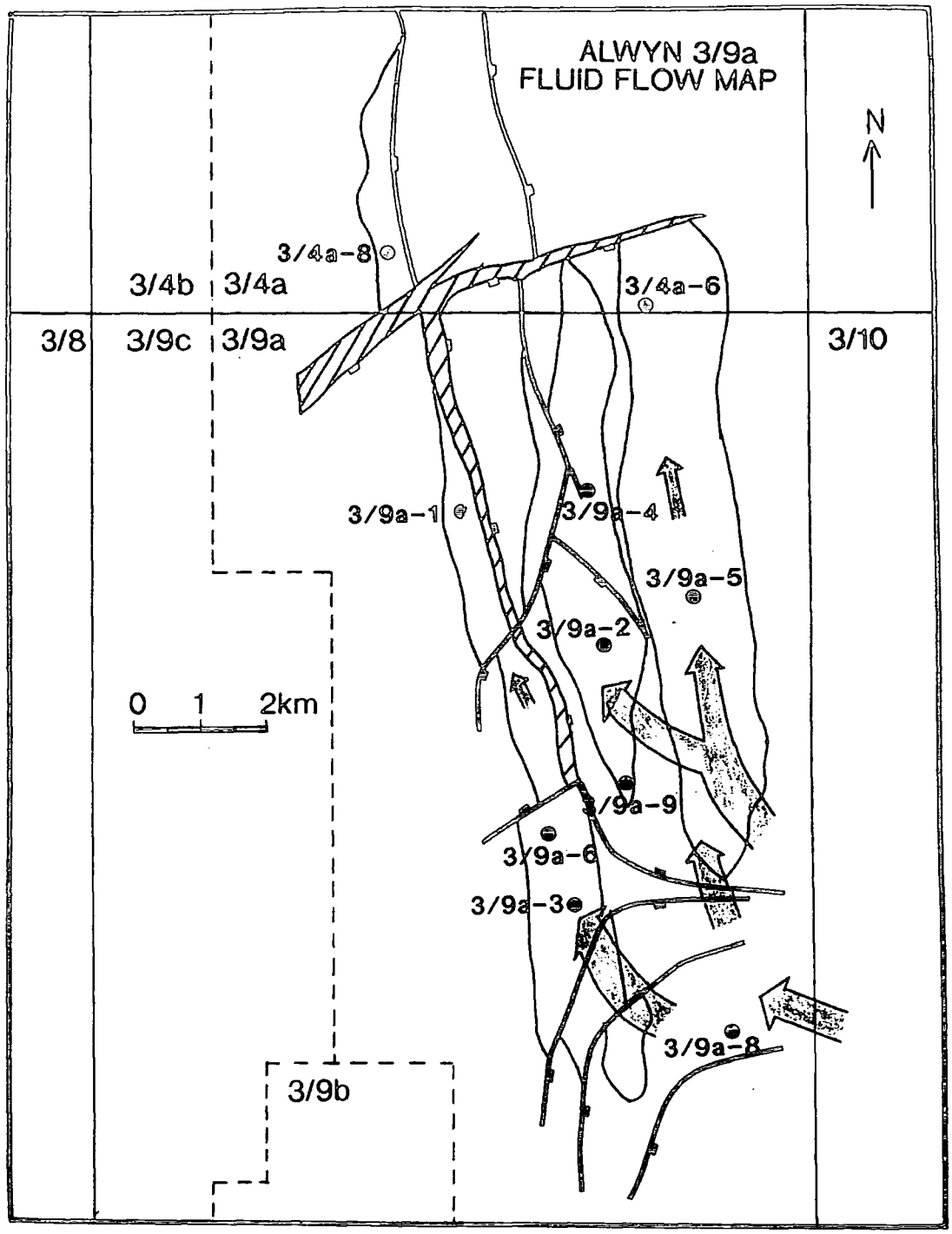

Geochemical Parameter

Well	Illite Ages	Tm/Ts	Ts/Tm+Ts	D/D+G	Ip
3/9a-3		0.3		54	1.5
3/9a-6	75-65	0.65	55.3	53	1.4
3/9a-2		0.75	54	52	1.1
3/9a-5		0.65	53	53	1.15
3/9a-4	75-65	1.3	50.4	50.5	0.85
3/9a-1	75-65				1.1

Illite data from Jourdan, et al. (1987)

Fig.3.6.12b - Fluid flow map for Alwyn North constructed the combination of illite age dates, geochemical maturity modelling, diagenetic interpretation and basin modelling

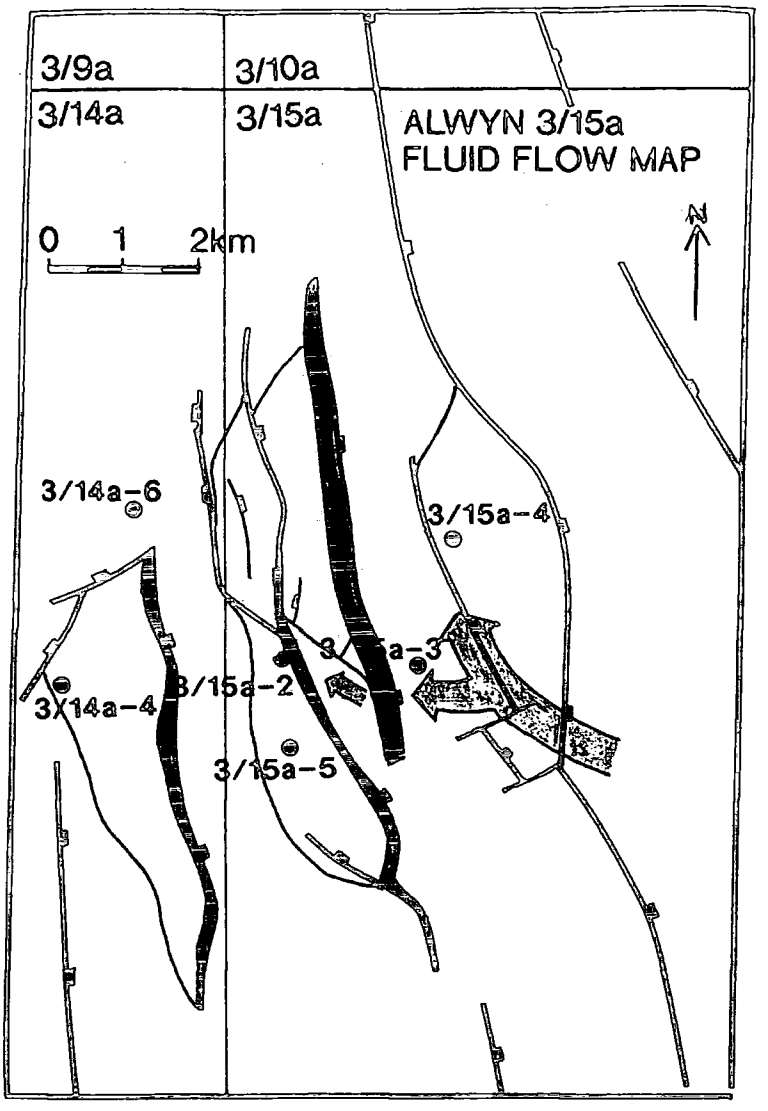

Geochemical Parameter

Well	Illite Ages	Tm/Ts	Ts/Tm+Ts	D/D+G	Ip
3 15-3					1.6
3 15-4	55-45				1.55
3 15-2	55-45				1.45

Illite data from Jourdan, et al. (1987)

Fig.3.6.12c - Fluid flow map for Alwyn South East constructed the combination of illite age dates, geochemical maturity modelling, diagenetic interpretation and basin modelling

thermal transformation of liquid hydrocarbons to gas (sections 2.4 and 3.5.6.2) has been identified as an important primary source of overpressure (Barker, 1987) and, in this study, the Viking Graben basin has been modelled to be in an increasing state of maturation since approximately 90Ma (Fig.3.5.6.3a) with the onset of gas generation (for the Kimmeridge Formation) and thus potential overpressure development at 53Ma. Also, conditions for the mineral transformation of smectite to illite (Boles and Franks, 1979) with an associated volume increase (Bruce, 1984; Colten-Bradley, 1987) are favourable with peak ordered illite formation documented as being in the range of 110-120°C (Boles and Franks, 1979) being timed at 80-74Ma and 87-80Ma (Fig.3.5.6.3a) for the key shale rich horizons of the Kimmeridge Clay and Heather Formation respectively in the Viking Graben depocentre. So the potential for overpressure generation in this basinal area can be recognised.

Any excess pressure developed in the system would try to escape as the system will constantly try to re-equilibrate in order to reachieve a state of pressure equilibrium. This means, then, that any overpressure developed would tend to dissipate. A conduit or avenue for pressure transference or release out of the basin deep can be envisaged as the most accessible, porous and continuous aquifer. In relative terms, the pressure developed in the organic rich, argillaceous and deeply buried Kimmeridge, Heather Formations and lower Cretaceous shales would tend to focus released pressure and released fluids through the sand members of the Brent Group and Statfjord Formation. These sands of the Brent Group are regionally extensive and could easily be seen to act as a continuous conduit out of the depocentre to more distal updip areas such as the fault blocks east and west of the Viking Graben trough. One of these trapping fault block systems is the Alwyn field. Since the source of the fluids responsible for reservoir diagenesis are interpreted to have a distal rather than local source (section 3.6.10, 3.6.12) transference of any pressure would drive these associated fluids through the reservoir sands. These fluids can be identified in the diagenetic sequence. These type of fluids have been widely recognised as forming fluid inclusions (Rhoedder, 1984) in the diagenetic sequence. These inclusions are commonly trapped in diagenetic mineral overgrowths such as quartz, calcite, feldspar, barite and ankerite.

The diagenetic relationships of mineral phases have largely been discussed in section 3.6 with respect to fluid movements in a relative temporal sense. Identification of fluid inclusions - whether they are hydrocarbon or brine rich - in respective mineral phases and fractures can be interpreted in terms of fluid type being trapped and precipitated coincidentally with a certain diagenetic mineral phase. This means, then, that if the temperature of these fluid inclusion phases can be calculated, a constraint can be made

regarding temperature in the reservoir/temperature of fluid flow through the reservoir at a particular time in the diagenetic history. However, by making assumptions and following criteria as initially postulated by Narr and Burrus (1984), the pressure of these inclusions can also be estimated. Identification of palaeopressure of fluid inclusion populations in the diagenetic mineral phases, and therefore the paragenetic sequence, can lead to the construction of a pressure history of the reservoir. When coupled with maturation studies, burial history and secondary mineralogical observations, these fluid inclusion studies can provide a unique interpretation in terms of pressure and the relationship with diagenesis in the reservoir section.

3.7.2 Fluid Inclusion Equipment

The fluid inclusions were recognised, defined and attributed to a particular overgrowth population by means of normal petrographic techniques using a Nikon Optiphot microscope with a x15 ocular and a long distance substage condenser. The relatively complex zonation achieved by the use of hot-CL studies (Hogg et al., 1992) were not available.

3.7.3 Fluid Inclusion Selection

Samples selected for the inclusion study represented the main authigenic mineral phases. Selection was also based on density of inclusions in a single population to ascertain an unbiased range of temperatures. Selection was also based on a vertical interval which tried to encompass as much stratigraphic coverage in the reservoir section as possible. All fluid inclusion temperature data identified at specific diagenetic locations with associated wells and depths are documented in Appendix 4.3. Populations of inclusions were seen to cluster at certain depths observed by the mass of inclusions recorded in the QA2 overgrowth (section 3.6.3) at 3200m, 3240m and 3300m in the 3/9a-6 well, at 3440m and 3480m in the 3/9a-5 well, at 3359m in well 3/15-3 and at 3250m in well 3/15-4. Walderhaug (1990) identified the density of inclusions increasing toward the top of the reservoir section. No such observation was made in Alwyn but clustering of data was common as documented above. Fluid inclusions were identified, petrographically, exclusively in authigenic quartz overgrowths. Since quartz overgrowths featured largely throughout the three fields, it was possible to assimilate a large amount of data from Alwyn North and South East. Data collected from the South field provided insufficient and lacked consistency in overgrowth patterns (section 3.6.5) to make positive interpretations regarding the pressure history. However, Hogg et al. (1992) and Jourdan et al. (1987) have attempted an interpretation of the temperatures recorded in the South field based on fluid inclusion temperature data.

Fluid inclusions identified and used for interpretation in the pressure analysis study must conform to certain requirements . The inclusions must be trapped in an authigenic mineral phase - such as an overgrowth - to avoid interpretation of a detrital/allogenic mineral. The inclusions must still be intact and not have been subjected to any physical volume change or 'necking' (Rhoedder, 1984; Burley et al., 1989). For the purpose of pressure interpretation, a single population of inclusions must contain both 2 phase hydrocarbon and brine inclusions (Narr and Burrus, 1984).

3.7.4 General Features of trapped inclusions

The size of inclusions trapped in the diagenetic sequence of certain minerals, such as anhydrite, can exist up to the mm scale, as a consequence of the particular conditions of trapping. In the petroleum reservoir inclusions rarely exceed 50μm and commonly fall in a range of 0.5-10μm. Scanning electron microscope (SEM) work has identified many inclusions below this lower limit (Rheodder, 1984) but these are not visible under the standard optical equipment used in these microthermometry studies. The inclusions found in the Alwyn reservoir sands are found exclusively in quartz overgrowths and are less than 5μm, commonly having a median size of 1.5-2μm. For accurate measurements, it is obviously the larger inclusions which are used as the most dependable sources of the T(hom) -homogenisation temperatures - and T(f) - freezing temperatures. The morphology of these inclusions is variable but commonly the most reliable inclusions tend to be ovoid or oblate. However, the shape of the inclusions can lead to interpretations regarding the content and composition. Pagel and Poty (1984) report that aqueous inclusions often show an irregular shape, CO_2 rich inclusions tend to take the form of negative crystals and methane inclusions may have a very irregular shape. However, other factors alter the form of inclusions such as the degree of evolved temperature and pressure leading to 'necking down' or decrepitation phenomena. The inclusions in the diagenetic sequence in the Alwyn reservoir sands are commonly aligned along overgrowth boundaries with the long axis sub-parallel to the overgrowth boundary (Fig.3.7.4a, Plate p3.6.3c). However, less frequently inclusions located within the overgrowth tend to be a more regular ovoid shape (Fig.3.7.4a, Plate p3.6.7c). Identification and interpretation of the inclusion phases was achieved using the combination of optical microscopy (limited by microscope resolution) and ultra- violet (UV) fluorescence for hydrocarbon identification.

The number of physical phases identified in the inclusions were exclusively restricted to two - liquid and gas. No solid phases were identified in the Alwyn samples. Occasionally one phase inclusions were observed but these are seen to be metastable in

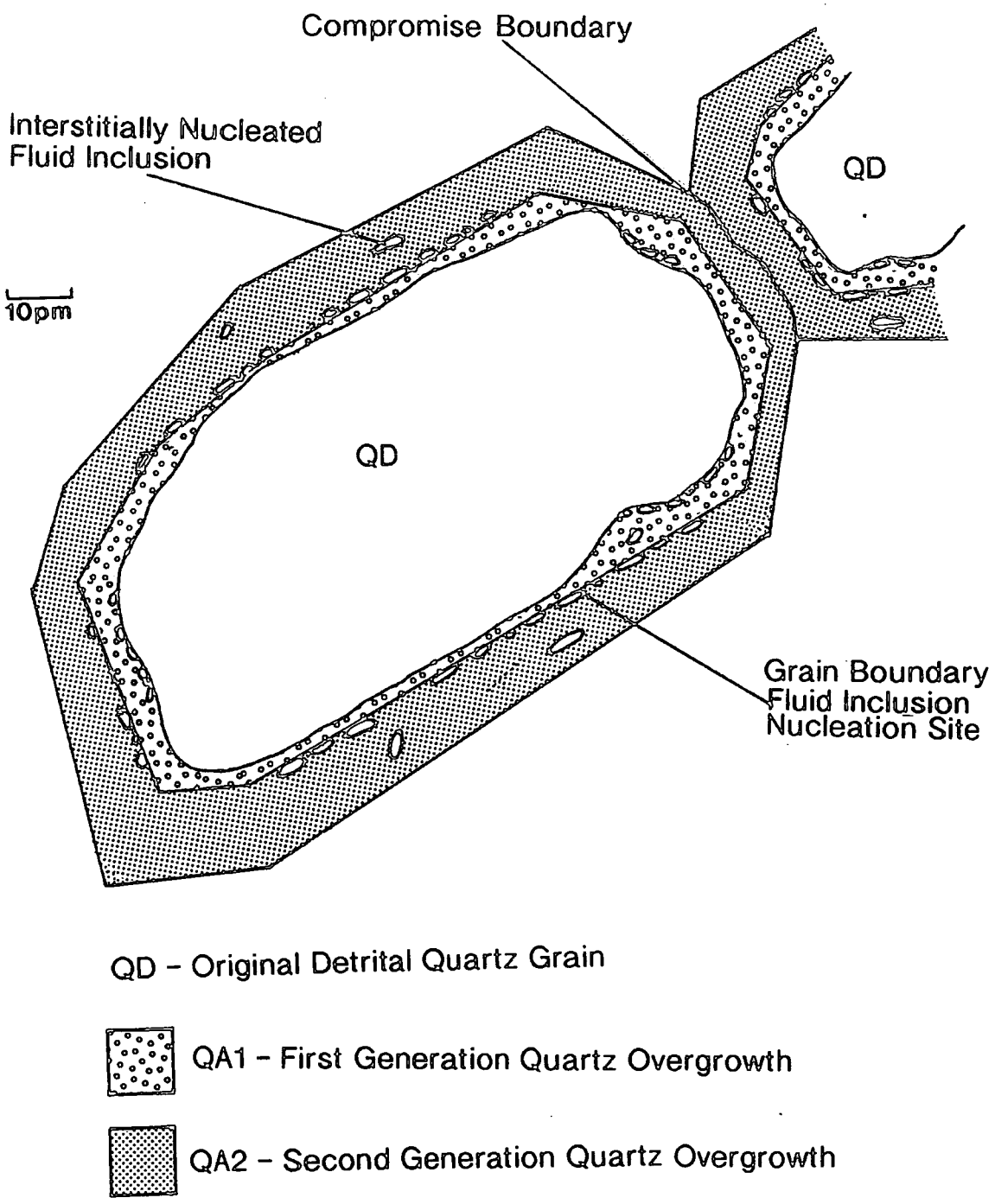

Fig.3.7.4a - The diagenetic position and notation of fluid inclusions nucleated in quartz overgrowths typically seen in reservoir sands of Alwyn South East

which the gas bubble may only seed at low temperatures or that these inclusions had been subjected to some sort of physical decrepitation. The chemical composition of the inclusions will be dealt with more thoroughly in the microthermometry section (3.7.6) especially with regard to specific hydrocarbon composition. Aqueous inclusions were the most frequently occurring fluid inclusions. Salinities were constant and reflected the presence of a saturated brine. Methane (CH_4) is assumed to be intimately connected and dissolved in the identified hydrocarbon phase.

3.7.5 Chronology and Paragenesis of the fluid inclusions

Since the common observation was that the majority of inclusions were nucleated at the interface of detrital grains and the first overgrowth or subsequent interfaces in the authigenic mineral phase, rather than being interstitial through the overgrowth, the populations have been documented with respect to overgrowth generations (Fig.3.7.4a) For instance, the temperature range for the fluid inclusion population QA1 equates to the generation of inclusions of inclusions nucleated between the detrital grain and the 1st quartz overgrowth (in common with observations and terminology in section 3.6.3). The 1st quartz overgrowth common to all reservoir sands in the Alwyn North area has been recognised as a thin pendant or peloidal cement (section 3.6.3) which tends to envelope rather than follow any epitaxial growth pattern onto free pore space. The populations and generations which have been observed in sufficient quantities and interpreted correspond to the QA2 in the Alwyn North Brent reservoirs and the QA1 and QA2 diagenetic positions in the Alwyn South East Brent reservoir sands (section 3.6.7).

3.7.6 Microthermometry

Certain assumptions regarding fluid inclusion observations and subsequent interpretations are necessary to avoid misinterpretation of fluid inclusion data. It is assumed that fluids within the inclusions were trapped as a single homogenous phase and the density and composition of this fluid has not changed since inclusion formation (Narr and Burruss, 1984). Essentially, the physical volume of the cavity and its contents must have been free from any effects of physical or chemical change. Therefore, fluid inclusions must have maintained constant volume since formation. The interpretation of the fluid inclusion temperature data in terms of associated trapping pressure also are subjected to certain assumptions which follow below.

The temperature of homogenisation between the liquid and vapour phase (T(hom)) of a fluid inclusion occurs when the vapour phase dissolves in the liquid and is considered the minimum trapping temperature of the fluid inclusion. All temperatures

were recorded from inclusions in quartz and individual inclusions consistently recorded the same T(hom) on repeated heating runs. This is most likely due to the crystal habit of quartz in that quartz does not possess a cleavage in which any leakage could propagate (Rhoedder, 1985). It is normal to record a range of T(Hom) values which reflect the temperatures of entrapment exclusive to the that particulat condition of diagenetic growth and fluid entrapment. A narrow range of T(hom) data reflects a relatively rapid precipitation event.

Osborne and Haszeldine (1993), however, interpret that fluid inclusion data recorded in quartz overgrowths in North Sea reservoir sands is unreliable. Osborne and Haszeldine (1993) interpret the spread of T(hom) data as the result of constant resetting of the larger inclusions through time in response to further burial and higher temperatures. Robinson et al. (1992) report evidence, however, that fluid inclusions trapped in quartz overgrowths are valid indicators of trapping temperatures. Robinson et al. (1992) report T(hom) with narrow distributions that are compatible with independent illite K-Ar ages and petrography. It is these observations that combined with the recognition of inclusions in a single sample set which also retain T(hom) distributions compatible with their sequential origin that Robinson et al. (1992) question the resetting arguements proposed by Osborne and Haszeldine (1993).

Narr and Burruss (1984) state that if the pressure of fluid during trapping was greater than the equilibrium vapour pressure then measured T(hom)s can significantly underestimate the temperature of entrapment. Therefore, a correction for pressure must be made on the basis of the pressure-volume-temperature (PVT) properties of the particular inclusion fluid - be it aqueous or hydrocarbon - to obtain an accurate estimate of temperature and ultimately pressure. Burley et al. (1989) have also recognised the need for pressure correction and recognise the significant degree of error which might be incurred due to the presence of saturated methane associated with the aqueous fluid phase.

Narr and Burruss (1984) follow the approach of constructing a pressure correction diagram based on the density of the fluids which were calculated from superimposing T(f) measurements on the system H_2O-NaCl (see Fig.3.7.6a). This density data can be applied to a pressure-temperature diagram for the range of T(hom) recorded. Fig.3.7.6b shows a hypothetical example. Narr and Burruss' (1984) approach is perfectly valid but in the presence of methane saturation (as inferred in the study of fluid inclusions in the Tartan field (Burley et al. 1989) and in this study) certain allowances and assumptions must be applied.

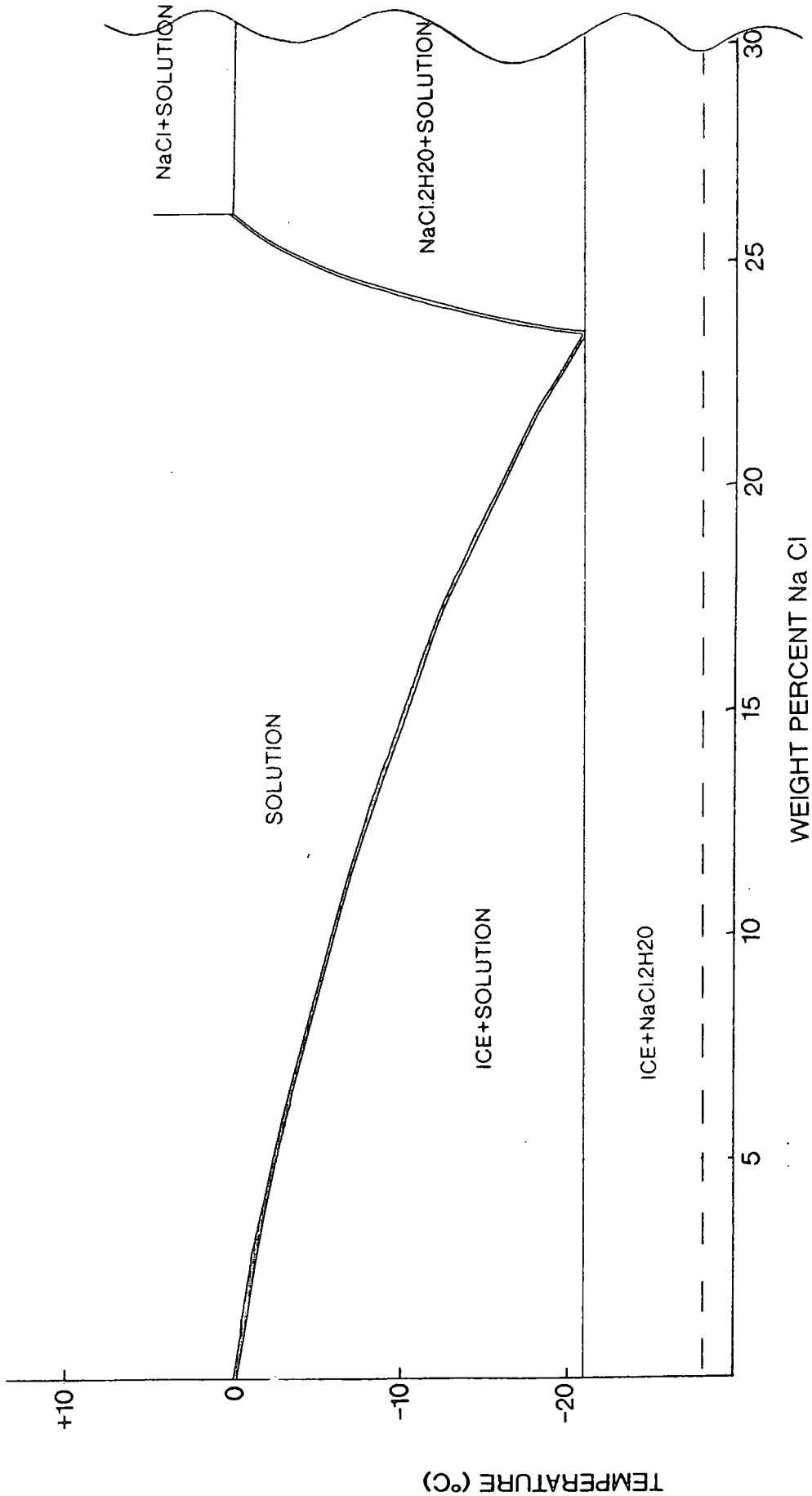

Fig.3.7.6a - The system H_2O - NaCl. To ascertain relative weight% NaCl of aqueous fluid inclsuion, freezing temperatures (T(f)) can be used. The recorded temperatures referenced on the y-axis can be projected horizontally across till it intercepts the coexistence/bubble point curve. This projects vertically downward to give the appropriate weight% NaCl for that particular brine

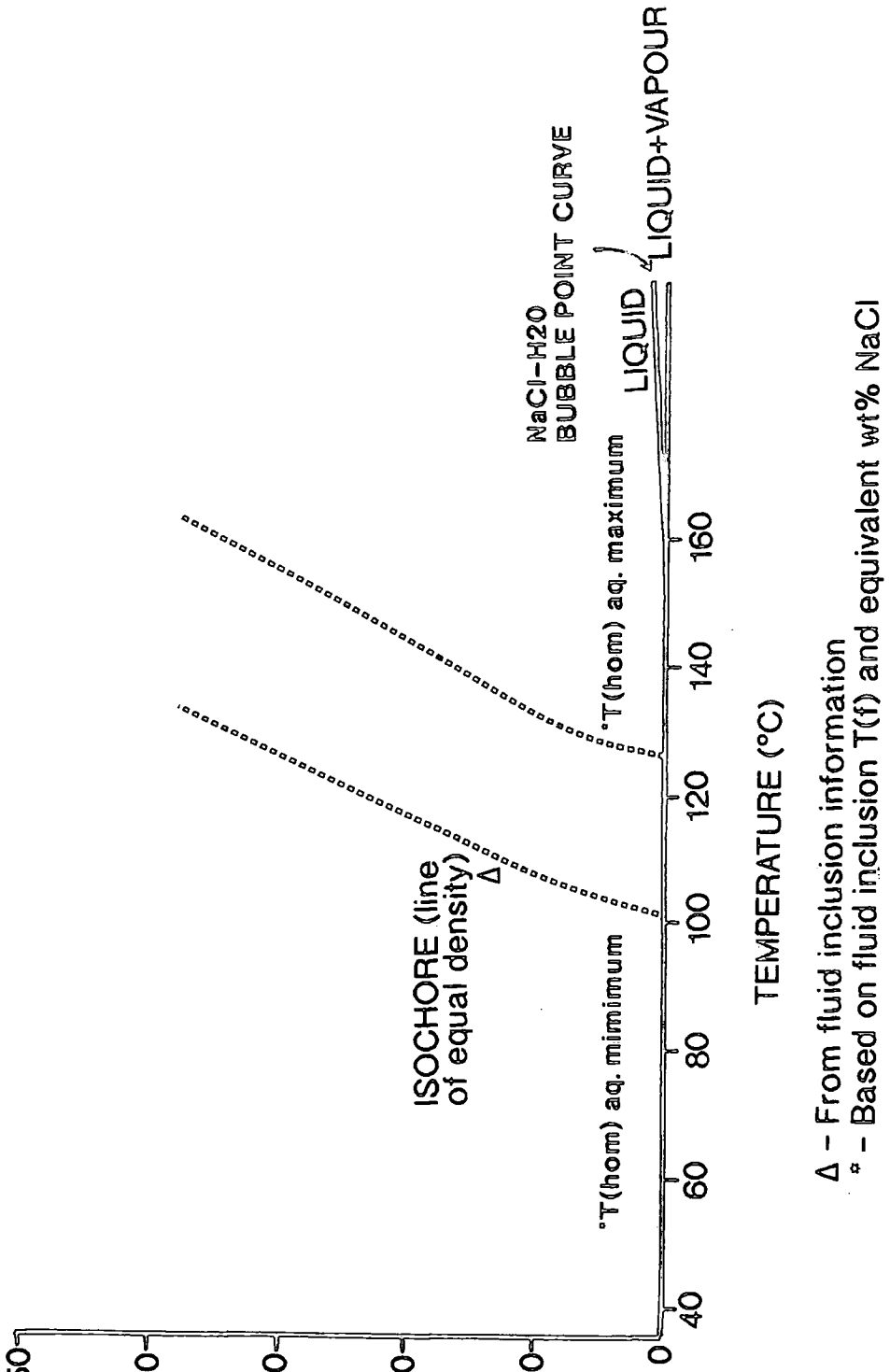

Fig.3.7.6b - Pressure versus temperature diagram showing a hypothetical example of isochores up from the bubble point curve, determined by their equivalent wt% NaCl (calculated from fluid inclusion T(f)

Burley, et al. (1989) state that, based on work by Mullis (1979) and applying data from Haas (1978), although the high levels of fluorescence preclude an estimation of CH_4 content within the trapped fluids, it is clear that significant quantities of CH_4 are associated with the hydrocarbons. Work conducted by Hanor (1980) and Burruss (1992) show that the effect of dissolved methane is to elevate the bubble point curve to a higher pressure regime in the pressure-temperature diagram so that the T(hom) would rise vertically to the new bubble point curve before the 'liquid only' field would be encountered and only then would the isochores deviate along the gradient dictated by their densities (see Fig.3.7.6c). Burley et al. (1989) introduced a 0.08wt% CH_4 into a theoretical example of temperature evaluation to illustrate that this amount comes close to saturation of the fluid. Therefore, based on the calculations by Burley et al. (1989), only a very small amount of methane associated with the trapped hydrocarbons is needed to saturate the fluid phase. This effect of methane saturation will become apparent when the recorded T(hom)s from the Alwyn reservoir sands are interpreted.

The QA2 generation inclusions in Alwyn North have the following information Fig.3.7.6d):
T(hom) of Aqueous Inclusions: 89-104°C
T(hom) of Hydrocarbon " : 69-79°C

The QA1 and QA2 generation inclusions in Alwyn South East have the following information Fig.3.6.7e):
T(hom) of Aqueous Inclusions: 116-128°C
T(hom) of Hydrocarbon " : 86-93°C

From petrographic observations in the reservoir sands of the North and South East fields at stratigraphic and depth intervals that varied across the field, there appears to be two distinct generations of inclusions with respect to their T(hom) temperature range. Material from the South field was not available for this type of interpretation. There appears to be an early set of inclusions trapped in QA1 overgrowths in the North field with a lower temperature range for both aqueous and hydrocarbon-rich inclusions than the inclusions at the QA1 and QA2 boundaries in the South East field which correspond to a higher temperature range. The distribution of T(hom) data is illustrated in Figs.3.7.6d and e.

Fluid inclusion homogenisation temperatures of aqueous and petroleum inclusions trapped simultaneously can provide information on the pressure of entrapment. Following a similar approach as utilised by Narr and Burrus (1984), the combination of

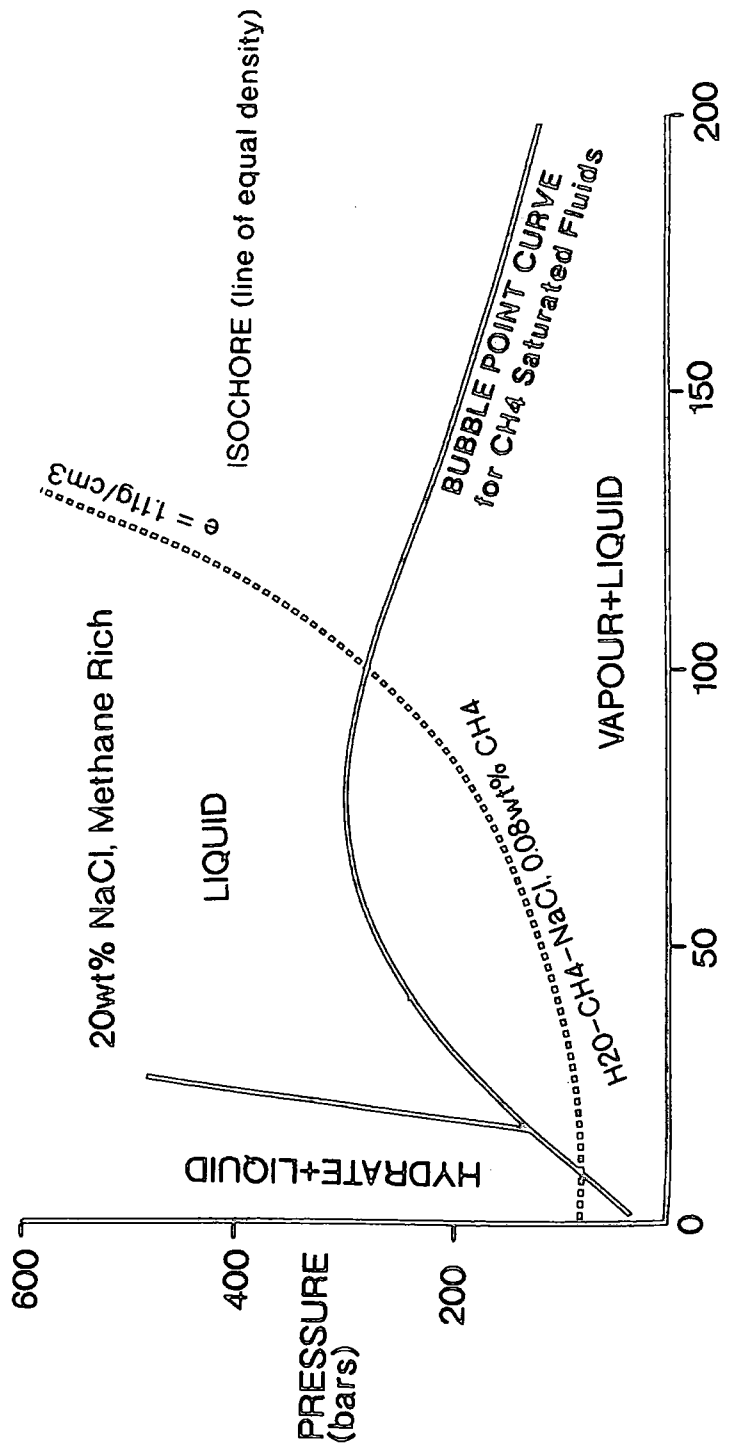

Fig.3.7.6c - Pressure versus temperature plot showing the bubble point curve for a methane saturated fluid with appropriate isochore of the system H_2O-CH_4-20wt%NaCl, 0.08wt% CH_4

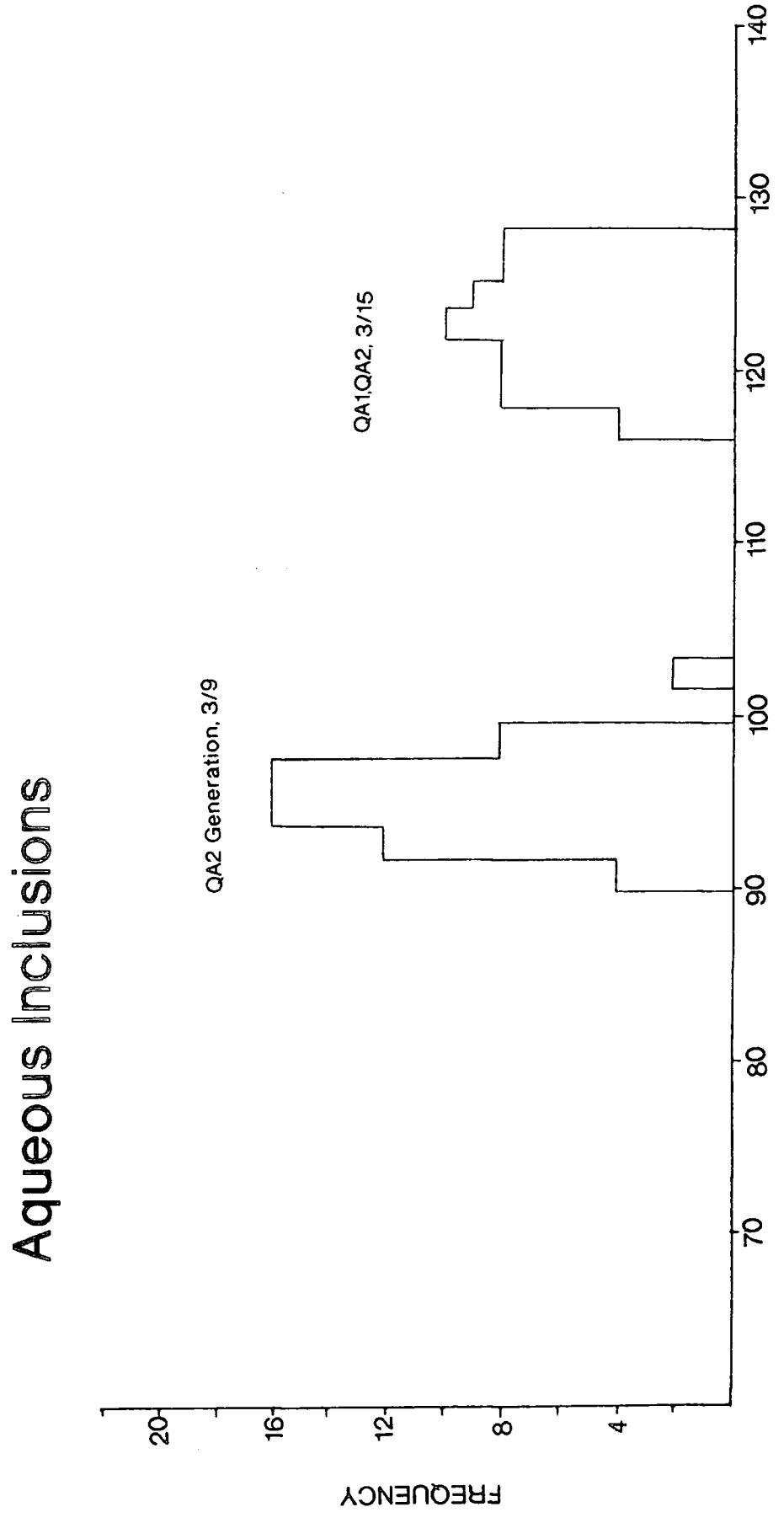

Fig.3.7.6d - Histogram representing homogenisation temperature (T(hom)) data range and frequency for aqueous fluid inclusions. Data collected from fluid inclusions in quartz overgrowths in Alwyn North and South East reservoirs

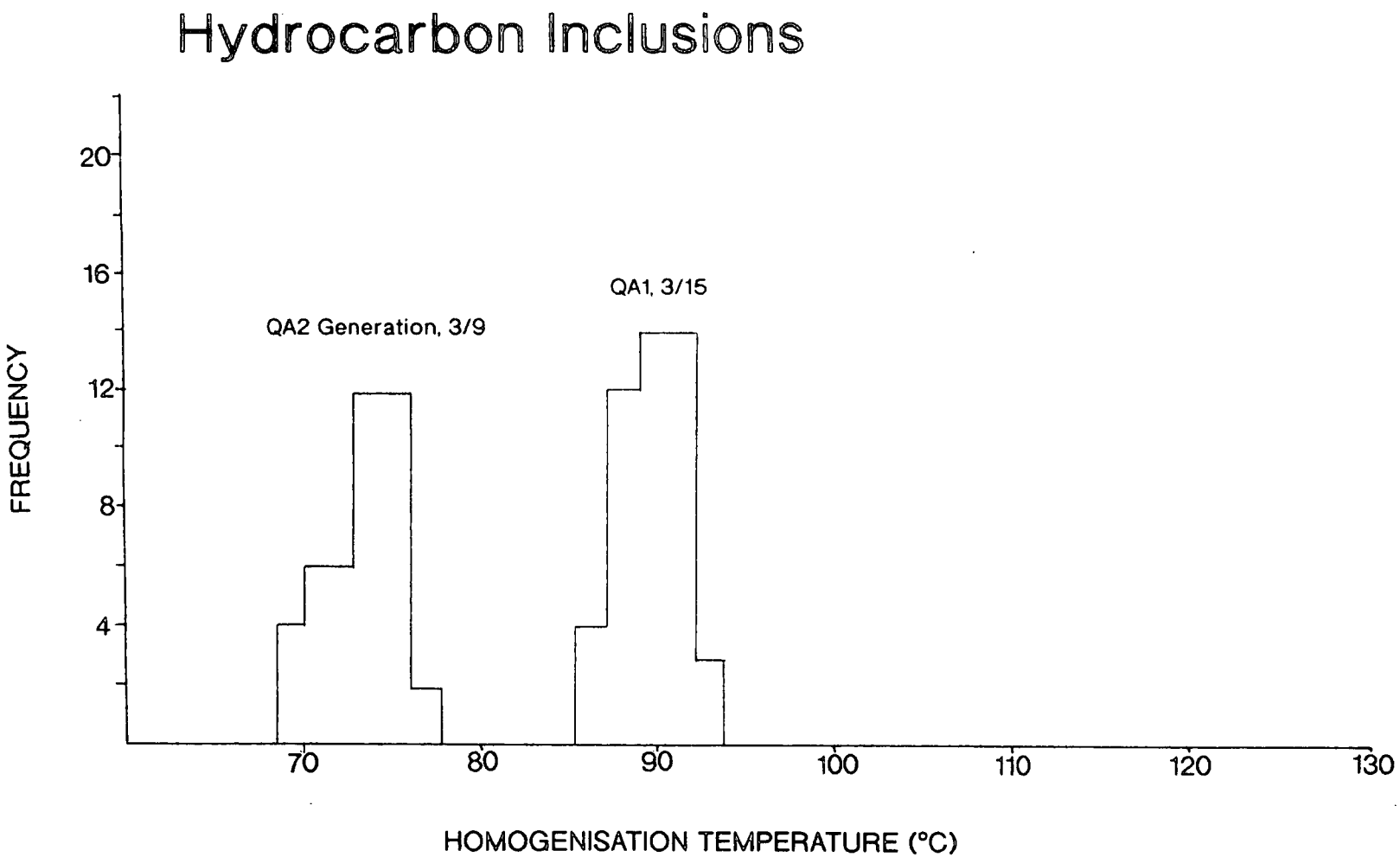

Fig.3.7.6e - Histogram representing homogenisation temperature (T(hom)) data range and frequency for hydrocarbon fluid inclusions. Data collected from fluid inclusions in quartz overgrowths in Alwyn North and South East reservoirs

aqueous and petroleum inclusion data can be used to approximate an envelope of likely P-T trapping conditions. Because of the differing PVT properties associated with aqueous solutions and hydrocarbons these two different phases will be dealt with separately.

3.7.6.1 Aqueous Fluid Inclusions

The QA2 generation inclusions in the Alwyn North field lie in a lower temperature range (89-104°C) than the higher temperature inclusions observed in the QA1 and QA2 overgrowths in the Alwyn South East field.

Observing the Alwyn North fluid inclusion dataset, it is possible to construct the appropriate P-T diagram applying a pressure correction for the saturation of the fluids with CH_4. Methane saturation in a brine associated with the hydrocarbon in a two phase fluid inclusion can have a very influential effect on the correct positioning of the bubble point curve. Bulk composition, weight % equivalent of CH_4 in typical North Sea black oils have been cited in the range 5 to 10% of total hydrocarbon composition (G.McLeod, pers.comm.). Although, the methane will be preferentially partitioned with the hydrocarbon phase of the fluid inclusion there must be an intimate relationship and saturation with the brine phase. Methane saturation increases with salt content (Hanor, 1980). In Alwyn, weight% equivalent of NaCl was observed from fluid inclusion freezing temperatures to be 5% NaCl (T(f) mean of -3°C, Fig.3.7.6.1a). A weight% equivalent saturation of only 0.28wt% CH_4 was used to position the bubble point curve to allow the T(hom) data for aqueous fluid inclusions (lowest value 89°C, highest value 104°C for aqueous inclusions in the Alwyn North data) to intercept the bubble point curve before the density of the fluids (calculated using Potter, 1977) would dictate the gradient of the respective isochores in the liquid only field (Fig.3.7.6.1b).

The CH_4 weight% equivalent of 0.28% is an extremely conservative estimate when considering the relative saturation of coeval brines in the Brent Province oil fields (G.McLeod, pers.comm.). Therefore, this constructed bubble point curve is likely to lie toward the lower extreme of the possible positioning which inherently depends upon actual values of saturated CH_4. Correlative pressure calculations for the positioning of the bubble point curve utilised correlative tables (Haas, 1978) requiring temperature information, relative saturation of methane (in ppm) and weight% equivalent NaCl. Pressure was corrected for the following temperatures assuming 50000ppm NaCl (weight% of 5%) and 0.28weight% CH_4:

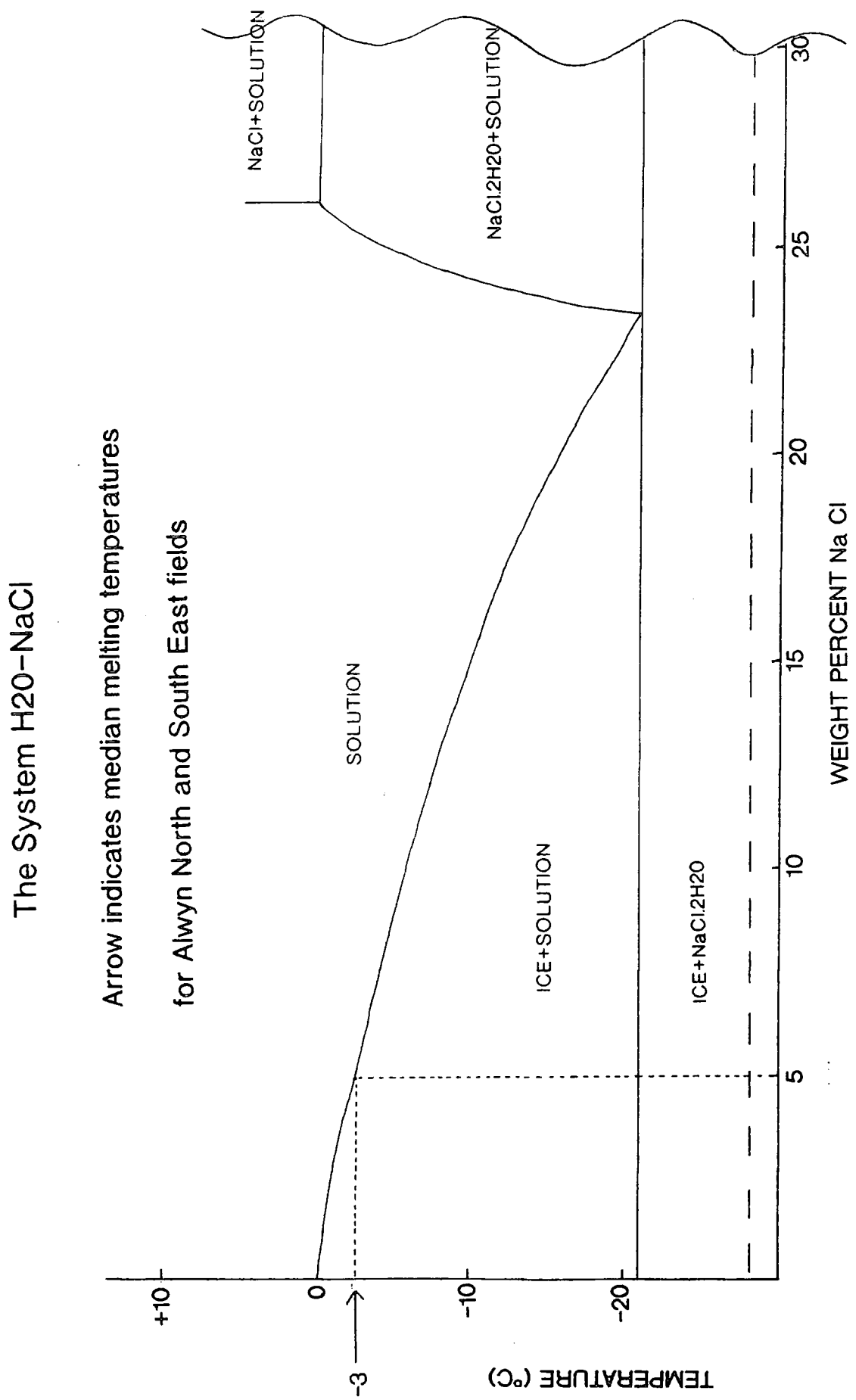

Fig.3.7.6.1a - Mean melting temperatures for aqueous fluid inclusions from Alwyn North and South east. the median T(f) of -3°C gives an equivalent wt% of 5wt% NaCl

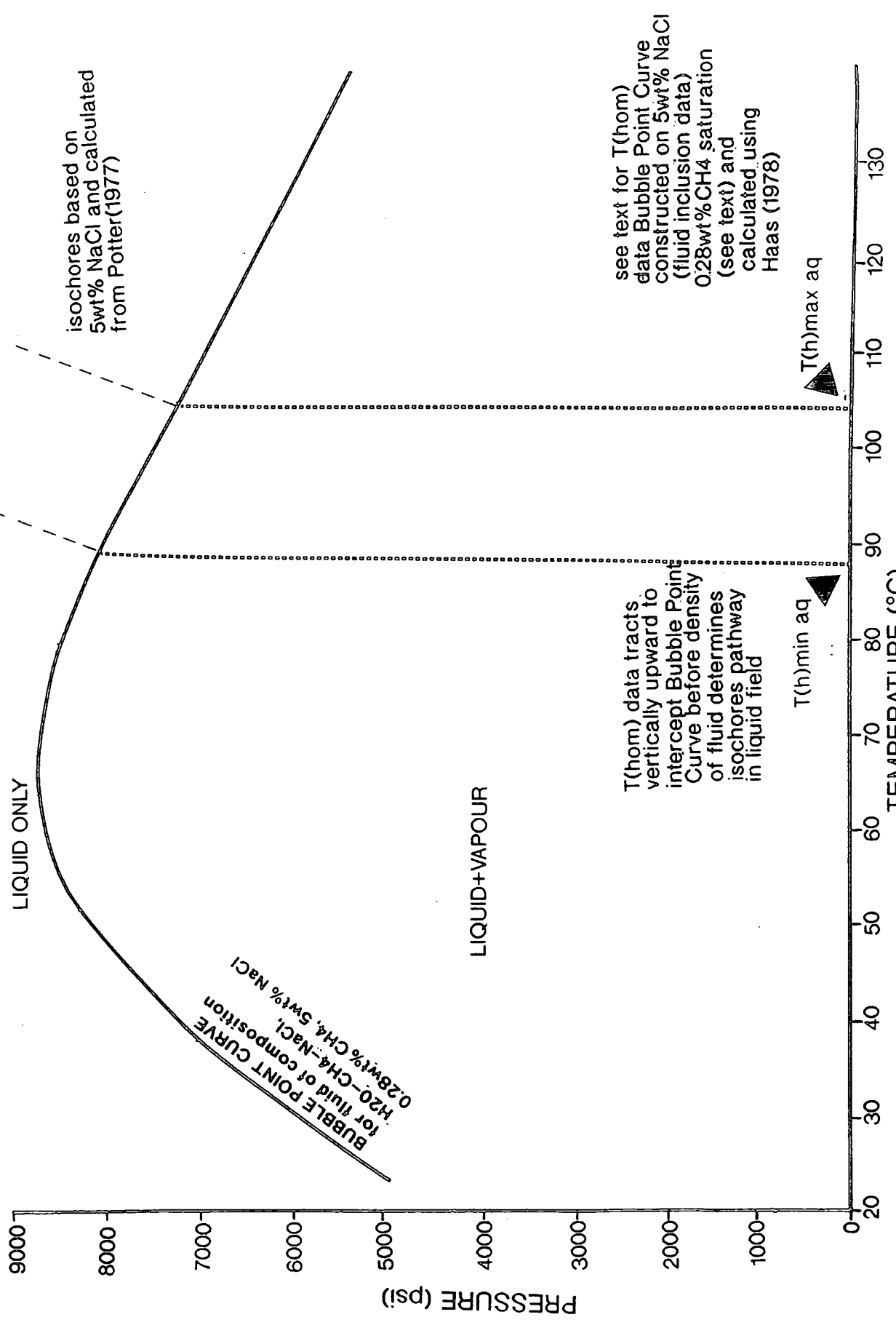

Fig.3.7.6.1b - Pressure versus temperature plot of aqueous fluid inclusion T(hom) data from Alwyn North. Bubble point curve based on 0.28wt% CH_4 and 5wt% NaCl (see text for discussion). Isochores for these aqueous T(hom) minima and maxima increase in temperature and pressure based on brine composition

Corrected pressures (accurate to 50psi) for the construction of the bubble point curve in Figs.3.7.6.1b and c using Haas (1978) -

Temperature	75°F(24°C)	100°F(38°C)	125°F(52°C)	159°F(66°C)	175°F(80)
Pressure(psi)	5100	7100	8250	8750	8500

Temperature	200°F(93°C)	225°F(107°C)	250°F(121°C)	275°F(135°C)	300F(149)
Pressure(psi)	7800	7150	6650	5500	4750

Therefore, Fig.3.7.6.1b shows the P-T diagram for corrected pressure for aqueous inclusions in the QA2 generation in the Alwyn North reservoir sands. This method has been applied to the data set from the QA1 and QA2 generation inclusions from Alwyn South East, summarised in Fig.3.7.6.1c.

3.7.6.2 Hydrocarbon Fluid Inclusions

Hydrocarbon rich fluid inclusions are identified in the diagenetic sequence using ultra-violet (UV) light. A white to yellow gold fluorescence typically identifies the included hydrocarbons in the samples observed.

The hydrocarbon inclusions in the QA2 population observed in the Alwyn North reservoirs yield a temperature range of 69-79°C and the measured T(hom) from the QA1 and QA2 generation inclusions from the South East field fell within the range of 86-93°C.

It is possible to follow a similar methodology to brine inclusions when correcting the T(hom) measurements for the hydrocarbon inclusions. However, phase relations with respect to PVT behaviour in the petroleum systems are complex. This is due to the amount of components that are possible in the composition of an oil and that each oil is unique in composition. Burruss (1992) describes how, depending upon the composition of the petroleum, multiple phase coexistence can extend from sub-zero temperatures to 100's of °C and 100's of bars pressure at the conditions of inclusion trapping. This then translates in the correct positioning of the bubble point curve. Therefore accurate temperature and pressure corrections are sensitive to the actual composition of the hydrocarbon trapped in the inclusion. This has obvious implications on any attempt to assess pressure using the combination of aqueous and hydrocarbon fluid inclusions.

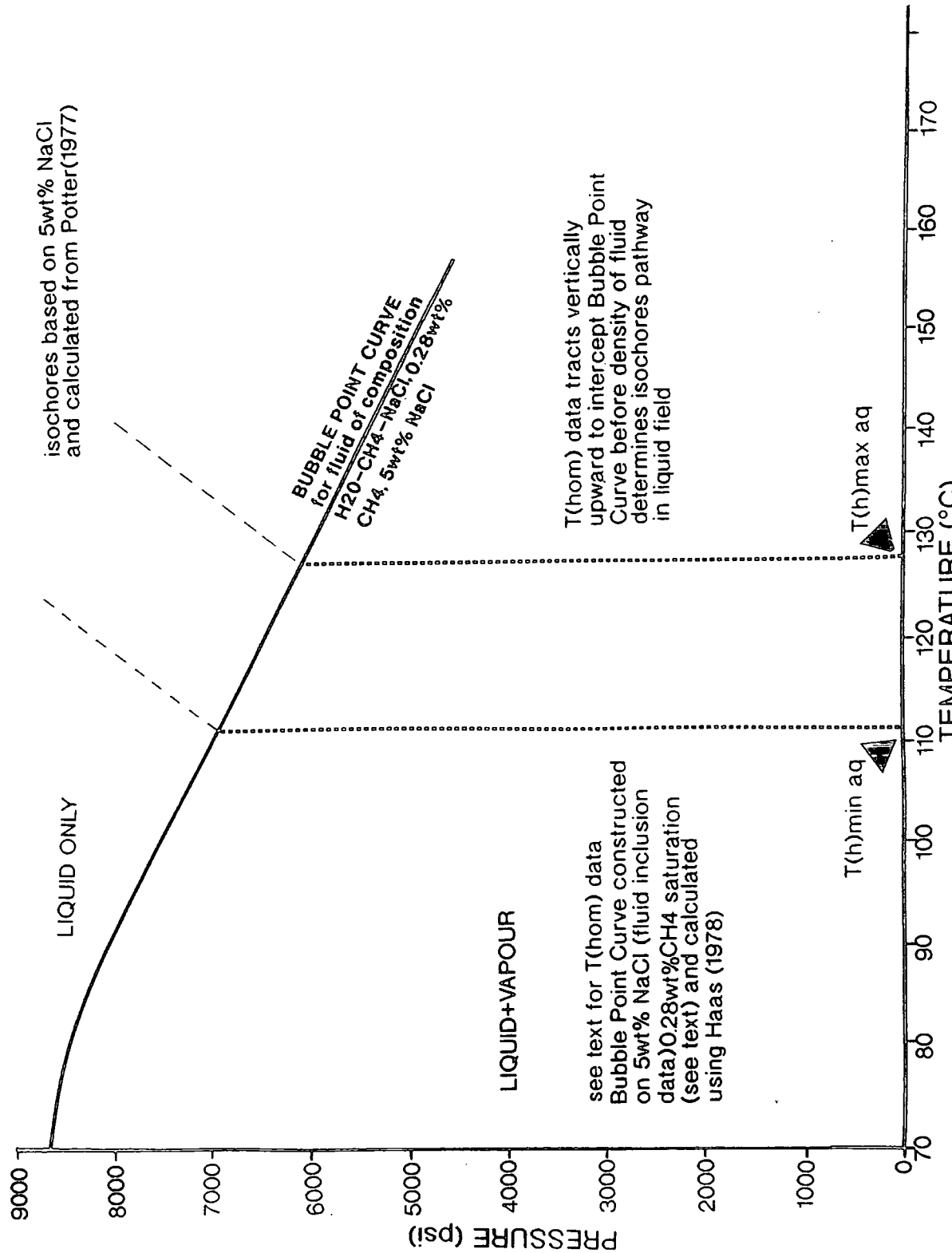

Fig3.7.6.1c - Pressure versus temperature plot of aqueous fluid inclusion T(hom) data from Alwyn South East. Bubble point curve based on 0.28wt% CH_4 and 5wt% NaCl (see text for discussion). Isochores for these aqueous T(hom) minima and maxima increase in temperature and pressure based on brine composition

Compositional analysis of hydrocarbons in fluid inclusions is extremely difficult due to the size of the individual inclusions, the risk of contamination during bulk crushing and overgrowth etching and the precision of available equipment. However, the bulk composition of multiple hydrocarbon inclusions concentrated from a number of samples can be analysed using conventional geochemical analytical techniques including GC and Iatroscan techniques.

Without accurate knowledge of the composition of the trapped hydrocarbons in terms of PVT properties, liquid-vapour coexistence (bubble point) curves and isochores for trapped hydrocarbon inclusions interpretation is difficult. Burruss (1992) has determined the bubble point curve for four petroleum fluids of known composition - black oil, volatile oil, gas condensate and gas - knowing in detail their composition (ie. C1 through to C7+ components - Table t3.7.6.2a). It was found, when isochores and T(hom) were calculated for each fluid, that the positions of the L+V (bubble point) curves shift to lower temperatures as the mole percent of CH_4 increases (Burruss, 1992). This is an effect of the increasing compressibility with increasing mole % CH_4 causing the isochores to decrease. Fig.3.7.6.2a (from Burruss, 1992) show these 4 'generic' fluids and their associated bubble point curves.

When considering the trapped hydrocarbons in the inclusions in the Alwyn reservoirs, these 'generic' bubble point curves from Burruss (1992) are considered to be reasonable to base the Alwyn hydrocarbons on. It has been determined from the fluid flow history, based on interpretations of maturity modelling, diagenesis and K-Ar dating of illites, that the first influx of oils into the reservoirs may approximate to the maturity of the early expelled oils from the source area. The Kimmeridge Formation in the Viking Graben depocentre is modelled as expelling early mature hydrocarbons (0.5-0.7%Ro) from approximately 90Ma (section 3.5.6). Given the transference time to account for the migration of these fluids into the Alwyn structural traps, the illite age determined oil fill-up at reservoir level would suggest that these early mature hydrocarbons would be trapped. From previous inferences based on Saigal et al. (1992) and Bjorlykke and Egeberg (1993) quartz diagenesis is retarded upon oil saturation. However, these early imported hydrocarbons are recorded in the diagenetic sequence as fluid inclusions. Since the hydrocarbon inclusions are assumed to approximate to an early mature crude, from a predominantly Type II kerogen source rock (Kimmeridge Shale Formation), a generic bubble point curve constructed from a combination of data from the black oil data (Burruss, 1992) and from PVT data based on an early mature oil (unpublished North Sea data). However, a fuller explanation for

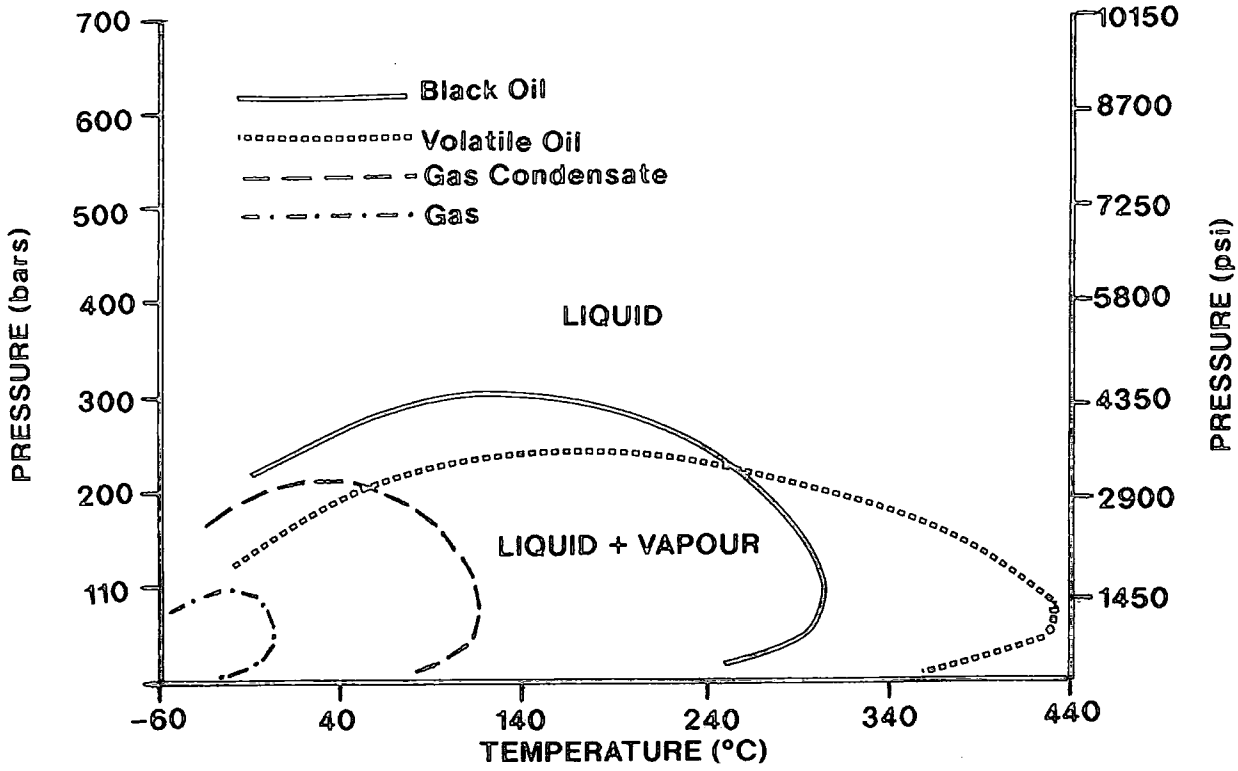

Fig.3.7.6.2a - Pressure and temperature phase relations of four 'type member' hydrocarbons based on PVT data from Burruss (1992) (see table t3.7.6.2a)

Component	Black Oil	Volatile Oil	Gas-Condensate	Gas
C1	48.3	64.36	87.07	86.67
C2	2.75	7.52	4.39	7.77
C3	1.93	4.74	2.29	2.95
C4	1.60	4.12	1.74	1.73
C5	1.15	2.97	0.83	0.88
C6	1.59	1.38	0.60	
C7+	42.15	14.91	3.80	
Gas-Oil Ratio (SCF/bbl[1]):	625	2000	18 200	no liquid
°API gravity	34.3	50.1	60.8	no liquid
Properties of C7 fraction:				
Molecular weight	225	181	112	
Average Carbon Number	16	13	8	
Boiling Point (°C)	277	227	107	
Specific gravity (g/cm^3)	0.840	0.800	0.745	
Homogenisation behaviour:				
Temperature (°C)	82	81	12	-51
Phase:	liquid	liquid	vapour	liquid

[1]Volumetric ratio, standard cubic feet of gas per barrel of oil

Table t3.7.6.2a - Compositional analyses of four 'type member' hydrocarbons. Data from Burruss (1992)

this assumption with regard to possible variation in geochemistry is given further below (section 3.7.8.4).

By plotting the homogenisation temperature range for each set of inclusions, the correct isochores and bubble point curve can be constructed to allow for the calculation of the corrected temperature and ultimately, when combined with the aqueous inclusion data, pressure under which the fluids were trapped. Fig.3.7.6.2a shows the isochore gradients reflecting the PVT properties of the trapped hydrocarbons projected into the LIQUID only part of the P-T diagram from the associated bubble point curve. As previously stated, the bubble point curve was plotted in conjunction with PVT data for an early mature oil which is likely to reflect the first trapped oils in this part of the diagenetic sequence in the Alwyn reservoirs. This diagram (Fig.3.7.6.2b) shows the isochore pathway for a range of temperature data for the QA2 (Alwyn North) inclusion data of 69-79°C. Similarly, the temperature range of 86-93°C measured from inclusions in the QA1 and QA2 generations in Alwyn South East gives respective isochore positions in Fig.3.7.6.2c.

3.7.7 Interpretation of Fluid Inclusion analyses in terms of palaeo temperature and pressure

The combination of the interpreted isochores for both aqueous and hydrocarbon inclusion data allows the interpretation of temperature and pressure of these fluids which were co-eval and which were moving through the trapping medium at a particular time. It must be remembered that the interpretation of the flow of aqueous and hydrocarbon fluids through the rock framework will reflect the palaeo conditions of the fluids rather than the ambient reservoir rock conditions. Since both fluids yield a range of homogenisation temperatures, an envelope of possible P-T conditions at the time of trapping is generated from the intersection of the 4 isochores from the minimum and maximum temperature ranges.

For the co-eval fluids trapped in the QA2 overgrowth generation in Alwyn North, Fig.3.7.7a describes the combination, intersection and interpretation of these isochores on a P-T diagram. The combination of Figs.3.7.6.1a and 3.7.6.2b give an envelope of likely palaeo fluid flow conditions at this particular time in the diagenetic sequence as having temperature range of 89-104°C which is the T(hom) range of the measured aqueous range. A pressure correction was unnecessary due to the presence, saturation and effect of dissolved methane in the system . The interpreted pressure conditions of 3750-5750psi (258.6-396.5 bars, 21.6-39.6MPa), when referenced against the

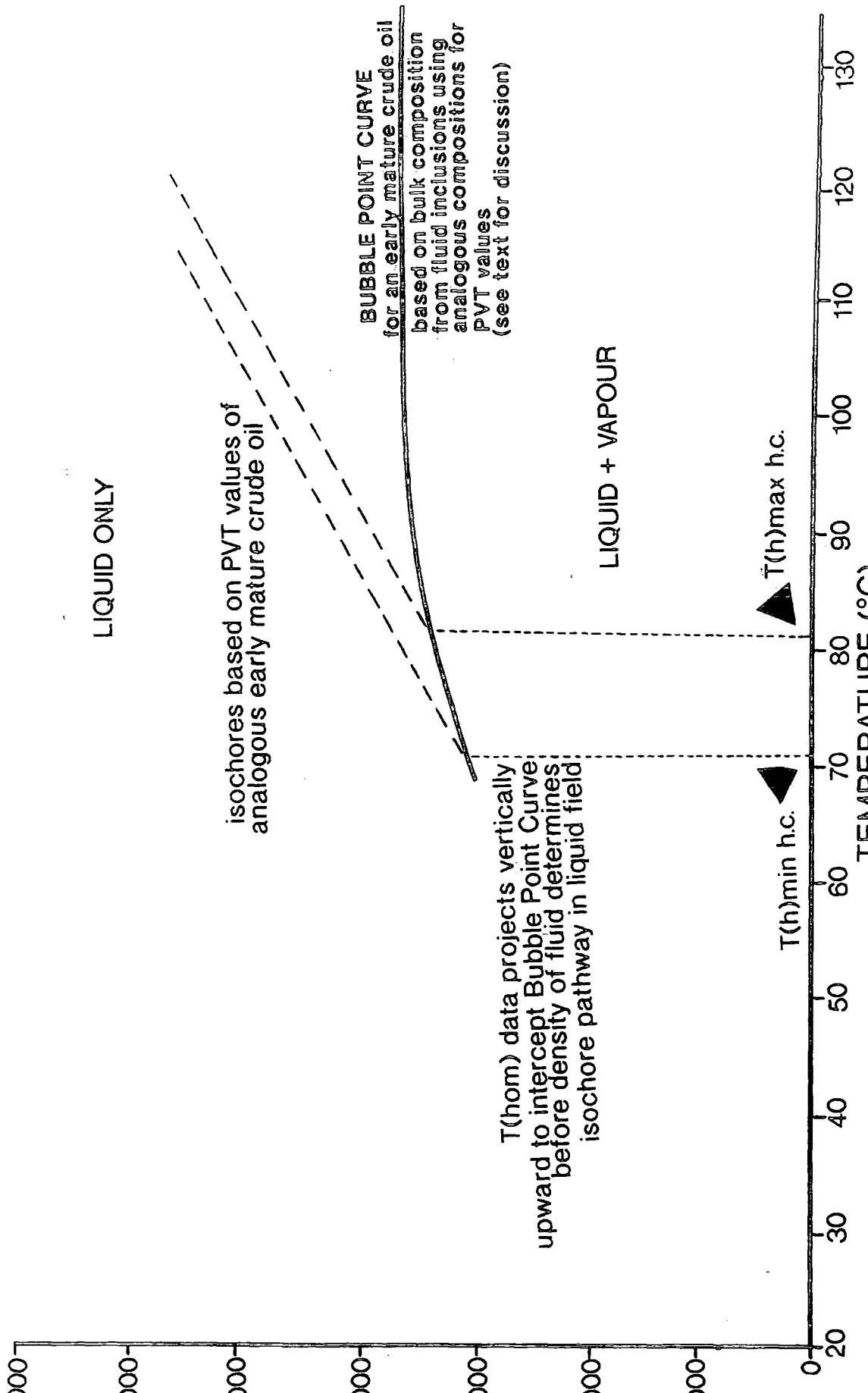

Fig.3.7.6.2b - *Pressure versus depth plot of hydrocarbon fluid inclusion T(hom) data from Alwyn North*

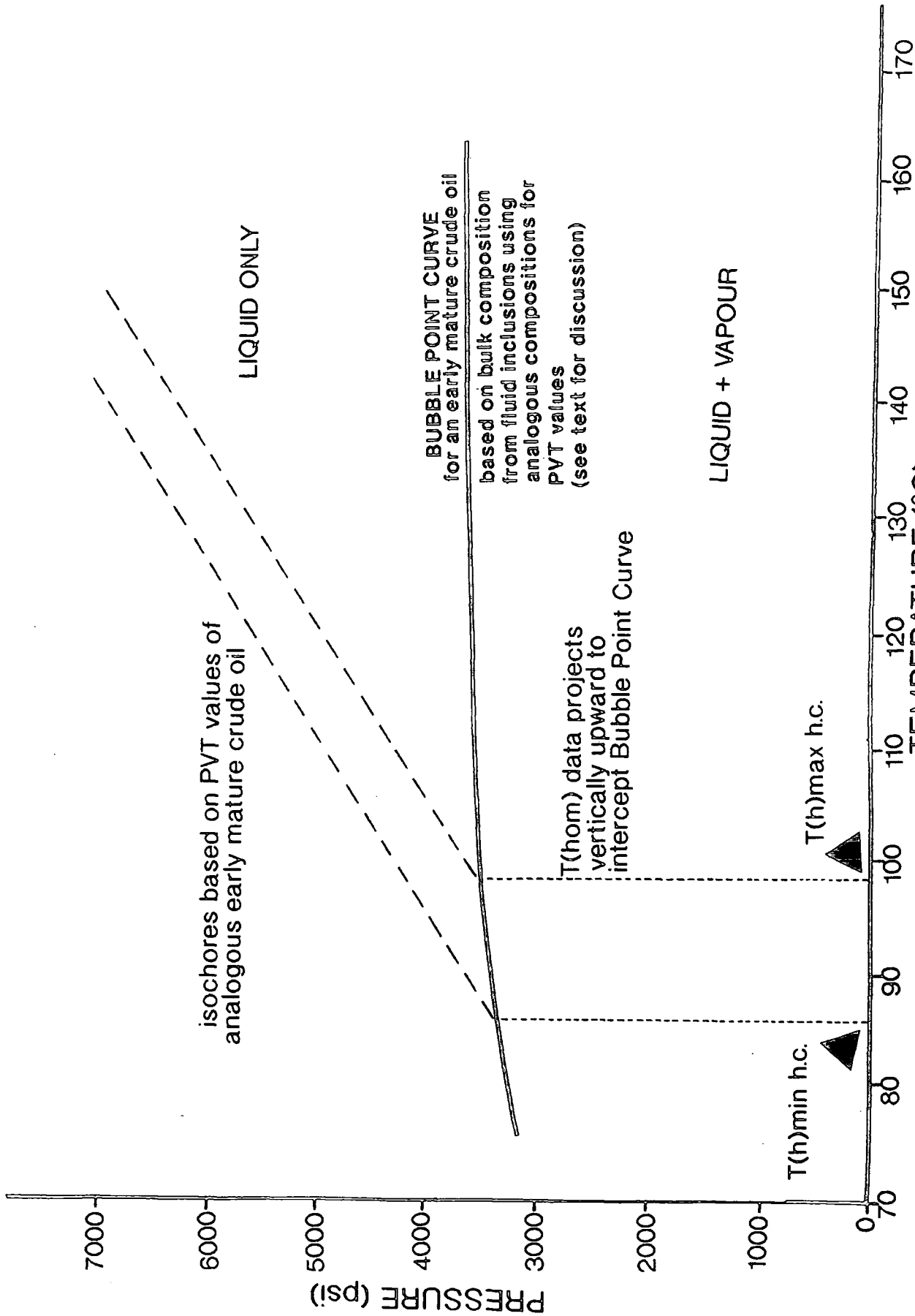

Fig.3.7.6.2c - Pressure versus depth plot of hydrocarbon fluid inclusion T(hom) data from Alwyn South East

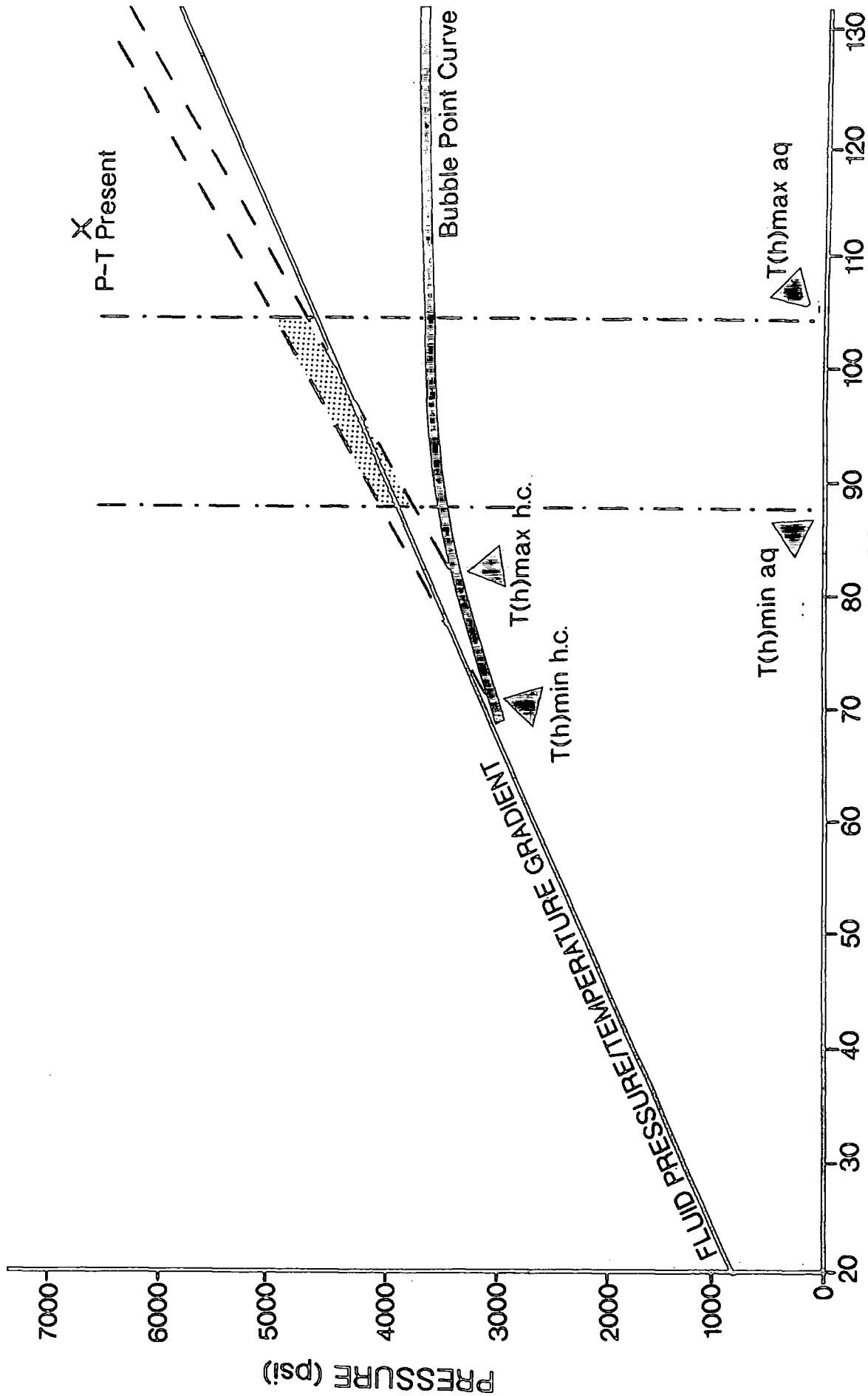

Fig.3.7.7a - Pressure versus depth plot on which a combination of aqueous (Fig.3.7.6.1a) and hydrocarbon (Fig.3.7.6.2b) fluid inclusion data for Alwyn North define an envelope of trapping temperature and pressure conditions

effective hydrostatic, lies close to normal pressure conditions. Normal pressure conditions are calculated for this temperature range at:

89°C (at geothermal gradient of 34°C/km) = 2618m
2618m (at hydrostatic gradient of 1.47645psi/m) = 3865psi (266.6bars, 26.6MPa)

104°C (at geothermal gradient of 34°C/km) = 3059m
3059m (at hydrostatic gradient of 1.47645psi/m) = 4517psi (311.5bars, 31.5MPa)

This can be inferred, then, for this period of fluid flow and hence an early diagenetic phase in the Alwyn North reservoirs and first trapping of hydrocarbons in the reservoir occurred close to or at hydrostatic pressure conditions.

For the fluid flow conditions under which the inclusion population belonging to the QA1 and QA2 diagenetic phase in the Alwyn South East reservoirs, a combination of Figs.3.7.6.1c and 3.7.6.2c produces an envelope of entrapment conditions (Fig.3.7.7b). The aqueous range of 116-128°C reflects the actual temperature conditions, as a pressure correction is not necessary due to assumed methane saturation. Pressure conditions were observed on Fig.3.7.7b at between 4100-5485psi (282.8-403.5bars, 28.3-40.3MPa). When compared to the fluid pressure-temperature gradient the envelope of pressure entrapment falls, once again, similar to observations made for the QA2 inclusion population in Alwyn North, close to the hydrostatic pressure condition. Normal pressure conditions for the temperature of entrapment are calculated at:

116°C (at geothermal gradient of 34°C/km) = 3412m
3412m (at hydrostatic gradient of 1.47645psi/m) = 5038psi (347.5bars, 34.7MPa)

128°C (at geothermal gradient of 34°C/km) = 3765m
3765m (at hydrostatic gradient of 1.47645psi/m) = 5559psi (383.4bars, 38.3MPa)

Therefore, again it would appear from this interpretation that fluid flow through the reservoir coincidental with the QA1 and QA2 phases of the diagenetic sequence in Alwyn South East occurs near to or at hydrostatic pressure conditions.

The observation, then, that both sets of inclusions for reservoir sands in different structural levels and positions and developed at different times were trapped close to normal conditions. In both interpretations of fluid trapping and reservoir diagenesis with respect to pressure of entrapment, the common observation is that diagenesis is

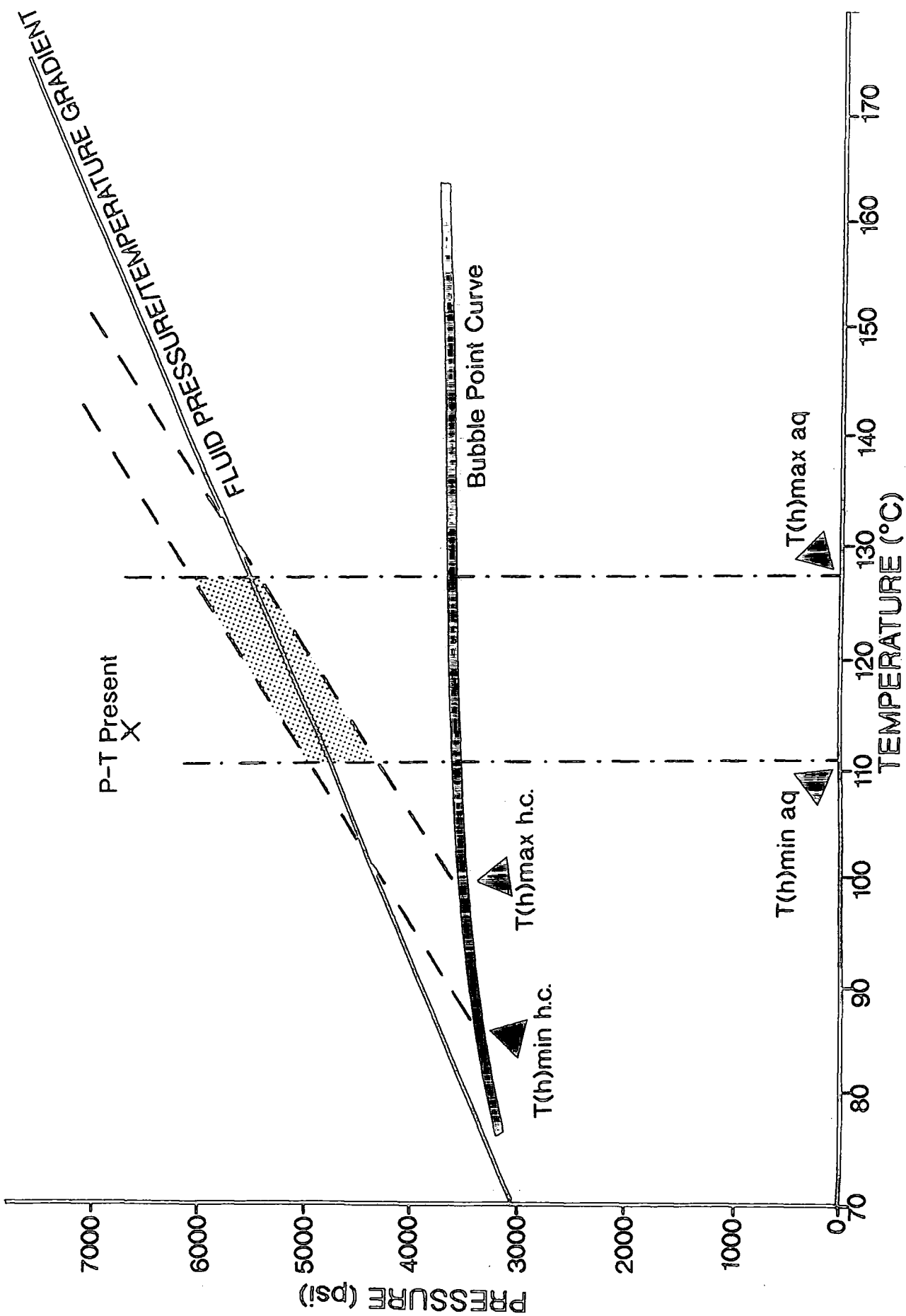

Fig.3.7.7b - Pressure versus depth plot on which a combination of aqueous (Fig.3.7.6.1c) and hydrocarbon (Fig.3.7.6.2c) fluid inclusion data for Alwyn South East define an envelope of trapping temperature and pressure conditions

taking place under normal to near normal pressure conditions. This may be a result of necessary conditions appropriate for solute precipitation from fluids in the reservoir sands. Even though it is thought that the primary control on diagenetic precipitation and mineralisation is temperature, diagenetic fluids under higher pressure conditions may restrict precipitation whereas lower hydrostatic pressures may favour minerals coming out of solution as a direct result of a pressure drop.

3.7.8 Assumptions in the interpretation of inclusion P-T trapping conditions

3.7.8.1 The PVT properties of the aqueous phase:

The main debate in this study of fluid inclusion pressure/temperature is the position of the bubble point curve and associated lines of equal volume/density (isochores). If no methane is associated with the system and the application of the pure system H_2O-NaCl is used the T(hom) represents the minimum temperature on the bubble point curve for brine and will not equal the actual trapping temperature until a pressure correction has been made. However, in this study, as the aqueous fluids were seen to be co-eval with hydrocarbons trapped in the same diagenetic phase, many authors (Hanor, 1980; Burley et al., 1989 and Burruss, 1981) recognise that experimental and theoretical work carried out by workers such as Haas (1978) has shown that only a very small % of dissolved methane in the aqueous solution will shift the bubble point curve to a sufficiently high pressure regime that no pressure correction is needed such that T(hom) equals T(trapping). Therefore, this study followed the observation made by Burruss (1992) who states that no pressure correction is required for aqueous homogenisation temperatures where there is evidence of simultaneous trapping of aqueous and petroleum fluid inclusions.

3.7.8.2 The PVT properties of the hydrocarbon phase:

Imperative to the successful interpretation of the trapping pressure of two phase fluid inclusions within a reservoir sandstone is the correct positioning of the bubble point curve for the trapped aqueous and hydrocarbon phase. The assumptions and variables in defining the hydrocarbon curve are complex. This is due to the accuracy in determining the composition of the trapped hydrocarbons and their PVT properties.

Standing (1947) describes that the complexity of multi-component hydrocarbon systems are varied and are defined by three relatively simple parameters: gas gravity, oil gravity and gas-oil ratio (GOR). Standing (1947) postulates a relationship which combines the above parameters to calculate the bubble point pressure of an oil. The relationship is described by:

$$P_b = \Phi\ (GOR, \psi g, T, API)$$

where:

P_b = bubble point pressure (psi, absolute)

GOR = gas-oil ratio (ft^3/bbl)

ψg = gravity of dissolved gas (air = 1)

T = temperature (°F)

Φ = a function of.....

Standing (1947) has created graphical relationships and nomograms to describe the above relationship which allows immediate facilitation of the parameters to assess bubble point pressure (Fig.3.7.8.2a).

Fig.3.7.8.2b shows the nomogram in operation for calculating the bubble point pressure or solubility. The procedure for calculating the bubble point pressure runs with the example given in Fig.3.7.8.2b and the following commentary: Required: Bubble Point Pressure at 200°F of a liquid, having a gas-oil ratio of 350CFB (cubic feet of gas per barrel of oil) a gas gravity of 0.75 and tank oil gravity of 30°API. Procedure: Starting at the left side of chart, proceed horizontally along the 350CFB line to a gas gravity of 0.75. From this point drop vertically to the tank gravity scale to 30°API. Proceed along the horizontal till the 200°F line. Drop vertically down from the 200°F line to find the bubble point pressure. The required pressure is found to be 1930psi.

However, only a small change in any variable in this relationship is sufficient to dramatically affect the bubble point pressure. A likely scenario in a compositional change in the oil, an increase of 15% on the amount of polar compounds in the hydrocarbon phase is sufficient to increase the API gravity of the oil by 10°API (Larter, 1993). Thus, the calculation of the bubble point curve by this variation in the gravity of the oil is the raising of the bubble point curve by over 1000psi (Fig.3.7.8.2b). This obviously has serious implications for assigning a bubble point curve necessary in the interpretation of palaeopressure and temperature calculated from fluid inclusion data. If the included oils are rich in polar compounds relative to the assumptions made then the assumed position of the bubble point curve used in the previous pressure interpretation (section 3.7.7) may be incorrectly positioned. Therefore, the pressure interpretations of the fluid inclusions may be erroneous.

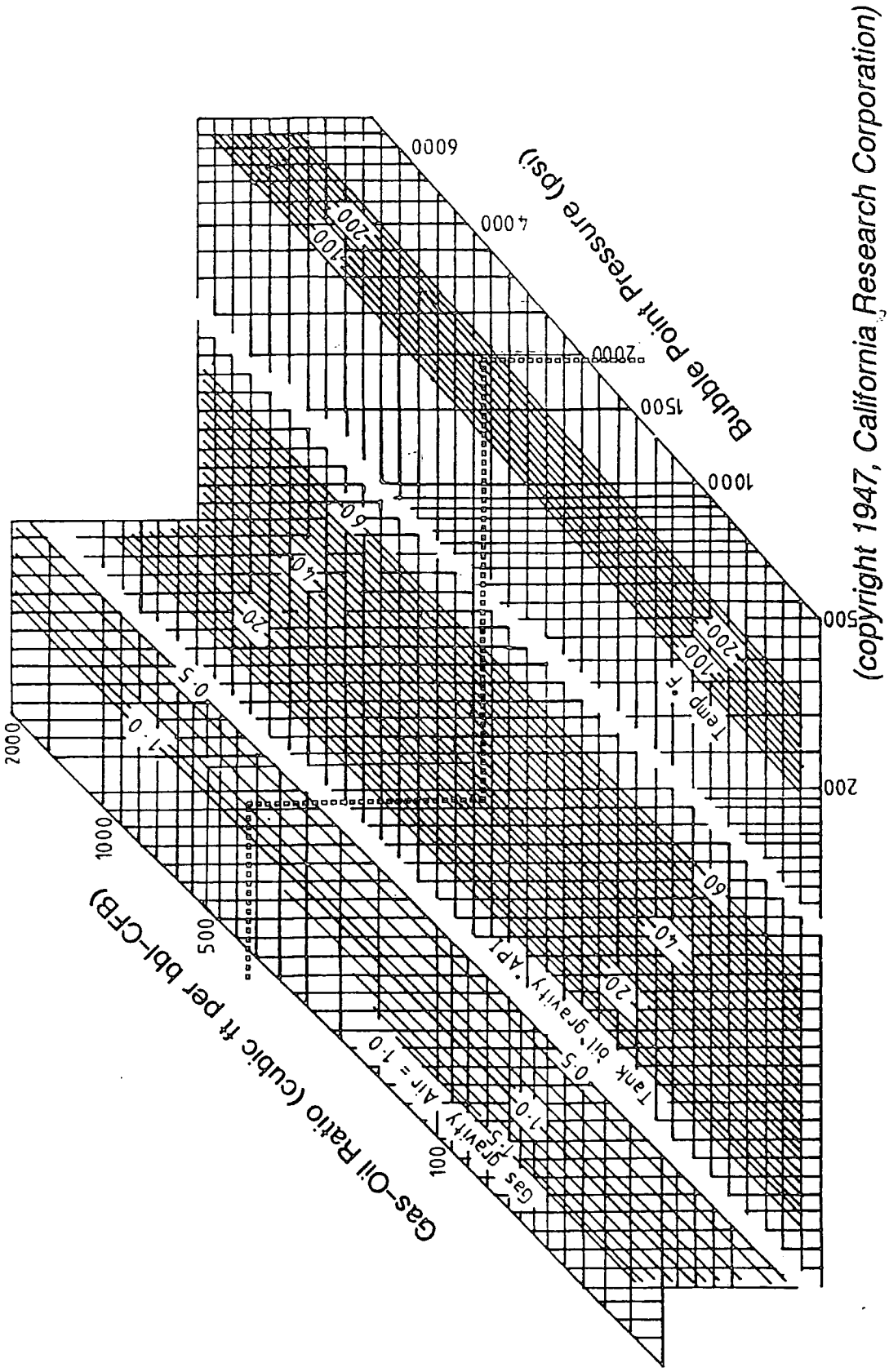

Fig.3.7.8.2a - Nomogram describing the relationship of gas solubility as a function of pressure, temperature, gas gravity and oil gravity (see text for discussion). Modified from Standing (1947)

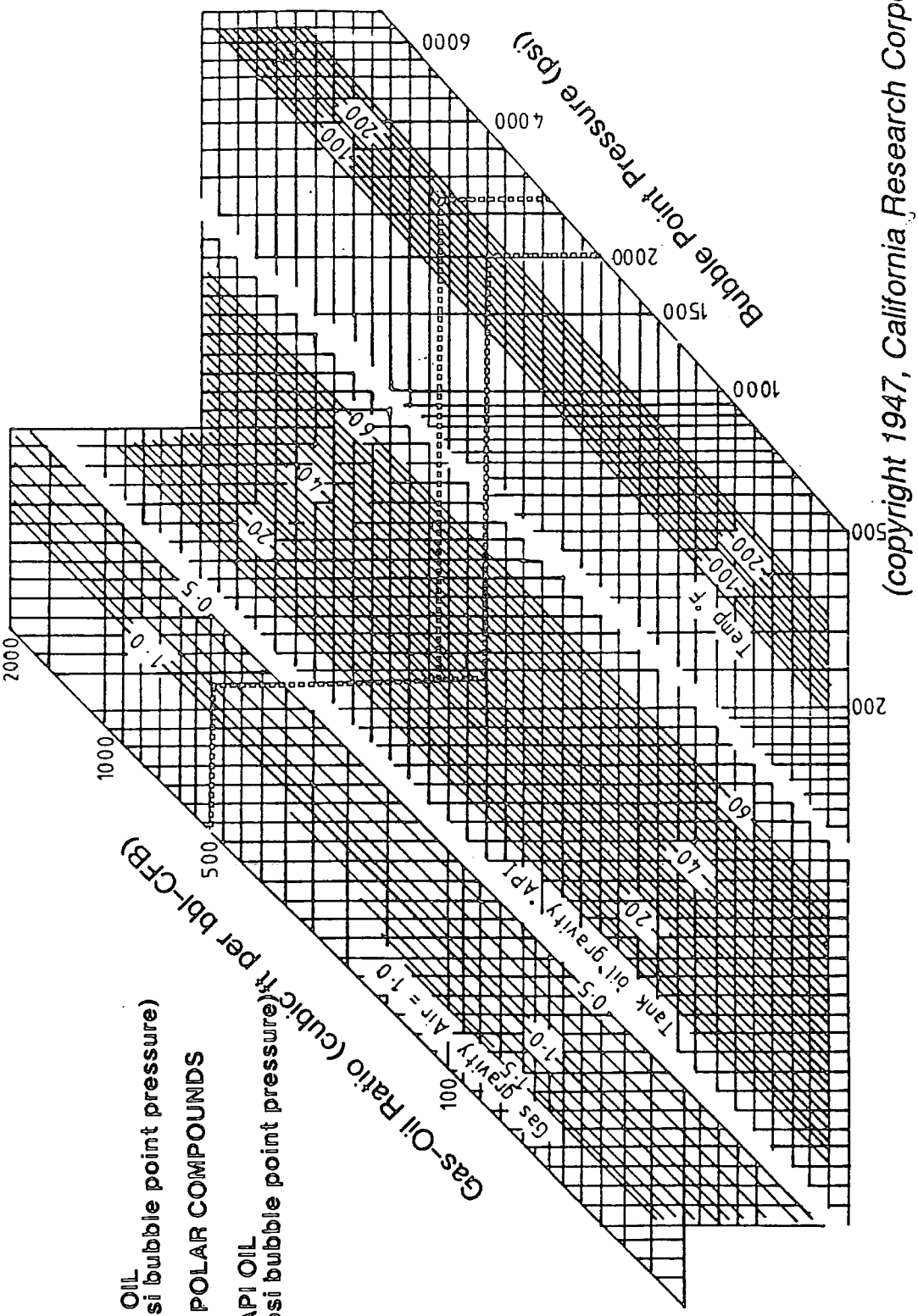

Fig.3.7.8.2b - Standing's (1947) nomogram utilised to show the effect of increasing the polar compounds of a 35°API oil with respect to its bubble point pressure (see text for discussion)

It is supposed that the entrapped hydrocarbons resemble an early mature crude as being the primary phase of oil migration into the reservoir at the time the inclusions were formed. PVT properties similar to the bubble point curve and isochores used in this study were taken from a combination of unpublished North Sea data of an early mature light oil and the black oil data developed by Burruss (1992). Also, the following section interprets the geochemistry of the trapped hydrocarbons and although the process of assigning an API gravity to these oils is difficult (G.McLeod, pers.comm.), the various other parameters conform to the assumed characteristics made in the interpretation of the included oils.

Larter (1993) reviews the partition of organic nitrogen, sulphur and oxygen species (NSO) between phases as control parameters in the formation and interpretation of fluid inclusions. Larter (1993) states that the partition of petroleum non-hydrocarbons (NSO compounds) onto mineral surfaces or into water phases has implications for all processes involving petroleum or water fluid flow in sedimentary basins. Larter (1993) reports that NSO compounds are chemically more attractive to nucleate on an inclusion surface and therefore may change the PVT values of entrapped hydrocarbons. NSO compounds may then preferentially site on mineral surfaces and become intimately associated with the hydrocarbons trapped as fluid inclusions. Preferential enrichment in NSO and polar compounds will alter the PVT properties of the included oil relative to the reservoir oil and when, in the context of Standing's (1947) graphical calculations, alter the bubble point pressure. Thus the potential trapping conditions may not represent the assumed early mature crude which the previous interpretations are based upon. To represent the effect of NSO and polar compounds and the hydrophilic nature of these members in the way that will readily nucleate on the surface of a mineral (a typical site for fluid inclusion nucleation), an example is given (Fig.3.7.8.2b). An oil of constant gas gravity (0.8gm/cc), temperature (205°F) and GOR (500ft^3/bbl) is subjected to the introduction of polar compounds by 15%. The effect of this chemical change in the oil is to increase the viscosity and gravity of the oil and Larter (pers. comm.) has calculated that an oil of 35 °API gravity with the above constant parameters will, upon 15% polar compound increase, increase the gravity of this oil to 25°API. The introduction of polar compounds will effect the oil viscosity/gravity as shown by Glasø (1980). Using Standing's (1947) graph to represent gas solubility as a function of pressure, temperature, gas gravity and oil gravity, it is calculated that the effect on the bubble point pressure is to increase the pressure by approximately 700psi.

The isochores and bubble point curve used in the palaeopressure interpretation of the Alwyn hydrocarbon inclusions were based on data from Burruss (1992) and unpublished data of an early mature light crude from the North Sea, average °API was approximately 35. Figs.3.7.7a and b shows the original interpretation of trapping temperature and pressure using isochores and bubble point pressures based on this gravity and associated PVT properties. The effect of increasing the polar compounds by 15% would shift the bubble point pressure by approximately 700psi; the isochores defined by the new PVT properties will steepen. The combined effect will be to produce an envelope of entrapment which lies in the overpressure region of this diagram. Indeed, using the fluid pressure-temperature gradient this new modification would indicate entrapment of fluids in an overpressured state. Present hydrocarbons recovered from the Brent reservoirs in the Alwyn North field average a tank gravity of 41°API (Inglis and Gerard, 1992). The assumption in this study of using an oil with a 35°API gravity seems justified then, as compared to the present day recovered hydrocarbons, the assumed oil has a 6°API more dense gravity approximately equal to 7% increase in polar and primary NSO compounds (Larter, pers.comm) compared to the present day recovered oil. This would seem entirely reasonable as the present day °API gravities will reflect lighter compounds in the oil which were not available during initial oil influx recorded in the fluid inclusions. Therefore the position of the bubble point curve and associated isochores used in the interpretation of the fluid inclusion data can be justified.

Due to the richness and abundance of hydrocarbon inclusions in the Alwyn samples and the success in developing crushing and extraction equipment a successful attempt was made to extract and analyse the entrapped hydrocarbons from the quartz overgrowths. Analyses were carried using GC (Gas Chromatography) and Flame Ionisation Iatroscan techniques developed and executed by Newcastle Research Group (NRG). The results of the experimentation and analyses is detailed in section 3.7.8.4 (Geochemistry of the hydrocarbon inclusions).

3.7.8.3 Fluid Pressure/Temperature Gradient:

This important reference line is used as the ambient normal pressure and temperature conditions as a function of depth. The gradient rises with depth at 1.47645psi/m and 34°C/km. These figures and gradients are based on and resemble present day conditions (section 2.1 and 2.2).

This assumption, as far the pressure gradient is concerned, that the present hydrostatic pressure gradient would be an identical representation of the conditions at fluid

entrapment (approximately 65-75Ma for the QA2 generation inclusions - Alwyn North, and approximately 45-55Ma for the QA1 and QA2 generation inclusions - Alwyn South East, Jourdan et al 1987) is justified as palaeo-geographic, climatic and structural configuration would approximate to the present day. The hydrostatic pressure gradient is known to vary due to the pore water salinity which affects the density of the medium (section 2.1). The North Sea at the present day is recognised as a failed rift basin, fully connected seaway with an average sea temperature of 5°C and a salinity of 50 000ppm (Buhrig, 1989).

Buchardt (1978) has calculated sea floor temperatures from North sea rocks from the Palaeocene to the present day (section 3.5.5). Buchardt (1978) calculated from $\delta^{18}O$ values that the period of the Eocene (approximately 45-55Ma corresponding to the QA1 and QA2 generation inclusions from Alwyn South East) that palaeoclimatic conditions would be in the range of 15-21°C (main non-glacial temperature). Kennet (1977) reports convincing evidence that indicates a drastic global cooling event at the end of the Eocene, probably triggered by the development of the cryosphere. This combined with the onset of cold water circulation in the Norwegian-Greenlandic Sea, initiated by the opening of the strait between Greenland and Svalbard, at approximately this time. The likelihood of the illite age dating is for the Alwyn South East inclusions to be pulled toward the lower end of the age range (45Ma, from Hamilton et al 1989). This will tend to bias the mean temperature of 18°C to the lower extreme of maximum error of 4°C to bring the mean temperature for this period of entrapment for the Alwyn South East inclusions close to present day conditions.

Sea level temperatures were thought to be slightly higher in the period 65-75Ma reflecting a more humid climate (Hancock and Scolle, 1975) but in both periods associated with this study, no major tectonic events associated with volcanism in the Northern North Sea have been recorded and therefore the assumption of the present ambient heat flow and geothermal gradient of 34°C/km can be used in this study's calculation of palaeo P-T entrapment conditions.

3.7.8.4 Geochemistry of the hydrocarbon phase in Alwyn Field fluid inclusions:
If the maturity and composition of the trapped oils could be ascertained then the previous assumptions used in section 3.7.7 can be confirmed as valid or erroneous. Previous attempts to qualify the maturity and composition of hydrocarbon bearing fluid inclusions have been attempted by McLimans (1987) and Karlsen et al (1992). However, each fluid inclusion data from a specific oil field set must be treated

individually to accurately assess the maturity and composition of the specific hydrocarbons.

Crushed Gas Chromatography (GC), Flame Ionisation Iatroscan and Ultra-Violet (UV) Fluorescence Spectra techniques were employed at Newcastle Research Group (NRG) to analyse the hydrocarbons trapped in authigenic quartz overgrowths in the Alwyn 3/9a-6 well. The samples from this well were taken from core at a depth of 3190 to 3220m. Preparation techniques and the experimental programme was developed in-house and at this time remain confidential.

Flame Ionisation Iatroscan analyses repeatedly observed the masking effect of diesel fuel which presumably was used in the washing of the core to strip the oil based drilling fluid from the core. Therefore, this technique observed suppressed peaks due to the high contamination and inability to entirely clean the sample of diesel.

Gas Chromatography (GC):
Fluid inclusion rich quartz grains were etched and cleaned for purpose of the crushed GC analyses. Samples were then crushed in a vacuum leading to the flame unit of the GC. Fig.3.7.8.4a shows the GC trace of the crushed sample whereby the GC recognises all detectable hydrocarbon groups. The trace shows that sample 3/9a-6 (3200m) contains the full array of compounds found in a conventional crude oil with a high amount of C1-C7 with a relatively high response at C3/C4 (propane/butane). This would suggest and agree with the assumptions that there is an association of light end hydrocarbons in the included hydrocarbons; in particular, the assumption of a methane rich hydrocarbon seems justified on this evidence. Therefore, calculations based on a methane saturated hydrocarbon in assessing the palaeo-pressure of hydrocarbon/brine fluid inclusions seems justified on this GC data.

UV Fluorescence Spectra:
The fluorescence spectra of the hydrocarbon bearing inclusions can be used to address the maturity of the hydrocarbon (McLimans, 1987) and the API gravity (Lang and Gelfand, 1985). Using an excitation wavelength calibrated and corrected for white light (G.Mcleod, Pers.Comm.), the analysed spectrum is assigned x and y co-ordinates with respect to the 1931 CIE chromaticity diagram to determine the fluorescence colour (Deaton, 1987). CIE x and y co-ordinates quantify the hue, value and chroma of the fluorescence (Deaton, 1987). The following data has been observed for 3/9a-6 (3200m):

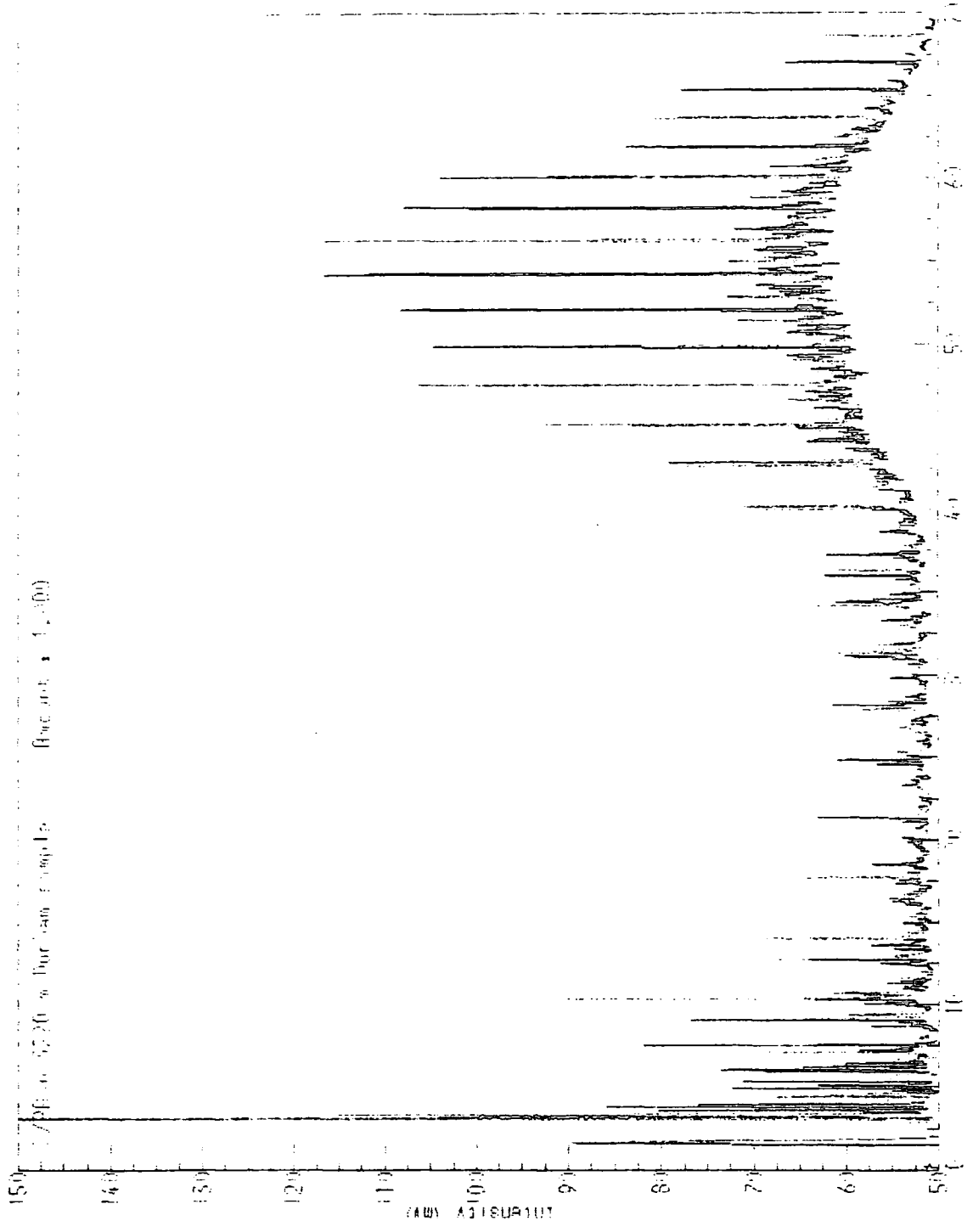

Fig.3.7.8.4a - Gas Chromatography (GC) trace of included hydrocarbons from sample from well 3/9a-6 (3200m)

Analyses 1	x = 0.3884	(Gain = 3, A/D = 40%)
	y = 0.3886	
Analyses 2	x = 0.3940	(Gain = 3, A/D = 40%)
	y = 0.3998	

Plotting this data on the CIE diagram (Fig.3.7.8.4b) to assess the locus of the dominant wavelength of the fluorescence spectra, both analyses show dominant wavelengths of between 460-470nm. By extrapolating the co-ordinates through point C, which represents the dominant excitation wavelength for white light, the spectra falls between 460-470nm. These dominant wavelengths are confirmed by the fluorescence maximum intensities (Figs.3.7.8.4c and d) which observes maximum fluorescence at approximately 450nm for both sample 1 and sample 2.

This dominant wavelength and maximum intensity can be used to estimate the API gravity. Lang and Gelfand (1985) have constructed a correlative chart between the fluorescence of colour and API gravity. Samples 1 and 2 have been observed to have a peak intensity of between 450-470nm. These observed wavelengths and CIE coordinates corresponds to a colour approximating to gold-yellow when using the spectral fluorescence defined by Altman (1967). Using this chroma to correlate an API gravity (Fig.3.7.8.4e), the 3/9a-6 included oils, at a core depth of 3200m, have an API gravity of 25-34°API. This, then, suggests an oil of early mature origin corresponding approximately to the black oil defined by Burruss (1992) which was used in the calculation of palaeo-pressure in this study (section 3.7.7). This assumption of defining PVT properties on an early mature crude seems be confined by geochemical analysis.

CIE co-ordinates calculated for the Alwyn oils were also applied to observations made by McLimans (1987). Using data from oils from the Wealdon basin, McLimans (1987) observed that oils with decreasing x y co-ordinate values correlate to an increasing maturity (Fig.3.7.8.4f). Superimposing the CIE co-ordinates for the Alwyn samples, shows the oils from Alwyn correspond to an early mature phase on McLimans (1987) diagram.

Biomarker Analyses:

Maturity calculations based on biomarkers have been conducted. The specific biomarker ratios used are the MPI-3 (Methyl Phenanthrene Index) and the MeNa ratio (Methyl Napthalene). The biomarker ratios returned the following information:

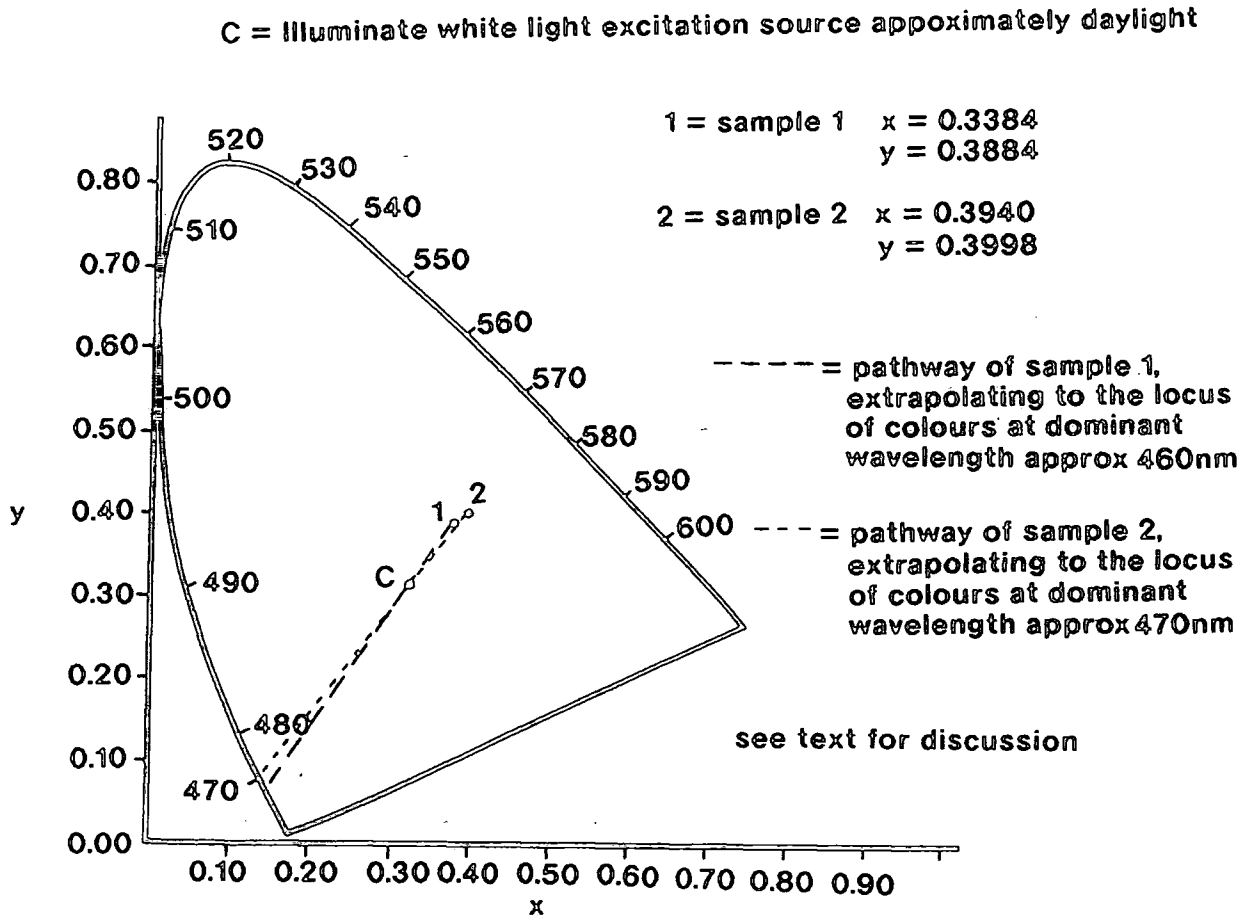

Fig.3.7.8.4b - Chromaticity diagram showing the locus of spectral colours (solid line) according to the 1931 standard observer. Samlples 1 and 2 represent CIE co-ordinates of Alwyn North included oils. Their spectra are determined by extrapolating a line through the excitation source (daylight). Modified after Deaton (1987).

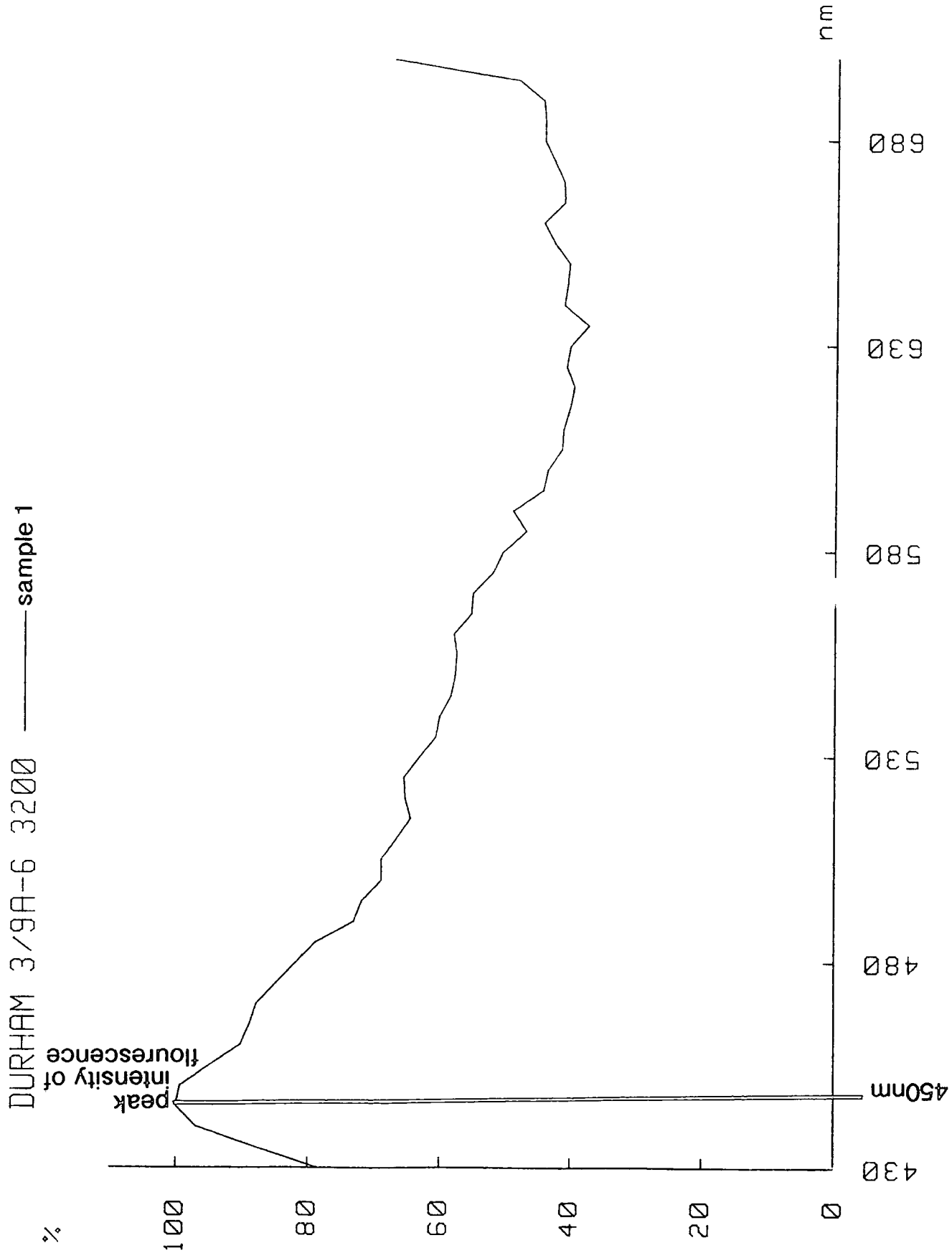

Fig.3.7.8.4c - Dominant wavelength of maximum intensity of flourescence, sample 1 (3/9a-6, 3200m)

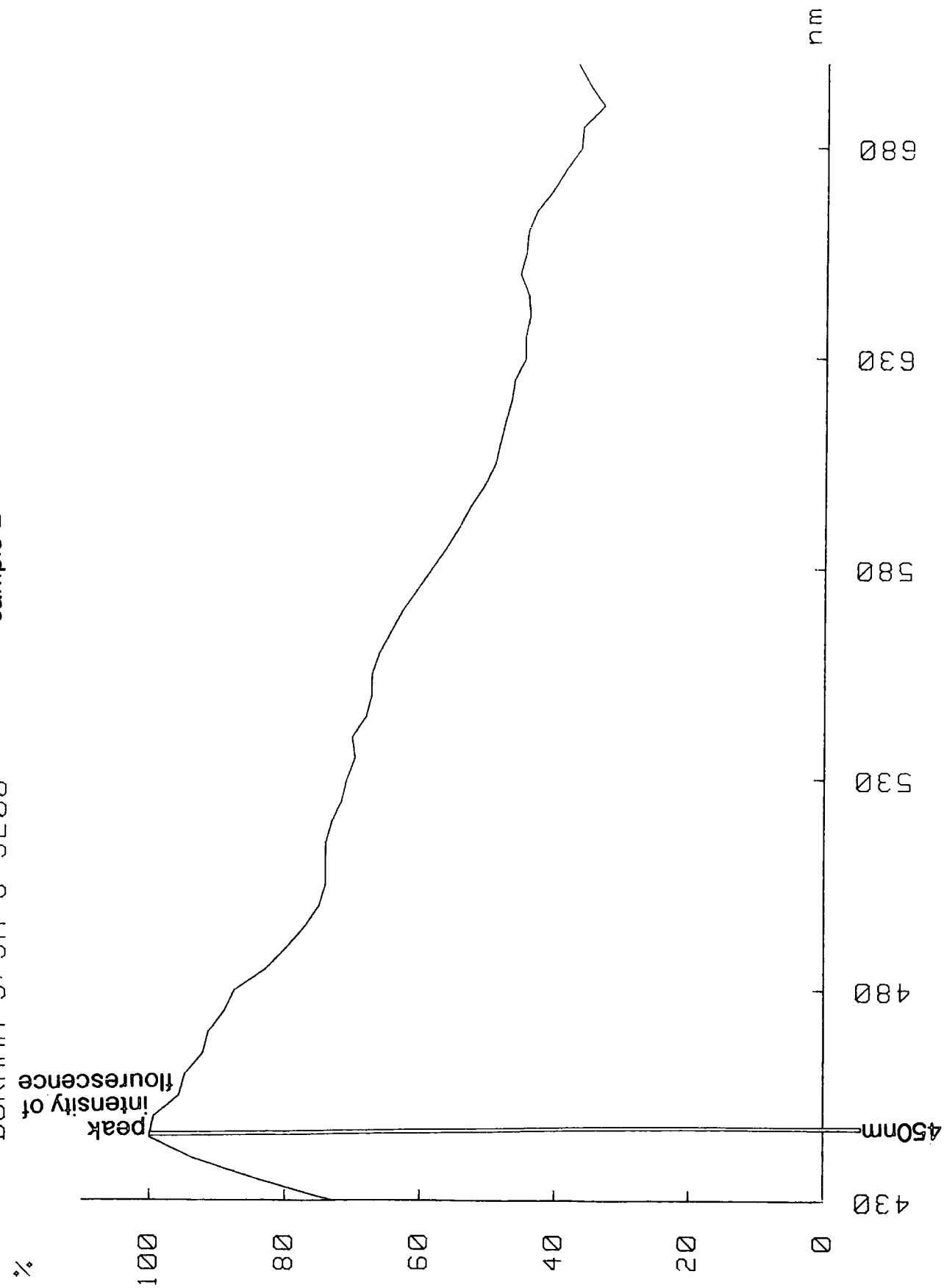

Fig.3.7.8.4d - Dominant wavelength of maximum intensity of flourescence, sample 2 (3/9a-6, 3200m)

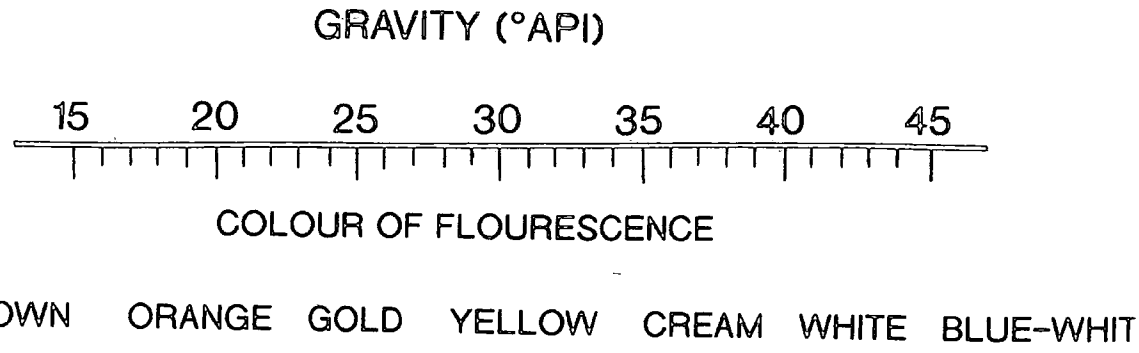

Fig.3.7.8.4e - °API oil gravity determined by spectral flourscence of hydrocarbons. After Lang and Gelfand (1985)

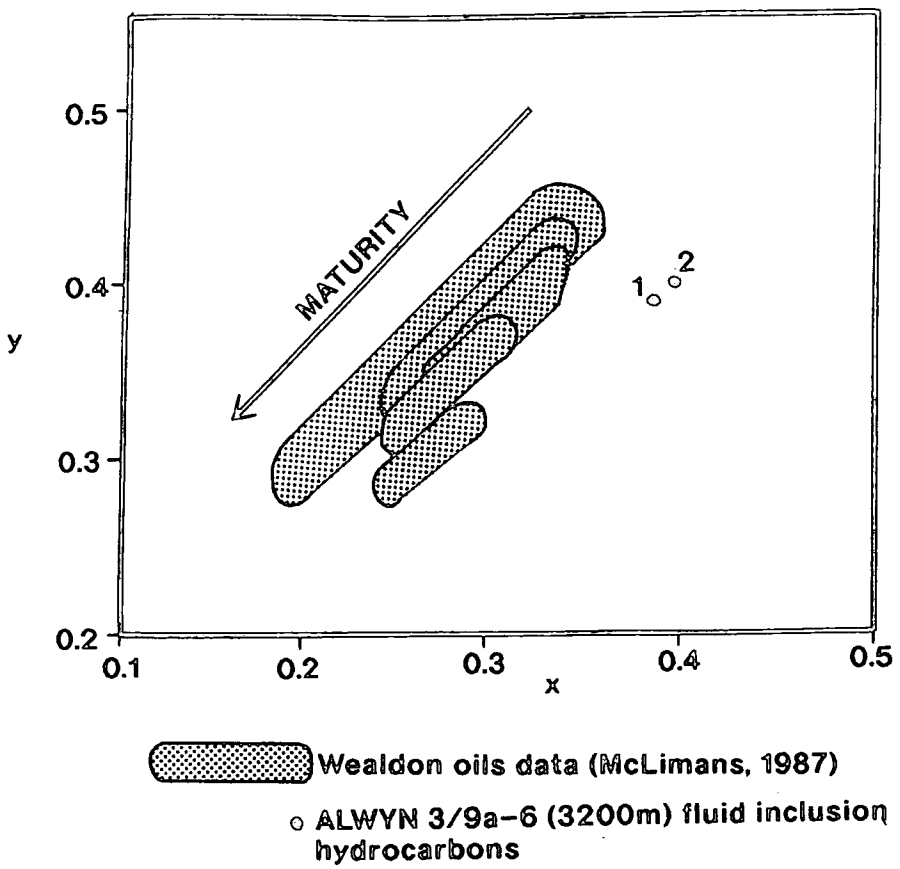

Fig.3.7.8.4f - Included hydrocarbons from Alwyn North (3/9a-6, 3200m) plotted as CIE co-ordinates. Compared to oils analysed by McLimans (1987) and assessed in terms of maturity. Modified from McLimans (1987)

	MPI-3	2MeNa/1MeNa
3/9a-6, 3190m	0.53	1.64
3/9a-6, 3220m	0.47	1.45

Although these data are not conclusive, the calculations of these ratios and indices for the Alwyn oils suggest that the included hydrocarbons are at the beginning of the oil window (early mature - Peters and Moldowan, 1992). This set of analyses agress with the GC and fluorescence analyses to strengthen the assumption made for bubble point curve selection of an early mature oil and hence the calculations of palaeo-pressure using hydrocarbon bearing inclusions.

3.7.9 Temporal Constraints on Fluid Inclusions

The K-Ar dating of the three Alwyn fields has been used to date the entrapment of oil influx into the reservoirs (section 3.6.11). It has also been recognised that hydrocarbon fluid inclusions also represent the first hydrocarbon flow into the reservoir contained within the diagenetic sequence. This, then, has implications for the previous interpretation of pressure and temperatures associated with respective inclusion populations and the actual timing of this fluid influx.

All of the age dates interpreted from separate studies conducted on reservoir sands in the Alwyn area (Sommers, 1975; 1978; Jourdan et al., 1987; Liewig et al., 1987; Hogg et al., 1992; Fig.3.7.9a) conform to previous interpretations made on the fluid flow history and reconstruction of fluid movements made by the geochemical and organic geochemical interpretations (section 3.6.12). It is inferred further that the Alwyn North field was exposed to hydrocarbon fill-up first, from a distal source. The effect of this early trapping is to preserve primary porosity and prevent continued diagenesis. Jourdan et al. (1987) ascribe an age date of 76-65Ma to this event. Recent work by Hamilton et al. (1992) have documented an increasing bias toward the younger end of the time scale with more accurate separating and analytical techniques with control provided by XRD and SEM observations. This would tend to pull Jourdan et al. (1987) data, since the clay fraction analysed in his study was using <0.2μm granulometric fractions as opposed to the <0.1μm fraction used by Hamilton et al (1992), toward the lower end of Jourdan et al. (1987) age ranges. Following Hamilton et al. (1992) observations and interpretation, the Alwyn data would still conform to distinct age ranges with respect to their structural position but that age dates assigned to the wells are more likely to be accurate toward the lower (younger) end of the range. Therefore, in Alwyn North lower end of the 75-65Ma range is most plausible for termination of diagenesis in this structure.

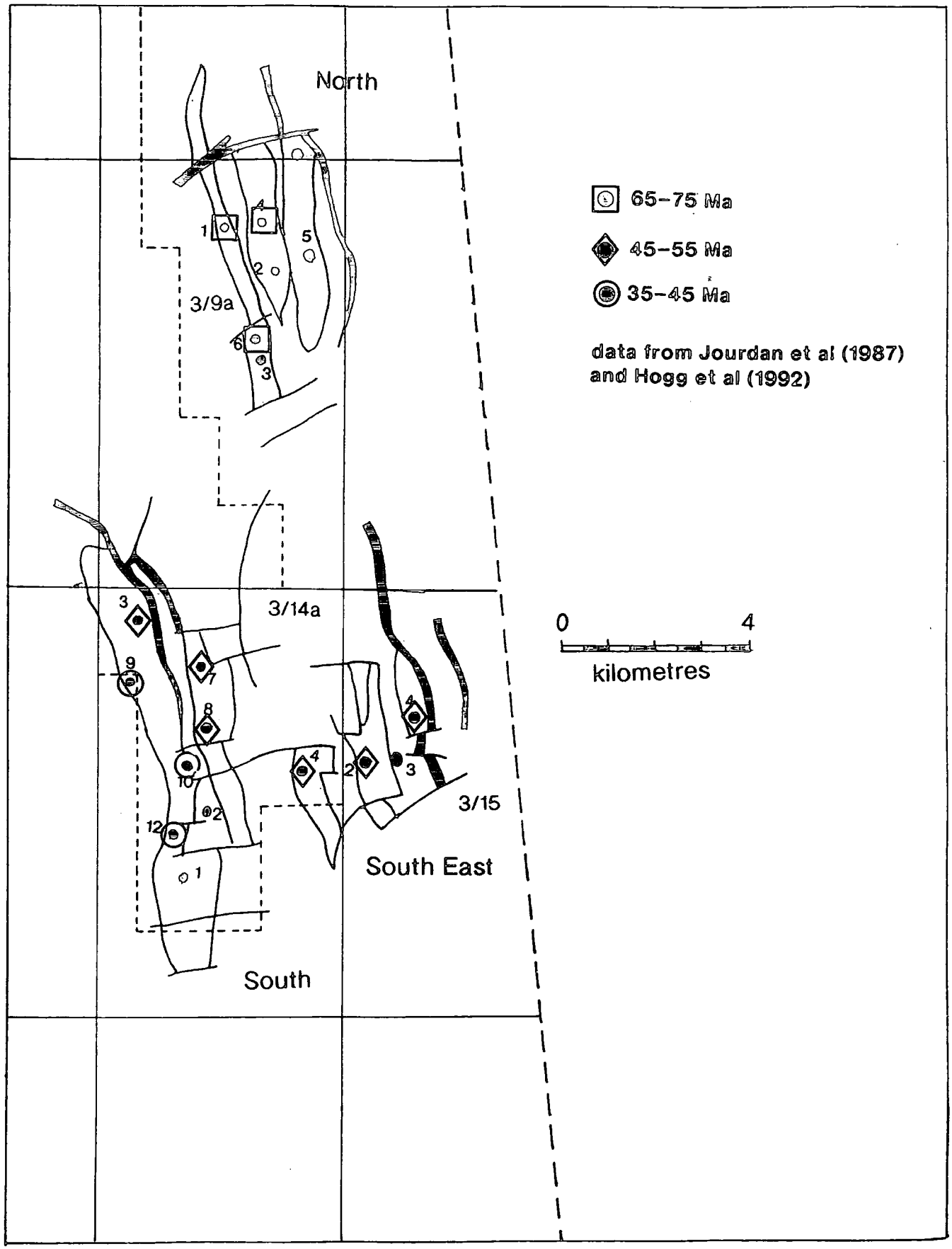

Fig.3.7.9a - Average ages of <0.1μm (Hogg et al., 1992) and <0.2μm (Jourdan et al., 1987) granulomteric illite fractions

*It is important to reiterate, however, that the thermal model may be wrong and the use of palaeo temperatures from the calculated burial and thermal histories may be invalid. It is assumed that heat flow is constant . Thermal conductivity may vary through time due to compaction effect of the lithological sequences. Also, the choice of compaction equation will have an effect on the thermal conductivities of the rocks through time. Palaeo-temperatures used for comparison to the fluid inclusion temperatures assume constant heat flow through time.

One principal benefit in constraining the primary influx and saturation of hydrocarbons into the reservoirs with respect to an absolute age is to be able to date the fluid inclusion populations and therefore the pressure and temperature interpretations. The QA2 aqueous and hydrocarbon inclusion population in the Alwyn North field represents the primary trapping of hydrocarbons and when combined with the age dating from Jourdan et al. (1987), these inclusions are dated as being trapped at 75-65Ma. This period of flow and hydrocarbon influx occurs close to or at hydrostatic pressure conditions and at temperatures of 89-104°C (section 3.7.7). Similarly, the period of fluid flow and entrapment of the QA1 and QA2 inclusions in the Alwyn South East are dated at 55-45Ma (more plausibly 45Ma). Pressure estimates observed for these inclusions reflect normal pressures and temperatures of 4300-5700psi and 112-126°C respectively.

It is possible to estimate the palaeo temperatures corresponding to the radiometric ages by considering the depth of burial of the reservoir at the time and the palaeo geothermal gradient. This temperature estimate can be compared with the fluid inclusion temperature data. Similarly hydrostatic pressures can be compared if the depth is calculated from the burial history curve and pressure gradient is known. Comparison will indicate whether the inclusions were part of a fluid flow phase at ambient reservoir conditions or were at elevated or reduced temperatures.*

Using BasinMod™ software program to reconstruct the burial history and palaeo temperatures, the reservoir section in the Alwyn North field is interpreted at 75-65Ma as being buried to a depth range of 1200-1450m (Fig.3.5.1a) with a reservoir temperature of 58.8-67.3°C. A surface temperature of 18°C is assumed (Anderton et al., 1980) and the present day geothermal gradient of 34°C/km) the temperature does not compare with T(hom) recorded for fluid entrapment (89-104°C) in the reservoir at this time. A possible explanation for these elevated temperatures recorded in the fluid inclusions may suggest that the fluids were from a hotter source. Another, but more unlikely, explanation is that the illite age dates are incorrect and do not date the oil emplacement, that the fluid inclusions have been reset (Osborne and Haszeldine, 1993; section 3.7.6) or a significantly higher geothermal gradient existed at the this time. However, diagenetic and geochemical observations tend to verify and support these dates with respect to relative oil emplacement.

Similarly, when the reservoir section in the Alwyn South East field (3.5.1b) is modelled with respect to ambient temperature due to background heat flow, the modelled temperatures do not correlate with the recorded T(hom) range and hence T(trapping)

for the QA1 and QA2 generation inclusions identified as being nucleated in the diagenetic sequence at approximately 45Ma. Indeed and interestingly, the trapping temperatures (112-128°C) record higher mean temperatures then the present bottom hole conditions (116°C - 3/9a-2). Since there is no evidence of uplift, it must be inferred that hot fluids were circulating and flowing through the reservoir sands during fluid inclusion entrapment if other explanations documented above are dismissed.

To summarise the pressure history, it is evident from the combination of diagenesis, fluid inclusion microthermometry, geochemical and K-Ar dating observations that two periods of hydrostatic pressure conditions, at 75-65Ma and 55-45Ma have been identified in the Alwyn North and South East field respectively. Therefore, fluid flow and diagenesis at these periods of normal pressure could infer periodic pulsing of fluids into the reservoir section. This pulsing theory is coincidental with the petrographic observations of distinct overgrowth boundaries attributed to distinct diagenetic phases. These diagenetic phases may indeed be controlled by the pressure differential between the distal source and the reservoir section. This would control the amount of fluid transfer and therefore the ability of diagenetic fluids to precipitate diagenetic minerals in the sands. Although the temperature has long been recognised as one control on the solubility of chemical diagenesis, the pressure differential that operates between source and sink for these fluids may control the actual availability of any fluids flowing into the reservoir. To test the reality of this theory of differential pressure control on the diagenesis in the reservoir, quantification of pore pressure through time is necessary. Although K-Ar dating methods have identified and allowed the interpretation of fluid inclusion data to describe pressure conditions at two periods in the geological history of the reservoir, an independent pressure modelling approach was also used to model the potential of pressure build up, retention and dissipation through time.

3.7.10 Overpressure mechanics and pressure history in the reservoirs

It is possible to quantify pore pressure development through time due to the mechanism of disequilibrium compaction. This mechanism relies on the inability of compacting pore fluids to escape quickly enough to maintain a pressure equilibrium in the porous medium (Magara, 1974; Dutta, 1986; Mann and Mackenzie, 1988). The main controls of this mechanism lies in permeability linked to the rate of loading (overburden stress).

Pore pressure versus time has been modelled utilising the BasinMod™ software program. The software recognises the existence of pressure generation due

compaction disequilibrium but does not consider the possibility of contributions from any other overpressure mechanism (section 2.2).

The burial history profile for the 3/9a-2 well (Fig.3.5.1a) is used to represent the average burial history of the Alwyn North and South East fields, with Fig.3.7.10a a reconstruction of the pressure profile in response to the burial history for the Kimmeridge Shale Formation and Brent reservoir sections. The profile shows that a normal hydrostatic gradient is maintained over the first 1300m (approximately) of burial to the end of the Cretaceous (65Ma) in response to the ability of the pore fluids to escape in a compacting sequence modelled as moderate enough for normal sediment compaction.

Contemporaneous maturation of the Kimmeridge Formation in the distal Viking Graben downfaulted to the east has been modelled and the onset of maturation occurs as early as 85Ma (Fig.3.5.6.3a). At this time, modelling observes no maturation of source rocks in the field area (Fig.3.5.1a). However, transference of fluids out of the depocentre up dip to flank trap areas such as Alwyn could be envisaged for these maturing hydrocarbons in the Viking Graben. A lag time of <20Ma for migration is entirely feasible to transport these fluids moving under the combined effect of buoyancy and water flow (England et al., 1987) to the Alwyn North reservoir at 75-65Ma time frame. England et al. (1987) describe petroleum migration and direction in terms of fluid potential and states that excess water pressure is the dominant mechanism in controlling fluid potentials at depths greater than 3km. Thus, differential pressure is documented as a primary drive mechanism in the transference and migration of petroleum, at depths greater than 3km, from source area to reservoir. These fluids have also been interpreted to be operating and trapping under normal pressure but at elevated temperatures at 75-65Ma in Alwyn North (due to the inferred distal source of the fluids - section 3.6.8). When this normal/hydrostatic pressure period of precipitating diagenesis and oil trapping in the Alwyn North reservoir is plotted on the pressure versus time profile, it is seen that this period pre-dates the development of overpressure in the reservoir from pressure modelling. However, immediately after this phase of entrapment at 65Ma, rapid burial of the reservoir section in response to increased sediment supply and subsidence caused an anomalous build up of pressure. The period of overpressure due to compaction disequilibrium developed at 65Ma and continued to peak at the approximately 55Ma. Peak overpressure modelled with this mechanism approximates to 7MPa (Fig.3.7.10a). It would appear, when coupled with the dating of diagenesis, oil in-migration and reservoir pressure conditions, that a period of diagenesis and associated primary hydrocarbon influx was operating under

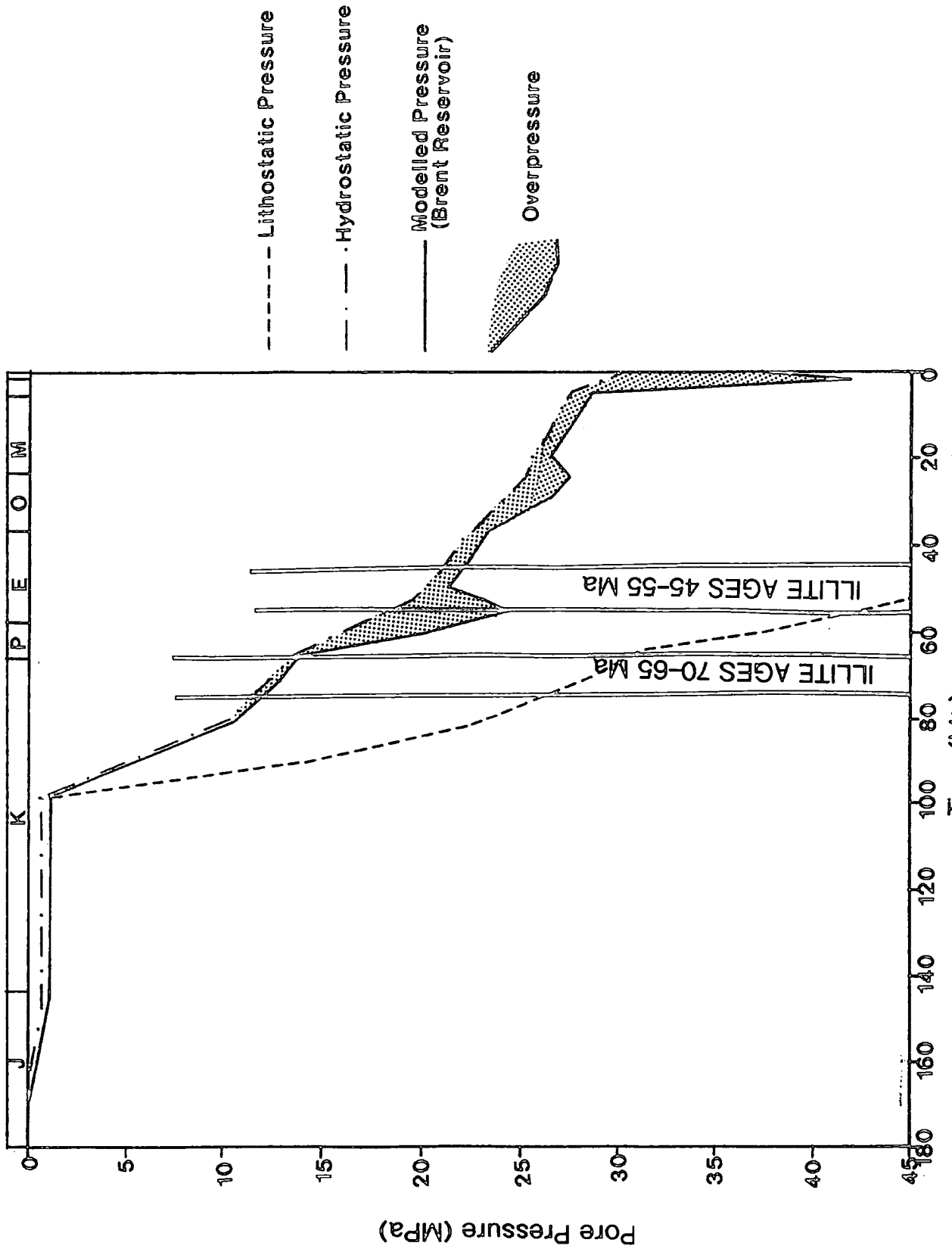

Fig.3.7.10 - Pore pressure history of the Kimmeridge Shale Formation and Brent reservoir based on the burial history plot of 3/9a-2 (Fig.3.5.1a) taken as representative of the burial history of the Alwyn North and South East fields

hydrostatic conditions. These processes appear to terminate when reservoir pressure increased to an overpressure state inhibiting fluid flow and availability of precipitating mineral solutes into the reservoir. The model shows gradual reduction in excess pressure when the rate of burial decreases, and normal pressure is re-established by approximately 50Ma.

Again, analysing this period in the history of the reservoir diagenesis, this is approximate to the timing of the onset of primary trapping of hydrocarbons and the early diagenetic phase in the Alwyn South East field. Illite ages of 55-45Ma (Jourdan et al 1987) date the retardation and termination of diagenesis coincidental and simultaneous with the saturation of hydrocarbons in the reservoir. However, the model shows overpressure still in operation till 50Ma (Fig.3.7.10a). But when considering the refined work on illite age dating by Hamilton et al. (1992) the lower/younger end of the age range is favoured (45Ma).

When this interpreted period of temporally constrained diagenesis, hydrocarbon saturation and hydrostatic reservoir conditions are correlated with the independently generated simulation of pressure versus time, a similar pattern emerges. Both pressure interpretation methods agree that this period of diagenesis in the Alwyn South East field at approximately 45Ma is taking place at or close to normal pressure conditions. At approximately 37Ma, pressure conditions in the reservoir respond to a slightly higher/more rapid burial rate (Fig.3.5.1a). This may cause pressure to increase again. Permeability would be less at this depth (approximately 2300m) due to increased mechanical and chemical diagenesis. The period of rapid burial between 37-25Ma (Fig.3.5.1a) responds with a second overpressure peak of approximately 3-4MPa before a stabilised pressure condition is resumed in response to a further change in the burial rate at 22Ma. The profile maintains a gradient reflecting hydrostatic increase until approximately 7Ma. There is then a dramatic increase of overpressure to the order of approximately 20MPa due to rapid burial which appears to be have existed to the present day. This late phase of very substantial overpressure development will be assessed in section 3.7.11.

From the computer simulation of pressure history in the reservoir section, it is/was possible to combine and correlate interpreted observations regarding rock data and simulated pressure profiling using lithological, stratigraphic and other supplementary data. Both methods have been used to construct a history which infers and postulates a theory of diagenetic and fluid flow control in response to the pressure state in the reservoir. It is inferred that fluid flow is retarded during periods of reservoir

overpressure, itself developed by the mechanism of disequilibrium compaction in response to rapid burial in the subsiding basin, and diagenesis will occur exclusively within periods of fluid flow (pressure differential between source and sink; that is, between the Viking Graben depocentre and the structural traps). Hydrocarbons which have been trapped and interpreted to be in a normal pressure state have also been dated in these periods of pressure quiescence.

This observation and theory is based on the observations and pressure interpretations from both the diagenetic sequences in Alwyn North and South East. It also represents the sensitivity and the delicate balance required to achieve normal pressure conditions. This sensitivity increases with depth as permeability and porosity diminishes. A slight increase in the burial, deposition and/or loading rate over the equilibrium threshold amounts to the development of pressure in the section.

3.7.11 Quaternary - Recent pressure history (Figs.3.7.10a, 3.7.11a, b and c - the modelled pressure histories of Alwyn South , North and South East respectively)

An important observation from the computed pressure history is the apparent large development of overpressure during the last 10-5Ma in response to rapid burial. However, the sensitivity and amount of anomalous pressure build up in the model is highly accentuated during this stage of burial. This is due to the very low permeability at this depth. At approximately 7Ma, the model predicts the reservoir section at approximately 3050m (Fig.3.5.5a). Baldwin and Butler (1985) estimates from a porosity/depth function that average porosity would be 12.4% and the model simulates a permeability (using the modified Kozeny-Carman model) of 0.0077md for the base of the Kimmeridge Formation/top of the Brent.

One major problem is the lack of reliable age dates in the top 800m of the well stratigraphy. This, traditionally, is a problem due to the well logging process in the North Sea basins as the top 500m of section is usually drilled with little regard to cuttings returns and recorded lagged data. There is no great significance in detailing the top hole stratigraphy and thus little importance is given to the accurate dating and picking of formation tops. Due to the sensitivity of the model during this phase and amount of overpressure response returned by the software, it was necessary to constrain the stratigraphy and hence the thickness of each formation. Since the thickness of each major stratigraphic unit in this section - Oligocene, Miocene, Pliocene and Quaternary - are vital in the correct modelling of overpressure generation due to compaction disequilibrium, an accurate correlation was necessary.

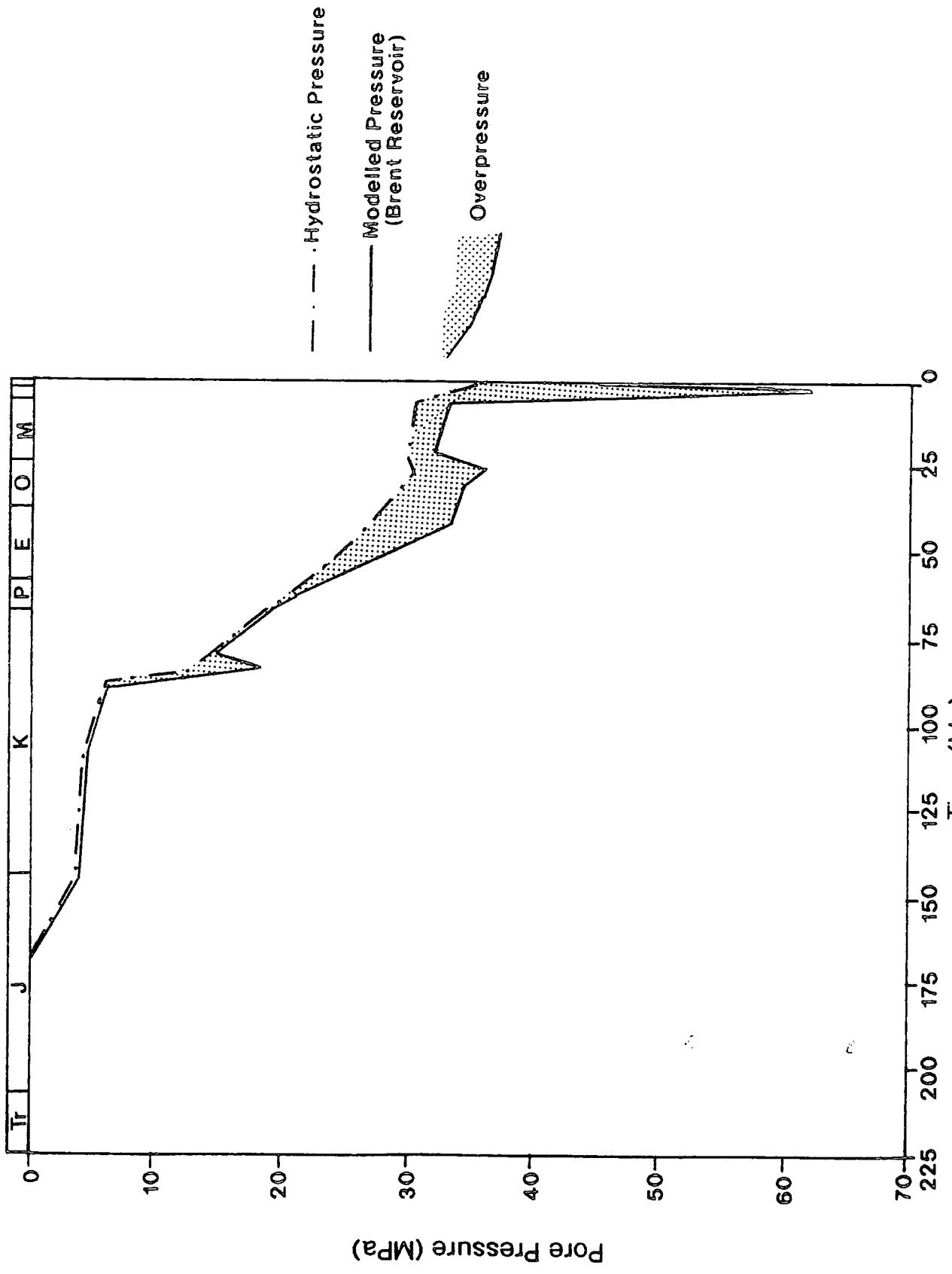

Fig.3.7.11 - Pore pressure history of the Alwyn South field (the Kimmeridge Formation and Brent reservoir) based on the burial history plot of 3/14a-8 (Fig.3.5.1b)

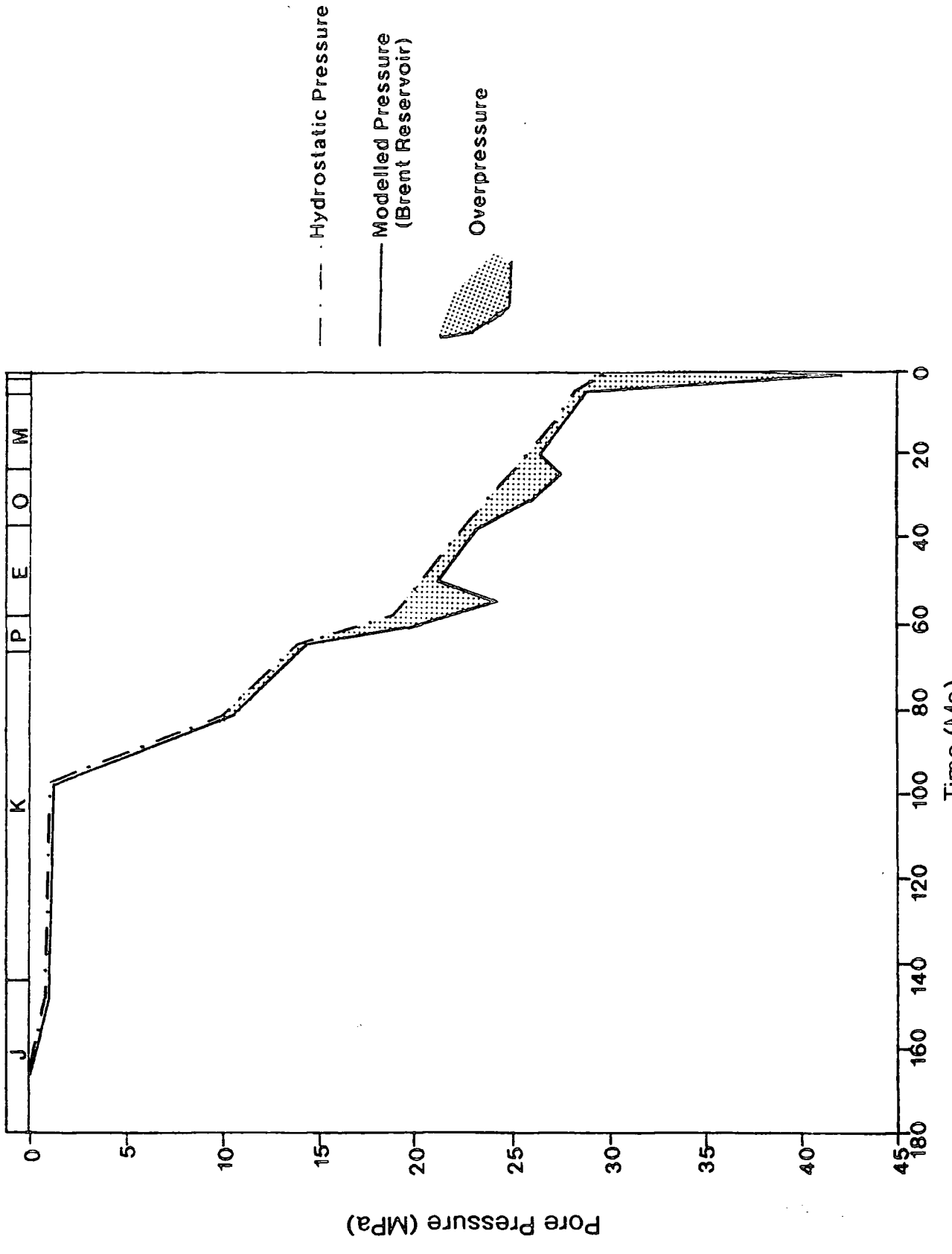

Fig.3.7.11b - Pore pressure history of the Alwyn North field (the Kimmeridge Formation and Brent reservoir) based on the burial history plot of 3/9a-2 (Fig.3.5.1a)

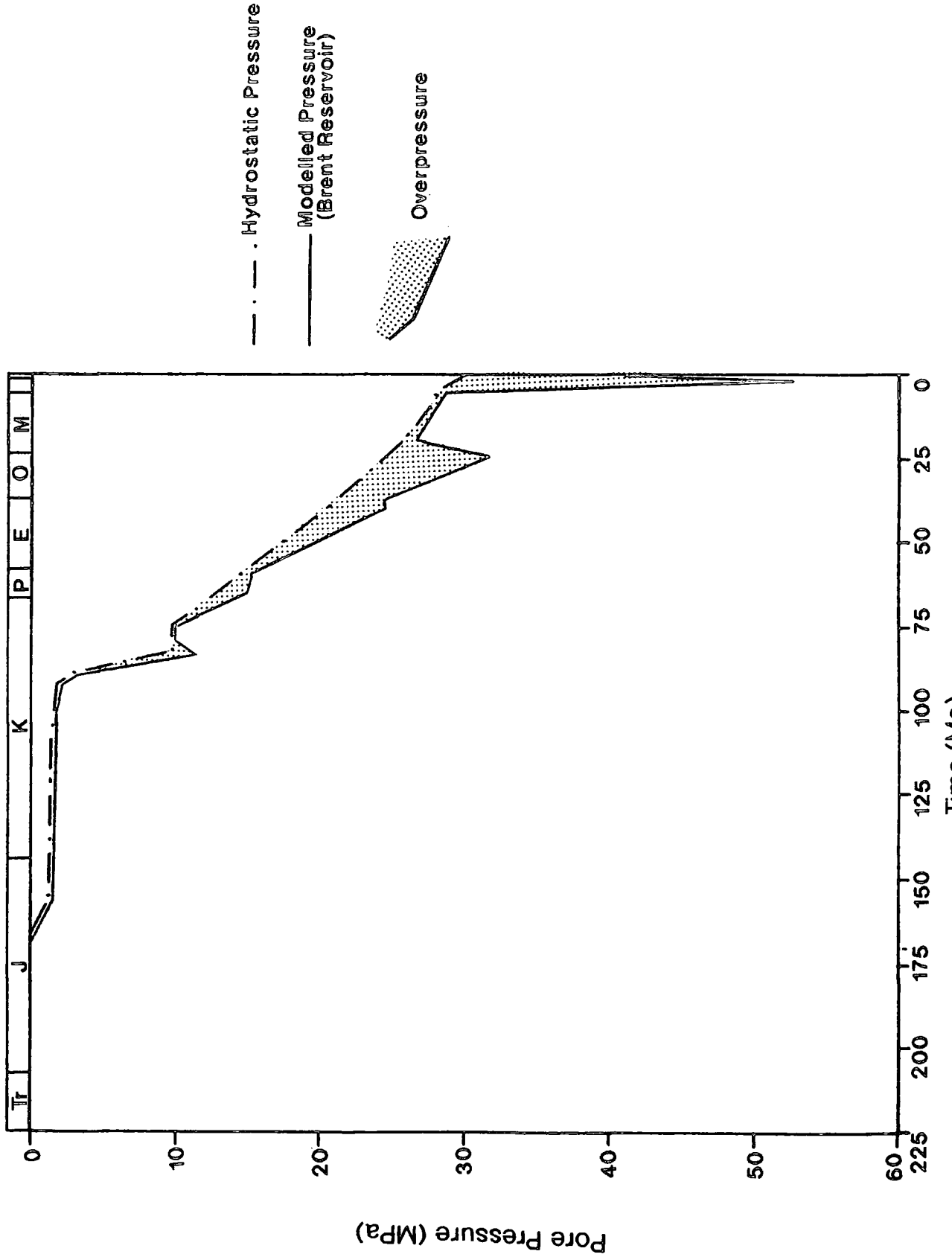

Fig.3.7.11c - Pore pressure history of the Alwyn South East field (the Kimmeridge Formation and Brent reservoir) based on the burial history plot of 3/15-4 (Fig.3.5.1c)

Since some electric logs are available through the top hole section, correlations were drawn from the log response between wells and regionally across the field area (Figs.3.7.11e and d). The stratigraphic section was subdivided and correlated using gamma ray response (Fig.3.7.11d) and a combination of gamma ray, resistivity and sonic response (Fig.3.7.11d). Although accurate age determination is not possible using these methods, lithostratigraphic consistency is possible. The lithological transition at the top Pliocene/base Quaternary saw a sharp increase in argillaceous sediments. This sharp deflection in the amount of compacting shales affected the log parameters as a sharp deviation to a negative response on the gamma ray (γ) log from the ambient conditions of relatively high γ in the Quaternary. Since the gamma ray tool responds to the amount of absorbed natural radiation emitted from the open formation, the more clay rich and argillaceous Quaternary section gave a background and average response of 15-20 cps (counts per second). A sharp kick in the log profile returning <5cps was seen to be a constant observation in each well throughout the Alwyn fields following the ambient conditions in the Quaternary. The depth of this correlation and log kick ranged across the fields from 250m TVD KB (well 3/15-5) to 333m TVD KB (well 3/9a-N3). Fig.3.7.11a shows a schematic reconstruction of the profile and response of the γ ray at the top of the subsequently interpreted Pliocene. The wells depicted in Fig.3.7.11d are representative of all wells and associated log response.

The γ ray profile was not sufficient alone to identify the stratigraphic boundary at base Pliocene/top Miocene. This is most likely due to a similar amount of clay content and therefore an accurate pick utilised a combination of γ ray, resistivity and sonic responses. Indeed, the base of the Pliocene/top Miocene is interpreted on the basis of an approximately 20m thick section deflecting the profile from low values of γ ray, resistivity and sonic to a marked kick peaking with values of 85cps (γ ray, well 3/9a-2), 5 ohms/m (resistivity, well 3/14a-8) and high sonic transit times (85 µsec/ft, well 3/15-4). This leads to an interpretation of a consistent marker, possibly high clays/argillaceous content, across the field giving such a response. This interval of 20m and associated anomalous profile suggests a major lithological change in an otherwise monotonous lithological profile. However, flanking this kick in the profile in the Pliocene are similar but of less magnitude responses. Therefore, the Miocene/Pliocene boundary is picked and interpreted at the major lithological shale boundary as suggested by the major deviation in the electric log profile. Thus the base of the Pliocene/top of the Miocene ranges from 618m (TVD KB) in well 3/9a-2 to 655m (TVD KB) in well 3/15-4.

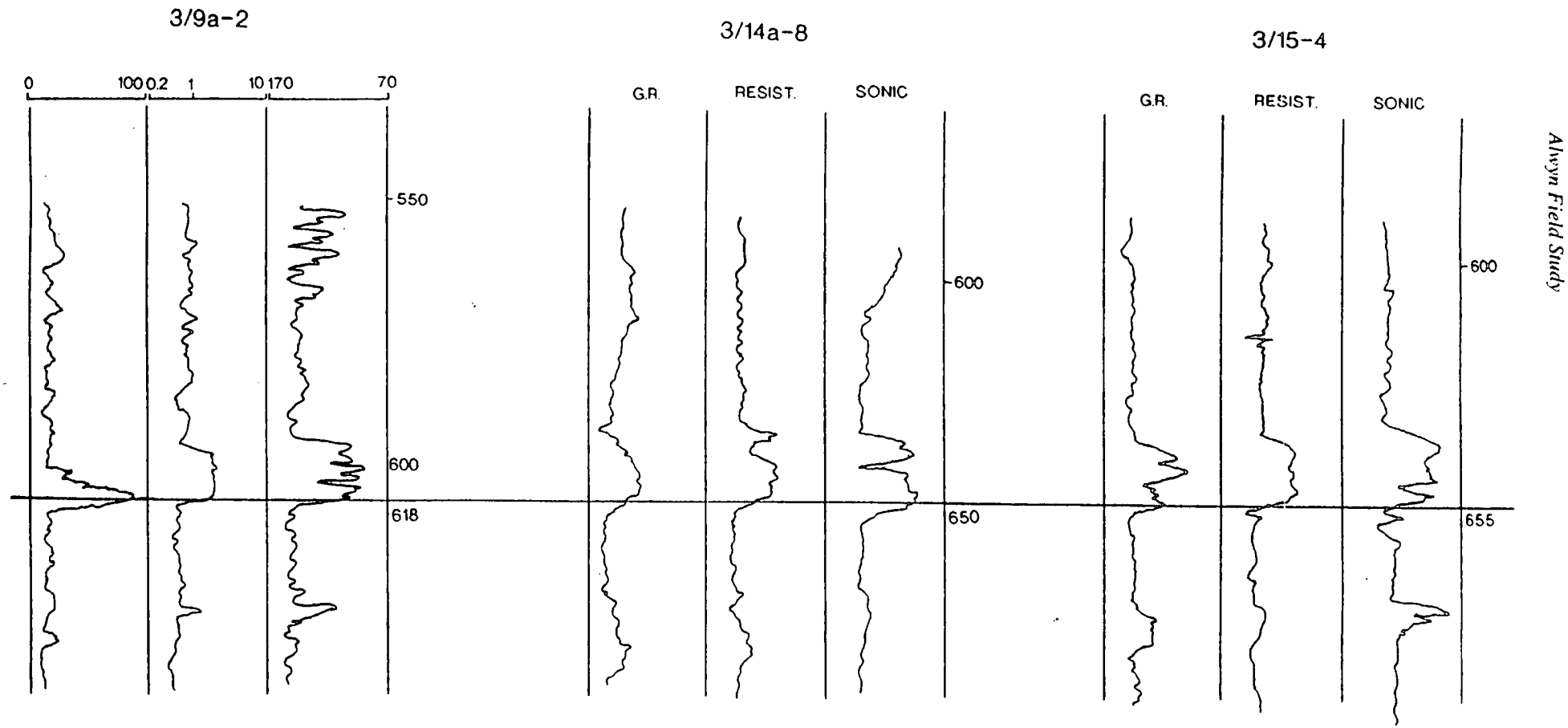

Fig.3.7.11e - Interpreted Miocene stratigraphic pick based on gamma ray, resistivity and sonic correlation across the three Alwyn fields

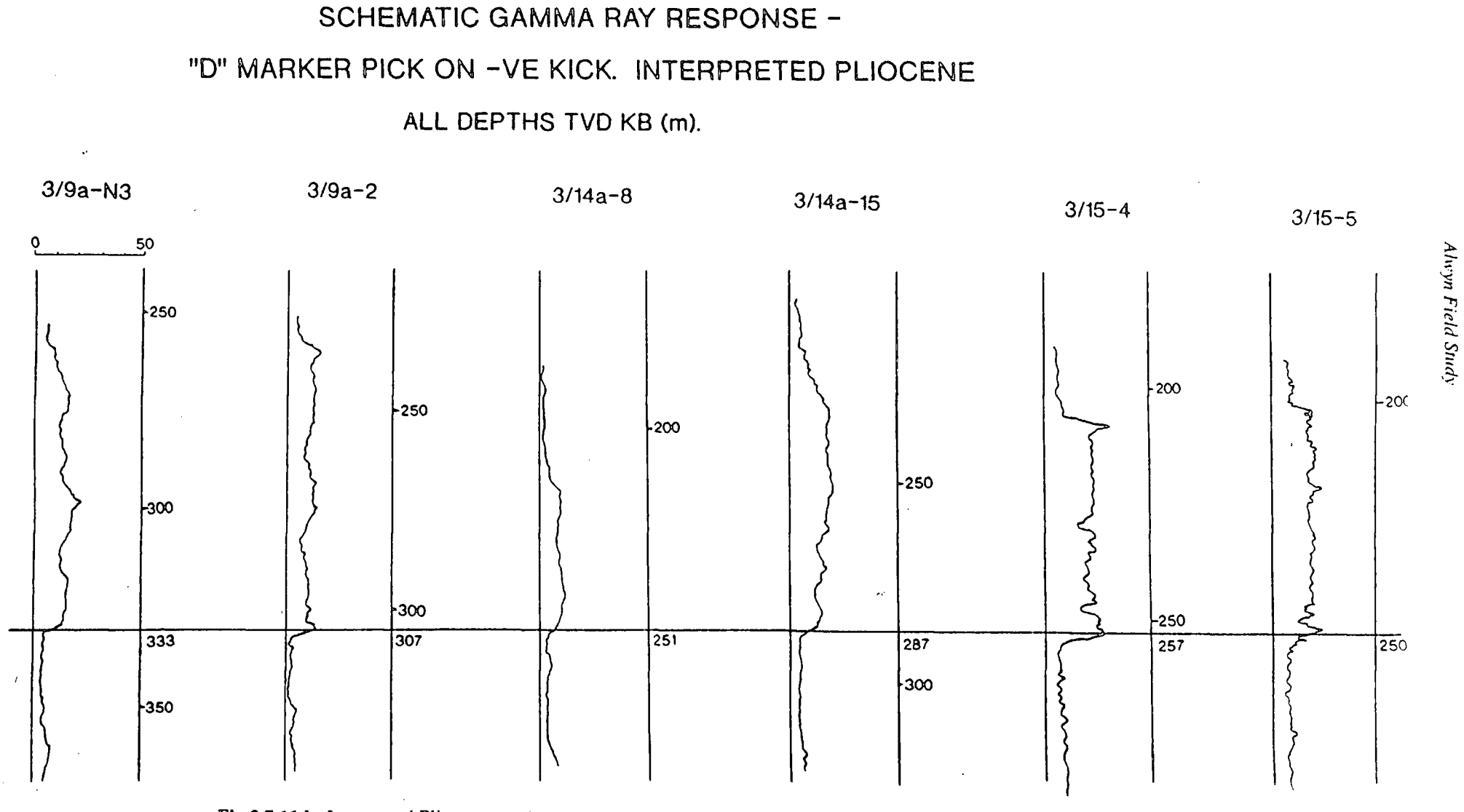

Fig.3.7.11d - Interpreted Pliocene stratigraphic pick on gamma ray correlation across the three Alwyn fields

This determination and lateral consistency of the electric log markers provides the stratigraphic control in the top hole section utilised by the basin modelling package. Although the actual chronostratigraphy of these electric log picks are unknown, the correlation does provide a level of consistency in lithostratigraphic boundaries across the three fields. Thus, confidence in calculating an accurate pore pressure at the time interval 10Ma-recent is much higher.

With the top hole stratigraphy constrained, the pore pressure developed in response to the last phase of burial was observed to be a similar magnitude across the Alwyn area. In response to the more rapid phase of burial, the permeability and porosity associated with the large argillaceous section which lies stratigraphically above the reservoir allows the anomalous build up of pressure of the order of 8.5MPa (3/9a-2) to 11.5MPa (3/15-4) present day (Figs.3.7.11a and c) with peak overpressure developing approximately at 4-5Ma of the order of 12.5MPa (3/9a-2) to 27MPa (3/14a-8 - Fig.3.7.11b) before loading relaxation to bring the pressure to its present state. Therefore, modelling overpressure through time using computer generated plots based on lithological, stratigraphical, porosity and permeability relationships, real-time well and engineering data allows the interpretation of pressure generation due to the mechanism of compaction disequilibrium. It has been seen to be useful in correlating diagenetic observations, K-Ar illite dates and basin modelling. It is also useful in providing a comparison between present day overpressure predicted by the modelling and real time information from RFT, FIT and DST data.

Using compaction disequilibrium as the generating mechanism, it is seen that the overpressure that developed in response to this last phase of burial is a regional phenomenon affecting the 3 fields in the same manner generating approximately 8.5MPa (1223.5psi) - 11.5MPa (1668.8psi) at the present day. So, from approximately 10-5Ma, a blanket overpressure effect due to regional rapid burial has created 8.5MPa - 11.5 MPa overpressure.

However, pressure distribution and differential in the Alwyn area must be accounted for. Modelling compaction disequilibrium yield a similar contribution of overpressure in each of the three fields and therefore other mechanisms need to be considered to explain the variability of overpressure that is experienced at the present day. As previously identified, overpressure is defined into 3 pressure cells (section 3.2) with the Alwyn North field experiencing lowest overpressure in the region of 1500-1900psi through the intermediate overpressure of the Alwyn South filed to a range of 2900-3400psi in the Alwyn South East field. Therefore, if the amount of overpressure

created by the calculated compaction disequilibrium effect is accurate, the shortfall must be accounted for; as well as a mechanism and parameter for pressure differential control.

The contributions of potential overpressure from other mechanisms to account for the present day distribution is discussed in the following section (3.8).

3.8 Other Overpressure Contributory Mechanisms

From the preceeding section, it was seen that although overpressure was modelled to have developed in the last 5-10Ma in response to rapid burial, the overpressure distribution in the Alwyn field requires an explanation as the compaction disequilibrium derived overpressure modelled during the final phase of burial was seen to have affected the three Alwyn fields approximately equally. Therefore, other potential mechanisms of overpressure generation are discussed and evaluated in their respective potential to develop overpressure.

3.8.1 Hydrocarbon Thermal Maturation

This mechanism operates to generate overpressure by exposing a suitable organic rich source rock to temperature conditions whereby a thermal reaction causes the cracking of liquid hydrocarbons to gas with an associated increase in volume (Barker, 1985; section 2.1). If the volume of the system is restricted, excess pressure will be created. Section 3.5.2 documents the maturation characteristics of the likely source areas for hydrocarbons trapped in the reservoirs of the Alwyn fields.

Section 3.5 calculated the overpressure potential of the source formations in the Viking Graben (Fig.3.5.6.3a) and the East Shetland Basin (Fig.3.5.6.2a). Although the calculations are purely theoretical and probably inaccurate due to assumptions made regarding the seal retention ability of the formations (poroperm and mechanical relationships) and the lack of input regarding kerogen types, specific hydrocarbons, solubilities of oil/gas and that any developed gas would be purely methane, the calculations do suggest a vast amount of overpressure generated in these basinal areas.

Since the identification of the source area is distal to the Alwyn field, a transporting medium for fluids must be proposed. Laterally continuous sand horizons plus fault zones could act as avenues of pressure transference out of the depocentre with an associated progressive leak off of fluid and pressure. Work conducted by Buhrig (1989) and Paxton et al. (1993) show a progressive reduction in the amount of overpressure away from the Viking Graben axis. This would then, simplistically,

assume a decrease in pressure away from both a deeper and hydrocarbon generating area. It is interesting to note that within the Alwyn area it is the Alwyn South East field which is the most structural and areally proximal to the Viking Graben and also experiences the highest overpressures. Similarly, the more distal and structurally higher elevated reservoirs of Alwyn North contain the lowest range of overpressures.

Although not modelled in detail, overpressure could have developed in response to gas charge in the Viking Graben from approximately 55Ma to the present day with transference up dip to the Alwyn field area. The more proximal South East field would be subjected to higher overpressure with a progressive leak off of overpressure through semi-sealing faults to the structurally more elevated Alwyn South and North fields if the faults were more permeable than the top seal. This would account for the pressure distribution between the Alwyn structures and support the concept of pressure compartments with faults as lateral pressure and fluid seals. These faults would be seen to be transitionary phenomena in their ability to retain pressure. The faults will have a physical finite limit of mechanical coherence dictated by various parameters such as magnitude and throw of the fault, angle of heave, component fault gouge, amount of previous diagenesis along the fault plane, competence of wall rock and response to imposed compressive and tensile stress.

3.8.2 Mechanism of overpressure retention and transference

A controlling mechanism of fluid and pressure transference from source to reservoir as well as in field overpressure distribution must be in existence. Illite intensity identified in the diagenetic sequence within the reservoir (Hogg et al., 1992), elevated fluid inclusion temperatures and pressure distribution suggest that faults determine and control fluid migration from source to individual reservoirs. These faults, which offset reservoir levels and simplistically divide the Alwyn field into 3 structures of Alwyn North, South and South East have been described as a Viking Graben sub-parallel NNW-SSE system complimenting secondary E-W cross faults (section 3.2). Both fault sets are common and repetitive features throughout the region and the faulting style generates the necessary rotation to provide the structural trapping style of the Alwyn fault blocks (Inglis and Gerard, 1991). There are various indications in the diagenesis to suggest the involvement of faults in the transference mechanism:

3.8.2.1 Diagenetic sequence

It has been reported in previous sections that the diagenetic sequence in the reservoir sands of the Brent Group members suggest diagenetic cyclicity. Zonation and style of quartz cementation has been described by Jourdan et al. (1987), Hogg et al. (1992) and

in this study (section 3.6). The common observation is zoned syntaxial or epitaxial quartz overgrowths in optical discontinuity reflecting differing pulsing and influx of precipitating mineralisation phases. This would be best explained by a fluid pulsing perhaps with an external valve mechanism, possibly faults, controlling the influx of fluids and pressure.

3.8.2.2 Fluid conduit continuity

It has been documented previously (section 3.3) that the main carrier beds for the fluids and pressure has typically been the sand members of the Brent Group and the Statfjord Formation. These members all conform to a largely identical lithostratigraphy irrespective of structural level (Morton et al., 1992). However, at different structural levels, common diagenetic features and coincidental fluid inclusion observations have been identified in reservoir sands of similar stratigraphic interval (section 3.7) which then suggests a common lateral transport conduit. Since the sands of the Brent Group and Statfjord Formation are laterally continuous over much of the Viking Graben (Morton et al., 1992), it is proposed that the vertical distance achieved by the fluids and pressure generated in the graben is by utilising normal faults. Burley et al. (1989) also indicate that large scale vertical movement is most readily accomplished along major faults.

3.8.2.3 Intense diagenesis in wells near faults

Jourdan et al. (1987) and Hogg et al. (1992) report intense diagenesis occurring in well 3/14a-8 (Alwyn South). Hogg et al. (1992) used cathodoluminescence to identify complex zoning in the diagenetic sequence of this well which was more profound than in wells of close proximity. Hogg et al. (1992) describes intense illitisation in this well suggesting focused flow and possibly an entry for acidic fluids circulating to cause this intense diagenesis. Jourdan et al. (1987) documents anomalously high trapping temperatures for fluid inclusions in the quartz overgrowths and attributes this phenomenon to the close proximity of a nearby major fault. It is postulated that this fault, representative of others in the area, could provide access for deeper and distally derived fluids and pressure.

3.8.2.4 Pressure modelling

The relationship of differential pressure control and its effect on the timing of reservoir diagenesis is described in section 3.7. It was inferred that reservoir diagenesis preferentially occurred during phases of normal pressure conditions at reservoir level and that the build up of overpressure at reservoir level would inhibit and retard diagenesis. Although temperature is the main control on diagenesis (Burley et al.,

1989; Saigal et al., 1992), if fluid is stagnant in a reservoir section then replenishment of precipitating minerals to induce further diagenesis is restricted and ultimately starved.

A common model of fluid and pressure transference is the utilisation and re-activation of a fault plane involving dilation of a fault zone. This concept was initiated by Sibson (1975) in the sub-crustal regime but its application to the sedimentary environment is plausible. Burley et al. (1989) have described the diagenesis in the Tartan structure as being likely controlled by this seismic pumping and valving mechanism. The system is described more fully by Fig.3.8.2.4a and involves the build up of pressure against an impermeable barrier (fault plane) restricting fluid passage. Increased fluid flow from the source area at a point of focus between the carrier bed (likely to be a continuos sand horizon) and the fault plane would cause increased imposed stress on the fault plane before the mechanical capacity of the fault could no longer sustain this overpressure. Break out along the fault plane will result in a pressure drop, elevated temperature fluid transport and on structure cooling (Burley et al., 1989). The fault plane will resume a sealing capacity once pressure has dissipated and a suitable pressure regime is re-established at the point of fluid entry and exit along the fault plane. Multiple repetitions of this process will provide the fluid flow pattern necessary to generate the observed diagenetic sequence seen in the Alwyn reservoirs. Hogg et al. (1992) reports that in Alwyn South, the relative complexity of CL textures in 3/14a-8 relative to shallower up flank and crestal wells may be due to thermal and compositional homogenisation of the incoming hot basinal fluids, utilising major faults, with existing reservoir waters. In such a case, it would follow that homogenisation would be more advanced resulting in a slower and more continuos cement growth in wells furthest from the point of entry (fault) of the diagenetic fluids.

The seismic pumping/valving scenario provides a convenient model of fluid and pressure build up and catastrophic release can account for the pressure distribution in the Alwyn field, whereupon the fault sets will act as transitionary in sealing ability in response to the overpressure generated by hydrocarbon maturation and thermal cracking to gas in the Viking Graben. This would allow higher pressures in the more proximal South East field leading to compartmentalisation of pressure away from the Graben with an associated loss of pressure to structurally higher levels and traps. The model would also fit with the diagenesis and intensity of mineral growth near to fault

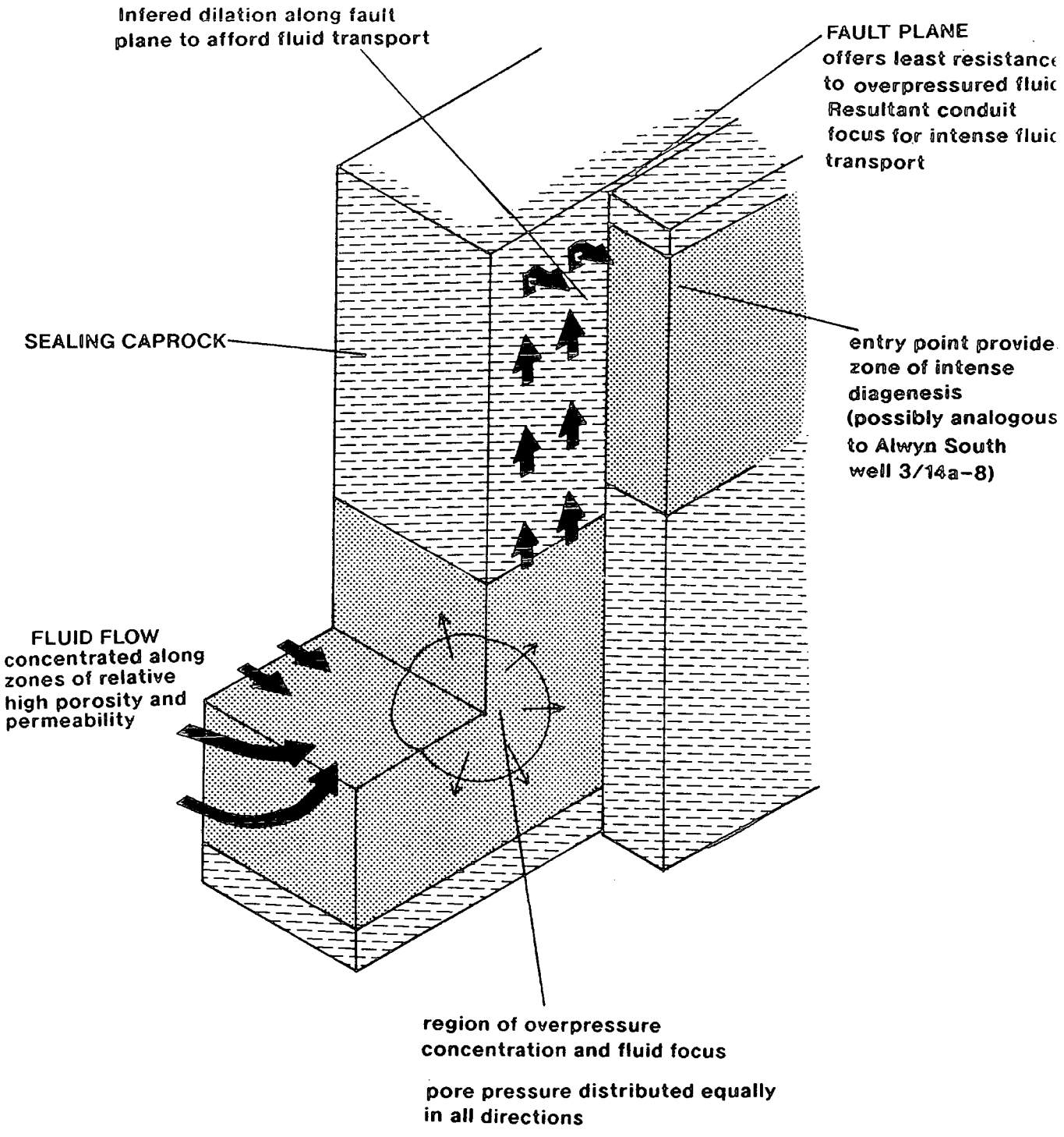

Fig.3.8.2.4a - Seismic pumping/valving mechanism as a possible source for periodic fluid flow and entry into the Alwyn field reservoirs. Based on Sibson (1975) and modified from Burley et al. (1989)

planes. However, the K-Ar dating of the diagenesis suggests that all diagenetic phases associated with the influx of deeper and distally derived fluids lie in the period of <75Ma. It is documented that these faults have remained inactive since the Kimmerian (150Ma, Inglis and Gerard, 1991) and that the faults identified on seismic do not penetrate the base Kimmeridgian at any point throughout the area (Johnson and Eyssautier, 1987; Jourdan et al 1987; Inglis and Gerard, 1991). Therefore, this would conflict with the timing of fluid influx into the Alwyn field. However, since the fluids are utilising the faults from structurally deeper, movement along the fault plane need not involve any component of vertical shear but rather operate in a dilational mode. This would be sufficient to facilitate movement of fluids and pressure along the fault zone.

Transportation of sufficient fluid volume by this method is not seen to be inhibited by fault planes acting as conduits. Analogies taken from modern earthquakes studies have shown in Idaho, the Borah Peak earthquake expelled greater than $1km^3$ of groundwater at <30°C over a 6 month period (Wood et al., 1985). These earthquakes were measured at depths of less than 2km showing the analogies that can be drawn from modern day examples.

3.8.3 Crystal transformation of smectite-illite

3.8.3.1 Introduction

Many authors have reported on this crystal reaction being a contributory cause of developed overpressure. Particularly in the Gulf Coast area, Burst (1969); Powers (1967); Bruce (1984) and Freed and Peacor (1989) have noted the depth of pressure transition from normal to overpressured state as being a function and effect of smectite chemically and physically altering to illite. The mechanism is reviewed in section 2.1 with respect to its potential in generating overpressure but simplistically operates to generate overpressure by expelling bound interlayer water held in the smectite crystal structure to free pore water during the reaction to illite.

In this study of Alwyn, it was necessary to analyse the major clay types found in the reservoir section. Due to the absence of core material in the overlying shale section only clays in the predominantly sand section of the Brent Group members were analysed. However, these clays would have been subjected to any temperature dependant reaction and with the availability of K from the dissolution of K-feldspar, the necessary parameters for illite formation from smectite are available. X-Ray Diffraction (XRD) techniques determined main clay fractions in the Alwyn reservoirs.

It is seen that authigenic illite is scarce in the Alwyn North field (section 3.6.5). This has been identified as an effect of diagenesis and early oil fill up. As authigenic illite is one of the latest phases to form in response to burial diagenesis before hydrocarbon invasion (Hogg et al., 1992), early invasion and percolation through the reservoir section by hydrocarbons will preclude the growth of illite crystals in the reservoir. The effect of this protection offered by this early oil with respect to reservoir quality is obvious in that porosity and permeability are protected by the growth of late-stage neoformational fibrous illite. Thus, the lack of authigenic illite in the Alwyn North field may be a consequence of early influx of oil.

When observing illite concentration and degree of overpressure in the South and South East fields, there appears to be no greater amount of authigenic illite clay fraction in the higher overpressured South East field. Fibrous illite growth in these two fields have already been documented as being a major influence on porosity and permeability (Jourdan et al., 1987; Hogg et al., 1992) as a direct result of late hydrocarbon invasion with respect to reservoir diagenesis. Indeed, the greatest concentration of the clay has been identified by Hogg et al. (1992) as occurring in the 3/14a-8 well. Hogg et al. (1992) interpret this well as being close to a fault zone and a point of entry for hot diagenetic fluids focused at this point. This would explain the intensity of diagenesis and degree of illitisation in 3/14a-8. This well does not show any anomalous pressure with respect to other wells in the vicinity away from the fault which experiences less intense illitisation. There appears also to be no pressure anomaly through the vertical profile of the well (section 3.4) indicating that the degree of the illitisation has no direct bearing on the potential overpressure generation in the wells or fields studied.

3.8.3.2 XRD Analyses

XRD analysis was of no great relevance to the identification of potential of overpressure generated by the smectite-illite transformation as only samples from the sand dominated reservoir section were available. XRD was useful in the compositional analyses of the clay fraction with respect to diagenesis and reservoir quality. However, the progress of the reaction from an assemblage dominated by smectite to randomly interstratified I/S to well ordered IS II to interstratified illite can be followed by XRD profiling (Reynolds and Hower, 1970; Hower et al 1976; Wilson, 1987).

Smectite alters to illite via a series of compositional changes with increasing temperature and associated dehydration and increased ordering, a gain of interlayer K, increasing substitution of Al for Si in the tetrahedral layer, loss of octohedral Mg and Fe and probable reduction of the octohedral ion from ferric to ferrous (Sroden and

Eberl, 1984). The chemical relationship between the compositional changes are summarised in Fig.3.8.3.2a.

These metastable states of the transforming clay are important with respect to XRD identification and the possible interpretation of these intermediaries as geothermometers. If these intermediate state clays can be determined, then a further possible control on the geothermal conditions at reservoir level may be determined. The reaction is non-reversible and therefore will record the latest and maximum stage of ordering, dehydration and potential thermal conditions. Various workers have used the ordering of the reaction and correlated the composition of the I/S clays with the thermal and burial histories of several sedimentary basins (Hower et al 1976; Hoffman and Hower, 1986; Hagan and Surdam, 1989).

Hoffman and Hower (1986) and Sroden and Eberl (1984) have plotted the composition of I/S versus temperature from data in different basin settings. Fig.3.8.3.2b and c shows that although the data follows a trend of increasing ordering and dominance of illite with temperature, the range afforded by the data suggests that other factors may also govern the absolute ordering and dehydration of smectite to illite. These parameters have been suggested including pore fluid composition, amount and availability of potassium ions (Boles and Franks, 1979), original smectite chemistry and reaction time (Hower, 1981) as well as temperature. However, despite these variables Pytte and Reynolds (1989) and Elliot et al (1991) conclude that temperature is the dependant and dominant control on the transformation.

Preparation techniques are documented in Appendix 2 and analysis were carried out on 10 samples from the three wells at different depths. These sample depths are listed in Appendix 4.2.

Therefore, by utilisation of XRD analyses, various ordered metastable states of I/S clays can be observed and referenced back to the diagram postulated by Sroden and Eberl (1984). According to 2θ angle on an X-ray diffractogram and relative abundance, certain ordered types of the clay can be seen:

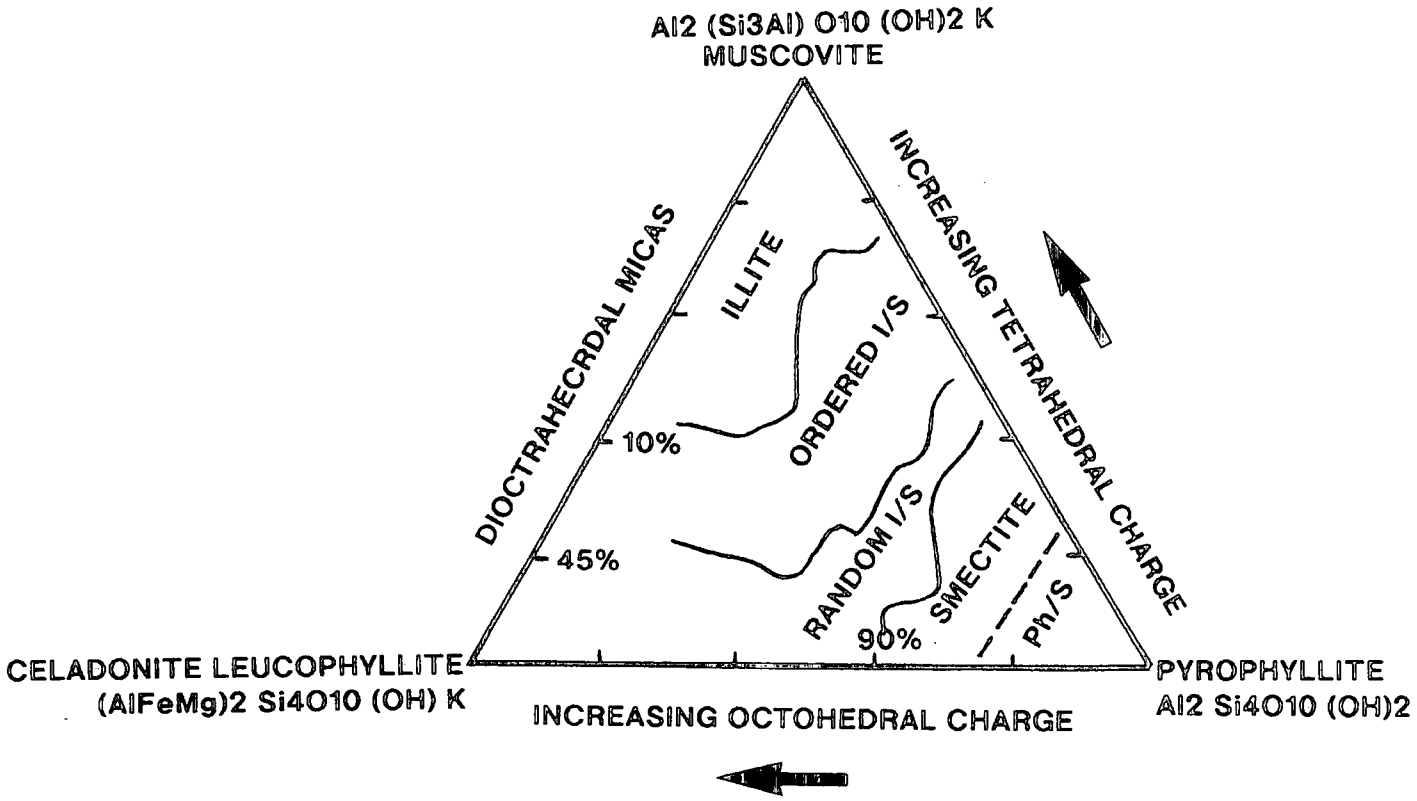

Fig.3.8.3.2a - The chemical relationships between illite and related minerals. Modified from Sroden and Eberl (1984)

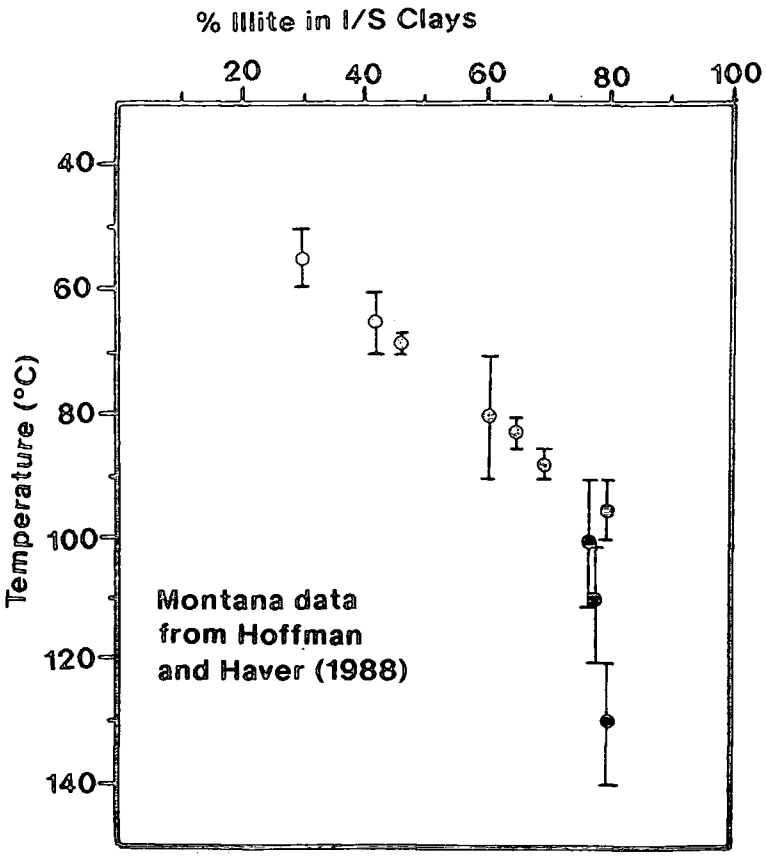

Fig.3.8.3.2b - Percentage of illite in I/S mixed layer clays with increasing temperature. Illite datapoints shows range of temperature. Data from Hoffman and Hower (1988)

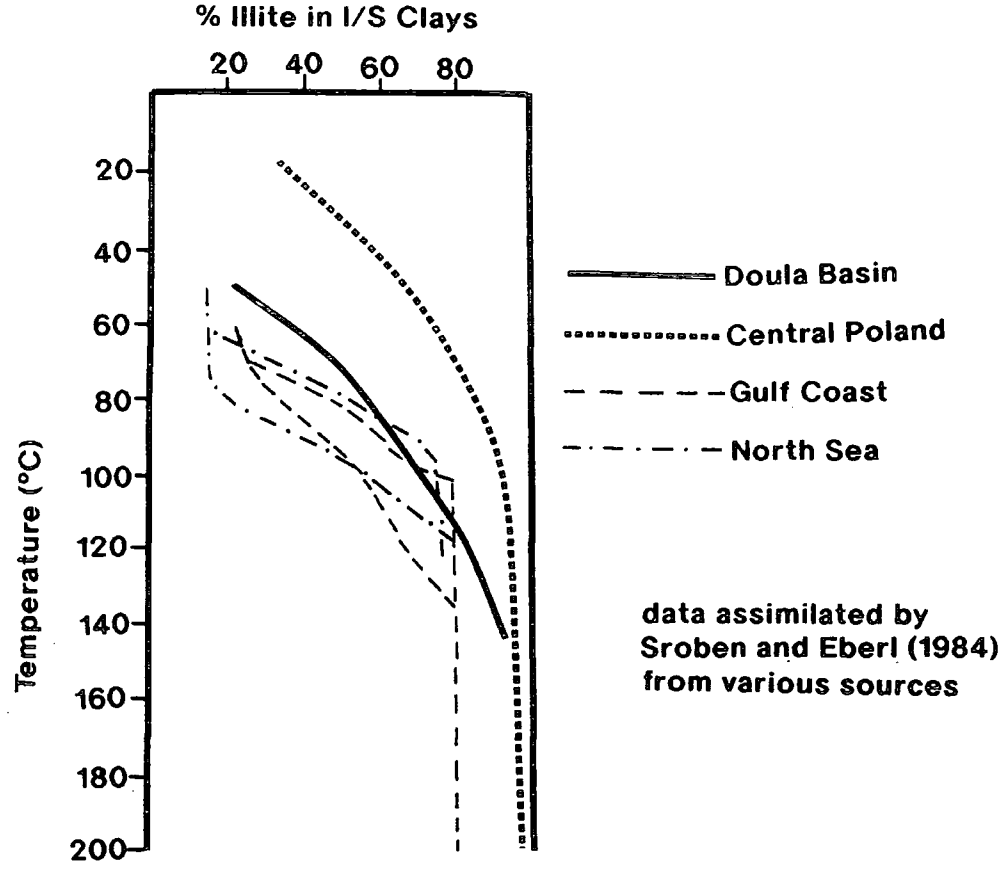

Fig..3.8.3.2c - Percentage illite versus temperature (as a function of depth) showing approximate increase of illite with increasing temperature. Data assimilated from four contrasting basins. From Sroden and Eberl (1984)

Crystallography	Ordering Definition	% illite	Formation Temp.
001 illite peak	I/S RANDOM	<65%	approx <100°C
001 illite peak	I/S ALLEVARDITE/ IM superlattice	65-80%	approx 100-125°C
001 illite peak	I/S KALKBERG/ IM II superlattice	>80%	approx >125°C

See Reynolds (1970) for further definitions of these ordering types. Figs.3.8.3.2d, e and f show the appropriate diffractogram profile for each of the above ordered I/S types.

Fitting the profile to established X-ray diffractograms such as the ones described above shows the effect of fluid flow, proximity to fluid entry points, relative time of exposure to chemical diagenesis and the effect that early oil influx into the reservoir can exert on the clay fractions of the Alwyn reservoirs. However, several interesting inferences and correlations with previous geothermometry indicators - fluid inclusion and vitrinite reflectance data- can be drawn.

Well 3/14b-9: The XRD profile fits an ALLEVARDITE/RANDOM type of I/S ordering. A suppressed Id (discrete illite) peak rises to dominant twin peak I/S and Sm (discrete smectite). This suggests the ordering of approximately <65% illite to smectite (Wilson, 1987). This may infer relative protection from hot circulating fluid and exposure to fluids rich potassium solutes necessary for the smectite-illite reaction to readily occur (Boles and Franks, 1979). The relative position of the well in proximity to a fault/point of fluid entry and fluid source being further from the Viking Graben could possibly explain the high relative 'expandability' (amount of residual smectite) of the clay fraction in this well. When correlated with the % illite/temperature graph suggested by Sroden and Eberl (1984) (Fig.3.8.3.2b), and it suggests diagenetic temperatures operating at less than 100°C.

Well 3/14a-3: The VRD profile follows an ALLEVARDITE configuration with an increased peak in discrete illite, dominated by an I/S peak. Although distal to the Viking Graben its relative close proximity to a major fault zone - The Ninian Fault (Hogg et al., 1992) - promotes the idea of a conduit for deeper derived and hotter fluids rich in diagenetic minerals including potassium. This would enhance the reaction to discrete illite. However, the areal and structural position of the well would also suggest partial protection from the over-saturation of these distal fluids. The inferred temperature range for this identified I/S configuration as described by Sroden and

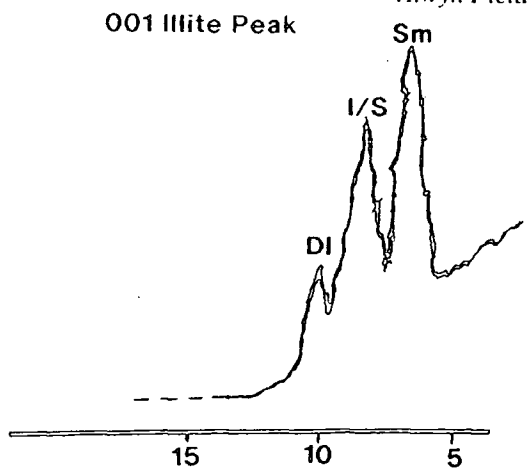

I/S RANDOM >65% Illite

Approx. <100°C neoformation

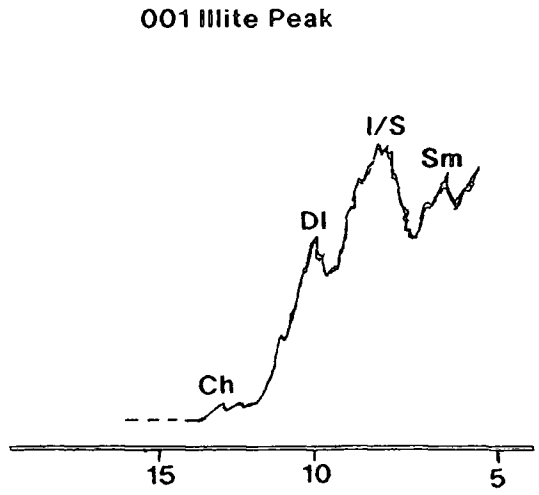

I/S ALLEVARDITE

(I/M SUPERLATTICE)

65–80% Illite

Approx. 100–125°C neoformation

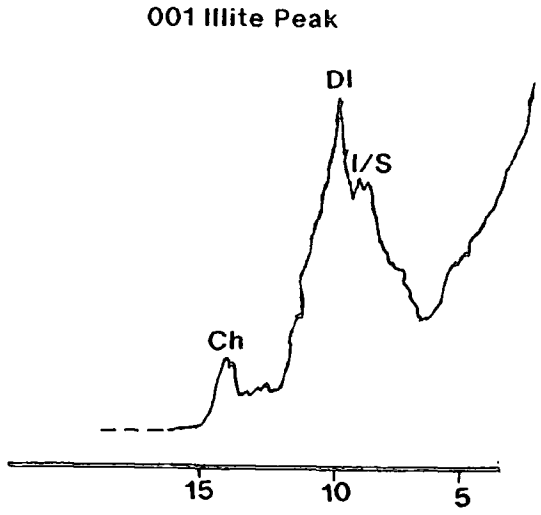

I/S KALKBERG

(IM II SUPERLATTICE)

<80% Illite

Approx. >125°C neoformation

2Ø ANGLE

Ch = Chlorite
I/S = Mixed Layer Illite/Smectite
DI = Discrete Illite
Sm = Smectite

Figs.3.8.3.2d, e and f (top to bottom) - d) Typical XRD profile of I/S RANDOM ordered I/S clays
e) Typical XRD profile of I/S ALLEVARDITE order I/S clays
f) Typical XRD profile of I/S KALKBERG ordered I/S clays.
Classification from Wilson (1987)

Eberl (1984) is in the range of 100-125°C. This temperature range is generally higher than the modelled burial temperature at the time of this diagenesis (35-45Ma, Jourdan et al 1987; 97-103°C - Fig.3.8.3.2g). This would infer, if using the XRD analyses as the sole and critical palaeo-thermal indicator, that hotter fluids were circulating in the reservoir to achieve this type of ordering in the mixed layer clays. It would follow that the major fault close to 3/14a-3 did act as an avenue of fluid percolation and recharge from a distal fluid source down dip from the structure.

Well 3/14a-8: The XRD profiles for this well show an increasingly ordered I/S with depth. Although only 4 samples were run from this well, a consistent observation is that ordering and transformation to discrete illite increases with depth. Peak illitisation occurs at sample ASC8 at a depth of 3560m. At this depth, ordering pattern and 2θ angle fits the KALKBERG profile (Wilson, 1987) whereby the illite to smectite ratio is >80% illite. At this value, Sroden and Eberl (1984) attribute a temperature range of ordering at >125°C. With its close proximity to a major fault and therefore a potential fluid conduit it can be postulated that the clay diagenesis has been temperature controlled using the vertical throw of the nearby fault as a conduit and transport medium. Hogg et al. (1992) suggests that this well is a main entry point for focused fluid flow via the 'Ninian Fault' (Fig.3.6.12a) causing the intense illitisation in this well.

Well 3/15-3: The XRD prolfile follows a similar profile as that of 3/14b-9. The composition of the mixed layer I/S, with 65-80% illite within the I/S, suggests an exposure to a temperature range of 100-125°C if the relationship between temperature and % illite as suggested by Sroden and Eberl (1984) using data from a variety of basins is used (Fig.3.8.3.2c). This infers that well 3/15-3, being areally closer to the fluid source, has been exposed to higher temperatures than those inferred by ambient reservoir conditions calculated by basin modelling (Fig.3.8.3.2h) at the time of illite precipitation in Alwyn South East (55-45Ma, Jourdan et al., 1987). However, by virtue of the age dating and relatively early oil fill up with respect to the structures of Alwyn South, the clay diagenesis and therefore the illite transformation has been halted prematurely in comparison to more distally located Alwyn South reservoirs.

The above XRD analyses support the conclusions drawn from fluid inclusion (section 3.7) and organic geochemical data (section 3.7) suggesting distal fluids being introduced into the reservoirs and recording temperatures of fluid flow higher than the expected ambient geothermal reservoir temperatures at that time.

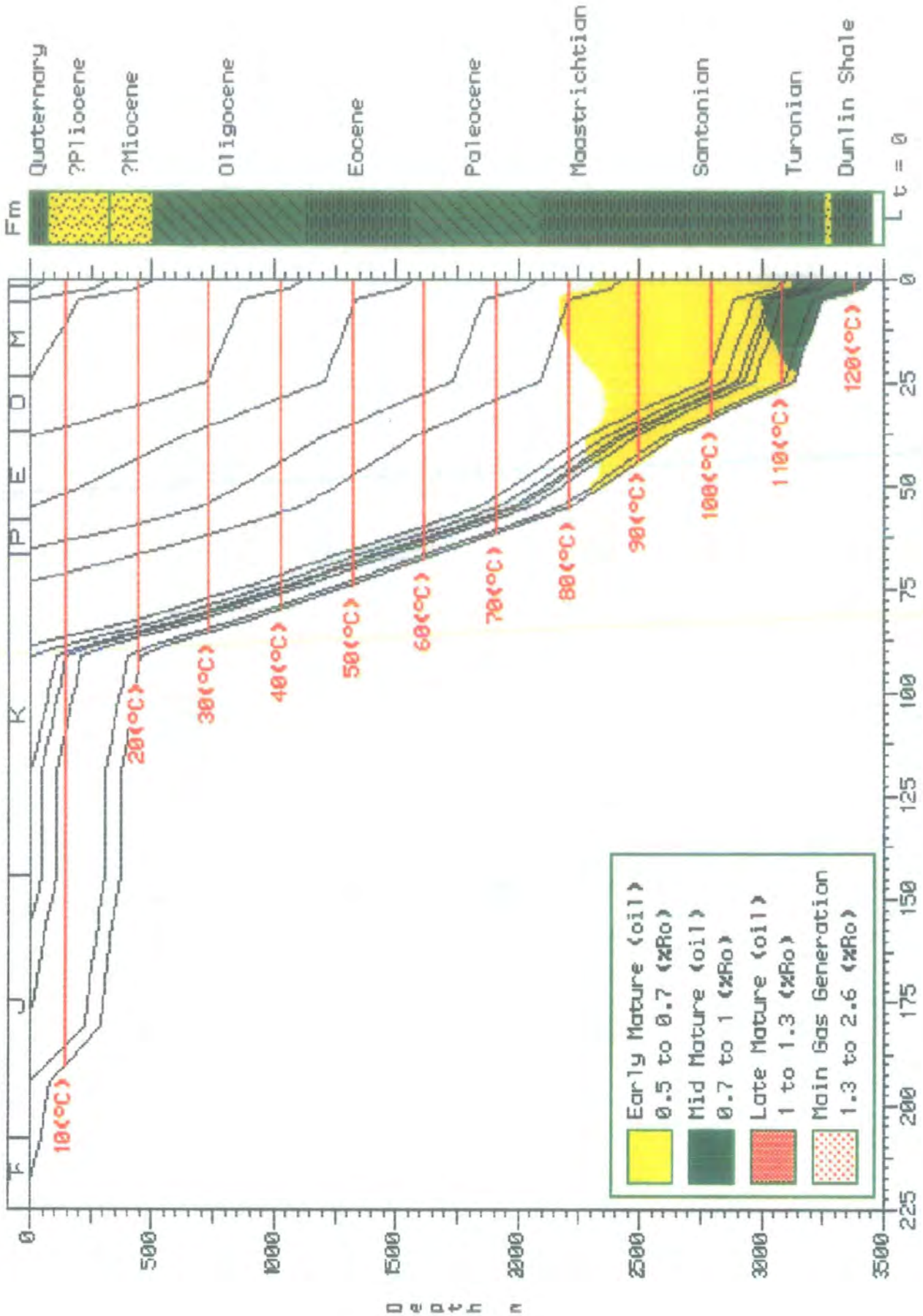

Fig.3.8.3.2g - Burial history plot of Alwyn South well 3/14a-3 with superimposed maturity windows.

Assumptions identical to those used in 3.5.5c (3/14a-8)

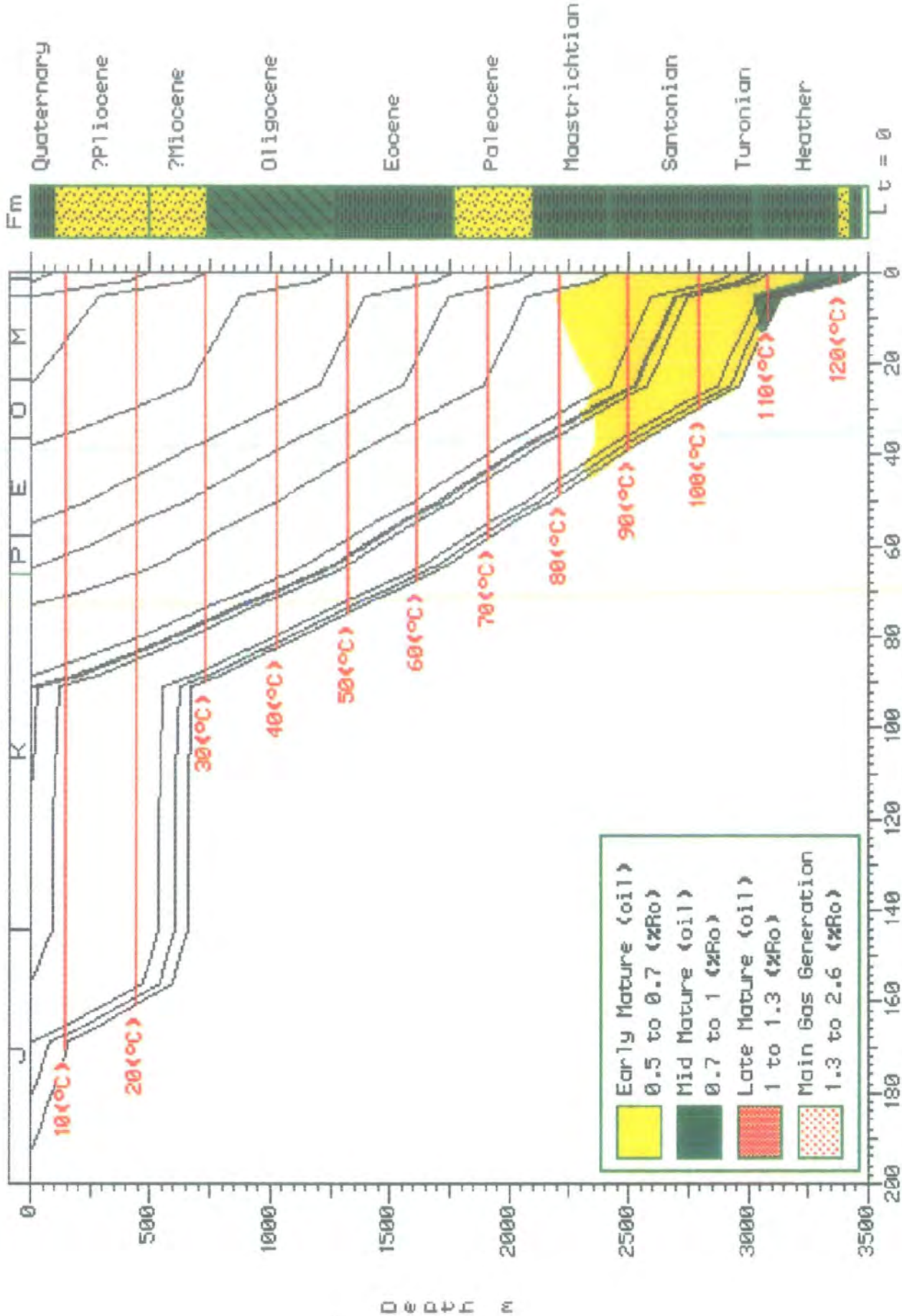

Fig.3.8.3.2h - Burial history plot of Alwyn South East well 3/15-3 with superimposed maturity windows. Assumptions identical to those used in 3.5.5e (3/15-4)

With respect to overpressure generation in the reservoir, it must be concluded that the illite formation in the Alwyn reservoir sands are controlled mainly by temperature, mostly at the local level caused by circulating and percolating fluids. There appears to be no apparent greater concentration of discrete illite in the highly overpressured South East field than any other proximal well in the South or North fields. The concentration of discrete illite and intermediate I/S clays seems to a function of areal and structural position to the fluid source and proximity to likely fluid conduits (faults).

3.8.4 Aquathermal Pressuring

This process has been described as a potentially significant overpressure generating mechanism in shallow basins with high geothermal gradients (Daines, 1982). Barker (1972) describes the theoretical pressure increase associated with a small relative increase in temperature acting on a sealed body of fluid. However, Barker (1972) does not make reference to scale or other phenomena likely to occur in the natural system. The process of generating overpressure by this mechanism has already been described in section 2.1.

The likelihood of this mechanism contributing in the Alwyn area to both palaeo reservoir and present day overpressure is remote for a number of reasons:

1) The mechanism requires a temperature increase acting on a completely sealed volume of fluid. Therefore, if burial is acting as the variable and function of temperature then the geothermal gradient and heat flow would be the parameters of temperature controlling the heating rate of the fluid. Assuming a rise of 10's of °C (using a geothermal gradient of 34°C/km), the geological time frame involved in this amount of heating is unlikely to support the idea of a completely sealed unit free from tectonic effects and local fracturing which would act to release any overpressure caused by this mechanism.

2) A requirement of constant pore volume and fluid density (Mouchet and Mitchell, 1989) is unfeasible given the ionic transfer and chemical diagenesis operating within a continually subsiding mineral sequence such as the vast shale sequences in the Alwyn field area and over much of the Northern North Sea region (Glennie and Brookes, 1982). With the chemical changes associated with burial diagenesis, the effect on pore fluid volume would not be constant and therefore the effect of temperature on the fluid could not be accurately assessed as Barker (1972) had previously calculated.

3) The rarity of a totally impermeable lithological section early in the burial history of a basin before temperature can act on the system is probable. At low temperatures (in the range of 20-40°C), porosities and permeabilities would not support the isolation and sealing effect necessary for the mechanism to initiate.

4) The presence of major faults in the area as reported and described in section 3.3 are evidence of major tectonism to offset and afford the trapping style of the reservoirs. Thus, any overpressure developed by this mechanism must have developed after 150Ma (end Kimmeridgian) and would therefore require the mass transfer of pressure and associated fluid from sedimentary sequences structurally higher in the section. There have been no recorded observations of any fluid and pressure effects from younger rocks into the reservoir section.

It is concluded that aquathermal pressuring is not only governed by thermal conditions and water density but more particularly by the permeability of the environment and the time factor (Mitchell and Mouchet, 1989). Magara (1975) and Lou and Vassuer (1993), however, explain that, given the correct environment and conditions, the effect and potential of the mechanism is significant. Daines (1982) concludes that any overpressure developed by this mechanism would be geologically transient. The overall contribution to the generation and maintenance of pressure in the reservoirs is considered negligible in the Alwyn area due to improbable conditions afforded by the thermal and structural configuration.

3.8.5 Osmosis

Previously documented in Chapter 2.1, this process is thought be secondary and minor in generating overpressure. Because of the variability and uncertainty as to the lateral continuity, uniformity and ion exchange of the enveloping shale horizon above the Brent reservoirs this mechanism must be thought of as being insignificant in overpressure development in the Alwyn fields.

There are no salt domes or structures in the region to set up such an ionic and osmotic potential and the role of the Kimmeridge Shale acting as an efficient semi-permeable membrane must be thought of as unlikely due to the unconformable contact and local irregularity of shale rich facies across the area of the Alwyn field. Shales also have been reported as highly inefficient due to the possible existence of microcracks, large pore sizes, weakly charged pore throats and a relatively high concentration of fine silica in the clay interstices (Young and Low, 1965).

3.8.6 Tectonism

Where deformations occur due to tectonic stress, they can cause modifications in fluid pressures (Grauls and Cassignol, 1993). This means that tectonics may create pressure anomalies or restore pressure to normal conditions. Tectonic effects recorded in the Northern North Sea Viking Graben province and locally in the Alwyn field are limited normal and occasional reverse faulting associated with a failed rifting phase in response to extension (Inglis and Gerard, 1991). No diaparism (shale or salt) is evident and due to the lack of carbonate accumulations in the sedimentary sequence, rafting is not seen. Therefore the documented effects and resultant overpressure potentially created cannot be attributed to the Alwyn field area.

The only possible effect on overpressure through tectonism has already been documented by utilising fault zones as semi-sealing transient features creating the pressure differential and compartmentalised nature of the overpressure distribution across the Alwyn field at the present day (section 3.4). These faults are also envisaged as acting as fluid and associated pressure conduits and entry points of hydrocarbons into the different structural levels in the field. Therefore, the faults and their associated configuration are seen as vitally important in the emplacement of fluid and pressure. However, the lack of compressional flexure, diaparism, evaporites and carbonates must therefore put the effect of tectonism on developing overpressure as insignificant and negligible.

3.9 Conclusions and synthesis of petrographic, geophysical, geochemical and pressure modelling data on the overpressure history and distribution in the Alwyn field

Incorporating all of the general observations from the initial recognition of overpressure and its distribution through the field at the present day to modelling overpressure through time and its relationship with reservoir diagenesis, a summary and model regarding overpressure in the Alwyn structures has been developed.

3.9.1 Pressure recognition and stratigraphy

Broadly, the Alwyn field can be subdivided into 3 distinct pressure cells or compartments. These are Alwyn North, South and South East experiencing lowest to highest degrees of overpressure respectively. Pressure information was gathered from DST, RFT and FIT data in the Brent and Statfjord reservoirs. The Brent member reservoirs are filled with oil whereas the underlying Statfjord is sealed with respect to the Brent Group and contains gas condensate. The main focus of the study has been

the Brent reservoirs due to core availability. In addition the presence of hydrocarbon fluid inclusions identified in the diagenetic sequence was restricted to the Brent, a pre-requisite of the study.

3.9.2 Fluid flow and maturation modelling

In order to understand the source of the trapped hydrocarbons and associated fluids, it was necessary to evaluate the maturity of the reservoired oils with respect to local organic rich rocks on structure to assess the source of the hydrocarbons. By using various organic geochemical parameters it was seen that the reservoired oils did not match the geochemical information of local organic rich rocks except for the possibility of Alwyn South.

Biomarker analyses indicate the Viking Graben is the source of the fluids. Regional seismic data across the Alwyn structure into the Viking Graben allowed the depocentre to be modelled, via depth conversion and computer reconstruction, in terms of burial history and maturation characteristics. There, it was observed that oil source rocks reach maturity from approximately 90-85Ma with peak gas generation at approximately 35Ma onwards (Kimmeridge Formation). It is envisaged that these fluids would be displaced and transferred up-dip to structural traps such as Alwyn. Associated overpressure may also have been generated in this graben area due to the thermal alteration of oil to gas.

3.9.3 Diagenesis

The diagenetic sequence of the three Alwyn structures of North, South and South East differed on the basis of intensity of diagenesis and porosity loss. Alwyn North boasted the greatest reservoir parameters with the sands of Alwyn South being most severely degraded in terms of reservoir potential which reflected peak diagenesis and exposure to intense illitisation. After modelling the burial history and correlating the structural and areal position of the fields to the depocentre, it is thought that the invasion of oil controlled the preservation of the reservoir quality of the sands by its ability to retard and terminate diagenesis once saturation of the oil had occurred.

Both aqueous and hydrocarbon inclusions simultaneously trapped in quartz cements were co-eval with illite in the reservoirs of Alwyn North and South East. An attempt to interpret palaeo temperature and pressure was made to reconstruct the conditions at the time entrapment, using published age dates to time the diagenesis.

3.9.4 Pressure modelling

The inclusion sets of Alwyn North and South East were interpreted with respect to their trapping temperature and pressure. Several assumptions were made but justified and it was seen that the inclusions and therefore the first invasion of hydrocarbons into the respective reservoirs of Alwyn North and South East were trapped at elevated temperatures with respect to ambient reservoir temperature but at normal hydrostatic pressure conditions. A temporal constraint, using previously documented K-Ar illite age dates, was assigned to these primary influxes of hydrocarbons and therefore an interpretation of the conditions with respect to absolute age was possible. Hydrostatic pressure conditions were in operation at 75-65Ma for the first invasion of hydrocarbons into Alwyn North and 55-45Ma for this influx into Alwyn South East.

Computer generated modelling of pressure history through time in the reservoir was conducted, using compaction disequilibrium as the sole generating mechanism. The times of hydrostatic pressure from the rock data coincided with the computer simulation indicating that fluid flow in the reservoir could be controlled by the pressure differential between fluid source and sink. Further, major faults in the area were identified as likely avenues of fluid and pressure percolation but controlled by the stress and pressure imposed upon them. Therefore, these faults were seen to be semi-sealing and transient in their role as fluid and pressure conduits.

3.9.5 Overpressure mechanisms

The interpretation and correlation of the rock data with the computer simulated maturation history in the Viking Graben suggest pressure distribution in the Alwyn field controlled by the proximity of each pressure cell to the Viking Graben. However, accurate modelling of the final burial sequence in the field (10Ma-present day) shows a blanket overpressure effect of between 9-11MPa subjected across the three Alwyn fields. Therefore, the overpressure distribution in the Alwyn structures has likely been in operation, with major faults acting as lateral seals, for a substantial period of geological time. Then, from approximately 7Ma to the present day, reservoir overpressure has increased uniformly across the field in response to rapid burial. Compaction disequilibrium can account for the majority of the overpressure observed in the Alwyn field (generated during the period of 7Ma to the present). However, gas generation is a probable supplementary mechanism.

Other mechanisms of overpressure generation such as smectite-illite clay transformation and aquathermal pressuring are likely to be negligible in the contribution to the overpressure in the Alwyn field both in the past and at the present day.

Chapter 4
The burial, maturation and pressure history and the emplacement of Gilsonite veins in the Uinta Basin, Utah

4.1 Introduction

Gilsonite, a solid hydrocarbon residue which occurs in both a brittle and plastic form dependant upon its specific chemistry, stage of maturity and amount of volatiles, is found in a series of vertical dykes in the eastern part of the Uinta Basin, Utah (Fig.4.1.1a).

These unique features trend NW-SE across the basin in a relatively concentrated swarm at the surface fracturing the upper units of the Eocene Green River Formation. The majority of dykes strike within a range of 40°N - 70°W and were emplaced vertically. The width of the Gilsonite dykes range from 2cms to over 5m. The length of strike varies from approximately 1km to over 20km (Plate p4.1a) and the veins have a vertical interval of up to 1000m (down to the proposed source rock for these hydrocarbon veins - Verbeek and Grout, 1992).

Gilsonite is exposed as a viscous to brittle highly volatile, predominantly aromatic asphaltite (Hunt, 1963) which has a chemical make up of 85-86%C, 8.5-10%H, 2.2-3.4%N, 0.2-0.5%S and approximately 0.2%O (Abraham, 1945; Hunt, 1963). This highly versatile hydrocarbon has been successfully mined for over 100 years and because of its qualities has been used as a thermal insulator and as both a reactant and catalyst in a variety of hydrocarbon derivatives such as paints and volatiles.

There has been considerable debate over the mechanics of emplacement of the dykes. Studies (Eldridge, 1901; Monson and Parnell, 1992) have focused on both slow intrusion of the Gilsonite seeping into pre-existing fractures initiated by the Laramide tectonic extension and on near instantaneous, high pressure forced injections creating fractures and space due to large overpressures in the organic rich source rock at depth.

The source of the hydrocarbon has been verified by various authors after the initial discovery and definitive recognition by Hunt (1963). The source rocks for the Gilsonite is recognised as the organic rich lacustrine shales of the Upper Green River Formation - more locally and specifically, this unit is recognised as the Mohogany Oil Zone (MOZ) which is also suggested as a marker horizon. The MOZ is both stratigraphically and laterally consistent in thickness at the base of the Upper Eocene Uinta Formation and at the top of the Douglas Creek Member of the Green River

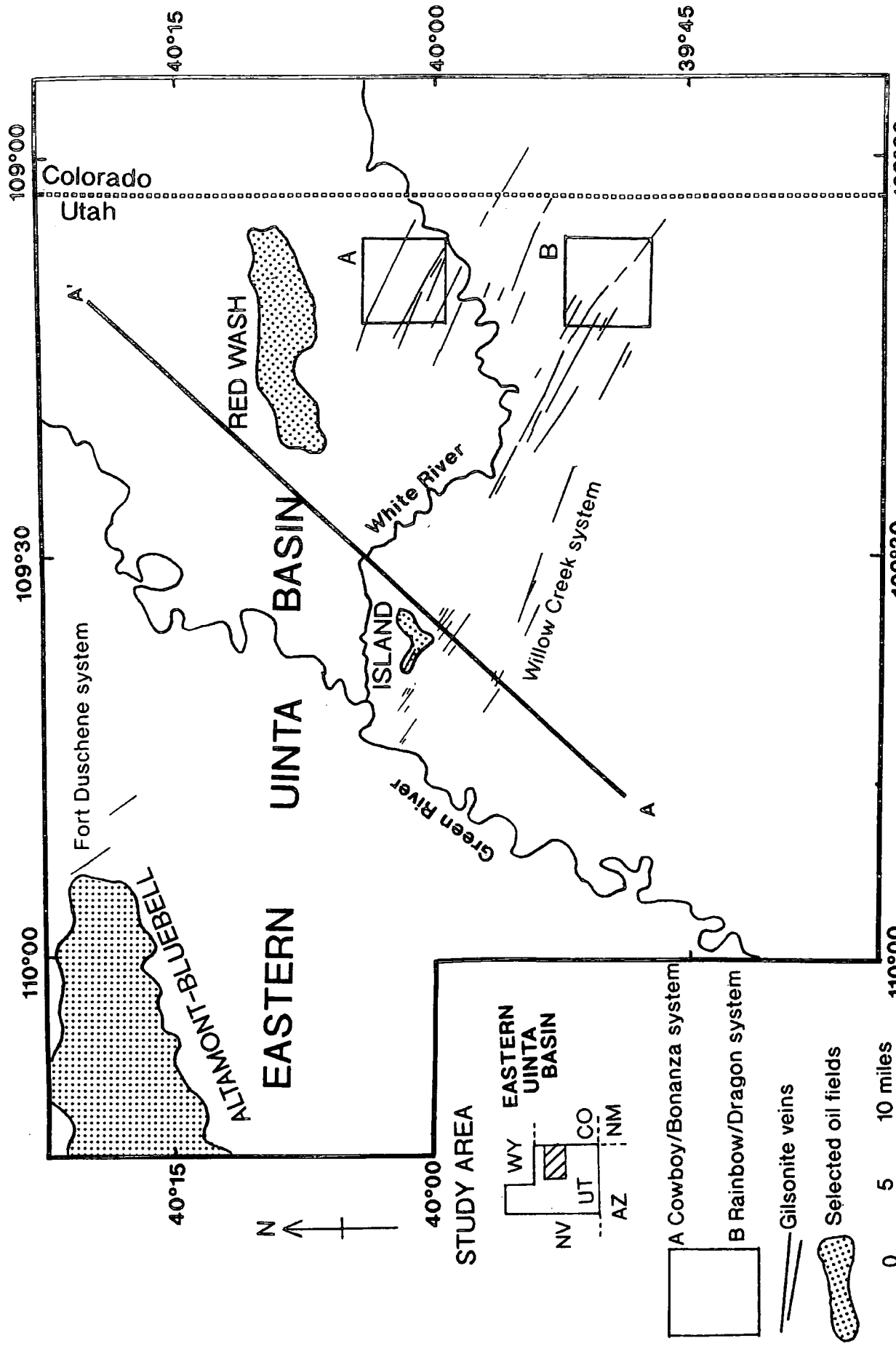

Fig.4.4.1a - Location map of the Uinta Basin showing named Gilsonite vein systems ans selected oil fields. Line a-a' depicts cross section (fig.4.2.2)

Plate p4.1a - Mined out trench of Cowboy vein looking north-east toward the hori zon. Width of the vein is approximately 4m.

Formation. The stratigraphy is summarised in Fig.4.1.1b and acts as the basis for stratigraphic observations and references throughout this chapter. Individual named and observed veins which will be referred to in subsequent sections are detailed in Figs.4.1.1c and d with respect to their areal occurrence. Figs.4.1.1c and d refer to the inserts termed A and B on Fig.4.1.1a.

The aim of this study was to investigate the claim that these dykes are caused by hydrocarbon induced overpressure (Monson and Parnell, 1992) and to try to ascertain both the timing and mechanisms of emplacement.

4.2 Geological Setting

The Gilsonite dykes are exposed at the surface and are most concentrated in the south eastern flank of the shallow dipping asymmetric Uinta Basin (Fig.4.2.1a). Surface outcrop show the basin axis exposing the Oligocene and Top Eocene Duschene River Formation giving way to the south and east in a progressively older sequence as follows: Upper Eocene Uinta Formation, Eocene Green River Formation to the basin margin Lower Eocene/Top Palaeocene Wasatch Formation. A structural cross-section illustrates the asymmetrical style of the basin (Fig.4.2.2a).

The south west limb of the basin dips between 2-8° whereas the NE limb has undergone more flexure in response to the upthrust of the Uinta Mountains - a product of the Cretaceous-early Tertiary Laramide orogeny and dips at 10-13° (Pitman, et al., 1982). The Uinta Basin comprises up to 16,400ft of Cretaceous to Palaeogene lacustrine and fluvial sediments.

The hydrocarbon recovery and potential of the Green River Petroleum System (GRPS) in the Uinta Basin is sizeable with >400 million bbls of oil and 1.3 TCF of gas being produced to date (Fouch, et al., 1992). Recovery is mostly from lenticular sandstone pods within the GRPS and the underlying Wasatch and Colton Formations. Reservoirs are provided by diagenetically enhanced fluvial to marginal lacustrine lenses of sand which possess reservoir qualities enhanced by secondary porosity. Oil production from deeper and highly overpressured (fluid pressure gradient >0.5psi/ft - Lucas and Drexler, 1976; Spencer, 1987) strata (Wasatch and Colton Formations) located along the axis of the basin is made possible by a series of fractures which link to form a permeable network that provide recovery from otherwise conventional tight sandstones which experience low matrix porosity at depths down to 9000ft (Spencer, 1987).

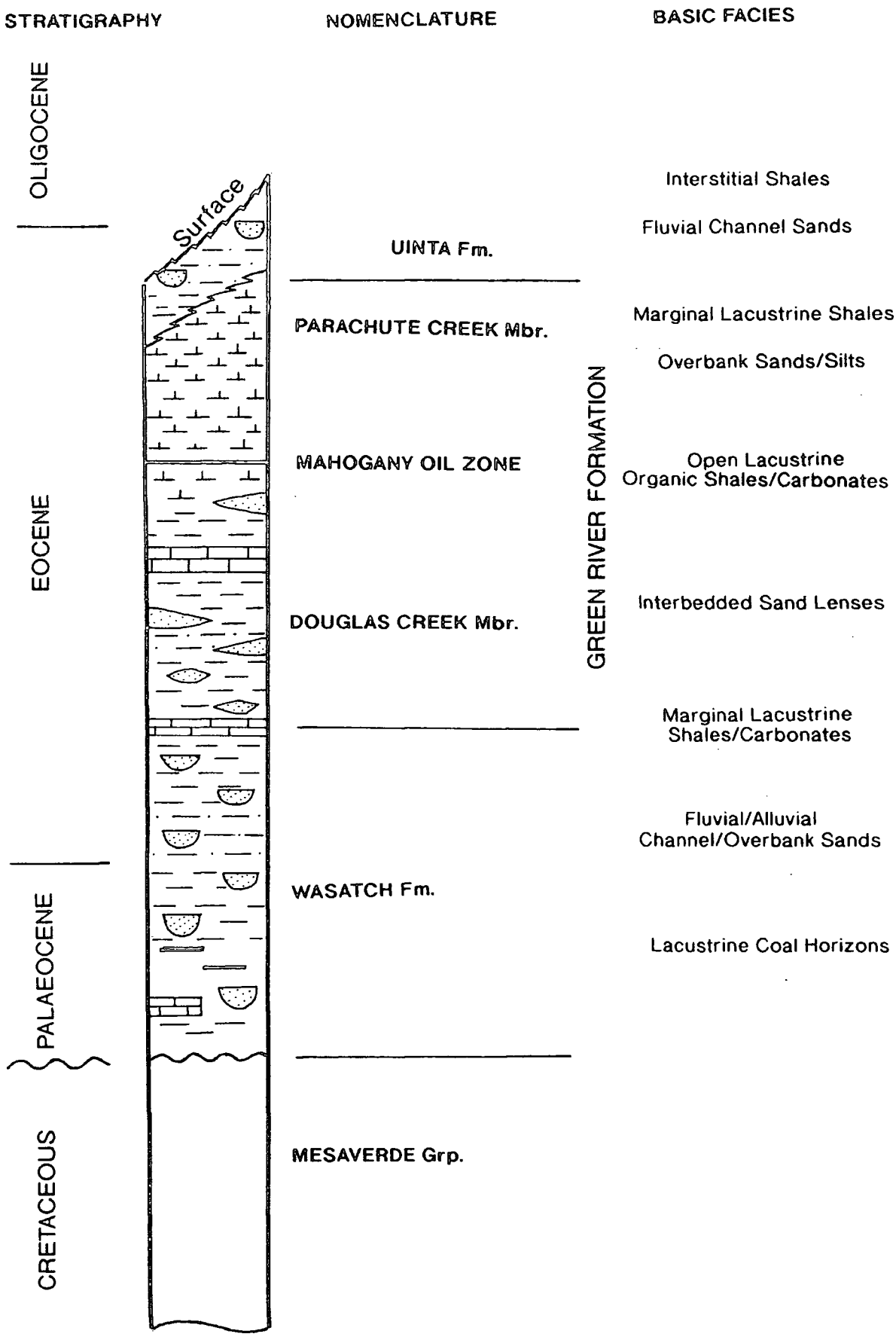

Fig.4.1.1b - Generalised stratigraphic column and nomenclature for the the Uinta Basin showing formation of direct relevance to this study. Modified from Osmond (1992)

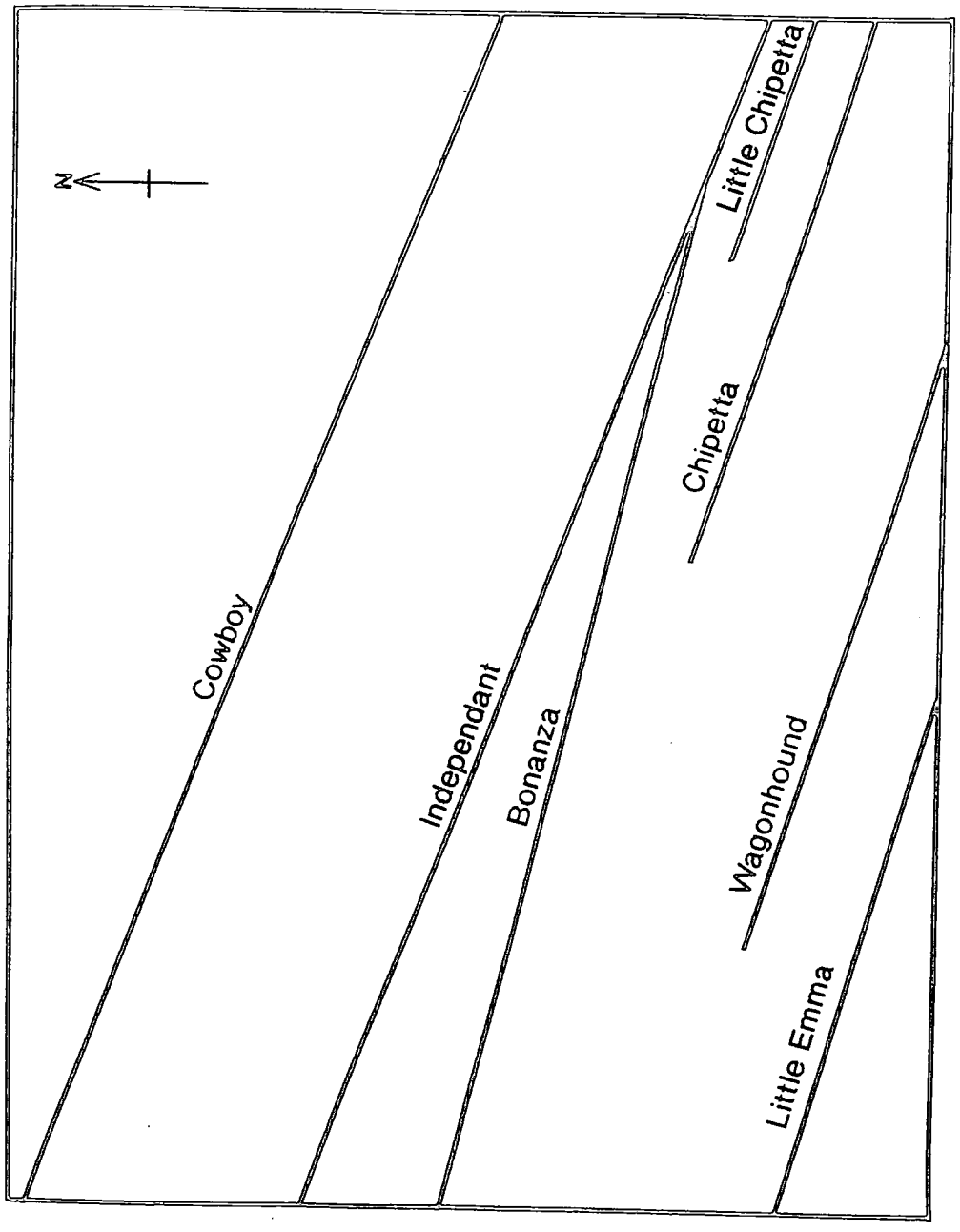

Fig.4.1.1c - Cowboy/Independent Gilsonite vein system (Insert A on Fig.4.1.1a)

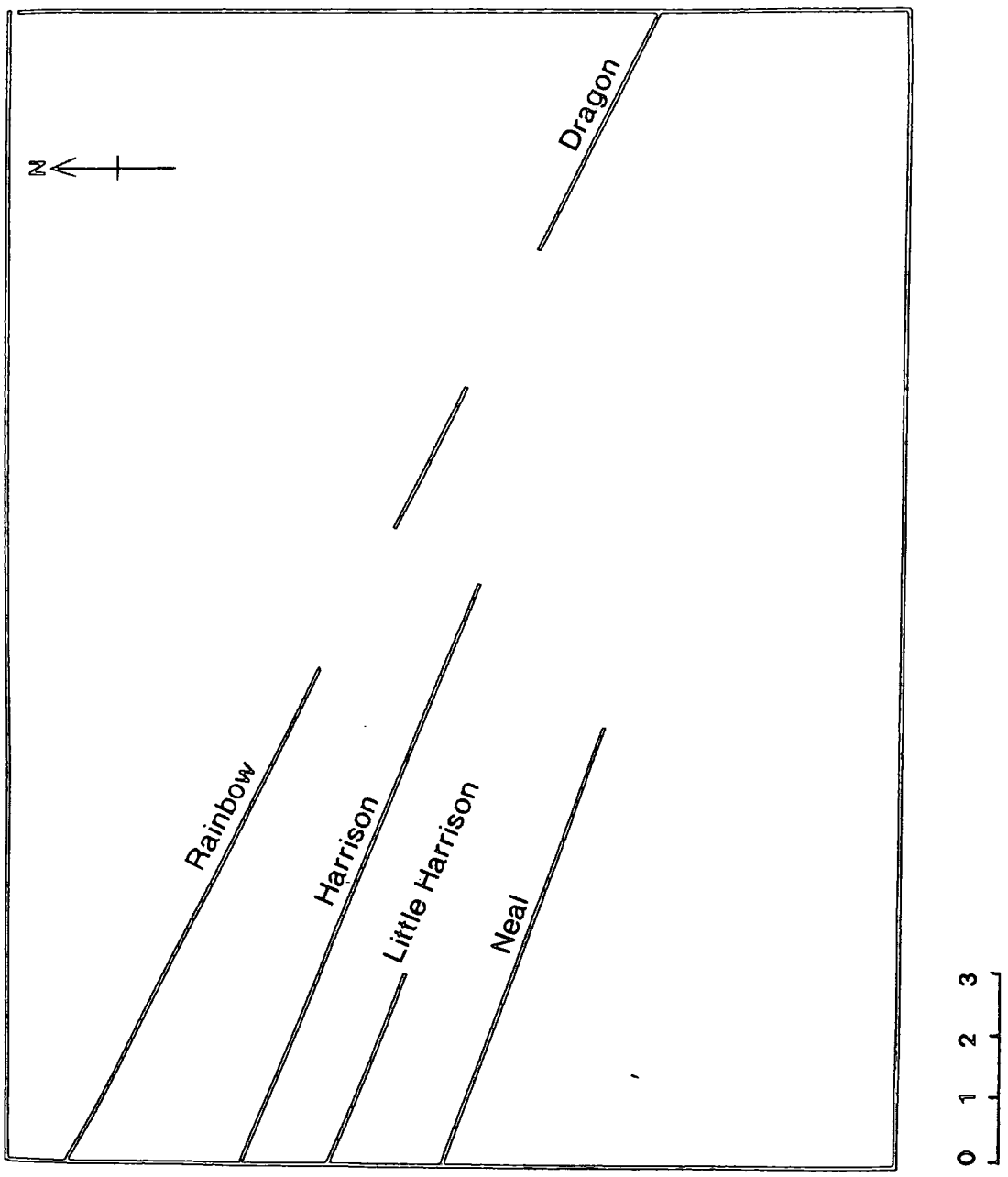

Fig.4.1.1d - Rainbow/Dragon Gilsonite vein system (Insert B on Fig.4.1.1a)

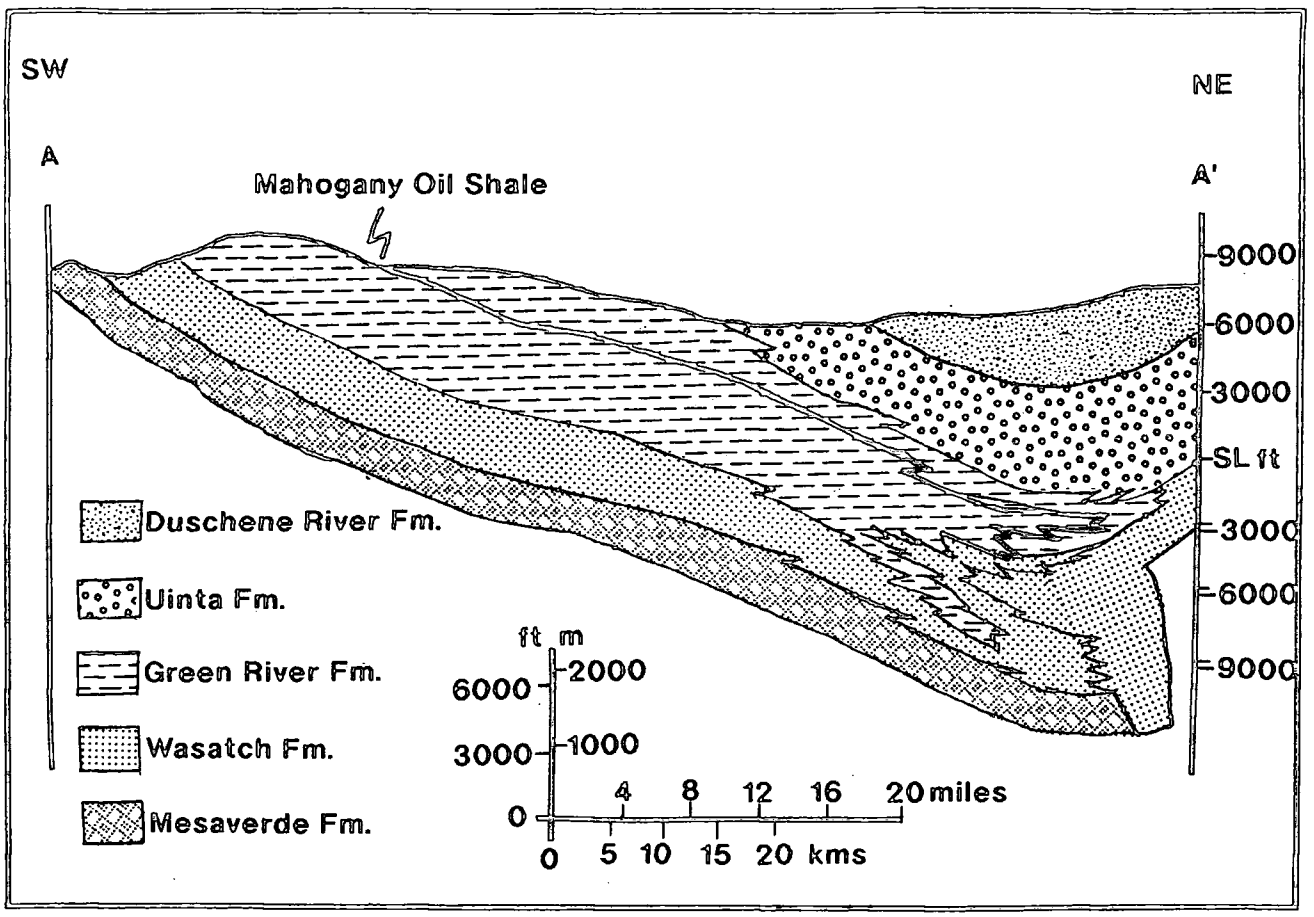

Fig.4.2.2a - Structural cross section showing Tertiary Formations and Cretaceous Mesaverde Formation (section runs A-A' on Fig.4.1.1a). Modified from Fouch et al. (1992)

Lateral continuity of reservoirs in the GRPS is not common due to the lenticular sand pods which act as ponded and isolated reservoir units. However, Lower Eocene sandstone bodies, by virtue of their lateral extent, do provide migration pathways for hydrocarbon fractions to move structurally up-dip (Fouch, et al., 1992). Migration of hydrocarbons through these bodies are represented at surface where oil bearing bituminous sandstones are exposed in the northern part of the basin.

The Uinta Basin began to develop in Latest Cretaceous time with the deposition of the North Horn Formation (Gwynn, 1992). The main tectonic factors in its development were the rise of the Uinta Mountains block and the simultaneous subsidence of the synclinal axis of the basin (Osmond, 1964). During most of the Cretaceous, episodes of thrust faulting and folding associated with the development of the Sevier orogenic belt created major highlands in eastern and southern Nevada and western Utah (Fouch et al., 1983). Detritus from Precambrian, Palaeozoic and Mesozoic sedimentary rocks eroded from these tectonically active highlands was shed eastward into the Cretaceous foreland basin, where it accumulated in fluvial, coastal-plain, marine and marginal-marine depositional environments (Pitman et al., 1982). Lakes developed between the eroding Sevier highlands to the west and the rising Laramide-age Uinta Mountains, Uncompahgre uplift, and San Rafael Swell to the north, east and south respectively (Chidsey and Laine, 1992). This then provided the closed hydrological basin in which the Tertiary sedimentation took place before reactivation of the Uncompahgre uplift at approximately 10Ma (Anders et al., 1992) structurally elevated the basin to its present level.

The major structural elements that existed at some period in the late Cretaceous to early Tertiary and that contributed sediment to the area of the central and eastern Uinta Basin are summarised by Fig.4.2.2b.

4.3 Facies types and depositional environments

The stratigraphic system in the Uinta Basin province is limited to the existence and geographic extent of the ancient depositional system - Lake Uinta. Its margins fluctuated through time due to climatic change, tectonic activation and reactivation of regional faults such as the subsurface Basin Boundary Fault of Campbell (1975) along the north flank of the basin, sediment input and drainage of a closed hydrological system. Because the lake system had no outlet, the chemistry and geometry of the water mass were especially sensitive to external factors such as those listed above and these changes, according to Fouch et al. (1992), provided a continuing mechanism for

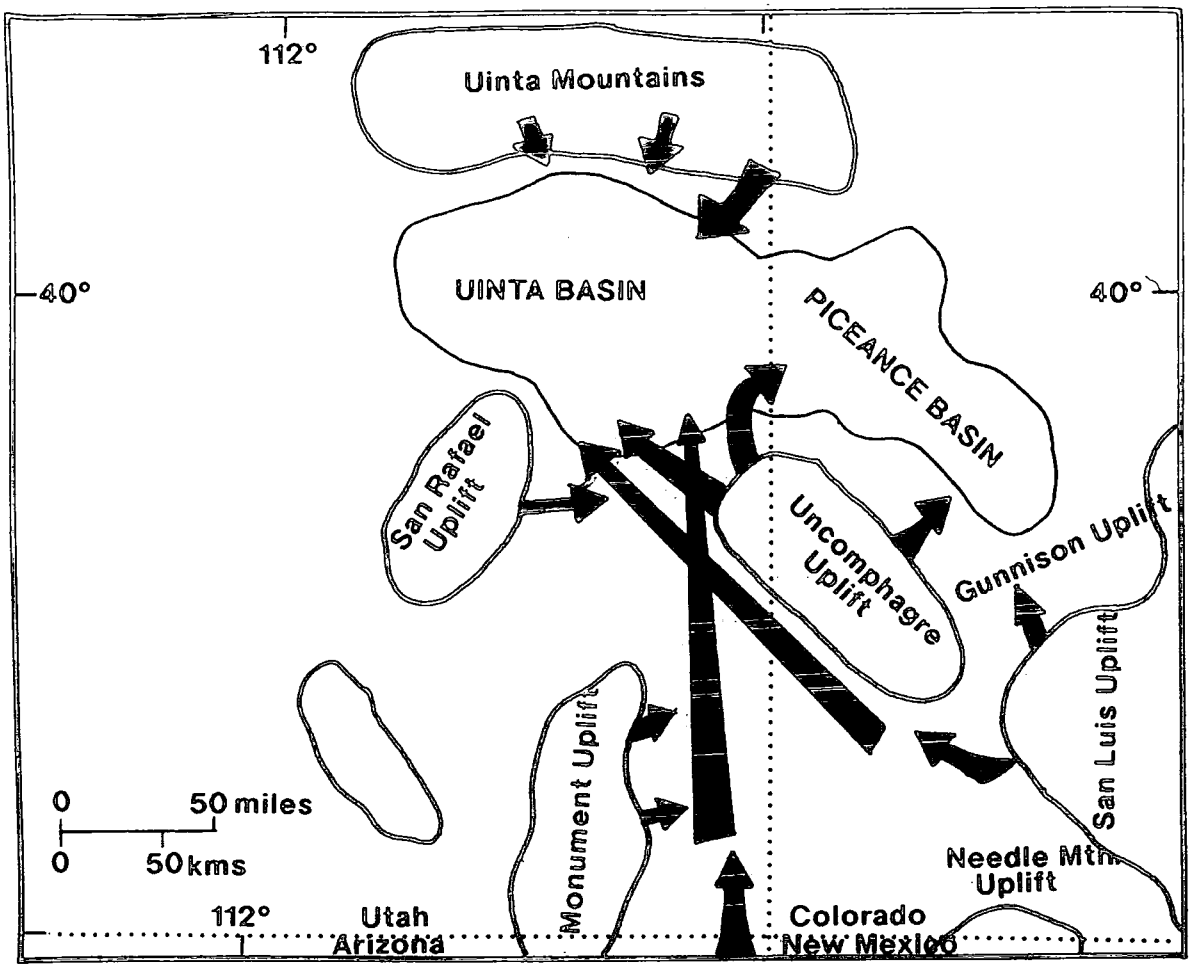

Fig.4.2.2b - Major structural elements that existed at some period in the late Cretaceous to early Tertiary and that contributed sediment to the area of the central and eastern Uinta Basin. From Fouch et al. (1992)

the production and preservation of intercalated petroleum reservoir and source rocks in the Tertiary sequence.

Most regionally extensive reconfigurations were probably in response to faulting which commonly expanded the hydrological and topographic basin giving rise to relatively thick (several hundred metres) areally extensive sequences. Fouch et al., (1992) interpret the smaller development of sedimentary cycles (approximately 10m thick) as the result of simultaneous changes in the climate brought on by variations in solar radiation to initiate the rapid rises and falls of lake level to develop these cycles.

It is not the brief of this study to interpret the sedimentary successions of the Uinta Basin in a sequence stratigraphic framework. It is, however, necessary to briefly describe the facies types of the possible organic source horizons and make a brief attempt to interpret the depositional environments of the sedimentary sequences and their influence on the Gilsonite veins.

4.3.1 Field Observations

The Gilsonite veins have been recorded as penetrating strata in all depositional systems in the Eocene Green River Formation through to the Oligocene Uinta Formation (Osmond, et al., 1992; Monson and Parnell, 1992; Verbeek and Grout, 1992).

Sedimentary logging provided the basis on which the observations and interpretations were made. The logging was systematic: starting in the Tertiary Wasatch and lower Green River Formation and running, where outcrop allowed, going vertically upward to the Oligocene lower Uinta Formation. The logging was not detailed enough as to provide a high resolution descriptive and interpretative analysis of facies packages, stacking patterns and sequence stratigraphic framework but did allow an assessment of major facies types and likely depositional environments.

Fig.4.3.1a shows the graphical log profile depicting the grain size distribution and internal structure of the sediments from the upper Wasatch Formation to the lower Green River Formation. At the base of the log, recognition of fining upward grain sizes is obvious. Corresponding with this observation is a gradational change of cross bedded, occasionally dewatered (flame structures and water escape disconformities and terminations are common) and occasionally burrowed sands giving way to more silty, less well structured and well defined sands. These units, which approximate 6-9m in thickness, grade upward to a finely laminated organic and carbonate rich shale of approximately 0.5-2m which defines the top of the cycle (Plate p4.3.1a). An abrupt

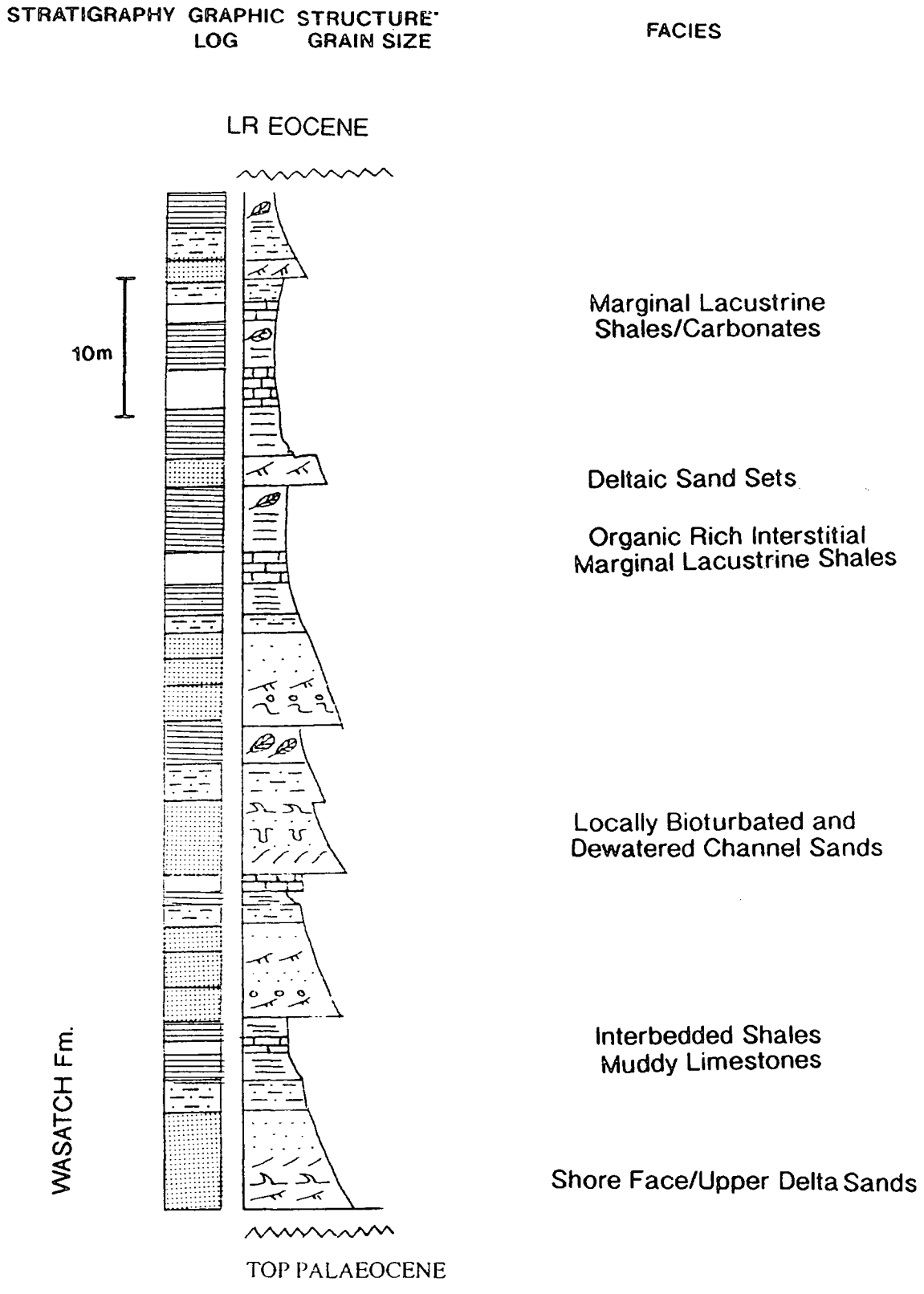

* Sedimentary structures depicted are standard symbols in accordance with Shell Standard Legend (1976)

Fig.4.3.1a - Graphic log of sediments in the top Palaeocene Wasatch Formation to the lower Eocene Green River Formation

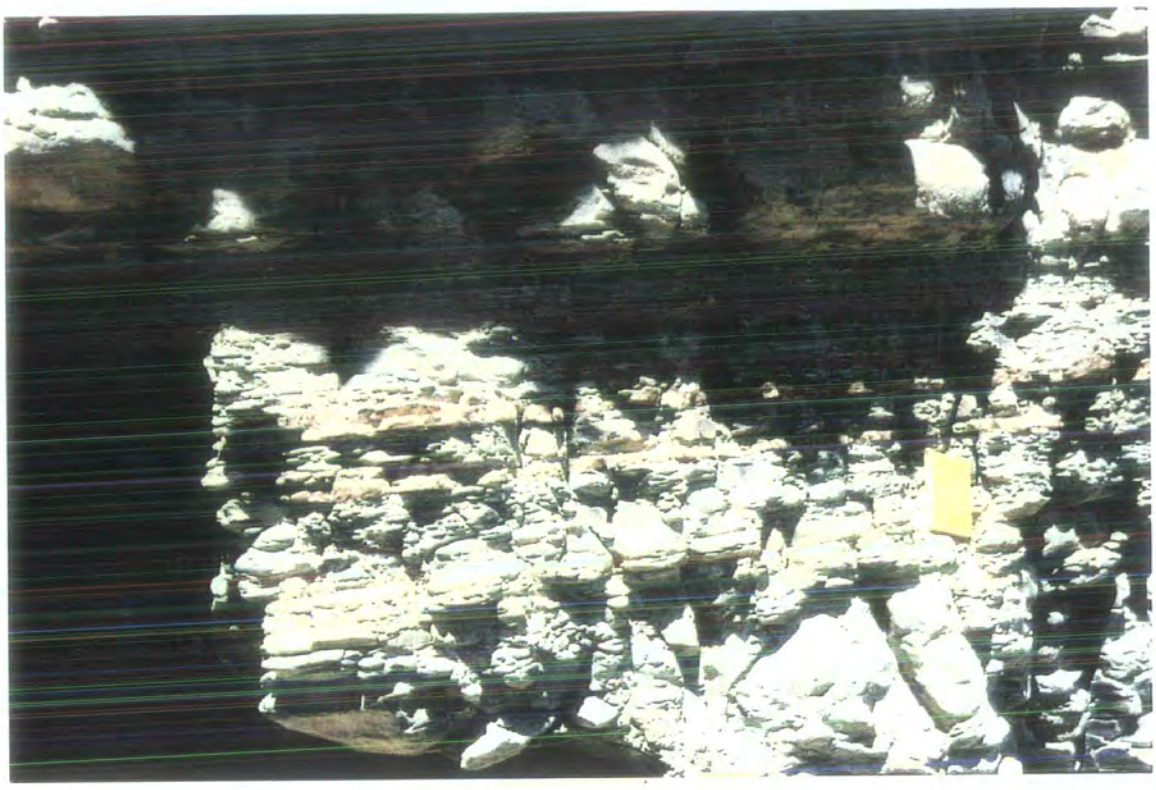

Plate p4.3.1a - Finely laminated organic and carbonate rich shale (middle to upper of photograph) overlain by more massive carbonate beds (top of photograph). Field notebook for scale. Location Atchee Ridge.

change with little or no gradation back to the cross stratified and dewatered sandstones is observed immediately above and comformably overlying the organic carbonate rich shale. These cycles are typically recorded as being 8-13m over a vertical interval with the arenaceous content dominating each cycle at the base of this log. The upper most shale markers of each cycle vary in carbonate content from cycle to cycle but retain an increasing organic content and thickness with each cycle moving vertically up the sequence into the Green River Formation. Also associated with the progression into the Green River Formation is the increase in fines in each cycle and a consequential overall decrease in grain size. Each cycle, however, is still recognisable as containing the basal sand rich facies grading upwards into the argillaceous dominated shale and carbonate rich units. Cyclicity remains approximately of the same order of thickness moving upward into the Green River Formation.

Fig.4.3.1b illustrates the graphic log with associated structures and grain size for the lower to middle Green River Formation which records the log profile of the Douglas Creek Member and the Mahogany Oil Zone (MOZ) (Plate p4.3.1b). This log was recorded in the well exposed creek walls of Hells Hole Canyon. Following on from the defined cycles of sedimentation in the previous log, this log again records cyclicity but the definition of each cycle boundary becomes increasingly more difficult as the carbonate rich shaley muds and organic rich shales become the dominant lithologies. Only the identification of an increasingly thinning sandstone and siltstone interstitial unit (0.5-1m) identifies the basal boundary of each cycle. The organic content in the shales increases to a petroliferous dark oil shale at its peak intensity over approximately 2-3 cycles in the middle Green River Formation (Plate p4.3.1c). These units are collectively known and identified as the Mahogany Oil Zone (MOZ). Distinct carbonate rich horizons and the organic rich shales are masked in definition between the two end members such is the apparent intimate relationship of the two lithologies. The carbonate horizons are fissile and retain much of the structureless features of the organic shales but occasionally appear as massive (0.2m) units (Plate p4.3.1d).

Fig.4.3.1c depicts the graphic log of the sedimentary succession from the middle Green River Formation (immediately above the MOZ) to the lower Uinta Formation recorded in Parachute Creek. The cyclicity which appears to dominate and define the sedimentary sequence through the previous two logs is retained and becomes more apparent in this log with the increase in sand rich units and the decline in organic rich shales. The carbonate rich units increasingly lose the fissile character and organic richness characteristic of the facies in previous log (Fig.4.3.1b), The carbonate units become increasingly massive (0.4m), are bluff-yellow in colour in contrast to the light

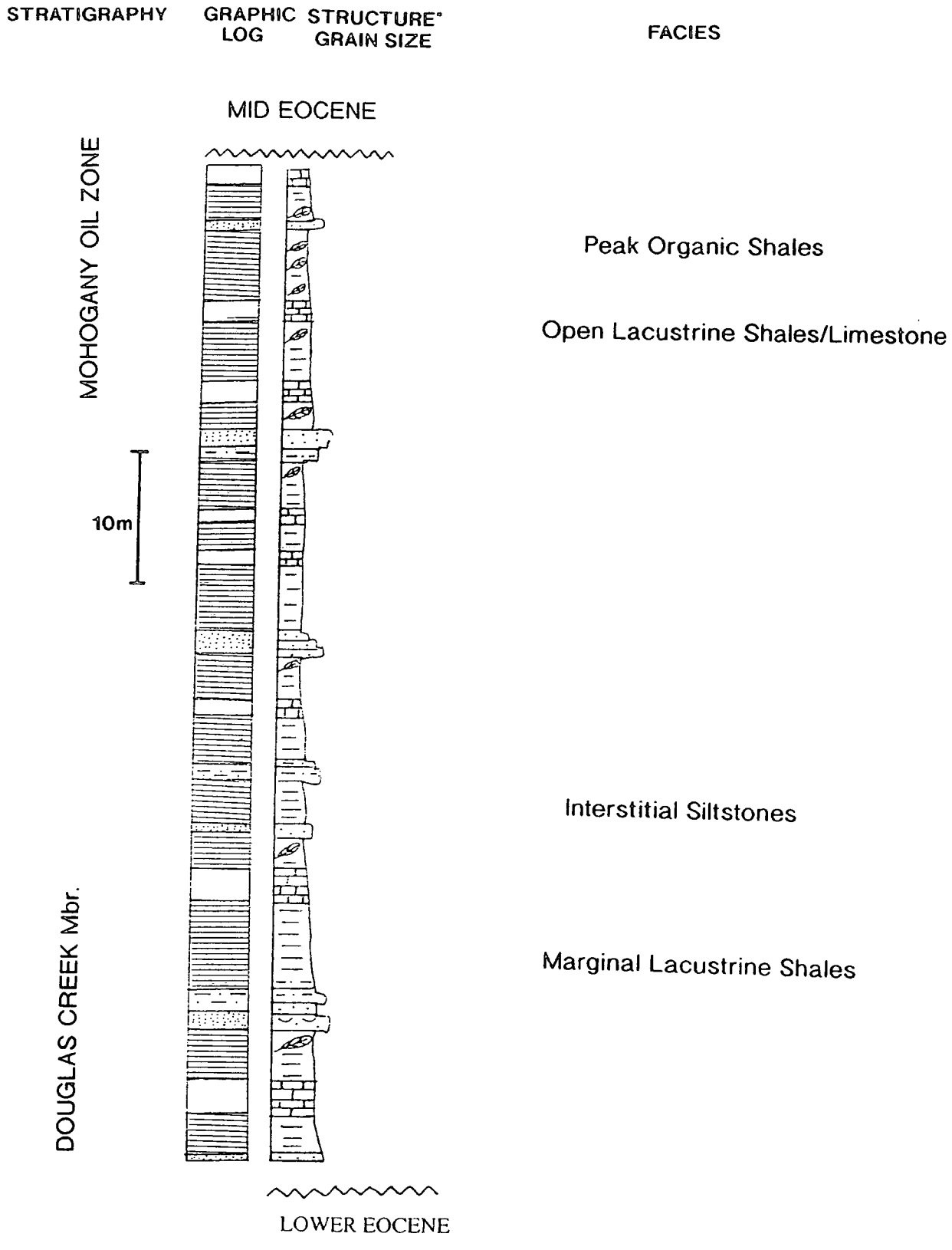

* Sedimentary structures depicted are standard symbols in accordance with Shell Standard Legend (1976)

Fig.4.3.1b - Graphic log of sediments identified in the lower Eocene Douglas Creek Member to the middle Eocene Mahogany Oil Zone of the Green River Formation

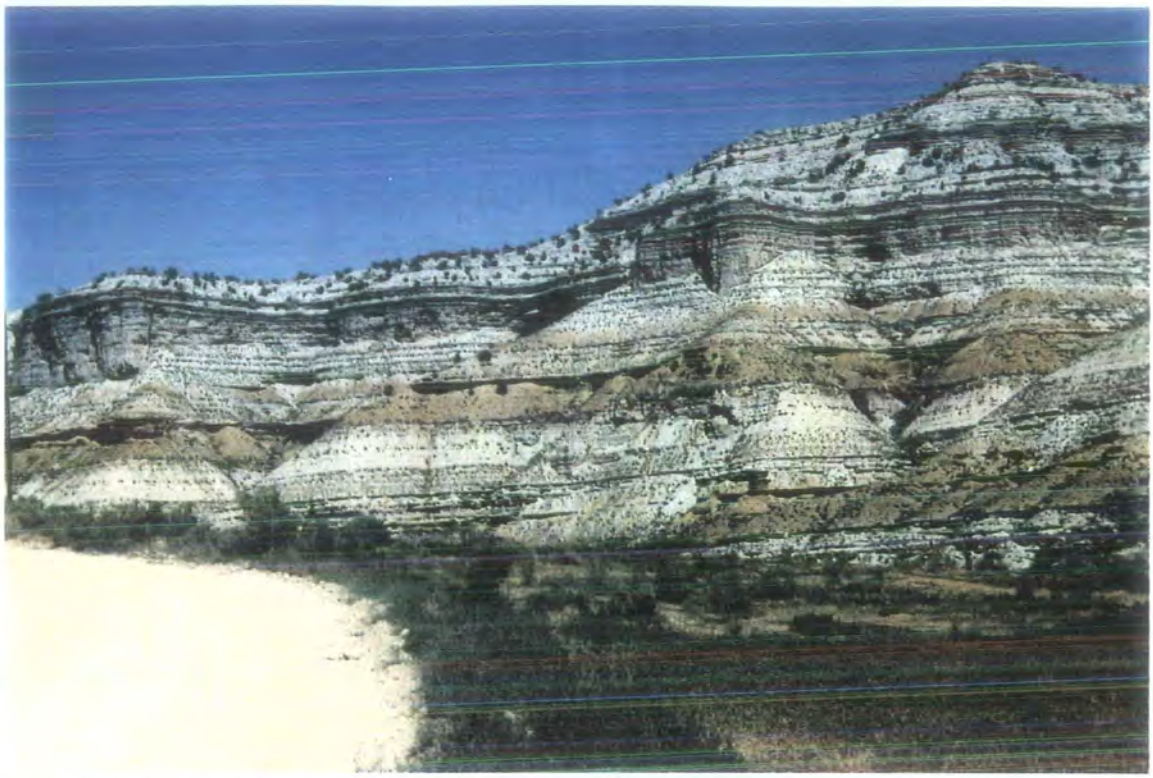

Plate p4.3.1b - Douglas Creek Member of lower Green River Shale Formation at the base of the cliff section grading upward through a series of cycles (see text for description) to the MOZ (darker to black shale horizons at the top of the cliff). Vertical section approximately 100m. Location Evacuation Creek.

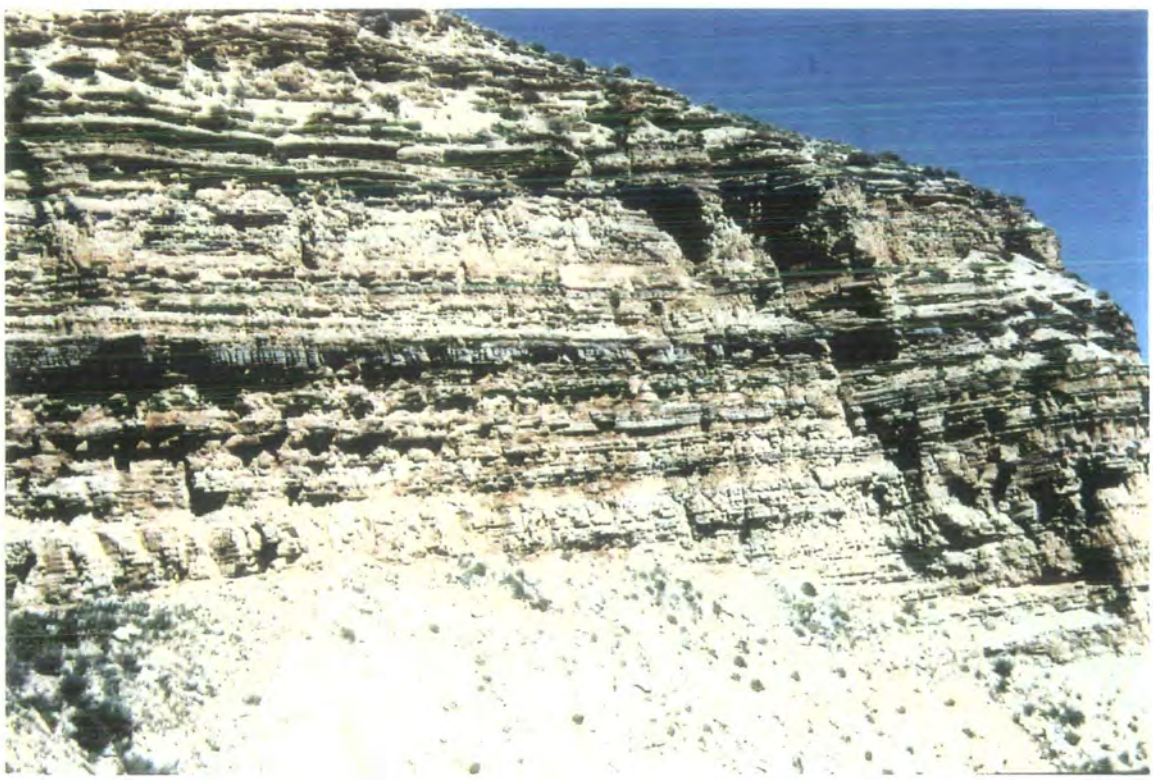

Plate p4.3.1c - MOZ represented by dark oil shales (dark horizons) of approximately 0.25m thickness. Top of the photograph shows gradation into the carbonate rich shales of the Parachute Creek Member. Location Hells Hole Canyon.

Plate p4.3.1d - Fissile carbonate rich shales dominate the base of the Prarchute Creek Member immediately above the MOZ (base of the photograph). Hammer for scale. Location Hells Hole Canyon.

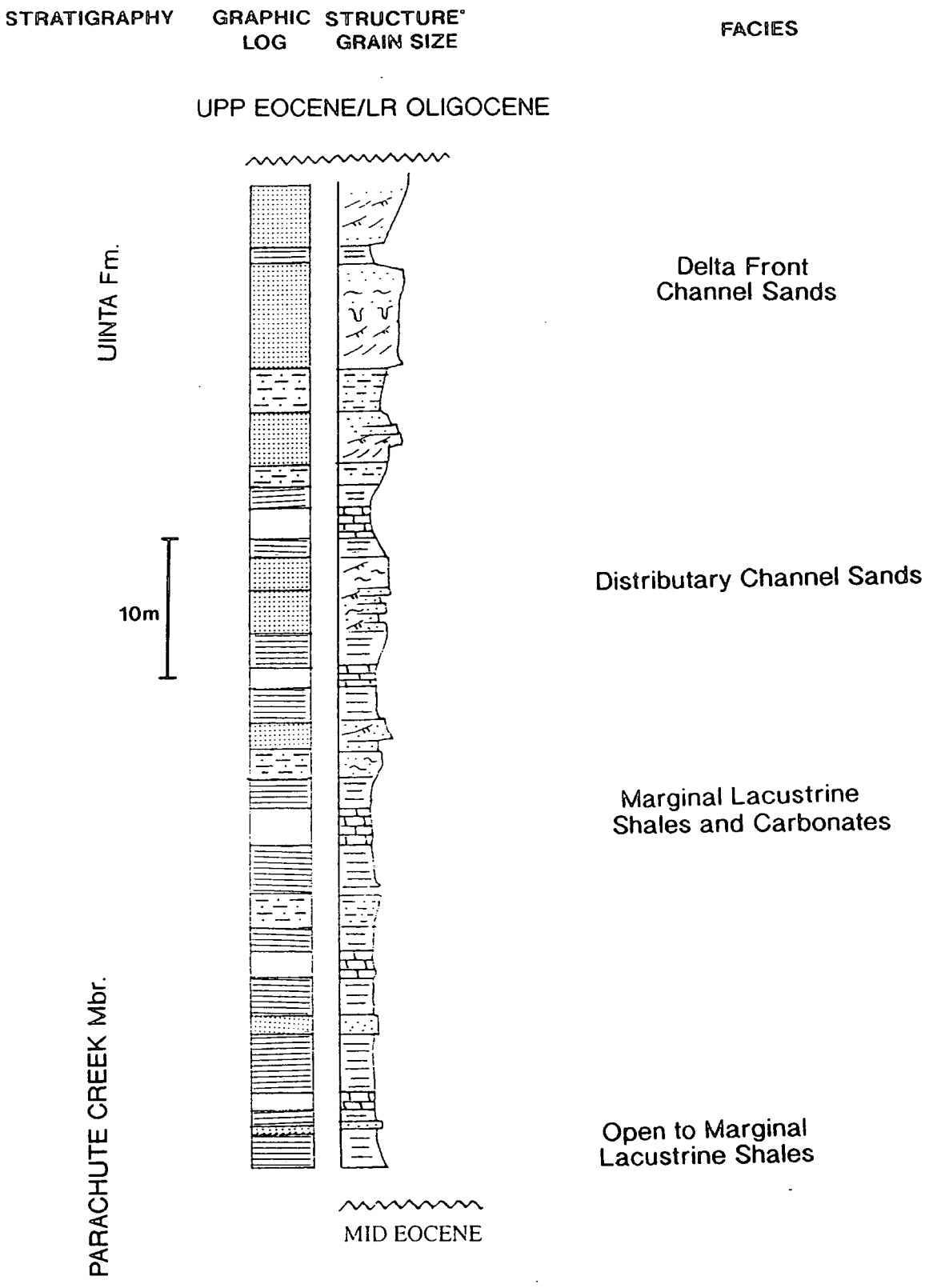

° Sedimentary structures depicted are standard symbols in accordance with Shell Standard Legend (1976

Fig.4.3.1c - Graphic log of sediemnts identified in the upper Eocene Parachute Creek Member of the Green River Formation to the lower Oligocene Uinta Formation

grey of those identified in the previous log recorded in Hells Hole Canyon and possess an erosional structure of cavities (Plate p4.3.1e) which has been described by Bradley (1931) as the Bird's nest zone. The increasingly arenaceous content of the sand and silt dominated units become thicker and internal structure is more defined (Plate p4.3.1f). Cross stratification and slump, collapse and dewatering structures are common (Plate 4.3.1g). These sand units increase to the point where the Uinta Sandstone Formation is firmly established and identified as burrowed, dewatered and cross bedded pink to light brown medium grained sandstones (Plate p4.3.1h). These sandstones take on a more massive character (0.2-0.3m) at the top of the logged section and interstitial shale horizons at this point in the succession are almost depleted and cyclicity, which was the dominant overall feature of the entire section from the top Wasatch to the lower Uinta Formation is unrecognisable.

4.3.2 Depositional environments and sedimentation patterns

Although the field logging and intensity of observations could not underpin a sequence stratigraphic interpretation, the observations made on the apparent cyclicity, facies types and sedimentation patterns could be used as a basis for an interpretation of the likely major depositional environments.

The cyclicity identified here and observations made by Fouch et al. (1992) and Fouch and Pitman (1991) is likely to be a response to recurrent and continuing climatic change initiating very rapid expansions and contractions (and rises and falls) of the lake (Fouch et al., 1992). Also, Fouch et al. (1992) interpret the climate-induced sedimentary and geochemical cycles as similar in style to tectonic cycles except that they commonly record thicknesses of 3-30m which is the common observation made on the logged sections. Each cycle begins with an arenaceous sand dominated unit which, at the top Wasatch/lower Green River Formation, is interpreted to represent a shore face or deltaic channel sands grading upward into interbedded shales and muddy limestones. Each cycle conforms to this pattern but the overall stacking pattern records an increasingly greater amount of fines and, correspondingly, shales and carbonate units increase and begin to dominate the individual cycles progressively upward towards the middle Green River Formation. This is likely to be a result of drowning of the basin associated with an increase in relative lake level. Therefore, tectonically induced response of the lake would be to transgress and drown over the area of deposition and force the shoreline outward. The increase in organic content of the shale units and finely laminated/stratified carbonate units are possibly the result of being deposited at the lake bottom in a relatively quiet water environment. The peak organic units recorded in the MOZ are likely to be the response of an algal bloom or similar organic

Plate p4.3.1e - Erosion cavities termed the Bird's Nest Zone (Bradley, 1931). Hammer at base of photograph for scale. Location Parachute Creek.

Plate p4.3.1f - Bird's Nest Zone of the upper Parachute Creek Member grading from fissile and massive carbonates to sand dominated beds of the Oligocene Uinta Formation (top of photograph). Vertical section 60m.

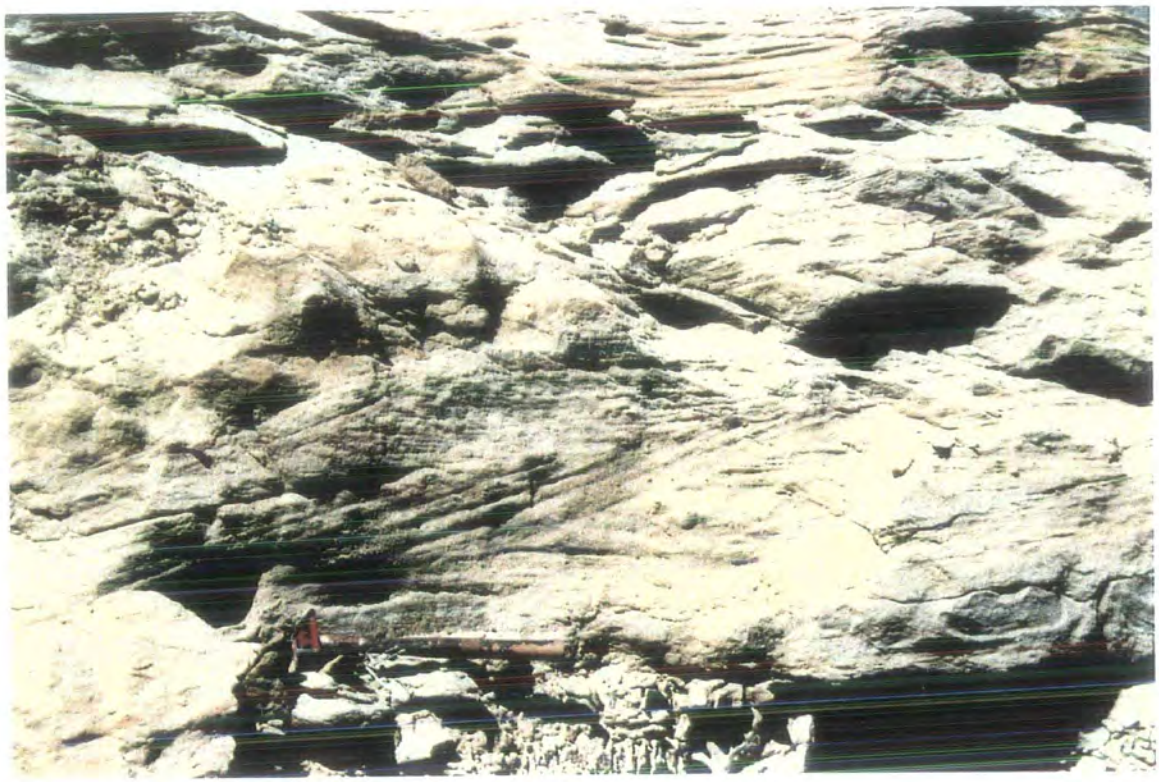

Plate p4.4.1g - Cross stratified and slumped sandstones of the Uinta Formation. Hammer for scale. Location White River Oil Shale Project entrance.

Plate p4.4.1h - Flame structure in massive pink sandstones of the Uinta Formation. Photograph (base to top) approximately 2m. Location White River Oil Shale Project entrance.

material flourishing in the upper phototrophic levels of the lake before extinction and mass deposition at the base of the lake. Fig.4.3.4 depicts the possible scenario of the marginal-open lacustrine environment of deposition at this time when the MOZ is deposited.

The sequence recorded from the MOZ to the lower Uinta Formation shows the cyclicity increasing in arenaceous input; accumulating with the recognition of identifiable sandstones in the cycles once again. This intensifies as the log and profile of the succession progresses into the Uinta Formation which is dominated by channel sandstones and dewatered and slumped delta front or distributary channel sands. This sequence likely records an aggradational sequence whereby the depositional environment has changed from a marginal to open lacustrine setting to a deltaic and ultimately a fluvial/alluvial environment (Fig.4.3.5). Again, this change in overall environment is a possible response to tectonic uplift through the reactivation of the Uncompahgre and Uinta Uplifts (Fig.4.2.2b) which have been identified at this time of deposition (Whitney and Andrews, 1983).

The more subtle but definitely recognisable cycles which increasingly fine upward but which are then overlain by a sharp gradation to medium-coarse grained basal sand units are more likely to be the product of climatic influences on the depositional environment to produce the subsequent patterns of sedimentation which are recorded in these cycles.

4.4 Structure of the Gilsonite veins

The occurrence of Gilsonite dykes and associated fracture systems developed in Tertiary formations have been noted and interpreted by various workers (Verbeek and Grout, 1992; Monson and Parnell, 1992). In addition, the nature and style of the veins and their apparent relation to other documented subsurface natural fracture systems has also been recorded (Lucas and Drexler, 1976; Narr and Currie, 1982). Before modelling and evaluation of emplacement and the geological processes which affect the system in the cycle of burial, diagenesis. organic maturation, uplift and erosional unloading, the characteristics of the veins and their morphology must be documented. This will access information that can be elucidated with respect to host rock interaction with the Gilsonite dykes, wall rock accommodation and mechanical reaction and any indicators which tell of precursor fracturing predating fluid influx into the vein. Also the character and morphology of the veins can reveal much about the stress conditions both in a regional tectonic setting and at the local scale. Therefore, observations of the dyke wall relationships, the strike and offset of the fractures and any shear/tensile

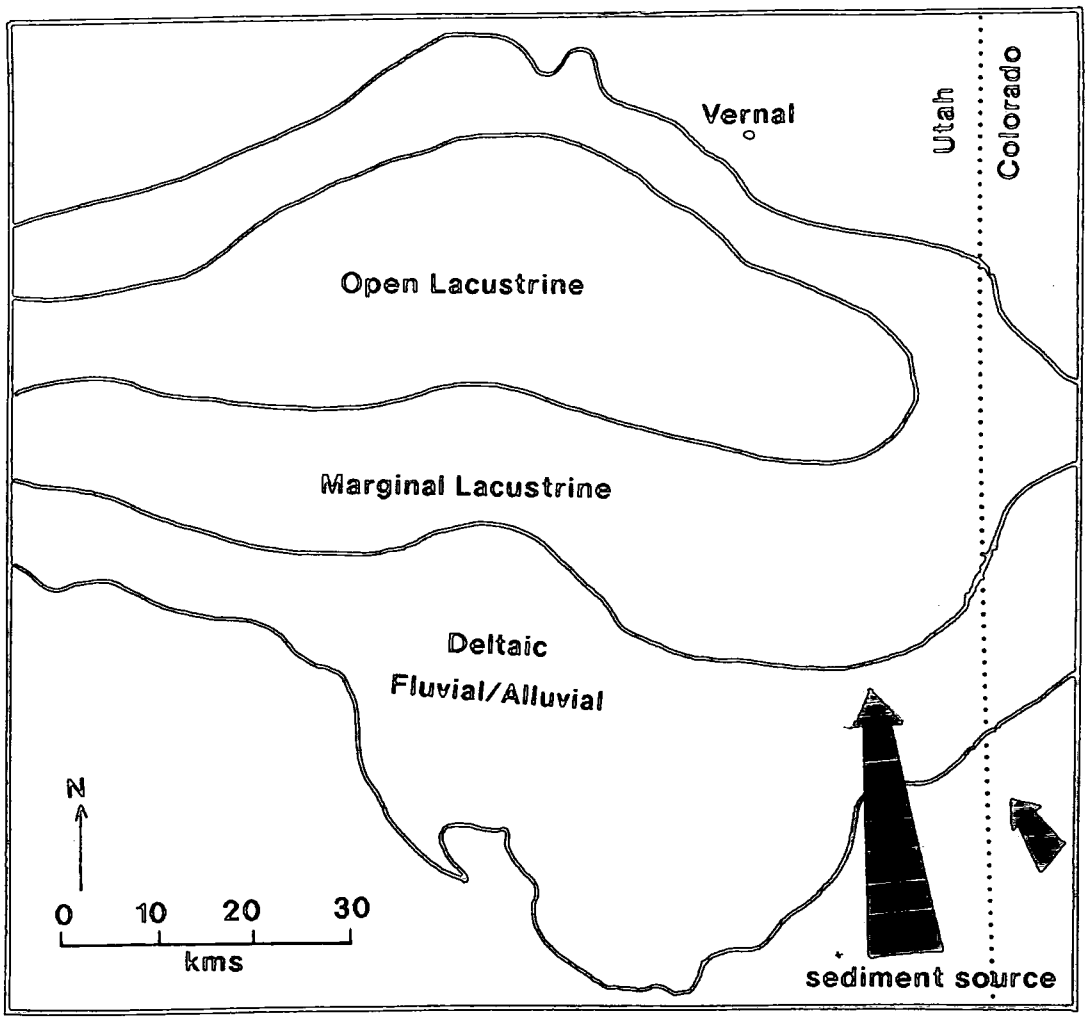

Fig.4.3.4 - Palaeogeographic map including depositional facies equivalent to the MOZ of the Green River Formation (modified from Fouch et al., 1975)

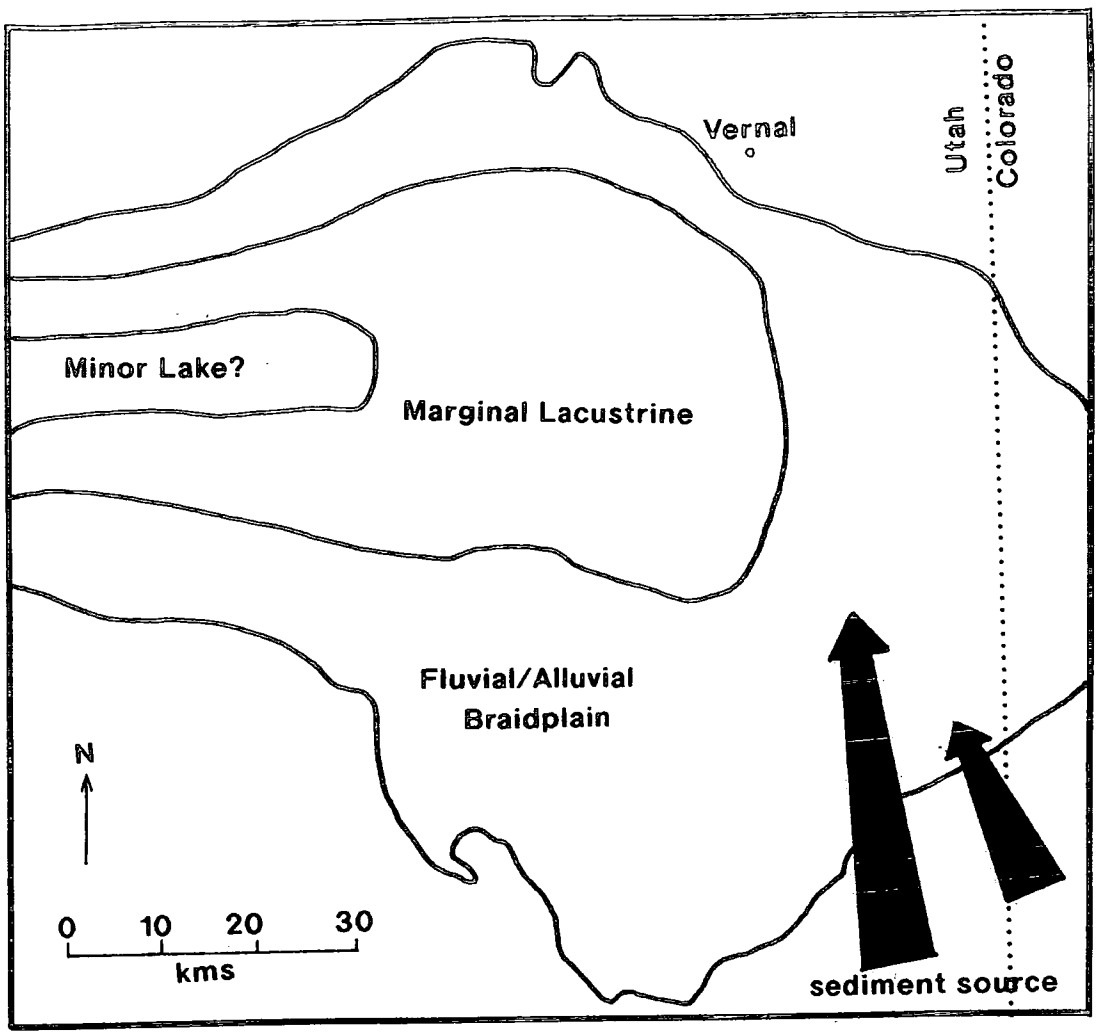

Fig.4.3.5 - Palaeogeographic map including depositional facies equivalent to the base of the Uinta Formation (modified from Fouch et al., 1975)

indicators can provide a valuable starting point for the interpretation of the emplacement and timing of these hydrocarbon deposits.

The most impressive feature of the veins is that they strike, without deviation with respect to their width, along an orientation between 264-279° (trend NW-SE) for up to 16km mapped on the surface (Plate p4.1a) (Cashion, 1967). The ratio of length of these features to their width (range of <0.02m to >10m) is suggestive of regional tectonism applying directed stress, and inducing fractures which would allow this repetitive orientation over such a large area, apparently irrespective of host medium. It would appear that if these veins were possibly accommodating space for fluid escape and residual emplacement then differential and favoured fracture patterns would emerge with respect to lithology and stratigraphic framework. However, since these veins are not consistent in their width along strike, the host wall rock might dictate to some degree the accommodation of these hydrocarbons. Whether this occurs as an early stage of high fluid pressure and ductility contrasts, hydraulic conductivity and porosity and permeability relationships offered by the host medium or as a late stage mechanical reaction to time dependant strain (creep) of the solidifying residue, remains to be seen.

4.4.1 Wall rock relationships with respect to host medium

Following the approach of Verbeek and Grout (1992) the response and characteristics of the host rocks and their relationship to the veins can be divided into the major rock types in which the Gilsonite veins occur:

1) **Lower Uinta Formation:** Marginal-lacustrine, fine grained sandstones (section 4.3.2)

This part of the sequence is dominated by a fairly cyclical repetition of fine grained sandstones punctuated by siltstones increasing to well sorted arenaceous components up the sequence.

Commonly the Gilsonite is well developed and has been extensively mined at certain locations. However, due to the transitional nature of the facies in both an areal and vertical sense, the width of the veins range from the cm to the metre scale suggesting that the width of the veins may be controlled to some extent by the facies. Well developed surface features are expressed both on the main fracture face (Plate p4.4.1.a) and also in complimentary sub-parallel anastomising fractures which step in both directions along strike. These sub-parallel fractures also decrease in intensity sharply away from the main fracture/vein (approximately 10m each side of the main vein). Heavily stained mineralisation is visible on these parasitic fractures indicative of

Plate p4.4.1a - Surface fractures in the lower Uinta Formation wall rock. Gilsonite has exploited these fractures. Hammer for scale. Loaction Cowboy vein.

precursor fluid flow prior to the phase of Gilsonite emplacement. These stained surfaces have been identified as limonite (Verbeek and Grout, 1992) and leaching of fluids saturated in minerals such as iron and diagenetic phases such as silica (Monson and Parnell, 1992).

On the actual vein bounding wall rocks, various structures indicative of parasitic fracturing are well developed. Plate p4.4.1.b shows the Cowboy vein which has been mined out and trenched exposing several important features. The presence of plumose structures and markings are interpreted as subtle surface features that form during fracture growth (Narr and Currie, 1982). These features are identifiable as tapered markings that branch at low angles from the main dyke which allow the pervasion and solidification of Gilsonite on the 'shadow' side of these features (Plate p4.4.1.b). Verbeek and Grout (1992) refer to these structures as 'twist and hackle' faces and steps. These plumose features would likely be unpreserved and destroyed if any elements of shear were in operation (Narr and Currie, 1982). Their existence infers that these joint surfaces were the result of extensional stress. Whether this extensional component is entirely regionally induced or a combined effect of local fluid and tectonic interaction is still to be deduced. Fluid would be inferred as being sourced from directly downward through the sequence from the source horizon (MOZ) of the Middle Green River Formation.

Lateral jogs into the wall rock are also seen at the Cowboy vein locality (Plate p4.4.1.c). Evidence of this vertical component is also suggested by a major 1.5 metre offset and the existence of subordinate fractures in the B600 level of the underground shaft of the Bonanza vein (Fig.4.4.1.c). This observation at the B600 level in the underground Bonanza vein again conforms to the lithological classification of the Lower Uinta formation and is possibly a lateral equivalent of the feature seen at the Cowboy locality.

Several theories have been postulated for the existence of these Gilsonite filled sub fractures which seem to offshoot along these apparent en echelon type gashes. These features are thought to initiate due to post dyke movement along transverse faults (Verbeek and Grout, 1992) but no evidence of disturbance or overprinting of this faulting has been recorded in the fault line or in the Gilsonite itself. These lateral jogs are probably the lateral expression of anastomising vertical fractures caused by high fluid pressure injection taking advantage of joint sets sub-parallel to the main conduit. This theory envisages a main vertical movement of fluid with its lateral expression visualised at the surface in the Cowboy vein. Therefore, if vertically

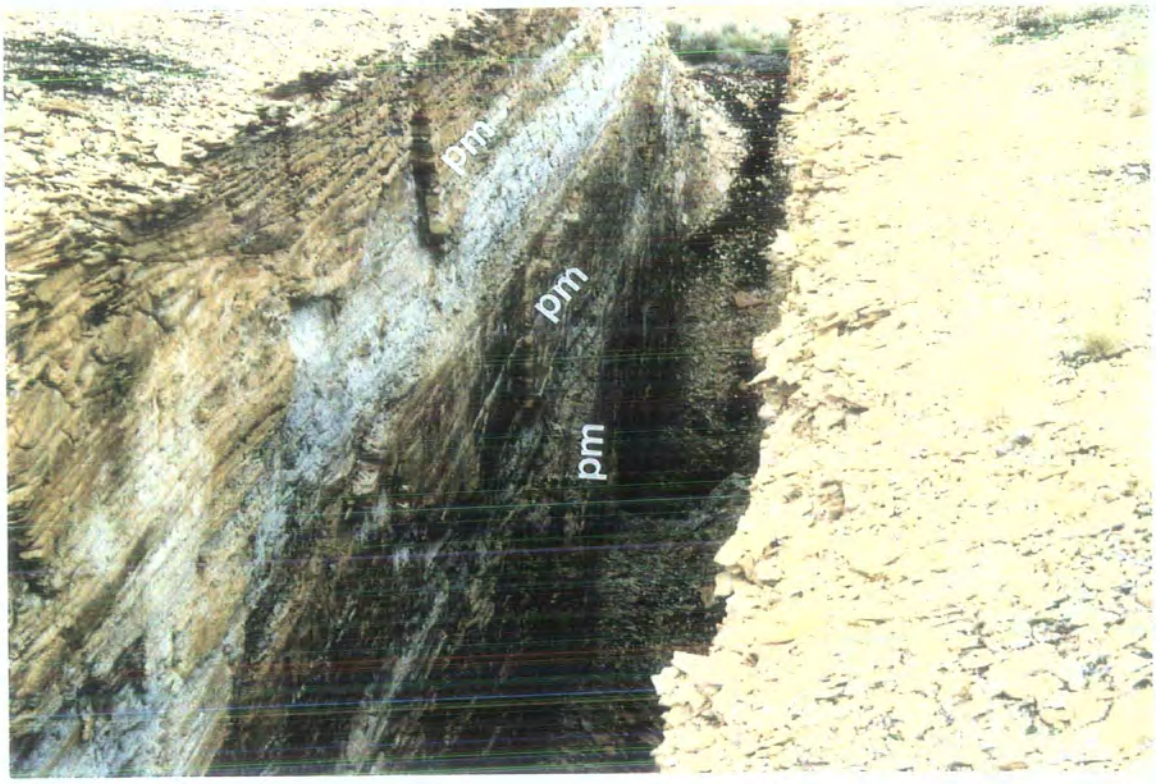

Plate p4.4.1b - Cowboy vein (mined out) showing plumose markings identified as pm. These features taper at low angles and occassionally retain Gilsonite on the 'shadow' side of these features. Vein width approximately 4m.

Plate p4.4.1c - Lateral jog of Gilsonite exploiting sub-parallel 'en echelon' type fracture into the wall rock. Hammer for scale. Location Cowboy vein. See text for discussion).

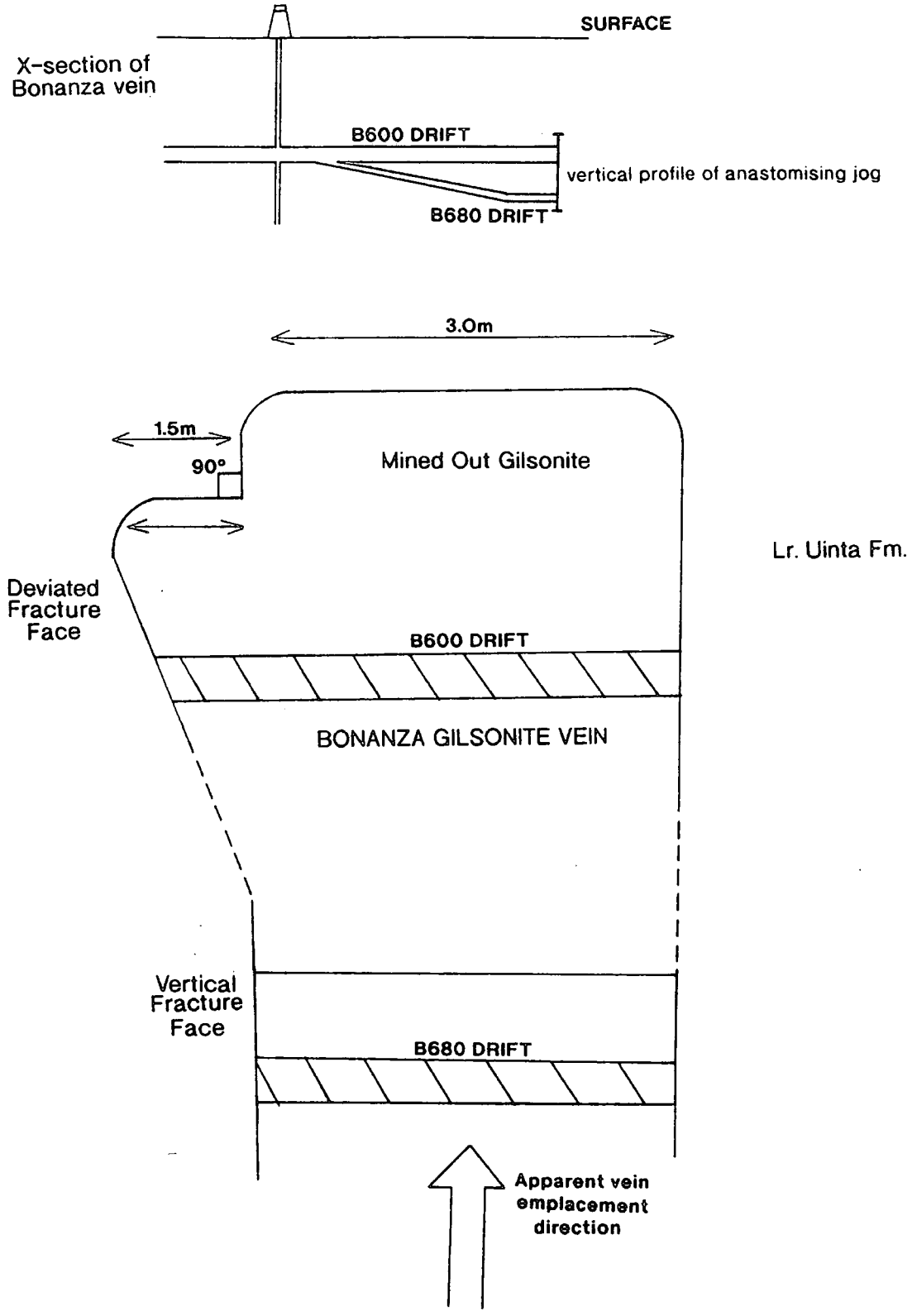

Fig.4.4.1c - Vertical deviated offset in the Bonanza vein at the B600 level of the underground workings

migrating fluids were to preferentially exploit an offset, the lateral expression of this at surface could be seen as this lateral jog.

Verbeek and Grout (1992) suggest the existence of these lateral jogs as a consequence of dyke propagation and dilation into non-coplanar fractures. However, no evidence of lateral propagation of the Gilsonite is observed and no logical theory is postulated as to why propagation and migration of the expelling fluids and hydrocarbons should have a pathway expressed in a horizontal plane perpendicular to the main lithological and stratigraphic stacking pattern and inferred fluid conduits.

2) **Mid Uinta Formation:** Deltaic-fluvial/alluvial medium-coarse grained sandstones (section 4.3.2)
The veins and fractures in these host rocks are relatively simple with regard to fracture faces and subordinate structures which are apparent in the lower part of the Uinta formation documented in the above section. The dilational component observed by mineralisation on the faces of the joint sets is not obvious and extensional movement is more difficult to imply in these occurrences of predominantly medium grained sandstones hosting the Gilsonite. A less well cemented matrix combined with the relatively well enhanced reservoir properties of porosity and permeability afforded by the constituent grains in this part of the Uinta formation has given rise to low relief walls which lack the structural complexity of the dyke walls lower in the section (Verbeek and Grout, 1992). It is these dyke-wall relationships which have been observed and described by Davis (1957) and Henderson (1957) as smooth and featureless.

An important feature is the presence of Gilsonite in the pores of the sandstone, decreasing in intensity away from the main vein. The main control is the porosity and permeability relationship of the host rock relative to the vein. In the Mid Uinta formation at the eastern end of the Main Chipetta vein, the impregnation of the wall rock extended to approximately 40m each side of the main vein. The intensity of Gilsonite impregnation decreases with distance from the vein observed in the field by rock colour and also mineralogically (section 4.4.5). It is interesting to note that the Main Chipetta vein at this locality is not well developed being approximately 2-4cm in width. This relationship has been noted by Monson and Parnell (1992) at the Black Dragon vein at the eastern extremity of the vein outcrop and is reported to extend to a margin of 50cm in the proximity of the main vein. This relationship occurs at the Main Chipetta vein but at migration distances far greater than reported by Monson and Parnell (1992). This suggests the possible invasion of precursor and volatile

hydrocarbons into the formation from the main fracture before the emplacement of the residual Gilsonite in the pore space of the Uinta formation at these reported localities.

3) **Upper Uinta Formation:** Fluvial/Alluvial medium grained sandstones with interstitial mudstones (section 4.3.2)
The introduction of mudstones into the sedimentary succession is important with respect to the behaviour of the Gilsonite and the space provided by these shale interbeds.

Dyke walls in these localities typically exhibit pinch and swell features of non linear bulbous dilations along the strike of the vein (Plate p4.4.1.d). Differential distortion of the wall rocks suggest mechanical reaction of an incompletely lithified host rock and the interaction of fluids causing such irregularities. However, the presence and consistent relationship of strike of the vein following a linear pattern in these facies as in other brittley fractured Uinta formation facies (Lower and Mid Uinta formation sandstones) infer that the fractures are complete and non deviational along strike and through the lithostratigraphic sequence. Also, previous observations of residual Gilsonite in the brittley deformed Mid Uinta sandstone formation away from the main veins have not been recorded in the Upper Uinta formation. This is probably a direct result of the permeability contrast of the interbedded shales and mudstones of this succession. Plumose structures are absent on the dyke walls in these host rocks due to the ductile behaviour and inability of the mudstones to act brittely with respect to the emplacement of the Gilsonite.

If the fractures were to initiate in a non lithified ductile sequence, then accommodation of any structural or tectonic feature in the form of fractures would show deviation along strike and would possibly be buffered and the stress would be taken up by competent mudstone horizons. The mechanical response to emplace the fractures in such a fashion exhibited at localities such as Independent/Bonanza vein junction would infer brittle deformation before time dependent strain of the residual Gilsonite could differentially distort the wall rock to allow the formation of pinch and swell structures. Verbeek and Grout (1992) attribute the existence of this wall rock pattern to the semi ductile nature of the mudstone at the time of dyke intrusion but the consistency of the vertical and lateral attitude of the veins in both the older sandstone members and the Upper Uinta formation mudstones suggest a lithified sequence prior to fracturing and vein intrusion. This mechanical operation of Gilsonite emplacement with respect to wall rock mechanical state and capability is investigated in section 4.7.

Plate p4.4.1d - Pinch and swell feature/bulbous dilations of Gilsonite deforming host rock differentially. Hanging wall shows slight deviation but is mostly coherant along strike. Gilsonite deforms foot wall differentially with coherant sandstone block apperaing as an 'in lier' in the Gilsonite vein. Location Bonanza vein.

4.4.2 Existence and occurrence of Gilsonite sills

The Gilsonite has been recorded principally in vertical fractures with associated subordinate features such as the vertical offsets. However, small Gilsonite sills (Plate p4.4.2.a) have been identified and inferred to be fed from the main vertical dykes (Monson and Parnell, 1992; Verbeek and Grout, 1992). Thus, the structure of the veins and their likely emplacement history is not as apparently simple when this component of the structural feature is considered. The existence of these sills suggests concordant emplacement exploiting fissility along shale laminations. This then infers that precursor hydrocarbons may have been forcibly injected along these laminations and did not vertically fracture the formation as the common observations of the veins observe.

The Gilsonite sills are located in argillaceous sections possibly due to the competence of these shaley sections to accommodate and deform in such a manner. The permeability and associated hydraulic conductivity offered by the shales and mudrocks in the succession may result in dilatancy in the horizontal plane. The lateral expression of the emplacement of high pressure fluids in low permeability horizons may be seen as sills which trend perpendicular to the main vertical vein (Plate p4.4.2.a). These occurrences are common in the Green River shale sequence and has been noted by Verbeek and Grout (1992) in the Pariette system of Gilsonite dykes. The main locality for the exposure of these features in the Green River shales is at the Rainbow and Black Dragon veins (Monson and Parnell, 1992). Due to the fissile nature and laminar stacking pattern offered by the shale horizons, it is feasible that high pressure fluid forced these laminations apart to accommodate the volume of injected hydrocarbons.

4.4.3 Structural overprinting - post Gilsonite injection

Several features of post Gilsonite structural overprinting have been identified and are important in allowing constraints to be placed on the hydrocarbon emplacement with respect to basin history.

Stratigraphic and geomorphic data summarised in Verbeek and Grout (1992) bracket the times of formation of three primary joint sets at 43-10Ma; The two youngest sets date from the time of regional uplift beginning at approximately 10-15Ma (Whitney and Andrews, 1983). It is these most recent expressions of tectonic overprinting that are of interest to this study.

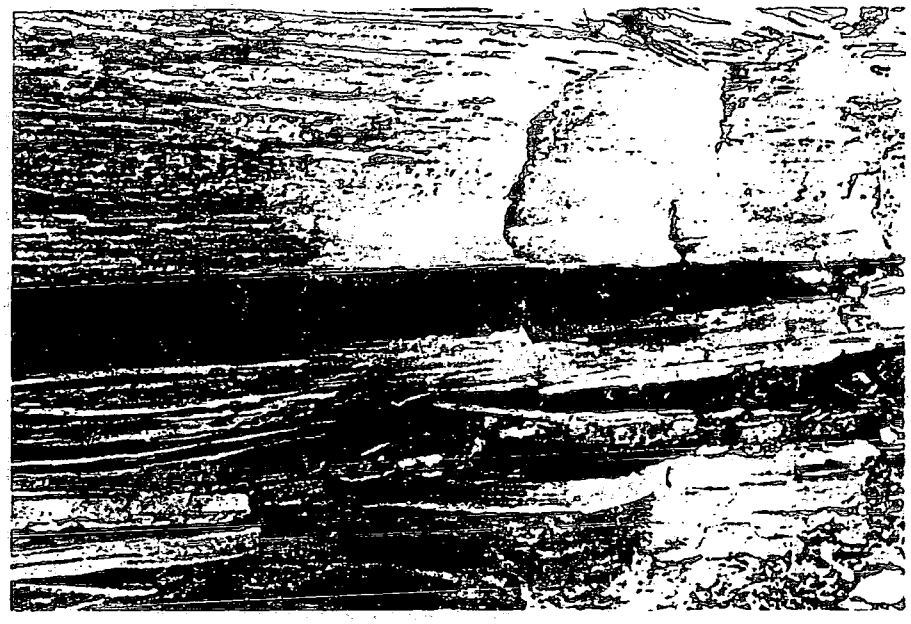

Plate p4.4.2a - Gislonite sills on finely laminated marlstone and lean oil shale in the Green River Formation near the south-east end of the Rainbow vein. Pencil for scale. Reproduced from Verbeek and Grout (1992)

4.4.3.1 Pencillated joint sets (Fig.4.4.3.1a)

A diagnostic tool in determining any post Gilsonite tectonic influence in the Uinta Basin is seen by the existence of platey columnar joint sets which fracture the Gilsonite at certain localities (Plate p4.4.3.1a). These pencillated joint surfaces typically exhibit fractures separately on the mm to cm scale not generally exceeding 2cm in width. Again, in common with the earlier dyke fractures, no sense of shear was evident an any of the examples studied. The orientation of these fractures range from 035°-052° coincidental with the F_4 joint set observed by Verbeek and Grout (1992). The expression of these joints in the surrounding country rocks are similar in structure but preservation is degraded. These features have been recorded by Eldridge (1901), Davis (1957), Pruitt (1961), Cashion (1967) and Verbeek and Grout (1992). Various origins have been postulated by these authors ranging from cooling characteristics of bituminous hydrocarbon, near surface weathering and compression due to dyke readjustment. However, what they have in common implies an overprinted joint set accentuated and preserved in the Gilsonite which is also observed in surrounding country rocks.

Since these joint sets are seen as relatively late stage features, the Gilsonite can be thought of as also being a relatively late feature as none of the previous joint sets observed by Verbeek and Grout (1992) overprint the Gilsonite veins. No shear sense indicators were present and thus the orientation and trend of these fractures suggest an extensional response to uplift which commenced from approximately 10Ma (Whitney and Andrews, 1983). If the joint sets are parallel to the direction of the least imposed stress then fracturing associated with extension can be envisaged (Lucas and Drexler, 1976). If this is the case then the extension is directed along a NNW-SSE trend which is comparable and coincidental to the envisaged uplift at this time (Narr and Currie, 1982).

4.4.3.2 Dyke offset associated with differential uplift and rotation (Plate 4.4.3.2a)

An apparent lateral offset was observed in the Main Chipetta vein with an observed apparent dextral offset of approximately 4cm along the south fracture wall. The corresponding northern contact face was not disturbed along strike and the overprinted pencillated structures were seen to be contemporaneous with this apparent offset. The influence of dextral shear indicates a component of shear stress which is not noted elsewhere is the veins or the outcrops studied. Monson and Parnell (1992) attempt to explain offsetting in the veins to be a result of apparent sinistral offset due to the extensional stress operating on an already existing kinked fracture but fail to expand the theory to explain the reason for the original fracture deviation. Tip line

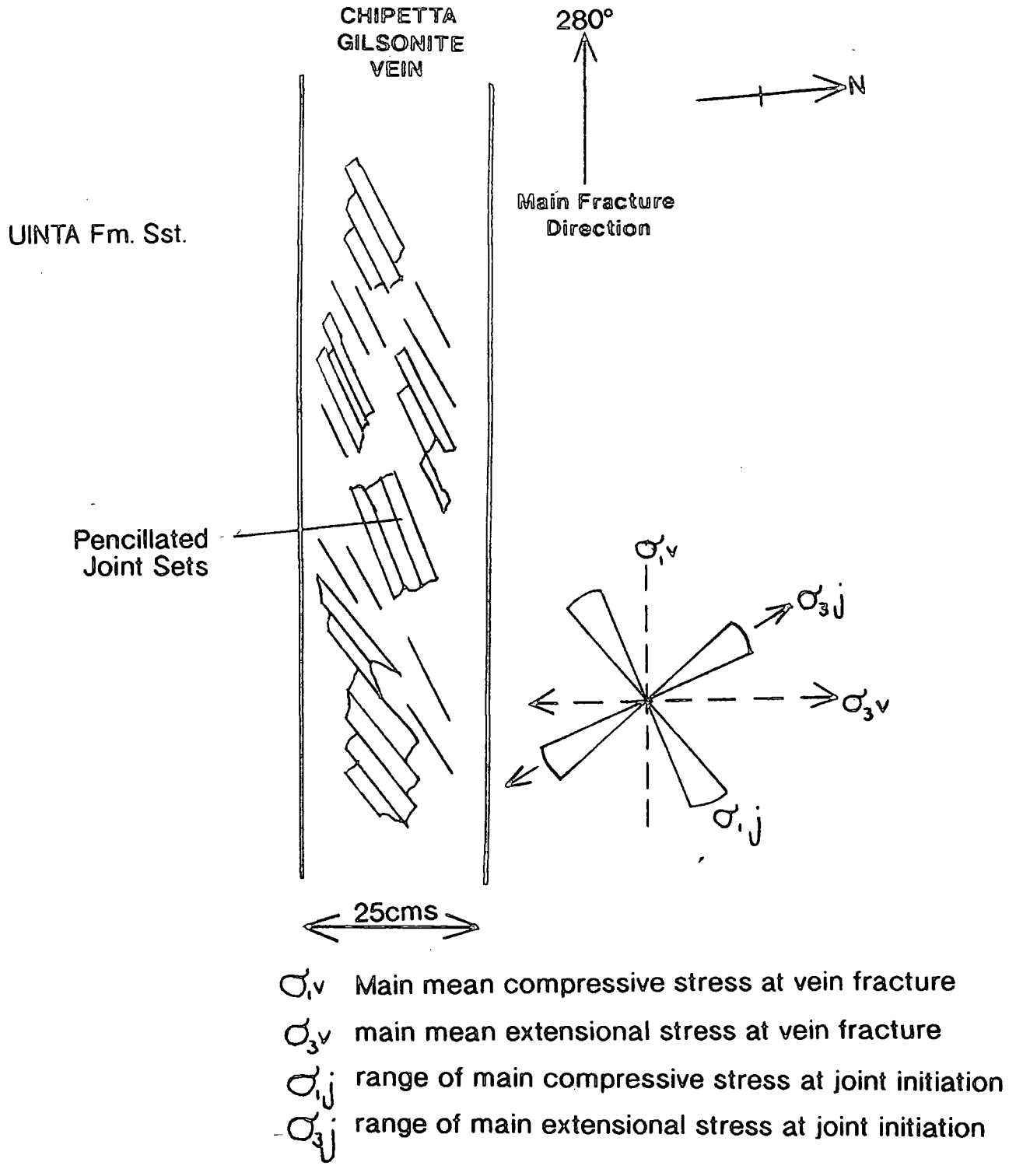

Fig.4.4.3.1a - Pencillated joint sets identified in the Little Chipetta and Wagonhound veins

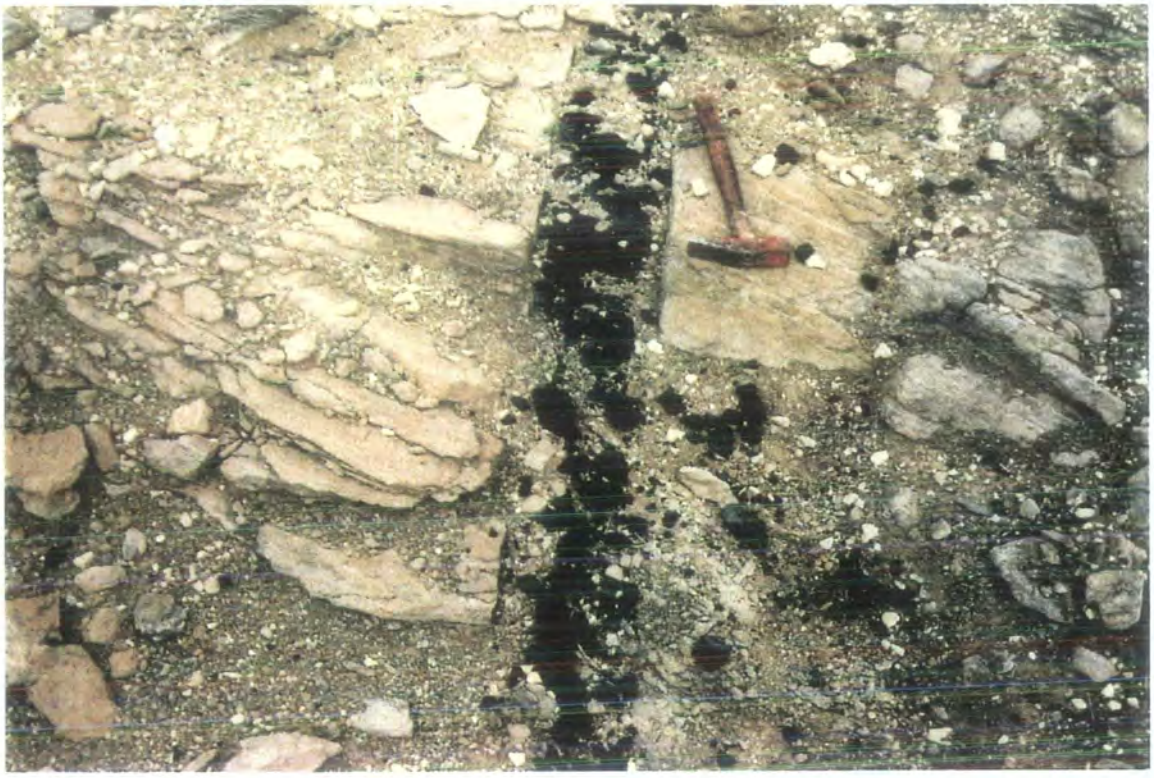

Plate p4.4.3.1a - Pencillated joint sets in the Gilsonite trending approximately 30-45° to the main trend of the vein. Location Little Chipetta vein.

Plate p4.4.4.3.2a - Apparent offset of wall rock showing abutting relationship of Uinta sandstone with Gilsonite either as a result of differential uplift and associated rotation or as an effect of mechanical strain of solidifying Gilsonite. Location Wagonhound vein. See text for discussion.

propagation due to stress amplification could cause kinking in the original fracture for future extensional stress to act upon but again this was not observed in the field or documented by Monson and Parnell (1992). The apparent offset in the example (Plate p4.4.3.2a) is more likely an expression of differential unloading during uplift to cause uneven distribution of extensional stress. The possibility exists that local stress amplification occurs at certain focus points along the country rock at fracture or plumose terminations. The result would be a minor offset or rotation with associated breccia as seen at this locality. The abutting relationship of this structure could also be the result of the interaction of younger extension fractures terminating against older ones arising from the fact that a tensile tress cannot be transmitted across a cohesionless boundary as suggested by Verbeek and Grout (1992).

Therefore, it would appear that vein emplacement is determined largely on the utilisation of pre-existing fractures in the sedimentary succession created by regional extension and possibly enhanced by high fluid pressure in the compacting sedimentary pile. Precursor mineralisation on the walls of these veins point to early percolation and fluid flow but actual emplacement of the Gilsonite with respect to mechanical and physical interaction with the host rock largely dependant on the characteristics and ability to host or disperse the hydrocarbons. Brittle deformation and lateral anastomising jogs appear to occur in the Lower Uinta marginal-lacustrine sandstones taking advantage of dyke parallel joints and fractures. The sandstones typical of the Mid Uinta Formation appeared to allow percolation and invasion of the hydrocarbons to a zone peripheral to the main vein due to the porosity and permeability characteristics offered by these rocks. Plastic and ductile wall rock response in the Upper Uinta Formation is more likely to be a result of strain on the wall rock due to the emplacement of residual Gilsonite. No shear sense indicators were visible at any locality and all overprinted structures such as the pencillated joint sets and lateral offsets are inferred to be a product of extension late in the history of basin evolution.

4.5 Mineralisation of the wall rock

It is necessary to examine the mineralisation and associated diagenetic history of the wall rock to the dykes to assess the relative timing of events with respect to mineralisation and hydrocarbon invasion. Evidence has already been reported for precursor mineralisation and fluid flow bleaching and altering the Gilsonite vein wall rocks (section 4.4.1; Verbeek and Grout, 1992). Gilsonite impregnation of the host rocks is a common feature and is pronounced adjacent to certain main veins such as the Main Chipetta (section 4.4.1 and Fig.4.4.1a). Wall rock mineralisation has been described by Verbeek and Grout (1992) as a smearing of limonite rich minerals on the

fracture faces in the Mid Uinta Formation. This could not be verified by field observations. Bleached zones are conspicuous in the reddish-brown to maroon mudstones and siltstones of the upper part of the Uinta Formation, which in many places have lost all vestige of their original red colour adjacent to dykes and are now pale grey to tan (Verbeek and Grout, 1992). This colouration and intensity around the vein-wall rock contacts suggest the possibility of iron oxide staining inferring some aqueous flow to cause this differential weathering at the vein-wall rock contacts.

For an appreciation of timing of this fluid invasion with respect to wall rock diagenesis, an examination has been made on the petrography of the authigenic phases of sands adjacent and peripheral to the main dykes; Monson and Parnell (1992) have interpreted the diagenetic sequence in the host sandstones as being a fairly continuos event of mineral precipitation and dissolution with overlap between certain phases (Fig.4.5.1a). They cite compaction as only being influential in mechanically reducing the sediment pile and affecting quartz precipitation by the mechanism of pressure solution and remobilisation of this solute. Monson and Parnell (1992) state that the paragenetic sequence indicates that Gilsonite impregnation of the sandstone wall rocks occurred relatively late in the diagenetic history (Fig.4.5.1a). Although this is intrinsically true, this observation does not necessarily define the relationship between the diagenesis and the impregnation of the Gilsonite. Monson and Parnell (1992) infer that impregnation is mechanical and does not interact with the mineral phases. However, it is seen that Gilsonite (a brown interstitial material in thin section) occurs in a decreasing amount peripheral to the Main Chipetta vein in the Mid Uinta sandstones in a zone of approximately 40m (Fig.4.5.1b, Plates 4.5.1a, b, and c). It is not conceivable to suggest that Gilsonite possessed a viscosity high enough to permeate mechanically through the sandstone once in a state of solidification. Therefore, the Gilsonite must be thought as a residual bitumen compound of low viscosity which was part of a higher volatile carrier compound which escaped through the relatively high porous network. Therefore, solidification of the Gilsonite can be thought of as a relatively late stage mechanism.

Petrographic observations on the Uinta Formation sandstone host rocks adjacent to the Little Chipetta vein showed epitaxial overgrowths on the detrital quartz grains which contained fluid inclusions but which were no greater than 2μm and did not fluoresce under UV light suggesting that the trapped fluids are aqueous and do not contain any hydrocarbon phase. Therefore, it is possible to conclude that hydrocarbons did not invade these rocks until after the quartz diagenesis had ceased.

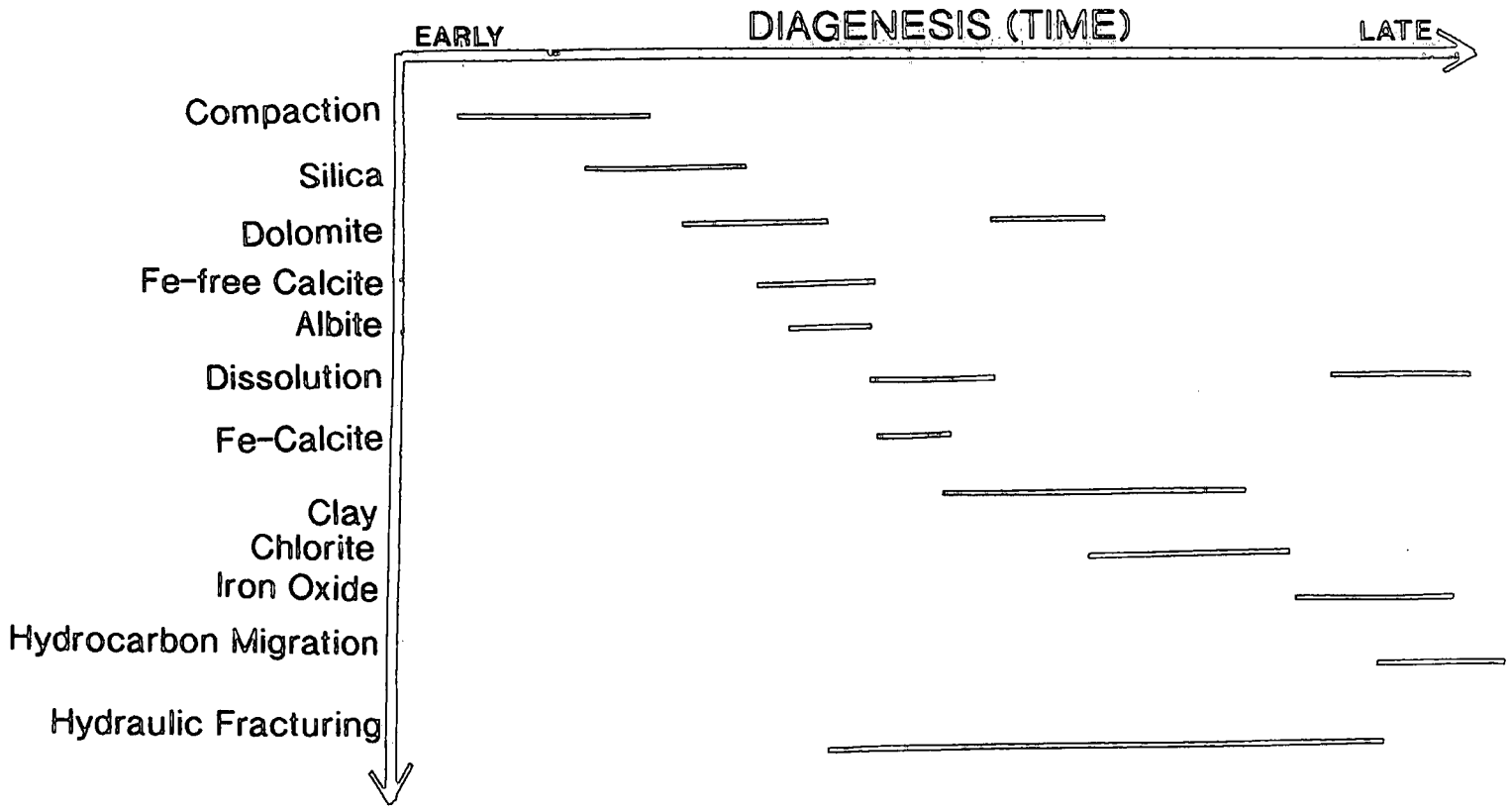

Fig.4.5.1a - Paragenetic sequence of the Uinta Formation host sandstone. Modified from Pitman et al. (1982) and Monson and Parnell (1992)

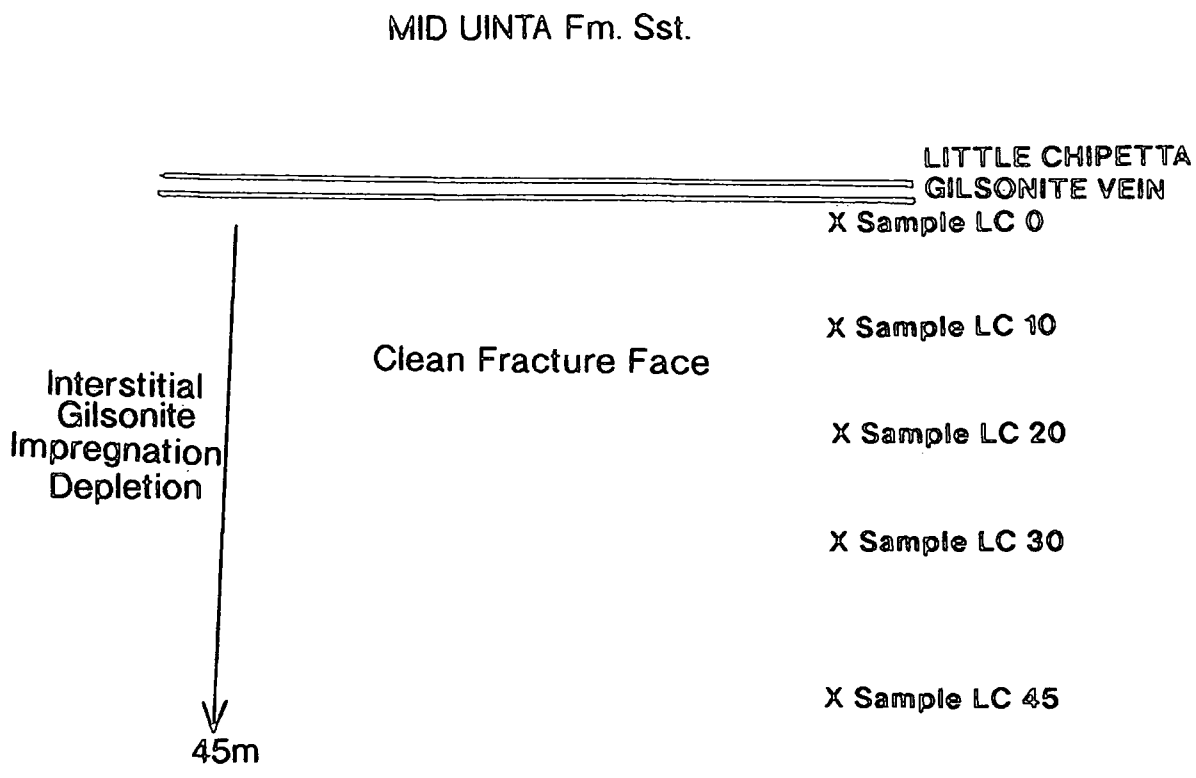

Fig.4.5.1b - Sampling locations and relationship of impregnated wall rock with distance from the Little Chipetta vein

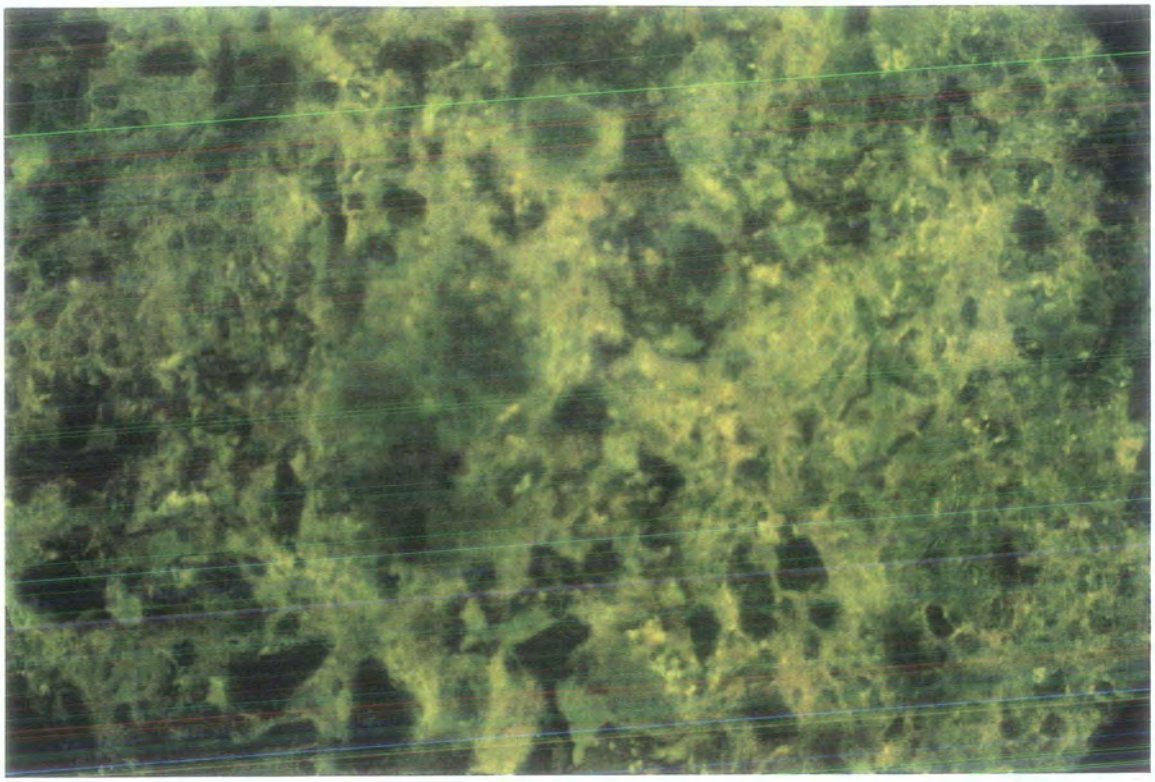

Plate p4.5.1a - sample LC0 (see Fig.4.5.1a). UV photomicrograph showing high yellow-gold fourescence due to high saturation of Gilsonite. Gilsonite is dominant over the subordinate sandstone minerals. Field of view1.2mm

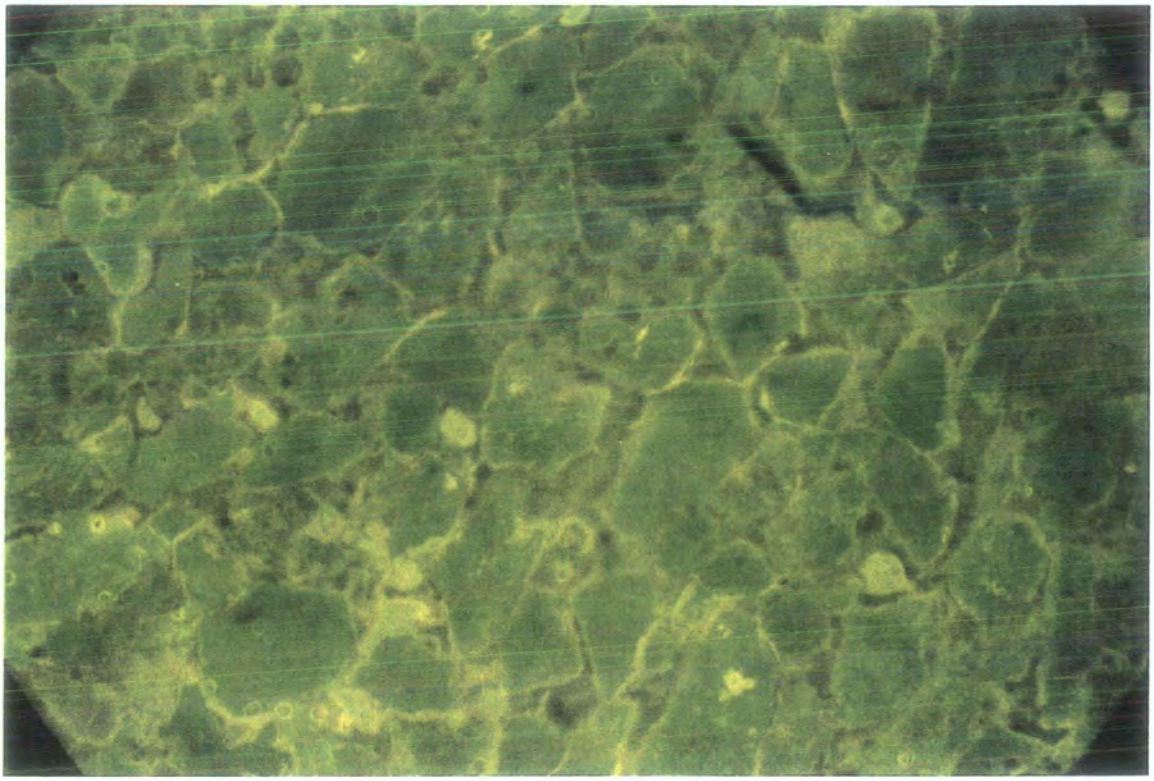

Plate 4.51b - sample LC20 (see Fig.4.5.1a). UV photomicrograph of Uinta sandstone host rock 20m away from the Little Chippeta vein. High flourescence due to interstial Gilsonite but quartz grains are easilt recognisable. Field of view1.2mm

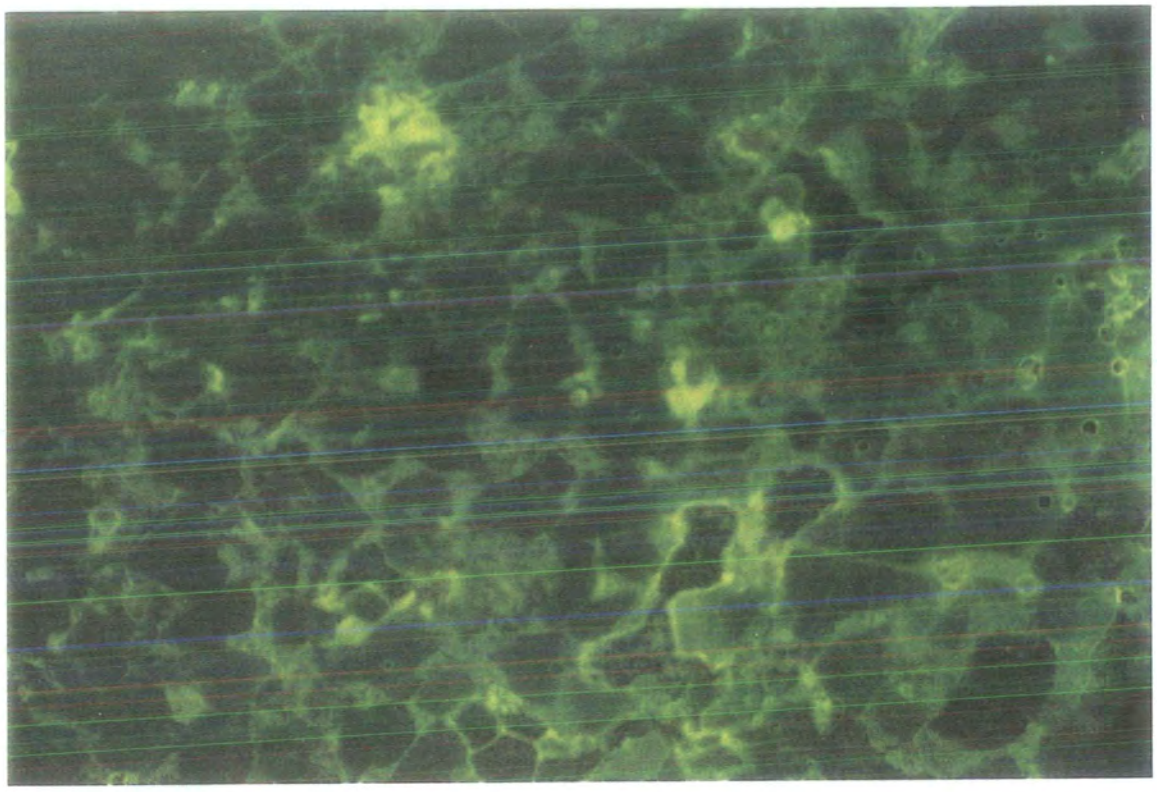

Plate p4.5.1c - sample LC40 (see Fig.4.5.1a). UV photomicrograph of Uinta sandstone host rock 40m away from the Little Chipetta vein. Interstitial Gilsonite now relatively depleted. Field of view 1.2mm

Pitman et al. (1982) have analysed and interpreted the isotopic signatures of the pore water from the carbonate component (calcite) of this part of the diagenetic sequence, and concluded that authigenic carbonate formed at low temperatures (<60°C) in the presence of meteoric waters by a process of solution precipitation. Therefore, since quartz precipitation is thought to predate the calcite mineral phase (Fig.4.5.1a), the source of the quartz must be thought of as being meteoric in origin or a result of remobilised silica due to grain rearrangement as an effect of early mechanical compaction. Therefore, any entrapped fluid within the quartz overgrowth generation must be from a source not associated with any precursor fluid immediately prior to the hydrocarbon generation and expulsion by virtue of the fact that the quartz precipitation ceased relatively early in the compactional history of the sandstone.

The major difference between the Uinta Formation sandstones acting as vein host rocks and hydrocarbon reservoir rocks elsewhere in the basin (Fouch et al., 1975) is the clay component (Pitman et al., 1982; Monson and Parnell, 1992). It is seen that mixed layer I/S clays make up the clay fraction of reservoir sandstones as opposed to the main clay being chlorite in the Gilsonite vein host sandstones. Since the vein hosting sandstones have been buried to depths no greater than time equivalent facies elsewhere in the basin, another reason must be inferred for the existence of chlorite. Chlorite, by the nature of its favoured environment of formation, requires a high association with fluids rich in Mg^{2+} ions suggesting that the fluids being expelled through the host sandstones were rich in such minerals to cause the alteration to chlorite. Chlorite is also a hydrous mineral forming in conditions where water, especially at elevated temperatures, have been exposed to micaceous minerals to cause their alteration. Therefore, a transitionary fluid rich in Mg^{2+} ions, possibly being sourced from deeper in the section (to benefit from elevated temperatures), late in the diagenetic sequence and using these main fractures as conduits through the argillaceous section of the Green River Formation before acting on the sandstones of the Uinta Formation can be inferred to accommodate the observations seen and the events interpreted.

4.6 Origin of the Gilsonite

One of the problems associated with the identification of the source rocks from which the Gilsonite and indeed other hydrocarbon deposits are derived is a limited understanding of the thermal evolution of the basin (Anders et al., 1992). Temperature is the most sensitive parameter in hydrocarbon generation (Tissot et al., 1987) and reconstructing the thermal history is of paramount importance when evaluating hydrocarbons and their likely source. It was necessary to understand the emplacement

history, timing and maturation of the Gilsonite and to evaluate whether the veins were under stress due to the rapid expulsion rate and small range of activation energy associated with the kerogen type (Type I) - Tissot et al. (1987) (Fig.4.6.1a); Sweeney et al. (1987) - or were under stress due to regional tectonism. In order to reconstruct the burial, thermal and maturation history for this particular part of the basin, it is necessary to identify the depths and time when the likely source horizon was in a state of maturation, what thermal maturity the Gilsonite was equivalent to (in order to trace any maturity trends from present day reservoired hydrocarbons) and the unequivocal identification and correlation of the Gilsonite with its source rock.

Only fluid inclusions can be used to measure directly a palaeotemperature (section 3.6). Other methods and indices measure the thermal maturity of rocks and/or hydrocarbons. The measurable parameters include Vitrinite Reflectance (Ro), Rock-Eval (Tmax), Transformation Ratio, Spore Colour, Light Hydrocarbon Yield and Biomarkers associated with isomerisation reactions.

According to Khavari-Khorasani (1984) and Hunt (1979) Gilsonite is believed to be derived from oil shales in the middle to upper Green River Formation. The organic fraction of oil shale consists largely of bitumen and kerogen (Hatcher, et al., 1992). Bitumen is a complex mixture of organic compounds which, by definition, are soluble in organic solvents, whereas kerogen is a macromolecular biopolymer which can be thermally decomposed but is insoluble in organic solvents (Hatcher, et al., 1992). Bitumen comprises many separate components including aromatic and heterocyclic compounds but, importantly with respect to its relationship with kerogen and its physical properties, asphaltenes. According to Prost and Rondelez (1991) bitumen is a colloidal solution in which the asphaltenes are the solute particles and the saturated paraffins, aromatic oils and resins constitute the solvent. Therefore, if the Gilsonite can be correlated with the bitumen component of the oil shale in the Green River Formation by way of indirect or direct maturity signatures such as biomarkers (Hatcher, et al., 1992) identification and correlation can be inferred between the oil shales and the Gilsonite. There are also various other approaches toward the identification of the Gilsonite with respect to its source rock. These include:

1) Field observations
2) Isomerisation and aromatisation of biomarkers (Anders et al., 1992)
3) Total and single ion current chromatography of biomarkers (Hatcher et al., 1992)
4) Basin modelling based on stratigraphic information and thermal indicators (Anders et al., 1992).

4.6.1 Direct Field Observations

As previously described, the Gilsonite deposits (both veins and sills) are associated with the upper Green River Shale Formation where the highly organic Mahogany Oil Zone (MOZ) occurs. Especially around the Black Dragon and Rainbow veins, the Gilsonite deposits form anastomising networks of veins, sub veins and perpendicular sills which exploit the fissility provided by the shale members of the Green River Formation (section 4.4). Although there is no one locality where a Gilsonite vertical vein can be linked directly to the organic horizons of the mid and upper Green River shales, the presence and stratigraphic correlation of the Gilsonite to the oil shales are intimate.

The areal distribution of the Gilsonite veins, being located in the eastern side of the basin, suggests some response of the kerogen specific chemistry to the depositional system in this part of the basin. It has already been documented that this part of the succession - the upper Green River shales - is in an organised facies associated with peak shoreline encroachment of lake level. An algal bloom and lipid rich sapropelic organisms may flourish at this areal position of the lake and provide the necessary organic type for the future hydrocarbon deposits in this area. The oxygen versus hydrogen index Van Krevelen diagram (Fig.4.6.1a) observes a Type I kerogen with a high hydrogen index relative to oxygen and the Green River Shales have been plotted (data from Tissot et al., 1987) on as corresponding to Type I kerogen. A Type I kerogen is commonly documented as having an organic precursor such as lacustrine borne algae. Therefore, from the depositional environment inferred for the MOZ (section 4.3) this is a distinct possibility that lacustrine borne algae may provide the organic basis from which the kerogen of the Green River Formation are derived.

4.6.2 Thermal maturity using Ro equivalent indicators (isomerisation and aromatisation of biomarkers)

The unique response of the parent kerogen dominant in the organic rich Green River Formation to thermal maturation gives a very obvious profile when correlated against the kerogen. Being of a sapropelic/lipid rich Type I kerogen (Tissot et al., 1987), the response of the various thermal maturity indicators show that the activation energy and kinetics needed for catagenesis is in a very narrow range (Fig 4.6.2a) with the mean energy being approximately 55kcal/mole (Tissot, et al., 1987). The subsequent result when observing the Rock-Eval temperature indices (Tmax) against the transformation ratio (S1/{S1 + S2}) - Fig 4.6.2b, the transformation ratio against Ro (Fig.4.6.2c) and Tmax against Ro (Fig.4.6.2d) show that the kerogen changes very little during the immature stage of maturation (Anders, et al., 1992 - 0.3 to 0.6% Ro). The result then

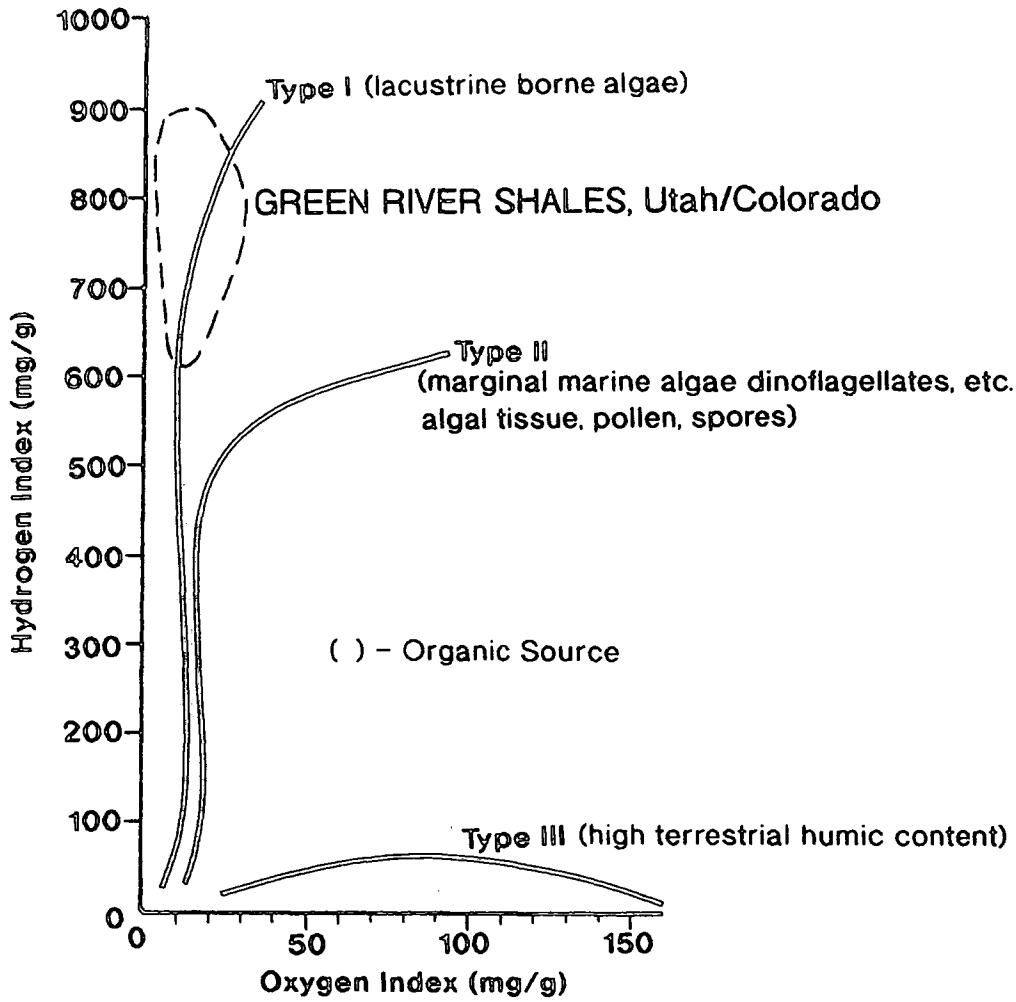

Fig.4.6.1a - Van Krevelen Diagram showing the kerogen type for the Green River Shales. Modified from Monson and Parnell (1992)

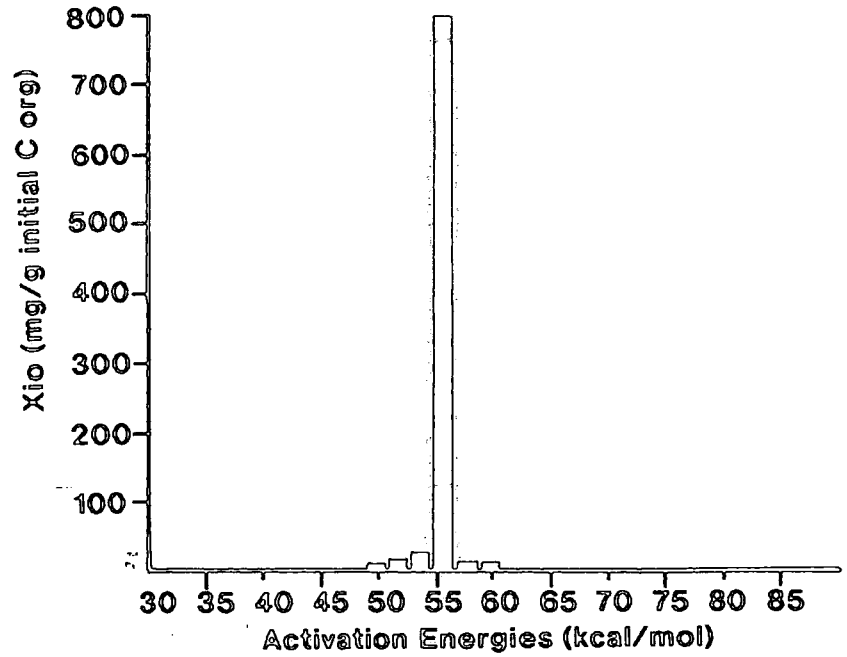

Fig.4.6.2a - Distribution of activation energies specifically calibrated on the Green River Formation shales using Rock-Eval Pyrolysis data only. From Tissot et al. (1987)

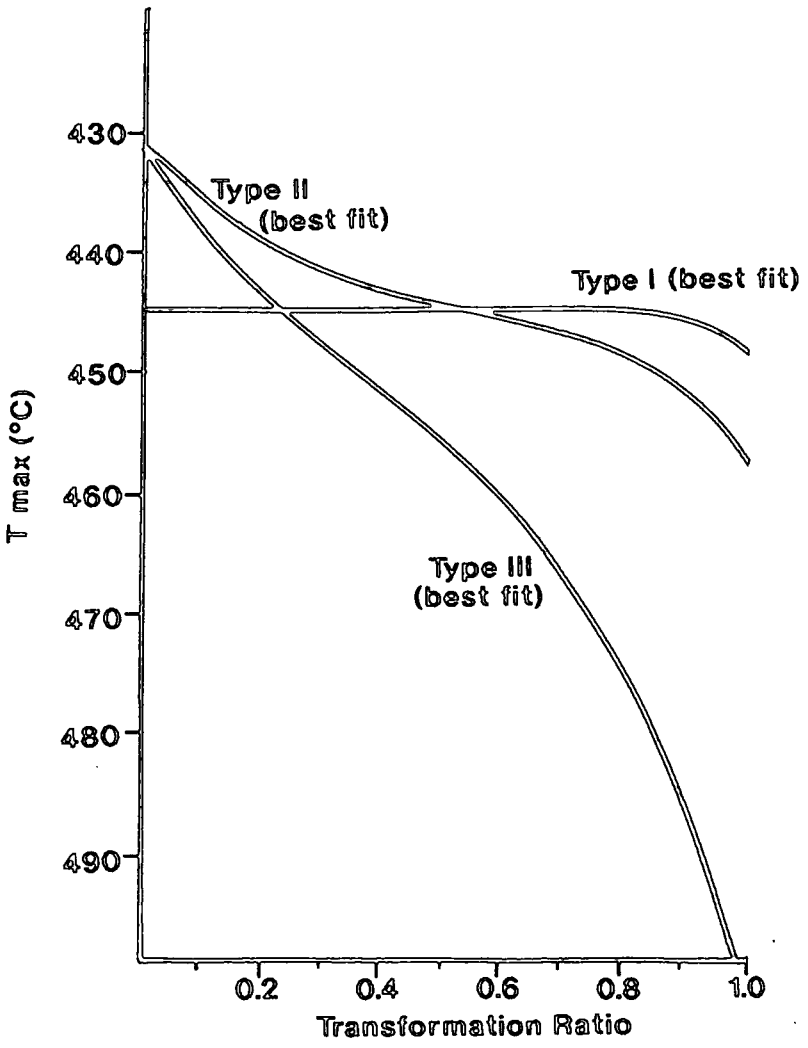

Fig.4.6.2b - Relationship between Tmax and the transformation ratio of the main kerogens types based on data from Rock-Eval Pyrolysis of subsurface samples obtained by Espitalie et al. (1985). From Tissot et al. (1987)

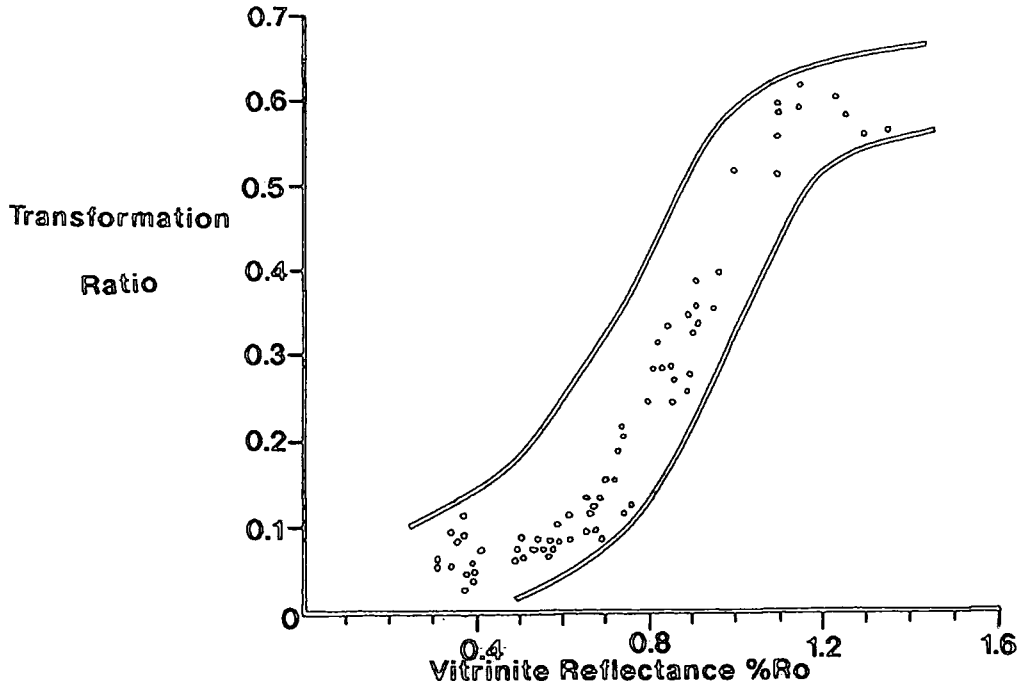

Fig.4.6.2c - Transformation ratio versus Vitrinite Reflectance (Ro) of Green River Formation rocks. From Anders et al. (1992)

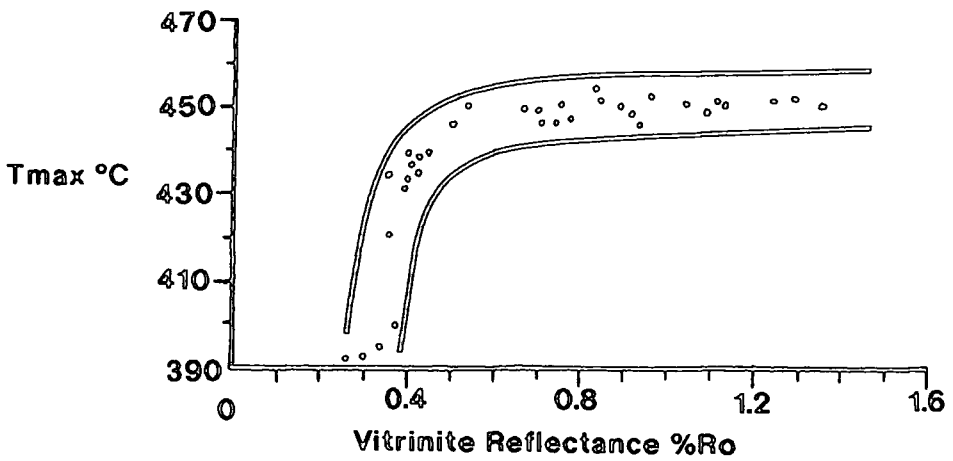

Fig.4.6.2d - Rock-Eval Pyrolysis (Tmax) versus Vitrinite Reflectance (Ro) of Green River Formation rocks. From Anders et al. (1992)

is a very energetic and rapid maturation of the kerogen when the initial kinetics have been realised. The main parameter of maturity index - Ro - is used to assess the thermal stage of the Gilsonite. However, since vitrinite is a coal and no such material was recovered from the Gilsonite veins, a vitrinite reflectance equivalent (VRE) was used. By utilising organic biological markers present in the complex make up of the Gilsonite, maturity indicators were made available to be expressed in terms of VRE. In the study made by Anders, et al. (1992) two isomeric ratios were used:
The 22S and 22R diasteromers of the $C_{32}17\alpha(H)$, $21\beta(H)$ extended hopane (pentacyclic triterpane) and
The 20S and 20R diasteromers of the $5\alpha(H)$, $14\alpha(H)$, $17\alpha(H)$ C_{29} sterane.

Selected data from the study by Anders, et al. (1992) reads

Location	Depth (ft)	C_{32} hopanes*	C_{29} steranes*	VRE
Bonanza vein	450	57	31	0.5%
Cowboy vein	surface	56	22	0.5%
Rainbow vein	surface	57	31	0.5%
Eureka vein	surface	58	31	0.5%

* S/S + R (%)

The above data show the biomarker ratios that, when plotted against VRE fall into the thermally 'early' mature category as intense oil generation from type I kerogen is judged to occur at 0.7% Ro (Anders and Gerrild, 1984; Tissot, et al., 1987). Also, the n-alkane distributions in the Gilsonites are indicative of hydrocarbons associated with thermally immature organic matter (Hollerbach and Hagemann, 1981), in that the n-alkanes are dominated by n-C_{17} with minor amounts of n-alkanes in the C_{22}-C_{31} region (Anders, et al., 1992).

4.6.3 Thermal maturity using total and single ion current chromatography (Pyrolysis Gas Chromatography/Mass Spectrometry - GC/MS)

Hatcher, et al. (1992) have conducted a thorough Pyrolysis GC/MS set of analyses on various hydrocarbons in the Uinta Basin including the oil shales from the Upper Green River Formation, the Gilsonite, tar sands and also crude oils from the Altamont-Bluebell and Red Wash fields. By analysing both the MS profile and single ion fragmentograms for specific ion masses, certain conclusions can be drawn.

Observing, and with reference to tables t4.6.3a and b, the profile of the total ion chromatogram for the oil shale (MOZ) in the range of pristane, steranes and carotane (Figs.4.6.3a and b), the major peaks are identified as pristane, a series of steranes and a

Peak No.	Formula	Identification
1	$C_{27}H_{46}$	22, 29, 30-trisnor-18α(H)-hopane (Ts)
2	$C_{27}H_{46}$	22, 29, 30-trisnor-17α(H)-hopane (Tm)
3	$C_{27}H_{46}$	22, 29, 30-trisnor-17β(H)-hopane
4	$C_{29}H_{50}$	30-nor-17α(H), 21β(H)-hopane
5	$C_{29}H_{50}$	30-nor-17β(H), 21α(H)-moretane
6	$C_{30}H_{52}$	17α(H), 21β(H)-hopane
7	$C_{30}H_{52}$	17β(H), 21α(H)-moretane
8	$C_{31}H_{54}$	22S and R-30-nomo-17α(H), 21β(H)-hopane
9	$C_{30}H_{52}$	Gammacerane
10	$C_{32}H_{56}$	22S and R-30, 31-bishomo-17α(H), 21β (H)-hopane

Table t4.6.3a - Major components in Triterpane fragmentograms based on identification made by Philp (1984), Rullkotter (1985), Zumberge (1987) and Philp et al. (1989). From Hatcher et al. (1992)

Peak No.	Formula	Identification
1		24-methyl-13α, 17β-diacholestane (20S) and 14α, 17α-cholestane (20S)
2		24-methyl-13β, 17α-diacholestane (20S) and 14β, 17β-cholestane (20R)
3	C27H48	14α, 17α-cholestane (20R)
4	C29H50	24-ethyl-13β, 17α-diacholestane (20R)
5	C29H50	24-ethyl-13α, 17β-diacholestane (20S)
6		24-ethyl-13α, 17β-diacholestane (20R) and 24-methyl-14β,17β-cholestane (20R)
7	C28H50	24-methyl-14β,17β-cholestane (20S)
8	C28H50	24-methyl-14α,17α-cholestane (20R)
9	C29H52	24-ethyl-14α,17α-cholestane (20S)
10	C29H52	24-ethyl-14β,17β-cholestane (20R)
11	C29H52	24-ethyl-14β,17β-cholestane (20S)
12	C29H52	24-ethyl-14α,17α-cholestane (20R)

Table t4.6.3b - Major components in Sterane fragmentograms based on identification made by Philp (1984), Rullkotter (1985), Zumberge (1987), Philp et al. (1989) and Riedeger et al. (1989). From Hatcher et al. (1992)

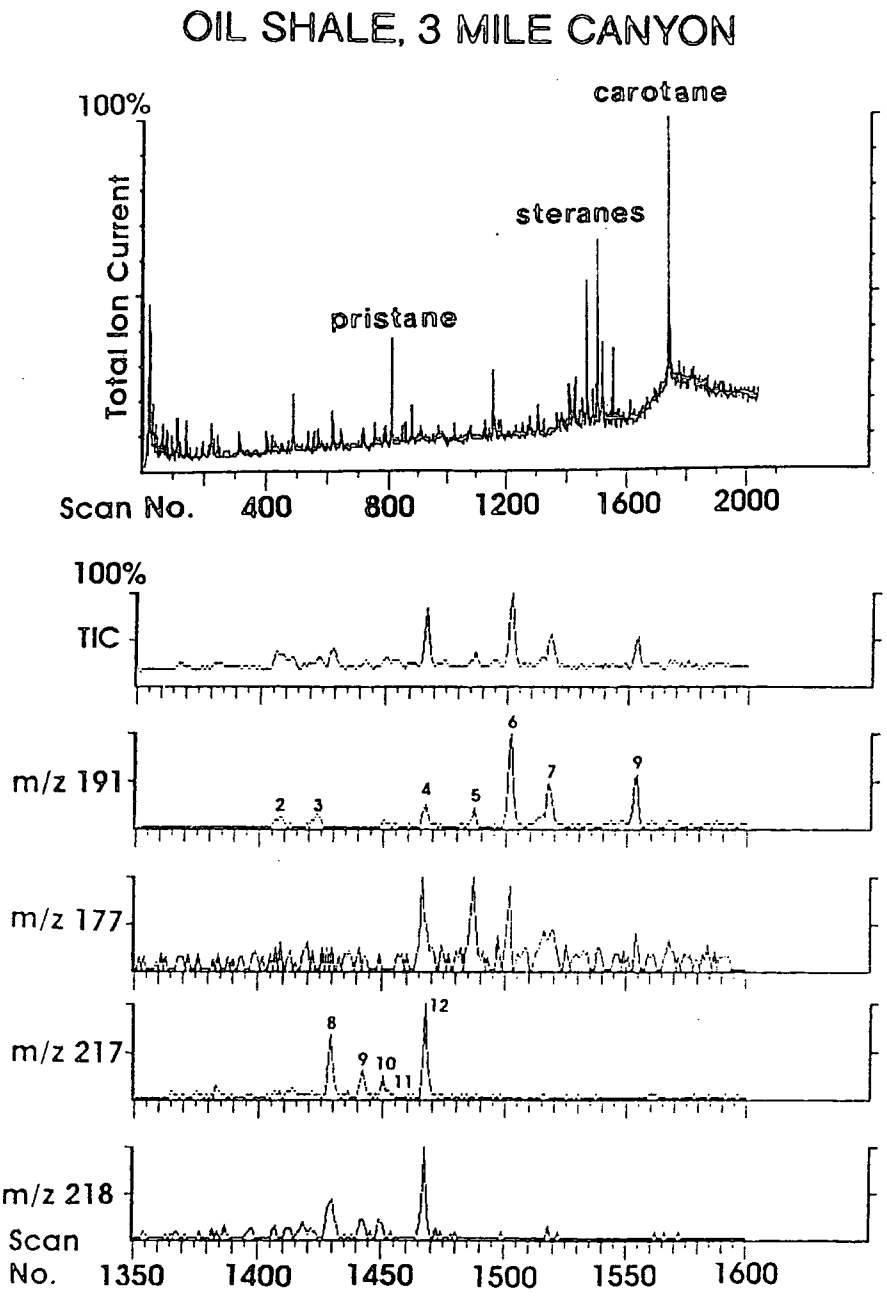

Figs.4.6.3a (top) and b (bottom) - **a)** Total ion current chromatogram of oil shale (MOZ) from Three Mile Canyon (location - T12S R25E Sec.4) **b)** Single ion current fragmentogram for triterpane m/z191, m/z177 and sterane m/z217, m/z218

large peak representing carotene. Since steranes are indicators of biodegradation (Philp, 1985b) formed by the reduction of originally sediment deposited steroids (Hatcher et al., 1992) they can be useful in determining source area and they offer the most consistent and reliable maturity indicator. When the single ion masses for the constituent sterane groups are detailed, the profiles for the atomic mass m/z 217 (Å) and the triterpane m/z 191 are the bench mark profiles to which the profiles of the Gilsonite and the crude oils are compared.

The profiles of the chromatograms of the Gilsonite from the Bonanza vein (Figs.4.6.3c and d) show a similar pattern of peaks for the occurrence of the pristene, steranes and carotene on the total ion current chromatogram. The analyses and scan profile for the member single ion masses of m/z 191 and m/z 217 show a similar response to the profile of the oil shale and are almost identical to the Gilsonite from the Three Mile Canyon (Figs.4.6.3e and f). This suggests then that the geochemical signatures of the biomarker components (steranes and triterpanes) of the Gilsonite are similar to that of the oil shale. However, the overall profile of the total ion current chromatograms of all 3 samples are very similar. It is inferred that the geochemistry points toward a common source for the Gilsonite being the oil shale of the upper Green River Formation.

When considering the sterane pattern in the above samples with the waxy crude oil in the Red Wash field (Figs.4.6.3g and h) it is seen that the response and ion peaks are similar to the oil shale and the Gilsonites. The common sterane pattern suggests a common source.

The general area where the Gilsonite veins occur lies in apparent association with the specific parent oil shale. However, the Red Wash field also contains paraffinic petroleum and waxy crude containing similar sterane profiles as the Gilsonite from the Bonanza and Three Mile Canyon veins and also the MOZ oil shale located in Three Mile Canyon. Since the bitumen and Gilsonite found in these veins are largely compounds of solvents containing paraffins, aromatic oils and resins and solutes primarily being asphaltenes with the physical properties of the suspension primarily dependant upon the volume fraction of asphaltenes, Prost and Rondelez (1991) have calculated that bitumen with 15% asphaltene is solid at 25°C but fluid at 60-100°C. Therefore, the similar sterane patterns associated with the possibility of fluid mobilisation at low temperatures (pre-maturation temperatures) combined with the information which gives the Gilsonite a VRE of 0.5% (Anders et al., 1992) suggest that pre-maturation temperatures could mobilise the bitumen and other early

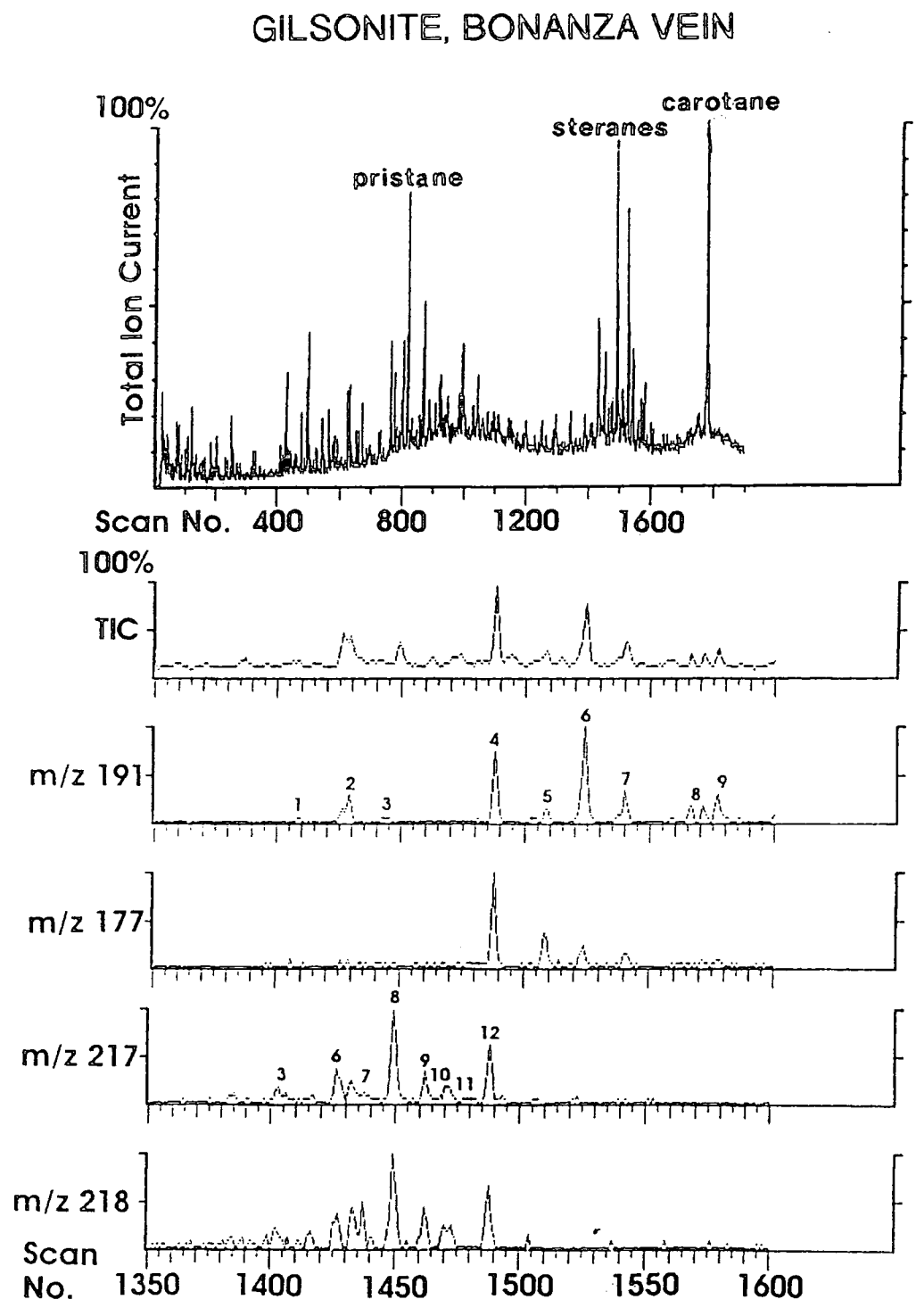

Fig.4.6.3c (top) and d (bottom) - **c)** Total ion current chromatogram of Gilsonite from the Bonanza vein (location - T9S R24E Sec.16) **d)** Single ion current fragmentogram for triterpane m/z191, m/z177 and sterane m/z217, m/z218

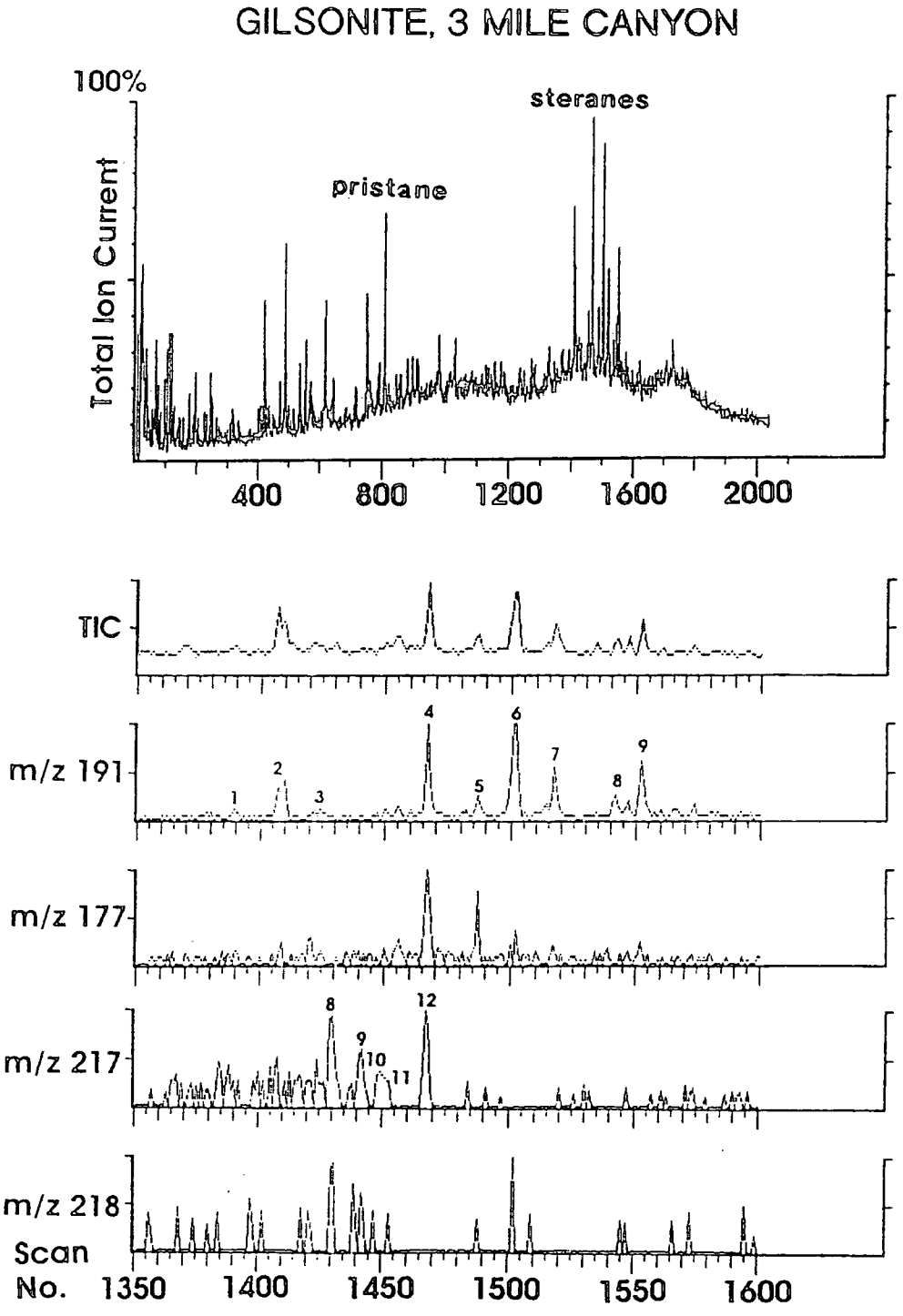

Fig.4.6.3e (top) and f (bottom) - e) Total ion current chromatogram of Gilsonite from Three Mile Canyon (location - T12S R25E Sec.4) f) Single ion current fragmentogram for triterpane m/z191, m/z177 and sterane m/z217, m/z218

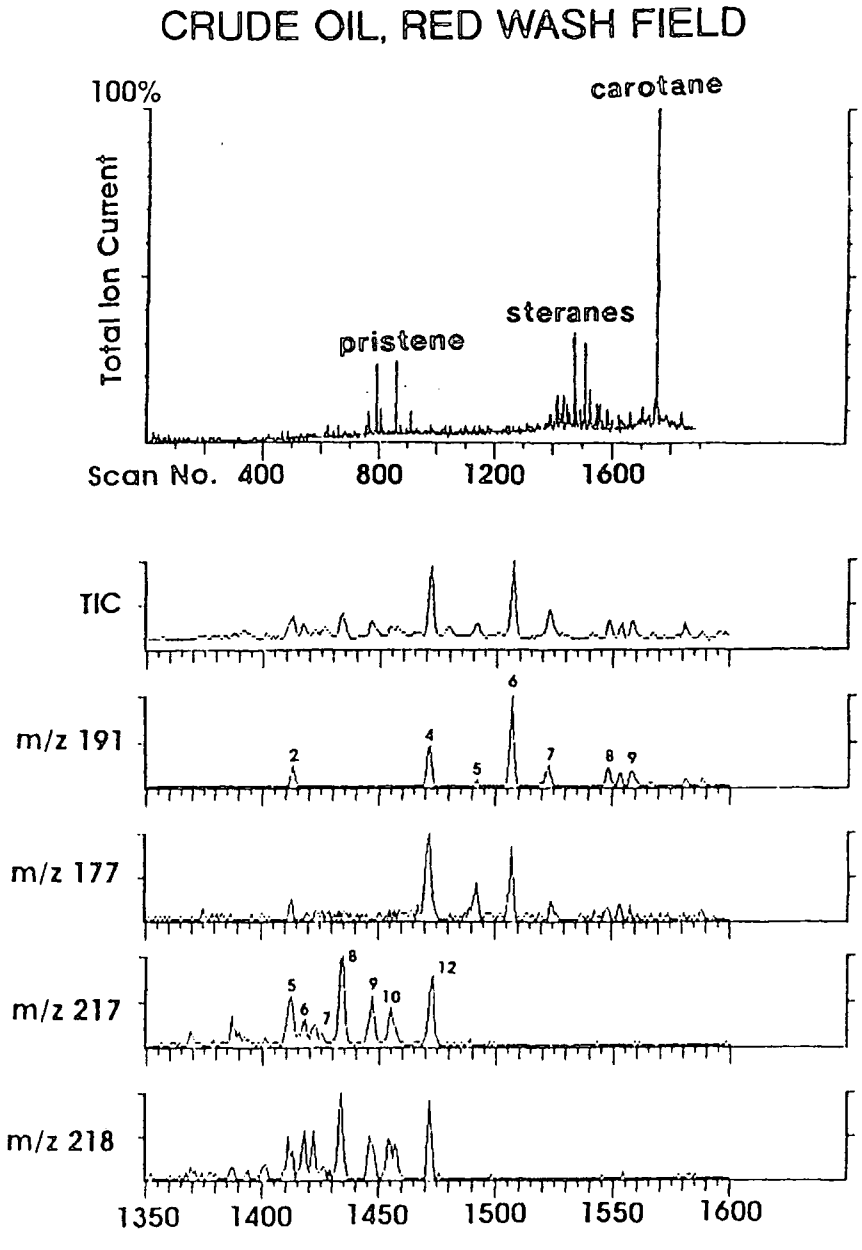

Fig.4.6.3g (top) and h (bottom) - g) Total ion current chromatogram of crude oil sample, Red Wash field (location - T6S R3W Sec.31) h) Single ion current fragmentogram for triterpane m/z191, m/z177 and sterane m/z217, m/z218

hydrocarbon products. Therefore, expulsion of the solvents and solutes through a complex migration route could account for the residual asphaltene rich compounds solidifying in the veins where they are seen at the present day but the paraffinic, aromatic and resinous volatile components would be dispersed far more readily through a porous medium before being reservoired in the stratigraphic and structural traps of the Red Wash field and other similar proximal traps. The sterane profiles, being similar, link the two residual hydrocarbons as being sourced from the MOZ of the Green River Formation. Therefore, this early mature residual hydrocarbon can be traced to a temperature regime and, through use of specific biomarkers, a common source is inferred.

4.6.4 Computer simulated maturation modelling (1-D kinetic modelling)

To calculate the maturation potential of the source horizon and the onset of organic maturation, the burial history has to be calculated. Important variables include geothermal gradient, stratigraphy and lithology.

4.6.4.1 Geothermal Gradient

The geothermal gradient is a product of thermal conductivity and is affected by burial. Heat flow can be affected by other geothermal and structural activity such as faulting, meteoric drainage patterns and igneous intrusions. The Uinta Basin has been observed in terms of present heat flow and Chapman et al. (1984) have noted anomalies of heat flow with increasing geothermal gradients north to south. The result is a systematic change in thermal gradients from 0.6°F/100ft in the north to 2.1°F/100ft in the south of the basin (Anders et al., 1992). In the locale of the Gilsonite veins, the mean thermal gradient is 1.8°F/100ft (data taken from corrected bottom hole temperatures - Anders, et al., 1992). Willet and Chapman (1987) conclude that this thermal heat flow is heterogeneous and is likely to be a combination of conductive effects and advection by a groundwater flow system driven by high topography north of the basin (the Uinta Mountains acting as the run off watershed) to best explain the present temperature field. Anders et al. (1992) noted that the geothermal gradient pattern observed by Chapman et al. (1984) mimics the thickness of organic rich sediments but the explanation offered by Willet and Chapman (1987) is more conceivable given the asymmetric structure of the basin with faulting along the mountain-basin interface focusing any meteoric run from the topographic high of the Uinta Mountains. From detailed work on the thermal resistivity and heat flow on the Duschene River, Uinta, Green River, Wasatch and Mesaverde Formations, Willet and Chapman (1987) described differing geothermal gradients for each formation which can give a more accurate and confident prediction of the burial history and palaeo-heat flow. Although

in the general vicinity of the Gilsonite veins the temperature (surface) through time varies only by a small amount (see table t4.6.4.1) indicating stable thermal conditions, it is still useful to input the available information. Willet and Chapman (1987) calculated the following thermal gradients:

Table t4.6.4.1

Formation	°C/100m	Surface temperature (°C)
Duschene River	2.8	20
Uinta	2.9	20
Green River	3.0	20
Wasatch	2.8	20

Surface temperature has been observed to have remained relatively constant since the Eocene but has been described by Sweeney et al. (1987) as being 5°C in contrast to Willet and Chapman's calculation of 20°C. There is an insufficient explanation provided by Sweeney et al. (1987) for using 5°C and thus the more substantiated 20°C estimate of Willet and Chapman (1987) will be used in this study.

4.6.4.2 Stratigraphic information

Obviously constraints must be put on the stratigraphic succession with respect to formation thickness, time interval and therefore burial rate. This information is traditionally taken from well information from drilling operations in the area. The nearest accurate information which could be relied on and available for this study was from the Mount Fuel Island #3 well (Anders et al., 1992) and the Red Wash #32 well (USGS central files) which are both located in the general vicinity of the Gilsonite veins and therefore assumed to have undergone a similar burial history. The main concern with respect to the stratigraphy is the amount of uplift which has occurred and hence the amount of sediment which could have been eroded. Various authors have already postulated the intensity of uplift and erosion. Narr and Currie (1982) calculated 1825m to be representative of the amount of sediment removed data from the basin. Narr and Currie (1982) analysed temperatures from fluid inclusions taken from core samples from the Altamont field and estimated a range of 510-2890m of overburden removed. Tissot et al. (1978) use 1780m for the amount of erosion at the Shell 1-23B4 Brotherson well but they do not determine how the value was deduced. Pitman et al. (1982) used reconstructed thicknesses of the Uinta and Duschene River Formations to estimate a maximum of 1000m of removal in the Pariette Bench field. The amount of variance in this overburden removal and the accuracy of the uplift inputted into the burial history will greatly influence the

maximum burial depth and therefore the maximum temperatures attained by the organic rich and kerogen bearing rocks in the Uinta Basin.

Based on a method demonstrated by Magara (1978) using shale compaction data and correlation with downhole acoustic logs, Sweeney et al. (1987) use the interval velocity in shales as being a parameter of their porosity. Due to the fact that compaction is almost irreversible, porosity will record a maximum burial depth. Therefore by comparing the porosity with the present day depth of burial with the porosity/depth expected for the measured porosity, an estimate of depth anomaly and therefore uplift and erosion. Estimated values for removed overburden of approximately 1800m in the Shell 1-11B4 Brotherson well and 1410m in the Chevron 250 Red Wash well resulted in very good agreement between predicted and measured maturity (vitrinite data) levels (Sweeney et al., 1987).

Anders et al. (1992) have adjusted their erosional estimates to bring the estimated maturation curves into agreement with the measured maturities taken from rock data at the present day using vitrinite data. For the Mount Fuel Island #3 well, Anders et al. (1992) recalculate the amount of erosion as 488m. However, this estimate is calculated by bringing the predicted maturity profile to fit maturity data using only one vitrinite reflectance measurement. Because of the investigation made by Sweeney et al. (1987) and the correlation made with electric log data and its successful application to a geochemical model, this study will base any burial history and maturation modelling on the data provided by the erosional estimates of the Red Wash 250 well (1410m - Sweeney et al, 1987) and the well tops provided by the Red Wash #32 well which is nearby (data from USGS files).

4.6.4.3 Lithology

Specifying the lithology is important with respect to a number of parameters including thermal conductivity and its affect on heat flow but most importantly, with respect to pressure modelling, the effect of compaction on the specified lithology. As previously documented by a series of workers on the Uinta Basin (Lucas and Drexler, 1976; Fouch et al., 1976; Pitman et al., 1982), the lithologies of the Uinta Basin are well constrained. For the purpose of basin modelling, the input parameters for the formations are based upon the dominant lithologies for each formation taken from various studies on the lithologies of the Uinta Basin (Fouch et al., 1975; Lucas and Drexler, 1976; Pitman et al., 1982; Fouch et al., 1992; Osmond, et al., 1992) and utilise the standards offered by BasinMod™ library and, as noted in Chapter 2, are summarised as follows:

Formation	Lithology
Duschene River	Sandstone
Uinta	Sandstone
MOZ*	Shale
Douglas Creek*	Shale
Wasatch	Sandstone
Mesaverde	Shale

*MOZ represents Upper Green River Formation

*Douglas Creek represents Lower Green River Formation

4.6.4.4 Modelling of the Red Wash #32 well with 1410m uplift

The burial history profile of the Red Wash #32 well was selected as documenting a well constrained history in the general vicinity of the Gilsonite. The formation thicknesses and lithologies of this well were taken from USGS central files and the basin modelling inputs requirements have been summarised in Chapter 2. The burial history of the well was modelled with 1410m (4626ft - Fig.4.6.4.4a) of uplift and erosion. The formations of interest to maturation and potential overpressure are the Douglas Creek and Mahogany (MOZ) members of the Green River Formation due to the argillaceous dominated nature of the these two members and the possible contribution to abnormal pressure through rapid loading and compaction disequilibrium. Also, the MOZ has been identified as the likely source rock for the Gilsonite and other hydrocarbons reservoired in the Red Wash field reservoirs (section 4.6). These two members follow a similar rate of burial being rapid in the first 3000ft of burial before assuming a more rapid but still relatively constant burial path. A hiatus, or period of non deposition, occurs at approximately 25Ma (Sweeney et al., 1987). This time constraint provided by the hiatus, when correlated with the start of deposition of the Duschene River Formation, can approximate an idea of burial rate. With the assumption of 1410m (4626ft) of uplift, the Duschene River Formation commenced at 35Ma until the hiatal onset at 25Ma (Sweeney et al, 1987). Therefore, during a period of 10My, approximately 7200ft of compacted sediment has been deposited - an equivalent rate of 720ft per 1My. The hiatus is interpreted to be a product of the Laramide Orogeny and associated termination of basin subsidence in the late Eocene to early Oligocene (Anders et al., 1992). This emergence and non deposition of the Duschene River Formation continued to approximately 10Ma when uplift and erosion removed 1410m (4626ft) of the Duschene River Formation to bring this well to its present day level.

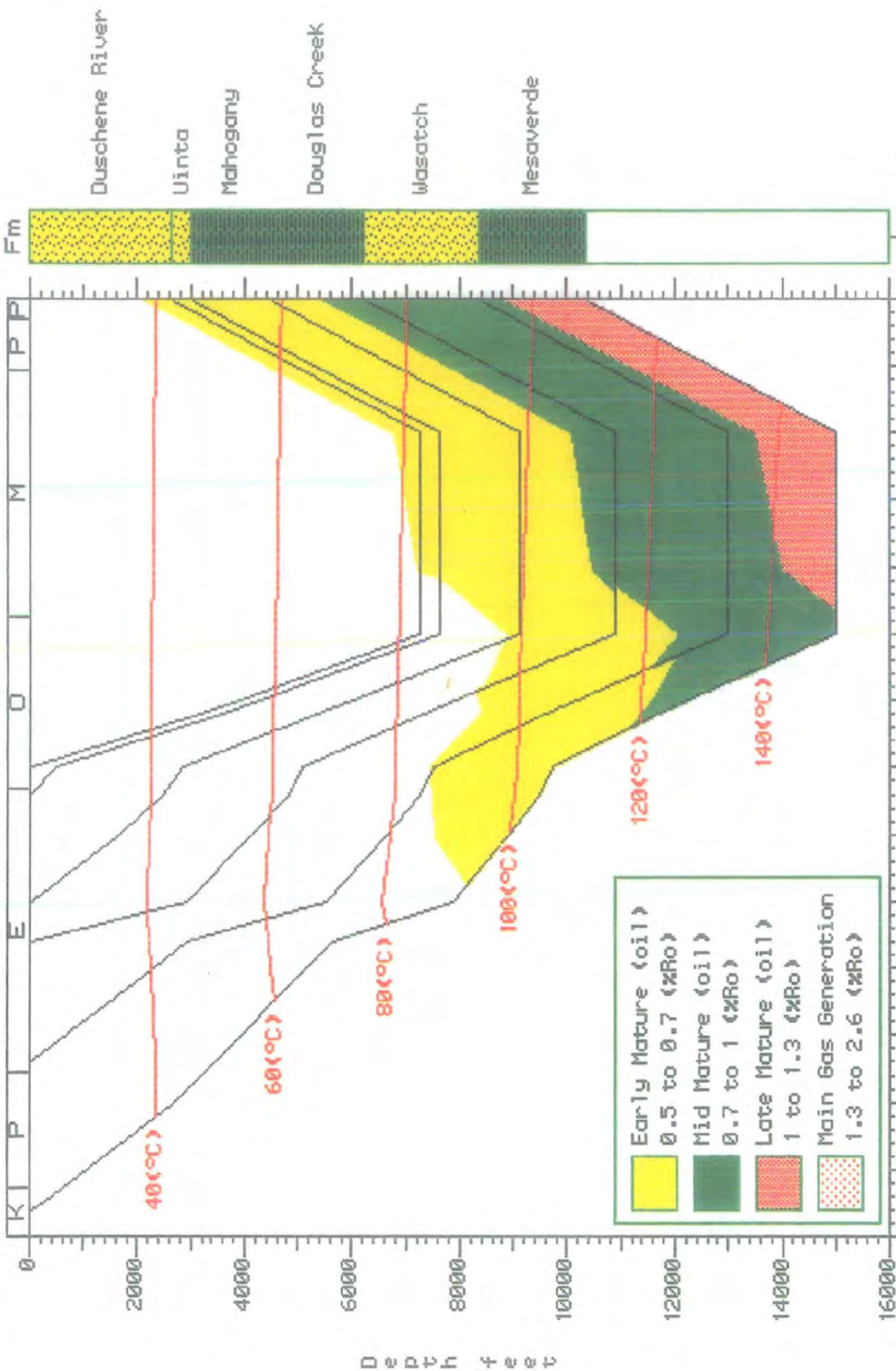

Fig.4.6.4.4a - Burial history profile of the Red Wash #32 well with 1410m of uplift. Superimposed kinetics (illustrated as Ro equivalent maturity)

Superimposing the maturation potential and kinetics onto the burial history (Fig.4.6.4.4a), the kinetics have been calculated using the thermal and organic parameters previously specified and described. It appears that the base of the organic rich MOZ enters the early mature stage of maturation (VRE of 0.5 to 0.7%) at approximately 20Ma with the base of the MOZ/top of the Douglas Creek member entering the early mature window at 26Ma. Therefore, from approximately 26-20Ma, the organic rich MOZ has been stimulated by parameters of time and temperature to evolve and thermally mature to expel early hydrocarbon products. It is only the mid to lower part of the Douglas Creek Formation which appears to enter the main phase of oil maturation (0.7 to 1.3% VRE). At approximately 25Ma the kinetics of a Type I kerogen indicates rapid maturation of the source rock and therefore expulsion of these early mature hydrocarbons would be inferred to have expelled at a relatively vigorous rate and during a short period of time if burial and increase in temperature were also rapid. It is assumed that the expulsion, transport and accommodation of the maturing hydrocarbons after primary migration would exploit any pre-existing conduits such as high permeability carrier beds of interstitial siltstone or sandstone beds or by utilisation of structural heterogeneities such as faults or fractures. Therefore, expelling early hydrocarbon products at approximately 25Ma would permeate any suitable conduit to commence secondary migration.

4.6.4.5 Modelling of the Red Wash #32 well with 488m uplift (Fig.4.6.4.5a)

The profile, using an uplift of 488m (1601ft) as suggested by Anders et al. (1992) and basing this uplift on a corrected maturation profile to equal available rock data (Ro data) in the Mountain Fuel Island #3 well situated in the Island field (Fig.4.1.1a), was also modelled in terms of burial history and maturation. When this amount of uplift is assumed, the succession is obviously not buried to the same maximum depth and therefore this will have consequences in terms of maturation in the key horizons of the MOZ and Douglas Creek members of the Green River Formation. The simulation of burial history with superimposed maturation shows only the basal section of the MOZ entering the early mature window at approximately 12Ma. The Douglas Creek member does not reach the mid mature stage as it had previously done in the well modelled with 1410m of uplift (Fig.4.6.4.4a). This obviously has implications when considering the source of the Gilsonite and the chemically related volatile components which are reservoired in the Red Wash and Island fields (Hatcher et al., 1992).

It has already been inferred from multiple geochemical studies that the Upper Green River Formation, in particular the MOZ, has matured and provided these early products and thus a control on the maturation modelling can be provided. The

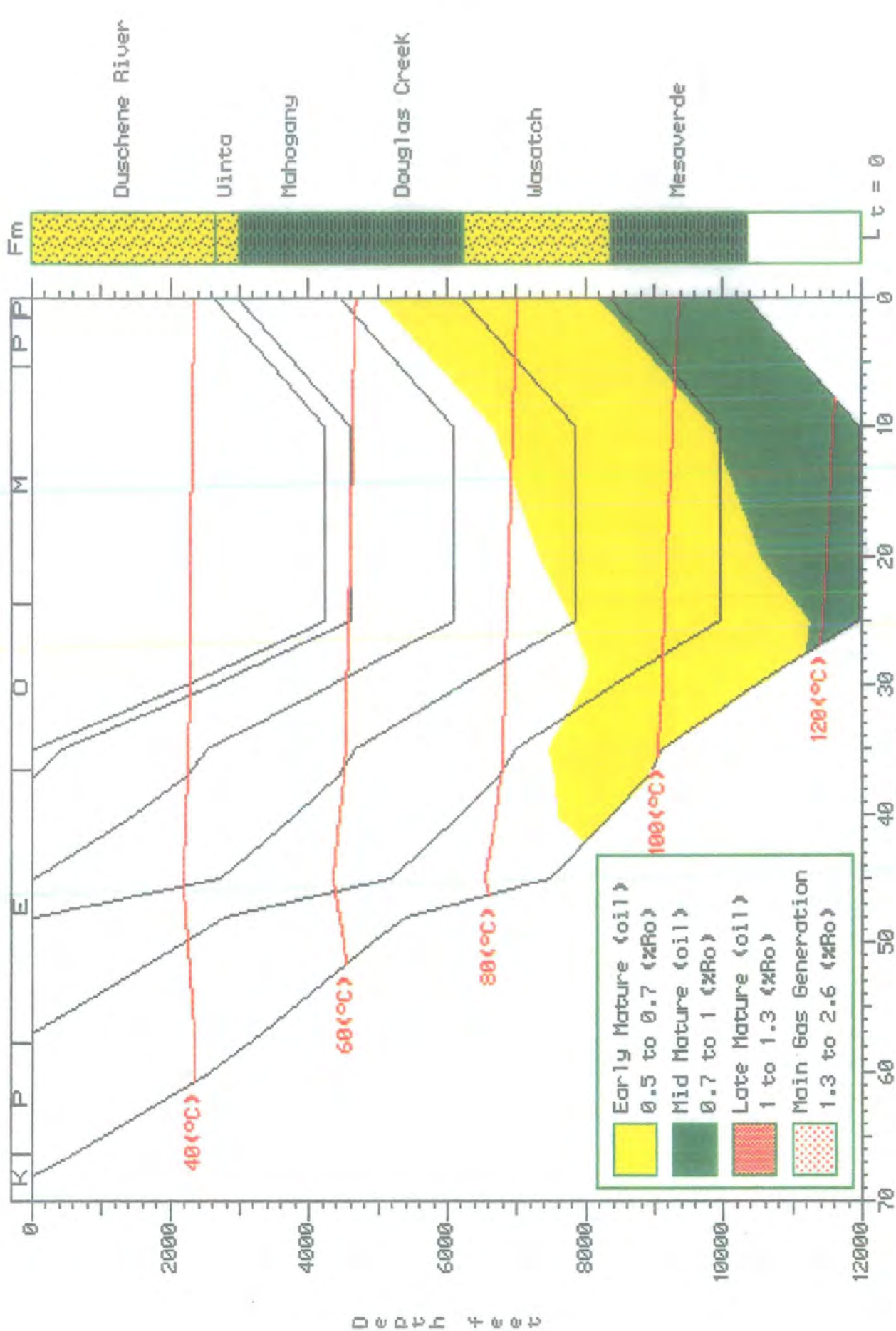

Fig.4.6.4.5a - Burial history profile of the Red Wash #32 well with 488m of uplift. Superimposed kinetics (illustrated as Ro equivalent maturity)

Gilsonite VRE combined with the hydrocarbons recovered from the Red Wash field suggest a maturity equivalent of 0.5 to 0.7% Ro. This is what the simulated maturation history shows the maturation state of the MOZ at approximately 26-20Ma when 1426m of uplift is assumed whereas 488m of uplift, taken as being accurate by Anders et al. (1992), does not allow the entry of the organic source rock (top MOZ) into any defined maturity window.

4.6.4.6 Predicted maturity profiling

Using the burial history profiles of the Red Wash #32 well with differing amounts of uplift, the sensitivity to the predicted maturity model when varying the erosional estimates isshown to beas being critical to the ability to accurately plot data. Fig.4.6.4.4a shows the predicted maturity of a burial profile assuming 1426m of uplift. The early maturity phase commences at a depth of approximately 2100ft (640m) whereas when 488m is taken as the eroded section, the maturity profile predicts a depth of approximately 5000ft (1524m) before the critical organic rich horizons enter the early mature phase.

It has already been seen that field observations and maturation modelling can be used to infer the likely source rocks for the Gilsonite (section 4.5). By matching geochemical profiles considering indices such as specific steranes and triterpanes, the oil shale of the MOZ is considered to be the probable source horizon for the asphaltene rich Gilsonite with its associated properties of high viscosity and temperature dependant mobilisation. The paraffinic, aromatic and resinous compounds trapped in the Red Wash field reservoirs have also been geochemically traced to the MOZ in the locale of the Gilsonite veins (section 4.5; Hatcher et al., 1992). Direct field observations have also linked the vein deposits to the organic rich shales of the Upper Green River Formation (section 4.4 and 4.5). There appears to be definite link between the chemistry of the oil shale of the MOZ and different hydrocarbon products including the Gilsonite and reservoired oils in the Red Wash field. This, then, provides evidence that MOZ is indeed the source rock for the Gilsonite. The MOZ can then be confidently used as the source horizon to build the maturation history around in the independent basin modelling analyses to estimate the time and rate of maturation and the effect of variables such as erosion effects.

To Summarise, geological modelling using the BasinMod™ software programme provided an efficient way to integrate geological, geochemical and geophysical data to independently assess the potential of the likely source horizons in terms of maturation and kinetics (using the LLNL Easy %Ro calculation - see Chapter 2). The

hydrocarbon components of the Gilsonite show that the VRE maturity corresponds to the profile modelled for the MOZ simulated by the software. However, only when using the Sweeney et al. (1987) calculation of overburden removal of 1410m from the Red Wash field did the MOZ enter the early mature window. Anders et al. (1992) estimate of 488m underestimates the amount of erosion and uplift as the modelling did not simulate maturation of the Upper MOZ at any point throughout the burial history of the well. It is inferred by correlating these independent utilities of basin modelling, geochemical analyses and field observations that the Gilsonite is a product of early maturation of the MOZ in the south eastern part of the Uinta Basin. Expulsion of these early compounds and subsequent migration and trapping would, it seems, largely depend upon the individual hydrocarbon chemistry which would dictate its physical mobility and viscosity.

4.6.5 Pressure history

Another important facility offered by the computer programme and simulation of the burial history is the ability to observe pore pressure at specific horizons through time. Following similar methods and applying the same controlling parameters described in Chapter 2 and in the Alwyn study (section 3.6), pore pressure is largely dependant upon the burial rate and permeability relationship of the compacting section with respect to maintaining a pressure equilibrium or developing overpressure by the mechanism of disequilibrium compaction. It is the shale dominated sections of the Mahogany and Douglas Creek members which are of interest in generating overpressure as pressure in the overlying Uinta and Duschene River Formations will remain at hydrostatic pressure throughout their burial cycle by virtue of its hydraulic connectivity provided by the sands which constitute the formations.

4.6.5.1 Pressure modelling of the Red Wash #32 field (1410m uplift) - Fig.4.6.5.1a

Using the calculated hydrostatic and lithostatic gradients (3.101×10^{-3} MPa/ft and 6.891×10^{-3}MPa/ft respectively - BasinMod™ defaulted values), the simulated pore pressure for the specified argillaceous section can be modelled. The base of the MOZ/top of the Douglas Creek member is used to model the burial through time. This section is most abundant in argillaceous sediments and can be envisaged as being an almost complete shale section (section 4.3) and therefore most likely to develop any overpressure by compaction disequilibrium. With reference to this aforementioned lithostratigraphic section and Fig.4.6.5.1a, the initial burial phase, from 45 to 37Ma, of approximately 2600ft shows the pressure profile at hydrostatic, inferring that the rate of burial and compaction is sufficient enough to maintain normal pressure in the sediment pile. However, at approximately 37Ma the pressure profile deviates due to a change in

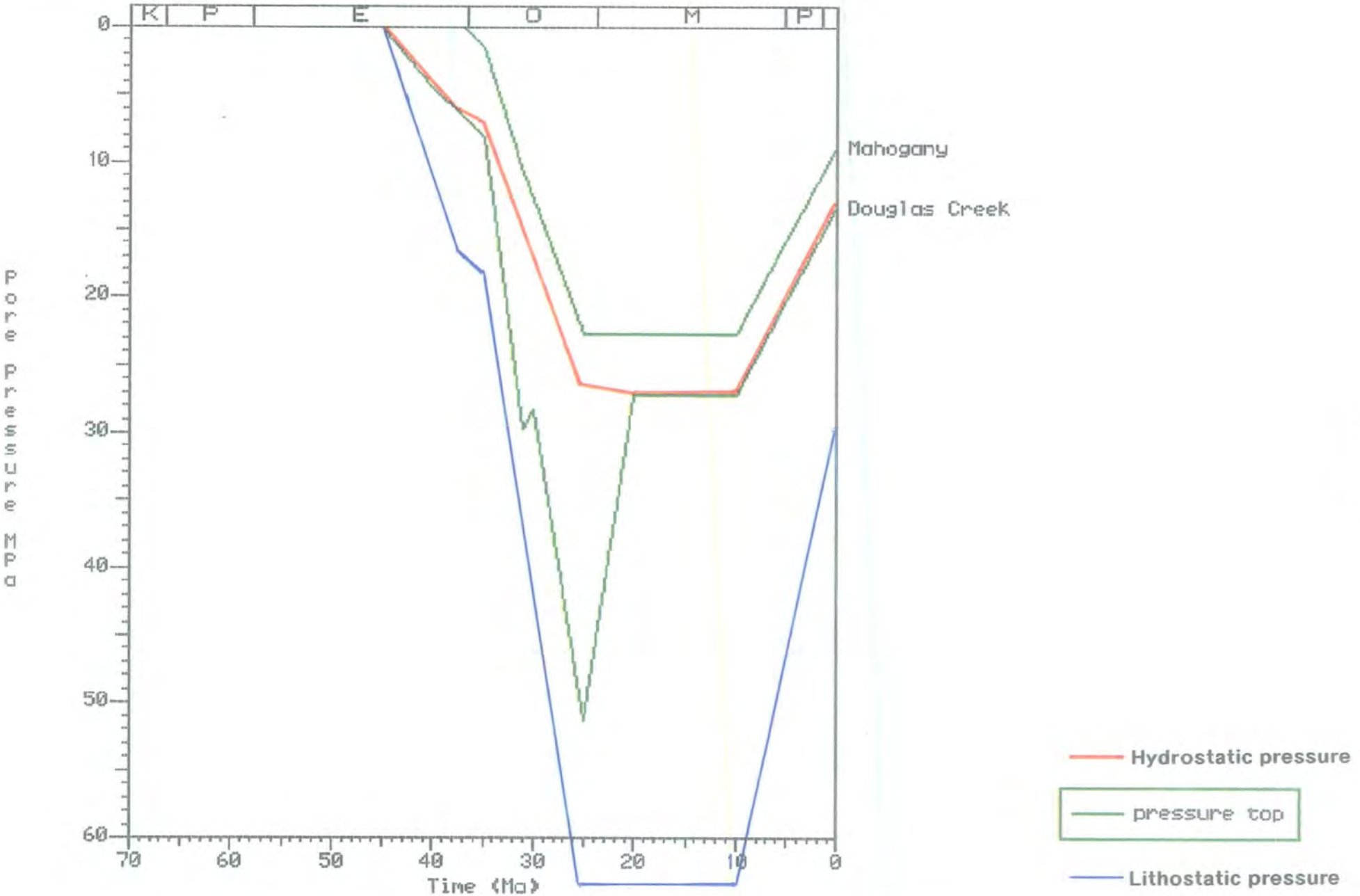

Fig.4.6.5.1a - Pressure versus time based on the burial history profile of the Red Wash #32 well (see text for discussion). Organic rich base MOZ and top Douglas Creek Member is the reference horizon

the burial rate, itself acting in response to regional tectonism, to build a small amount of overpressure (approximately 1MPa). The major deviation in the burial rate occurs at 35Ma. The response of the sediment is to create an increasing overpressure at an identical rate to the lithostatic gradient (6.891×10^{-3} MPa/ft). The porosity calculated for this section is 27.3% (using the porosity versus depth function proposed by Falvey and Middleton, 1981). A reduction in permeability would obviously be a consequence of this compaction and therefore the burial rate at this time outstrips the ability of pore fluids to escape and thus the internal pore pressure of the sediment would increase abnormally with respect to the hydrostatic pressure gradient. This is amplified at approximately 35Ma where the burial rate increases. This new rate of burial and pressure increase is constant until the period of non deposition marked on the profile as a horizontal line between 25-10Ma. The response of the sediment is to take advantage of a pressure differential between the overpressured argillaceous section and the hydrostatic regime and dynamically dissipate the overpressure to return to the hydrostatic equilibrium. The model allows the pressure to return at a linear rate symmetrical to the gradient of pressure build. Thus, the model suggests pressure dissipation in the region of 24MPa over 6My. The actual reality of the situation may not follow this suggested pathway. Pressure would possibly transmit away from the section as a function of specific depth, porosity and permeability afforded by the section at maximum burial and may not return to hydrostatic conditions in a linear fashion as depicted by the model. The period of uplift from 10Ma to the present day determines that the pressure profile follows a hydrostatic gradient. Calculated pressure at the present day for the base MOZ in the Red Wash #32 well assuming 1410m of uplift is approximately 13.5MPa (Hydrostatic pressure calculated at this depth of burial using a hydrostatic gradient of 3.101×10^{-3} MPa/ft = 14.3MPa). Therefore, the model slightly undercalculates the present day hydrostatic pressure at this depth. This is a possible result of computational errors and functions used such as the compaction function and ability to model uplift).

4.7 Emplacement Mechanisms

To appreciate the migration phase of expelling early hydrocarbons from the source rock in a given geological situation, the mode of available transport will dictate the transmission of fluids and hydrocarbon. Therefore the particular geological scenario must be assessed in terms of stratigraphic and structural setting at the time of source rock maturation and burial. Another important consideration is the mechanical state and response of the sealing cap rock. Therefore, addressing the problem of pore pressure, effective stress, any effective directional compressive stress due to dipping beds, regional tectonic influence, local lithological heterogeneities, permeability,

cohesion, internal friction of the cap rock and overall stress state must be seen as a natural progression in the study of the timing and emplacement of the Gilsonite veins.

It has been inferred from simulated pressure modelling (section 4.6.5.1), that pore pressure in the MOZ and Douglas Creek Member, which also contain the main organic horizons thought to be the source rock, is at a pressure state near to lithostatic at approximately 26Ma (section 4.6.5.1). It has been recognised by various workers that hydraulic fracturing can be induced by water; Snarsky (1962), Price, (1974) and Price, et al. (1978) have suggested the role of hydrocarbon expulsion from source rocks as being paramount in causing hydraulic fissures. Du Rochet (1981) emphasises the importance of capillary pressure differential between invading hydrocarbons and pore water in opening vertical fractures in the cap rock when oil is squeezed from kerogen by compaction following oil generation. Evidence has been cited by Stoneley (1983) for hydraulic fractures occurring in response to overpressuring and being subsequently filled by fibrous calcite. Stoneley (1983) attributes the overpressure generation mechanism to disequilibrium compaction in thick shale sequences and suggests fluid escape along lines of weakness such as bedding. Within the confines of the overpressured system, this would permit freedom of movement of fluids from which calcite would be precipitated and on return to hydrostatic conditions, the volume occupied by these fibrous calcite deposits will mark the volume otherwise lost to compaction. No such evidence for mineral precipitation in the Gilsonite sills were recorded but bleaching and observations were made by Verbeek and Grout (1992) that limonite is smeared on the fracture faces and subordinate veins. However, this does not suggest a similar type of process as described by Stoneley (1983).

Therefore, it would seem plausible to reconstruct the inferred stress state on the source rock at various times throughout the burial history of the Red Wash #32 well to appreciate any stress conditions imposed upon the sedimentary succession to aid dissipation of compactional fluids and maturing hydrocarbons. The Red Wash #32 well is thought to represent the stress state imposed in the vicinity of the Gilsonite veins. The general situation in the basin at various indicated times is also considered as regional extensional stresses associated with the uplift and erosional phase considerably altered the overall stress of the rock sequence. It has been reported previously (sections 4.4 and 4.5) that the Gilsonite is emplaced in pre-existing fractures and various lines of evidence have been put forward to explain this conclusion. However, this is not to imply that these fractures were hydraulically induced exclusive to the effects of regional tectonism. Natural hydraulic fractures are extension fractures. This means that the rock is separated by fluid pressure, which therefore has to overcome the

tensile strength (positive) and to push aside the rock walls against the action of the total rock stress (Mandl and Harkness, 1987). Fluid induced extensional fractures require that the effective normal stress (total stress minus the pore fluid pressure) puts the stress state in a tensile condition and therefore that the pore fluid pressure exceeds the total stress component. This means that pore fluid pressure exceeds the lithostatic gradient and pressure dissipation is achieved by fracturing the rock matrix.

4.7.1 Stress State - Upper Eocene

Fig.4.7.1a schematically represents the depositional system with horizontally stacked sequences with primary compaction effects progressing at a rate to sustain a pore pressure equilibrium in the shale dominated sequences of the Douglas Creek Member and the MOZ. Essentially the depositional interface would have observed flocculating clays undergoing initial reorganisation into primary clay structures with an associated loss of interlayer water through the first few metres of compaction. The shales of the Douglas Creek Member and MOZ would be in a physical state whereby there would possess relatively high internal friction between the layers due to ionic attraction of bound water (section 2.2). Compaction is inferred to be slow enough to maintain a hydrostatic pressure condition at this point in the burial profile (Fig.4.6.5.1a). However, due to the porosity of these normally compacting shales through this depth range of 100-3000ft/30.5-914.4m which corresponds to a porosity range (using the function proposed by Falvey and Middleton, 1981) of 56.5-25.7% giving a high internal fluid volume and therefore the cohesion of the interpore network must be considered as being relatively low.

Because of the lacustrine depositional system (section 4.3) planar sequences of sediment can be envisaged at this time. The consequence of this is that the system would only be operating in uniaxial compression with σ_1 being applied as the overburden stress. There is no element of bed dip at this time and therefore no resolved or resultant σ_3 can be applied. Uniaxial compression due to overburden stress puts the system in a simple stress state. The pore pressure of the sediments at this time infers that the system is draining the compacting sequence efficiently and therefore the effective stress must be thought to equal the uniaxial compressive stress. This description is depicted by use of Mohr's circle of stress (Fig.4.7.1a).

4.7.2 Stress State - Lower to Mid Oligocene

Stratigraphically this period shows a major shift in the burial rate from the lower to mid Oligocene (Fig.4.7.2a). With the loss of porosity with depth, compacting pore fluids in the sediment will have increasing difficulty in escaping to maintain a pressure

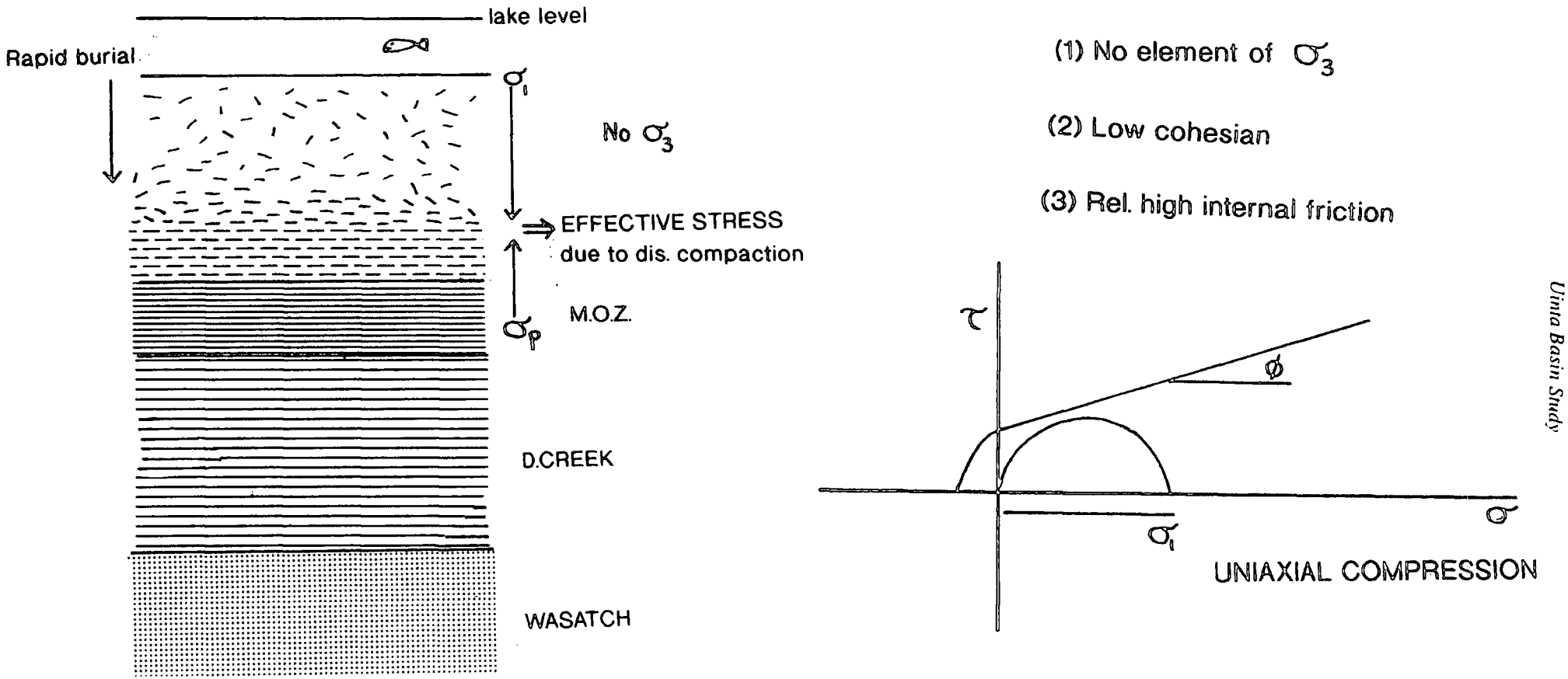

Fig.4.7.1a - Interpreted stress state at the upper Eocene (approximately 36Ma) in the Hells Hole Canyon area (Fig.4.3.2) described diagramatically and by Mohr's circles of stress

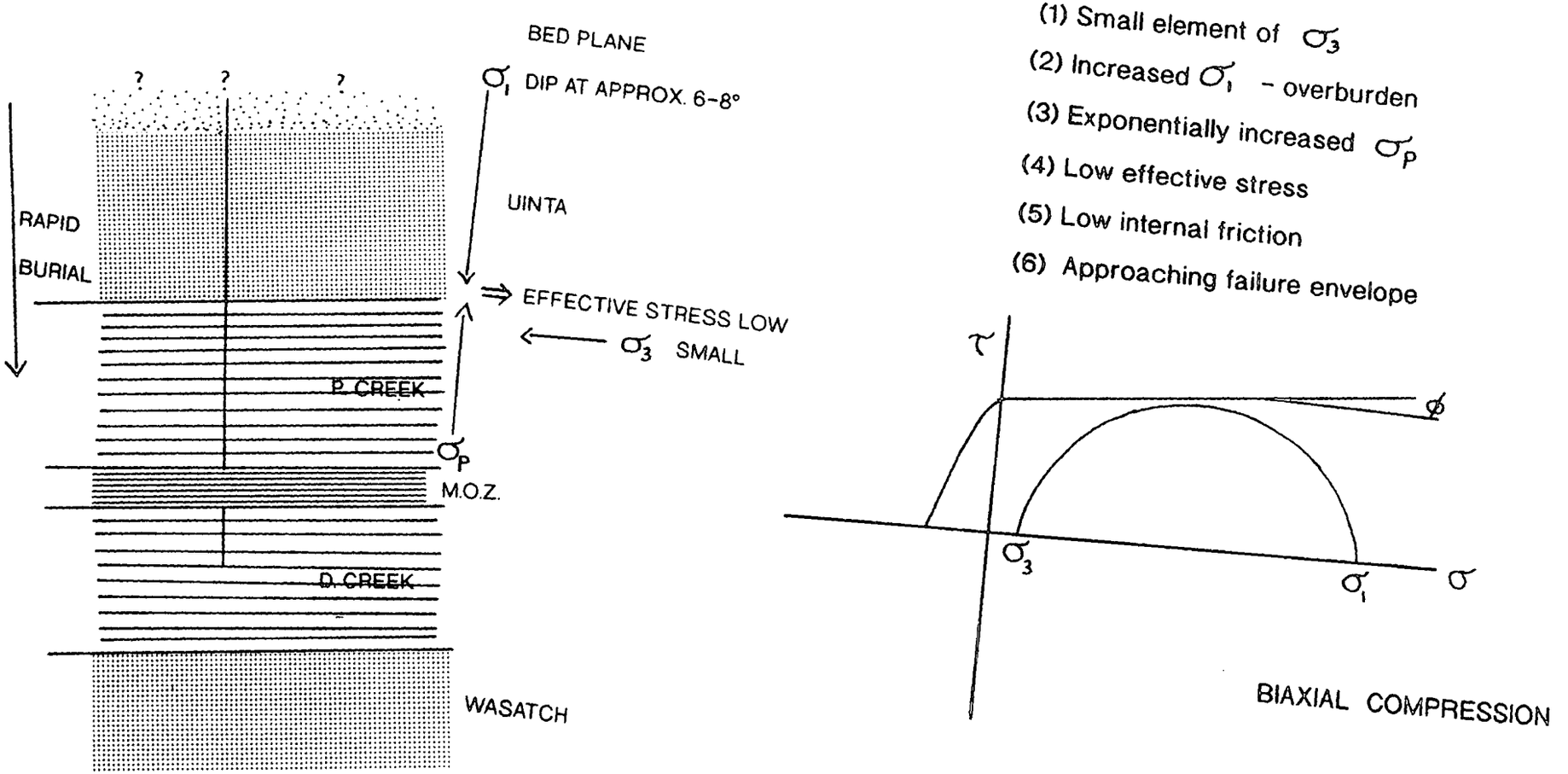

Fig.4.7.2a - Interpreted stress state at the lower Oligocene (approximately 27Ma) in the Hells Hole Canyon area (Fig.4.3.2) described diagramatically and by Mohr's circles of stress

equilibrium. The result of the burial rate outstripping the ability of dispersing pore fluids in the compacting sequence will cause the internal pore pressure of the system to rise (Fig.4.6.5.1a). The deviation away from the hydrostatic as depicted by the pressure profile (Fig.4.6.5.1a) suggests that abnormal pressure is building quickly and assumes a pressure rise comparable to the lithostatic gradient (6.891×10^{-3}MPa/ft). Although the pressure profile never breaches the theoretical lithostatic gradient, the critical pore pressure (which describes the state of the pore fluids which are able to support the overburden stress to attain an effective stress which approaches zero - section 2.1) may be reached. This would lower the internal friction of the sediment toward zero with a resultant state of near buoyancy whereby the pore fluids would support the entire weight of the overburden.

In mid Oligocene times (approximately 27Ma), the Uinta Formation would be progressively depositing at the depositional interface and the shales of the Green River Formation would be undergoing progressive compaction and compactional effects. Regional tectonics would be acting to influence the system as the structural configuration of the basin would change in response to possible renewed extension to cause bed tilting (Campbell, 1979; Pitman et al. 1982). This slightly complicates the stress state as it will move from an effective uniaxial compressive state to a biaxial compressive state (Fig.4.6.5.2a) due to directed and imposed σ_3. In addition, σ_1 has increased due to increased sediment deposition. The effect of the inability of efficient shale dewatering is to rapidly increase the pore pressure to create an effective stress almost approaching zero or a state of near non friction. The representative Mohr's stress diagram (Fig.4.6.5.2b) shows the biaxial compressive stress state circle with an envelope of failure dictated by low effective stress and low internal friction. With the gradual introduction of this high pore pressure cancelling any compressive stress from the overburden, the stress circle would move toward the field of pure shear and in doing so will intercept the failure envelope. Resultant interception of the failure envelope will be to produce fractures in the rock framework to facilitate and accommodate the vast amount of generated pressure due to compaction disequilibrium (Fig.4.6.5.1a). This amount of generated overpressure due to compaction disequilibrium working in combination with the stress state at this time, then, when considering the timing of onset of maturation of the source rock in the basin (approximately 25Ma, Fig.4.6.4.4a), is prior to initial hydrocarbon maturation and expulsion. Therefore, this mechanism of fracture initiation is inferred to preceed hydrocarbon maturation.

Geological processes such as compaction and diagenesis are considered to be inelastic and unrecoverable and therefore stresses, pore pressures and strains that exist in the rock framework to cause structural heterogenieties must be seen to be permanent in the rock record. According to Mandl and Harkness (1987), in the absence of tectonic extension, friction between individual beds will generally be sufficient to provide a lateral constraint and therefore there will be no change in horizontal strain parallel to the fracture walls. In this case, the role of tectonic extension has to be considered and thus a possible change in strain parallel to the fracture walls is envisaged. The maintenance of separation of vertical fracture walls has to be achieved.

The above tectonic stress scenario depicts a time frame of mid to upper Oligocene coincident with maximum burial. At the end of this maximum burial and the onset of the hiatus, pore pressure relaxes to reachieve the equilibrium (Fig.4.6.5.1a). However, the kinetics involved in the maturation of any material is such that the activation energy is critical for the thermal alteration to oil have reached (50 kcal/mole in the case of a Type I kerogen, Tissot et al., 1987). The transformation to oil is rapid when considering a Type I kerogen (Fig.4.6.2a - Tissot et al., 1987; Anders and Gerrild, 1988). The onset of early organic maturation of VRE 0.5-0.7% Ro for the MOZ is between 21-17 Ma. This time period occurs after the modelled large pore pressure and inferred associated hydraulic fracturing generated by disequilibrium compaction acting in unison with regional extensional stress. Associated with kerogen transformation to these early hydrocarbon products, which have geochemical signatures similar to those observed in the vein Gilsonites and the waxy crudes of the Red Wash field, is an increase in pressure if the rock cell in which the transformation is taking place is severely restricted (Barker, 1990). Therefore, to alleviate anomalous pressure build up and utilise secondary migration conduits, it is likely that these hydrocarbons which are thought to be mobile in the temperature range of 60-100°C (Prost and Rondelez, 1991) - if the specifics of the bitumen are similar - would permeate through these dykelets. In the scenario depicted by Mandl and Harkness (1987), dykelets will temporarily close and stop growing until the hydrocarbon derived pressure has built up again and that the growth of these dykelets is likely to be spasmodic. However, the combination of the rapid kinetics generated by the Type I kerogen associated with a large penecontemporaneous pressure event caused by disequilibrium compaction means it is likely that these fractures remained open and that hydrocarbons migrated quickly through the network. Mandl and Harkness (1987) impose several restrictions on the conditions of fracture formation but do recognise that large scale formation of hydrocarbon dykes may be drastically advanced by a regional or local tectonic extensional stress that reduces the horizontal stress and consequently the value of

parameter Ko (the ratio for original rock stresses which existed at the onset of source rock maturation). Mandl and Harkness (1987) then expect strong rocks, such as lithified shales, to respond with a drastic drop in Ko when subjected to horizontal extension which has clearly happened in the Uinta Basin at this time (Pitman et al., 1982).

4.7.3 Process of dyke formation

It has already been reported (section 4.4 and 4.5) that the Uinta Basin contains both vertical and lateral heterogeneities with respect to facies, structure, source rock potential and also temperature. Therefore, the conditions acting upon the physical state of the compacting sequence and, in particular, the overpressured shale units must be concerned with local differences and anomalies in the above parameters. Although the overall stress imposed due to high internal pore pressure working in combination with tectonism will act upon an area as a whole, local amplifications of stress will be set up, for instance, along bedding plane irregularities. However, through pore pressure modelling (section 4.6.5) and structural inference that the basin was undergoing an extensional phase at the mid to upper Oligocene (Crawford, 1979), the conditions for fracture initiation have been satisfied. The actual process of dyke formation can be envisaged :

Mandl and Harkness (1987) suggest that the rate at which fractures propagate is controlled by the rate of fluid supply to the fracture tip. An expression is given for the growth rate as

$$V \sim {}^{3}/_{4} (P_{hc} - \sigma_H)^3 L/(\eta_{hc} E^2)$$

where V = fracture growth rate
P_{hc} = fluid pore pressure
σ_H = horizontal total rock stress
L = fracture length
η_{hc} = fracture fluid viscosity
E = Young's modulus

or, in words, the growth rate is proportional to the fracture length and to the cube of the excess pressure in the fracture and inversely proportional to the squared Young's modulus of the rock and to the viscosity of the fracture fluid. Mandl and Harkness (1987) suggest that a fracture growth rate of increase in length by $^{1}/_{10}$th (of initial fracture length) in approximately 1 second is not unreasonable. However, the rate would primarily be dependant upon fluid supply and that this fluid would be in overbalance with respect to overburden and other imposed and directed stresses. This means that there must be a constant supply of highly pressured fluid to allow continous

fracture propagation. This infers, that in this scenario whereby the fractures propagate in response to compaction derived overpressure working with regional stress conditions, that the compaction driven overpressure must be very high and sustained or that another supplementary overpressure source is operating. It is possible that, due to the rapid kinetics associated with a maturing type I kerogen identified in the Uinta Basin, a high fluid pressure may be maintained. The maturation of the source rock has been interpreted as commencing at approximately 25Ma (Fig.4.6.4.4a) which is approximately the same time period when overpressure due to compaction disequilibrium reaches a peak (Fig.4.6.5.1a). If the internal fluid pressure and fluid supply to the fracture tip could not be maintained by maturing hydrocarbons and compactional fluid then fracturing would be envisaged as being spasmodic in its growth.

Actual propagation of fractures is thought to be controlled by the difference in the hydrostatic pressure gradient of the fracture fluid and the actual pore pressure to realise effective pore pressure which would induce tensile stresses in the upper tip regions (Twiss and Moores, 1992). These tensile stresses will break interparticle bonds of the rock and allow the fractures to extend in the vertical direction (Mandl and Harkness, 1987). If the sealing rocks (shale units of the MOZ and Douglas Creek Member) possess a uniform strength vertically propagating fractures may be expected to maintain a length which is just sufficient to overcome the tensile strength of the rock ahead of the fracture tip.

Using a formula for the width of independently growing fractures, Mandl and Harkness (1987) utilise Hooke's law which describes the undrained compression of the rock to calculate the horizontal distance between non interfering fractures as being approximately 3 times the fracture length (in the vertical direction). However, field observations show the spacing between major veins of the Bonanza, Independent, Little Chipetta, and Chipetta (which all occur within a lateral distance of <2km, Fig.4.2a) are closer spaced than 3 times the fracture length. The vertical interval of the MOZ to the Uinta Formation in which these mentioned veins are seen at the present day is up to 3000ft/915m (Verbeek and Grout, 1992) which would give a fracture spacing, according to Mandl and Harkness (1987), between individual non interfering fractures of 9000ft/2743m. Taking the surface spacing interval of these 4 above mentioned veins (Fig.4.2a), the veins all occur within 2400m and have an average spacing of 800m between each vein. therefore, the Gilsonite veins of the Uinta Basin do not conform to the theory proposed by Mandl and Harkness (1987) When compensating for uplift and erosion of the missing Uinta and Duschene River

Formations, this estimate for fracture spacing increases as the vertical interval of the veins would increase but the actual horizontal distance and spacing between individual veins would remain constant. Thus the estimates made by Mandl and Harkness (1987) would become more unreasonable. The estimates made by Mandl and Harkness (1987) may be reasonable when considering a homogenous set of conditions and lithologies but does not fit with the lithologies observed at surface. The facies have already been described (section 4.3) as homogenous through a vertical section and regional differential stress conditions have been inferred to be operating at different times throughout the basin history (Crawford et al., 1979; Pitman et al., 1982; Fouch et al., 1992). These irregularities and heterogenieties may be sufficient to explain as to why the model of Mandl and Harkness (1987) of fracture spacing does not agree with observations on Gilsonite veins.

In summary, bedding plane irregularities or other lithological or stratigraphic perturbations are likely focus points of stress amplification which any imposed pressure or stress can operate. Abnormal pore pressure generated by compaction disequilibrium of a thick shale sequence and the rapid maturation characteristics of a Type I kerogen resident in the same thick shale sequence can be seen to combine with regional stress conditions acting extensionally in the direction ENE-WSW, to provide additional horizontal extensional stress on any heterogeneity. The resultant effect of these two independent applied stresses would cause the initiation of the vertical fractures and dissipation of locally derived fluid and pressure. The propagation and spacing of the fracture sets would progress in a fashion dictated by fluid pressure properties, fluid supply and local lithological and structural heterogenieties.

4.7.4 Process of sill formation

When pore pressure equals the total maximum compressive stress, the effective stress is zero (in the absence of any other applied stress field) and the internal friction of the system also approaches zero. This condition arises when the primary overpressure is generated by the thick shale sequence during rapid loading and when any additional pressure is generated by hydrocarbon maturation. Thus, bedding planes which act as lines of inherent weakness and fissility are exploited by fluids in a condition whereby the stress state has been shifted toward the field of pure shear. Expulsion of the hydrocarbons have already been described in terms of specific chemical composition and associated physical properties and kinetics. It may be inferred that vertical fractures could not propagate quickly enough to maintain the necessary space for the maturing hydrocarbons and therefore bedding plane parallel intrusions of these early mature hydrocarbons would form interstitially in the shale sequences. Again, local

focus points where the smallest compressive stresses occur would be utilised and exploited.

Mandl and Harkness (1987) postulate that unlike igneous sills which are limited in lateral extent by the cooling properties of the fluid, hydrocarbon sills can only be terminated by lithological barriers, an increase in total rock pressure on the bedding plane or by leakage from the sill into the sealing rock. However, it has been reported (section 4.6) that these early mature compounds do depend highly on temperature conditions with respect to their mobility and ability to flow. Thus, asphaltene-rich bitumen which is physically sensitive over a narrow temperature range (dependant upon actual chemistry) may indeed act similarly to igneous fluids in that temperature will primarily dictate their lateral extent along the bedding planes. This mobility is emphasised when dipping beds are considered. If the exploitation of this shale fissility by the early mature hydrocarbons is taken as occurring at maximum burial depth then a temperature range can be estimated allowing a temperature constraint to be placed on the hydrocarbons. This would allow an assessment of its mobility if the chemistry of the asphaltene-rich hydrocarbons is similar to that described by Prost and Rondelez (1989) in assessing the physical properties of the hydrocarbons at this depth of sill emplacement.

Field observations have identified these sills in the Douglas Creek Member of the lower Green River Formation. When using the burial history profile of the Red Wash #32 well (Fig.4.6.4.4a) as being accurate the Douglas Creek Member would be at depth of approximately 9000ft/2743m under ambient temperature conditions equal to approximately 96°C (assuming thermal conditions as used in the basin modelling in Fig.4.6.4.4a). This temperature could easily allow the hydrocarbons to assume a low viscous state (if the early mature hydrocarbons area assumed to be asphaltene-rich) and flow could be envisaged. Therefore, only when uplift occurred and temperature decreased, due to the entire basin undergoing a thermal relaxation, would the solidification of the residual compounds occur.

Flow of these hydrocarbons along bedding planes must have been halted by local lithological or stratigraphic deviations, by the change in the total stress state or the migrating fluids intercepting the main vertical fractures dispersing any overpressured fluids and maturing hydrocarbons more efficiently. This last scenario is most probable as during the hiatus, there would be overpressure relaxation associated with a static burial profile. Therefore the fracture network would have time to re-establish a pressure equilibrium and dynamically reduce and dissipate the overpressured fluid that

was generated during the 25-17Ma time frame (the period of maximum developed overpressured due to compaction disequilibrium coinciding with any developed overpressure associated with the entry of the MOZ source rock and subsequent maturation into the early maturation window).

4.7.5 Significance of expulsion rate versus hydrocarbon dissipation

Structurally concordant hydrocarbon filled sills, then, are a likely product of early expelled hydrocarbons generating at a rate more rapid than the propagation of vertical fractures. Although there is a very narrow range of activation energies required for a Type I kerogen to mature (Tissot et al., 1987), the transformation ratio of the Green River shale kerogen at the depth of maximum burial of the MOZ (approximately 9200ft/2804m) will yield only a relatively small amount of hydrocarbons (less than 0.1 according to Tissot et al., 1987). However, since the kinetics of the reaction is also dependant upon time and not purely temperature (itself a function of depth), at different points in the burial history, a slightly differing rate of generation will be observed. Since the emplacement of these early mature hydrocarbons are of interest with respect to timing and final emplacement of the various products, including Gilsonite, the significance of hydrocarbon expulsion versus dissipation (a function of the mechanical and mineralogical competency of the rock) is investigated.

At the start of expulsion (initial entry into the early mature oil window, VRE 0.5%Ro) the source rock (MOZ) is modelled at approximately 25Ma (Fig.4.6.4.4a) with the porosity of the shale section calculated at 19.7%. However, since overpressure has been modelled to peak at this point to cause the initiation of hydraulic vertical fractures, it is rock matrix permeability which will primarily control the dissipation of any fluid into the surrounding country rock. Permeability is diagenetically sensitive and cannot be directly correlated to depth and therefore an accurate assessment of permeability cannot be estimated. However, at mid to upper Oligocene (28-24Ma), the fractures are inferred to have developed and thus any expelling fluids will preferentially access these conduits. The permeability afforded by the shale section of the Green River Formation would be expected to be far lower than that offered by the fracture network. Therefore fluids, including the early mature hydrocarbons, would migrate vertically upward via the fractures through the section until the sand dominated Uinta Formation is encountered. At this time the base of the Uinta Formation would be at approximately 7400ft/2256m (Fig.4.6.4.4a) with a porosity of 17.8%. On arriving at this widespread reservoir section any low viscosity fluids (volatile hydrocarbons) would escape leaving only the residual and higher viscosity components. Fractionation of the hydrocarbons is assumed to occur in the developed

fractures in the Uinta Formation. It is after temperature driven fractionation occurs that the more volatile hydrocarbon members will access and utilise the porous sand network leaving the heavier and relatively immobile compounds such as Gilsonite in the fractures.

It is only when the expulsion rate of hydrocarbons from the source rock has exceeded the dissipation rate into the surrounding host medium that deformation of the shales is thought to occur. This condition was probably the main mechanism by which the formation of the hydrocarbon sills formed seen in the lower Green River Formation occurred. At this stage, the compactional fluids and possibly early mature hydrocarbons were being expelled more quickly than the rock framework could dissipate these generating fluids. Fractures were not opening quickly enough to accommodate the expelling fluids or hydraulic fractures which were developing were terminated along bedding or structure due to a facies heterogeneity or sudden lithological change which could more easily contain this amount of imposed stress.

4.7.6 Post volatile escape - syn Gilsonite solidification

Emplacement of the solidifying Gilsonite within respective host rocks have already been seen to differ in fracture face contacts dependant upon the facies into which it was emplaced (section 4.4). The deformation of the wall rock and opening of these fractures to their present width must be inferred to be post hydraulic fracturing and hydrocarbon injection, because a series of veins such as those seen at the present day would be unlikely to be formed and maintained by just the release of compactional fluid. The amount of compactional fluid from disequilibrium compaction required to firstly create and maintain the overall volume provided by the present day veins over a period of approximately 25Ma cannot be reasonably be justified in the geological realm as the recharge and supply of fluid to maintain such features is unlikely given the limited amount of overpressure and associated fluid derived from compaction disequilibrium. Also, Fig.4.6.5.1a shows the depletion of overpressure through time due to the onset of non deposition at approximately 25Ma such that any compactional fluids would be in equilibrium with normal pressure conditions. The return to hydrostatic modelled by the software shows a rate of depletion symmetrical to generation. This profile generated by the software is likely to be unrealistic as porosity, permeability, rock matrix and imposed stress relationships will dictate the pressure dissipation profile to allow the pressure to rapidly decrease to a point whereby the rock matrix can contain the overpressure (below critical pressure gradient, section 2.1) before a more gentle dissipation rate will allow a return to hydrostatic. The dissipation of the overpressure is dependant upon permeability and seal efficiency.

The pressure dissipation would possibly follow an exponential curve of depletion with higher overpressures dissipating quickly but the rate would decline in response to the amount of overpressure such that the function would more likely be exponential rather than linear.

Some model must explain the deformation and space that the veins possess at the present day. The Gilsonite has a wall rock contact in every locality observed and, in places, permeates a zone up to 40m around the vein (section 4.5). This suggests that residual emplacement of the Gilsonite have accommodated through initial fractionation in the vein and then time to deform the wall rocks according to the facies type and associated mechanical response.

As discussed above, volatile escape of the lighter solvent components is likely to utilise the sand rich Uinta Formation after primary migration from the source horizons of the MOZ and DCM and secondary migration through network of the hydraulic fractures. The transporting fluid would likely be a colloidal solution containing many individual hydrocarbon compounds. During secondary migration, temperature would be lost as a direct result of moving up the rock and the migrating fluids would cool. A consequence of this cooling would be the fluid beginning to separate dependant upon physical properties of state with asphaltene rich compounds such as Gilsonite increasing in viscosity with decreasing temperature. As the maximum temperature of the Uinta Formation reached was approximately 87°C (base of the Duschene River Formation, Fig.4.6.4.4a) up to the surface (20°C), then these temperatures are within the range suggested by Prost and Rondelez (1991) who suggested a 15% asphaltene rich bitumen is fluid at 60°-100°C but would solidify at temperatures lower than this; such that at maximum burial, a bitumen of this type would begin to solidify at approximately 4600ft/1402m (Fig.4.6.4.4a).

Once the solidification process of the residual Gilsonite has initiated, the wall rocks can deform through time dependant strain or creep strain. This is a process whereby a primary, secondary and tertiary state of deformation is recognised by the relative state of elasticity of the deforming medium. In this case, the deforming medium is the host rock.

Fig.4.7.6a diagramatically describes creep strains through time with the following steps representing the state of the Gilsonite and wall rock deformation:

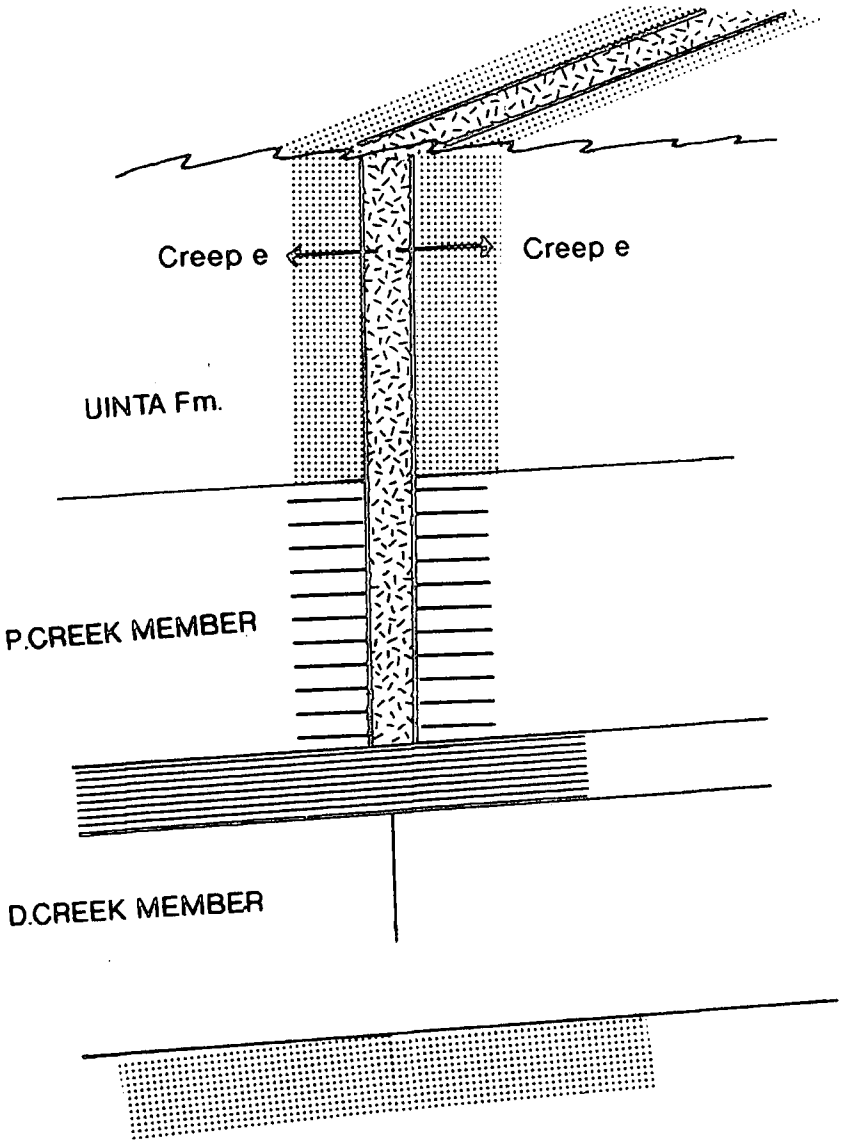

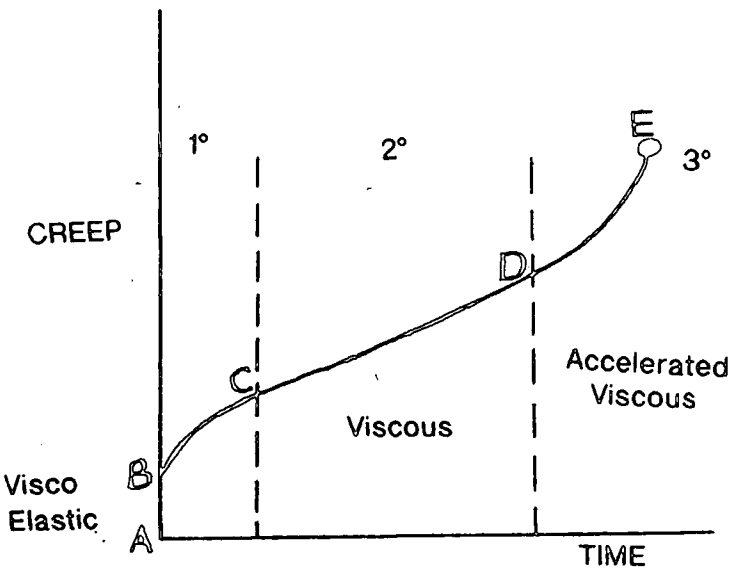

AB - Initial strain taken by wall rocks

BC - Initial injection of gilsonite, pores close

CD - Constant strain rate

Wall rocks accomodate accordingly

Approx. C-D uplift, erosion and stress relief

Non recoverable plastic strain

Fig.4.7.6a - Description of wall rock deformation through time dependent strain (creep strain)

Stage	Activity
AB	Initial strain imposed upon the wall rocks by emplacing fluid hydrocarbons. Wall rocks still capable of some elastic recovery due to residual and regional horizontal stress conditions.
BC	Irrecoverable deformation of the wall rocks as volatile components percolate away from the fracture. Initial solidification causes directed stress on the wall rock fracture face. If, as in many cases, the wall rock is sandstone, deformation of the wall rock will occur and pore throats will decrease in size due to this directed stress.
CD	A stage of linear increase in strain with time in this viscous deformation field. A constant rate of strain increase with time would be envisaged with continued cooling higher up the sequence with hydrocarbon recharge from the maturing source rocks lower in the section. It is approximately at this strain state that uplift, erosion and associated regional stress relief is thought to commence. However, since non recoverable plastic strain has occurred no level of mechanical rebound is envisaged.

The tertiary field of accelerated viscous creep (DE) whereby strain exponentially increases with time is unlikely to have occurred due to the relief offered by regional uplift which is indicated to have began at approximately 10Ma (Fig.4.6.4.4a). This accelerated viscous stage of strain is usually associated with failure as the host material would have entered a zone above a second critical value of stress known as failure stress (Park, 1989). There is no evidence of stress induced failure due to the emplacement of the Gilsonite and although the yield stress has been surpassed and the viscous stage of creep reached, the imposed stress and associated permanent strain must have relaxed before the accelerated viscous stage. Relaxation of this stress may be a product of retarded hydrocarbon input which is unlikely as the kinetics of the source rock, with a kerogen yield of approximately 1000mg/g (Tissot et al., 1978) and a hydrocarbon yield of approximately 15gal/ton oil shale (Cashion, 1967), is inferred to have continued and indeed increased to the present day (Spencer, 1987) (Fig.4.6.4.4a). The other more probable explanation of stress relaxation is the effect of uplift on the regional stress conditions at approximately 10Ma. The confining stress from both overburden (σ_1) and horizontal imposed stress (σ_3) would be reduced by uplift and creep strain would have therefore reached its maximum at this point in the burial history.

Twiss and Moores (1992) discuss in detail the strain rate of specific materials in differing environments of temperature and pressure and cite various terms dependant upon the environment of deformation. Microfabrics have been used to identify these dislocations due to creep but most of the ductile deformation that Twiss and Moores (1992) describe belong to very high temperature fields. Only the zone that is described as dislocation glide can represent the type of creep strain which is occurring at the levels envisaged for the Gilsonite veins in the Uinta Basin. Dislocation glide describes deformation of solids by dislocation through the crystal lattice, a process called 'cold working' (Twiss and Moores, 1992). At the lattice scale, silicates (which are the minerals predominantly composing the host rock) contain largely covalent bonds and therefore resistance to stress is high. When several slip systems operate simultaneously, dislocations gliding on different slip systems inevitably intersect introducing 'kinks' and 'jogs' into the medium (Twiss and Moores, 1992). This might explain the post Gilsonite kinking and pinch and swell features seen in the fracture faces of the shale rich and heterogeneous host rock fracture faces (section 4.4).

4.8 Conclusions and synthesis of the burial, maturation and pressure history and the emplacement of Gilsonite veins in the Uinta Basin, Utah

The Uinta Basin with its relatively simple burial and thermal history allowed the production of a model with regard to developing a temporal history of overpressure generation, fracture development, regional tectonism, hydrocarbon maturation and expulsion and the process of Gilsonite emplacement.

4.8.1 Stratigraphic Interpretation

Field logs recorded for the upper Palaeocene Wasatch through the Eocene Green River Formation to the lower Oligocene Uinta Formation represent a facies distribution acting in response to regional tectonism with regard to a relative depositional environment. No eustatic influence has been recorded as Lake Uinta has always been a closed hydrologic basin (Fouch et al., 1992). Local cyclicity is thought to represent the response of sediment deposition to climatic change throughout the depositional history. Logs were organised into facies types and from the inferred stacking patterns which emerged, it was suggested that the overall sequence of the Green River formation fitted an overall fining upward sequence. The result being an increasingly more marginal to open lacustrine sequence which peaked at the MOZ in the mid-upper Green River formation coinciding with maximum organic flourish, possibly representing an algal bloom. Tectonic and climatic influence at the end Eocene

initiated an apparent aggradational sequence in the upper Green River formation/lower Uinta formation with an increasing amount of coarse terrigenous sediment. This represents the majority of the Uinta formation which was interpreted to have been deposited in the marginal lacustrine to fluvial/alluvial environment. The highly organic rich horizons of the MOZ are interpreted to constitute the likely source horizons for the Gilsonite veins.

4.8.2 Structure of the veins

The occurrence and exposure of the Gilsonite veins revealed a number of structural features. Most significantly, no sense of shear was recorded at any locality suggesting that fracturing occurred under extension only. Subordinate parallel and sub-parallel fractures in close proximity to the main veins were recorded as well as offset anastomising lateral and vertical jogs. Overprinted pencillated structures visible in the Gilsonite suggest a late stage post solidification being a product of late stage extension in the basin history. Pinch and swell structures along the strike of mudstone rich wall rock were likely a result of fluid percolation and the ability of the host rock to accommodate and allow flow of compactional fluids. Clean fracture faces were typical of the porous Uinta formation sandstones which would offer access to any low viscosity fluid. However, these host rocks were susceptible to brittle deformation and contained many of the lateral and vertical jogs and sub-parallel fractures described.

4.8.3 Mineralisation of the wall rocks

Syntaxial quartz overgrowths recorded only the presence of aqueous fluid inclusions and isotope information suggested a meteoric source of water trapped in authigenic carbonate minerals (Pitman et al., 1982). This combined to suggest diagenesis was an early phenomenon in the burial history and that it had received little effect from overpressure derived fluids. However, bleaching of the wall rock (Verbeek and Grout, 1992) in sub parallel veins suggests some mineralisation of the wall rock prior to hydrocarbon migration.

4.8.4 Origin of the Gilsonite

A suite of biomarker analyses were undertaken (Anders et al., 1992; Hatcher et al., 1992) which, when observing the degradationally resistant sterane and triterpane single ion masses, suggest that the oil shale from the MOZ have very similar GC-MS profiles to the Gilsonite and the crude oils of the Red Wash field. This infers that the MOZ oil shale is the source horizon for these hydrocarbon occurrences. VRE taken from transformation ratios, atomic H/C ratios and Rock Eval Tmax indices put the Gilsonite at 0.5%Ro indicating an immature maturity status. However, for a Type I kerogen of

the Uinta Basin, the Rock Eval Tmax does not significantly change with maturation (Tissot, et al., 1987) and therefore cannot be used as a reliable indicator of maturity.

Independent maturation, kinetic and pressure modelling used available constraints from stratigraphical, lithological and thermal information with any assumptions likely to cause major deviations in the profile justified. Amount of uplift and erosion, heat flow, compaction factor, geothermal gradient and specific kerogen type were all significantly important in impact on the resultant profiling for maturation and kinetics. These were constrained accordingly. Maturation and kinetic simulation revealed that organic rich horizons of the MOZ and Douglas Creek Member entered the early mature oil window at approximately 25Ma coinciding with the last phase of burial before the onset of the hiatus. When correlated with the pressure profile for the same burial history, at approximately 25Ma, maximum overpressure had developed in the shale dominated section due to the mechanism of disequilibrium compaction.

So two independent lines of evidence point to the Gilsonite pertaining to an early mature identity and that maximum overpressure developed immediately prior to entry of the base MOZ into the early mature oil window (VRE 0.5-0.7%Ro). This timing of maturation at this time is coincidental with maximum overpressure developed by disequilibrium compaction and may, due to the kinetics of the kerogen and rapid transformation to hydrocarbon, contribute to the overall overpressure.

4.8.5 Emplacement mechanisms

It is concluded and inferred that initial hydraulically induced fracturing of the Green River and overlying formations was a result of combined overpressure due to disequilibrium compaction at approximately 25Ma and regional extension with a possible contribution from the maturation of the source rock. This mechanism disagrees with the main conclusion drawn by Monson and Parnell (1992) who infer the initiation of the fractures as a result of forced hydrocarbon break out upon the maturation of the source rock. This study recognises that the hydrocarbon was emplaced under a high pressure regime with evidence cited as the existence of hydrocarbon sills forcibly injected along pre-existing hydraulically induced fractures. After initial fracturing, maturation of the organic rich horizons provided the early mature products which utilised and pervaded these conduits before individual hydrocarbon physical properties dictated whether dissipation away from or residence in these fractures occurred. Highly viscous and immobile residual hydrocarbons thus accommodated in the fractures through time dependant deformation. In contrast the more volatile components accessed the porous sandstone network of the Uinta and

Duschene River formations until they were halted by structural and stratigraphic trapping.

Chapter 5
Multiple Failure State Compression Tests and X-Ray Diffraction Analyses on Shale Materials from the Green River Formation, Uinta Basin, Utah

5.1 Introduction

The thick Tertiary sequences of the Uinta Basin, Utah have already been described in Chapter 4 and include the Eocene Green River Formation. This particular formation and its individual members and units support evidence for being an important organic source (section 4.6) which primarily acts as the main hydrocarbon source formation maturing hydrocarbons that are expelled and trapped in stratigraphic units such as the Palaeocene Wasatch and time equivalent Colton Formations. The stratigraphic framework implies migration of maturing hydrocarbons both upward (evidence being the presence of Gilsonite veins in the Oligocene Uinta Formation, Chapter 4) and downward (oil and gas reservoired in the Palaeocene Wasatch and Colton Formations, Lucas and Drexler, 1976; Spencer, 1987; Fouch et al., 1992) from the Green River Formation. There is also the possibility of organic maturation and the issuing of hydrocarbons from the shales of the Cretaceous Mesaverde Formation (Pitman et al., 1982; Fouch et al., 1992). The Green River Formation has been described and modelled in terms of overpressure potential. Section 4.6 infers overpressure generation due to the primary mechanism of disequilibrium compaction and the likely contribution from the thermal maturation of hydrocarbons. The thickness of the Green River Formation (up to 3000ft in some parts of the basin, Fouch et al., 1992) combined with its consistent lithostratigraphic organisation (primarily marginal to open lacustrine shale units with interspersed carbonates and sand/silt horizons - section 4.3) also act to provide the necessary top seal to contain the reservoired hydrocarbons.

The Wasatch and Colton Formation reservoirs have been targeted for exploitation but high pore fluid pressure within these formations has presented the need to plan drilling procedures carefully. Typical overpressures in these Tertiary reservoirs exceed hydrostatic (0.433psi/ft, Spencer, 1987) by 4500psi at 13000ft (Shell 1-11 B4 Brotherson well, Bluebell-Altamont field; source of information - Spencer, 1987). The Green River Formation provides the seal for this overpressure.

This chapter investigates the triaxial compression properties (in the drained configuration) of the Green River Formation to determine the peak strength and deformation characteristics of a selection of shale materials acting as the top seal for the reservoir units of the Wasatch/Colton Formations. These physical parameters were

then assayed against the bulk mineralogical composition of the individual shale materials to determine any relationship between mineralogical composition and mechanical characteristics.

In this chapter, the results of nine 5-stage multiple failure state drained triaxial compression tests are discussed. Samples were collected from preserved core from 2 wells in the Uinta Basin, Utah which penetrated the thick Green River Formation (seal) and the Wasatch/Colton Formations (reservoirs). These tests were conducted at ambient room temperature and at zero pore pressure, to determine the peak strength and deformation characteristics of a selection of shale materials from 2 well cores obtained from the Wexpro #3 well and the Island Unit #5 well in the Uinta Basin, Utah (core supplied by the Utah Geological Survey core store, Salt Lake City, Utah).

Peak compressive strengths were determined for each sample at confining stresses of 5MPa, 10MPa, 20MPa, 30MPa and 40MPa. Axial and Radial deformations were measured at a confining stress of nominal 5MPa to determine Young's moduli and Poisson's ratios. The peak compressive strengths were used to define a failure envelope for each sample in terms of Mohr-Coulomb and Hoek-Brown criteria.

The mineralogical bulk compositions were determined for each sample utilising X-ray diffraction profiles. D-spacing and crystal lattice peak intensity identified both major and minor minerals in respective samples.

The following sections summarise the test procedures, data obtained, results, discussion and any correlative parameters between the two independent test programmes. The results include the physical properties of the shale samples, the deformation curves obtained and analyses of the peak compressive strength data. A description of the triaxial cell used for the test programme is given in Appendix 2.6.

The tests were carried out to show any relationships of mineralogy to the rock strength of a known overpressure sealing formation. Any such relationships or correlation may have implications for the capacity of the sealing formation to contain and retain overpressure. These relationships may provide a basis to constrain the amount of maximum overpressure in a reservoir where the seal capacity is known or constrained.

5.2 Glossary of terms and definitions used in this study

Axial Stress — The principle stress axis parallel to the test cylinder axis

Radial Stress — The principle stress axis perpendicular to the test cylinder axis

Confining Stress — The stress applied by the surrounding fluid and that of the fluid (non applicable in drained testing) in the pore spaces

Axial Strain — The associated change in the dimensions of the sample parallel to the cylinder axis. Also termed **shortening**

Radial Strain — The associated change in the dimensions of the sample perpendicular to the cylinder axis

Two elastic constants which characterise the elastic behaviour of an isotropic (whose mechanical properties are the same in all directions) material are:
Young's modulus (E) and **Poisson's ratio (v)**

Young's modulus (E) is the constant of proportionality whereby in a uniaxial state of stress, the magnitude of the elastic extension parallel to the applied stress is directly proportional to the magnitude of the stress.

That is, a uniaxial compressive stress decreases the length of the specimen, thereby producing a negative extension. Thus, Young's modulus is a negative number. For most rocks, E has values in the range of -0.5×10^5MPa to -1.5×10^5MPa. The extreme value of the extension that most materials can reach before they fracture is generally quite small - a few % at most and usually much less (Twiss and Moores, 1992).

Poisson's ratio (v) is the absolute value of the ratio given by the extension perpendicular to an applied compressive stress ($\hat{e}\perp$), divided by the extension parallel to an applied compressive stress ($\hat{e} \parallel$)

$$v = \frac{\hat{e}\perp}{\hat{e} \parallel}$$

If a material were perfectly incompressible, v would equal 0.5. Poisson's ratio for most rocks, however, range from 0.25 to 0.33.

Coulomb Fracture Criterion is the straight line approximation to the shear fracture envelope described by $o_s = c + \mu o_n$ where $\mu = \tan\phi$

and where
c = cohesion (the resistance to shear fracture on a plane across which the normal stress is zero)
μ = coefficient of internal friction
ϕ = angle of internal friction

5.3 Experimental materials, preparation and procedures

The shale material tested in this study was obtained, via the UGS* core store, from two wells penetrating the Tertiary strata of the Uinta Basin, Utah. The specific wells from which the core was obtained are:

* Utah Geological Survey

Well Name - Island Unit # 5
County - Uinta Field - Island
Location - Township10S Range18E Section11
Core Denomination/Identification - IU
Depth of Coverage - 4690 - 4812ft
Formation of Coverage - Green River

Sample Identification (depth - ft)	General lithological description
IU 6 (4765)	Laminated Shale
IU 8 (4806)	Laminated Silty Shale

Well Name - Project EX-1(Wexpro #3)
County - Uinta Field - Pariette Bench
Location - Township 9S Range 20E Section36
Core Denomination/Identification - EX
Depth of Coverage - 1770 - 3010ft
Formation of Coverage - Green River

Sample Identification (depth - ft)	General lithological description
EX 1 (1782)	Laminated Silty Shale
EX 5 (2182)	Inter laminated Silt/ Dominantly Shale
EX 6 (2280)	As Above, increasing shale
EX 7 (2385)	As Above, increasing sand
EX 8 (2480)	Inter laminated Sandy Silt/Shale
EX 9/2583 (2583)	Heterogeneous Silt/Sand
EX 10 (2680)	As Above, increasing Shale laminations

The preparation and testing of the samples were carried out on dedicated machinery in the Rock Mechanics Laboratory, Department of Mineral Resources Engineering, Royal School of Mines, Imperial College, London. Core plugs having diameters of nominal 38mm ($1\,^1/2$") were diamond cored from the core sections, in a direction normal to the primary laminations in the samples. The plugs were trimmed to nominal height:diameter ratios of 2:1, and were end-ground to ensure standards of sample preparation within the tolerances suggested by the International Society for Rock Mechanics (I.S.R.M.) (1983) for triaxial test specimens. An 5% aqueous solution of NaCl was used as the cutting fluid to inhibit swelling in any clay minerals present in the shales and, prior to testing, the samples were saturated with the same 5% NaCl solution using an evacuation and immersion technique (I.S.R.M., 1979). The dry bulk density, saturated bulk density and effective porosity of each sample was also determined by the saturation and calliper techniques (I.S.R.M., 1979), taking into account the relative density of the saturating fluid used.

The triaxial compression tests were conducted following I.S.R.M. (1983) suggested procedures for type II multiple failure triaxial tests, using a closed-loop, servo controlled, rock mechanics test system incorporating an 2000kN capacity loading frame (ESH Testing, Ltd.) and an instrumented, multi-core diameter, Hoek-type triaxial cell (Robertson Geologging - see Appendix 2.6).

Mean axial deformation during the first loading cycle was measured using a pair of linear variable differential transformers (LVDTs), mounted diametrically opposite one another between steel loading platens adjacent to the faces of the samples. Measurements made with these devices were corrected for any axial deformation occurring in the loading platens. Radial deformation was measured using a pair of electronic cantilever devices mounted onto stand-offs at mid height around the circumference of the samples. Axial load on the specimens was measured using an electronic load cell device, and readings from the measurement devices were recorded using a dedicated micro-processor system. Confining stress on the samples was generated and maintained using the triaxial cell in conjunction with a closed-loop, servo-hydraulic, pressure intensifier and electronic pressure transducer. All the measurement devices employed in test programme were calibrated 'in house' prior to the tests, using devices having calibrations traceable to national standards of measurement.

To ensure drained behaviour in all the tests, loading was conducted in axial strain control at a nominal axial strain rate of 10 millistrains/hour and excess pore pressures generated during loading were allowed to drain to atmosphere via fluid ports in the loading platens. In addition, side-filter drains and end-filter drains with ceramic porous discs were employed to assist the drainage and distribution of excess pore pressure.

The testing carried out in the drained configuration allowed any evolved fluids developed during the test to escape and thus a neutral pore pressure was maintained. This series of tests then conflicts with those of Zeuch (1983) who carried out undrained axial compressive experiments in an attempt to simulate pore pressure build up as a result of incipient pyrolysis of kerogen in the oil shale samples that were being tested. The reason for testing under completely drained conditions was simply to bypass effects experienced in other studies on hard, low porosity rocks. Swan et al. (1989) working on the Kimmeridge Shale have reported that the ratio of pore pressure to confining pressure increases generated by loading dominates the decrease generated by dilatancy. This effect is not applicable in the drained situation. Also, Swan et al. (1989) report that rises in strength with strain rates is an intrinsic property of the shale rather than the particular drainage condition. Drained testing also allows effective stresses to be measured.

The Green River Formation is recognised as containing organic rich rocks thought to yield hydrocarbons reservoired in Tertiary units of the Uinta Basin (section 4.6). Although, Sellers et al. (1972) recognises that both the compressive strength and Young's modulus of oil shale are quite sensitive to kerogen content, no procedure or equipment was made available to account for the possible kerogen content variation in the specimens. However, Total Organic Content (TOC) was ascertained (section 5.5.8) and thus a constraint on the organic carbon was introduced.

5.4 Results of the Triaxial Multi-Stage Compression Tests

5.4.1 Introduction

A summary of the physical and mechanical properties were determined for the shales are presented in Table t5.4.1a. The Young's moduli (E) and Poisson's ratios (v) quoted are 'average' values E_{av} and v_{av} as defined by the I.S.R.M. (1979), and were determined for the first loading cycle on each sample at a confining stress of nominal 5MPa. The linear Mohr-Coulomb peak strength parameters and the Hoek-Brown peak strength parameters for each sample were determined from their axial stresses σ_1 and confining stresses $\sigma_2 = \sigma_3$ at failure.

Sample	Condition at testing		Physical properties			Peak strengths		Deformation parameters		Linear Mohr-Coulomb peak strength parameters		Hoek-Brown peak strength parameters			
	Moisture	Laminations wrt axial loading	Dry bulk density (kg/cu.m)	Saturated bulk density (kg/cu.m)	Effective porosity (%)	Confining stress (MPa)	Peak axial stress (MPa)	Average Young's modulus (GPa)	Average Poisson's ratio	Cohesion (MPa)	Internal friction angle (degrees)	Estimated uniaxial compressive strength (MPa)	Estimated tensile strength (MPa)	Strength parameter m	Strength parameter s
EX 1	Saturated 5% NaCl	Perpendicular	2530	2535	0.5	4.5	247.8	30.3	0.34	51.9	40.6	215.7	-20.2	10.8	1.00 (intact rock)
						10.0	270.6	----------	----------						
						20.0	323.4	----------	----------						
						30.0	365.7	----------	----------						
						40.0	414.5	----------	----------						
EX 5	Saturated 5% NaCl	Perpendicular	2447	2449	0.2	5.1	261.8	32.8	0.30	60.9	36.1	233.5	-30.8	7.5	1.00 (intact rock)
						10.0	276.5	----------	----------						
						20.0	314.9	----------	----------						
						30.0	354.9	----------	----------						
						40.0	395.3	----------	----------						
EX 6	Saturated 5% NaCl	Perpendicular	2174	2177	0.2	5.2	86.7	9.9	0.20	18.4	33.7	51.1	-4.1	12.2	
						10.0	104.9	----------	----------						
						20.0	138.8	----------	----------						
						30.0	172.1	----------	----------						
						40.0	209.8	----------	----------						
EX 7	Saturated 5% NaCl	Perpendicular	2551	2593	4.2	4.9	268.5	39.1	0.32	Insufficient test data available *		Insufficient test data available *			
EX 8	Saturated 5% NaCl	Perpendicular	2371	2385	1.3	5.1	88.6	13.4	0.24	15.6	39.4	20.5	-0.4	48.6	1.00 (intact rock)
						10.0	110.3	----------	----------						
						20.0	156.5	----------	----------						
						30.0	201.2	----------	----------						
						40.0	244.1	----------	----------						
EX 10	Saturated 5% NaCl	Perpendicular	2546	2556	1.1	5.1	238.3	35.6	0.26	50.9	40.4	211.7	-20.3	10.3	1.00 (intact rock)
						10.0	271.4	----------	----------						
						20.0	318.5	----------	----------						
						30.0	365.6	----------	----------						
						40.0	402	----------	----------						
IU 6	Saturated 5% NaCl	Perpendicular	2676	2686	1.0	5.0	139.6	18.4	0.28	29.3	38.8	108.9	-9.2	11.8	1.00 (intact rock)
						10.0	166.5	----------	----------						
						20.0	216.1	----------	----------						
						30.0	254.7	----------	----------						
						40.0	291.1	----------	----------						
IU 8	Saturated 5% NaCl	Perpendicular	2365	2377	1.2	5.0	72.6	7.5	0.32	16.0	31.4	40.4	-3.5	11.4	1.00 (intact rock)
						10.0	89.6	----------	----------						
						20.0	120.3	----------	----------						
						30.0	149.9	----------	----------						
						40.0	185.1	----------	----------						
2583	Saturated 5% NaCl	Perpendicular	2435	2515	8.0	5.0	214.1	32.4	0.30	45.7	40.0	186.9	-17.9	10.4	1.00 (intact rock)
						10.0	242.6	----------	----------						
						20.0	293.6	----------	----------						
						30.0	338.1	----------	----------						
						40.0	372.8	----------	----------						

Notes : * Sample EX 7 failed catastrophically at end of first loading stage

Table t5.4.1a - Summary of physical and mechanical test results

One sample, EX 7, failed catastrophically at the end of its first loading cycle at a confining stress of nominal 5MPa. Hence, no further loading stages could be conducted, and subsequently the peak strength parameters for this shale material could not be determined.

Measurements for determining the physical properties of the shale materials are given in Table t5.4.1b. Plots of

1) Axial stress versus mean axial strain
2) Mean radial strain versus mean axial strain
3) Applied confining stresses versus mean axial strain

are given throughout the text. Analyses of peak strength data given in Mohr-Coulomb linear strength criterion and Hoek-Brown empirical strength criterion are represented as failure envelopes on σ_1 versus σ_3 plots.

5.4.2 Discussion on the mechanical response and properties of the tested samples **EX6, EX8** and **IU8**

Representative plots of mean axial strain versus axial stress, radial strain and complimentary confining stress have been chosen to illustrate any emergent patterns of deformation, partial recovery and ultimate failure of certain samples. With reference to Figs.5.4.2a, b and c samples **EX6**, **EX8** and **IU8**, when first considering the plot of axial stress versus mean axial strain, show similarities in the profiling of stress build up and accommodation of increased stress. Initial imposed stress is taken up, at 5MPa compressive stress, as being almost linear in its relationship with the shortening deformation; that is, mean axial strain responds and increases in equal increments with increases in axial stress. However, the relationship acquires a more geometric increase above an imposed axial stress of 50MPa. As axial stress and loading increases parallel to the cylinder axis, axial strain increases with increasingly less amounts of axial stress. This would indicate the test material approaching failure as axial stress increases toward the yield point of the sample whereupon the cohesion and internal friction of the material is lost and the system fails. The complimentary plot of mean axial strain versus radial strain shows an increase in radial strain on the section of the curve where the axial stress versus axial strain adopts a geometric relationship. Radial strain is a measure of the 'outward barrelling' of the specimen around the diameter of the cylinder. Thus, as axial stress is increasing at small increments, approaching yield, the magnitude of radial strain increases more rapidly as the specimen reaches a cohesionless state. At this point (marked (1) on Figs.5.4.2a, b and c, the

Sample ref	Laminations wrt core axis	Condition	Mean Diameter (mm)	Height (mm)	Air-dry mass (g)	Fluid-sat mass (g)	Pore fluid mass (g)	Pore fluid relative density	Pore volume (cc)	Dry bulk density (kg/cu.m)	Saturated water content (%)	Saturated bulk density kg/cu.m	Effective porosity %
EX 1	Perpendicular	Saturated 5% NaCl	38.00	77.86	223.4	223.9	0.5	1.050	0.5	2530	0.21	2535	0.54
EX 5	Perpendicular	Saturated 5% NaCl	38.07	77.98	217.2	217.4	0.2	1.050	0.2	2447	0.09	2449	0.21
EX 6	Perpendicular	Saturated 5% NaCl	38.02	78.26	193.2	193.4	0.2	1.050	0.2	2174	0.10	2177	0.21
EX 7	Perpendicular	Saturated 5% NaCl	37.98	78.57	227.1	231.0	3.9	1.050	3.7	2551	1.64	2593	4.17
EX 8	Perpendicular	Saturated 5% NaCl	37.65	77.31	204.1	205.3	1.2	1.050	1.1	2371	0.56	2385	1.33
EX 10	Perpendicular	Saturated 5% NaCl	37.99	71.94	207.6	208.5	0.9	1.050	0.9	2546	0.41	2556	1.05
IU 6	Perpendicular	Saturated 5% NaCl	37.94	72.26	218.6	219.5	0.9	1.050	0.9	2676	0.39	2686	1.05
IU 8	Perpendicular	Saturated 5% NaCl	38.05	72.43	194.8	195.8	1.0	1.050	1.0	2365	0.49	2377	1.16
2583	Perpendicular	Saturated 5% NaCl	37.98	77.61	214.1	221.5	7.4	1.050	7.0	2435	3.29	2515	8.02

Table t5.4.1b - Physical properties of the tested samples

5-stage multiple failure state drained triaxial compression test - EX 6

Sample reference : EX 6

Pore pressure zero

Laminations normal to axial loading

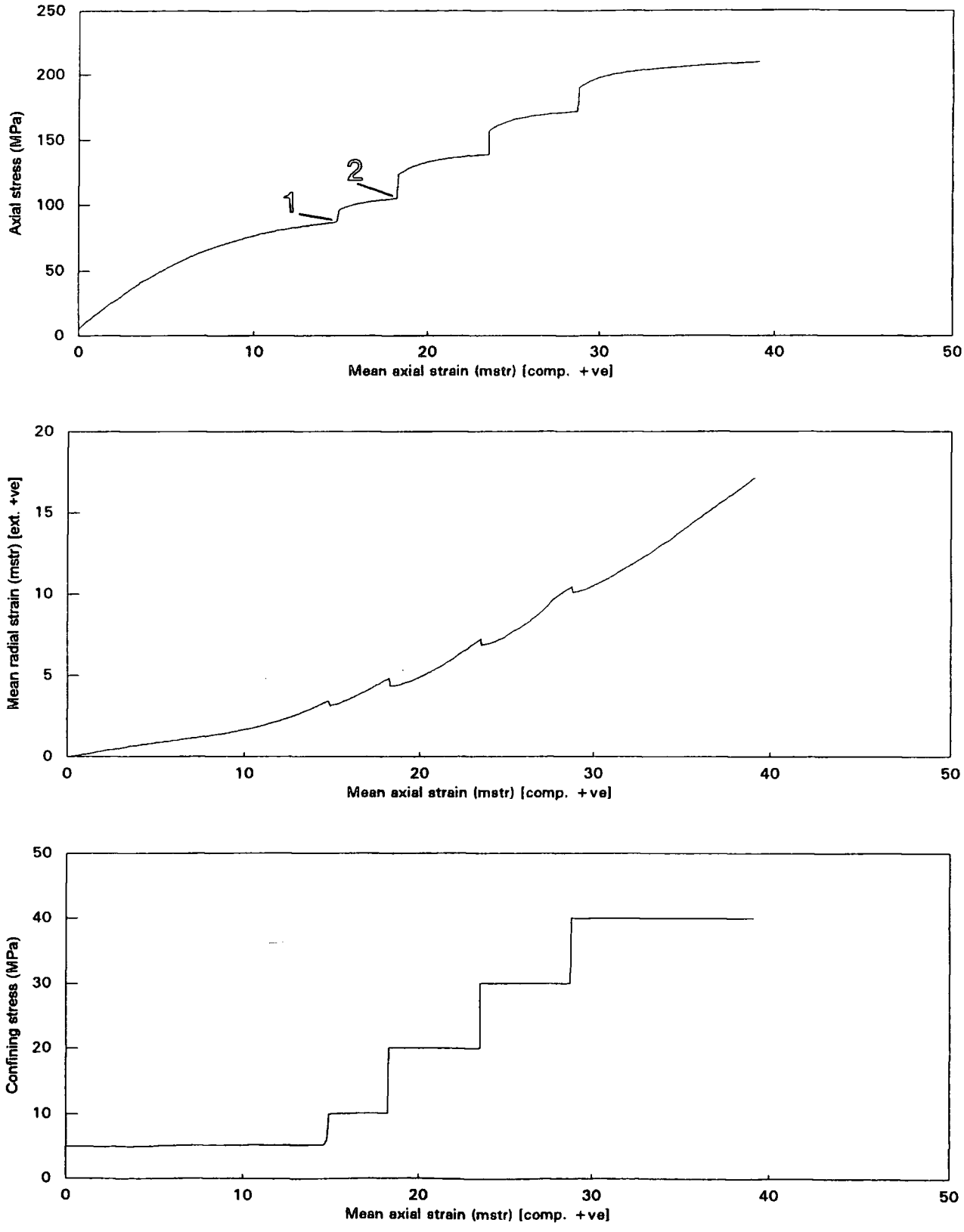

Fig.5.4.2a - Top) Axial stress versus axial strain **Centre)** Mean radial strain versus axial strain **Lower)** Confining stress versus axial strain

5-stage multiple failure state drained triaxial compression test - EX 8

Sample reference : EX 8

Pore pressure zero

Laminations normal to axial loading

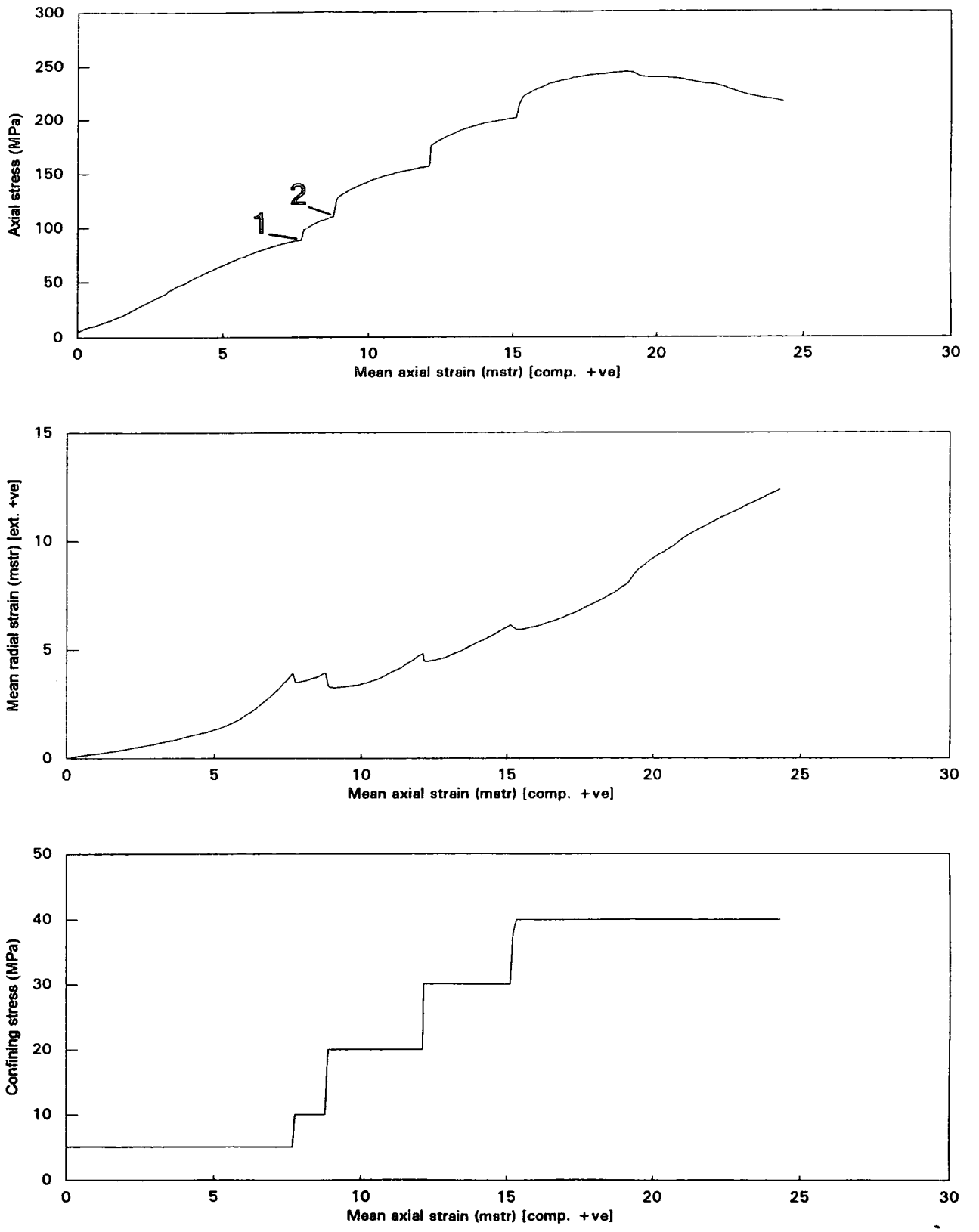

Fig.5.4.2b - Top) Axial stress versus axial strain **Centre)** Mean radial strain versus axial strain **Lower)** Confining stress versus axial strain

5-stage multiple failure state drained triaxial compression test - IU 8

Sample reference : IU 8

Pore pressure zero

Laminations normal to axial loading

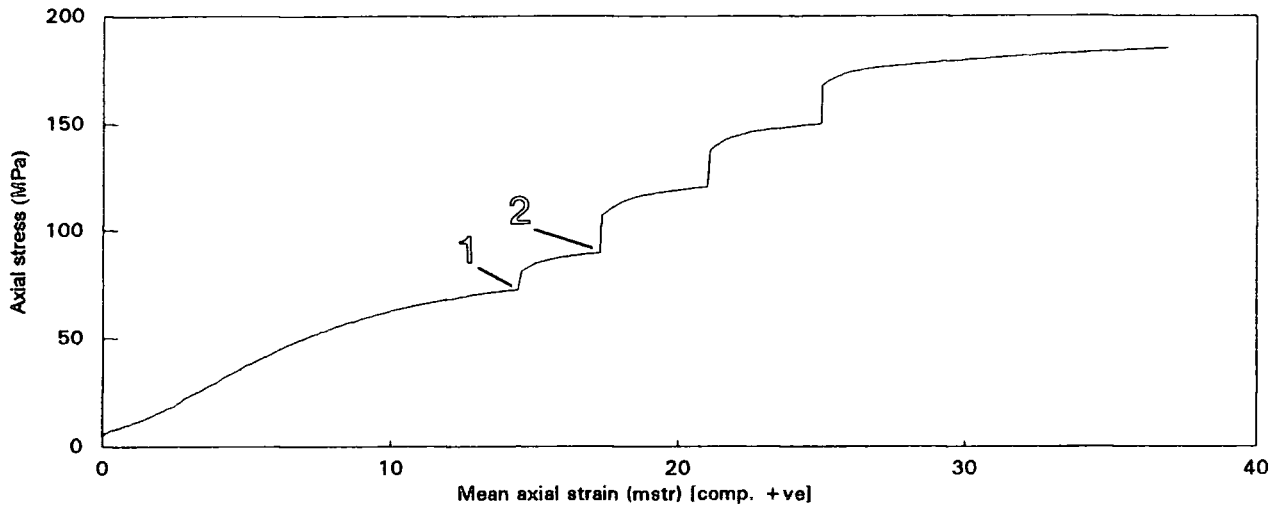

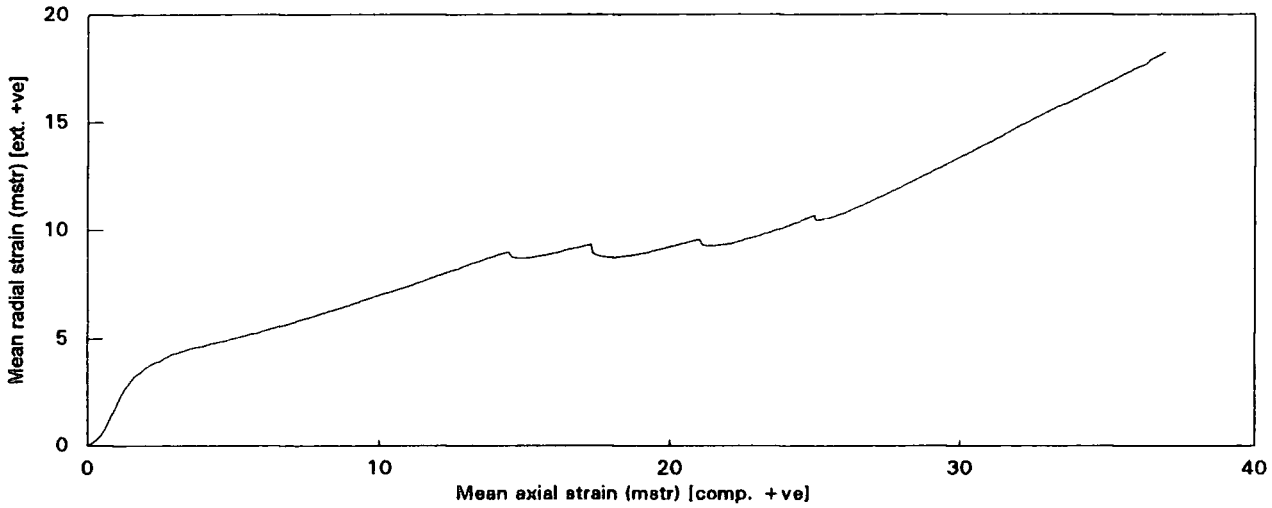

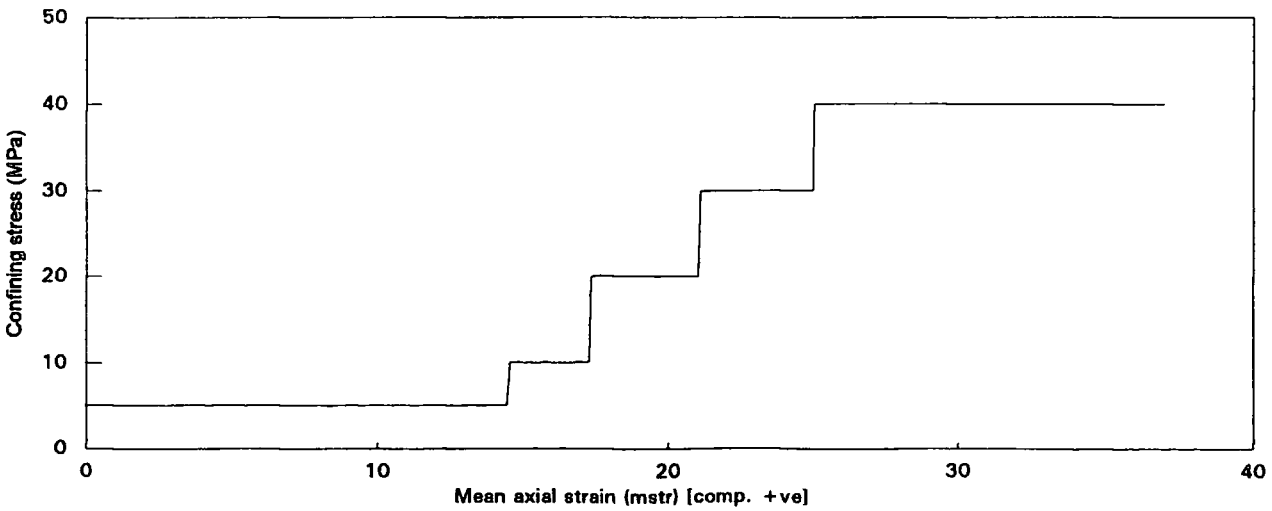

Fig.5.4.2c - Top) Axial stress versus axial strain **Centre)** Mean radial strain versus axial strain **Lower)** Confining stress versus axial strain

instrumentation recognises this point as being the maximum imposed axial stress that can be allowed before failure in the compressive stress state of 5MPa. In each case, EX6, EX8 and IU8 record this point (1) for peak axial stress at 86.7, 88.6 and 72.6MPa respectively and mean axial strain in a range of 13.5 to 15millistrains. Therefore, peak strengths for an initial loading at a confining stress of 5MPa are in a similar range for the three samples.

At point (1), the instrumentation immediately adjusts the system and conditions to increase the compressive stress to 10MPa. The effect on the tested cylinder is to allow an instantaneous but small amount of recovery in radial strain reflecting the elasticity of the material when an increase in compressive stress is imposed and a drop in the effective stress is allowed. Mean axial strain/shortening does not increase at this point as confining stress operates to confine and restrict the effectiveness of the imposed axial stress. Therefore axial strain will only increase again once the axial stress is increased to a point where strain and deformation is once again effected. The shape of the stress versus strain curves in both the axial stress and radial strain conditions resume the profile recorded for initial loading at 5MPa confining pressure. The geometric relationship allows the curve to approach the horizontal describing a relationship of near flow (cohesionless) whereby no increase in axial stress is needed to justify an asymptotic increase in axial strain (Marsden, pers. comm.). This is the case approaching point (2). At point (2) the confining stress is increased to 20MPa and axial stress is increased once more. This pattern of loading continues until 40MPa where axial stress is increased until the cylinder catastrophically fails or the system is unloaded (dependant upon the overall programme load time). Immediate stress relaxation at this magnitude of loading very often has the effect of initiating horizontal fractures parallel to laminations as recorded also by Zeuch (1983). Failure, otherwise, is usually described by conjugate shear fractures at angles <45° (Twiss and Moores, 1992).

A recognisable trend that is apparent and important in the profiles of **EX6**, **EX8** and **IU8** is the confining stress increment increase of 5MPa through to 40MPa at intervals of 10MPa, 20MPa and 30MPa against the mean axial strain. At point (1) confining stress is increased to 10MPa and the sample materials of **EX6**, **EX8** and **IU8** shortens and strain increases due to increasing axial stress loading by 2-3 millistrains before confining stress is increased to 20MPa. Between confining stress references 20MPa to 30MPa, axial strain increases to 5 millistrains in **EX6**, **EX8** and 7 millistrains in **IU8**. Between 30MPa and 40MPa, deformation recorded as axial strain is again 5 millistrains in **EX6** and **EX8** and 7 millistrains in **IU8**. Therefore, in each sample, the

deformability of the material adopts a predictable behaviour throughout initial loading to approaching yield and cohesionless flow. This apparent predictability and similar profiling is investigated in terms of physical properties and Mohr-Coulomb and Hoek-Brown peak strength parameters.

Figs.5.4.2a', b' and c' show the Mohr-Coulomb linear strength criterion and the Hoek-Brown empirical strength criterion as plotted as envelopes on σ_1 and σ_3 respectively for EX6, EX8 and IU8. Common data appear to be the computed cohesion (range of 15.5 to 18.5MPa), angle of internal friction (range of 31 to 39.5°) and the tensile strength of the material (range of -0.4 to -4.2MPa). Therefore, the combination of a relatively low cohesion and low tensile strengths are common criteria to correlate the stress and strain profiles for these samples. The deformation parameters of E_{av} (7.4 to 13.4) and a v_{av} (0.2 to 0.34) are very low values for these isotropic parameters.

The low cohesion cannot be attributable to internal pore pressure generation by trapped evolving pore fluids as these 5-stage compression tests were carried under minimal strain rate and completely drained conditions. No structural heterogenieties or other obvious anisotropies can readily explain both the peak strengths, deformation parameters and apparent predictability of these materials.

5.4.3 Physical Properties

With reference to table t5.4.2b, it is observed that samples **EX8** and **IU8** have approximately similar effective porosities and dry and saturated densities. Cohesion, as a parameter of peak strength, for **EX8** and **IU8** are 15.6 and 16.0MPa respectively indicating that cohesion and physical properties may have an inherent relationship. However, the friction angle of **EX8** is higher at 39.4° than that of **IU8** (31.4°) and Poisson's ratio calculated for these two samples puts (0.32) at a value reflecting its relative incompressibility with respect to 0.24 of **EX8**. Also, the behaviour of axis stress and radial strain versus mean axial strain (Figs.5.4.2b and c) shows a high initial amount of radial strain (barrelling) with relatively little shortening under initial loading for **IU8**. **EX8** follows an accelerated radial strain pattern as axial stress load is increased toward point (1)/yield (Fig.5.4.2b). This is likely an effect of initial deformability determined by initial stress accommodation by the internal structure and fabric rather than being dictated by densities or porosities (as effective porosity and density for **EX8** and **IU8** are almost identical). **EX8** also responds to increasing confining stress of 10MPa and 20MPa (Fig.5.4.2b) with a relatively large radial elastic recovery before effective stress (by virtue of increasing the total amount of axial stress) overcomes this effect. This all suggests there are other parameters at work in

Analysis of peak strength data - EX 6

Mohr-Coulomb linear strength criterion [ref: Hoek, E. & Bray, J.W. (1981), Rock Slope Engineering, pp 333-334]
Hoek-Brown empirical strength criterion [ref: Hoek, E. & Brown, E.T. (1980), Underground Excavations in Rock, p 513]

Sample reference : EX 6

Test number	Sig3 MPa	Sig1(max) MPa
Loading stage 1	5.21	86.73
Loading stage 2	10.03	104.92
Loading stage 3	20.00	138.82
Loading stage 4	30.01	172.15
Loading stage 5	40.02	209.84

These data yield the following models :

Mohr-Coulomb linear strength criterion :	Cohesion c	=	18.410	MPa
	Friction angle	=	33.731	degs
	Correlation r	=	1.000	
Hoek-Brown empirical strength criterion :	UCS	=	51.054	MPa
	Parameter m	=	12.238	
	Parameter s	=	1.000	(intact rock)
	Tensile strength	=	-4.144	MPa
	Correlation r	=	0.993	

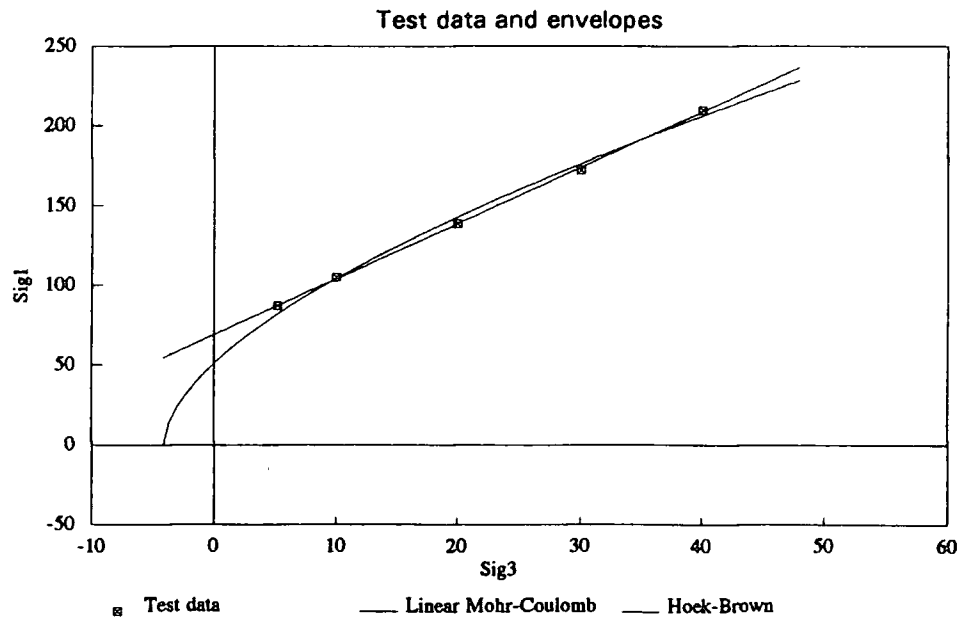

Fig.5.4.2a' - Mohr-Coloumb and Hoek-Brown strength criteria described as peak strength envelopes

Analysis of peak strength data - EX 8

Mohr-Coulomb linear strength criterion [ref: Hoek, E. & Bray, J.W. (1981), Rock Slope Engineering, pp 333-334]
Hoek-Brown empirical strength criterion [ref: Hoek, E. & Brown, E.T. (1980), Underground Excavations in Rock, p 513]

Sample reference : EX 8

Test number	Sig3 MPa	Sig1(max) MPa
Loading stage 1	5.08	88.59
Loading stage 2	10.02	110.28
Loading stage 3	19.99	156.53
Loading stage 4	30.01	201.24
Loading stage 5	40.02	244.09

These data yield the following models :

Mohr-Coulomb linear strength criterion :	Cohesion c	=	15.634	MPa
	Friction angle	=	39.385	degs
	Correlation r	=	1.000	
Hoek-Brown empirical strength criterion :	UCS	=	20.452	MPa
	Parameter m	=	48.630	
	Parameter s	=	1.000	(intact rock)
	Tensile strength	=	-0.420	MPa
	Correlation r	=	0.995	

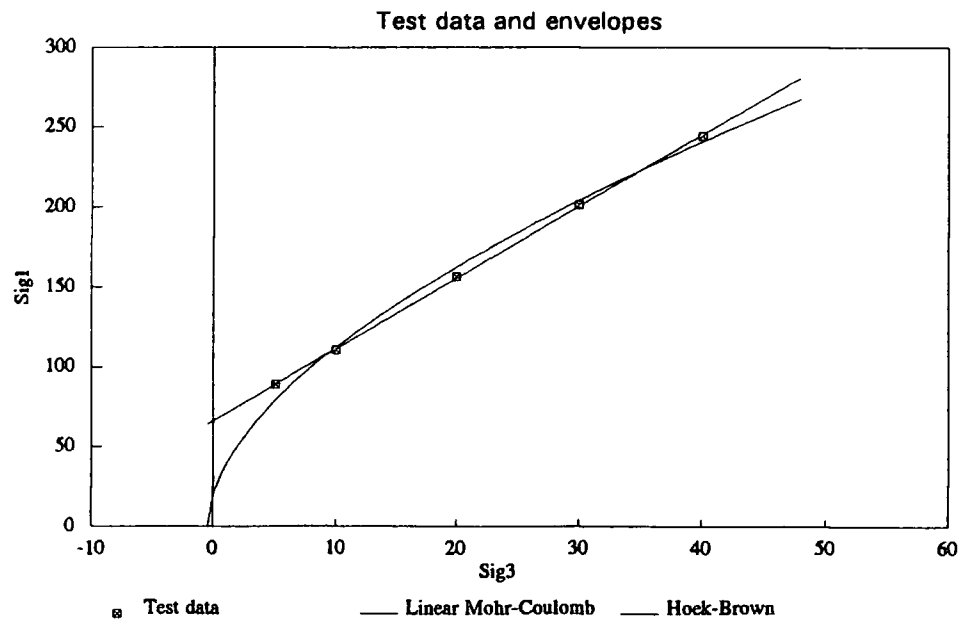

Fig.5.4.2b' - Mohr-Coloumb and Hoek-Brown strength criteria described as peak strength envelopes

Analysis of peak strength data - IU 8

Mohr-Coulomb linear strength criterion [ref: Hoek, E. & Bray, J.W. (1981), Rock Slope Engineering, pp 333-334]
Hoek-Brown empirical strength criterion [ref: Hoek, E. & Brown, E.T. (1980), Underground Excavations in Rock, p 513]

Sample reference : IU 8

Test number	Sig3 MPa	Sig1(max) MPa
Loading stage 1	5.03	72.62
Loading stage 2	10.02	89.63
Loading stage 3	20.02	120.35
Loading stage 4	30.00	149.93
Loading stage 5	40.01	185.06

These data yield the following models :

Mohr-Coulomb linear strength criterion :	Cohesion c	=	15.963	MPa
	Friction angle	=	31.373	degs
	Correlation r	=	1.000	
Hoek-Brown empirical strength criterion :	UCS	=	40.362	MPa
	Parameter m	=	11.377	
	Parameter s	=	1.000	(intact rock)
	Tensile strength	=	-3.521	MPa
	Correlation r	=	0.991	

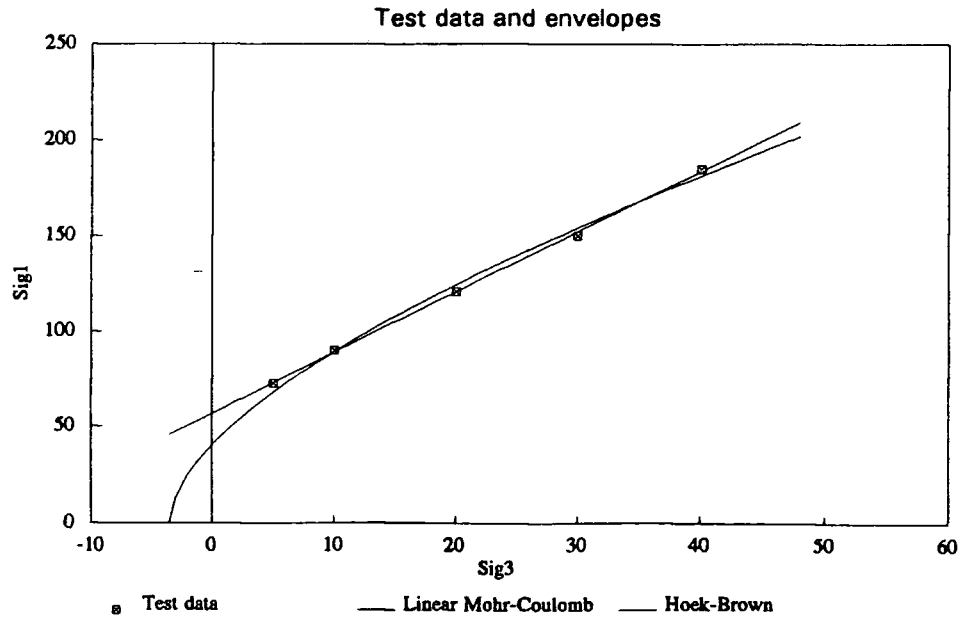

Fig.5.4.2c' - Mohr-Coloumb and Hoek-Brown strength criteria described as peak strength envelopes

determining the response to multistage loading and peak strengths than the physical parameters of bulk density and effective porosity.

When considering EX6 (Fig.5.4.2a), the axial stress and radial strain versus mean axial strain profiles of loading have already been described as similar to EX8 and IU8. However, EX6 demonstrates this similar predictable behaviour with a lower bulk density (2174kg/cu.m dry density and 2177kg/cu.m saturated density) but with a very low effective porosity (0.2%). This similar loading and accommodation behaviour suggests, then, that effective porosity does not have any obvious effect on peak strength or deformation in the configuration where laminations are normal to imposed axial stress. With reference to Table t5.4.1b, this inference agrees with observations made with sample 2583 (8.0% effective porosity, peak axial stress at 5.0MPa confining stress = 214.1MPa) and EX1 (0.5% effective porosity, peak axial stress at 4.5MPa = 247.8MPa). This would seem reasonable in a drained configuration whereby any evolved fluids and pressure developed and accommodated in the rock porosity would be allowed to escape (due to a very low strain rate of 10millistrains/hr) such that any stress imposed on a tested cylinder would be accommodated and taken up by the grain framework and ultimately borne by the mineral crystal lattice. This suggests then that the composition and possibly the fabric of the material being tested is more important in determining the peak strength of the material than physical parameters such as porosity. This, however, would be the reverse under undrained conditions whereupon internal pore pressure would largely dictate the peak physical strength (Swan et al., 1989).

5.4.4 Discussion on the deformation patterns of samples IU6, 2583, EX10, EX5 and EX1

The deformational response of samples EX6, EX8 and IU8 seem to follow a coherent pattern of stress loading and reciprocal accommodation and strain. This has been correlated to the cohesion of the material as well as the isotropic deformation parameters of E_{av} and v_{av}. The predictable behaviour of stress accommodation in these 3 samples is not repeated as obviously as in other tested samples. However, the relationship of increasing cohesion with peak strength seems to hold true for all samples tested and that cohesion has marked effect on the tensile strength of the material also (EX6, EX8 and IU8 have estimated tensile strengths of -4.1, -0.4 and -3.5MPa respectively - Figs.5.4.2a, b and c).

Sample IU6 (Figs.5.4.4a, a')

With a cohesion of 29.3MPa and deformation parameters of E=18.4 and v=0.28, this material lies intermediate in peak strength capacity and deformation capability between sample set EX6, EX8 and IU8 and the remainder of the tested cylinders. Axial stress versus mean axial strain (Fig.5.4.4a) shows a capacity of approximately 140MPa at 5MPa confining stress following an almost linear relationship with strain. However, radial strain behaviour is observed to be largely unpredictable showing differing amounts of recovery at points of increasing confining stress and appears to be no coherence in the ability to accommodate radial strain in any definable relationship. Similarly, confining stress versus mean axial strain shows no inherent relationship of when the material is approaching yield. This would infer that internal fabric and structural heterogenieties of the material were possibly influencing the deformation pattern.

Samples 2583 (Figs.5.4.4b, b') and EX10 (Figs.5.4.4c, c')

Cohesion in the range of 45-51MPa, internal friction angles at 40°, E_{av} of 32-36GPa and v_{av} of 0.26-0.30 and tensile strengths in the range of -17.9 to -20.3MPa, the deformation patterns of these two materials are similar in the initial loading toward (1), as having an approximate linear relationship between axial stress at various confining stress plateaux of 10-20MPa and 20-30MPa in both cases, and the response at 40MPa shows a relatively high amount of axial stress needed to overcome the confining stress and effective stress. At 40MPa, this is explained by the lack of elastic rebound observed as radial strain. This would infer elasticity is increasingly lost and at this point, even by increasing the confining stress from 30-40MPa, radial recovery is almost negligible. As previously mentioned 2583 has an affective porosity of 8% but follows a similar profile to EX10 which has an effective porosity of 1.1%. This supports the inference that effective porosity and bulk density have no correlative effect on the peak strength and deformation characteristics in these tested materials.

Samples EX5 (Figs.5.4.4d, d') and EX1 (Figs.5.4.4e, e')

The deformation patterns of these two materials are very different to those previously documented samples. These two materials record the highest estimated uniaxial compressive strengths - 215.7MPa (EX1) and 233.5MPa (EX5). These two materials also record the highest estimated tensile strengths (-20.2MPa and -30.8MPa), cohesion (51.9MPa and 60.9MPa) and peak axial stress at 40MPa confining stress (414.5MPa and 395.3MPa for EX1 and EX5 respectively). The deformation profiles shows a high imposed axial stress before the yield point is approached at approximately 11millistrains (mean axial strain). Increasing the confining pressure to 10MPa has little effect and only a slight increase in axial strain is observed before

5-stage multiple failure state drained triaxial compression test - IU 6

Sample reference : IU 6

Pore pressure zero

Laminations normal to axial loading

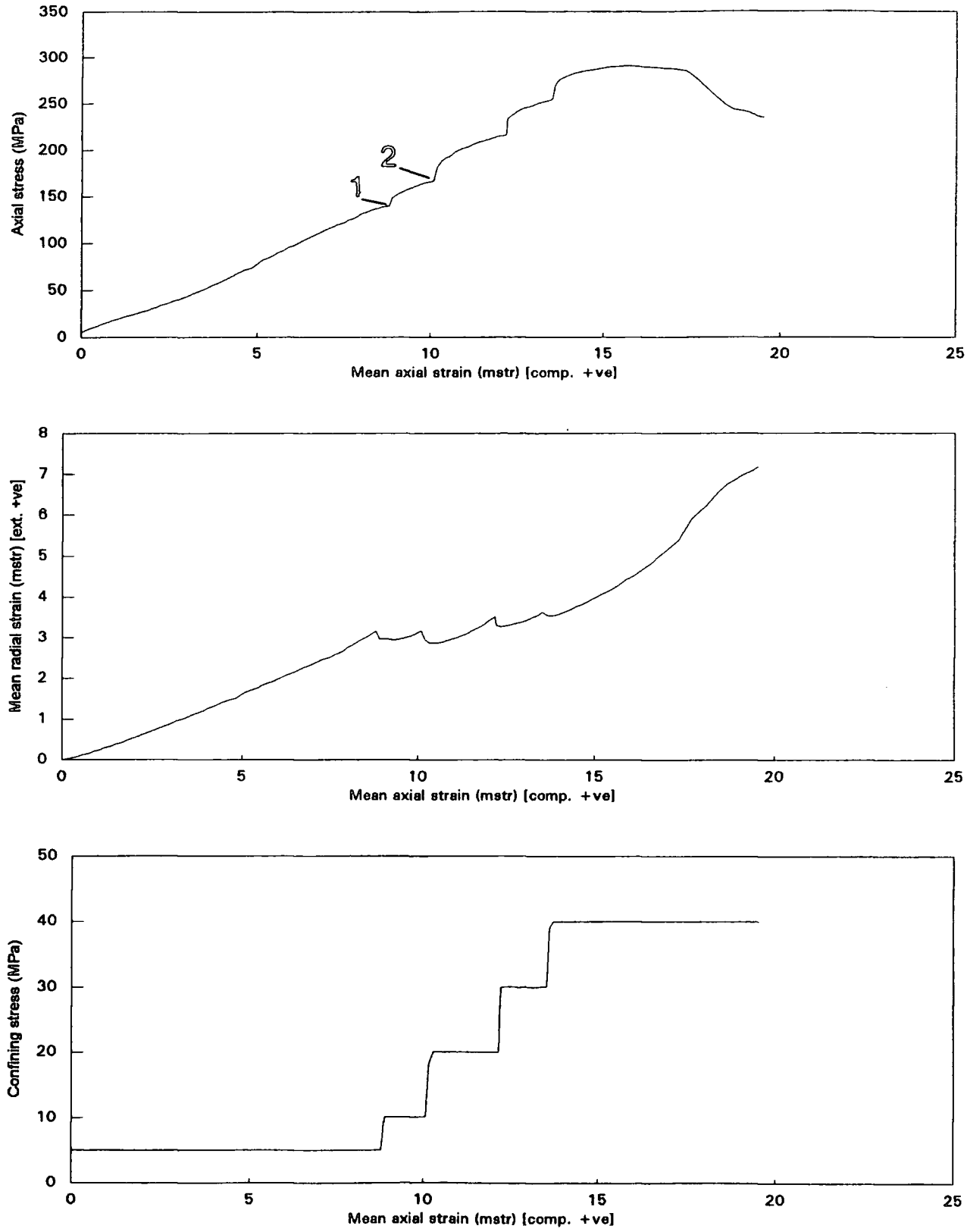

Fig.5.4.4a - Top) Axial stress versus axial strain **Centre)** Mean radial strain versus axial strain **Lower)** Confining stress versus axial strain

Analysis of peak strength data - IU 6

Mohr-Coulomb linear strength criterion [ref: Hoek, E. & Bray, J.W. (1981), Rock Slope Engineering, pp 333-334]
Hoek-Brown empirical strength criterion [ref: Hoek, E. & Brown, E.T. (1980), Underground Excavations in Rock, p 513]

Sample reference : IU 6

Test number	Sig3 MPa	Sig1(max) MPa
Loading stage 1	5.04	139.62
Loading stage 2	10.02	166.51
Loading stage 3	20.02	216.08
Loading stage 4	30.01	254.73
Loading stage 5	40.00	291.05

These data yield the following models :

Mohr-Coulomb linear strength criterion :	Cohesion c	=	29.293	MPa
	Friction angle	=	38.766	degs
	Correlation r	=	0.997	
Hoek-Brown empirical strength criterion :	UCS	=	108.924	MPa
	Parameter m	=	11.816	
	Parameter s	=	1.000	(intact rock)
	Tensile strength	=	-9.153	MPa
	Correlation r	=	1.000	

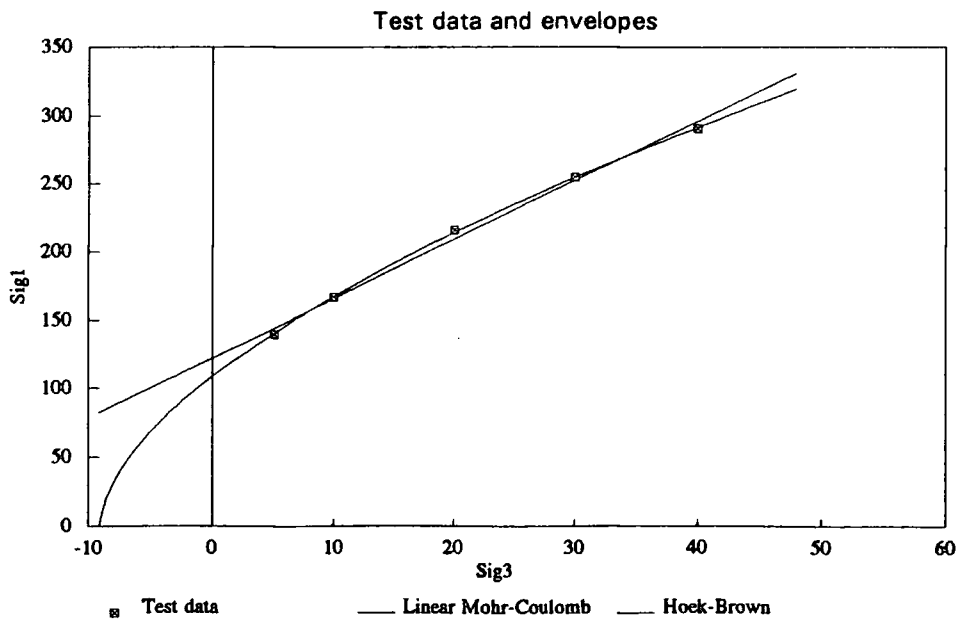

Fig.5.4.4a' - Mohr-Coloumb and Hoek-Brown strength criteria described as peak strength envelopes

5-stage multiple failure state drained triaxial compression test - 2583

Sample reference : 2583

Pore pressure zero

Laminations normal to axial loading

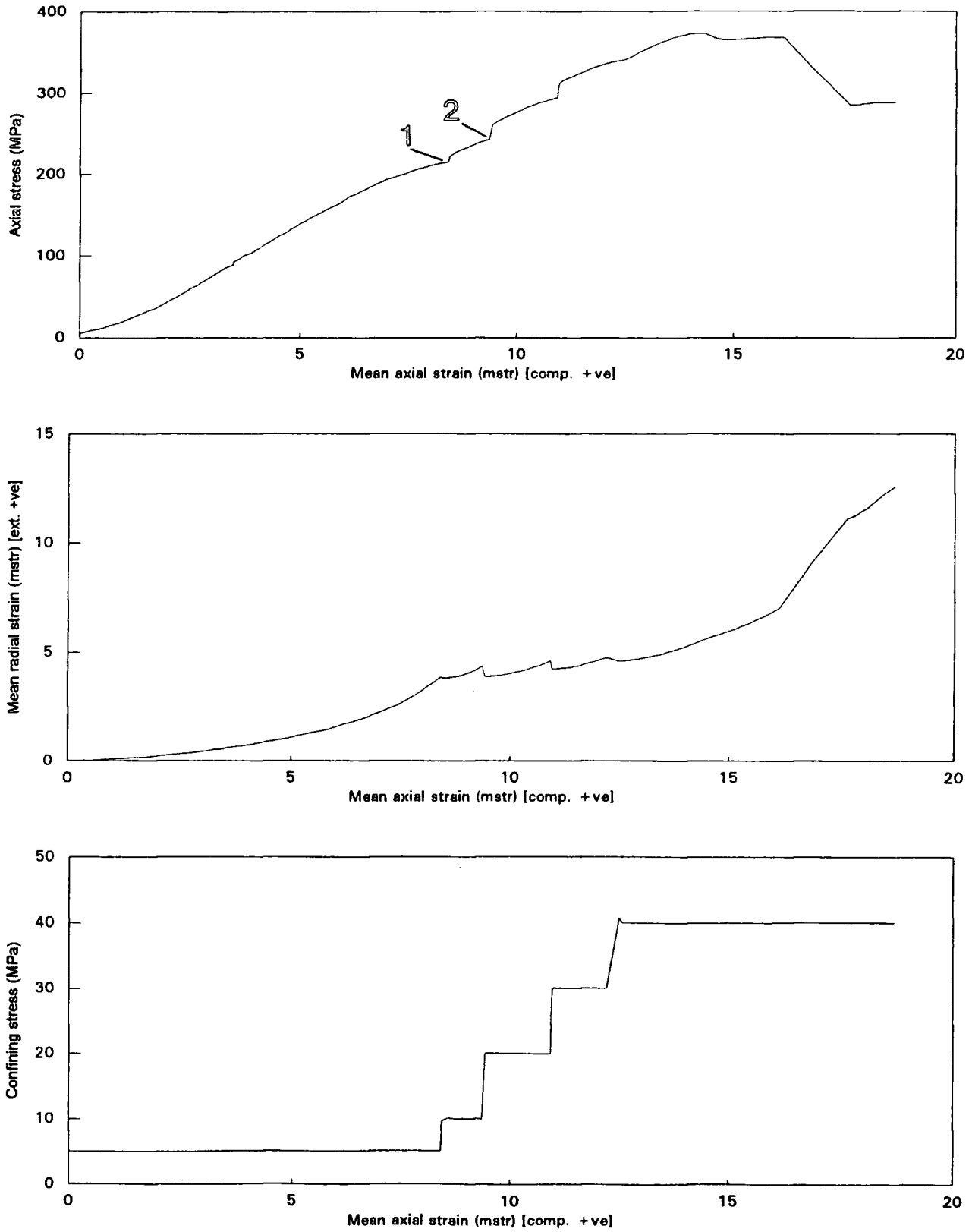

Fig.5.4.4b - Top) Axial stress versus axial strain **Centre)** Mean radial strain versus axial strain **Lower)** Confining stress versus axial strain

Analysis of peak strength data - 2583

Mohr-Coulomb linear strength criterion [ref: Hoek, E. & Bray, J.W. (1981), Rock Slope Engineering, pp 333-334]
Hoek-Brown empirical strength criterion [ref: Hoek, E. & Brown, E.T. (1980), Underground Excavations in Rock, p 513]

Sample reference : 2583

Test number	Sig3 MPa	Sig1(max) MPa
Loading stage 1	5.04	214.09
Loading stage 2	10.00	242.63
Loading stage 3	20.02	293.64
Loading stage 4	30.04	338.07
Loading stage 5	40.02	372.80

These data yield the following models :

Mohr-Coulomb linear strength criterion :	Cohesion c	=	45.677	MPa
	Friction angle	=	39.960	degs
	Correlation r	=	0.996	
Hoek-Brown empirical strength criterion :	UCS	=	186.907	MPa
	Parameter m	=	10.364	
	Parameter s	=	1.000	(intact rock)
	Tensile strength	=	-17.869	MPa
	Correlation r	=	0.999	

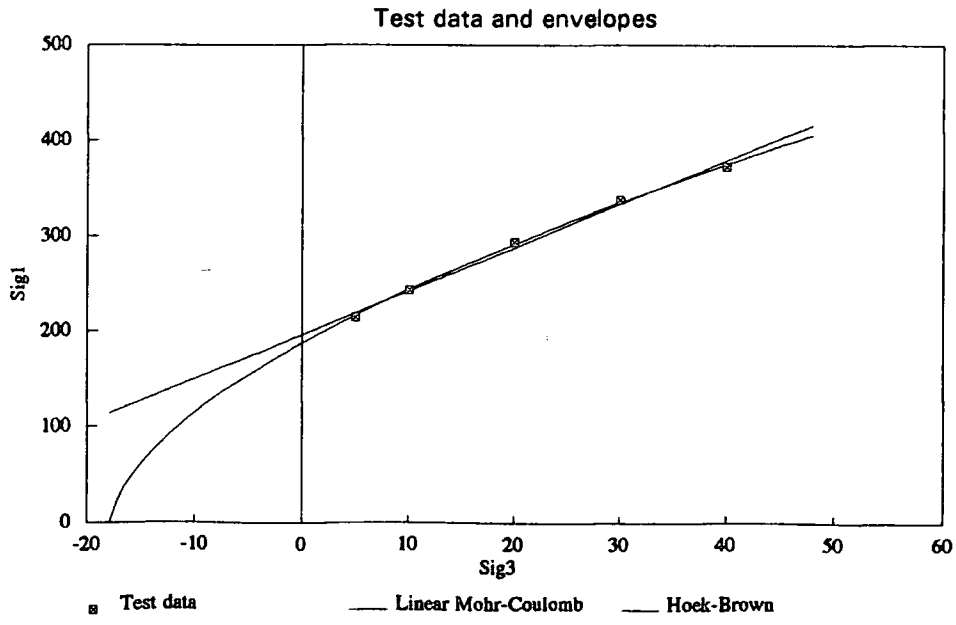

Fig.5.4.4b' - Mohr-Coloumb and Hoek-Brown strength criteria described as peak strength envelopes

5-stage multiple failure state drained triaxial compression test - EX 10

Sample reference : EX 10

Pore pressure zero

Laminations normal to axial loading

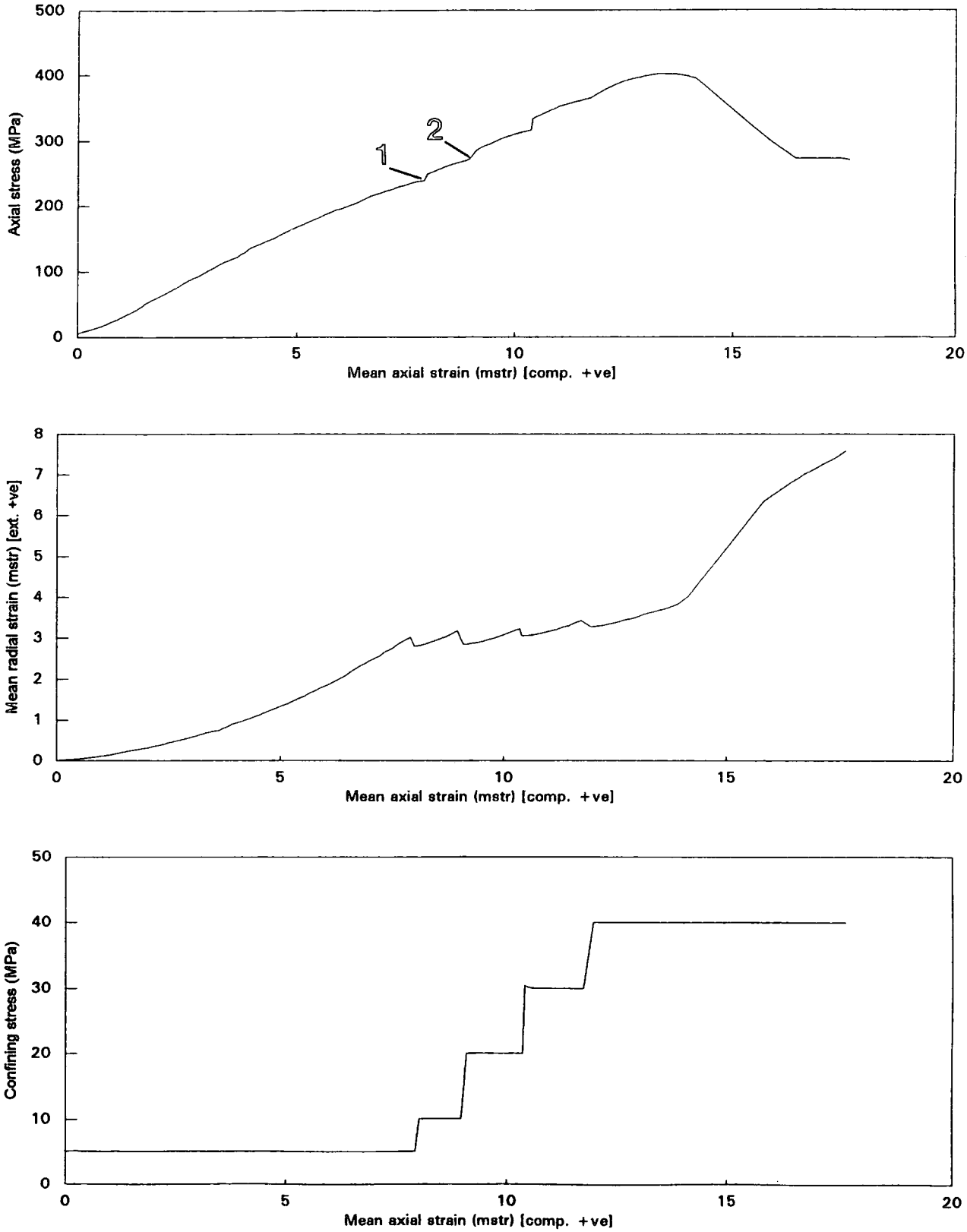

Fig.5.4.4c - Top) Axial stress versus axial strain **Centre)** Mean radial strain versus axial strain **Lower)** Confining stress versus axial strain

Analysis of peak strength data - EX 10

Mohr-Coulomb linear strength criterion [ref: Hoek, E. & Bray, J.W. (1981), Rock Slope Engineering, pp 333-334]
Hoek-Brown empirical strength criterion [ref: Hoek, E. & Brown, E.T. (1980), Underground Excavations in Rock, p 513]

Sample reference : EX 10

Test number	Sig3 MPa	Sig1(max) MPa
Loading stage 1	5.07	238.34
Loading stage 2	10.03	271.40
Loading stage 3	20.01	316.47
Loading stage 4	29.99	365.57
Loading stage 5	40.02	401.95

These data yield the following models :

Mohr-Coulomb linear strength criterion :	Cohesion c	=	50.878	MPa
	Friction angle	=	40.405	degs
	Correlation r	=	0.997	
Hoek-Brown empirical strength criterion :	UCS	=	211.694	MPa
	Parameter m	=	10.342	
	Parameter s	=	1.000	(intact rock)
	Tensile strength	=	-20.281	MPa
	Correlation r	=	0.998	

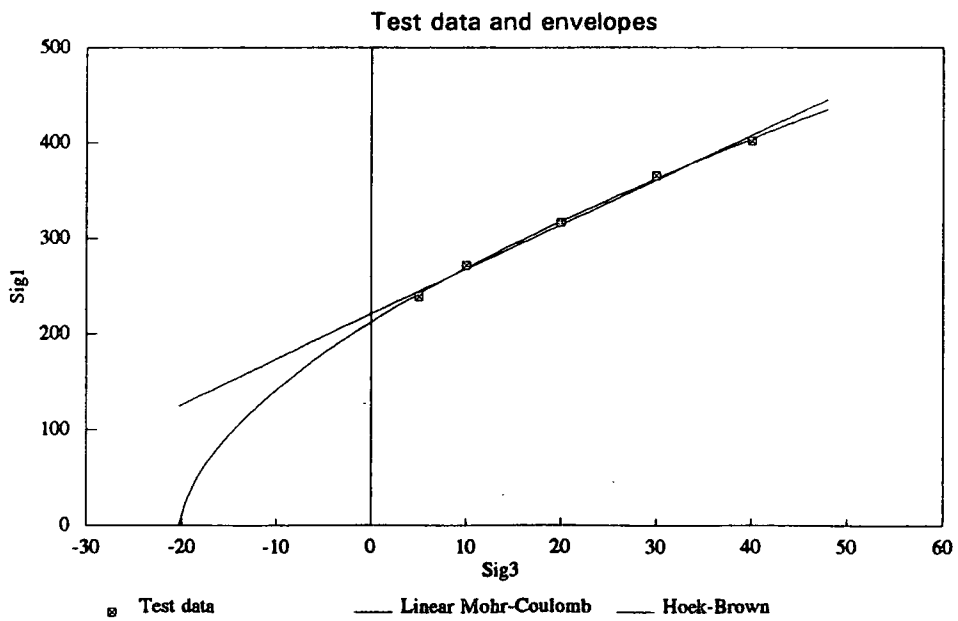

Fig.5.4.4c' - Mohr-Coloumb and Hoek-Brown strength criteria described as peak strength envelopes

5-stage multiple failure state drained triaxial compression test - EX 5

Sample reference : EX 5

Pore pressure zero

Laminations normal to axial loading

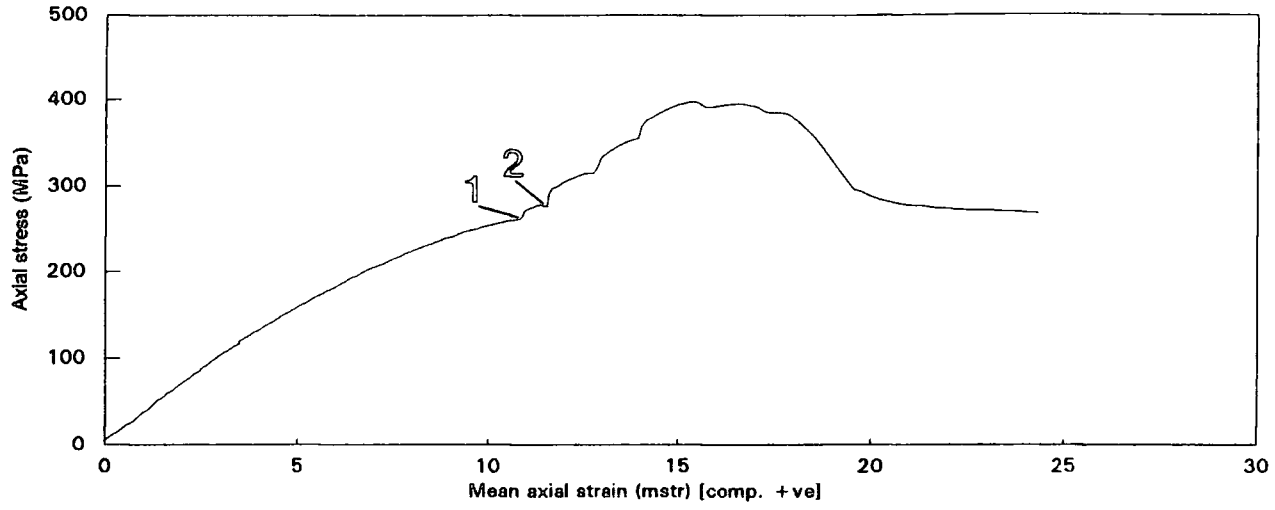

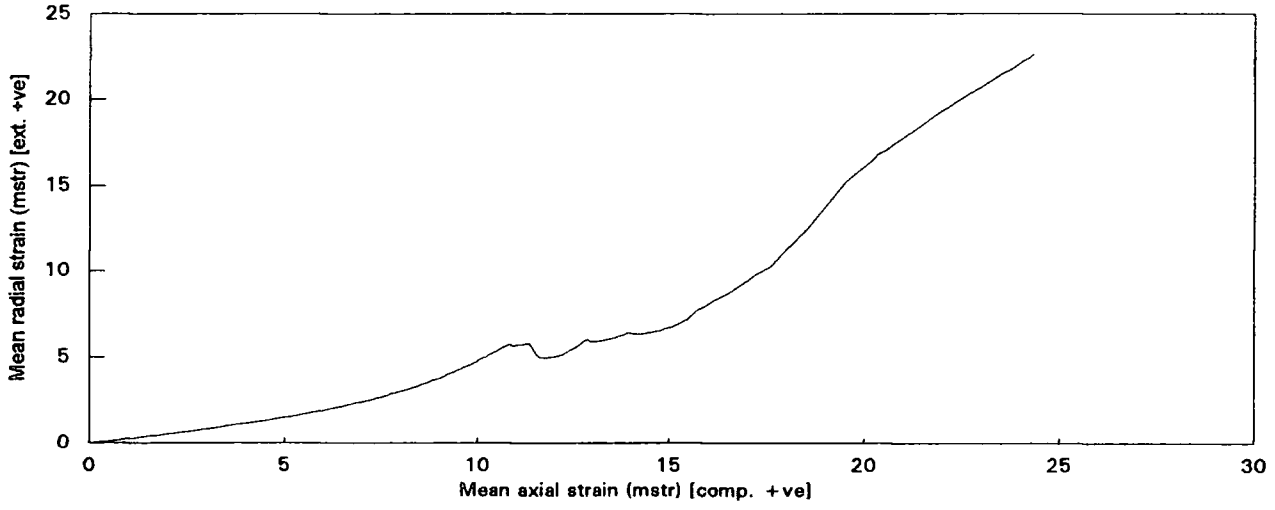

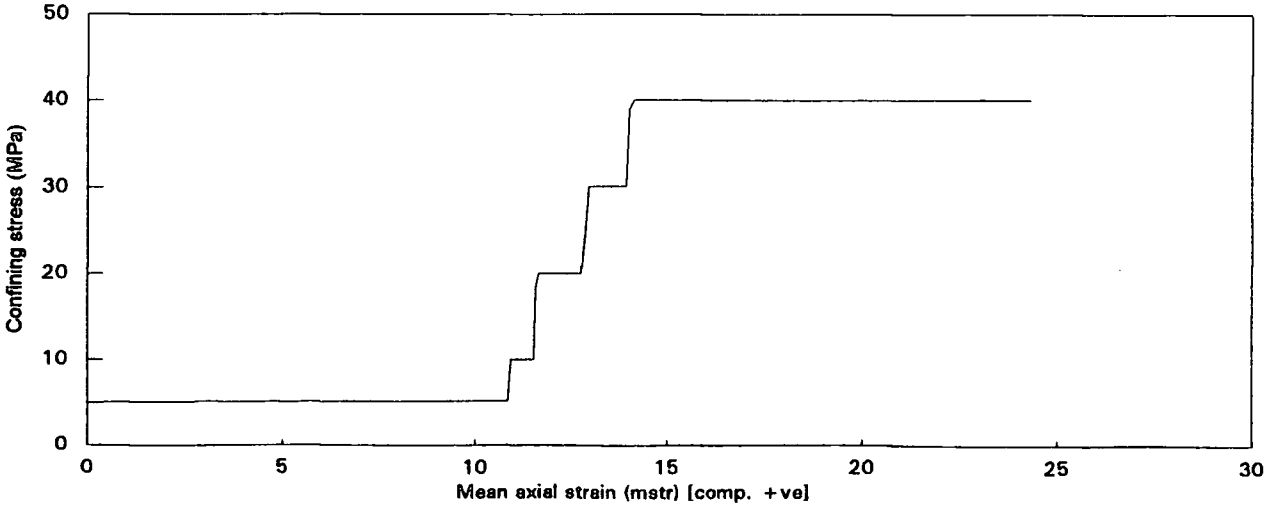

Fig.5.4.4d - Top) Axial stress versus axial strain **Centre)** Mean radial strain versus axial strain **Lower)** Confining stress versus axial strain

Analysis of peak strength data - EX 5

Mohr-Coulomb linear strength criterion [ref: Hoek, E. & Bray, J.W. (1981), Rock Slope Engineering, pp 333-334]
Hoek-Brown empirical strength criterion [ref: Hoek, E. & Brown, E.T. (1980), Underground Excavations in Rock, p 513]

Sample reference : EX 5

Test number	Sig3 MPa	Sig1(max) MPa
Loading stage 1	5.11	261.78
Loading stage 2	9.99	276.49
Loading stage 3	19.99	314.92
Loading stage 4	30.02	354.92
Loading stage 5	40.02	395.29

These data yield the following models :

Mohr-Coulomb linear strength criterion :	Cohesion c	=	60.914	MPa
	Friction angle	=	36.069	degs
	Correlation r	=	0.999	
Hoek-Brown empirical strength criterion :	UCS	=	233.497	MPa
	Parameter m	=	7.458	
	Parameter s	=	1.000	(intact rock)
	Tensile strength	=	-30.765	MPa
	Correlation r	=	0.996	

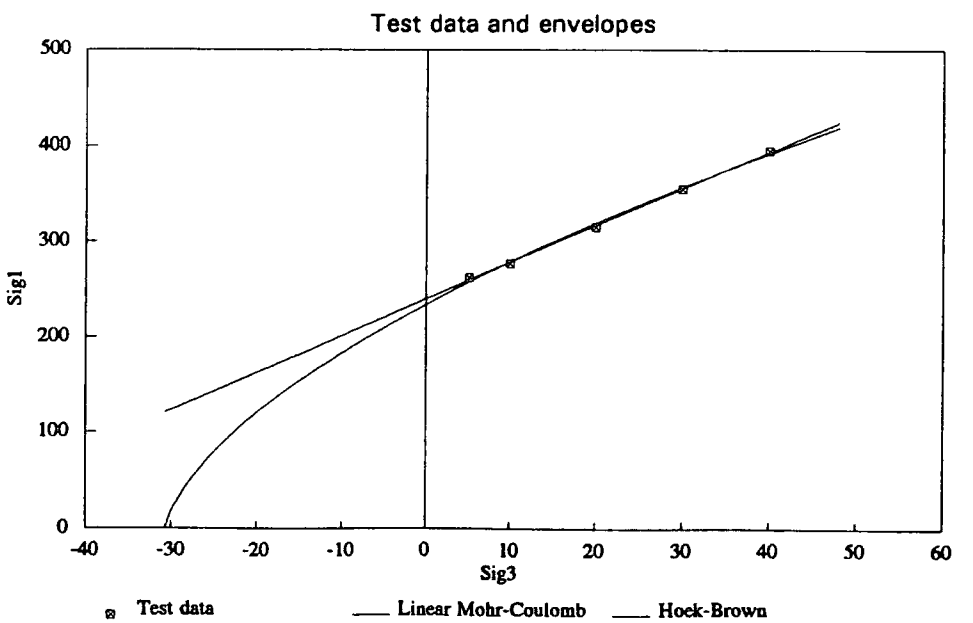

Fig.5.4.4d' - Mohr-Coloumb and Hoek-Brown strength criteria described as peak strength envelopes

5-stage multiple failure state drained triaxial compression test - EX 1

Sample reference : EX 1

Pore pressure zero

Laminations normal to axial loading

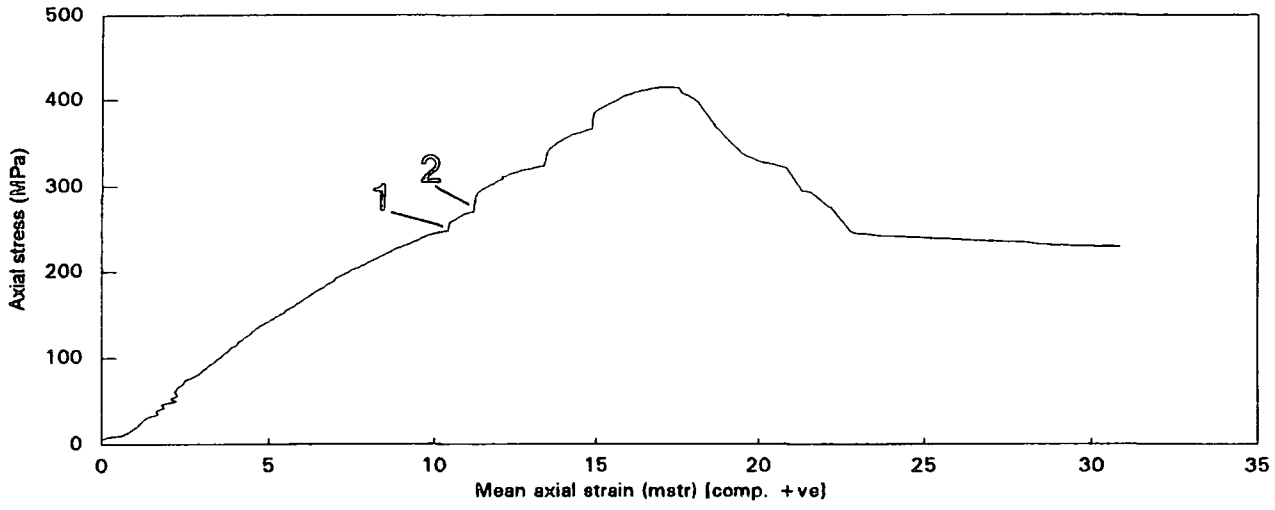

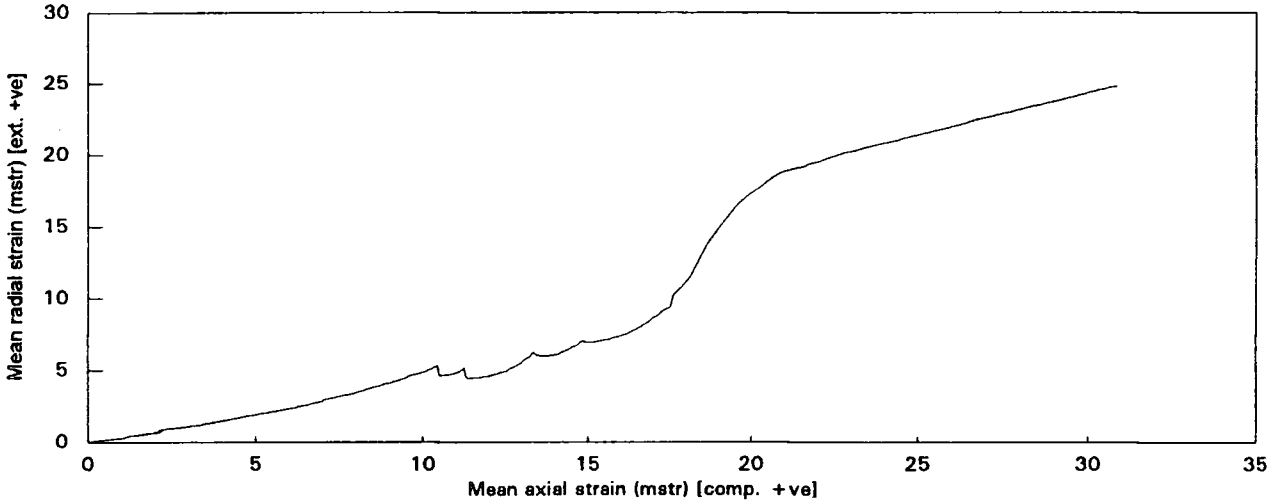

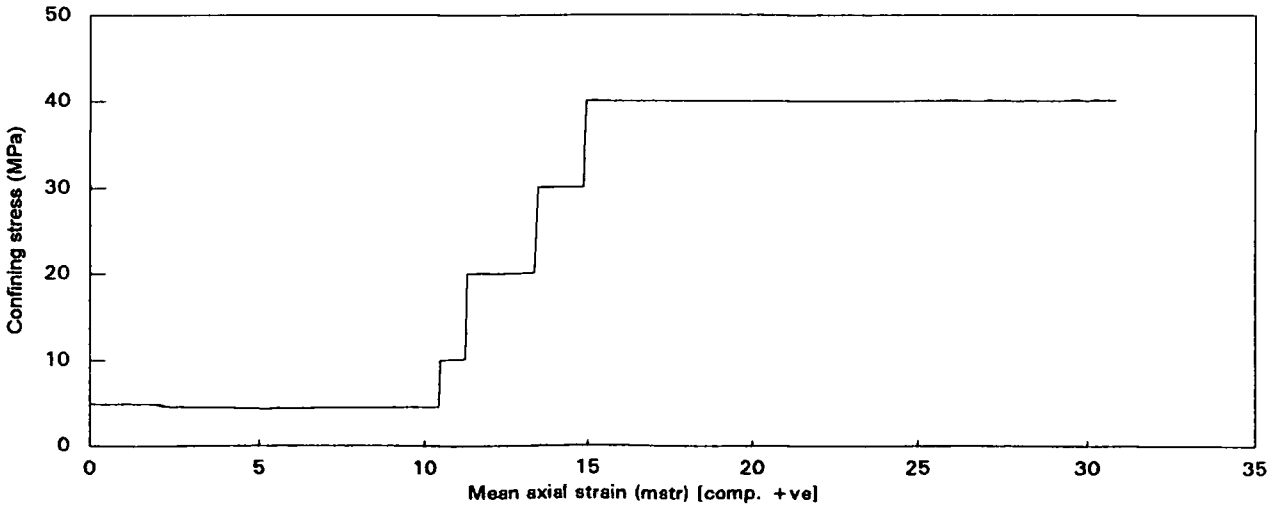

Fig.5.4.4e - Top) Axial stress versus axial strain **Centre)** Mean radial strain versus axial strain **Lower)** Confining stress versus axial strain

Analysis of peak strength data - EX 1

Mohr-Coulomb linear strength criterion [ref: Hoek, E. & Brey, J.W. (1981), Rock Slope Engineering, pp 333-334]
Hoek-Brown empirical strength criterion [ref: Hoek, E. & Brown, E.T. (1980), Underground Excavations in Rock, p 513]

Sample reference : EX 1

Test number	Sig3 MPa	Sig1(max) MPa
Loading stage 1	4.53	247.76
Loading stage 2	10.03	270.55
Loading stage 3	20.05	323.41
Loading stage 4	30.01	365.74
Loading stage 5	40.01	414.55

These data yield the following models :

Mohr-Coulomb linear strength criterion :	Cohesion c	=	51.895	MPa
	Friction angle	=	40.583	degs
	Correlation r	=	0.999	
Hoek-Brown empirical strength criterion :	UCS	=	215.703	MPa
	Parameter m	=	10.609	
	Parameter s	=	1.000	(intact rock)
	Tensile strength	=	-20.155	MPa
	Correlation r	=	0.998	

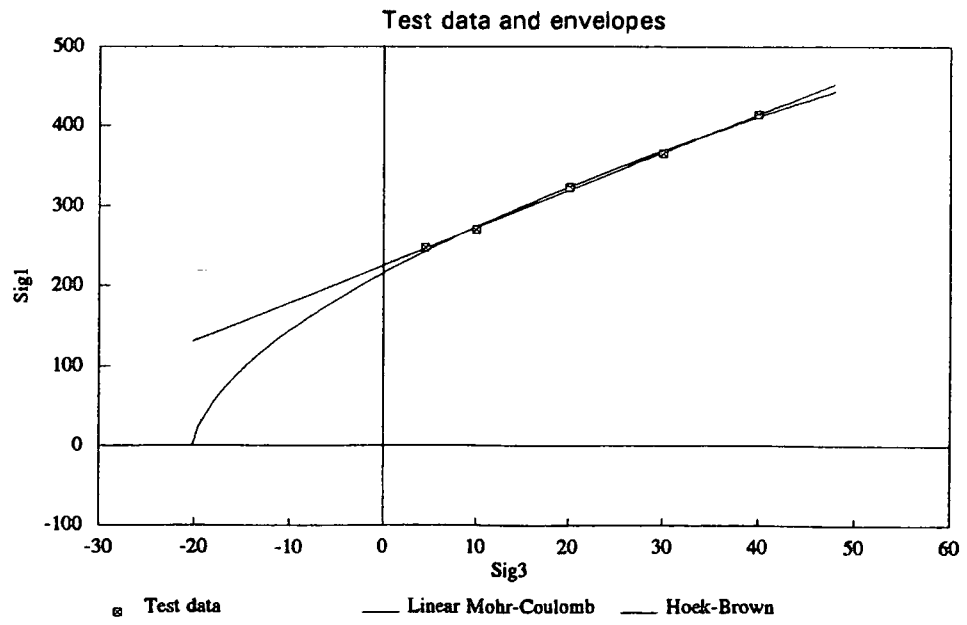

Fig.5.4.4e' - Mohr-Coloumb and Hoek-Brown strength criteria described as peak strength envelopes

confining stress is increased to 20MPa. Confining stress is raised from 5MPa to 40MPa in less than 5millistrains showing the capacity and strength of these materials to accommodate high amounts of imposed axial stress without the radial and axial strain response seen for other less capable materials. Both samples were tested to catastrophic failure by conjugate shear at the confining pressure plateau of 40MPa.

Sample EX7 (Figs.5.4.4f)
This cylinder failed catastrophically at the end of the first stage of loading and therefore does not return the data or profiles needed to accurately assess the deformation parameters or characteristics. Also, peak strength parameters could not be calculated due to insufficient test data.

5.5 X-Ray Diffraction and Total Organic Carbon analyses of whole rock to determine bulk mineralogy

5.5.1 Introduction

All samples which were multi-stage triaxially tested were also analysed for bulk mineralogy to compare with results from the mechanical test programme. To ascertain the relative abundance of the composite mineralogy, X-ray diffraction techniques were employed. Total Organic Carbon (TOC) analyses resolved any organic carbon that may have been a constituent in the bulk composition of the samples. Clay separates were also analysed to determine any relationship between individual clay groups and the mechanical test information.

5.5.2 Preparation Techniques

All XRD samples were run on a Philips PW 1330 3Kw X-ray diffractometer, using CoKα, running at 50KV and 25Ma. Samples were cleaned using distilled water and initially crushed using a fly wheel bulk crusher. Hand crushing using an agate pestle and mortar powdered the fragments down to a fine fraction. Using a 45μm sieve, the <45μm fraction was caught. To control the XRD analyses, 10% weight of Boehmite (Aluminium Oxide Hydrate) (12.5° 2θ peak) was added and homogenised into the powder. The powder was then applied to glass slides using acetone as a neutral mounting medium (for bulk analyses). All samples were run in an air dried state.

The clay fraction was separated and analysed to differentiate any clay peaks which were seen to be suppressed and blanketed during the bulk composition run. The separation technique utilised the suspension of <45μm which was allowed to settle in 100ml of distilled water for 4 hours. A glass slide was then carefully placed in the bottom of the beaker and the solution was dried at room temperature. The glass slide

5-stage multiple failure state drained triaxial compression test - EX 7

Sample reference : EX 7

Pore pressure zero

Laminations normal to axial loading

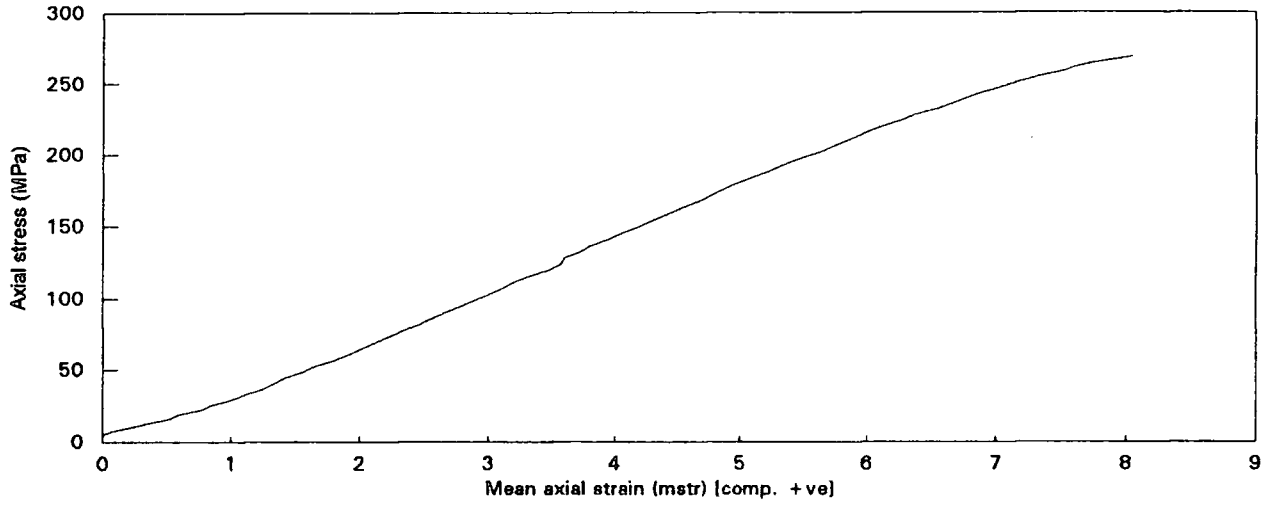

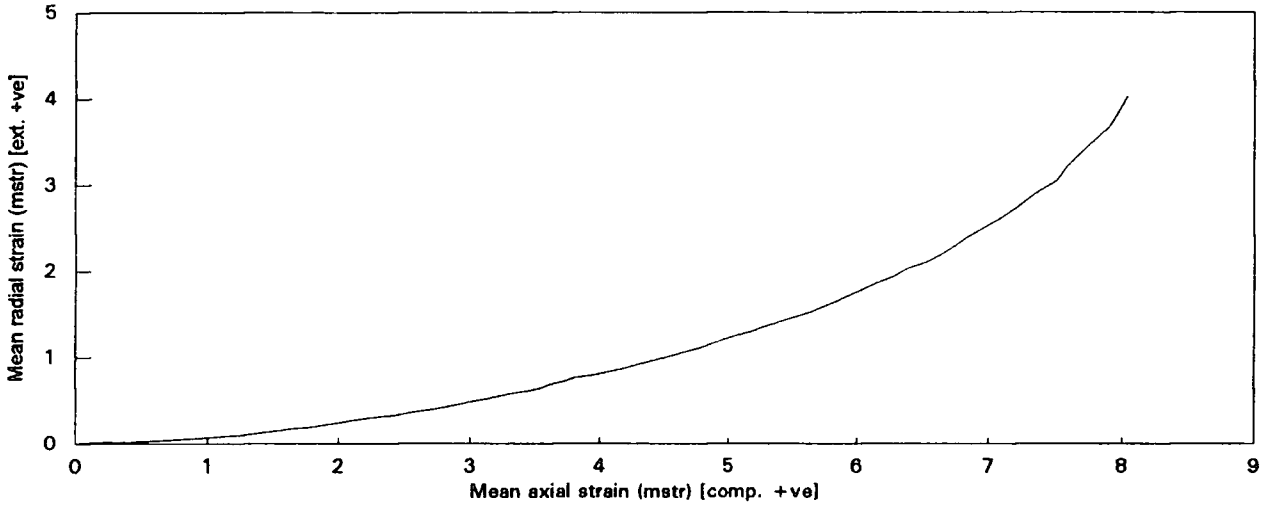

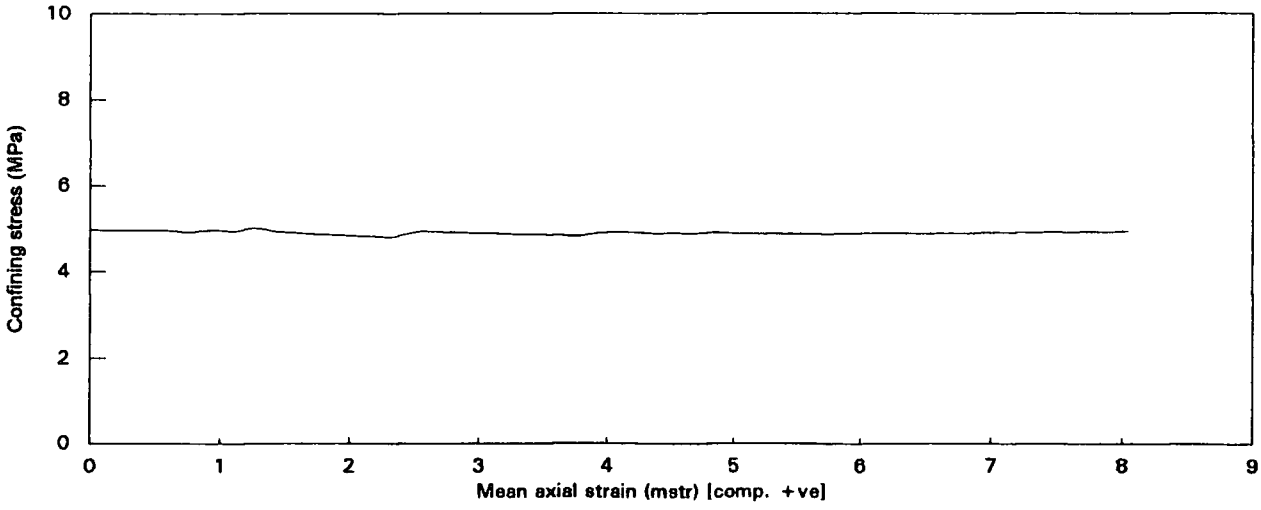

Fig.5.4.4f - Top) Axial stress versus axial strain **Centre)** Mean radial strain versus axial strain **Lower)** Confining stress versus axial strain

then caught the suspended and finest fraction which was then analysed over a 2θ angle range of 2°-14° (where most of the primary clay peaks occur).

The TOC of each sample was determined by taking relative weight % of powdered sample before and after heating. The powdered fractions were <600μm and 1g of powder was heated in a ceramic crucible. Two heating runs were employed: The first which heated the sample at a constant 350°C for 3 hours; the second run utilised a temperature of 950°C for 20 hours to break down and burn off any residual carbon that may have remained after the first heating run. Weights were taken after both heating runs. All preparation and analyses were carried out at the Department of Geological Sciences , University of Durham.

5.5.3 Results of the XRD bulk analyses and supplementary clay separates

XRD analyses utilised a 2θ range of 2° to 60° to analyse and record all major minerals likely to be present in these samples (60° onwards records mainly exotic and secondary and tertiary peaks). A summary of the relative % quoted minerals were determined for all samples in Table t5.5.3a. In addition, reference Table t.5.5.3b lists the quoted major identified minerals with their respective diffraction peaks in terms of 2θ angle, d-spacing (Å) and if the particular peak reflects the primary or secondary peaks.

Table t5.5.3a

MINERALS	PEAKS - data (2θ angle(°)/d-spacing (Å), peak type -primary/secondary)
QUARTZ (Q)	26.7/3.342 (Primary)
	20.9/4.257 (Secondary)
CALCITE (C)	29.5/3.035 (Primary)
	39.4/2.285 (Secondary)
FERROAN DOLOMITE (FD)	31.0/2.899 (Primary)
BOEHMITE (B) - Control 10wt%	14.5/6.11 (Primary)
	28.2/3.164 (Secondary)
	38.4/2.346 (Secondary)
DOLOMITE (D)	30.8/2.886 (Primary)
	41.2/2.192 (Secondary)
MIXED LAYERED CLAYS (MLC)	5→14 - see separate data set
PLAGIOCLASE FELDSPARS (PF)	28.0/3.112 (Primary)
	22.1/4.001 (Secondary)
ORTHOCLASE (O)	26.9/3.31 (Primary)
	23.6/3.77 (Primary)

21.05/4.24 (Secondary)

UNIDENTIFIED BACKGROUND
(UB)

Table t5.5.3b Bulk Analyses (%) taking major named minerals

Sample	Q	C	FD	B	D	MLC	PF	O	UB
EX1	25	15	-	10	20	15	5	2	8
EX5	24	10	13	10	9	12	4	6	12
EX6	19	8	14	10	8	13	8	4	13
EX8	20	9	13	10	7	15	7	4	15
EX10	24	9	-	10	18	16	6	4	14
IU8	18	18	-	10	12	15	10	3	17
IU6	26	13	-	10	14	9	4	4	23
2583	26	14	-	10	18	11	10	3	9

5.5.4 Discussion of bulk composition results

Primary peaks identified on the XRD profiles were fairly consistent throughout the sample set with the quartz 26.7°, calcite 29.5° and the ferroan dolomite/dolomite 31.0° /30.8° 2θ angles being dominant. Boehmite, was injected and homogenised at 10wt% into each sample for reference and control purposes and recorded the expected primary peak at 14.5° 2θ. The clay peaks which included basal chlorite, kaolinite, montmorillonite, illite (Im and tetragonal) and smectite mixed layer clays were consistently observed as a series of high background but suppressed individual peaks in the range of 2-14° 2θ. For this purpose, this range was grouped together as mixed layer clays but a supplementary analysis of the finer fraction was conducted to differentiate any peaks suppressed by the bulk mineralogy.

Feldspars of both the plagioclase series and orthoclase were identified and typically constituted joint values of less 14% bulk composition. Background peaks which were not prominent enough to extract an accurate identification were classified as unidentified background minerals. Sulphide peaks were checked as were minerals such as glauconite, to ascertain any information regarding the oxidising/reducing environment of mineral formation, but no prominent peaks were seen for these minerals. Quartz, in relative % terms, is consistently the largest mineral fraction in all samples with ranges between 18% (EX10) and 26% (2583). Calcite primary peaks and associated secondary peaks observes a range of 8% (EX6) to 18% (IU8). Ferroan Dolomite seems either to occur in relatively large amounts (13-14%, EX5, EX6 and EX8) or is completely absent (or in negligible amounts) in all other samples.

Background profiling accounts for up to 23% (IU8) but typically has a mean value of 13%.

5.5.5 Relationship of bulk composition (XRD determined) with mechanical parameters

Section 5.4 defined 3 groups of samples upon the peak strength parameters, deformation capabilities and style/patterns of deformation with respect to stress accommodation and recovery.

Sample Set EX6, EX8 and IU8:

This sample set characteristically displayed relatively low peak strength parameters associated with low cohesion values and tensile strengths. Their respective deformation patterns, with increasing imposed axial stress and confining stress fell into a recognised pattern and predictability (section 5.4). Samples EX6 and EX8 show very similar compositions and both are rich in ferroan dolomite at the apparent expense of pure dolomite and calcite. Sample IU8 appears devoid of ferroan dolomite and thus no relationship can be drawn from the presence/abundance of this mineral. The only consistently highly occurring mineral common to all three samples is quartz/silica in abundances of 19%, 20% and 18% for samples EX6, EX8 and IU8 respectively.

Sample Set IU6, 2583 and EX10:

This sample set is seen as having common deformation and mechanical patterns and a similar range of mechanical capacities (section 5.4). This sample set has similar compositions of calcite and dolomite with IU6 and 2583 having markedly higher quartz values of 24% and 26% respectively. EX10, however, only records 18% quartz/silica. Again, no definite pattern emerges for this sample set when correlating the XRD determined bulk analyses against the mechanical properties which define the grouping of these samples.

Sample Set EX1 and EX5:

EX5 contains ferroan dolomite whereas this mineral is absent from EX1. This relationship has an effect on pure dolomite where EX5 has a relatively low amount and EX1 is relatively enriched. The only mineral composition which shows a consistency in relative amounts is quartz/silica. This amount of quartz (24-25%) is markedly higher than that recorded for sample set EX6, EX8, IU8 (18-20%) but is approximately in the same range as IU6 and 2583.

5.5.6 Discussion of the Sample Sets

It has already been observed that EX6, EX8 and IU8 are less coherent with respect to deformation parameters than all other samples. These samples also show a consistently lower relative composition of quartz with respect to the samples belonging to the higher mechanically capable sample sets. Although this observation could be coincidental with only a small data set quartz and neomorphose silica would be expected to affect the peak strength of materials. Since quartz/silica does not have a preferred orientation of fracture, neomorphic silica which could act to bridge pore space and seal free floating grains, thereby possibly attaining a higher mechanical capacity. The effect of neoformational silica may also limit the amount of grain slippage on the application of stress and thus increase the cohesion. Clearly EX6, EX8 and IU8 have low cohesion and tensile strength properties which might be linked to relative amount of quartz and, in particular, neoformational silica. However, this might be a product of fabric rather than of mineralogy and investigative techniques such as Scanning Electron Microscopy (SEM) may be of use in testing such theories. Indeed, sample EX10, which displays high deformation parameters and a deformational pattern which is categorised along with other mechanically coherent samples, has a low amount of quartz. This quartz may be composed of different polymorphs and thus may give different results. However, no clear correlation can be drawn between peak strength and relative % quartz in the bulk composition of these materials.

5.5.7 Results and Discussion of the Clay Separates (2→14° 2θ unless stated)

Table t5.5.7a

MINERALS	PEAKS - data (2θ angle(°)/d-spacing (Å), peak type -primary/secondary)
ILLITE (Im) (I)	8.8/10.0 (Primary)
	8.9/9.964 (Primary)
SMECTITE-KAOLINITE (SK)	12.2/7.24 (Primary)
KAOLINITE (K)	12.4/7.1 (Primary)
	25.0/3.56 (Secondary)
CHLORITE (001 basal) (C)	6.2/14.2 (Primary)
MONTMORILLINITE (M)	5.9/15.0 (Primary)
	6.5/13.6 (Primary)

Table t5.5.7b Clays Analyses (%) taking major named clays (ML - Mixed Layered Clays)

Sample	I	SK	K	C	M	ML
EX1	15	7	-	-	11	77
EX5	12	8	8	4	10	58
EX6	8	10	6	8	18	56
EX8	12	8	4	2	17	57
EX10	14	8	4	-	-	74
IU6	23	6	26	-	28	17
IU8	28	9	-	-	16	47
2583	28	9	-	-	16	47

Even using separating techniques to bias the clay peaks, the analyses show that unidentified mixed layered clays dominate and mask/suppress any individual peaks. Sample IU6 returned a profile with sizeable peaks at the illite, kaolinite and montmorillinite positions. The sample set of EX6, EX8 and IU8 consistently returned low amounts of illite but of no great difference to the other analysed materials. Illite is recognised as a permeability occluding mineral, in its 'hairy' form, and its neoformational growth is random thus effectively reducing free pore space. It is, however, unlikely that this fabric and morphology of this clay could affect the strength of a material. However, the growth of illite might be seen to increase cohesion and decrease grain slippage by virtue of its growth character. There is insufficient data in this study to draw any relationship between clay type and mechanical strength.

5.5.8 Results and Discussion of Total Organic Carbon (TOC) Analyses

Table t5.5.8a

SAMPLE	TOC (weight %)
EX1	1.88
EX5	1.98
EX6	3.00
EX8	3.12
EX10	1.14
IU6	0.79
IU8	2.66
2583	1.24

Observing the above data, it is clear that certain samples contain different amounts of organic carbon. Importantly, samples EX6, EX8 and IU8 contain TOC's of 3.00%,

3.12% and 2.66% respectively which are, on average, are 32% more enriched in organic carbon than the next enriched sample (EX5 - 1.98% TOC). Samples EX6, EX8 and IU8 also belong to the sample set identified as having the lowest peak strength values, deformation parameters, cohesion and internal friction angles. All other samples analysed for TOC show an approximate correlation with peak strength and cohesion/tensile strength correlating with decreasing TOC.

Although accounting for the lack of data to substantiate such a correlation, Sellars et al. (1972) recognised the significance of kerogen in determining the compressive strength and Young's Modulus. Sellars et al. (1972) and Zeuch (1983) explained the variation and scatter of data, notably compressive strength decreasing with increasing kerogen content, as a consequence of 'in situ' organic carbon.

Depending upon the specific composition and chemistry of the organic carbon and its physical state, it is insufficient to conclude that organic carbon content will affect the inherent strength of a rock. Detailed work regarding the precursor organic material, state of thermal maturity and any hydrocarbon potential could further define a relationship. However, organic carbon may be inferred to reduce cohesion by its physical state (viscous, non viscous, gaseous) and its particular mineral crystal lattice (by possessing cleavage planes). The interaction with other fluids in the material could also be an important factor in the reduction of the peak strength. R.Marsden (pers.comm.) reported that, simulating drilling fluid interaction with wall rocks, in alkaline conditions, organic carbon acts as a catalyst in making the alkaline fluids act as a dispersant and a reactant with the clays in the material. This dispersing effect would reduce the cohesion, friction angle and tensile strength of a clay rich material and increasing the TOC would increase this effect. This theory may be crucial in explaining the results found in this study.

5.6 Conclusions and synthesis of the study of triaxial compression tests with XRD and TOC analyses of shale samples from the Uinta Basin, Utah

5.6.1 Deformation patterns and physical parameters

The effects of elevated axial stress and confining pressures on the deformational patterns, parameters and peak strength parameters (both Mohr-Coulomb and Hoek-Brown criteria) were investigated at ambient room temperatures and under drained conditions. Peak Strength was seen to increase with increasing confining stress but the relationship of this stress accommodation (linear, geometric or polynomial) was recognised as differing and several sample sets were defined upon their deformation relationship of stress versus strain. Three samples EX6, EX8 and IU8 followed a

predictable deformation pattern of strain with increasing axial stress. These samples show an initial strain of 2-3 millistrains during the 10-20MPa confining stress load period. This changes to 5 millistrains during 20-30MPa confining stress and remains at this rate of deformation until the 40MPa maximum confining stress is reached. Similarly, the pattern of stress accommodation has an initial approximately linear relationship with strain but adopts a more exponential relationship as axial stress is increased. At high axial stresses, these samples require little increased axial stress in order to deform and record increased strain until confining stress adjusts the effective stress imposed on the material which allows some component recovery. Three samples have very low cohesion values, friction angles, deformation parameters and tensile strengths.

Samples IU6, 2583 and EX10 have cohesion values in the range of 29-51MPa and have an approximate loading linear relationship between axial stress and axial strain. However, at high confining stress (eg. radial recovery becomes increasing small possibly reflecting the loss of elasticity of the material).

Sample set EX1 and EX5 record highest estimated uniaxial compressive strengths and also display highest tensile strengths. The capacity to accommodate imposed stress is also high observing 11 millistrains before yield is approached. Confining stress was increased through the entire test range of 5-40MPa in less than 5 millistrains, reflecting the capacity and strength of these two materials, up to the peak strengths of 414.5MPa (EX1) and 395.3MPa (EX5).

5.6.2 XRD correlation with mechanical strength

When relative mineral compositions were calculated using X-ray diffraction to identify constituent minerals, no clear emergent pattern could be drawn when correlating mineralogy with the deformation and mechanical data. However, a coincidental relationship of quartz/silica abundance showed that the lowest amounts of quartz were identified in sample set **EX6**, **EX8** and **IU8** (19%, 20% and 18% respectively) and increased with samples **EX5** and **EX1** (24% and 25% respectively). It has been argued that quartz and, in particular, neoformational silica could possibly increase the mechanical cohesion and capacity by effectively bridging free pore space and thus increase internal friction by limiting grain slippage under stress. However, this relationship is unclear and the size of the dataset does not support a conclusive theory.

Clay separates were analysed but recognisable peaks were suppressed as a result as a result of the high percentage of mixed layer clay. This is indicative of the growth of

amorphous clays (R.Hardy, pers.comm.). Again, no relationship could be drawn from the clay analyses and the mechanical capacity of these samples.

5.6.3 TOC correlation with mechanical strength

The analyses of Total Organic Carbon (TOC) showed a relatively good relationship with the mechanical test data. The sample set EX6, EX8 and IU8 (which were observed to be the most mechanically weak materials) recorded markedly higher %TOC, values in the region of 2.6-3.1%. These values were much higher than all of the other analysed samples and a relationship between the amount of organic carbon and the strength of the material is thought to exist. This is possibly a result of the interaction of alkaline fluids with organic carbon to produce a dispersant which then acts upon and causes a reduction of cohesion of residual clays.

5.6.4 Overall Conclusions

Although a relationship between TOC and mechanical capacity of core material from the Green River Formation in the Uinta Basin, Utah, is observed in this study, further investigation would possibly reveal more positive and conclusive trends. Organic Carbon would be sensitive to temperature. Increasing temperature would increase the ductility and decrease the compressive strength of an oil shale (Swan et al., 1989). Further investigation (eg. SEM) would help clarify these relationships, but were beyond the scope of this study.

Chapter 6
Principle conclusions to the chapters and of this thesis

6.1 Conclusions regarding the overpressure genesis, likely processes and distribution in the Alwyn Field

Present day observations of reservoir pressure define 3 distinct pressure cells that operate to compartmentalise the Brent reservoir in the Alwyn Field of the Northern North Sea. These are the Alwyn North, South and South East fields experiencing lowest to highest overpressures respectively. A study of maturity indices and biomarker trends reveal the Viking Graben as the most likely source area for the reservoired hydrocarbons. Maturity has been modelled in this source area and the potential for generating and expelling hydrocarbons from 90Ma to the present day is proposed.

Aqueous and hydrocarbon fluid inclusions identified at specific diagenetic positions have been used to estimate palaeo-temperature and pressure conditions in the reservoir at the time of diagenesis and fluid flow. Interpretation of the inclusion data indicate entrapment of fluids in the reservoirs at elevated temperatures but at hydrostatic pressures. A constraint on the timing of these events was made possible using illite age dates. Therefore, it was concluded that hydrostatic pressure conditions were operative at 75-65Ma in the Alwyn North field and 55-45Ma in the Alwyn South East field. Independent pressure modelling through time utilising a 1-D software programme also showed hydrostatic conditions likely at these times.

Fluid flow into the reservoir was inferred to be controlled by the pressure differential between fluid source and sink with faults acting as transient seals and conduits to account for the pressure distribution.

The combination of the rock data and computer based simulations of maturation and pressure history suggested the pressure distribution observed in the Alwyn Field as a result of the proximity of each pressure compartment to the gas generative Viking Graben. In addition, an elevation of overpressure, during the final phase of burial from approximately 10Ma to Present, of approximately 9-11MPa was observed to affect the entire Alwyn area due to compaction disequilibrium.

The Alwyn Field study has utilised both real time and rock data and the interpretation provided by independent computer simulations to assess the fluid flow and pressure history that has been operating both regionally and locally. Organic geochemistry,

diagenetic observations and basin modelling provided the basis on which the study developed. The Alwyn study has shown that the lines of investigation are available to constrain and assess the generation, maintenance and distribution of overpressure within and outwith an oil field.

6.2 Conclusions regarding the burial, maturation and pressure history and the emplacement of gilsonite veins in the Uinta Basin, Utah

Direct field observations of gilsonite veins in the Uinta Basin acted as a reliable source of information to which interpretation regarding likely emplacement mechanisms could be fed back into the geochemical, burial and kinetic modelling. The Uinta Basin, with a relatively simple tectonic and thermal history, allowed a model to develop to incorporate a temporal history of overpressure generation and depletion, fracture development, regional tectonism, hydrocarbon expulsion and migration and the process of gilsonite vein emplacement.

Organic maturity indicators identified the likely source area for both the gilsonite and other distally reservoired hydrocarbons as the Mahogany Oil Zone (MOZ) of the Green River Formation. Maturation and kinetic modelling of the organic source horizons of the Douglas Creek Member and the Mahogany Oil Zone of the Green River Formation correlated with the geochemical information in assigning an early mature (VRE 0.5-0.7 %Ro) signature to the source horizons at the computer derived point where maximum overpressure was generated due to compaction disequilibrium.

Hydraulic fracturing of the Green River Formation and the overlying formations was inferred to be a result of combined overpressure due to compaction disequilibrium at approximately 25-20Ma and regional extension operating NE-SW. After this initial fracturing, early mature products pervaded these vertical fractures. Dependant upon individual physical properties, fractionation of these early mature compounds took place which left the immobile and viscous compounds (gilsonite).

The Uinta Basin study took advantage of field exposures to observe likely emplacement mechanisms and host rock relationships. The Uinta Basin study incorporated regional fluid flow, stratigraphic and thermal information.

6.3 Conclusions of the study of triaxial compression tests and XRD and TOC analyses of shale samples of the Green River Formation, Uinta Basin

Several sample sets were defined upon the deformation patterns they exhibited under increasing axial and radial loading. A relationship between mechanical capacity and

physical parameters was an obvious correlation showing samples with lowest mechanical capacities having lowest cohesion values, friction angles and tensile strengths.

When attempting to demonstrate some association between rock strength and mineralogy of the tested samples, XRD analyses of both bulk composition and clay separates did not show any conclusive relationship. Although, increasing percentage of silica did provide a very loose relationship with peak strength. This was deemed a possible effect of neoformational quartz increasing internal cohesion by bridging free pore space.

A better correlation was seen by the TOC analyses. Sample set EX6, EX8 and IU8 (which were observed to be the most mechanically weak materials) recorded markedly higher TOC values in the region of 2.6-3.1%. A relationship between the amount of organic carbon and the strength of the material is therefore thought to exist. This is possibly the result of the interaction of alkaline fluids with organic carbon to produce a dispersant which then acts upon and causes a reduction in the cohesion of the residual clays.

The study was undertaken to observe the physical parameters of a sealing formation (the Green River Formation). The study incorporated markedly different investigative techniques than the previous studies on the Alwyn Field and the Uinta Basin. Although these studies recognised the need to combine data to realise the overpressure history and distribution of an oil field and basin, an understanding of the capacities of the sealing formation was deemed important enough to observe any potential correlation between the mechanical strength and the compositional differences in the sealing formation.

6.4 Overall Conclusions

The studies and models presented here are considered to be reasonable representations of the fluid flow and pressure evolution of selected oil fields in the North Sea and Uinta Basin. These models are not unique solutions. A reasonable model is one which is plausible or satisfactory in most respects given the information and interpretative techniques available. Modelling by definition is a representative simulation of a process for which it is not possible to verify all the input parameters. This is purely due to the dataset and the uncertainty about the choice of values for certain parameters and the necessary chosen assumptions.

References

Abraham H. (1945) Asphalts and allied substances - *their occurence, modes of production, using the arts and methods of testing: 5th edition.* D.Van Nostrand Co. New York 1, 887p.

Altman J. (1967) Spectral flourescence charts. *SPE Paper* **606**, 75-89.

Anders D.E. and Gerrild P.M. (1988) Hydrocarbon generation in lacustrine rocks of Tertiary age, Uinta Basin, Utah - organic carbon, pyrolysis yield and light hydrocarbons. in: Woodward J., Meisnner F.F. and Clayton J.L. (eds.) *Hydrocarbon source rocks of the greater Rocky Mountain region.* Denver Rocky Mtn. Assoc. of Geologists, 513-529.

Anders D.E., Palacas J.G. and Johnson R.C. (1992) Thermal maturity of rocks and hydrocarbon deposits, Uinta Basin, Utah. in: Fouch T.D., Nuccio V.F. and Chidsey T.C Jr. (eds.) *Hydrocarbon and mineral resources of the Uinta Basin, Utah and Colorado.* Utah Geol.Assoc. Guidebook **20**,

Anderton R., Bridges P.H., Leeder M.R. and Sellwood B.W. (1980) *A dynamic stratigraphy of the British Isles.* Allen and Unwin, London, 301p.

Aplin A.C., Warren E.A., Grant S.M. and Robinson A.G. (1993) Mechanisms of quartz cementations in North Sea reservoir sandstones: constraints from fluid compositions. in: Horbury A.D. and Robinson A.G. (eds.) *Diagenesis and basin development.* AAPG studies in Geology **36**, 7-22.

Audet M. and McConnell D. (1992) Forward modelling of porosity and pore pressure evolution in sedimentary basins. *Basin Research* **4**, 147-162.

Baldwin B. and Butler C.O. (1985) Compaction curves. *Am.Assoc.Pet.Geol.Bull.* **69**, 622-626.

Barker C. (1972) Aquathermal pressuring - a role of temperature in development of abnormal-pressure zones. *Am.Assoc.Pet.Geol.Bull.* **56**, 2068-2071.

Barker C. (1987) Development of abnormal and subnormal pressures in reservoirs containing bacterially generated gas. *Am.Assoc.Pet.Geol.Bull.* **71**, 1404-1413.

Barker C. (1990) Calculated volume and pressure changes during the thermal cracking of oil to gas in reservoirs. *Am.Assoc.Pet.Geol.Bull.* **74**, 1254-1261.

Bethke C.M. (1986) Inverse hydologic analysis of the distribution and origin of Gulf Coast type overpressured zones. *Journal Geophys. Res.* **91**, 6535-6545.

Bjorlykke K. and Egeberg P.K. (1993) Quartz cementation in sedimentary in sandstones, North Sea and Haltenbanken basins. *Am.Assoc.Pet.Geol.Bull.* **77**, 1538-1548.

Boles J.R. and Franks S.G. (1979) Clay diagenesis in Wilcox sandstones of south west Texas: Implications of smectite diagenesis on sandstone cementation. *J.Sed.Pet.* **49**, 55-70.

Bostick N. (1973) Time as a factor in thermal metamorphism of phytoclasts (coaly particles). *Congr.Int.Strat.Geol.Carbon.* Krefeld Maastricht **2**, 183-193.

Bradley W.H. (1931) Origin of microfossils of the oil shale of the Green River Formation of Colorado and Utah: U.S.G.S. *Professional paper* **168**, 58p.

Brigaud F. and Vasseur G. (1989) Mineralogy, porosity and fluid control on thermal conductivity of sedimentary rocks. *Geophys. Journal* **98**, 525-542.

Brooks J. and Glennie K.W. (1987) eds. *Petroleum Geology of North West Europe.* Graham & Trotman, London.

Bruce C.H. (1984) Smectite dehydration - its relation to structural development and hydrocarbon accumulation in northern Gulf of Mexico basin. *Am.Assoc.Pet.Geol.Bull.* **68**, 673-683.

Buchardt B. (1978) Oxygen isotope palaeotemperatures from the Teriary period in the North Sea area. *Nature* **275**, 121-123.

Buhrig C. (1989) Geopressured Jurassic reservoirs in the Viking Graben: modelling and geological significance. *Marine and Pet.Geol.* **6**, 31-48.

Burnham A.K., Braun R.L. and Gregg H.R. (1987) Comparison of method from measuring kerogen pyrolysis rates and fitting kinetic parameters. *J.Energy and Fuels* **1**, 452-458.

Burnham A.K. and Braun R.L. (1990) Development of a detailed model of petroleum formation, destruction and expulsion from lacustrine and marine source rocks. *Adv.Org. Geochem.* **16**, 27-39.

Burnham A.K. (1991) Oil evolution from a self purging reactor: kinetics and composition at 2°C/min and 2°C/hr. *J.Energy and Fuels* **5**, 205-214.

Burley S.E., Mullis J. and Matter A. (1989) Timing diagenesis in the Tartan Reservoir (UK North Sea): constraints from combined cathodoluminescence microscopy and fluid inclusion studies. *Marine and Pet.Geol.* **6**, 98-120.

Burrus R.C (1992) Phase behaviour in petroleum-water (brine) systems applid to fluid inclusion studies (abs.). Presented at the *4th biennial Pan-American conference on research on fluid inclusions*, May 1992, 116-118.

Burst J.F. (1969) Diagenesis of Gulf Coast clayey sediemnts and its possible relation to petroleum migration. *Am.Assoc.Pet.Geol.Bull.* **53**, 73-93.

Campbell J.A. (1975) Structural geology and petroleum potential of the south flank of the Uinta Mountain uplift, north east Utah. *Utah Geology* **2**, 129-132.

Carstens H. and Dypvik H. (1981) Abnormal formation pressure and shale porosity. *Am.Assoc.Pet.Geol.Bull.* **71**, 368-388.

Cashion W.B. (1967) Geology and fuel resources of the Green River Formation, southeastern Uinta Basin, Utah and Colorado. *US Geol.Surv. Professional Paper* **548**, 48p.

Chapman D.S., Keho T.H, Bauer M.S and Picard M.D. (1984) Heat flow in the Uinta Basin detremined from bottom hole temepartures (BHT's) data. *Geophysics* **49**, 453-466.

Chidsey T.C. and Laine M.D. (1992) The fractured Green River and Wasatch Formations of the Uinta Basins, Utah: Targets for horizontal drilling. in: Fouch T.D., Nuccio V.F. and Chidsey T.C Jr. (eds.) *Hydrocarbon and mineral resources of the Uinta Basin, Utah and Colorado.* Utah Geol.Assoc. Guidebook **20**.

Colton-Bradley V.A. (1987) Role of pressure in smectite dehydration - effects on geopressure and smectite to illite transformation. *Am.Assoc.Pet.Geol.Bull.* 71, 1414-1427.

Crawford A.L. (1979) (ed) Oil and Gas possibilities of Utah re-evaluated. *Utah Geol. Mineral Surv. Bull.* **54**.

Crawford A.L., Praitt R.G. and Campbell J.A. (1979) Gilsonite and other mineral resources of Central Uinta County, Utah. in: Crawford A.L. (ed) Oil and Gas possibilities of Utah re-evaluated. *Utah Geol. Mineral Surv. Bull.* **54**, 215-224.

Daines S. (1982) Aquathermal pressuring and geopressure evaluation. *Am.Assoc.Pet.Geol.Bull.* **66**, 931-939.

Dalrymple G.B and Lanphere M.A. (1969) *Potassium-Argon dating.* W.H. Freemann San Francisco 258p.

Davis L.J. (1957) Geology of gilsonite. *Intermountain Assoc.Pet.Geol.* 8th Annual Field Conference, 152-156.

Deaton B.C. (1987) Quantification of rock color from Munsell chips. *J.Sed.Pet.* **57**, 774-776.

Didyk B.M. and Simoneit B.R.T. (1989) Hydrothermal oil of Guaymas Basin and implications for petroleum formation mechanisms. *Nature* **342**, 65-68.

Du Rochet J. (1981) Stess fields, a key to oil migration. *Am.Assoc.Pet.Geol.Bull.* **65**, 79-99.

Dutta N.C. (1983) Shale compaction, burial diagenesis and geopressures: a dynamic model, solution and some results (abs.). *53rd annual meeting of SEG*, Las Vegas, 149-172.

Dykstra J. (1987) Compaction correction for burial history curves: application to Lopatin's method for source rock maturation determination. *Geobyte* November, 16-23.

Eldridge J. (1901) The apshalt and bitumenous rock deposits of the United States. in: Walcott C.D. (ed.) *US Geol.Surv. 22nd annual report*, 209-464.

Elliot W.C., Aronson J.L., Matisoff G. and Gautier D.L. (1991) Kinetics of the smectite to illite transformation in the Denver Basin: clay minerals, K-Ar data and the mathematical model results. *Am.Assoc.Pet.Geol.Bull.* **75**, 436-462.

England W.A., Mackenzie A.S., Mann D.M. and Quigley T.M. (1987) The movement and entrapment of petroleum fluids in the subsurface. *J.Geol.Soc.* **144**, 327-347.

England W.A. and Mackenzie A.S (1989) Some aspects of the organic geochemistry of petroleum fluids. *Geologische Rundschau* **78**, 191-208.

Espitalite J., Deroo G. and Marquis F. (1985) La pyrolyse Rock-Eval et ses applications. *Revue de L'Institut Francais du Petrole* **40**, 563-579.

Falvey D.G. and Middleton M.F. (1981) Passive continental margins: evidence for a pre-breakup deep crustal metamorphic subsudence mechanism. *Oceanol.Acta.* **5**, 103-114.

Faure G. (1986) *Priciples of isotope geology.* 2nd edn. Wiley, New York, 589p.

Forbes P.L., Ungerer P. and Mudford B.S. (1992) A two-dimensional model of overpressure development and gas accumulation in Venture Field, eastern Canada. *Am.Assoc.Pet.Geol.Bull.* **76**, 318-338.

Fouch T.D., Cashia W.B., Ryder R.T. and Campbell J.A. (1975) Lthofacies and related hydrocarbon accumulations in Tertiary strata of the western and central Uinta Basin, Utah. in: Bolgard, D.W. (ed.) *Symposium on deep drilling frontiers in the central Rocky Mountains.* Rocky Mtn.Assoc.Geol.Bull., 163-173.

Fouch T.D., Wandrey C.J., Pitman J.K., Nuccio V.F., Schomker J.W., Rice D.D., Johnson R.C. and Dolton G.L. (1992) Natural gas accumulations in low permeability Tertairy and Cretaceous rocks, Uinta Basin, Utah. *US Department of Energy Contract* A121-83MC 20422, 64p.

Fouch T.D., Nuccio V.F., Osmond J.C., MacMillan L., Cashion W.B. and Wandrey C.J. (1992) Oil and gas in uppermost Cretaceous and Tertiary rock, Uinta Basin, Utah. in: Fouch T.D., Nuccio V.F. and Chidsey T.C Jr. (eds.) *Hydrocarbon and mineral resources of the Uinta Basin, Utah and Colorado.* Utah Geol.Assoc. Guidebook **20**, 9-47.

Freed R.L. and Peacor D.R. (1989) Geopressured shale and sealing effect of smectite to illite transformation. *Am.Assoc.Pet.Geol.Bull.* **73**, 1223-1232.

Glaso O. (1980) Generalised pressure - volume - temperature correlations. *Journal of Pet. Tech.*, 785-795.

Grauls D. and Cassignol C (1993) Identification of a zone of fluid pressure-induced fractures from log and seismic data - a case history. *First Break* **11**, 12-23.

Haas J.L. (1978) An empirical equation with tables of smoothed solibilities of methane in water and aqueous sodium chloride solutions up to 25 weight percent, 360° C and 138MPa. *US Geol.Surv. Open File Report* 78-1004, 41p.

Hagan E.S. and Surdam R.C. (1989) Thermal evolution of Laramide-style basins: constraints from the northern Bighorn Basin, Wyoming and Montana. in: Naeser N.D. and McCulloh T.H. (eds.) *Thermal history of sedimentary basins: methods and case histories* 277-296, Springer-Verlag, New York.

Hamilton P.J., Giles M.R. and Ainsworth P. (1992) K-Ar dating of illites in Brent Group reservoirs: a regional perspective. in: Morton A.C., Haszeldine R.S., Giles M.R. and Brown S. (eds.) *Geology of the Brent Group. Geol.Soc.Spec.Pub.* 61.

Hamilton P.J., Kelly S. and Fallick A.E. (1989) Isotopic constraints on diagenetic processes: radiometric dating of illite in hydrocarbon reservoirs. *Clay Minerals* 24, 215-231.

Hancock J.M. and Scolle P.A. (1975) Chalk of the North Sea. in: Woodland A.W. (ed.) *Petroleum and the continental shelf of north west Europe*, 3-28.

Hanor J.S. (1980) Dissolved methane in sedimentary brines: potential effect on the PVT properties of fluid inclusions. *Econ.Geol.* 75, 603-617.

Hanshaw B.B. and Zen E. (1965) Osmotic equilibrium and overthrust faulting. *Am.Assoc.Pet.Geol.Bull.* 76, 156-165.

Harland W.B., Armstrong R.L., Cox A.V., Craig L.V., Smith A.G. and Smith D.G. (1990) A geologic timescale 1989. *Cambridge University Press, Cambridge.*

Haszeldine R.S., Brint J.F., Fallick A.E., Hamilton P.J. and Brown S. (1992) Open and restricted hydrologies in Brent Group diagenesis: North Sea. in: Morton A.C., Haszeldine R.S., Giles M.R. and Brown S. (eds.) *Geology of the Brent Group.* Geol.Soc.Spec.Pub. 61, 377-400.

Hatcher H.J., Meuzelaar H.L.C. and Urban D.T (1992) A composition of biomarkers in gilsonite, oil shale, tar sand and petroleum from threemile canyon and adjacent areas in the Uinta Basin, Utah. in: Fouch T.D., Nuccio V.F. and Chidsey T.C Jr. (eds.) *Hydrocarbon and mineral resources of the Uinta Basin, Utah and Colorado.* Utah Geol.Assoc. Guidebook **20**, 9-47.

Henderson J.H. (1957) The Gilsonite refining project of the American Gilsonite Company. ,*8th Annual Field Conference. Intermountain Assoc. of Geologists,* 157-160.

Hermanrud C. (1993) Basin modelling techniques - an overview. in: Dore A.G. (ed.) *Basin modelling: advances and applications.* NPF Spec.Pub. 3, 1-34.

Hogg A.J.C., Hamilton P.J. and Macintyre R.M. (1992a) Mapping diagenetic fluid flow within a reservoir: K-Ar dating in the Alwyn area (UK North Sea). *Marine and Pet.Geol.* **10**, 279-294.

Hogg A.J.C., Sellier E. and Jourdan A.J. (1992b) Cathodoluminescence of quartz cements in Brent Group sandstones, Alwyn South, UK North Sea. in: Morton A.C., Haszeldine R.S., Giles M.R. and Brown S. (eds.) *Geology of the Brent Group.* Geol.Soc.Spec.Pub. 61, 421-440.

Hoffman J. and Hower J. (1986) Clay mineral assemblages as low grade metamorphic geothermometers: apllication to the thrust faulted disturbed belt of Montana, USA. in: Scolle P.A. and Schluger P.R. (eds.) *Aspects of diagenesis.* Soc.Econ.Min.Spec.Pub. 26, 55-79.

Hollerbach A. and Hagemann H.W. (1981) Organic geochemical and petrological investigations into a sreies of coals with increasing ranks. *Proceedings Int.Conf. on Coal Science.* Dusseldorf 1981, Gluckauf GmbH, 80-85.

Horsfield B., Disko U. and Leistner F. (1989) The micro scale simulation of maturation: outline of a new technique and its practical applications. *Geol. Rundsch.* 78, 361-374.

Horstad I, Larter S.R., Dypvik H., Aagaard P., Johansen P.E. and Erikson S. (1990) Degradation and maturity on oil field petroleum colunm heterogeneity in the Gullfaks field, Norwegian North Sea. *Organic Geochemistry* 16, 497-510.

Hottman C.E. and Johnson R.K. (1965) Estimation of formation pressures from log-derived shale properties. *J.Pet.Tech.* 17, 717-722.

Hower J., Eslinger E.V. and Perry E.A. (1979) Mechanics of burial of metamorphism of argillaceous sediment: mineralogical and chemical evidence. *Geol. Soc. Am. Bull.* 87, 725-737.

Hubbert M.K. (1953) Entrapment of petroleum under hydrodynamic conditions. *Am.Assoc.Pet.Geol.Bull.* 37, 1954-2026.

Hunt J.M. (1963) Composition and origin of the Uinta Basin bitumens. Utah *Am.Assoc.Pet.Geol.Bull.* 54, 249-273.

Hunt J.M. (1979) Petroleum geochemistry and geology, San Francisco. W.H. Freeman, 617p.

Hunt J. (1990) Generation and migration of petroleum from abnormally pressured fluid compartments. *Am.Assoc.Pet.Geol.Bull.* 74, 1-12.

Hunt J.M., Lewan M.D. and Hennet R.J.C. (1991) Modelling oil generation with respect to time temperature index graphs based on the Arrhenius equation. *Am.Assoc.Pet.Geol.Bull.* 75, 795-807.

Inglis I. and Gerard J. (1991) The Alwyn North field, blocks 3/9a, 3/4a, UK North Sea. in: Abbotts B. (ed.) *United Kingdom oil and gas fields, 25 years commemorative volume.* Geol.Soc.Memoir 14, 21-32.

International Society for Rock Mechanics (1979) Suggested mthods for determining water content, porosity, density, adsorption and related properties and swelling and slake-durability index properties. *International Journal of Rock Mechanics, Mineral Science and Geomechanics* **16**, 141-156.

International Society for Rock Mechanics (1983) Suggested methods for determining the strength of rock materials in triaxial compression: revised version (abs.). *International Journal of Rock Mechanics, Mineral Science and Geomechanics* **20**, 283-290.

Jansa L.F. and Noguera Urrea V.H. (1990) Geology and diagenetic history of overpressured sandstone reservoirs, Venture gas field, offshore Nova Scotia, Canada. *Am.Assoc.Pet.Geol.Bull.* 74, 1640-1659.

Johnson A. and Eyssautier M. (1987) Alwyn Nort field and its regional geological context. in: Glennie K. and Brookes J. (eds.) *Petroleum geology of north west Europe*, 963-977.

Jones P.H. (1969) Hydrodynamics of geopressures in the northern Gulf of Mexico basin, *J.Pet.Tech.*

Jourdan A., Thomas M., Brevart O., Robson P., Sommer F. and Sullivan (1987) Diagenesis as the control of the Brent sandstone reservoir properties in the Greater Alwyn area (East Shetland Basin). in: Glennie K. and Brookes J. (eds.) *Petroleum geology of north west Europe*, 963-977.

Kappelmyer O and Haenel R. (1974) *Geothermics with special reference to application.* Borntraeger, Berlin, 238p.

Karlsen D.A. (1990) Petroleum heterogeneities in clastic reservoirs. *Unpublished Ph.D. Thesis, University of Oslo, Norway.*

Karlsen D.A. and Larter S.R. (1991) Analysis of petroleum fraction by TLC-FID: applications to petroleum reservoir description. *Organic Geochemistry* 17, 603-617.

Karlsen D.A., Nedkvitn T., Larter S.R. and Bjorlykke K. (1992) Hydrocaarbon composition of authigenic inclusions: application to elucidation of petroleum reservoir filling history. *Geochim.Cosmochim.Acta* 57, 3641-3659.

Karweil J. (1955) Die metamorphose der Kohlen vom Standpunkt der Physikalischein Chemie. *Z.Dtsh.Geol.Ges.* **107**, 132-139.

Klomp U.C. and Wright P.A. (1990) A new method for the measurement of kinetic parameters of hydrocarbon generation from source rocks. *Adv. in Organic Geochem.* **16**, 49-60.

Kent P.E. (1975) The tectonic development of Great Britain and the surrounding seas. in: Woodland A.W. (ed.) *Petroleum and the continental shelf of the north west Europe*, 3-28.

Khavari-Khoramsami G. (1989) Free hydrocarbons in Uinta Basin, Utah. *Am.Assoc.Pet.Geol.Bull.* **68**, 1193-1197.

Lang W. and Gelfand J.C. (1985) Evaluation of U.V. co-ordinates of potential deep-sea wild cat wells. *Log Analyst* **26**, 13-22.

Larter S.R., Bjorlykke K., Karlsen D.A., Nedkvitne T., Eglinton T., Johnson P.E., Leythaeuser D., Mason P.C., Mitchell A.W. and Newcombe G.A. (1990) Determination of petroleum accumulation histories: examples from the Ula field, Central Graben, Norwegian North Sea. in: Buller A.T. (ed.) *North Sea oil and gas reservoirs II*, Graham and Trotman, London 319-330.

Larter S.R. (1990) Molecular characterisation of kerogen - applications to primary and secondary migration studies and to maturation modelling. *Review of Palaeobotany and Palynology* **65**, 379-391.

Larter S.R. (1993) Petroleum reservoir fluid geochemistry - implications for understanding basin to pore scale phenomena (ads.). in: Parnell J., Ruffell A.H. and Moles N.R. (eds.) *Geofluids '93* conference, Torquay, England, 66-67.

Lerche I. (1993) Theoretical aspects of problems in basin modelling. in: Dore A.G. (ed.) *Basin modelling: advances and applications*. NPF Spec.Pub. **3**, 1-34.

Liewig N., Clauer N. and Sommer F. (1987) Datation isotopique K-Ar d'argiles diagenetique de reservoirs greseux: mise en evidence d'anomalie thermique du Lias inferieur on Europe nord-occidentale. *C.R. Acad.Sci. Paris* **304 II**, 707-711.

Lopatin N.V. (1971) Temperature and geological time as factors in coalification. *Izv.Akad.Nauk.SSSR, Ser.Geol.* **3**, 95-106.

Lou X. and Vassuer G. (1992) Contributions of compaction and aquathermal pressuring to geopressure and the influence of environmental conditions. *Am.Assoc.Pet.Geol.Bull.* **76**, 1550-1559.

Lou X. and Vassuer G. (1993) Contributions of compaction and aquathermal pressuring to geopressure and the influence of environmental conditions: reply. *Am.Assoc.Pet.Geol.Bull.* **76**, 1550-1559.

Lucas P.T. and Drexler J.M. (1976) Altamont-Bluebell - a major naturally fractured stratigraphic trap: *Am.Assoc.Pet.Geol. Memoirs* **24**, 121-135.

Ludvigson A., Gran K, Palm E. and Bjorlykke K. (1993) Effects of convection - currents on heat transfer in sedimentary basins. in: Dore A.G. (ed.) *Basin modelling: advances and applications*. NPF Spec.Pub. **3**, 1-34.

Lundegard P.D. and Travena A.S. (1990) Sandstone diagenesis in the Pattani Basin: history of water-rock interaction and comparison with the Gulf of Mexico. *Applied Geochemistry* **5**, 669-685.

Lundegard P.D., Travena A.S. and Land D.S. (1987) Influence of fluid chemistry and high geothermal gradient on sandstone diagenesis: Pottanu Basin, Gulf of Thailand (abs) *Am.Assoc.Pet.Geol.Bull.* 71, 586.

McLimans R.K. (1987) The application of fluid inclusions to migration of oil and diagenesis in petroleum reservoirs. *Applied Geochemistry* 2, 585-603.

Magara K. (1968) Subsurface fluid pressure profile, Nagaoka Plain, Japan. B*ulletin of the Japanese Petroleum Institute* 10, 1-7.

Magara K. (1974) Aquathermal fluid migration. *Am.Assoc.Pet.Geol.Bull.* 58, 283-290.

Magara K. (1975) Reevaluation of montmorillonite dehydration as the cause of overpressure and hydrocarbon migration. *Am.Assoc.Pet.Geol.Bull.* 59, 292-302.

Magara K. (1978) *Compaction and fluid migration - practical petroleum geology.* Elsevier, Amsterdam, 11-25.

Mandl G. and Harkness R.M. (1987) Hydrocarbon migration by hydraulic fracturing. in: Jones M.E. and Preston R.M.F. (eds.) *Deformation of sedimentary and sedimentary rocks.* Geol.Soc.Spec.Pub. 29, 39-53.

Mann D.M. and MacKenzie A.S. (1990) Prediction of pore fluid pressures in sedimentary basins. *Mar. and Pet. Geol.* 7, 55-65.

Meisnner F.F. (1987) Regional hydrocarbon generation, migration and accumulation patterns of Cretaceous strata, Powder River Basin. (abs) *Am.Assoc.Pet.Geol.Bull.* 69, 856.

Miller T.W and Luk C.H. (1993) Contributions of compaction and aquathermal pressuring to geopressure and the influence of environmental conditions: discussion. *Am.Assoc.Pet.Geol.Bull.* 76, 1550-1559.

Morton A.C., Haszeldine R.S., Giles M.R. and Brown S. (1992) (eds.) *Geology of the Brent Group.* Geol.Soc.Spec.Pub. 61.

Mouchet J.P and Mitchell A. (1989) Abnormal pressures while drilling: origins - prediction - detection - evaluation. Manuels techniques elf aquitaine 2. *Elf Aquitaine Edition, Boussens,* 264p.

Monson B. and Parnell J. (1992) The origin of gilsonite vein deposits in the Uinta Basin, Utah. in: Fouch T.D., Nuccio V.F. and Chidsey T.C Jr. (eds.) *Hydrocarbon and mineral resources of the Uinta Basin, Utah and Colorado.* Utah Geol.Assoc. Guidebook 20, 257-270.

Montigny R. (1985) Method classique potassium-argon. in: Poty B. and Roth E. (eds.) *Methods de dataion par les Phenomenes Nuclearities Naturels: applications.* Masson/ commissariat a l'Energie Atomique, Paris, 309-340.

Mudford B.S. (1990) A one-dimensional, two phase model of overpressure generation in the Venture gas field, offshore Nova Scotia. *Can.Pet.Geol.Bull.* 38, 246-258.

Mullis J. (1979) The system methane-water as a geologic thermomter and barometer from the external part of Central Alps. *Bull.Mineral.* 102, 526-536.

Narr W. and Burruss R.C. (1984) Origin of reservoir fractures in Little Knife Field, North Dakota. *Am.Assoc.Pet.Geol.Bull.* 68, 1087-1100.

Narr W. and Currie J.B. (1982) Origin of fracture porosity - example from Altamont field, Utah. *Am.Assoc.Pet.Geol.Bull.* 66, 1231-1247.

Osborne M. and Haszeldine S. (1993) Evidence for resetting of fluid inclusion temperatures from quartz cements in oildields. *Marine and Pet.Geol.* 9, 568-572.

Osmond J.C. (1964) New gas pipeline spurs, Uinta Basin exploration. *The oil and gas Journal,* April 1964, 130-134.

Osmond J.C. (1992) Greater Natural Buttes Gas Field, Uinta County, Utah. in: Fouch T.D., Nuccio V.F. and Chidsey T.C Jr. (eds.) *Hydrocarbon and mineral resources of the Uinta Basin, Utah and Colorado.* Utah Geol.Assoc. Guidebook 20.

Park R.G. (1989) *Foundations of structural geology.* Blackie, London, 130p.

Paxton S.T., Nardin T.R., Converse D.R. and Cayley G.T. (1993) North Sea fluid pressure distribution and effects upon Brent Group reservoir quality (abs.). *Conf. on diagenesis, overpressure and reservoir quality.* Cambridge, England.

Pearson M.J. and Small J.S. (1988) Illite-smectite diagenesis and palaeotemperatures in northern North Sea Quaternary to Mesozoic shale sequences. *Clay Minerals* 23, 109-132.

Peters K.E and Moldowan J.M.(1992) *The Biomarker Guide.* Prentice Hall, New Jersey, USA, 363p.

Philp B. (1985) Fossil fuel biomarkers. in: *Methods in Geochemistry and Geophysics.* Elsevier, Amsterdam, 294p.

Philp R.P., Jinggui L. and Lewis C.A. (1989) An organic geochemical investigation of crude oils from Shanganning Jianghan, Chaidamu and Zhungeer Basins.1 *Uinta Organic Geochemistry* 14, 447-460.

Pitman J.K., Franczyk K.J. and Anders D.E. (1982) Marine and non-marine gas bearing rocks in Upper Creraceous Blackhawk and Neslen Formations, eastern Uinta Basin, Utah: sedimentology, diagenesis and source rock potential. *Am.Assoc.Pet.Geol.Bull.* 71, 76-94.

Pittion J.L. (1987) *Synthesis of the organic geochemical studies in the Alwyn area.* Unpublished company report, Total CFP, Paris.

Plumley W.J. (1980) Abnormally high fluid pressure - survey of some basic pricipals. *Am.Assoc.Pet.Geol.Bull.* 64, 414-430.

Potter R.W. (1977) Pressure corrections for fluid inclusion homogenisation temperatures based on the volumetric properties of the system NaCl-H_2O. *J.Res. US Geol.Surv.* 5/5, 603-607.

Pagel M. and Poty B. (1984) The evidence of composition, temperature and pressure of sedimentary fluids over time: a fluid inclusion reconstruction. in: Durand B. (ed.) *Thermal phenomena in sedimentary basins*. Technip, 71-88.

Powers M.C. (1967) Fluid release mechanisms in compacting marine mudrocks and their importance in oil exploration. *Am.Assoc.Pet.Geol.Bull.* 51, 1240-1254.

Price N.J. (1974) The development of stress systems and fracture patterns on undeformed sediments. in: *Advances on rock mechanics 3rd International Congress on Rock Mechanics, Denver* 1, 497-508.

Price N.J., Fyfe W.S and Thompson W.S. (1978) *Fluids in the Earth's Crust.* Elsevier, Amsterdam, 308p.

Price L.C. (1982) Time as a factor in organic metamorphism and the use of vitrinite reflectance as an absolute palaeogeothermometer. *Am.Assoc.Pet.Geol.Bull.* 66, 619-620.

Price L.C. (1983) Geologic time as a parameter in organic metamorphism and vitrinite reflectance as an absolute palaeogeothermometer. *J.Pet.Geol.* 6, 5-38.

Prost J. and Rondelez F. (1991) Structures in colloidal physical chemistry. *Nature* 350, 11-23.

Pruitt R.G. (1961) The mineral resouces of Uinta County, Utah. *Utah Geol.Min. Survey Bull.* 71, 101p.

Pytte A.M. and Reynolds R.C. (1989) Thethermal transformation of smectite to illite. in: Naeser N.D. and McCulloh T.H. (eds.) *Thermal history of sedimentary basins: methods and case histories* 133-140, Springer-Verlag, New York.

Reynolds R.C. and Hower J. (1970) The nature if interlayering in mixed-layer illite montmorillonite. *Clays and Clay Minerals* 18, 25-55.

Reynolds J.G., Crawford R.W. and Burnham A.K. (1991) Analysis of oil shale and petroleum source rock pyrolysis by triple quadrupole mass spectrometry: comparisons of gas evolution at a heating rate of 10°C/min. *J. Energy and Fuels* 5, 507-523.

Riediger C.L., Fowler M.G., Brooks P.W. and Snowdon L.R. (1990) Triassic oils and potential Mesozoic source rocks, Peace River Arch area, Western Canada. in: Advances in Organic Geochemistry. 1989. *Org. Geochem.* 16, 295-305.

Ritzma B. (1974) Cross-section of south east Asphalt Ridge, Uintah County. in: Utah, energy and resources of the Uinta Basin. *Utah Geol.Assoc.Pub.* 4, 60p.

Robinson A. and Gluyas J. (1992) Duration of quartz cementation in sandstones, North Sea and Haltenbanken basins. *Marine and Pet.Geol.* 9, 324-328-7.

Robinson A., Grant S. and Oxtoby N. (1992) Evidence against natural deformation of fluid inclusions in diagenetic quartz. *Marine and Pet.Geol.* **9**, 568-572.

Roedder E. (1984) *Fluid Inclusions. in: Reviews in mineralogy* **12**. Mineral Soc.Am., Washington DC, 644p.

Rubey W.W. and Hubbert M.K. (1957) Overthrust belt in geosynclinal area of western Wyoming in light of fluid pressure hypothesis. *Geol.Soc.Am.Bull.* **70**, 167-206.

Rullkotter J., Spiro B. and Nissembaum A. (1985) Biological marker characteristics of oils and asphalts from carbonate source rocks in a rapidly subsiding graben, Dead Sea, Israel. *Geochem. et Cosmochimica Acta* **47**, 785-794.

Rybach L. (1986) Amount and significance of radioactive heat sources in sediments. in: Burrus J. (ed.) *Thermal modelling in petroleum in sedimentary basins.* Technip, Paris 311-322.

Saigal G.C., Bjorlykke K and Larter S.R. (1992) The effects of oil emplacement on diagenetic processes - examples from the Fulmar reservoir sandstones, Central North Sea. *Am.Assoc.Pet.Geol.Bull.* **76**, 1024-1033.

Schneider F., Burrus J. and Wolf, S. (1993) Modelling overpressures by effective stress/porosity relationships in low permeability rocks: empirical artifice or physical reality?. in: Dore A.G. (ed.) *Basin modelling: advances and applications.* NPF Spec.Pub. **3**, 1-34.

Sclater J.G. and Christie P.A.F. (1980) Continental stretching: an explanation of the post-mid Cretaceous subsidence of the Central North Sea basin. *J.Geophysics Res.* **85**, 3711-3739.

Sellers J.B., Haworth G.R. and Zambas P.G. (1972) Rock mechanics research on oil shale mining. *Trans. of the Am.Inst. of Mining, Metall. and Pet. Eng.* **252**, 222-232.

Shell Standard Legend (1976) Shell Internationale Petroleum Maatschappij B.V., The Hague.

Sibson R.H., Moore J. and Rankin A.H. (1975) Seismic pumping - a hydrothermal fluid transport mechanism. *J.Geol.Soc.* **131**, 635-359.

Smith J.E. (1971) The dynamics of shale compaction and the evaluation of pore fluid pressures. *Math.Geol.* **3**, 239-263.

Smith L. and Chapman D.S. (1983) On the thermal effects of ground water flow. Regional Scale Systems. *J.Geophys.Res.* **88**, 593-608.

Snarsky A.N. (1964) Relationship between primary migration and compaction of rocks. *Pet.Geol.* **5**, 362-364.

Sroden J. and Eberl D.D. (1984) Illite. in: Bailey S.W. (ed.) Micas. Reviews in mineralogy **13**, 495-544. *Mineralogical Soc.Am.*, Washington DC.

Spencer C.W. (1987) Hydrocarbon Generation as a mechanism for overpressuring in the Rocky Mountain Region. *Am.Assoc.Pet.Geol.Bull.* 71, 368-388.

Sommer F. (1978) Diagenesis of Jurassic sandstones in the Viking Graben. *J.Geol.Soc.* 135, 63-67.

Standing M.R. (1947) A pressure-volume-temperature correlation for mixtures of California oils and gases. *Presented at the 1947 meeting of the Pacific Coast District, division of production*, Standard Oil Company of California.

Stoneley R. (1983) Fibrous calcite veins, overpressures and primary oil migration. *Am.Assoc.Pet.Geol. Notes* 1983, 1427.

Stuart P. (1960) *Geopressures.* Shell Oil Company Production Department, New Orleans.

Swan G., Cook, J., Bruce S. and Meehan R. (1989) (abs.) Strain rate effects in Kiimerdige Bay shale. *International Journal of Rock Mechanics, Mineral Science and Geomechanics* 26, 135-149.

Sweeney J.J., Burnham A.K. and Braun R.L. (1987) A model of hydrocarbon maturation Type I kerogen: application to the Uinta Basin, Utah. *Am.Assoc.Pet.Geol.Bull.* 71, 967-985.

Sweeney J.J. and Burnham A.K. (1990) Evaluation of a simple model of vitrinite reflectance based on chemical kinetics. *Am.Assoc.Pet.Geol.Bull.* 74, 1559-1570.

Taylor J.M. (1950) Pore space reduction in sandstones. *Am.Assoc.Pet.Geol.Bull.* 34, 701-716.

Terzaghi K. (1923) Die Berechnung der durchlassigkeitsziffer des tones aus dem verlauf der hydrodynamischen spannungserscheinungen sitzungsgber. *Akad.Wiss.Wien.Math.Naturwiss.* 132, 125-138.

Terzaghi K. (1948) Soil mechanics in engineering practice. Wiley, New York, 566p.

Tissot B. (1969) Premieres donnees sur les mechanisms et al cinetique de la formation du petrole dans les sediments. *Rev.Inst.Fr.Pet.* 24, 470-501.

Tissot B. and Espotalie J. (1975) L'evolution thermique de la matiere organique des sediemnts: applications d'une simulation mathematique. *Rev.Inst.Fr.Pet.* 30, 713-777.

Tissot B., Deroo G. and Hood A. (1978) Geochemical study of the Uinta Basin - formation of petroleum from the Green River Formation. *Geochem. Cosmochim. Acta* 42, 1469-1489.

Tissot B.P., Pelet R. and Ungerer P.H. (1987) Thermal history of sedimentary basins, maturation indices and kinetics of oil and gas migration. *Am.Assoc.Pet.Geol.Bull.* 71, 1445-1466.

Tucker M.E. (1981) *Sedimentary Petrology - an introduction.* Blackwell Scientific Publications, 252p.

Twiss and Moores (1992) *Structural Geology.* WH Freeman, London, 532p.

Ungerer P., Burrus J., Doligaz B., Chenet P.Y. and Bessis F. (1990) Basin evaluation by intergrated two-dimensional modelling of heat transfer, fluid flow, hydrocarbon generation and migration. *Am.Assoc.Pet.Geol.Bull.* 74, 309-355.

Ungerer P. (1993) Modelling of petroleum generation and expulsion - an update to recent reviews. in: Dore A.G. (ed.) *Basin modelling: advances and applications*. NPF Spec.Pub. 3, 1-34.

Verbeek E. and Grout M. (1993) Structural evolution of gilsonite dikes, eastern Uinta Basin, Utah. in: Fouch T.D., Nuccio V.F. and Chidsey T.C Jr. (eds.) *Hydrocarbon and mineral resources of the Uinta Basin, Utah and Colorado.* Utah Geol.Assoc. Guidebook 20, 237-256.

Walderhaug O. (1990) A fluid inclusion study of quartz-cemented sandstones from offshore Mid-Norway - possible evidence for continued quartz cementation during oil emplacement. *J.Sed.Pet.* 60, 203-210.

Waples D.W. (1980) Time and temperature in petroleum formation: application to Lopatins method of petroleum exploration. *Am.Assoc.Pet.Geol.Bull.* 64, 916-926.

Whitney J.W. and Andrews E.D. (1983) Past and present geomorphic activity in the Piceance Creek drainage basin, north west Colorado. in: Gary J.H. (ed.) *16th oil shale symposium proceedings*. Colorado School of Mines Press, 566-577.

Whittaker J. (1980) Evaluation of abnormal formation pressures. *Exlog series of manuals, Houston.*

Willet S.D. and Chapman D.S. (1987) Analysis of temreratures and thermal processes in the Uinta Basin. in: Beaumont C. and Tankard A.J. (eds.) Sedimentary basins and basin forming mechanisms. *Can.Soc.Pet.Geol. Memoir* 12, 447-467.

Williamson M.A. (1992) The subsidence, compaction, thermal and maturation history of the Egret Member source rock, Jeanne d'Arc Basin, offshore Newfoundland. *Can.Pet.Geol.Bull.* 40, 136-150.

Williamson M.A. and Smyth C. (1992) Timing of gas and overpressure generation in the Sable Basin, offshore Nova Scotia: implications for gas migration dynamics. *Can.Pet.Geol.Bull.* 40, 151-169.

Wilson M.J. (1987) (ed.) *A handbook of determinative methods in clay mineralogy.* Blackie, London, 308p.

Wilson J.C. and McBride E.F (1988) Compaction and porosity evolution of Pliocene sandstones, Ventura Basin, California. *Am.Assoc.Pet.Geol.Bull.* 76, 664-681.

Wood, S.H., Wurts C., Lane T., Ballenger N., Shalteen M., Tortorica D. and Waag C. (1985) Increased groundwater discharge caused by the 1983 Idaho (USA) earthquake. in: *Proceedings of the 17th Int.Congr.Assoc.Hydrologists*; Hydrology of rocks of low permeability, 741-751.

Young A. and Low P. (1965) Osmosis in argillaceous rocks. *Am.Assoc.Pet.Geol.Bull.* 49, 1004-1007.

Yükler M.A. and Dahl B. (1993) (abs.) Future potential of basin modelling techniques. in: Dore A.G. (ed.) *Basin modelling: advances and applications.* NPF Spec.Pub. 3, 1-34.

Zeuch D.H. (1983) The mechanical behaviour of Anvils Point oil shale at elevated temperatures and confining pressures. *Can.Geotech.Jour.* 20, 344-352.

Zumberge J.E. (1987) Prediction of source rock characteristics based on terpane biomarkers in crude oils: a multivariate statistical approach. *Geochem. et Cosmochimica Acta* 51, 1625-1937.

UNIV DUNELM

Erratum: References associated with Fig.2.4.1a (Page 25)

Athy L.F. (1930) Compaction and oil migration *Am.Assoc.Pet.Geol.Bull.* 14 (1) 1-24.

Deming D. and Chapman D.S. (1989) Thermal histories and hydrocarbon generation: an example from the Utah-Wyoming thrust belt *Am.Assoc.Pet.Geol.Bull.* 73 (12) 1455-1471.

Dickinson G. (1953) Reservoir pressures in Gulf Coast Louisiana *Am.Assoc.Pet.Geol.Bull.* 37 (2) 410-432.

Doligez B.F. , Bessis J., Burrus J., Ungerer P. and Chenet P.Y. (1986) Intergrated numerical modelling of sedimentation, heat transfer and fluid migration in a sedimentary basin: the THEMIS model. in: Burrus J. (ed.) *Thermal Modelling of Sedimentary Basins*, Technip, Paris, 173-195.

Foster J.B. and Whalen H.E. (1966) Estimation of formation pressures from electrical surveys - offshore Louisiana *Jour.Pet.Tech.* 18 (2) 165-171.

Ham H.H. (1966) New charts help estimate formation pressures *Oil and Gas Journal* 64 (51) 58-63.

Hedberg H.D. (1936) Gravitational compaction of clays and shales *Am.Jour.Sci.* 231 (184) 241-287.

Hermanrud C., Eggen S., Jacobsen T., Carlsen E.M. and Pallensen S. (1990) On the accuracy of modelling hydrocarbon generation and migration: the Egersund Basin oil find, *Norway Org.Geochem.* 16 (1-3) 389-399.

Hosoi H. (1963) First migration of petroleum in Akita and Yamagata Prefectures Japan.Assoc.Mineral.Petrol.Econ.Geol.Jour. 49 (2) 43-55; 49 (3) 101-114.

Lerche I. (1990) Basin Analysis. Quantitative Methods, Vol.1 Academic Press, San Diego, 562pp.

Meade R.H. (1966) Factors influencing the early stages of compaction of clays and sands - review *Jour.Sed.Pet.* 36 1085-1101.

Proshlyakov B.K. (1960) Reservoir properties of rocks as a function of their depth and lithology *Geol.Nefti.Gaza.* 12 24-29.

Weller J.M. (1959) Compaction of sediments *Am.Assoc.Pet.Geol.Bull.* 43 (2) 273-310.

Appendix 1

Reference and conversion tables to commonly used units in this thesis

Standard Temperature and Pressure (STP): T = 273K
P = 1 atmosphere (atm)

Units of Pressure:

1 Pascal (Pa) = 1 Newton/metre^2 (N/m^2)
1 MegaPascal (MPa) = 10^6 N/m^2
1 GigaPascal (GPa) = 10^9 N/m^2
1 bar = 10^5 N/m^2
1 kilobar = 10^5 N/m^2
1 atmosphere = 1.01325 x 10^5 N/m^2
1 pound/square inch = 6891 Pa
1 bar = 14.5435 psi

Units of Distance:

1 foot = 0.3048 m
1 metre = 3.281 ft

Units of Temperature:

0°C (centigrade) = 273 K
0°K (Kelvin) = -273 K
°C (9/5) +32 = °F (Fahrenheit)

Appendix 2

Analytical Techniques

2.1 Microprobe Analyses

2.1.1 Equipment

All microprobe determinations were made at the microprobe/SEM laborotory, Department of Geology, University of St. Andrews. The combined SEM/microprobe machinery used was a JOEL 223 Superprobe using the analyses of 9 major elements. Magnification using the SEM was set to x2400 and was used in back scattered mode.

2.1.2 Sample Preparation

Samples were cut from core, supplied by the British Geological Survey (Edinburgh), to a thickness of 50μm and glass monted. The samples were then graphite coated to allow electrical conduction for a back scattered image.

2.2 X-Ray Diffraction

2.2.1 Equipment

All samples were run on a Philips PW 1130 3Kw X-Ray Diffractometer, using CoKα, running at 25ma.

2.2.2 Whole Rock Preparation

Samples were initially bulk crushed using a fly wheel titanium plated crusher. Then, to obtain the finer fraction, samples were hand crushed using a pestal and mortar. The <45μm fraction was caught using seiving techniques before adhering the powder to a glass slide using acetone as the neutral mounting medium.

2.2.3 Clay Seperates Preparation

This technique and preparation is discussed in the text and is identical to those employed in the Triaxial Compression Test study (section 5.5.2).

All XRD samples were run in their air dried state as to preserve any delicate mineral structures otherwise broken down by increased temperature. Control samples were run in duplicate to ascertain if results could be reproduced which, in the event, proved they could be.

2.3 Fluid Inclusion Microthermometry

2.3.1 Equipment

All fluid inclusions were petrographically identified and thermometrically measured using a Nikon Optiphot adapted microscope using a x400 lens for accurate identification and observation under heating and cooling runs. The heating and cooling runs were performed using a USGS adapted Reynolds gas flow heating stage. A temperature sensitive probe which was in constant contact with the specimen linked to a LED trendicator measuring temperature and ambient and forced air and Nitrogen flow (in cooling runs only). Capacity of the machinery allowed heating to >700°C (when silica windows were used) and cooling >70°C but in this study never breached 150°C and -10°C. A U.V. sodium light source was intergrated in the microscope which enabled identification of hydrocarbon rich inclusions.

2.3.2 Sample Preparation

Samples were firstly cut using a rock saw from the original core. The saw cut at minimum speed under constant water saturation to aid cooling and prevent any heat alteration and cracking of any fluid inclusions. The sections were mounted on glass slides to allow grinding to 40μm thickness. The resin used to hold the rock onto the slide was Araldite™ as it is heat stable up to 170°C and is non flourescent under U.V. light and therefore would not produce any anomalous effects during microscopic observation. The 40μm wafers were then dismounted from the glass slides for observation and analyses.

2.4 Gas Chromotography Analyses of Included Fluids

Wafers prepared in the way described in Appendix 2.3.2 were used to isolate individual mineral grains which recorded hydrocarbon bearing fluid inclusions. These mineral grains were then individually etched and then washed in detergent to remove any residual drilling fluids and potential contaminants which were recorded on primary runs. Bulk crushing of these etched grains were then analysed under specifically constructed machinery at N.R.G. which allowed the analyses of the bulk hydrocarbons in a GC column under vacuum conditions.

2.5 TOC Analyses

These analyses and preparation techniques are described in section 5.5.2

2.6 Triaxial Compression Testing

2.6.1 Equipment

The equipment used in the determination of triaxial compression response in Chapter 5 was a Robertson Geologging Multiple Core Diameter Instrumented Hoek-Type Triaxial Cell. The equipment was developed from the well-known Hoek triaxial cell originally devised at Imperial College and modified to incorporate instrumentation which permits reliable and direct measurement of sample deformations without the need to strain-gauge individual samples. This capability makes the cells particularly suited to the testing of preserved, saturated and friable materials, and where samples are to be loaded beyond failure. The specification of the equipment is listed in 'Instrumented Hoek Cell' by Robertson Geologging Ltd., Gwynedd, Wales.

2.6.2 Sample Preparation

Description of the sample preparation is documented in section 5.3

Appendix 3

Sedimentary graphic logs through the Tertiary section of the Uinta Basin

In localities with excellent vertical, continous and accessible exposure, the Tertiary section of the Uinta Basin was logged in detail (section 4.3). The following are simplified locations where these logs were taken:

Log 3 (section 4.3.1, Fig.4.3.1a)
A vertical to inclined section located on the Book Cliffs located SW of the juntion of the Evacuation Creek to Apache Ridge track. The location is

Log 2 (section 4.3.1, Fig.4.3.1b)
A vertical section located on the walls of Hells Hole Canyon NE of the Baxter Pass to Evacuation Creek track. Hells Hole Canyon provided over 120m of continous exposure of the Green River Formation containing the Douglas Creek Member through the Mahogany Oil Zone (MOZ) and into the base of the Parachute Creek Member. The location is

Log 1 (section 4.3.1, Fig.4.3.1c)
A vertical section and track side exposure along the Baxter Pass track in Parachute Creek approximately 0.7miles SE of the main Bonanza to White River Mine road. The log scetion started in Parachute Creek and ended north of Parachute Creek heading NW toward the Bonanza/White River Mine road. The location is

Appendix 4.1

3/14a-2b			3/14a-3			3/14a-4			3/14a-7			3/14a-8				3/14b-9			3/14a-11			3/14a-15		
FIT	Pressure(psi)	Depth(m)	FIT	Pressure(psi)	Depth(m)	FIT	Pressure(psi)	Depth(m)	FIT	Pressure(psi)	Depth(m)	RFT	Pressure(psi)	Depth(m)	Fluids	RFT	Pressure(psi)	Depth(m)	RFT	Pressure(psi)	Depth(m)	RFT	Pressure(psi)	Depth(m)
	8048	3224		8056	3415		8620	3560		8404	3844		8332	3723	H.C.'s		8176	3558		8239	3602		8170	3556
	8069	3223		8061	3441		8620	3521		8235	3800		8337	3731	"		8174	3564		8243	3606		8177	3565
	8295	3383		8258	3538		8739	3672		8290	3797		8345	3739	"		8180	3567		8246	3611		8185	3575
	8103	3302		8634	3724		8536	3521	RFT	8204	3635		8338	3747	"		8179	3571		8249	3616		8193	3585
			DST	8602	3723	RFT	9000	3848		8219	3649		8355	3755	"		8181	3573		8253	3621		8195	3588
				8264	3540		9318	3881		8229	3663		8340	3749	"		8184	3579		8261	3633		8201	3596
				8048	3415		9000	3847		8242	3683		8342	3753	"		8135	3579		8264	3637		8209	3606
						DST	8621	3584		8248	3692		8352	3762	"		8194	3588		8270	3641		8215	3614
							8658	3575		8256	3700		8364	3771	"		8209	3601		8278	3650		8220	3621
							8634	3542		8234	3669		8355	3779	"		8209	3611		8287	3660		8224	3625
							8597	3542		8226	3656		8417	3787	OWC at		8210	3612		8297	3664		8229	3631
										8219	3643		8371	3808	3795		8254	3630		8312	3676		8247	3656
										8205	3625		8382	3813	Water		8480	3743		8308	3682		8252	3662
										8204	3621		8486	3866	"		8487	3746		8593	3796		8256	3670
										8198	3621		8487	3879	"		8488	3747		8614	3804		8260	3675
										8223	3652		8582	3912	"		8506	3763		8623	3810		8278	3698
										8247	3685		8552	3919	"	DST	8224	3632		8618	3835		8289	3705
										8275	3718		9081	4068	"		8207	3608		8624	3840		8286	3714
										8289	3738	DST	8386	3778	41.5 API		8184	3563		8669	3855		8288	3719
									DST	8257	3733		8318	3742	42.5 API				DST	8283	3665		8304	3729
										8277	3685				gor1617					8220	3627		8312	3740
										8208	3661				327BOPD								8330	3753
										8198	3601				0.529 x								8325	3754
															10to6SCF								8334	3764
															GAS								8336	3767
																							8351	3774
																							8388	3794
																							8373	3796

Pressure/Depth data

3 15-3			3 15-4				3 15-5			3/9a-1			3/9a-2			3/9a-3			3/9a-4			3/9a-5			3/9a-6		
FIT	Pressure(psi)	Depth(m)	RFT	Pressure(psi)	Depth(m)	Fluids	RFT	Pressure(psi)	Depth(m)	FIT	Pressure(psi)	Depth(m)	FIT	Pressure(psi)	Depth(m)	FIT	Pressure(psi)	Depth(m)	RFT	Pressure(psi)	Depth(m)	RFT	Pressure(psi)	Depth(m)	RFT	Pressure(psi)	Depth(m)
	8767	3635		8254	3247	H.C.'s		3031	2051		6543	3227		7573	3874		6698	3370		7602	3836		7129	3415		6502	3177
DST	8244	3274		8286	3264	conden-		3030	2045		6619	3308		7603	3869		6556	3246		7520	3814		7131	3425		6507	3183
	8242	3256		8318	3284	sate?		3029	2041		6559	3257		7371	3717		6541	3246		7487	3794		7138	3442		6513	3191
				8373	3323	"		3028	2032		7575	3868		6799	3435		6550	3224		7515	3784		7152	3453		6516	3197
				8412	3351	"		3027	2029		7389	3760		6643	3324		6463	3159		7446	3753		7152	3472		6520	3201
				8443	3370	"		3026	2026		6837	3476		6538	3265		6596	3274		7403	3702		7162	3492		6523	3205
				8476	3394	"		3028	2014		6546	3256		6539	3251		7515	3773		7370	3677		7178	3508		6526	3211
				8504	3413	"		3024	2032		6500	3255		6516	3227		7377	3675		7354	3674		7179	3527		6532	3218
				8611	3474	"		3022	2029	DST	6528	3230	DST	7432	3683		7290	3640		6768	3407		7182	3532		6537	3225
				8665	3512	"		3022	2026					6557	3268		7340	3635		6760	3401		7191	3554		6540	3230
				8753	3544	"		3021	2024					6493	3205	RFT	7694	3878		6659	3335		7209	3570		6543	3234
				9514	3807	G/OWC		8194	3167								7631	3861		6571	3272		7209	3580		6546	3238
				9529	3810	Water		8196	3170								7650	3847		6549	3257		7213	3589		6551	3242
				9650	3818	"		8197	3174								7570	3797		6524	3230		7223	3584		6557	3247
				9488	3828	"		8193	3177								7543	3772		6516	3221		7225	3600		6564	3254
				7393	3839	"		8200	3182								6801	3412		6494	3197		7235	3609		6590	3268
				9464	3848	"		8202	3186								6711	3381		6481	3182		7260	3620		6596	3273
				9722	4059	"		8204	3192								6693	3365		6464	3264		7275	3636		6609	3282
			FIT	9488	3957	"		8208	3194								6646	3329		7339	3667		7323	3668		6623	3292
				9492	3903	"		8209	3200								6617	3316		7315	3677		7266	3689		6675	3333
				9439	3848	"		8209	3207								6608	3302	DST	7291	3661		7381	3712		6721	3369
				9333	3827	"		8211	3211								6621	3296		6471	3219		7506	3732		6651	3313
				9421	3825	"		8215	3217								6573	3272		6489	3201		7226	3595		6738	3382
			DST	9451	3597	conden-		8219	3226								6559	3261		6498	3199		7208	3558		6788	3417
				9455	3600	sate		8220	3228								6567	3254		6454	3137		7132	3420		6800	3426
								8225	3230								6527	3238					7164	3486		6849	3459
								8226	3234								6509	3214					7174	3509		6540	3224
								8227	3236								6485	3182					7204	3562	DST	6554	3246
								8228	3238								6471	3160					7216	3586		6427	3176
								8231	3242							DST	6700	3371					7131	3605		6514	3182
								8235	3250								6515	3165					7335	3677			
								8274	3288														7392	3719			
								8278	3290														7214	3580			
								8280	3292														7230	3537			
								8285	3295														7165	3473			
								8308	3313														7143	3440			
								8341	3339														7163	3430			
								8223	3224														7133	3415			
								8275	3287														7183	3532			
								8348	3345														7226	3603			
								8359	3352													DST	7216	3581			
								8382	3363														7162	3555			
								8399	3371														7142	3513			
								8405	3379														7153	3462			
								8221	3226														7092	3367			
								8221	3227																		
								8224	3234																		
								8225	3236																		
								8227	3242																		
								8235	3249																		
								8234	3249																		
								8409	3391																		
								8891	3608																		
								8847	3614																		
								8853	3624																		
								8861	3635																		
								8865	3640																		

Pressure/Depth data

3/9a-8			3/9a-N1			3/9a-N2			3/9a-N3				3/9a-N4			3/9a-N5		
RFT	Pressure(psi)	Depth(m)	RFT	Pressure(psi)	Depth(m)	RFT	Pressure(psi)	Depth(m)	RFT	Pressure(psi)	Depth(m)	Fluids	RFT	Pressure(psi)	Depth(m)	RFT	Pressure(psi)	Depth(m)
	7171	3423		6592	3258		6506	3180		6440	3115	H.C.'s		7156	3445		6464	3142
	7167	3430		6607	3269		6511	3186		6444	3119	"		7161	3454		6465	3144
	7168	3434		6618	3277		6516	3191		6447	3122	"		7165	3463		6469	3147
	7171	3440		6226	3283		6522	3198		6451	3126	"		7167	3468		6471	3151
	7204	3445		6639	3292		6526	3202		6453	3129	"		7174	3481		6474	3154
	7205	3453		6647	3298		6531	3207		6459	3135	"		7178	3490		6476	3157
	7214	3457		6661	3307		6538	3213		6465	3141	"		7182	3498		6479	3161
	7220	3462		6671	3312		6541	3218		6471	3148	"		7186	3506		6482	3164
	7224	3466		6683	3322		6546	3222		6474	3151	"		7189	3513		6481	3167
	7246	3477		6690	3328		6548	3226		6477	3154	"		7192	3519		6485	3171
	7257	3485		6700	3337		6554	3231		6479	3156	"		7196	3527		6489	3174
	7371	3494		6728	3356		6561	3236		6481	3158	"		7199	3534		6492	3177
	7276	3503		6749	3372		6565	3240		6481	3160	"		7203	3541		6494	3181
	7292	3509		6767	3385		6577	3248		6483	3161	"		7207	3548		6497	3184
	7307	3516		6804	3400		6585	3254		6484	3163	"		7216	3563		6499	3187
	7308	3524		6800	3409		6613	3273		6488	3167	"		7226	3577		6502	3190
	7303	3529		6838	3437		6640	3293		6493	3172	"		7231	3584		6504	3193
	7311	3533		6854	3448		6681	3321		6497	3176	"		7262	3595		6507	3196
	7322	3541		6924	3490		6698	3334		6499	3178	"		7267	3607		6508	3198
	7327	3545		6970	3521		6793	3395		6501	3180	"		7281	3616		6511	3202
	7340	3557		6979	3529		6811	3408		6503	3184	"		7294	3629		6514	3205
	7348	3562		6988	3534					6518	3199	"		7315	3642		6516	3208
	7359	3572		7067	3563					6533	3214	"		7363	3672		6518	3211
	7377	3587								6546	3229	Approx.		7387	3689		6521	3214
	7386	3593								6556	3237	OWC					6523	3217
	7414	3604								6570	3247	Water					6525	3219
	7421	3608								6579	3254	"					6529	3223
	7445	3616								6591	3263	"					6531	3227
	7452	3627								6619	3283	"					6534	3230
	7448	3630								6644	3298	"					6539	3236
	7264	3504								6662	3312	"					6560	3253
	7420	3609								6723	3349	"					6560	3261
DST	7248	3472								6738	3361	"					6580	3267
	7153	3395								6748	3366	"					6589	3272
										6752	3373	"					6596	3278
										6761	3379	"					6622	3285
																	6628	3300
																	6649	3316
																	6564	3256

Appendix 4.2

LOCATION	WELL	CORE DEPTH(m)	T.V.D.	LITHOSTRAT.	ANALYSIS	SAMPLE NAME
Alwyn North	3/9a-5					
		3420		sst	TS FI	ANA1
		3440		sst	TS FI	ANA2
		3459		sst		ANA3
		3480		sst	TS FI	ANA4
		3500		sst/sh	TS FI	ANA5
		3520		sst	TS FI	ANA6
		3540		sst/sh	TS SEM	ANA7
		3560		sst	TS FI	ANA8
		3581		sst		ANA9
		3600		sst	TS FI	ANA10
		3620		sst	TS FI	ANA11
Alwyn North	3/9a-6					
		3168		sh	SEM XRD	ANB1
		3170		sh	SEM XRD	ANB2
		3180		sst	FI	ANB3
		3190		sst	TS	ANB4
		3200		sst	TS FI	ANB5
		3220		sst	FI	ANB6
		3230		sst	TS FI	ANB7
		3240		sst	TS FI	ANB8
		3252		sst/sh	TS SEM	ANB9
		3258		sh	SEM	ANB10
		3271		sh	SEM	ANB11
		3278		sst	TS FI	ANB12
		3288		sst	TS FI	ANB13
		3300		sst	TS FI	ANB14
		3309		sst	TS	ANB15
Alwyn South	3/14a-3					
		3410		sh	SEM XRD	ASB1
		3420		sst	TS FI	ASB2
		3430		sst	TS FI	ASB3
		3445		sh	SEM XRD	ASB4
		3450		sh	SEM XRD	ASB5
		3460		sh	SEM XRD	ASB6
		3550		sst	TS FI	ASB7
		3560		sst	FI	ASB8
		3571		sst	TS FI	ASB9
Alwyn South	3/14b-9					
		3561		sh	SEM XRD	ASA1
		3570		sst	TS	ASA2
		3579		sst	TS FI	ASA3
		3591		sst/sh	SEM XRD	ASA4
		3600		sst	TS	ASA5
		3610		sst	FI	ASA6
		3617		sst		ASA7
		3630		sst	TS FI	ASA8
		3640		sh	SEM XRD	ASA9
		3731		sst/sh	TS	ASA10
		3740		sst/sh	TS SEM	ASA11
		3751		sst	TS FI	ASA12
		3760		sst	TS FI	ASA13
		3779		sst/sh	TS SEM	ASA14
Alwyn S.E.	3/15-3					
		3311		sh	SEM XRD	ASEA1
		3318		sh	SEM XRD	ASEA2
		3352		sst	TS FI	ASEA3
		3359		sst	TS FI	ASEA4
		3363		sst	FI	ASEA5
		3830		sst	TS FI	ASEA6
		3838		sst		ASEA7
Alwyn S.E.	3/15-4					
		3250		sst	TS FI	ASEB1
		3258		sst	FI	ASEB2
		3266		sst	TS	ASEB3
		3274		sst/sh	SEM XRD	ASEB4
		3827		sst	TS FI	ASEB5
		3820		sst	FI	ASEB6
		3855		sst	TS	ASEB7
		3860		sst	TS FI	ASEB8

Fluid Inclusion data

Appendix 4.3

Well	Core Depth (m	Lithology	Overgrowth	T(hom) C	T(f) C	Well	Core Depth (m	Lithology	Overgrowth	T(hom) C	T(f) C
3/9a-5	3440	Sandstone	QA2	89.4		3/9a-5	3420	Sandstone	QA2	89.3	
			All aqueous	88.8					All aqueous	89.9	
				89.9						91.6	
				90.2	-2.8					92	
				90.3						92.8	
				90.7						92.9	
				91.8	-2.8					92.4	
				91.8						93.4	-2.9
				91.9	-3					93.6	-2.8
				91.6						93.8	
				92						93.9	
				92.3	-3					95	-3.1
				92.4						95.2	
				93						95.3	
				92.4						96.1	
				93.7						96.5	
				93.7						96.8	
				93.8						96.9	
				93.9						97.1	
				94.2	-2.7					97.3	
				95						98	-3.1
				95.1						98	
				95.1						98.4	
				95.3	-3.2					99	
				95.4						99.3	-3
				95.4						102.3	-3
				95.5						104.4	
				95.5							
				95.6							
				96.2							
				96.4							
				96.8							
				96.9	-3.2						

Fluid Inclusion data

Well	Core Depth (m	Lithology	Overgrowth	T(hom) C	T(f) C	Well	Core Depth (m	Lithology	Overgrowth	T(hom) C	T(f) C
3/9a-5	3440	Sandstone	QA2	96.9		3/9a-6	3200	Sandstone	QA2	91	
			All aqueous	97					All aqueous	92.4	
				97.4						92.4	
				98						92.8	
				98.1						92.9	
				98.5						93	-2.9
				98.5						93.5	
				99.2						93.8	-3.2
3/9a-5	3520	Sandstone	QA2	90.6						93.9	
			All aqueous	92.9						95.1	
				93.3						95.2	-3.4
				93.8						95.7	
				93.9	-2.7					95.8	
				94						95.8	
				95.2	-3					98.4	
				95.8		3/9a-6	3220	Sandstone	QA2	91.8	
				95.9	-3.1				All aqueous	92.8	-2.8
				96.8						93	-3
				97	-3.2					93.9	-3.1
				99.1						95.1	
				102.6						95.1	
3/9a-6	3240	Sandstone	QA2	97.8						95.3	
			All aqueous	97.9						96	
				99.1						96.2	
				99.2						96.3	
				101.8						96.8	
				103						96.9	
				103.8						96.8	

Fluid Inclusion data

Well	Core Depth (m	Lithology	Overgrowth	T(hom) C	T(f) C	Well	Core Depth (m	Lithology	Overgrowth	T(hom) C	T(f) C
3 15-3	3352	Sandstone	QA1	115.9		3 15-3	3363	Sandstone	QA1	118	
			All aqueous	118.2					All aqueous	118.8	
				118.3	-2.8					118.9	-2.9
				119.9	-2.9					120.4	-2.6
			QA2	120.3						120.4	
			All aqueous	123.5						120.9	
				123.7						120.9	
3 15-3	3359	Sandstone	QA1	117						121.2	
			All aqueous	117.3						123	
				118.1	-3.1		3830	Sandstone	QA1	121.3	
				118.8	-3				All aqueous	121.4	
				118.9						125	
				118.9						125	-2.8
				119.5						125.2	-2.7
				119.6					QA2	123.2	
			QA2	116.3					All aqueous	123.1	
			All aqueous	118.2		3 15-4	3250	Sandstone	QA1	122.1	
				122.3	-3				All aqueous	122.4	-2.6
				122.4	-3					123.4	
				123.1						123.3	
3 15-4	3258	Sandstone	QA1	116.1						123.8	
			All aqueous	117	-3.2					123.9	
				120.1	-3.3					124.3	-3.1
				121.3					QA2	126.3	
				121.9					All aqueous	126.4	
				122		3 15-4	3827	Sandstone	QA2	125.6	
				123.3					All aqueous	126.6	
				125						126.7	
			QA2	125.1						127	
			All aqueous	125.3							
				126.5							

Fluid Inclusion data

Well	Core Depth (m	Lithology	Overgrowth	T(hom) C	T(f) C	Well	Core Depth (m	Lithology	Overgrowth	T(hom) C	T(f) C
3 15-4	3820	Sandstone	QA1	119		3 15-4	3860	Sandstone	QA1	115.8	
			All aqueous	119.2	-3				All aqueous	116.9	
				122.1	-2.9					118.1	-3
				124						118.3	
				124.3						119	-3
				124.8						121	-2.8
			QA2	123.1						121.4	-2.9
			All aqueous	124	-3					121.8	
				126.1						122.7	
				126.2						122.8	
				126.3						124.1	
				126.7						124.8	
				126.8							
				126.9							

Fluid Inclusion data

Well	Core Depth (m	Lithology	Overgrowth	T(hom) C	T(f) C	Well	Core Depth (m	Lithology	Overgrowth	T(hom) C	T(f) C
3/9a-5	3440	Sandstone	QA2	68		3/9a-5	3420	Sandstone	QA2	68.9	
			All Hyd.carb	68.1					All Hyd.carb	69.2	
				70.2						73	
				70.8						74.1	
				72.1						74.8	
				74.3						75.1	
				74.4						75.2	
				75.3						75.3	
				75.3						75.8	
				75.4						76	
				76.1						77.1	
				76.1							
3/9a-6	3200	Sandstone	QA2	71		3/9a-6	3220	Sandstone	QA2	68.1	
			All Hyd.carb	71.2					All Hyd.carb	68.3	
				72						69.3	
				72.3						69.8	
				72.4						69.9	
				73.1						70.5	
				74.9						70.8	
				75.1						70.9	
				75.6						72	
				75.7						72.3	
				77.9						72.9	
3/9a-6	3230	Sandstone	QA2	69.8						73	
			All Hyd.carb	70.1						74	
				70.3						74.1	
				72.6						74.9	
				72.7						75	
				74.7						77.3	
				75.9						77.5	

Fluid Inclusion data

Well	Core Depth (m	Lithology	Overgrowth	T(hom) C	T(f) C	Well	Core Depth (m	Lithology	Overgrowth	T(hom) C	T(f) C
3 15-3	3352	Sandstone	QA1	88		3 15-3	3359	Sandstone	QA1	85.8	
			All Hyd.carb	88.2					All Hyd.carb	86.2	
				90.1						88.5	
				90.3						88.9	
			QA2	91.4						91.3	
			All Hyd.carb	90.3						91.9	
				92					QA2	87	
				92.2					All Hyd.carb	91.3	
				94						91.9	
3 15-3	3363	Sandstone	QA1	87.8		3 15-3	3830	Sandstone	QA1	86.4	
			All Hyd.carb	87.9					All Hyd.carb	88.1	
				89.1						88.3	
				90.3						89.3	
				90.4					QA2	90.3	
				90.9					All Hyd.carb	90.4	
				90.9						91.3	
				91.6						92	
			QA2	89.4						92.3	
			All Hyd.carb	90.2		3 15-4	3250	Sandstone	QA1	88.1	
				91.3					All Hyd.carb	88.3	
				91.4						88.6	
3 15-4	3258	Sandstone	QA1	87.8						88.8	
			All Hyd.carb	88.8						91	
				90.1						91.3	
				90.3		3 15-4	3827	Sandstone	QA1	86.3	
			QA2	92.3					All Hyd.carb	87.1	
			All Hyd.carb	92.8						88.2	
3 15-4	3820	Sandstone	QA1	89						89.3	
			All Hyd.carb	89.9		3 15-4	3860	Sandstone	QA1	86.8	
				89.9					All Hyd.carb	87.2	
				91.2						87.8	
				92.3						87.9	
				92.4						89.3	

Fluid Inclusion data

Well	Core Depth (m	Lithology	Overgrowth	T(hom) C	T(f) C	Well	Core Depth (m	Lithology	Overgrowth	T(hom) C	T(f) C
3 15-4	3820	Sandstone	QA1	92.7							
			All Hyd.carb	92.9							
				94							
			QA2	89.8							
			All Hyd.carb	89.9							
				90.7							
				90.8							
				92							
				93.8